Gerbail T. Krishnamurthy
Shakuntala Krishnamurthy

Nuclear Hepatology

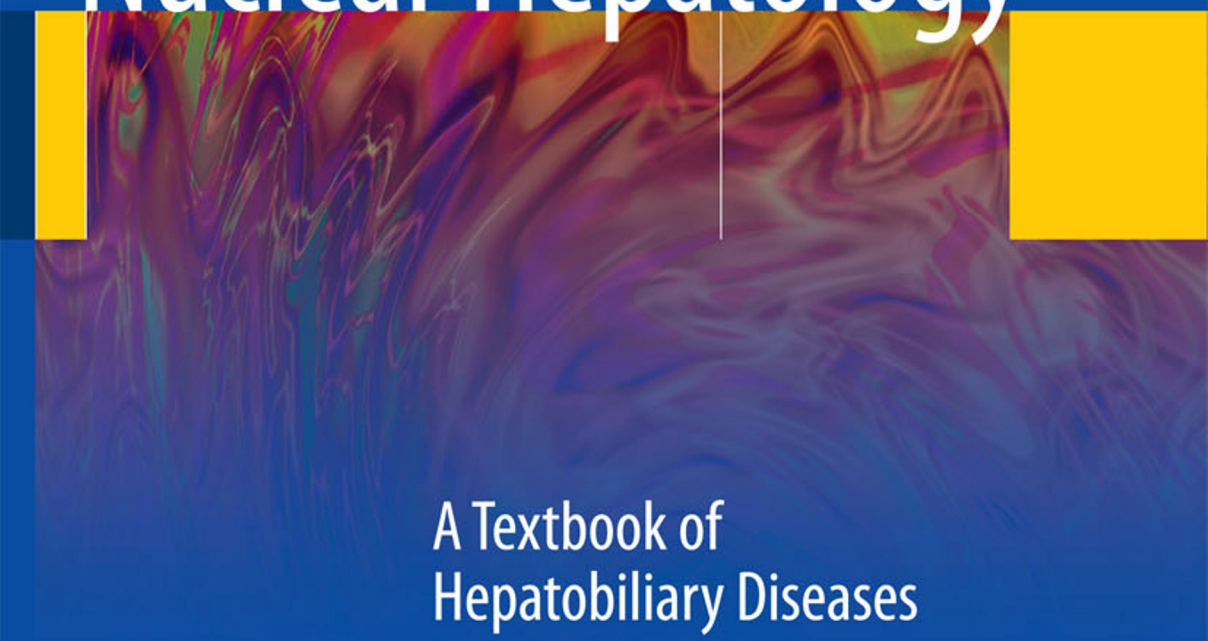

A Textbook of Hepatobiliary Diseases

Second Edition

Springer

Nuclear Hepatology

Gerbail T. Krishnamurthy • Shakuntala Krishnamurthy

Nuclear Hepatology

A Textbook of Hepatobiliary Diseases

Second Edition

Springer

Gerbail T. Krishnamurthy
Tuality Community Hospital
Hillsboro, OR 97123
USA

Shakuntala Krishnamurthy
Tuality Community Hospital
Hillsboro, OR 97123
USA

ISBN 978-3-642-00647-0 e-ISBN 978-3-642-00648-7
DOI 10.1007/978-3-642-00648-7
Springer Dordrecht Heidelberg London New York

Library of Congress Control Number: 2009926189

Cover design: eStudioCalamer

Printed on acid-free paper

Springer is part of Springer Science+Business Media (www.springer.com)

Dedicated with love and affection to our grandson Sachin Thomas Wheatley.

Preface to the Second Edition

Since the publication of the first edition of Nuclear Hepatology almost 10 years ago, new advances have taken place, both in our understanding of liver pathophysiology and various imaging modalities. A unique feature of imaging of physiology is that it enables quantification. Since liver physiology is complex, quantification has been a challenge. Many publications in the past have often included quantification based on home-made software not available for others. Thus, the comparison of results from one center to another becomes difficult, if not impossible. The second edition of Nuclear Hepatology addresses these issues. Sophisticated software for liver and gallbladder function has been tested and validated through many of our previous publications. Now that software is FDA approved and available for others through a commercial company, it is hoped that future publications of imaging of liver and gallbladder physiology would routinely include quantification.

Although the function of the hepatocyte is complex, it can be broadly divided into two main categories, substrate uptake at the basolateral border and intracellular transit prior to excretion into the canaliculi. The earliest manifestation of hepatocellular injury occurs in the form of prolongation of the intracellular transit time, which occurs long before the disruption of the basolateral border with subsequent rupture and death. The liver enzymes are released into circulation after the death of the hepatocyte. Hepatocyte function can be restored completely by treating the patient as soon as the intracellular transit is altered, but not after the rupture of the basolateral border (cell death). Measurement of intracellular transit time from a Tc-99m HIDA study enables early detection of the hepatocyte injury and early therapeutic intervention.

Most of the chapters include updated information. The second chapter describes the latest information related to liver physiology and Chap. 5 provides sophisticated software quantification of pathophysiology. Cholescintigraphic images are correlated with morphologic images obtained with ultrasound, CT or MRI. Since PET/CT imaging has currently become a standard in the care of the cancer patient, a detailed description is provided in Chap. 12. Latest information on biliary dyskinesia in adults and neonatal hepatitis in infants is updated. It is our firm belief that physicians, surgeons, and pediatricians caring for patients with liver and gallbladder disease would become more familiar with the latest advances in imaging technology and provide the best care for their patients, based on evidence from objective parameters.

Contents

Morphology and Microstructure of the Hepatobiliary System

1

1.1 Morphology

Liver and gallbladder disease is a common entity around the world and according to the World Health Organization estimation accounts for 46.1% of global disease [1]. Liver transplantation for end-stage liver disease, segmental resection for tumor, and therapeutic interventional maneuvers has made it necessary to have thorough knowledge of the morphology of the liver and biliary system in much greater detail than ever before [2]. With the widespread application of segmental liver resection for living donor liver transplantation or radioablation of liver tumors, thorough knowledge of internal structures is critical for radiologists, nuclear medicine physicians, and surgeons. Since the publication of the first edition of our book in 2000, many advances in liver disease therapy have taken place, making it necessary to provide more detailed anatomic and histopathological information. Anatomical details of the vascular and ductal structures are well depicted on a multidetector computer tomography (MDCT), magnetic resonance cholangiopancreatography (MRCP), and endoscopic retrograde cholangiopancreatography (ERCP), enabling identification of the third or fourth order branches on the images. Such detailed structural information is necessary for surgeons for segmental resection of the liver.

Embryology

The liver and biliary systems develop from an endodermal bud that arises during the 5th week of intrauterine life when the embryo is about 3 mm in length [3]. The bud originates from the ventral surface at the junction of the foregut with the midgut, and soon divides into cranial (pars hepatica) and caudal (pars cystica) branches. The ventral pancreas sprouts near the caudal bud, and the dorsal pancreas arises on the opposite side at the foregut–midgut junction (Fig. 1.1.1). When the embryo is about 5 mm in length, the cranial and caudal branches become further connected by a common stalk, which later becomes the common bile duct. By the time the embryo is about 7 mm in length, the cranial branch (pars hepatica) divides into two cellular columns, which later become the physiologic right and left hepatic lobes [4]. The gallbladder develops from the caudal branch (pars cystica) and continues its connection with the common stalk through a channel, which later becomes

G.T. Krishnamurthy and S. Krishnamurthy, *Nuclear Hepatology,*
DOI 10.1007/978-3-642-00648-7_1, © Springer-Verlag Berlin Heidelberg 2009

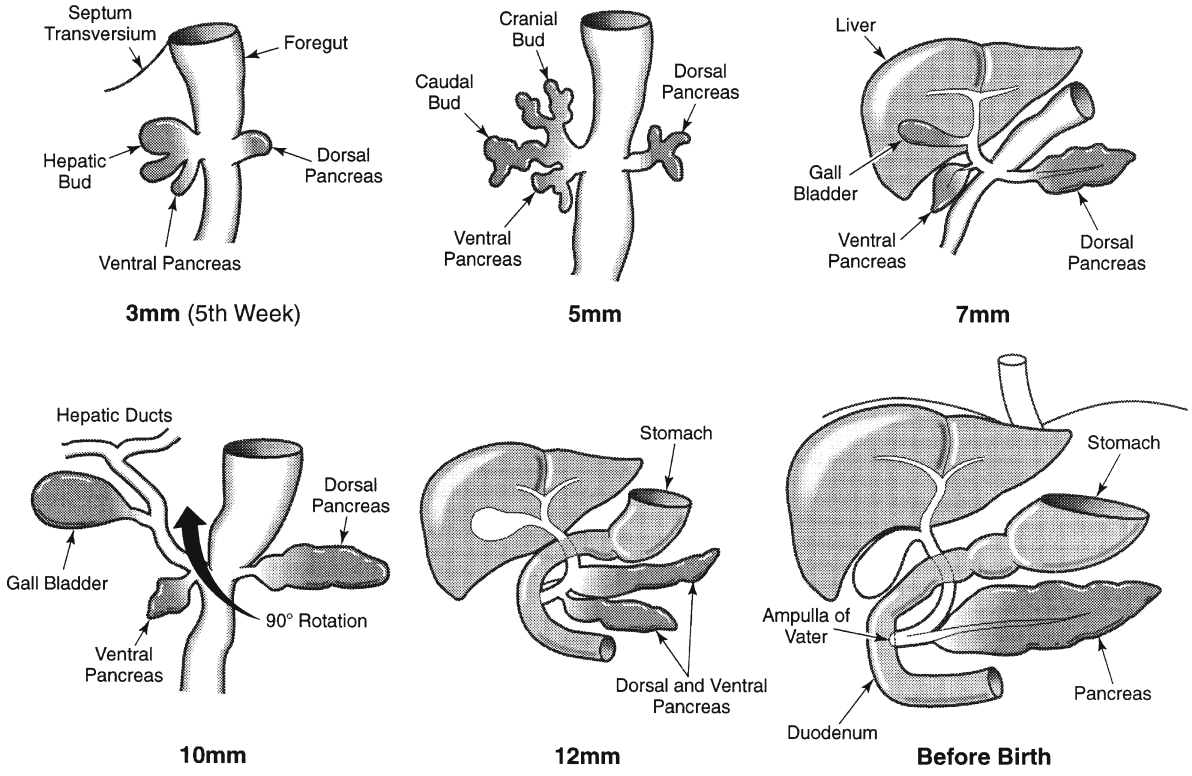

Fig. 1.1.1 Embryology of the hepatobiliary system. The hepatic bud arises from the endoderm of the primitive foregut at its junction with the midgut when the embryo is about 3 mm in length. The hepatic bud divides into cranial (pars hepatica) and caudal (pars cystica) branches when the embryo reaches 5 mm size. The ventral pancreas arises from the pars cystica, which later gives rise to the biliary system. After a 90° clockwise rotation (10 mm embryo), the ventral pancreas fuses with the dorsal pancreas. This rotation brings the common bile duct posterior to the duodenum (12 mm). The common bile duct opens into the duodenum at the postero-medial wall at an elevation called the papilla

the cystic duct. Canalization takes place to form a patent biliary tree (gallbladder, cystic duct, right and left hepatic duct, common hepatic duct, and the common bile duct). When the embryo is about 10 mm in length, the gut begins to make a 90° clockwise rotation and completes it by the time it is 12 mm in length, which brings the ventral pancreas in close contact with the dorsal pancreas, facilitating their fusion into a single pancreas before birth [5]. This rotation brings the common bile duct posterior to the duodenum. Many congenital abnormalities around this region are secondary to mal-rotation at this junction. The caudate lobe arises separately close to the inferior vena cava, independent of the right and left hepatic lobes. The liver begins bile secretion by the 12th intrauterine week, thus completing the formation of the hepatobiliary system, the most complex metabolic factory in the human body. In adults, the liver weighs about 1,500–1,800 g and forms about 1/50 of the body weight. In children, however, it forms a relatively much larger fraction (1/20) of the total body weight.

Liver Lobes and Surfaces

Most of the liver is situated in the right upper quadrant of the abdomen underneath the right hemi-diaphragm, with the superior border situated at the level of the right fifth intercostal space. Liver consists of five surfaces: anterior, posterior, right lateral, superior, and inferior. The anterior, right lateral, and posterior surfaces are smooth, and superior and inferior surfaces are rough with grooves and fissures for entry and exit of the vascular and biliary structures (Fig. 1.1.2). The liver is divided into right and left lobes on the basis of either anatomic or physiologic markers. Anatomically, the liver is divided into right and left lobes on the basis of the line of attachment of the falciform ligament. The anatomic division serves no useful purpose in the management of liver disease and hence has been given less importance in recent years. The physiologic division, on the other hand, has gained much more popularity as it follows embryologic development and delineates functional lobes and segments, whose line of demarcation is used for liver resection during transplant or tumor surgery. The physiologic division into right and left lobes is indicated on the inferior surface by a deep fissure called the plane of Sérégé-Cantlie that passes from the gallbladder fossa along the inferior border to the inferior vena caval groove along the superior border [5].

The falciform ligament, the marker of the anatomic right and left lobes, lies to the left of the deep fissure (Sérégé-Cantlie line) that divides the liver into physiologic right and left lobes. The caudate lobe situated posteriorly and quadrate lobe situated anteriorly form part of the anatomic right lobe, but both of these structures belong to the physiologic left lobe (Fig. 1.1.2). The anatomic right lobe is approximately six times larger (85%) than the anatomic left lobe (15%), whereas the physiologic right lobe is 70% and physiologic left lobe 30% in size. Thus, the physiologic left lobe is much larger than its anatomic counterpart. It is important, therefore, to be very specific while describing lobes of the liver, whether one is referring to the anatomic or to the physiologic division. Throughout this book, we will refer to the physiologic division unless otherwise mentioned.

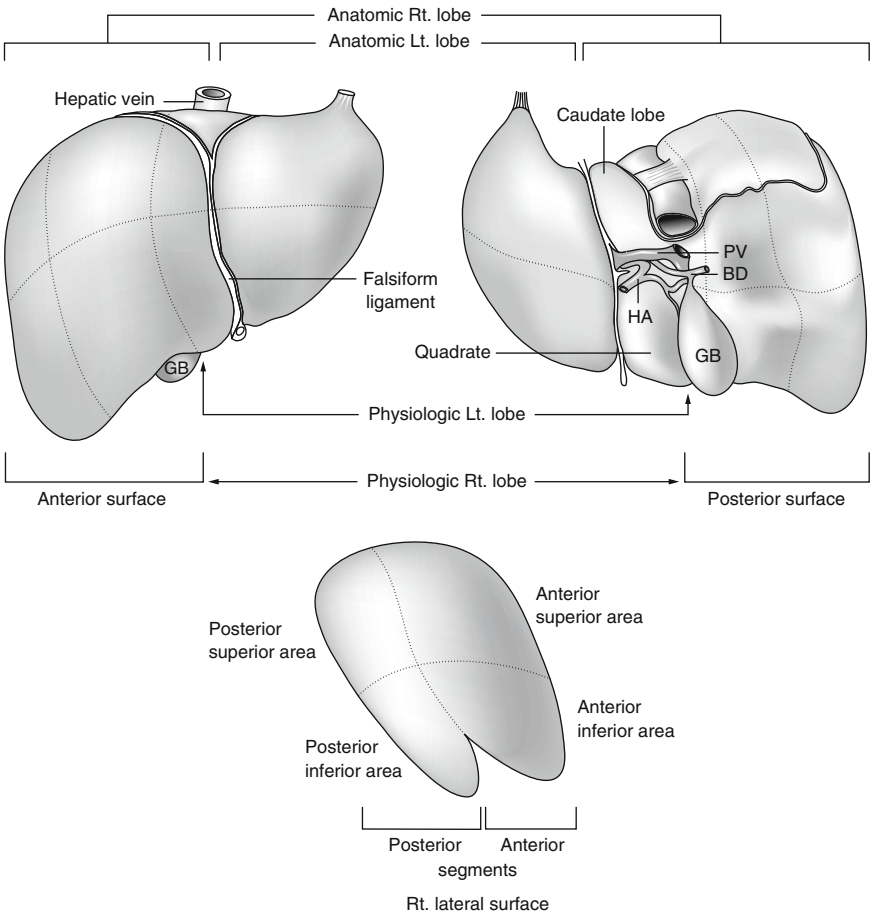

Fig. 1.1.2 Surfaces, segments, and lobes of the liver. The anatomic left lobe (divided by the falciform ligament) is much smaller than the anatomic right lobe, but the physiologic left lobe is much larger than the anatomic left lobe. The quadrate lobe, which forms a part of the anatomic right lobe, forms a part of the physiologic left lobe. Liver consists of three lobes (including the caudate lobe), four segments, and eight areas. *HA* hepatic artery, *BD* bile duct, *PV* portal vein, *GB* gallbladder

Segments and Areas

The liver is divided into lobes, segments, and areas. The division is made on the basis of either the vascular [6, 7] or the bile duct branches [8]. As both the vessels (hepatic artery and portal vein) and bile ducts travel together to every lobe, segment, and area of the liver, it usually makes no difference which structure is chosen as the reference point for the division. Segments are named by either numbers or given a directional nomenclature, similar to

Table 1.1.1 Nomenclature for hepatic segments and lobes as adopted by different authors

Liver lobes	Hjortsjo (5)	Healey and Schroy (8)	Couinaud (6)	Bismuth (9)
Caudate lobe	Dorsal segment	Lobus caudatus	I	I
Left lobe	Dorso-lateral segment	Lateral superior area	II	II
	Ventro-lateral segment	Lateral inferior area	III	III
	Central segment	Medial superior area	IV	IVA
	Dorso-ventral segment	Medial inferior area	IV	IVB
Right lobe	Ventro-caudal segment	Anterior-inferior area	V	V
		Posterior-inferior area	VI	VI
	Dorso-caudal + intermedio-caudal	Posterior-superior area	VII	VII
		Anterior-superior area	VIII	VIII
	Dorso-cranial + intermedio-cranial			
	Ventro-cranial			

the division of the lungs into lobes and segments. Couinaud [6] and Bismuth [9] used numbers, whereas Healey and Schroy [8] preferred directional nomenclature. The imaging technology (nuclear medicine, CT, MRI, and ultrasound) and surgeons prefer to use numerical segments for the division [10–16]. Table 1.1.1 shows names and numbers adopted by different authors. Starting from the caudate lobe (I), the numbers go clockwise covering the lateral (II, III) and medial (IVA, IVB) segments of the left lobe, and inferior (V, VI) and superior (VII, VIII) half of the right lobe. The directional nomenclature used by Healey and Schroy [8] is much easier to remember, whereas the numbers require memorization. Recent authors seem to prefer the numbers proposed by Couinaud and Bismuth [6, 9, 17].

Three major hepatic veins drain the liver blood into the inferior vena cava, left hepatic vein, middle hepatic vein, and right hepatic vein. The middle hepatic vein, which follows the direction of the Serege-Cantlie plane (from the gallbladder fossa below to the inferior vena caval groove above), divides the liver into physiologic right and left lobes. The right hepatic vein divides the right lobe into anterior (V and VIII) and posterior (VI and VII) segments. The left hepatic vein divides the left lobe into medial (IVA and IVB) and lateral (II and III) segments. The right and left branches of the portal vein, hepatic artery, or common hepatic duct divide the liver segments into superior and inferior areas. The liver, therefore, consists of two large lobes, four segments, and eight areas (Fig. 1.1.3). Recent studies, however, suggest that in the case of extended liver resection for malignancy, Hjortsjo's segmental division may provide better anatomic detail than Couinaud's classification [18]. The caudate lobe (I), despite being small in size, is considered as a separate lobe mainly because of its unique embryology and vasculature [19, 20]. It lies between the hilar structures and inferior vena cava and consists of three parts: Spiegel's lobe (left), the paracaval (middle) and caudate process (right).

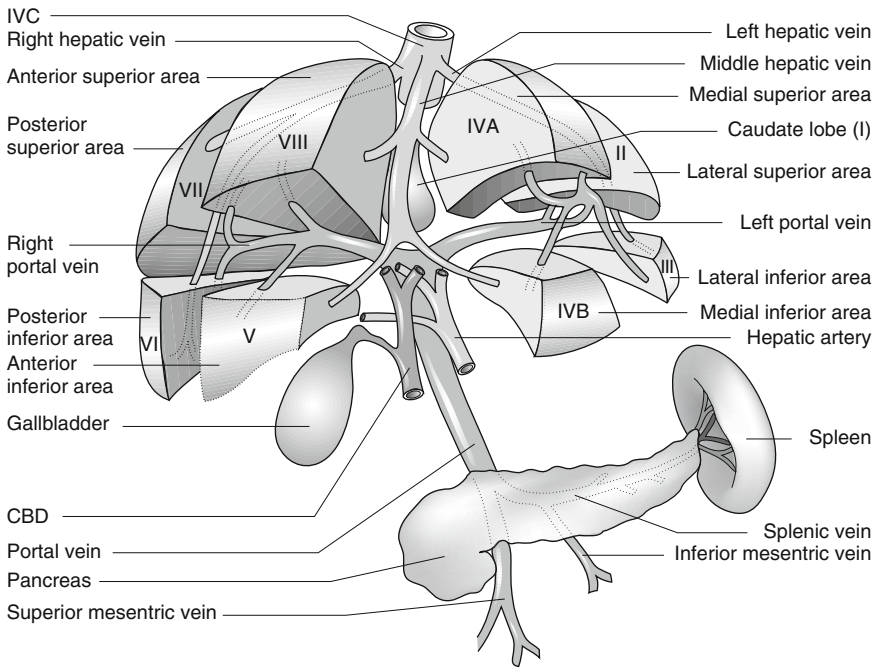

Fig. 1.1.3 Hepatic and portal venous system. The left hepatic vein, carrying blood from the lateral segment of the left lobe, joins the middle hepatic vein, carrying blood from the medial segment of the left lobe and anterior segment of the right lobe, to form a single venous trunk before joining the inferior vena cava. The right hepatic vein carries blood mostly from the posterior segment of the right lobe and joins the inferior vena cava separately. The portal vein is formed by the union of the superior mesenteric vein and splenic veins. It divides into right and left portal branches that travel in opposite directions and enter the parenchyma in the middle, dividing the liver into superior and inferior areas. (*CBD* common bile duct, *IVC* inferior vena cava)

Hepatic Artery

After arising from the celiac axis, the hepatic artery runs between the two layers of the hepatogastric ligament (lesser omentum) and enters the liver at the hilum. It is situated anterior to the portal vein and on the left side of the common bile duct (Fig. 1.1.3). In 90% of patients, the hepatic artery divides into right and left branches before entering the hilum of the liver. In the remaining 10%, the hepatic artery divides into three terminal branches, with the third branch entering the quadrate lobe (IV) directly. Wide variability is seen in the branching of the hepatic artery, portal vein, and bile ducts, and their clear delineation by imaging procedures (MDCT, ERCP, MRCP) is essential prior to segmental liver resection [21]. The hepatic artery supplies about 400 ml of arterial blood per minute at 100 mmHg systolic pressure and accounts for 25% of the total liver blood flow [22].

The cystic artery to the gallbladder usually arises from the right hepatic artery in the triangle of Calot, which is bordered by the inferior liver surface above, common hepatic duct to the left, and the cystic duct to the right. Often the cystic artery may arise from the

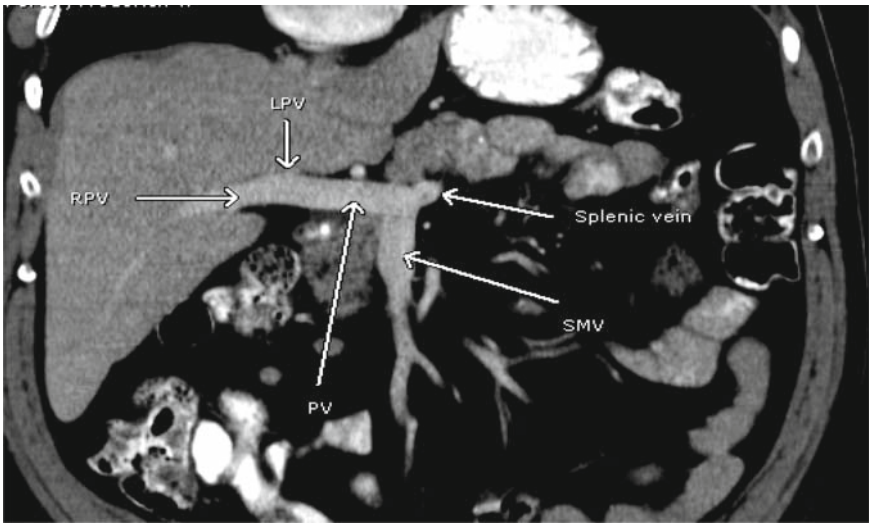

Fig. 1.1.4 Portal vein. Coronal section CT (with contrast agent) shows the formation of the portal vein (*PV*) by the union of the superior mesenteric vein (*SMV*) with splenic veins

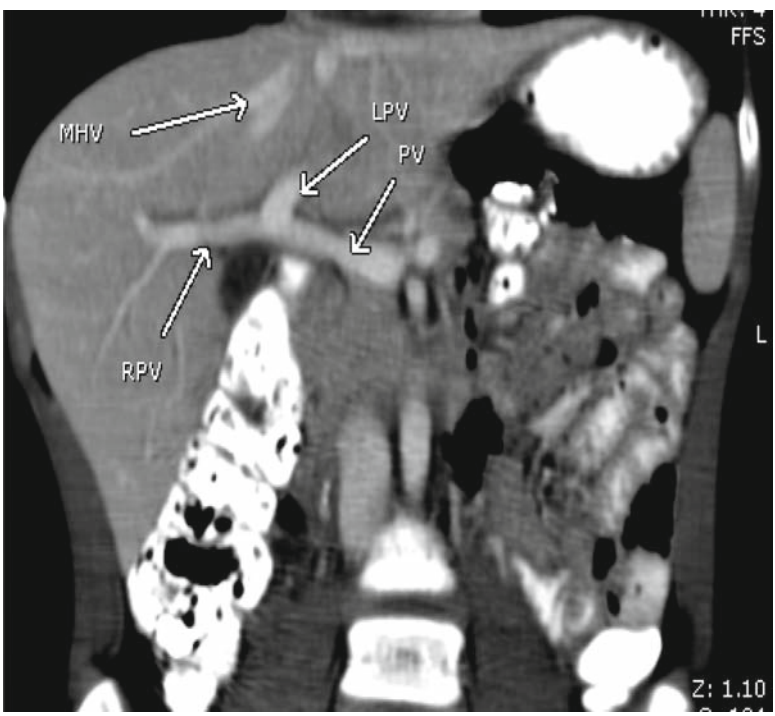

Fig. 1.1.5 Portal vein branches. Coronal section CT (with contrast agent) at the porta hepatis shows the branching of the portal vein (*PV*) into right portal vein (*RPV*) and left portal vein (*LPV*) at almost 90°. Middle hepatic vein (*MHV*) is seen entering the inferior vena cava at the superior liver margin

main hepatic artery, left hepatic artery, or the gastroduodenal artery. Soon after its origin, the cystic artery enters the gallbladder at its neck and divides immediately into a superficial and a deep branch, both of which were first identified by Vesalius in 1564 [5]. The superficial branch supplies blood mostly to the free inferior wall covered by the peritoneum, and the deep branch supplies blood to the superior wall, which lies in direct contact with the inferior liver surface.

Portal Vein

The portal vein is formed by the union of the splenic and superior mesenteric veins and measures about 5.5–8 cm in length; it enters the liver at the porta hepatis (Fig. 1.1.4). It usually divides at a 180° angle into the right and left portal vein branches, which enter the liver parenchyma in the middle, dividing the liver into superior and inferior areas. The right portal vein gives off anterior and posterior segmental branches, and the left portal vein gives off medial and lateral segmental branches (Fig. 1.1.5). At least one branch enters each area of the liver segment. On average, three small portal vein branches (varying from one to six) enter the caudate lobe. They may arise from the left, right, or portal vein bifurcation.

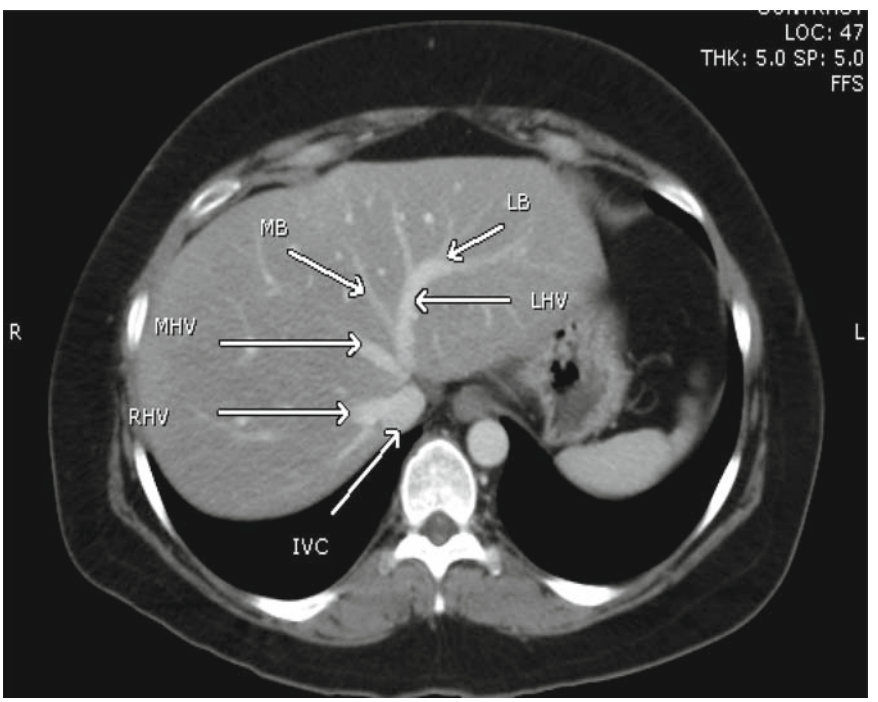

Fig. 1.1.6 Hepatic veins. Axial CT (with the contrast agent) at the upper part of the liver shows three hepatic veins. Left hepatic vein (*LHV*) has a medial (*MB*) and lateral (*LB*) branch and unites with the middle hepatic vein (*MHV*) before joining the inferior vena cava (*IVC*) as single trunk. Right hepatic vein (*RHV*) joins the IVC directly

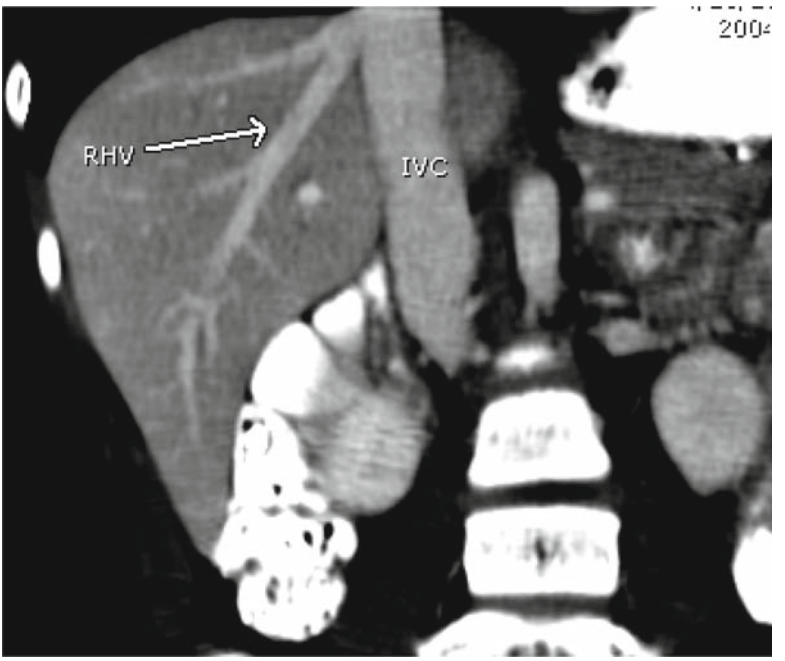

Fig. 1.1.7 Right hepatic vein. A coronal section CT with contrast agent at the middle of the right lobe shows the right hepatic vein (*RHV*) draining blood from the posterior (VI and VII) segment

The portal vein supplies about 1,200 ml blood per minute to the liver (75% of the total liver blood supply) at 7–10 mmHg systolic pressure [22].

Hepatic Veins

There are three distinctly separate hepatic veins: right, middle, and left (Fig. 1.1.6). They interdigitate and overlap with the portal venous system. The left hepatic vein has two tributaries, the medial and lateral branches. The medial branch drains blood from segments IVA and IVB, and the lateral branch drains blood from segments II and III (Fig. 1.1.6). The middle hepatic vein runs along the gallbladder fossa-inferior vena cava plane (Sérégé-Cantlie) and divides the liver into physiologic right (V–VIII) and left lobes (I–IV). It receives blood from the superior (IVA) and inferior (IVB) areas of the medial segment of the left lobe, and the superior (VIII) and inferior (V) areas of the anterior segment of the right lobe. The middle and left hepatic veins unite to form a single trunk before joining the inferior vena cava (Fig. 1.1.6). The right hepatic vein is the largest of the three veins and drains blood mostly from the superior and inferior areas of the posterior segment (VI and VII) of the right lobe (Fig. 1.1.7). Small tributaries are also received from the anterior segment. The right hepatic vein joins the inferior vena cava directly as a separate branch.

The major portion of the venous blood from the caudate lobe drains directly into the inferior vena cava through three short veins [19, 20]. Smaller veins also drain into the middle

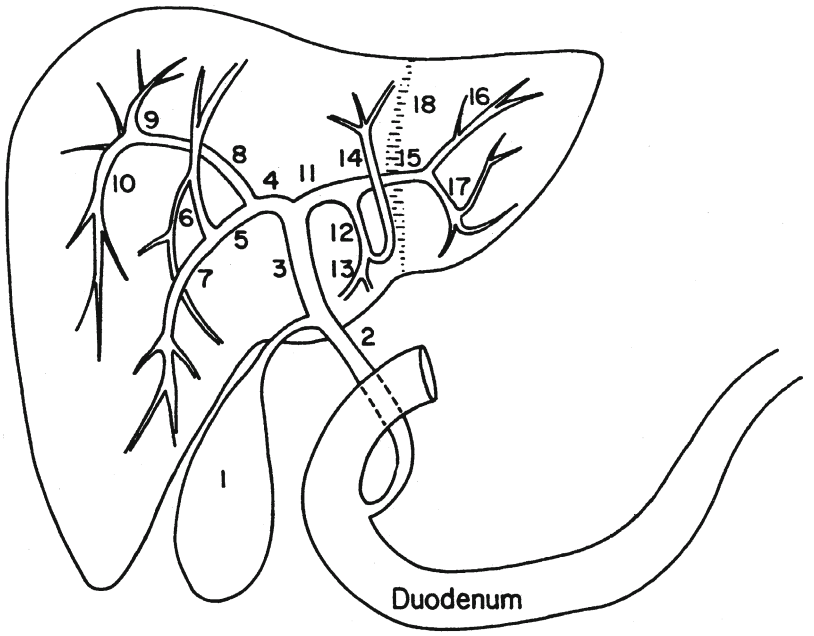

Fig. 1.1.8 Intra- and extra-hepatic ducts and gallbladder. *1* Gallbladder, *2* common bile duct, *3* common hepatic duct, *4* right hepatic duct, *5* anterior segmental duct, *6* anterior superior area duct, *7* anterior inferior area duct, *8* posterior segmental duct, *9* posterior superior area duct, *10* posterior inferior area duct, *11* left hepatic duct, *12* medial segmental duct, *13* medial inferior area duct, *14* medial superior area duct, *15* lateral segmental duct, *16* lateral superior area duct, *17* lateral inferior area duct, *18* falciform ligament

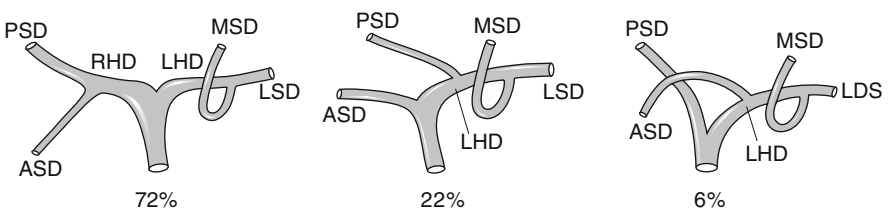

Fig. 1.1.9 Variations in bile drainage from the right lobe. The anterior segmental duct (*ASD*) usually joins with the posterior segmental duct (*PSD*) forming the right hepatic duct (*RHD*) in 72%. Sometimes either PSD (22%) or ASD (6%) may join the left hepatic duct directly. Both *RHD* and *LHD* unite to form the common hepatic duct

and left hepatic veins. Because of this separate venous pathway directly into the inferior vena cava, the caudate lobe often maintains normal function during thrombosis of the hepatic veins (Budd-Chiary syndrome). The patients with Budd-Chiary syndrome demonstrate a normal pattern of Tc-99m-sulfur colloid uptake by the caudate lobe, whereas the rest of the liver parenchyma may show marked reduction in radiocolloid uptake. The

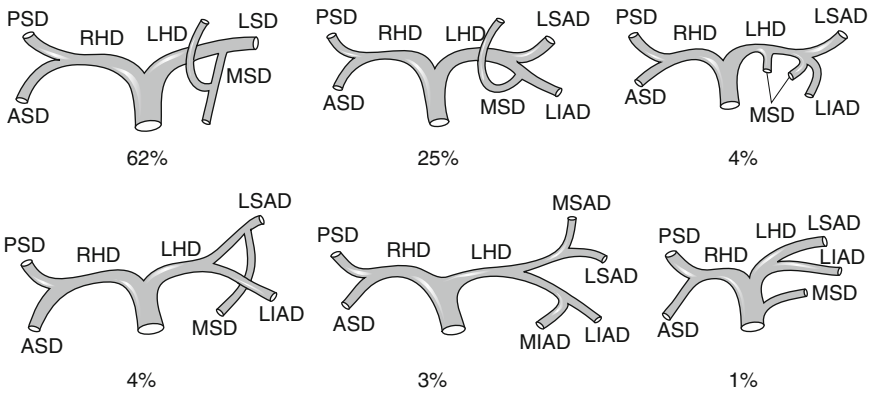

Fig. 1.1.10 Variations in drainage of bile from the left lobe. The medial segmental duct (*MSD*) usually unites with the lateral segmental duct (*LSD*) in 62%, forming the left hepatic duct (*LHD*), which later unites with the right hepatic duct (*RHD*), forming the common hepatic duct. In the remaining 38% of patients, the main difference in bile drainage pertains to variations in area ducts joining with each other. It is rare for either the left medial or the left lateral segmental duct from the left lobe to join directly with the right hepatic duct (*RHD*). (*LSAD* lateral superior area duct, *LIAD* lateral inferior area duct, *MIAD* medial inferior area duct, *MSAD* medial superior area duct, *PSD* posterior segmental duct, *ASD* anterior segmental duct)

venous blood from the gallbladder drains directly into the inferior vena cava. As the major portion of the caudate lobe falls on the left side of the Serege-Cantlie plane, it is usually included with the physiologic left lobe.

Bile Ducts

The biliary tree consists of a network of ductal systems progressively increasing in size and originating at the hepatocytes as the bile canaliculus (Fig. 1.1.8). Bile canaliculi from the adjoining hepatocytes unite to form the cholangioles (<20 μm), which in turn combine to form the interlobular ducts (20–100 μm) and later the area ducts (100–400 μm). Ducts from each area unite to form the segmental ducts (400–800 μm). The segments are positioned anterior and posterior in the right lobe, and medial and lateral in the left lobe [23]. The anterior segmental duct unites with the posterior segmental duct (72%) to form the right hepatic duct (Fig. 1.1.9). The right posterior segmental duct unites with the left hepatic duct directly in 22%, and in the remaining 6% of the cases, the right anterior segmental duct joins the left hepatic duct directly [8].

In the left lobe, the medial segmental duct usually unites with the lateral segmental duct (62%) to form the left hepatic duct. The left medial segmental duct joins the left inferior area duct in 25% of the cases. Other variations are less frequent (Fig. 1.1.10). It is rare for either the left medial or the left lateral segmental duct to join the right hepatic duct directly. The medial segmental duct drains bile from the quadrate lobe (IVA, IVB), and the lateral

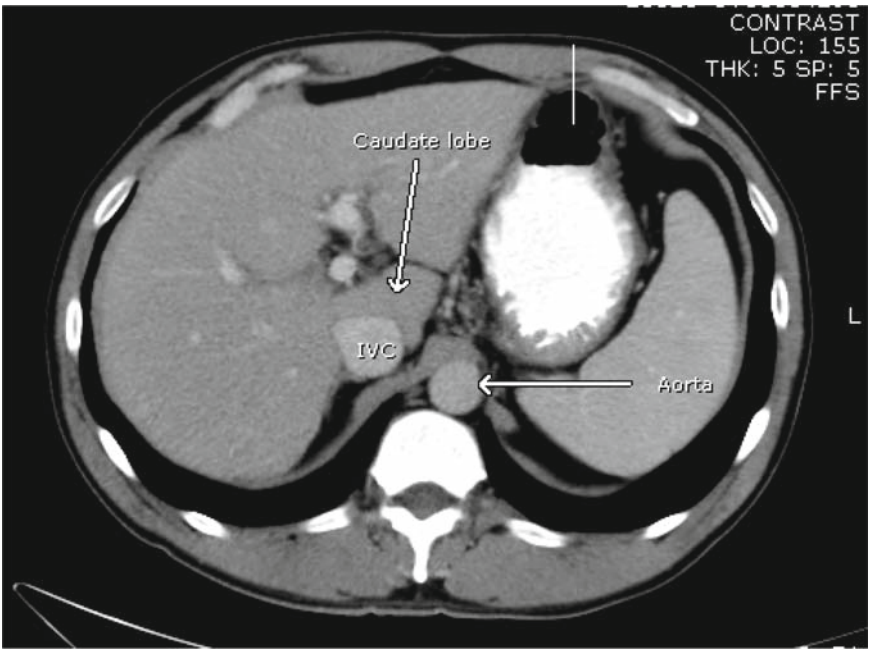

Fig. 1.1.11 Caudate lobe. Axial section CT with contrast shows the caudate lobe situated posteriorly, in between the inferior vena cava and vessels at the porta hepatis. The caudate lobe consists of three parts: (1) *right* (caudate process), (2) *middle* (paracaval), and (3) *left* (Spiegel's) lobe

segmental duct drains bile from the entire anatomic left lobe (II, III). In a Tc-99m-HIDA study, the medial segmental duct and the lateral segmental duct appear as separate trunks in an anterior view image, but the anterior and posterior segmental ducts of the right hepatic lobe are superimposed on one another in the anterior or posterior view of the liver. A right lateral view, therefore, is necessary to the separate bile drainage pattern of the anterior segmental duct from the posterior segmental duct of the right lobe (Fig. 1.1.2).

The caudate lobe (I) is divided anatomically into three parts: (1) the caudate process (right), (2) the paracaval (middle), and (3) Spiegel's (left) lobe (Fig. 1.1.11). Ducts from the caudate process are small, difficult to identify, and drain bile mostly into the right posterior segmental duct or right hepatic duct, and less often into the left hepatic duct. The duct from Spiegel's lobe is much larger in size, easy to identify at surgery, and drains bile mostly into the left hepatic duct. Ducts from the paracaval portion are small and variable in course [19, 20]. Because bile drainage from the caudate lobe is very variable and can occur into the left hepatic duct, right hepatic duct, or bifurcation, cancer of the hilar region can spread directly into the main lobes through the caudate lobe. Because of this unique feature, the caudate lobe is usually resected with a major lobectomy for Klatskin's tumor [19].

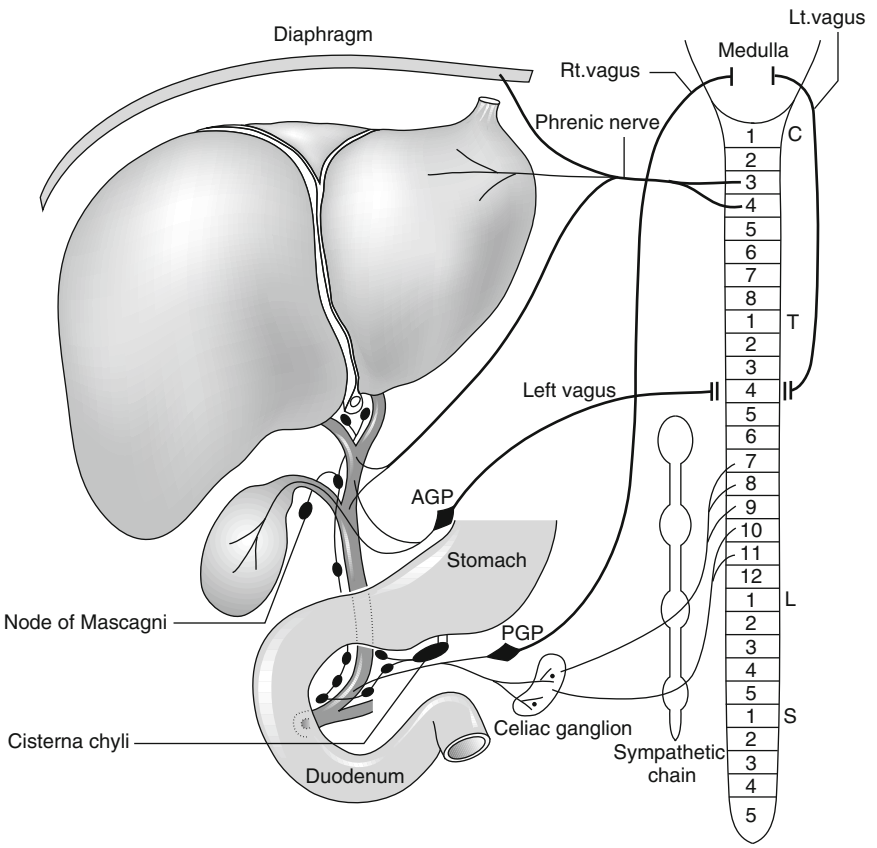

Fig. 1.1.12 Nerve supply and lymphatic drainage of the hepatobiliary system. The vagus (parasympathetic) nerve from the medulla descends along each side of the neck and mediastinum and enters the abdomen. The left vagus gives off branches to the anterior gastric plexus (*AGP*), from whence the vagal branches reach the liver and gallbladder and intrahepatic ducts. The right vagus gives off branches to the posterior gastric plexus (*PGP*), from whence the vagal branches are given off mainly to the common bile duct and the sphincter of Oddi. The phrenic nerve from cervical 3–4 supplies the liver capsule and the peritoneum covering the liver and gallbladder. Sympathetic nerve fibers reach the biliary system via the splanchnic nerves (T7–11) after passing through the celiac ganglion. The lymph from the gallbladder is drained to a node near the neck (node of Mascagni) and then to the nodes along the common bile duct, which also receive lymph from the lower half of the liver. The liver and gallbladder lymph vessels enter the peripancreatic lymph nodes and ultimately drain lymph into the cisterna chili

Lymphatics

The lymph vessels from the liver parenchyma generally follow the course of the blood vessels and bile ducts and join with the gallbladder lymph vessels at the porta hepatis, and later divide into two main lymph channels; one channel follows the course of the common

bile duct, and the other follows the course of the hepatic artery. Both channels pass through several lymph nodes. The channel following the course of the hepatic artery drains lymph primarily into nodes around the celiac axis, and the other channel, which follows the course of the common bile duct, drains lymph into lymph nodes around the pancreas [5]. The lymph from the liver parenchyma and bile ducts ultimately reaches the cisterna chyli (Fig. 1.1.12). The location of the liver lymph nodes is highly variable with the exception of one node situated at the junction of the gallbladder neck with the cystic duct (node of Mascagni). Enlargement of the node of Mascagni may cause cystic duct obstruction and block bile entry into the gallbladder, mimicking acute cholecystitis. Small lymph vessels around the central vein accompany the hepatic veins and inferior vena cava and drain lymph directly into the thoracic duct [24].

Nerves

The hepatobiliary system is supplied by both the somatic and autonomic nervous system. The somatic nerve supply comes from the lower thoracic intercostal nerves (T7–11) and the right phrenic nerve (C3, 4). The lower thoracic intercostal nerves supply the parietal peritoneum. The right phrenic nerve supplies the diaphragm and the peritoneum covering the liver and the gallbladder. The pain sensation due to distension of the liver capsule, gallbladder wall, and bile ducts is transmitted through these nerves (Fig. 1.1.12).

The autonomic nerve supply consists of both the sympathetic and parasympathetic nervous systems. The parasympathetic nerve fibers travel via the vagus, which arises from the medulla and traverses down on each side of the neck and mediastinum to reach the abdomen. Because of the clockwise rotation of the gut during early intrauterine life (Fig. 1.1.1), the left vagus nerve becomes the anterior and the right vagus the posterior trunk. Both of these nerve trunks were first identified and correctly described by Vesalius in 1543 [25]. The anterior trunk (left vagus) enters the anterior gastric plexus at the gastro-esophageal junction. A branch from the anterior gastric plexus, the anterior hepatic nerve, enters the porta hepatis and bifurcates; one branch supplies the intrahepatic and proximal extrahepatic bile ducts and blood vessels, and the other branch supplies the gallbladder. The posterior vagal trunk (right vagus) passes behind the stomach and enters the posterior gastric plexus. A few of its branches enter the celiac ganglion. From the posterior gastric plexus, the nerve fibers enter the distal common bile duct and the sphincter of Oddi (Fig. 1.1.12).

The parasympathetic nerve supply to the gallbladder comes primarily from the anterior trunk (left vagus). The distal common bile duct and the sphincter of Oddi receive their parasympathetic nerve supply primarily from the posterior trunk (right vagus). The parasympathetic motor function of the gallbladder, therefore, is controlled mainly through the anterior trunk (left vagus) and that of the sphincter of Oddi mainly through the posterior trunk (right vagus). An injury or section of the anterior trunk (left vagus) alone during vagotomy, therefore, has the same effect as complete vagotomy (cutting of both vagii) as far as the motor function of the gallbladder is concerned. Parasympathetic ablation enhances muscular relaxation and increases bile stasis within the gallbladder, promoting cholelithiasis [26–28]. Stimulation of the parasympathetic system, on the other hand, increases the tonicity of the gallbladder and promotes complete bile emptying.

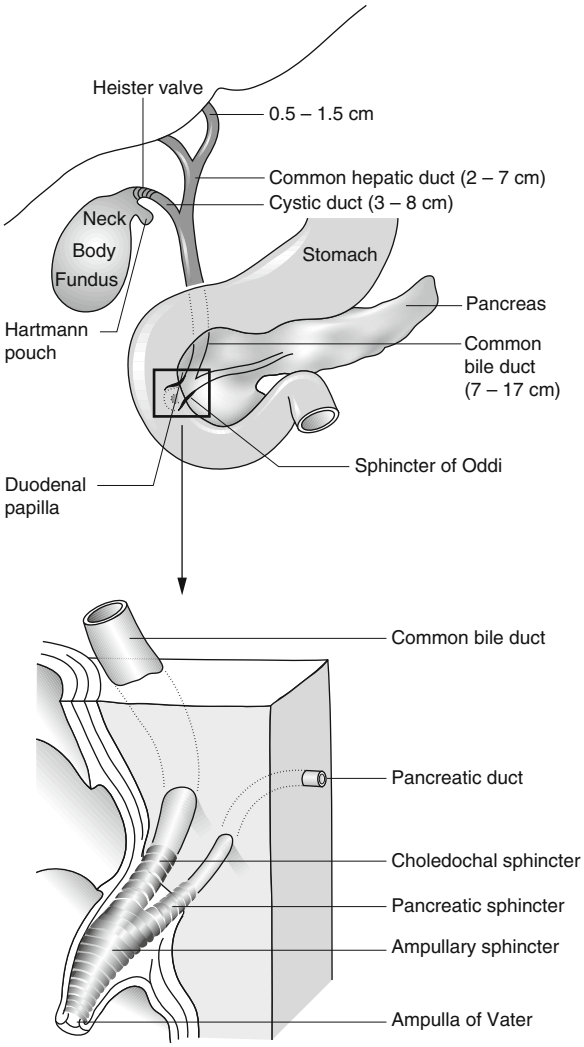

Fig. 1.1.13 Extrahepatic biliary tract. The distal one-third of both right and left hepatic ducts, and the entire common hepatic and common bile ducts, are extrahepatic in location. The gallbladder consists of a fundus, body, neck, and cystic duct. The mucous membrane in the neck and cystic duct is thrown into folds, acting as a valve (Heister's valve) for bile entry and exit. Gallstones often lodge in a pouch near the neck (Hartmann's pouch). The sphincter of Oddi (enlarged) at the distal end of the common bile duct consists of three separate sphincters. The distal common bile duct is surrounded by the choledochal sphincter (sphincter of Boyden). The distal pancreatic duct (duct of Wirsung) is surrounded by a separate pancreatic sphincter. The common channel formed by the union of two ducts is surrounded by the ampullary sphincter. The common channel (ampulla of Vater) opens into the duodenum at an elevation called the papilla. The name sphincter of Oddi refers to all three sphincters

The hepatobiliary system receives the sympathetic nerve supply via the greater splanchnic (T7–9) and lesser splanchnic nerves (T10–11). The axons from preganglionic sympathetic nerve cells in the lateral horn of the thoracic T7–11 segments travel via the greater and lesser splanchnic nerves and enter the celiac ganglion. The postganglionic sympathetic fibers from the celiac ganglion enter the liver, gallbladder, common bile duct, and the sphincter of Oddi. Sympathetic nerve stimulation relaxes the gallbladder wall. The hepatic artery and its branches are supplied by sympathetic nerves that control the vascular tone. The pain from the hepatobiliary system is carried to the central nervous system via both the splanchnic nerves and the branches of the right phrenic nerve (Fig. 1.1.12).

Biliary Apparatus

Intrahepatic Ducts

The hepatobiliary system is analogous to a tree. The hepatocytes can be considered to represent the leaves and canaliculi the trunk; area and segmental ducts represent the branches of the tree. The common hepatic duct and the common bile duct represent the trunk and the sphincter of Oddi the roots of a tree. The gallbladder is akin to a fruit [29]. Bile canaliculi from the hepatocytes join to form the cholangioles, which unite to form the interlobular bile ducts and then into larger area ducts. Ducts from each area unite to form the segmental ducts. The anterior and posterior segmental ducts from the right lobe unite to form the right hepatic duct, and the medial and lateral segmental ducts from the left lobe unite to form the left hepatic duct (Fig. 1.1.7).

Extrahepatic Ducts

The right and left hepatic ducts leave the liver parenchyma and proceed inferiorly for a distance of 0.5–1.5 cm before joining to form the common hepatic duct [8]. The common hepatic duct is 2–7 cm in length and joins with the cystic duct to form the common bile duct.

Gallbladder

The gallbladder lies along the inferior liver border in a groove between the right lobe and the quadrate lobe (medial segment of the left lobe; IVA, IVB). It consists of a fundus, body, and neck (Fig. 1.1.13). The gallbladder measures about 7–10 cm in length, 3–5 cm in width, and 40–50 ml in volume [30]. The superior third of the wall is in direct contact with the liver and hence lacks the peritoneal covering. The rest of the gallbladder wall is covered with the visceral peritoneum. The gallbladder is a pear-shaped, single-chamber organ with the extension of the fundus below the inferior liver margin. The position of the fundus, on the body surface, corresponds to the point of intersection of the lateral margin of the right rectus muscle with the right costal margin. A line drawn between the left anterior

superior iliac spine and umbilicus points to the fundus of the gallbladder when it is extended upwards to meet with the right costal margin. Gallstones often lodge in a pouch-like structure (Hartmann pouch) at the neck, initiating cystic duct obstruction and subsequent acute cholecystitis. The mucous membrane thrown into folds in the neck and cystic duct often acts as a valve (Heister valve) for bile entry into and exit out of the gallbladder. The cystic duct measures about 3–8 cm in length and less than 3 mm in diameter and joins the common hepatic duct at a 45° angle (80%) to form the common bile duct. Sometimes, the cystic duct may directly join the right hepatic or the left hepatic duct. There are many variations in the way the cystic duct joins with the common hepatic duct, right hepatic, or left hepatic duct [31]. The artery to the gallbladder (cystic artery) usually arises from the right hepatic artery (72%) or from its accessory branches (13%), and less often directly from the hepatic artery (6%) or the gastroduodenal artery.

The gallbladder is supplied by both the sympathetic and parasympathetic nervous systems, which control its tone, contraction, and relaxation. Parasympathetic stimulation causes contraction and bile emptying, and sympathetic stimulation results in relaxation and bile stasis. The gallbladder lymph, after passing through a node at the neck (node of Mascagni), enters the hepatic plexus and ultimately reaches the cisterna chyli (Fig. 1.1.7). The gallbladder is absent in 1:1,600 live births, and in about 8% of cases, it is entirely intrahepatic in location [32]. The C loop of the duodenum and the hepatic flexure of the colon are in close proximity to the gallbladder.

Common Bile Duct

This duct is formed by the union of the common hepatic duct with the cystic duct. It varies in length from 7 to 17 cm, and the lumen is less than 8 mm in diameter (Fig 1.1.13). The common bile duct is divided into the supraduodenal, retroduodenal, intrapancreatic, and intraduodenal segments. The supraduodenal segment is the longest and measures 2–4 cm in length. The retroduodenal and intrapancreatic segments each measure about 2.5–3 cm in length. The intradoudenal segment is the narrowest part of the common bile duct. The retroduodenal segment lies behind the duodenal bulb and may be non-visualized in a Tc-99m HIDA study if there is fluid collection in the duodenal lumen. The common bile duct enters the postero-medial wall of the second part of the duodenum and unites with the pancreatic duct (duct of Wirsung), forming a common channel, the ampulla of Vater, which finally enters the duodenal lumen at an elevation called the “papilla.” The papilla lies about 8–10 cm away from the pylorus of the stomach. The common bile duct joins with the pancreatic duct, forming a common channel of 10–12 mm length in 86% of cases. The two ducts join together at the ampulla just before opening into the duodenum in 6% of cases, and in the remaining 8%, both ducts open separately into the duodenum [32].

References

1. Williams R. Global challenges in liver disease. Hepatology 2006;44:521–526
2. Starzl TE. The saga of liver transplantation, with particular reference to the reciprocal influence of liver and kidney transplantation (1955–1967). J Am Coll Surg 2002;195:587–610

3. Linder HH, Green RB. Embryology and surgical anatomy of the extra hepatic biliary tract. Surg Clin N Amer 1964;44:1273–1285
4. Netter FH. CIBA collection of medical illustration, vol. lll, Digestive system, part lll. Liver, biliary tract, and pancreas. CIBA, Summit NJ, 1964
5. Hess W. Surgery of the biliary passages and the pancreas. D Von Nostrand Company Inc, Princeton NJ, 1965
6. Couinaud C. Le foie etudes anatomiques et chirurgicales, Masson, Paris, 1957
7. Reifferscheid M. Chirurgie der leber. Georg Thieme Verlag, Stuttgart, 1957
8. Haley JE, Schroy PC. Anatomy of the biliary ducts within the human liver. Analysis of the prevailing pattern of branchings and the major variations of the biliary ducts. Arch Surg 1953;66:599–616
9. Bismuth H. Surgical anatomy and anatomical surgery of the liver. World J Surg 1982;6:3–9
10. Goldsmith MA, Woodburn RT. Surgical anatomy pertaining to liver resection. Surg Gynecol Obstet 1957;141:429–437
11. Sugarbaker PH. En bloc resection of hepatic segments 4B, 5 and 6 by transverse hepatectomy. Surg Gynecol Obstet 1990;170:250–252
12. Sugarbaker PH, Nelson RC, Murray DR, Chezmar JL, Barnardino MF. A segmental approach to computerized tomographic portography for hepatic resection. Surg Gynecol Obstet 1990; 171:189–195
13. Nelson RC, Chezmar JL, Sugarbaker PH, Murray DR, Bernardino MF. Pre-operative localization of focal liver lesions to specific liver segments: utility of CT during arterial portography. Radiology 1991;181:443–448
14. Laforture M, Madore F, Patriquin H, Breton G. Segmental anatomy of the liver: a sonographic approach to the Couinaud nomenclature. Radiology 1991;181:443–448
15. Soyer P. Segmental anatomy of the liver: utility of a nomenclature accepted worldwide. AJR. Amer J Roentgenol 1993;161:572–573
16. Dodd GD lll. An American's guide to Couinaud's numbering system. AJR. Amer J Roentgenol 1993;161:574–575
17. Sutherland S, Harris J. Claude Couinaud–A passion for the liver. Arch Surg 2002;137:1305–1310
18. Kogure K, Kuwano H, Fujimaki N, Ishikawa H, Takada K. Reproposal for Hjortsjoo's segmental anatomy on the anterior segment in human liver. Arch Surg 2002;137:1118–1124
19. Abdalla EK, Vauthey J, Couinaud C. The caudate lobe of the liver. Implications of embryology and anatomy for surgery. Surg Oncol Clin N Am 2002;11:835–848
20. Kitagawa S, Murakami G, Hata F, Hirata K. Configuration of the right portion of the caudate lobe with special reference to identification of its right margin. Clinical Anat 2000;13:321–340
21. Varotti G, Gondoles G, Goldman J, Wayne M, Florman SS, Schwartz ME, Miller MM, Emre S. Anatomic variations in right liver living donor. J Am Coll Surg 2004;198:577–582
22. Sherlock S, Dooley J. Diseases of the liver and biliary system. 10th edition, Blackwell Science, Malden, MA, 1997
23. Roberts SK, Ludwig J, LaRusso NF. The pathology of biliary epithelia. Gastroenterology 1997;112:269–279
24. Jones AL. The architecture of bile secretion. A morphological perspective of physiology. Dig Dis Sci 1980;25:609–629
25. Holle F. Historical outline. In: Holle F, Anderson S. eds. Vagotomy: latest advances. Springer, New York, 1974
26. LaRusso D, Misciagno G, Noviello MR, Torantino S. Cholelithiasis after billroth ll gastric resection. Surgery 1988;103:579–583
27. Griffiths JMT, Holmes G. Cholecystitis following gastric surgery. Lancet 1994;2:780–782
28. Turunen M, Antila L. Gallbladder disease following gastrectomy. ACTA Chir Scand 1964;127:134–137

29. Krishnamurthy S, Krishnamurthy GT. Evolution of nuclear hepatology as a clinical subspeciality. J Nucl Med Technol 1995;23(Suppl):35S–45S
30. Gunnarson E, Investigation of the distension capacity of the human gallbladder. ACTA Radiol (Stockh) 1961;56:161–165
31. Goor DA, Ebert PA. Anomalies of the biliary tree. Report of a repair of an accessory bile duct and review of the literature. Arch Surg 1972;104:302–309
32. Boyden EA. The accessory gallbladder–An embryological and comparative study of aberrant biliary vesicles in man and domestic mammals. Am J Anat 1926;38:177–231

1.2 Microstructure

The liver is the largest organ in the body and consists of an intricate structure to carry out the complex exocrine (bile secretion) and endocrine (protein synthesis) functions efficiently. The organ shape and structure are well maintained despite the paucity of connective tissue.

The concept of the lobule as the basic micro-architectural unit of the liver prevailed for well over a century. A lobule is hexagonal in shape and consists of a tributary of the hepatic vein at the center surrounded by six portal triads (consisting of the terminal branch of the hepatic artery, portal vein, and bile duct) at the periphery, and the space in between is occupied by a single cell plate of hepatocytes and cells of the sinusoidal space. A new concept of an acinus as the basic liver unit was first proposed in 1958 and is now well accepted because it explains the function and regeneration of the liver in a much better way than the lobule model [1]. An acinus is diamond shaped with a portal triad at one corner and central vein (hepatic vein) at the other three corners. Hepatocytes are arranged in three zones. The cells in zone 1 towards the portal triad receive a much higher concentration of oxygen and other nutrients than cells in zone 3 towards the central vein. Zone 1 cells, therefore, can withstand hypoxia better and regenerate much faster than cells in zone 3. The liver consists of the polygonal cells (hepatocytes), sinosoidal cells, canalicular cells, and other supporting cells (Fig. 1.2.1). An adult liver consists of well over 250 billion cells, of which hepatocytes constitute 78% of the volume, non-hepatocytes 6.3% of the volume, 2.8% by endothelial cells, 2.1% by Kupffer cells, and 1.4% by stellate cells. The remaining 16% of liver volume is made up of extracellular space [2].

Vascular Compartment

This compartment is situated between two single layer plates of hepatocytes and consists of two spaces: (1) the sinusoidal space and (2) the perisinusoidal space of Disse (Fig. 1.2.1). The sinusoidal space is the much larger of the two and accounts for 2/3 of the vascular compartment. Four types of cells are found in the vascular space: (1) endothelial cells (sinusoidal lining cells), (2) Kupffer cells, (3) stellate cells (lipocyte or Ito cells), and (4) pit cells [3]. These four cells together constitute the functional unit of the hepatic sinusoid.

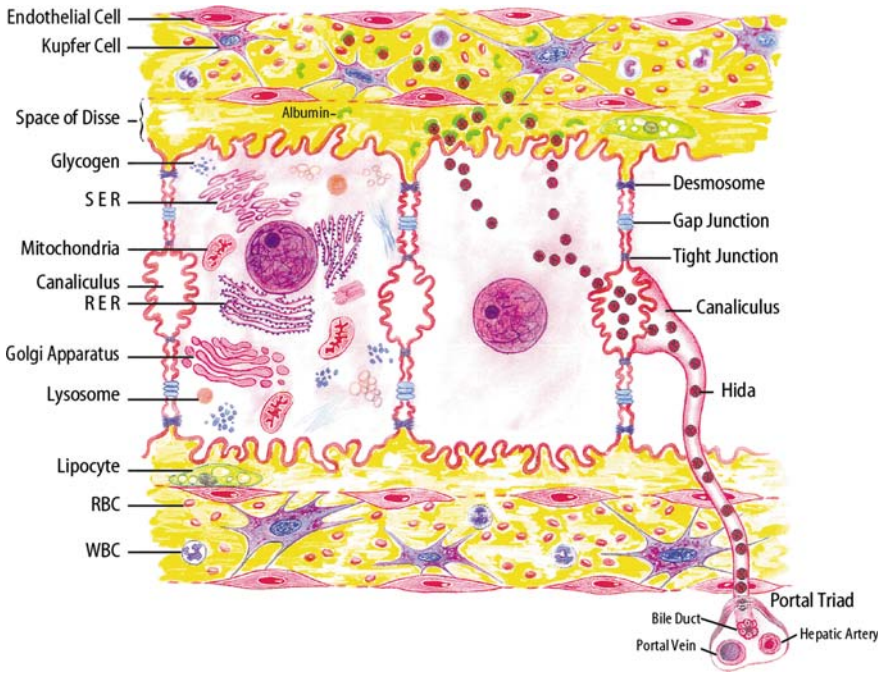

Fig. 1.2.1 Microstructure of the liver. The vascular space is divided into two compartments by the endothelial cells: (1) endothelial or sinusoidal space and (2) the perisinusoidal space of Disse. Kupffer cells are located in the sinusoidal space and stellate cells (Ito cells) in the perisinusoidal space of Disse. The basolateral border of the hepatocyte faces the space of Disse. Canaliculi are invaginations of the lateral wall of two adjacent hepatocytes. Canaliculi join to form the canal of Hering, which in turn unites with others to form the interlobular ducts. The portal triad consists of a branch of the bile duct, hepatic artery, and portal vein. Substrates move from the basolateral border to the canaliculi through the hepatocyte. *SER* smooth endoplasmic reticulum, *RER* rough endoplasmic reticulum

Endothelial Cell

These are flat cells lining the vascular space and consist of numerous holes or fenestrae in between [4]. The fenestrae vary in size from 0.1 to 3 μm in diameter and selectively allow certain plasma constituents to pass through from the sinusoidal space to the perisinusoidal space of Disse. The number of fenestrae decreases and the diameter of the hole increases in patients with alcoholic liver disease and cirrhosis [5–7]. The main function of the fenestrae is to act as a selective filter, allowing only those constituents that need to enter the perisinusoidal space of Disse and excluding others from the entrance. Red blood cells and leucocytes are excluded, whereas the electrolytes, plasma proteins (albumin), vitamins, and other essential nutrients are allowed free entry into the perisinusoidal space of Disse.

Kupffer Cell

Kupffer described two types of cells, one in 1876 [8] and the other in 1899 [9]. It was first thought that the cell described in 1876 was the reticuloendothelial cell bearing his name (Kupffer cell). However, in 1951, Ito showed that this cell is the fat-storing (lipocyte, Ito cell) cell situated in the perisinusoidal space of Disse, recognized now as the stellate cell [10]. The cell described by Kupffer in 1899 is now considered the Kupffer cell. The Kupffer cells are highly specialized macrophages distributed irregularly within the sinusoidal space. There is no direct connection between two adjacent Kupffer cells. Their surface is irregular with folds and ruffles. They are highly mobile scavenger cells often found within the space of Disse or may lie free within the sinusoidal space, unattached to the endothelial cell. The cytoplasm is rich in lysosomes, Golgi apparatus, and rough endoplasmic reticulum (Fig. 1.2.1). The Kupffer cells proliferate locally to maintain their population, but at times of greater need they increase their number by calling reinforcement from the bone marrow.

Stellate Cell

These cells, "the sternzellen of Von Kupffer," first described in 1876, are the resting fibroblasts in the perisinusoidal space of Disse that are now organized as the stellate cells [8]. They have been called by many names, such as lipocyte, hepatic pericyte, or Ito cells [10, 11]. For many years, it was thought that these star-shaped cells did not have any function in humans. Stellate cells are rich in vitamin A and are the storage site for retinoids. They become activated during liver injury and play a dominant role in angiogenesis, vascular remodeling, repair, and fibrosis [12]. The activation of stellate cells increases production of membrane metalloproteinase 1 and 2 (MMP-1 and MMP-2) and tissue inhibitors of metalloproteinases (TIMP). Metalloproteinases promote matrix degradation and subsequent replacement by interstitial collagen in the subendothelial space of Disse. Other accompanying effects include a reduction in the number of fenestrae and a loss of microvilli along the perisinusoidal surface of the hepatocytes, both of which result in decreasing the delivery of organic anions (including HIDA) into the perisinusoidal space of Disse.

Pit Cell

These cells are large granular T lymphocytes or natural killer cells found within the sinusoidal space. They are highly mobile killer lymphocytes and contain organelles necessary for removal of tumor cells and virus-infected hepatocytes. Activated natural killer cells promote hepatocyte proliferation and regeneration of the liver [14].

Hepatocyte

The hepatocyte is the largest cell in the liver and varies in size from 13 to 30 μm with an average diameter of 25 μm (Fig. 1.2.2). Each milligram of liver tissue consists of 202,000 cells. There are about 250 billion hepatocytes in an adult liver [15]. A hepatocyte is

polyhedral, multifaceted (as many as eight surfaces), and measures about 11,000 cubic μm in volume. Because of their relatively larger size, hepatocytes account for 78% of the liver by volume. Sinusoidal cells account for 6%, and the extracellular space occupies the remaining 16% of the liver volume. On the basis of function, the hepatocyte plasma membrane is divided into three domains: (1) the basolateral domain, (2) contact or contiguous domain, and (3) canalicular domain.

The basolateral domain faces the perisinusoidal space of Disse and accounts for 70% of the cell wall. It consists of 30–50 microvilli, which increase the absorptive surface by six times [16]. The microvilli extend along the paracellular space until the two adjacent hepatocytes come in close contact at the point of the desmosome. This surface is bathed in plasma filtered through the fenestrae of the sieve plate of the endothelial cells and allows metabolic exchange between the plasma and the hepatocyte. Organic anions, including Tc-99m-HIDA, enter the hepatocyte along the basolateral domain.

The contact domain accounts for 15% of the plasma membrane and is placed between two adjacent hepatocytes. The tight junction situated near the canaliculus prevents plasma constituents from entering the canalicular space directly from the space of Disse. The gap junction can be located anywhere along the lateral border and provides direct communication between adjacent hepatocytes on a selective basis.

The canalicular domain accounts for the remaining 15% of the cell surface and is situated at the center of two adjacent hepatocytes. It represents a specialized part of the hepatocyte. The canalicular wall consists of microvilli that increase the functional surface.

Hepatocyte contains a nucleus and a nucleolus that are rich in deoxyribonucleic acid. The smooth endoplasmic reticulum (SER) is made up of tubular structures containing microsomes and carries out bilirubin conjugation and detoxification of drugs and other organic anions. SER is steroid sensitive and participates in enzyme induction when phenobarbital is administered. The rough endoplasmic reticulum (RER) contains ribosomes and is responsible for protein synthesis, including albumin [13]. Lysosomes are cytoplasmic particles close to bile canaliculi and contain hydrolytic enzymes, including acid phosphatase [16]. Lysosomes perform a scavenger function and remove from blood excess material, including ferritin, bile pigments, and metals such as copper. The Golgi apparatus consists of particulates and vesicles and lies close to the bile canaliculus. The lysosomes and Golgi apparatus together perform the tasks of storage, entrapment, and final excretion into bile of various non-essential body constituents. The mitochondria, which participate in oxidative phospharilation, heme synthesis, and citric acid cycle, are scattered throughout the cell. The hepatocytes and cells in the sinusoidal and canalicular space are supported by a cytoskeleton consisting of microtubules and micro filaments. The cells of the sinusoidal and perisinusoidal space of Disse are supported by collagen, laminin, protoglycon, fibrinonectin, and heparan sulphate [15, 16].

Bile Canaliculus

Bile canaliculi are a simple convoluted border of the hepatocyte and account for 13% of the hepatocyte wall. The convolutions are microvilli that increase the surface area for bile secretion (Fig. 1.2.1). A canaliculus varies from 0.1 to 1 μm in diameter. At the periphery

Table 1.2.1 Function of various cells of the liver [15]

Hepatocyte	Endothelial cell	Kupffer cell	Stellate cell	Canalicular cell
Bile secretion	Plasma filtration	Phagocytosis of colloids, bacteria, endotoxin, tumor cells	Storage of fats, vitamin A, and retinoid	Bile transit
Phospharilation	Endocytosis	Receptor for Fc fraction, C3b complement	Collagen secretion	Water secretion
	Removal of collagen Fc fragment of IgG, C3b complement			
Hem synthesis				Electrolyte transfer
Protein synthesis				
Beta oxidation				
		Secretion of TNF-α		
Glycogenesis		Collagenase		
Bilirubin conjugation		Interleukins		
Drug detoxification		Arachidonic acid		
Lipoprotein synthesis		Erythroblastosis		
Storage of ferritin, vit B-12		Storage of iron, ferritin, hemosiderin, immune complex		

of a hepatic lobule several bile canaliculi join to form the canal of Hering, which acts as a transitional zone between intralobular and interlobular ductal systems. The interlobular ducts unite to form area ducts that drain bile from an area of the liver. Area ducts unite to form the segmental ducts, which in turn unite to form the lobar ducts. The cells lining the ducts (cholangioles) are cuboidal in shape and contain apical microvilli, which project into the duct lumen [17].

Gallbladder and Cystic Duct

The gallbladder wall consists of three layers: (1) the serosal layer, (2) fibromuscular layer, and (3) mucosal layer. The serosal layer is the peritoneum, which covers about 2/3 of the

gallbladder wall with the exception of the superior 1/3, which is in direct contact with the liver. The fibromuscular layer consists mostly of elastic fibrous tissue. The muscular layer is irregular and consists of longitudinal and circular muscle fibers, which are well developed around the fundus and infundibulum, and scanty over the body and neck of the gallbladder. The mucosa consists of a single layer of cells with three different cell types: columnar, pencil, and basal. The mucosal layer is thrown into folds that increase the surface area of the gallbladder. The columnar cells have microvilli, 0.7–0.8 μm in length, along the luminal surface. The intercellular space between two adjacent columnar cells is narrow at the luminal end, but is widely open towards the fibromuscular layer [18]. Water and electrolytes are continuously absorbed from the lumen, through these intercellular spaces, making room for entry of fresh hepatic bile into the gallbladder during fasting [19]. The wall is impermeable to bile acids, bilirubin, radiocontrast agents, and other organic anions, including Tc-99m-HIDA. The neck contains mucous-secreting cells. Pencil cells, which are long and narrow, are found mainly in the body and extend from the basement membrane to the lumen. Basal cells are small and are concentrated more towards the fibromuscular layer.

The water absorbed from the gallbladder lumen through the lateral intercellular spaces enters venous blood through several small veins that drain into the hepatic or portal veins. There is no one single large cystic vein. The venous blood from the free wall of the gallbladder drains into venous radicals, which eventually enter the portal venous system.

The cystic duct, common hepatic duct, and common bile duct possess a mucosa, submucosa, and muscularis. The mucosal cells are a continuation of the gallbladder mucosal cells and contain the columnar cells with a ciliated border. The walls of the common hepatic duct and common bile duct are composed of a thick layer of connective tissue interspersed with few muscle cells. This structural configuration is well suited for the bile ducts to participate in bile concentration and discharge.

Sphincter of Oddi

For well over a century, the study of this small segment of the biliary tract has fascinated anatomists, physiologists, and microscopists [20]. More recently, it has gotten the attention of gastroenterologists, hepatologists, and electron microscopists. For many years it was believed that the sphincter was a mere extension of the smooth muscle from the duodenal wall. Boyden's detailed work in 1937 clearly established it as a true sphincter, separate from the duodenal wall musculature [21]. The common bile duct enters the postero-medial wall of the second part of the duodenum tangentially and traverses for about 2 cm before joining the pancreatic duct (duct of Wirsung) to form a common channel, the ampulla of Vater. The common channel travels for 10–15 mm before entering the duodenal lumen at an elevation, the papilla, which is about 7–10 cm from the pylorus of the stomach (Fig. 1.1.13). The circular and longitudinal muscle fibers form a sphincter called the sphincter choledochus (sphincter of Boyden) at the distal end of the common bile duct before it joins the pancreatic duct. The sphincter is about 10–15 mm in length and mostly intramuscular. The contractions of this sphincter prevent reflux of pancreatic secretions into the common bile duct. The distal pancreatic duct (duct of Wirsung) is also surrounded

by a distinct sphincter called the pancreatic sphincter whose contractions prevent bile reflux into the pancreatic duct. The pancreatic sphincter is absent in about 20% of the subjects [22]. The common channel formed by the union of the common bile duct and the pancreatic duct is called the ampulla of Vater and is surrounded by a weak sphincter called the sphincter of ampulla (pylorus of Westpal). The name, "sphincter of Oddi," commonly refers to the function of all three sphincters situated at the distal end of the common bile duct and the pancreatic duct. Variations in the length, its union with the pancreatic duct, and opening into the duodenum of the common bile duct are frequent and are related to embryologic development [23]. The common bile duct opens through the ampulla of Vater into the lumen of the second part of the duodenum in 82% of the cases. The opening is lower than usual in 5%, or opens at an angle in 7%, or opens into the transverse duodenum (third part) in the remaining 6% of the patients [24].

References

1. Rapapport AM. The structural and functional unit in the human liver (liver acinus). Anat Rec 1958;130:673–689
2. Bloulin A, Bolender RP, Weibel ER. Distribution of organelles and membranes between hepatocytes and non-hepatocytes in the rat liver parenchyma. A stereological study. J Cell Biol 1977;72:441–455
3. Gendrault J, Montecino-Rodriguez, Cinqualbre J. Structure of the normal human liver sinusoid after perfusion fixation. In: Knook DL, Wisse E (eds). Liver sinusoidal cells. Elsevier Biomedical Press, Amsterdam, 1982;pp 93–100
4. Wisse E. An electron microscopic study of the fenestral endothelial lining of rat liver sinusoid. J Ultrastructure Research 1970;31:125–150
5. Toner PG, Carr KE. Ultrastructure of the liver and biliary apparatus. In: Marlow S, Sherlock S. Eds, Surgery of the gallbladder and bile ducts. Butterworth & Co Ltd, Boston, 1981, pp 19–65
6. Wisse E, DeZanger RB, Charles K, Van Der Smissen P, McCuskey RS. The liver sieve: considerations concerning the structure and function of endothelial fenestrae, the sinusoidal wall and the space of Disse. Hepatology 1985;5:683–692
7. Horn T, Christoffersen P, Henrikseen JH. Alcoholic liver injury: defenestration in non-cirrhotic livers. A scanning microscopic study. Hepatology 1987;7:77–82
8. Kupffer C Von. Uber die Sternzallen der Leber. Arch Mikr Anat 1876;12:353–357
9. Kupffer C Von. Uber die sogenanten Sternzellen der sangetheier Leber. Arch Mikr Anat 1899;54:254–260
10. Ito T. Cytological studies on stellate cells of Kupffer and fat storing cells in the capillaries of the human liver. ACTA Anat Nippon 1951;26:42 (abstract)
11. Lee JS, Semela D, Iredale J, Shah VH. Sinusoidal remodeling and angiogenesis: a new function for the liver-specific pericyte? Hepatology 2007;45:817–825
12. Friedman SL, Rockey DC, Bissell M. Hepatic fibrosis 2006: report of the third AASLD single topic conference. Hepatology 2007;45:242–249
13. Friedman SL, Basal MB. Reversal of hepatic fibrosis–fact or fantasy? Hepatology 2006; 43:S82–S88
14. Nakashima SL, Inui T, Habu Y, Kinishita M, et al. Activation of mouse natural killer cells accelerates liver regeneration after partial hepatectomy. Gastroenterology 2006;131:1573–1583
15. Sherlock S, Dooley J. Diseases of the liver and biliary system, 10th edn. Blackwell Science, Malden, MA, 1997

16. Feldman G. The cytoskeleton of the hepatocyte. J Hepatology. 1989;8:380–384
17. Jones AL, Schmucker DL, Reston RH, Murakami T. The architecture of bile secretion. A morphological perspective of physiology. Dig Dis Sci 1980;25:609–629
18. Eveff RD, Higgins JA, Brown AC. The fine structure of normal mucosa in human gallbladder. Gastroenterology 1964;47:49–60
19. Tormey JM, Diamond JM. Studies on the structural basis of water transport across epithelial membranes. Federation Proceedings 1966;25:692–707
20. Oddi R. D'une disposition a sphincter del'ouverture du canal cholique. Arch. Ital Biol 1887:8:317–322
21. Boyden EA. The sphincter of Oddi in man and certain representative mammals. Surgery 1937;1:25–37
22. Boyden EA. The anatomy of the choledochoduodenal junction in man. Surg Gynecol Obstet 1957;104:641–652
23. Linder HH. Embryology and anatomy of the biliary tree. In: Way LW, Pelligrini CA. (Eds) Surgery of the gallbladder and bile ducts. WB Saunders Co, Philadelphia, 1987;pp 3–22
24. Linder HH, Pena VA, Ruggieri RA. A clinical and anatomical study of anomalous termination of the common bile duct into the duodenum. Ann Surg 1976;184:626–632

Liver and Spleen Function 2

The liver is the largest organ and carries out the most complex biological functions in the body. It secretes bile, synthesizes proteins, metabolizes nutrients, hormones, and drugs, and detoxifies noxious endogenous and exogenous substrates. To accomplish all of these functions, the liver is located centrally in the body and endowed with well-designed architecture with a generous amount of blood supply. Secretion of bile is one of many important liver functions, and bile promotes digestion and absorption of essential nutrients; it also serves as a vehicle to get rid of biological waste products from the body. The biliary tree is designed not only for continuous bile secretion and flow, but also for periodic bile storage and discharge (gallbladder) at the time when food enters the small intestine. The spleen carries out many functions whose importance has been recognized only recently. This chapter will discuss the various functions of these two organs.

2.1 Liver Function

The liver secretes about 600–800 ml of bile per day, at 25–33 ml h^{-1} or 0.42–55 ml min^{-1} [1]. Under normal hydration, osmolality of the hepatic bile is similar to that of plasma and ranges between 290–320 $mOsm^{-1}$. Bile secretion is independent of hepatic perfusion pressure; thus, it differs from that of urine formation, which is very much dependent upon the glomerular filtration pressure in the kidneys [2]. The hepatic bile is composed of 98% water and 2% solutes, which include bile acids, phospholipids, cholesterol, conjugated bilirubin, electrolytes, and proteins (Table 2.1.1). Almost all of these functions are carried out mainly by the hepatocyte, which possesses all of the ingredients necessary for performing complex functions [3]. After extraction from blood in the space of Disse, some substrates are metabolized and transported through the hepatocyte to be secreted into canaliculi, while others may be secreted without any changes. All three domains of the hepatocyte plasma membrane participate in the uptake and excretion [4]. The uptake from the blood in the space of Disse takes place along the basolateral domain, which accounts for approximately 40% of the hepatocyte border. Bile secretion occurs at the canalicular domain, which constitutes 10% of the cell border. The lateral domain, the wall facing two adjacent hepatocytes, forms the remaining 50% of the cell border and plays a major role in water and solute transport and regulation of the total volume of bile secreted per day (Fig. 2.1.1).

G.T. Krishnamurthy and S. Krishnamurthy, *Nuclear Hepatology,*
DOI 10.1007/978-3-642-00648-7_2, © Springer-Verlag Berlin Heidelberg 2009

Table 2.1.1 Composition of human hepatic and gallbladder bile

Water (g/dl^{-1})	98	92
Na^+ (mEq/l^{-1})	150	130
K^+ (mEq/l^{-1})	5	10
Ca^{2+} (mEq/l^{-1})	5	23
$C1^-$ (mEq/l^{-1})	100	25
HCO_3^- (mEq/l^{-1})	28	10
Bile salts (g/dl^{-1})	1	6
Bilirubin (g/dl^{-1})	0.05	0.3
Cholesterol (g/dl^{-1})	0.1	0.6
Fatty acids (g/dl^{-1})	0.12	0.8
Lecithin (g/dl^{-1})	0.04	0.3

Bile formation in the hepatocyte can be divided into four major phases: *phase I*, uptake of substrates from blood (space of Disse) along the basolateral border; *phase II*, metabolism (hydroxylation); *phase III*, detoxification (conjugation); *phase IV*, excretion into bile canaliculi along the canalicular border. Both phases II and III take place intracellularly within the hepatocyte. A disease process can affect one, two, three, or all four phases at a time. The entire metabolic process is controlled by genes mainly through their nuclear receptors.

Basolateral (Sinusoidal) Domain

In the past decade, new knowledge has contributed to better understanding of the mechanisms involved in bile formation and flow. Basolateral and canalicular domains of the hepatocyte possess many polypeptide transporters that regulate the entrance and exit of substances across the plasma membrane (Fig. 2.1.1). Both sodium-dependent and sodium-independent pathways control the uptake of substrates along the basolateral border. The sodium-dependent pathway is regulated by sodium taurocholate cotransporting polypeptide (NTCP), which controls the majority of conjugated bile salts, a few sulfated steroids, and to a minor extent uptake of unconjugated bile salts. The sodium-dependent pathway also uses the Na^+/K^+ ATPase pump, which enables net movement of three Na^+ ions out of the hepatocyte for every two K^+ ions moving into the hepatocyte from the space of Disse [5]. The net effect of these electrolyte exchanges results in a higher concentration of K^+ inside than outside, and a higher concentration of Na^+ outside than inside of the hepatocyte. Due to this ion imbalance, the inside of the hepatocyte carries a much higher negative charge (–35 mV) than its outside environment [6].

Sodium-independent pathways are represented by several members of the superfamily of organic anion-transporting polypeptides (OATPs). Four of the OATPs located along the basolateral border include OATP1B1 (formerly OATP-C), OATP1B3, OATP1A2, and OATP2B1 [7]. In humans, the highest concentration of OATP1B1 and

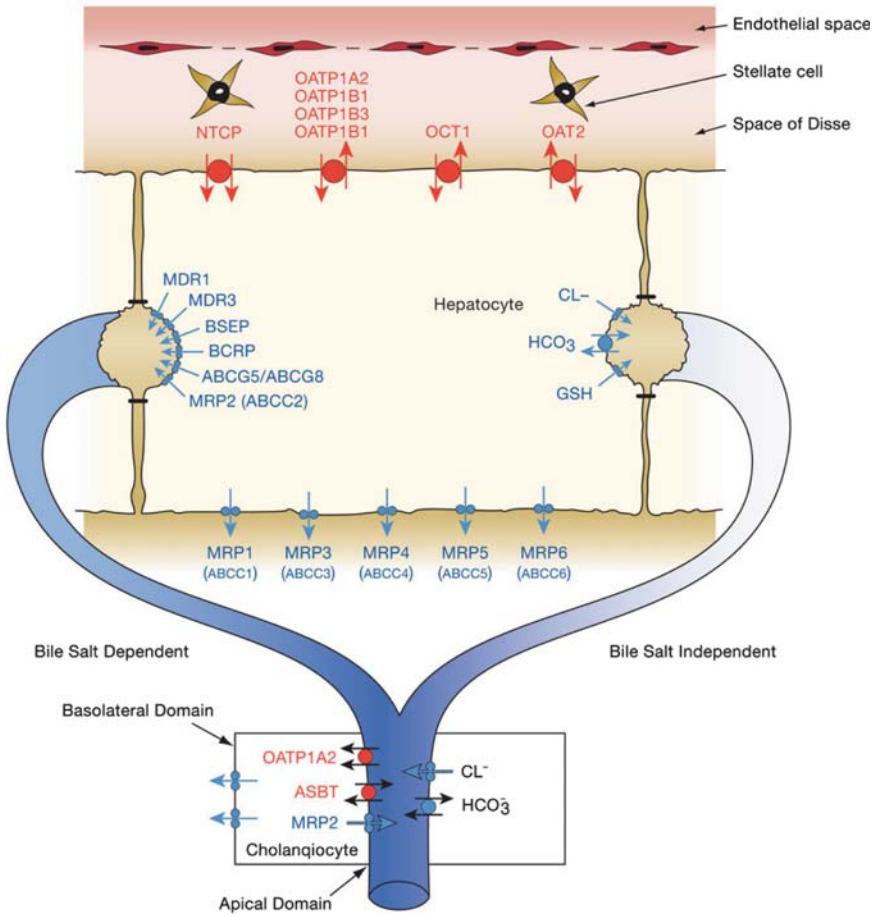

Fig. 2.1.1 Mechanism of bile secretion. Uptake of solutes from the space of Disse occurs along the basolateral domain of the hepatocyte through many different pathways controlled by different transporter proteins. Four organic anion transporter proteins (*OATPs*) and organic anion transporter-2 (*OAT2*) and organic cation transporter proteins (OCT1) control uptake of anions and cations along the basolateral border (*red*). Sodium-dependent bile salt uptake occurs via sodium taurocholate protein (*NTCP*). Five multidrug resistance-associated proteins (*MRPs*) control secretion (reflux) from the hepatocyte back into space of Disse (*blue*). After intracellular transit, solute secretion into bile takes place along the canalicular domain through MRP2, multidrug-resistant-1 p-glycoprotein (*MDR1* and *MDR3*), bile salt export pump (*BSEP*), breast cancer-resistance protein (*BCRP*), and flippases (*ABCG5*/*ABCG8*). Chloride channel, glutathione (*GSH*) transporter, and chloride (Cl^-)/ bicarbonate (HCO_3^-) exchange transporters also control excretion. Cholangioles absorb bile salts from the lumen through apical sodium-dependent bile salt transporter (*ASBT*) protein, and other anions are absorbed through OATP1A2. Exchange of Cl^- for HCO_3^- takes place. These substrates are secreted into the peribiliary plexus at the basolateral domain of the cholangiocytes mediated by MDR3, OST-1, and OST-2. Water enters the canalicular bile by three different routes: (1) transcellular, (2) paracellular, and (3) a combination of paracellular and transcellular

OATP1B3 is found in the liver. Bilirubin uptake is controlled mainly by OATP2B1. Three of the OATPs (OATP1B1, OATP1B3, and OATP1A2) have overlapping functions for conjugated and unconjugated bile salts, bromosulphophtalein, sulfates, glucoronides, and selected organic anions and organic cations. OATPs control uptake of many drugs, including radiotracers (Tc-99m-HIDA). OATP2B1 also controls uptake of bromosulfaphtalein (possible Tc-99m HIDA) and steroid sulfates. Other sodium-independent uptake systems, separate from OATPs, are the organic anion transporter2/organic cation transporter1 (OAT2/OCT1) gene family members, and they control uptake of organic anions and organic cations, respectively.

Besides the above group of uptake transporters, the basolateral domain has transporters that control excretion of substrates from the hepatocyte into blood (reflux) in the space of Disse (Fig. 2.1.1). These transporters belong to the adenosine triphosphate (ATP) binding cassette (ABC) family transporters called multidrug resistance-associated proteins (MRPs). Of the six known MRPs, five (MRP1, MRP3, MRP4, MRP5, and MRP6) are located along the basolateral border and play a role in the efflux of drugs and their metabolites (MRP4 and MRP5), drug conjugates (MRP1), and bile salts (MRP3) into the space of Disse. The sixth MRP (MRP2) is located along the canalicular border and controls excretion of bilirubin, bile salts, and other organic anions into the canaliculi.

Nuclear Receptors

Of the more than 100 nuclear receptor super-family members known in the mammalian cells, 49 have been identified in the human cell and are divided into four major classes [8]. Class I nuclear receptors are homodimers and include most steroid receptors (glucocorticoids, estrogens, androgens, mineralocorticoids, and progesterone). Class II receptors consist of eight heterodimer partners of RXR (retinoid X receptor) and include constitutive androstane receptor (CAR), farnesoid X receptor (FXR), liver X receptor (LXR), peroxisomal proliferator receptor (PPAR), pregnane X receptor/steroid, and xenobiotic receptor (PXR/SXR), retinoic acid receptor (RAR), thyroid hormone receptor (TR), and vitamin D receptor (VDR). Class II nuclear receptors play a major role in controlling the function of the hepatocyte. Class III nuclear receptors are orphan homodimers and include retinoid X receptor (RXR), chicken ovalbumin upstream promoter (COUP-TF), and hepatocyte nuclear factor 4 (HNF4), and class IV is monomers and includes liver receptor homologue1 (LRH1). The short heterodimer partner (SHP) is a nuclear receptor separate from the other class four types described (Table 2.1.2).

A typical nuclear receptor consists of five functional domains (Fig. 2.1.2). At the aminoterminal (N) end is the activation function 1 (AF1) region, which is responsible for ligand-independent transcriptional activation and coordination. DNA-binding domain (DBD) controls high affinity recognition with specific response. The hinge region in the middle facilitates coordination of multiple domains. Ligand-binding domain (LBD) determines specificity and affinity and is responsible for manifesting species variability. The C-terminal end contains activation function 2 (AF2), acts as a control switch, and maintains ligand-dependent transcriptional function [8].

Table 2.1.2 Nuclear receptors, ligands, and their target genes that influence uptake and excretion of organic anions by the hepatocyte

Nuclear receptor	Ligand (s)	Major target gene
RXR partners (class II receptors)		
FXR (farsenoid X receptor)	Bile acids, bilirubin	BSEP, SHP, UGTs, SULTS, MRP2, MDR3
PXR (pregnane X receptor)	Xenobiotics, UDC	CYP3A, OATP1B1, MRP2, MRP4, GST
CAR (constitutive X receptor)	Xenobiotics, phenobarb	CYP3A, OATP1B1, MRP2, MRP4, UGT, SULTs, GSTs
LXR (liver X receptor)	Oxysterols (metabolites of cholesterol)	CYP7A, CYP8B, ABCG5/8
RAR (retinoic acid receptor)	All-trans retinoic acid	NTCP, MRP2
PPAR (peroxisomal proliferators receptor)		
Others		
SHP-1 (short heterodimer partner)	None	Inhibits NTCP, CYP7A, CYP8B.
HNF-α (hepatocyte nuclear factor α)	None	NTCP, CYP7A.

Modified from Boyer [9]

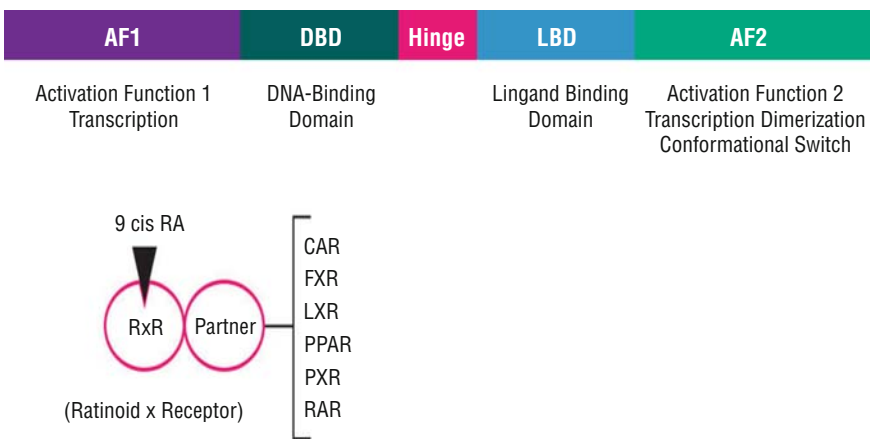

Fig. 2.1.2 Structure of class II nuclear receptors. A nuclear receptor consists of five functional domains. The aminoterminal (*N*) end is the activation function 1 (*AF1*) region, which controls the ligand-independent transcriptional activation and coordination. The DNA-binding domain (*DBD*) controls high-affinity recognition with a specific response. The middle region (*HINGE*) facilitates coordination of multiple domains. The ligand-binding domain (*LBD*) determines specificity, affinity, and species variability. The C-terminal end contains activation function 2 (*AF2*) and acts as a control switch to maintain ligand-dependent transcriptional function

Regulation of Basolateral Transporters

Class II nuclear receptors control many of the functions of the hepatocyte. By definition, class II nuclear receptors cannot act alone or as homodimers. They act by forming a heterodimer partner with retinoid X receptor (RXR). After complexing with RXR, class II receptors acquire DNA-binding capacity and regulation of transcriptional activity. Five (FXR, CAR, PXR, LXR, and RAR) of eight class II nuclear receptors play major roles in influencing hepatic uptake and excretion of organic anions (Table 2.1.2).

Cholestasis suppresses sodium taurocholate-cotransporting polypeptide (NTCP) through FXR (farnesoid X receptor)-mediated induction of short heterodimeric partner 1 (SHP1), which prevents further uptake of bile salts that may otherwise reach toxic levels. Cholestasis also downregulates OATP1B1 through bile acid-mediated activation of SHP1, which decreases hepatocyte nuclear factor α (HNFα). HNFα is one of the major activators of OATP1B1. Although cholestasis in general downregulates nuclear receptors, it stimulates OATP1B3 via activation of FXR, and thus provides an escape mechanism for clearance of xenobiotics from the body (Fig. 2.1.2). After the uptake, intracellular transit of both sodium-dependent and sodium-independent substrates is regulated by the cyclic adenosine monophosphate-mediated dephosphorylation process, which is controlled by protein kinase B. Uptake of toxins like phalloidin and microcystin is mediated by OATP1B1 and OATP1B3, whereas the uptake of the most toxic natural substance known, amanitin, is controlled solely by OATP1B3 [7].

Transport Through the Hepatocyte

After uptake along the basolateral border facilitated by NTCP, bile acids are hydroxylated and transported through the hepatocyte via a 33-kDa cytosolic protein, 3-α-hydroxysteroid dehydrogenase in phase II (Fig. 2.1.3.). After its uptake, bilirubin binds to glutathione-S-transferase and undergoes conjugation (phase III) by hepatic microsomal enzyme uridine-diphosphonate glucoronyl transferase (UGT) to form monoglucoronide and then diglucoronide [9]. The conjugation process converts hydrophobic salts into hydrophilic salts, which facilitates rapid excretion into bile canaliculi. Many organic anions (including Tc-99m-HIDA) are transported through the hepatocyte by yet undefined mechanisms.

Secretion into Bile Canaliculi

The quantity of solute transported across the canalicular membrane is the rate-limiting step in the volume of bile secreted per day. The canalicular membrane contains several ATP-dependent and ATP-independent transport proteins (pumps) to enable secretion of solutes from the hepatocyte into canaliculi [7, 10]. These pumps include ATP-dependent multidrug-resistance-1 p-glycoprotein (MDR1) and phospholipid transporter multidrug-resistance p-glycoprotein 3 (MDR3). The canalicular membrane also localizes multidrug resistance-associated protein 2 (MRP2), canalicular-bile-salt-export pump (BSEP or SGPG) and ABC half transporters, and breast cancer-resistance protein (BCRP), all of which facilitate

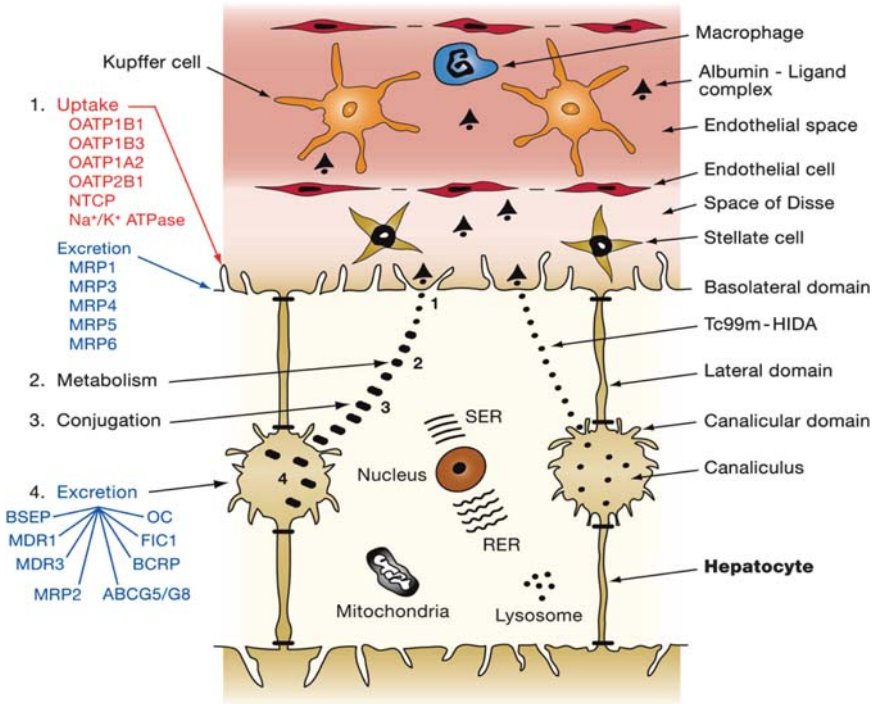

Fig. 2.1.3 Microenvironment and transporter proteins of the hepatocyte. Substrates are carried in blood loosely bound to albumin and delivered into the space of Disse. Basolateral domain of the hepatocyte has many transporter proteins that control uptake (*red*) and excretion (*blue*) of substrates from and into blood in the space of Disse. Uptake proteins (*red*) include four organic anion transporter proteins (*OATPs*), sodium taurocholate cotransporting peptide (*NTCP*), and sodium/potassium ATPase. It has five multidrug resistance-associated proteins (*MRPs*) that control reflux of substrates from the cytoplasm into blood. After the uptake, substrates are metabolized (phase 2), conjugated (phase 3), and excreted (phase 4) unchanged into bile canaliculi. Excretion is controlled by canalicular domain proteins, such as multidrug resistant p-glycoproteins (MDR1, MDR2), MRP2, bile salt export protein (BSEP), breast cancer-resistant protein (BCRP), organic cation (OC), and flippases (ABCG5/ABCG8), FIC1 protein

excretion of bile salts and xenobiotics into bile canaliculi. Flippases (ABCG5 and ABCG8) control cholesterol metabolism and excretion both by hepatocytes and intestinal cells. The ATP-independent transport systems include a chloride channel, a chloride-bicarbonate-anion exchanger, and a glutathione (GSH) transporter (Fig. 2.1.1). Secretion of other organic anions, such as bilirubin, BSP, indocyanin green, and glutathione (Tc-99m-HIDA), is controlled mainly by MRP2. The secretion of organic cations (e.g., cancer chemotherapy agents, cyclosporin A, calcium channel blockers, and other drugs) is mediated by MDR1–a 170 gene product [11]. After passing through the tight junction, sodium and other cations enter the canaliculi through the space between the lateral domain of two adjacent hepatocytes, and the water then simply follows the electrolytes by passive diffusion.

Regulation of Canalicular Membrane

Production of bile salt export protein (BSEP) and multidrug resistance glycoprotein 3 (MDR3) is controlled by a FXR-mediated process resulting in increased bile salt excretion into canaliculi, thereby facilitating formation of mixed micelles (Fig. 2.1.3). This action protects hepatocytes and cholangiocytes from toxic levels of bile salts. FXR also upregulates MRP2 and increases bile salt excretion into canaliculi. PXR (pregnane X receptor) upregulates MDR1, which is a key transporter protein in cellular excretion of many drugs and xenobiotics. LXR (liver X receptors α and β) controls flippases, ABCG5 and ABCG8, and transport proteins [9].

Cholangiocytes along the bile ducts further modify bile composition by selective absorption or secretion of bile solutes and water. Cholangiocytes absorb bile salts through apical sodium-dependent bile salt transporter (ASBT) and OATP1A2. After their uptake, bile salts are excreted through the basolateral membrane (via MRP3) into the peribiliary plexus where they reach the portal circulation. Bile acids and sterols also use organic solute transporters (OSTα/OSTβ) to be secreted into the peribiliary plexus through the basolateral domain. Unlike the basolateral border of the hepatocyte, which lacks MRP2, the basolateral border of the cholangiocyte contains MRP2 that controls excretion of organic anions into peribiliary plexus (Fig. 2.1.1).

Aquaporins

Of the daily total bile volume of 600 ml, 450 ml (75%) is secreted by hepatocytes, and 150 ml (25%) is added by the cells lining the canaliculi (cholangioles or cholangiocytes). Of a total of 450 ml hepatocellular bile, 225 ml (50%) is bile salt dependent, and the remaining 225 ml (50%) is bile salt independent (Fig. 2.1.1). Although the cholangiocytes account for only 3 to 5% of liver volume, they play a major role controlling daily bile volume mainly by secretion or absorption of water by either direct passive membrane passage or through special water-channel proteins called aquaporins (AQPs) located within the hepatocytes and cholangiocytes. AQPs are small (25–34 kDa) hydrophobic protein molecules consisting of 263–323 amino acids. Both amino and carboxy terminals are located intracellularly within the cytoplasm (Fig. 2.1.4). Each AQP monomer has six α helical transmembrane domains connected by five loops, A–E (Fig. 2.1.4A). Three of the connecting loops (A, C, E) are extracellular, and two (B, E) are intracellular [12]. When one intracellular and one extracellular loop, each containing Asp-Pro-Ala (NPA) amino acids, are juxtaposed to within the plasma membrane, AQP forms a tetramer containing four single water channels and allows molecules of 3 Å size or less to pass through (Fig. 2.1.4B). This enables water molecules (2Å) to pass through the tight junction readily. Figure 2.1.5 summarizes the mechanisms and carrier proteins that play a major part in the transport of water from blood into the hepatocyte and finally into bile canaliculi.

Water can pass either through the cell (transcellular) or between two adjacent (paracellular) cells. When electrolytes, bile salts, and other organic anions are transported from the basolateral to the canalicular border through the hepatocyte, and secreted into canaliculi, water follows passively through the cell via both channel-mediated and non-channel-mediated pathways. Of the 13 AQPs that have been identified in the mammalian cells,

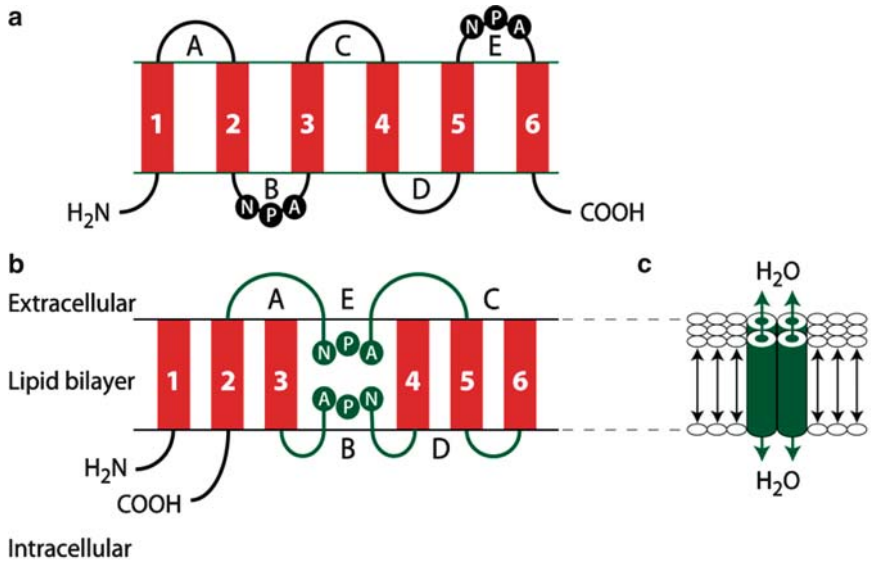

Fig. 2.1.4 Structure of aquaporins. Aquaporins are membrane proteins that regulate water movement. Each aquaporin has six alpha helical transmembrane domains connected by five loops, *A–E* (*top*). Three of the connecting loops (*A*, *C*, *E*) are extracellular and two (*B*, *E*) are intracellular. Each aquaporin forms a tetramer (four single water channels) when one intracellular and one extracellular loop, each containing Asp-Pro-Ala (NPA) amino acids, are juxtaposed within the plasma membrane and allows molecules of 3 Å size or less to pass through (*bottom*). This enables water molecules (2Å) to pass through the tight junction readily

seven (AQP0, AQP1, AQP4, AQP5, AQP8, AQP9, AQP11) are found within the hepatobiliary system [13]. Three of the AQPs (AQP0, AQP8, AQP9) are found in the hepatocytes, and two (AQP1, AQP4) are localized in the cholangiocytes. Four of them (AQP1, AQP4, AQP8, AQP9) play a major role in controlling water transport in the hepatobiliary tree. In the basal state, AQP8 and AQP1 are distributed free within the cytoplasm of the hepatocytes and cholangiocytes, respectively, and water diffuses passively through the lipid plasma membrane, facilitated by AQP9 and AQP4 water channels on the membrane (Fig. 2.1.5). In the stimulated state (CCK or secretin), hepatocyte AQP8 translocates to the canalicular border, and cholangiocytes AQP1 translocates to the apical border, allowing rapid passage of water from the cell into the bile duct lumen. Each AQP maintains its own rate of water transport; AQP0 is the slowest, while AQP1 and AQP4 allow 50–80 times more rapid flow of water. In the stimulated state, each AQP channel can increase its water transport ten times more rapidly than at the basal state.

Protein Secretion

Liver is the main source of plasma proteins, albumin, and globulins. Serum albumin synthesized entirely by the hepatocytes accounts for 60% of plasma proteins, is composed of 585 amino acids, and does not contain any carbohydrate moiety. In addition to controlling

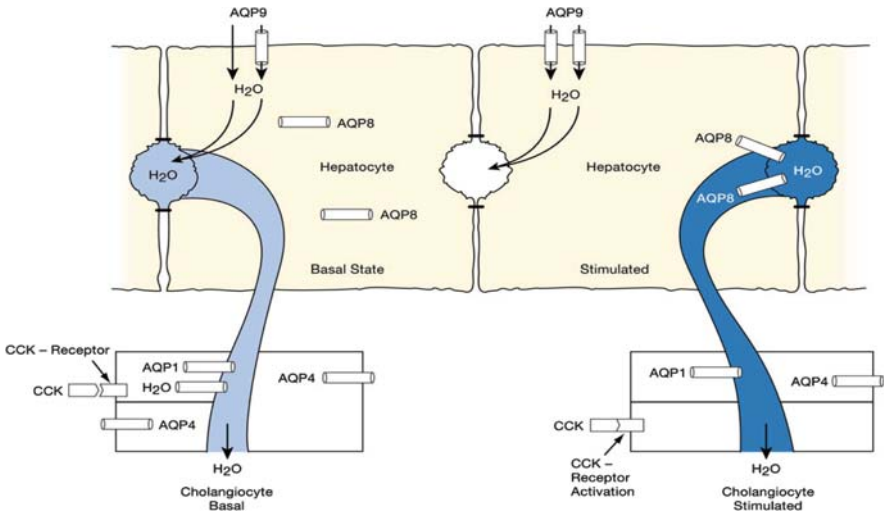

Fig. 2.1.5 Water movement within the hepatocytes and cholangiocytes. In the basal state, aquaporin 8 and aquaporin 1 are distributed free within the cytoplasm of the hepatocytes and cholangiocytes, respectively. Water passes passively through the lipid plasma membrane, facilitated by AQP9 and AQP4 water channels located on the membrane, respectively. When stimulated by cholecystokinin or secretin, hepatocyte AQP8 translocates to the canalicular border, and cholangiocyte AQP1 translocates to the apical border, promoting rapid passage of water from the cell into the bile duct lumen. In the stimulated state, each AQP channel can increase its water passage by more than ten times at its basal state

osmotic pressure, albumin functions as a carrier protein for drugs, metals, vitamins, amino acids, steroid, fatty acids, and Tc-99m-HIDA. Other proteins secreted by hepatocytes include α-1 anti trypsin, α-fetoprotein, α-2 macroglobulin, antithrombin lll, ceruloplasmin, C-reactive protein, fibrinogen, haptoglobin, hemopexin, and transferrin (Table 2.1.2). Most of these proteins are composed of a carbohydrate moiety and hence are called glycoproteins [14]. Hepatic bile is relatively more dilute (contains fewer bile salts, bilirubin, chloride, and bicarbonate per liter) than the gallbladder bile (Table 2.1.3).

Cell Death: Apopstosis or Necrosis

Liver, being metabolically very active, has mechanisms to increase or decrease the number of cells needed to carry out complex biological functions. It can get rid of unwanted cells through cell death or recruit new cells through regeneration. Liver can regenerate to its original size within a few weeks after resection of 60–70% of its volume. Cell death is a common phenomena associated with varieties of liver diseases, including viral hepatitis, cholestasis, ischemia/reperfusion injury, and hepatotoxins. Cell death occurs in one of two forms: necrosis or apopstosis. Both forms utilize a common pathway, but with different end results (Fig. 2.1.6). They involve participation of the plasma membrane, mitochondria, nucleus, endoplasmic

Table 2.1.3 Plasma proteins secreted by hepatocytes [11]

Protein	Molecular weight (kDa)	Function	Ligand binding	Plasma conc. (mg dl^{-1})
Albumin	66	Osmotic pressure Carrier protein	Hormones amino acids fatty acids, vitamins	4,500–5,000
Alpha-1 anti-trypsin	54	Trypsin and general Protease inhibitor	Present in serum & tissue secretions	1.3–1.4
Alpha Feto adults protein	72	Osmotic regulation Carrier protein	Hormones Amino acids	Undetectable in adults Present in fetal blood
Antithrombin lll	65	Protease inhibitor	Binding to Protease	15–60
Ceruloplasmin	134	Copper transport	6 copper atoms per mol	15–60
C-reactive protein	105	Tissue inflammation	Complement C1q	Increased in inflammation
Fibrinogen	340	Fibrin precursor during hemostasis.		200–450
Transferrin	80	Iron transport	Two iron atoms per mol	3–6.5
Haptoglobin	100	Transport of hemoglobin	Hemoglobin	40–180
Prothrombin	72	Hemostasis	Calcium chelation	10.0

reticulum, and lisosomes [15]. Necrosis is an acute process involving contiguous liver cells and takes place rapidly within a few minutes. Cells swell, forming blebs along the plasma membrane, disrupting its permeability, which ultimately results in its rupture with the release of cytosolic proteins, such as aspartate aminotransfarase (AST), alanine aminotransfarase (ALT), alkaline phosphatase (Alk.Phos), and lactic dehydrogenase (LDH), into blood. Necrosis is associated with acute inflammatory cell infiltration. Apoptosis, on the other hand, is a programmed cell death that occurs at a relatively a slow pace, requiring ATP. It affects cells at discontinuous locations, and death is characterized by chromatin condensation, DNA degradation, and shrinkage of cells with very little acute inflammatory cell infiltration [16]. Cytochrome c plays a central role in both processes (Fig. 2.1.6).

Hepatocytes, cholangiocytes, sinusoidal endothelial cells, stellate cells, and Kupffer cells express death receptors, such as tumor necrosis factor-alpha receptor 1 (TNFα-R1). The plasma membrane receives death signals through injury by toxins, ischemia/reperfusion injury, or toxic biological waste products. Death ligand and receptor interactions

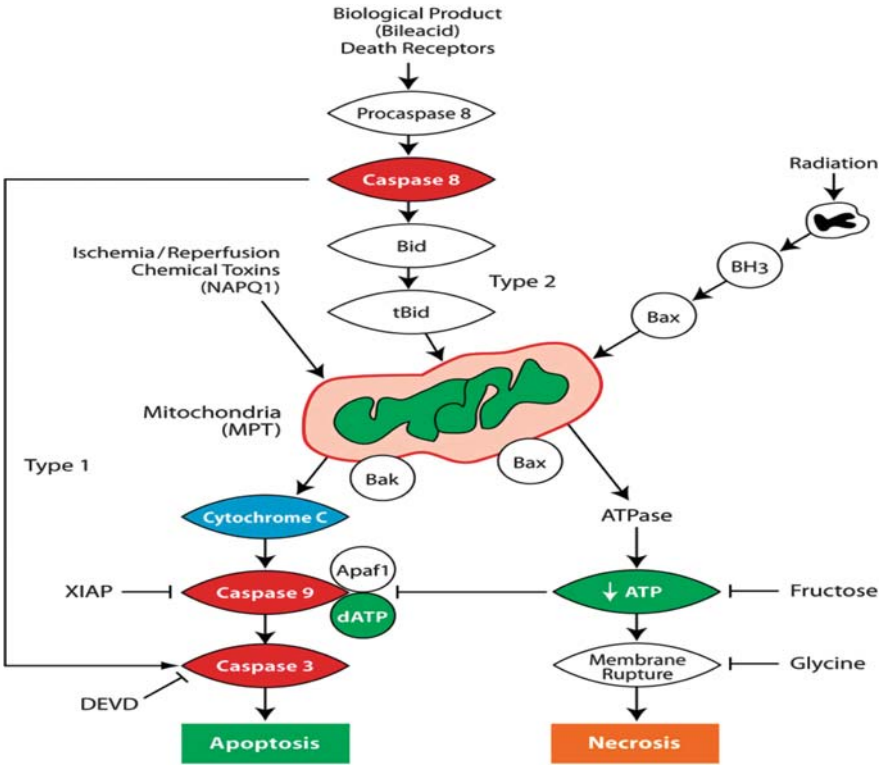

Fig. 2.1.6 Cell death through apoptosis or necrosis. Both forms utilize a common pathway, but with different end results. The process is initiated by interaction of death ligands with its corresponding receptor, which converts procaspase 8 to caspase 8. Caspase 8 can release caspase 3 directly in the type 1 mechanism. In the type 2 mechanism, caspase 8 converts Bid to tBid, which acts on the mitochondrial membrane, which releases cytochrome c. In the absence of ATP, necrosis sets in, involving contiguous liver cells, and takes place rapidly within a few minutes. Cells swell, forming blebs along the plasma membrane, disrupting its permeability, resulting in a rupture with the release of cytosolic proteins into the blood stream. Necrosis is followed by acute inflammatory cell infiltration. Apoptosis, on the other hand, is a programmed cell death that requires the presence of ATP and occurs at a relatively a slow pace. It affects cells at discontinuous locations, and death is characterized by chromatin condensation, DNA degradation, and shrinkage of cells with very little acute inflammatory cell infiltration (adopted from [16])

release adaptor proteins, TRADD and FADD, which in turn lead to activation of caspase 8 (*cysteine-aspartate proteases*). Caspase 8 can directly release the end product in the form of caspase 3 (type 1 signaling), which induces apoptosis (Fig. 2.1.7). Activated caspase 8 converts cytosolic inactive protein Bid to its active form, tBid, which translocates to the mitochondria and releases cytochrome c through activation of Bak and Bax, two members of the Bcl2 family (type 2 signaling). Type 2 signaling leads to opening of membrane permeability transition (MPT) pores in the inner membrane of the mitochondria. Opening of

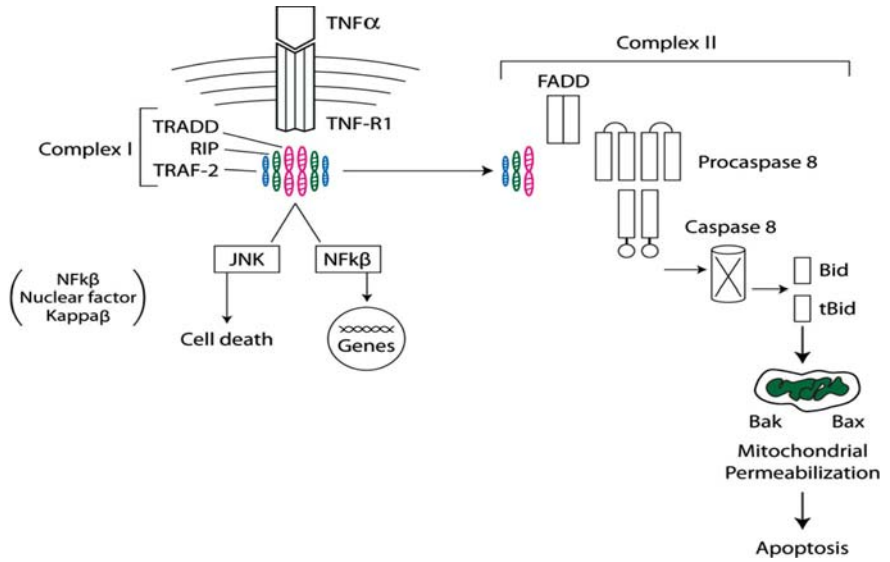

Fig. 2.1.7 Death ligand and receptor interaction. Plasma membrane receives death signals through injury by toxins, ischemia/reperfusion injury, or toxic biological waste products. Death ligand and receptor interactions release adaptor proteins, TRADD and FADD, which in turn lead to activation of procaspase 8 (*c*ysteine-*asp*artate prote*ases*) to caspase 8. Caspase 8 can directly release the end product caspase 3 (type 1 signaling) that induces apoptosis. Activated caspase 8 converts cytosolic inactive protein, Bid, to its active form, tBid, which translocates to the mitochondria and releases cytochrome c through activation of Bak and Bax (type 2 signaling). Type 2 signaling leads to opening of membrane permeability transition (*MPT*) pores in the inner membrane of the mitochondria. Opening of MPT starts the process of cell death, either through necrosis or apoptosis, depending upon the next sequence of events that follows. If the MPT opening is sudden due to death receptor-ligand interaction, which leads to ATP depletion and rupture of the outer membrane, necrosis is the outcome. Nuclear factor k beta in the genes controls cell death. In the presence of adequate amounts of ATP, cytochrome c releases caspase 9, which in turn releases caspase 3, which promotes apoptosis

MPT starts the process of cell death, either through necrosis or apoptosis, depending upon the next sequence of events that follows [17]. If the MPT opening is sudden due hepatotoxins, ischemia/reperfusion injury, or calcium overload, all of which lead to ATP depletion, the process leads to mitochondrial depolarization, disruption of oxidative phosphorylation, and mitochondrial swelling, rupture of the outer membrane, and necrosis [18]. In the presence of an adequate amount of ATP, cytochrome c releases caspase 9, which in turn releases caspase 3, which promotes apoptosis (Fig. 2.1.6).

Bile Entry, Storage, and Concentration by the Gallbladder

Hepatic bile that enters the gallbladder is of much lower osmolality than the bile that leaves the gallbladder after a meal (Table 2.1.1). A major portion (60–70%) of the hepatic

bile secreted during fasting enters the gallbladder, and a minor fraction enters the duodenum directly, depending upon the tonus of the sphincter of Oddi (Fig. 2.1.8). During a period of 10 h in the night, the liver produces about 250 ml of bile (25 ml h^{-1} or 0.42 ml h^{-1}), of which 175 ml (70%) enters the gallbladder (17.5 ml h^{-1} or 0.3 ml min^{-1}). An empty gallbladder can fill to its maximum capacity of 50 ml during a period of 6 h. A fully filled gallbladder continues to receive hepatic bile secreted during fasting by absorbing 0.3 ml of water per minute. This is accomplished primarily by absorption of water and electrolytes through the gallbladder wall. As much as 90% of water can be absorbed through the gallbladder wall during a 6-h period. Dietschy demonstrated that 100 ml of hepatic bile placed inside the gallbladder reduces to less than 10 ml in 6 h mainly through absorption of water (Fig. 2.1.9). As a consequence of this selective water absorption, the concentration of solutes increases in the gallbladder bile [19]. This process of selective absorption of water resulting in higher concentration of bile salts, bilirubin, cholesterol, fatty acids, and lecithin in the gallbladder bile than hepatic bile is called the concentration function of the gallbladder [20, 21]. A normal gallbladder can sequester all of 3–6 g total body bile salts within it after an overnight fast. Fresh hepatic bile enters the gallbladder along its central long axis and moves laterally to reach the wall as the space is made available through removal of water. It takes nearly 30 min for the fresh hepatic bile to reach the wall from the central long axis [21].

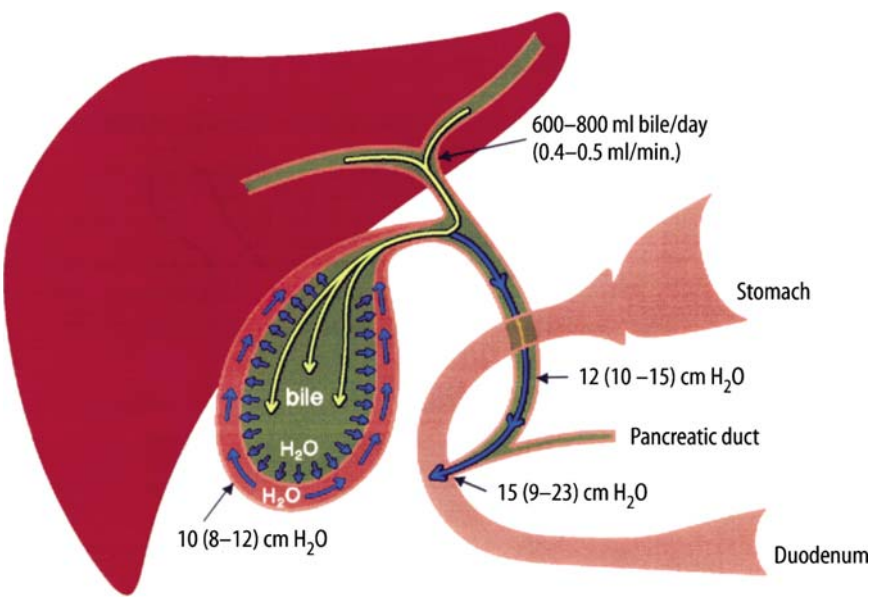

Fig. 2.1.8 Bile entry mechanism into the gallbladder. A higher mean (range) pressure at the sphincter of Oddi (15 cm of H_2O) than the pressure inside the gallbladder lumen and absorption of water through the wall during fasting facilitate constant hepatic bile inflow into the gallbladder

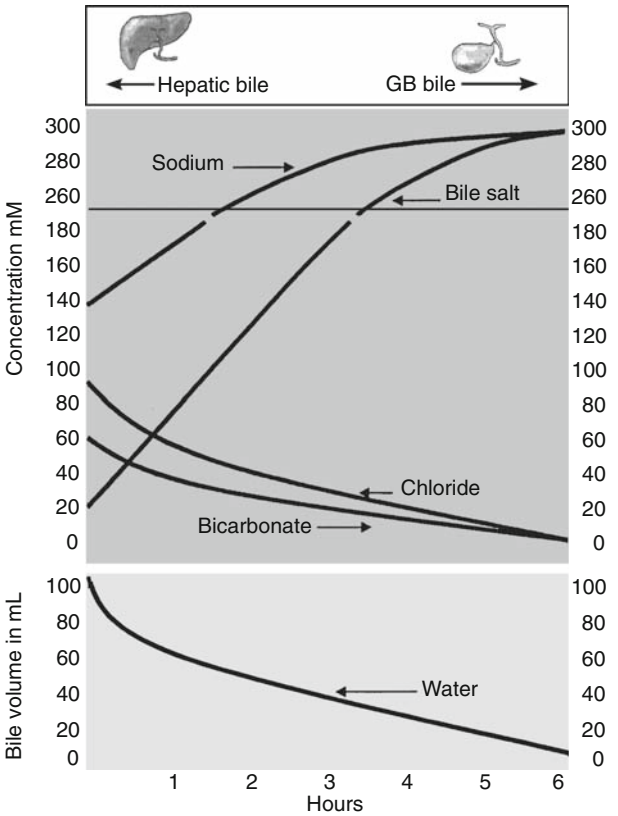

Fig. 2.1.9 Bile concentration. Mainly through different rates of absorption, gallbladder (rabbit) increases the concentration of sodium and bile salts and decreases the concentration of chloride and bicarbonate when compared to hepatic bile. Gallbladder bile volume decreases by 90% of its basal volume to achieve these concentrations [20]

The volume of hepatic bile that enters the gallbladder during fasting is controlled by two mechanisms, the tonus of the sphincter of Oddi and absorption of water through the gallbladder wall (Fig. 2.1.10). Under basal conditions, the mean pressure in the sphincter of Oddi is 15 cm of water, in the common bile duct, 12 cm of water, and in the gallbladder, 10 cm of water. By choosing the path of least resistance, the hepatic bile enters the gallbladder. The tonus of the sphincter of Oddi is dependent upon the frequency and amplitude of phasic wave contractions. The phasic wave frequency ranges from 1 to 13 per minute with an average of six contractions per minute [22]. High frequency contractions ($>8\,min^{-1}$) are relatively rare (14%). Sphincter of Oddi phasic wave contractions occur in conjunction with phase III of the migrating motor complex, which begins in the stomach and traverses through the duodenum and jejunum [23].

The second mechanism that promotes hepatic bile entry into the gallbladder is the rate of absorption of water through the gallbladder wall. During fasting, the lateral intercellular

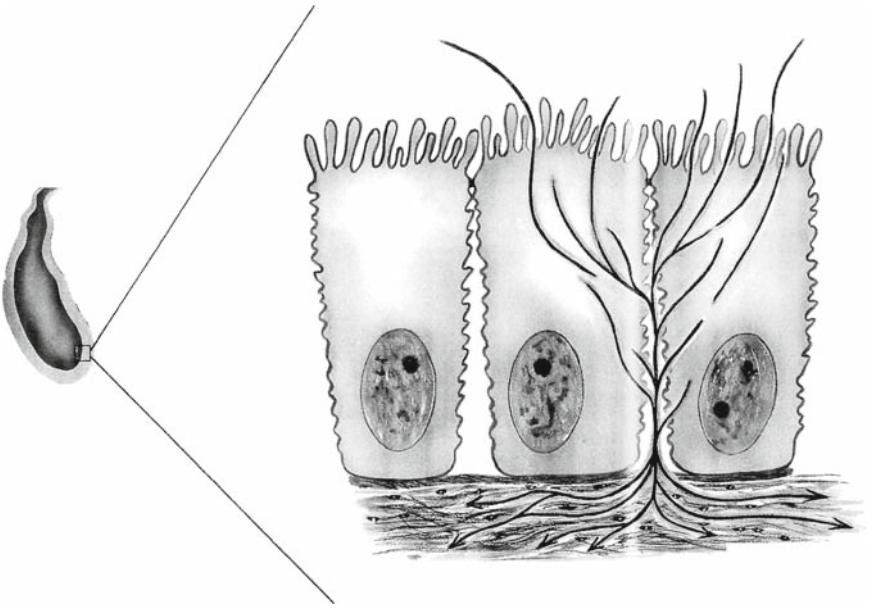

Fig. 2.1.10 Absorption of water through the gallbladder epithelium. Lateral intercellular channels between the columnar epithelial cells are widely open during fasting, allowing free passage of water from the lumen into the connective space. Water absorption creates space for constant entry of hepatic bile into the gallbladder during fasting [20]

channels between the columnar epithelial cells are widely opened, allowing the passage of sodium and water from the gallbladder lumen into the interstitial spaces and then the hepatic venous blood (Fig. 2.1.4). Constant removal of water allows steady entry of hepatic bile into the gallbladder (Fig. 2.1.11). These lateral intercellular spaces collapse when the gallbladder wall contracts following ingestion of a meal or injection of cholecystokinin. Quabain inhibits water transport across most epithelial membranes, including the gallbladder [20]. Spontaneous gallbladder emptying and refilling play a minor role in making room for the fresh hepatic bile. In large number of normal subjects monitored continuously for 2 h with Tc-99m-HIDA by the authors, spontaneous gallbladder emptying to the extent of 5–10% was noticed in less than 2% of the subjects. The bile that enters the duodenum during fasting normally moves antegrade towards the jejunum. Normally, there is no bile reflux from the duodenum into the stomach in the basal state.

Gallbladder Emptying

Emptying of the gallbladder is under both hormonal and nervous control, with hormonal control playing the major role. Nervous control is exerted through both the sympathetic and parasympathetic system as shown in Fig. 1.1.12 of Chap. 1. The cholinergic parasympathetic

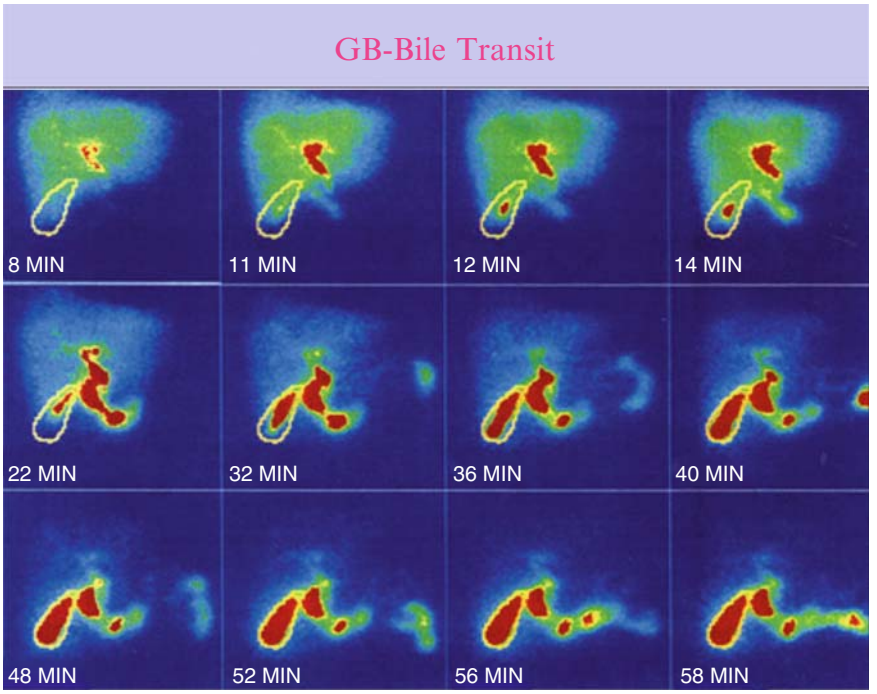

Fig. 2.1.11 Pattern of bile transit within the gallbladder. Fresh hepatic bile enters the gallbladder along its central long axis and moves laterally to reach the wall as water is removed by the lateral intercellular channels. It takes about 30 min for the fresh hepatic bile to reach the wall from the central long axis. Fully filled gallbladder outline is superimposed onto early frames to show how radiolabeled fresh bile moves inside. Radiolabed bile first enters at 12 min and reaches the wall at 48 min [21]

nerve fibers to the gallbladder come primarily from the anterior gastric plexus (left vagus) and control its contraction and emptying. The gallbladder response to sham feeding is mediated through these cholinergic nerve fibers and can be blocked with atropine or after vagotomy [24]. The parasympathetic cholinergic nerve fibers to the sphincter of Oddi come mainly from the posterior gastric plexus (right vagus). Sympathetic post-ganglionic nerve fibers from the celiac ganglion reach the gallbladder and the sphincter of Oddi. Sympathetic nerve stimulation relaxes the gallbladder wall and promotes hepatic bile entry.

The hormone-induced contraction and emptying of the gallbladder occur mainly through endogenous release of cholecystokinin (CCK), demonstrated first in 1928 by Ivy and Oldberg [25]. Cholecystokinin, a linear 33 or 39 amino acid polypeptide, is produced from a large precursor protein with 114 amino acids. Most of the biological functions of the hormone are confined to the last four carboxy terminal amino acids. A much shorter cholecystokinin with only eight carboxy terminal amino acids (CCK-8) carries out most of the biological functions of the parent molecule with 33 amino acids [26]. The contraction

and emptying of the gallbladder begin within 2–3 min after an intravenous administration of CCK-8, but it may take as long as 10–20 min to begin emptying following a meal [27]. This time delay in gallbladder emptying after a meal is due to a combination of time taken for the meal to pass from the stomach into the duodenum and the time taken for the CCK-secreting cells in the duodenal mucosa to release enough hormones into the blood stream. Cerulein, motilin, and other gastrointestinal hormones with an identical carboxy terminal tetrapeptide also induce gallbladder contraction and emptying [28].

References

1. Fitz JG. Cellular mechanism of bile secretion. In: Zakim D, Boyer TD, eds. Hepatology. A textbook of liver disease. Philadelphia, WB Saunders, 1996, pp 362–376
2. Brauer RW, Leong SF, Holloway RJ. Mechanism of secretion. Effect of perfusion pressure and temperature on bile flow and bile secretion pressure. Am. J Physiology 1954;177:103–106
3. Boyer JL, Klatskin G. Canalicular bile flow and bile secretary pressure. Evidence for a non-bile salt dependent fraction in the isolated perfused rat liver. Gastroenterology 1970;59:853–859
4. Jones AL, Schmucker DL, Renston RH, Murakami T. The architecture of bile secretion. A morphological perspective of physiology. Dig Dis Sci 1980;25:609–629
5. Sellinger M, Barrett C, Malle P, Gordon ER, Boyer JL. Cryptic Na+, K+-ATPase activity in the rat liver canalicular plasma membranes: evidence for its basolateral origin. Hepatology 1990;11:223–229
6. Meier PJ. Molecular mechanisms of hepatic bile salt transport from sinusoidal blood into bile. Am J Physiol 1995;269:G801–G812
7. Pauli-Magnus C, Meier PJ. Hepatobiliary transporters and drud-induced cholestasis. Hepatology 2006;44:778–787
8. Karpen SJ. Nuclear receptor regulation of hepatic function. J Hepatology 2002;36:832–850
9. Boyer JL. Nuclear receptor ligands: rational and effective therapy for chronic cholestatic liver disease. Gastroenterology 2005;129:735–740
10. Trauner M, Meier PJ, Boyer JL. Molecular pathogenesis of cholestasis. N Eng J Med 1998:339:1217–1227
11. Kamimato Y, Gatmaitan Z, Hsu J, Arias IM. The function of Gp 170, the multidrug resistance gene product, in rat liver canalicular membrane vesicles. J Biol Chem 1989;264:11693–11698
12. Masyuk AI, Marinelli RA, LaRusso NF. Water transport by epithelia of the digestive tract. Gastroenterology 2002;122:545–562
13. Masyuk AI, LaRusso NF. Aquaporins in the hepatobiliary system. Hepatology 2006;43:S75–S81
14. Donohue TM Jr., Tuma DJ, Sorrell MF. Plasma proteins metabolism. In: Zakim D, Boyer TD. Hepatology. A text book of liver disease, 3rd edn. Philadelphia, WB Saunders, 1996, pp 130–148
15. Lemasters JJ. Necrapopstosis and the mitochondrial permeability transition: shared pathways to necrosis and apoptosis. Am J Physiol 1999;276:G1–G6
16. Lemasters JJ. Dying of a thousand deaths: redundant pathways from different organells to apoptosis and necrosis. Gastroenterology 2005;129:351–360
17. Malhi H, Gres GJ, Lamaster JJ. Apoptosis and necrosis in the liver: a tale of two deaths? Hepatology 2006;43:S31–S44
18. Krishnamurthy G, Krishnamurthy S. Cholescintigraphic measurement of liver function: how is it different from other methods? Eur J Nucl Med Mol Imaging 2006;33:1103–1106

19. Dietschy JM. Water and solute movement across the wall of the everted rabbit gallbladder. Gastroenterology 1964;47:395–408
20. Wheeler HO. Concentrating function of the gallbladder. Am J Med 1971;51:588–595
21. Krishnamurthy S, Krishnamurthy GT. Hepatic bile entry into and transit pattern within the gallbladder lumen: a new technique quantitative cholescintigraphic technique for measurement of its concentration function. J Nucl Med 2002;43:901–908
22. Thune A, Scicchitano J, Roberts-Thompson I, Toouli J. Reproducibility of endoscopic sphincter of Oddi manometry. Dig Dis Sci 1991;36:1401–1405
23. Lee SK, Kim MH, Seo DW, Yoo BM, Lee MH, Myung SJ, Min YI. Frequency of phasic wave contraction is variable during long-term sphincter of Oddi manometry. Am J Gastroenterol 1996;91:2395–2398
24. Fisher RS, Rock E, Malmud LS. Gallbladder emptying response to sham feeding in humans. Gastroenterology 1986;90:1854–1857
25. Ivy AC, Oldberg E. A hormone mechanism of gallbladder contraction and evacuation. Am J Physiology 1928;86:599–613
26. Mutt V. Cholecystokinin: isolation, structure, and function. In: Jerzy Glass GB. ed. Gastrointestinal hormones. New York, Raven, 1980, pp 169–221
27. Bobba VR, Krishnamurthy GT, Kingston E, Turner FE, Brown PH, Langrell K. Gallbladder dynamics induced by a fatty meal in normal subjects and patients with gallstones: Concise communication. J Nucl Med 1984;25:21–24
28. Bloom SR, Adrian TE, Mitchenere P, et al. Motilin induced gallbladder contraction. A new mechanism. Gastroenterology 1981;80:1113

2.2 Spleen Function

The spleen is composed mostly of reticuloendothelial cells and lymphoid tissue. The spleen is usually seen during radionuclide imaging with radiocolloids and radiolabeled red blood cells, leucocytes, monoclonal antibodies, or peptides (somatostatin). As the spleen does not concentrate Tc-99m-HIDA, it is not seen during functional hepatobiliary imaging.

A normal spleen weighs between 80–200 gm with an average of 150 gm [1]. In the posterior view of a radiocolloid scan, the spleen normally measures 10.5 cm along the oblique axis. The spleen has to enlarge more than 2.5 times its normal size before it is palpable in the left upper quadrant during a routine physical examination. Most of the palpable spleens are enlarged, but not all non-palpable spleens are normal in size.

The spleen carries out many important functions (Table 2.2.1) that include: (1) hemopoiesis, (2) destruction of senescent red blood cells, leucocytes, and platelets, (3) culling and pitting, (4) phagocytosis, (5) reservoir function, and (6) immunologic function [2].

During the first 6 months of intrauterine life, the spleen functions as a major hematopoietic organ, and this function normally disappears by birth. In thalassemia and myeloid metaplasia, the spleen is capable of resuming its intrauterine function in adult life to produce red blood cells. The normal function in adults is one of destruction of senescent red blood cells, leucocytes, and platelets. Excessive destruction of blood cells by the spleen results in anemia, leucopenia, or thrombocytopenia. The volume of red blood cells in the

2

Table 2.2.1 Functions of the spleen

(1) Hemopoiesis
(2) Destruction of senescent red blood cells, leucocytes and platelets
(3) Culling and pitting
(4) Phagocytosis
(5) Reservoir function
(6) Immunologic function

body and their destruction by the spleen are measured by labeling the cells with chromium-51 [3]. During labeling, hexavalent chromium-51 (Na_2CrO_4) crosses the red cell membrane and attaches to hemoglobin after reduction into a trivalent form [4]. The physical half life of Cr-51 is 27 days. Random labeling, elution of Cr-51 and death of senescent red cells all account for the mean RBC survival half-time of 35 days (normal life span of RBC is 120 days). Chromium-51 released after RBC death is taken up by the reticuloendothelial cells, and it does not label other red blood cells in blood; hence, it serves as an ideal marker for RBC survival studies.

The selective removal of abnormal red cells by the spleen is called culling, and removal of intra-erythrocytic inclusions without destroying the RBC is called pitting. Howell-Jolly bodies, remnant of RBC nucleus, are removed from the red blood cells by the spleen. The appearance of Howell-Jolly bodies in the peripheral blood, therefore, is an indication of either splenectomy or of a non-functioning spleen [5]. Hypersplenism is documented by showing increased spleen/liver and increased spleen/precordial count ratio in association with decreased RBC survival time. Return of splenic function after splenectomy is attributed to auto-transplantation (due to spillage) of the splenic tissue on the peritoneal surface or an accessory spleen [6]. Imaging of the spleen with radiocolloids, a popular modality in the 1970 and 1980s, is largely replaced today by computerized tomography and ultrasound. Radiocolloid spleen imaging is now obtained occasionally to clarify an abnormality that has already been detected with CT or ultrasound or to confirm splenomegaly in the diagnosis of polycythemia rubra vera [7].

The spleen capsule has a thin muscle layer whose contraction squeezes out the sequestered RBC, WBC, and platelets into peripheral circulation. Injection of epinephrine induces smooth muscle contraction with a subsequent rise in peripheral cell count [3]. The spleen plays a protective role on the lung tissue, and pulmonary hypertension is shown to develop after splenectomy in some patients [8]. The immunologic function of the spleen is carried out by the lymphocytes and reticuloendothelial cells (phagocytosis). The spleen produces antibodies against many microorganisms, especially polysaccharide-encapsulated bacteria, such as pneumococci. Overwhelming infection sometimes follows after splenectomy in children. Human splenic autotransplantation produces significant antipneumococcal antibody in response to administration of pneumococcal vaccine [9].

References

1. Mattsson O. Scintigraphic spleen volume calculation. Acta Radiol [Diagn] (Stockh) 1982;23:471–477
2. Spencer RP, Pearson HA. The spleen as a hematological organ. Semin Nucl Med 1975;5:95–102
3. Gray SJ, Sterling K. The tagging of red blood cells and plasma proteins with radioactive chromium. J Clin Invest 1950;29:1604–1613
4. Pollycove M, Tono M. Blood volume. In: Sandler MP, Patton JH, Coleman RE, Gottschalk A, Wackers FJTh, Hopper PB. Diagnostic nuclear medicine, 3rd edn. Williams and Wilkins, Baltimore, 1996, pp 827–834
5. Crosby WH. Normal functions of the spleen relative to red blood cells. A review. Blood 1959;14:399–408
6. Pearson HA, Johnston D, Smith KA, Touloukian RJ. The born-again spleen. Return of splenic function after splenectomy for trauma. New Eng J Med 1978;298:1389–1392
7. Spencer RP. Spleen imaging. In: Sandler MP, Patton JH, Coleman RE, Gottschalk A, Wackers FJT, Hopper PB. Diagnostic nuclear medicine, 3rd edn. Williams and Wilkins, Baltimore, 1996, pp 865–874
8. Hoeper MM, Niedermeyer J, Hoffmeyer F, Flemming P, Fabel H. Pulmonary hypertension after splenectomy? Ann Intern Med 1999;130:506–509
9. Leemans R, Manson W, Snijder JAM, Smit JW, Klasen HJ, The TH, Timens W. Immune response capacity after human splenic autotransplantation. Restoration of response to individual pneumococcal vaccine subtypes. Ann Surg 1999;229:279–285

Imaging Agents 3

Historical evolution The introduction of radiocolloids in the 1940s, whose rate of clearance from the circulation was used as an indicator of liver function, gave birth to nuclear hepatology [1]. Imaging of the liver morphology began in 1954 with gold-198 colloid using an automated rectilinear scanner developed by Cassen [2, 3]. Imaging of morphology was supplanted by imaging of liver physiology with the introduction of I-131 rose bengal in 1955 by Taplin et al. [4]. Morphology imaging gained wide clinical popularity after the introduction of technetium-99m colloid in 1965 [5], and a rapid leap in imaging of physiology occurred with the introduction of technetium-99m-HIDA agents in 1976 [6].

3.1 Morphology and Physiology Imaging Agents

The liver carries out the most complex biological functions through the hepatocytes, Kupffer cells, endothelial cells, fat cells (Ito cells), blood vessels and biliary epithelial cells. The liver imaging agents are classified broadly into two groups: (1) those that identify pathology mainly through detection of changes in liver morphology and (2) those that identify pathology by identifying changes in liver physiology (Table 3.1.1). A wide variety of imaging agents now available enable the study of specific cell functions (Table 3.1.2). Radiocolloids are the most common agents for imaging morphology, and Tc-99m-HIDA compounds are the most preferred agents for physiology. Since liver morphology imaging is now carried out mostly with CT or ultrasound, imaging of physiology is currently the most common diagnostic procedure in nuclear hepatology. Since the publication of the first edition of our book, fluorine-18-labeled 2-fluoro-2–deoxyglucose (18-FDG) has become a major factor in the assessment of primary and metastatic lesions of the liver and is included in the current edition.

Radiocolloids

Radiocolloids are small particles, 5–1 μm size, that are removed from circulation by the reticuloendothelial cells of the liver, spleen and bone marrow. They carry a negative charge of –30 mV and do not pass through the dialysis membrane, which is permeable to ions.

G.T. Krishnamurthy and S. Krishnamurthy, *Nuclear Hepatology,*
DOI 10.1007/978-3-642-00648-7_3, © Springer-Verlag Berlin Heidelberg 2009

Table 3.1.1 Classification of liver imaging agents

(1) Morphology imaging agents	Radiocolloids (gold-198, Tc-99m-S colloid) gallium-67 citrate
(2) Physiology imaging agents	These agents can be further divided into four subgroups based on specific function
(a) Hepatobiliary agents	Tc-99m-HIDA, Tc-99m-PG, I-131 rose bengal, etc.
(b) Blood pool agents	Tc-99m-RBC, Tc-99m-albumin
(c) Receptor-specific agents	Tc-99m-GSA, In-lll octreotide, In-lll monoclonal antibody, Tc-99m-monoclonal antibodies
(d) Miscellaneous agents	Indium -lll WBC, Tc-99m-WBC(HMPAO), fluorine-18 2-fluoro-2-deoxyglucose (^{18}FDG) and other agents that are used primarily for imaging of other organs, but pass through the liver during their elimination, enabling imaging of the hepatobiliary system, e.g., Tc-99m-sestamibi, Tc-99m-tetrofosmin, Tc-99m-HMPAO, etc.

Table 3.1.2 The cell, mechanism of uptake, disposition and dose of radiolabeled agents for imaging of the liver and spleen

Agent	Uptake by	Mechanism of uptake	Excretion into bile	Dose
Tc-99-S colloid	Kupffer cell	Phagocytosis	No	2–5 mCi
Tc-99m-GSA	Hepatocyte	ASGP receptor	No	2–8 mCi
Tc-99m-HIDA	Hepatocyte	RME	Yes	2–8 mCi
Tc-99m-RBC	Hemangioma	Blood pool	No	10–20 mCi
Tc-99m HMPAO	Infection	Chemotaxis	No	10–20 mCi
In-111 WBC(oxine)	Infection	Chemotaxis	No	0.5–1.0 mCi
In-111 Octreotide	Somatostatin-	Receptor-ligand receptor	No interaction	3–8 mCi
In-111 MOAB	TAG-72	Antigen-antibody Interaction	No	2–5 mCi
Ga-67 citrate	Hepatocyte	Unknown	No	2–10 mCi
F-18 FDG	Hepatocyte	Glucose receptor	No	10–15 mCi

ASGP Asialoglycoprotein, *GSA*, galactosyl human serum albumin, *HIDA* hepatic iminodiacetic acid, *RME* receptor-mediated endocytosis.

However, they readily pass through an ion-exchange column and show no movement on paper chromatography [7]. Although Au-198 is no longer used for imaging, thorough understanding of its pharmacokinetics provides a sound basis for understanding the biokinetics of Tc-99m-S colloid and is described briefly below.

Gold-198 Colloid

Gold (Au)-198 colloid is one of the smallest radiocolloid particles known to nuclear medicine. The particles vary in size from 5 to 50 mμ, with an average size of 30 mμ, and clear from blood with a T ½ of 3 min. Gold-198 has a physical half life of 2.7 days, decays by a beta minus emission and emits a monoenergetic gamma photon of 411 keV for imaging. The adult dose ranges from 100 to 150 μCi in 25 μg to 2.5 mg gold. The three organs concentrating Au-198 colloid are the liver, spleen and bone marrow, with the smallest particles preferentially taken up by the bone marrow and the largest particles by the spleen [9]. The percent dose localized in each organ depends upon its function and size, and the size and electrochemical character of the radiocolloid particles. Normally, the liver weighs about 1,500–1,800 g, the spleen 150–200 g and the bone marrow ~1,500 g (Table 3.1.3). Normally, about 90% of the Au-198 colloid dose is taken up by the liver, 7% by the reticuloendothelial (RE) cells of the bone marrow and 3% by the spleen [10]. In moderate hepatocellular disease, the liver mass increases (2,400 g) because of fatty infiltration, and the mass of the spleen increases (250 g) because of portal hypertension. In advanced cirrhosis, the liver actually shrinks in size (1,400 g) because of fibrosis, whereas the spleen continues to increase in size (400 g) because of the increase in portal hypertension. The mass of reticuloendothelial cells in the bone marrow does not change. In moderate liver disease, the uptake by the liver decreases to 70%. In advanced cirrhosis when the liver shrinks in size, the radiocolloid uptake may fall below 35%. As the uptake of radiocolloid by the liver decreases, the uptake by the spleen and bone marrow increases in direct proportion to the degree of portal hypertension.

Technetium-99m-Sulfur Colloid

Technetium-99m-sulfur colloid particles are much larger, with a wider variation in size than Au-198 colloid particles, with an average size of about 300 mμ (Table 3.1.4). The usual dose for planar imaging in adults is 2–5 mCi. Liver perfusion and SPECT studies require a much larger dose, in the range of 5–10 mCi. Technetium-99m has a physical half life of 6 h and emits a gamma photon of 140 keV energy, which makes it ideal for imaging. Intravenously injected particles clear from blood with a T ½ of 2.5 min.

Table 3.1.3 Liver, spleen and bone marrow mass in normal subjects and patients with liver disease [10]

Clinical status	Mass of the organ in grams		
	Liver	Spleen	Bone marrow
Normal	1,807	174	1,500
Early to intermediate liver disease	2,400	250	1,500
Intermediate to advanced liver disease	1,400	400	1,500

Normally, about 85% of the injected dose of Tc-99m-S colloid is taken up by the liver, 7% by the spleen, 5% by the bone marrow and the remaining 3% by other organs, such as the lungs, stomach, etc. [11]. In moderate parenchymal liver disease, the radiocolloid uptake by the liver decreases, and the uptake by the spleen and bone marrow increases. In severe parenchymal liver disease (cirrhosis), when the liver shrinks in size, ~30% of the dose is taken up by the liver, and as much as 30% by the spleen, 25% by the red marrow and the remaining 13% of the dose by other organs, including the lungs, kidney and stomach (Table 3.1.5). As most of liver morphology imaging is currently obtained with CT, MRI or ultrasound, radiocolloid imaging is chosen primarily for delineating the functional characteristics of the lesion that have already been detected with one of the other imaging modalities. Radiocolloid spleen imaging is often obtained for accurate measurement of spleen size in the diagnosis of polycythemia rubra vera and other myeloproliferative disorders. Technetium-99m-S colloid preparations are also used in the measurement of gastric emptying time, evaluation of shunt (LeVeen) patency and for the detection of acute GI bleeding, gastro-esophageal reflux or pulmonary aspiration of gastric contents, etc.

The radiocolloid dose is used within 6 h of its preparation, and the particles are shaken vigorously just prior to injection to prevent settlement at the bottom of the vial. As free Tc-99m pertechnetate appears in breast milk, mothers are instructed not to feed their infants with breast milk for the next 24 h and to use formula milk instead. The breast milk expressed prior to radiocolloid injection and stored is preferable to formula milk. The usual pediatric dose is 15–75 μCi kg^{-1} (0.56–2.78 MBq kg^{-1}). For bone marrow imaging in pediatrics, the dose is 30–150 μCi kg^{-1} (1.1–5.6 MBq kg^{-1}). The minimum dose per study is 600 μCi (22.2 MBq). For gastroesophageal reflux and pulmonary aspiration studies, the Tc-99m-S colloid dose is given orally, mixed with a liquid or a semisolid meal.

Table 3.1.4 Characteristics of Tc-99m-S colloid

Parameter	
Half life	6.03 h
Blood clearance T½	2.5 min
Particle size range (μm)	100–1,000
Particle mean size (μm)	300
Decay constant	0.1149 h^{-1}
Mean disintegration	87%
G-rad μci^{-1} h^{-1}	0.0369
Adult dose	2–8 mCi
Dose to liver from a study	0.68–2.72 rads

Table 3.1.5 Relative distribution of Tc-99m-sulfur colloid (% injected dose) in normal subjects and patients with liver disease [11]

	Liver	Spleen	Marrow	Other
Clinical status				
Normal	85	7	5	3
Mild to moderate liver disease	67	13	12	8
Moderate to severe liver disease	32	30	25	13

Mechanism of Radiocolloid Uptake

Metchnikoff in 1884 first observed a process where highly mobile polymorphonuclear leucocytes ingested (phagocytosis) foreign particles, microorganisms and cellular debris, removing them from the circulation. Similar phenomena were observed in the cells lining the liver sinusoids [12]. Kupffer in 1899 described the nature of these cells in the hepatic sinusoids which today bear his name, the Kupffer cells [13]. Aschoff in 1924 introduced the concept of the reticuloendothelial system consisting of the mesenchymal cells distributed throughout the body [14]. Radiocolloid uptake is seen primarily in three organs in the body: the liver, spleen and bone marrow. Lung and other organ uptake normally is not high enough to be seen on the images.

The uptake of radiocolloids by the RE system cells is dependent upon various factors, including particle size, charge, dose, chemical composition and other factors. The maximum phagocytic capacity in humans is 1.07 mg min^{-1} kg^{-1} body weight [15]. The RE system acts as a biological filter by removing effete cells and foreign material from blood and thus restricting the general toxic effect on the body. The filtering mechanism becomes increasingly efficient in the spleen as the particle size increases. The smallest particles are removed preferentially by the bone marrow, medium-size particles by the liver and the largest particles by the spleen. As the Au-198 colloid particles are the smallest (30 μm), most of them are taken up by the liver and bone marrow, and very few particles by the spleen, explaining the reason why the spleen is usually not visualized well in the scans obtained with gold-198.

Upon intravenous injection, radiocolloid particles are coated by plasma opsonins, making them susceptible to phagocytosis. Radiocolloid-opsonin complex attaches to the RE cell membrane and initiates phagocytosis (Fig. 3.1.1). The cytoplasm of the RE cell flows around the opsonized radiocolloid particles as pseudopods, encircles the particle and ultimately incorporates into the cytoplasm, forming a phagosome [16, 17]. The ultimate fate of the radiocolloid in the phagosome depends upon its nature. The phagosome is either

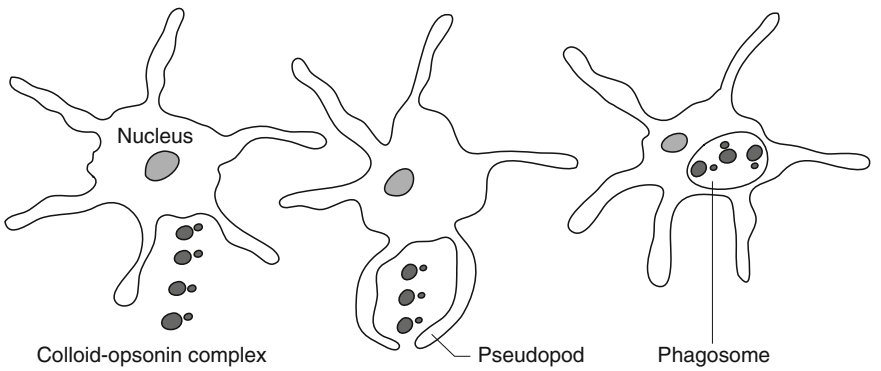

Fig. 3.1.1 Mechanism of radiocolloid uptake. After intravenous injection, radiocolloid comes in contact with plasma proteins forming a radiocolloid-opsonin complex. The complex is encircled by pseudopodes of the Kupffer cells in the liver and reticuloendothelial (RE) cells in the spleen and bone marrow. After complete engulfment, the radiocolloid forms a phagosome within the cytosol

destroyed and the contents stored in the cytosol or the phagosome is destroyed, digested and its contents released back into circulation. Gold-198 radiocolloids are stored intracellularly, whereas the Tc-99m-S colloids are digested and released into the circulation [18].

Dosimetry of Radiocolloids

The liver is the critical organ for radiocolloids and receives 39 rads mCi^{-1} of Au 198 and 0.34 rad mCi^{-1} of technetium-99m-S colloid (Table 3.1.6). From one imaging study, the liver receives 5.8 rads from Au-198 (200 μCi dose) and 0.68 rads from Tc-99m-S colloid (2-mCi dose). Radiation to the liver decreases as the severity of liver disease increases. The total body receives 1.4 rads mCi^{-1} with Au-198 and 0.019 rads mCi^{-1} with Tc-99m-S colloid. Introduction of Tc-99m-sulfur colloid in 1965 was a major breakthrough that revolutionized liver morphology imaging in the late 1970s and through the early 1980s.

Technetium-99m HIDA Agents

Functional imaging nuclear hepatology took a quantum leap with the introduction of Tc-99m-HIDA agents by Loberg et al. in 1976 [6]. Hepatobiliary diseases are quite common, and they often present clinically with dramatic suddenness requiring immediate diagnosis and therapy (acute cholecystitis). Technetium-99m HIDA agents fulfill the requirement for a rapid diagnosis.

Labeling

Technetium-99m-HIDA agents are lidocaine analogues. Lidocaine has been used in clinical practice for many years, and its pharmacokinetics are well understood. Liver is the primary site of uptake and metabolism of lidocaine and indocyanin green [19–21]. Lidocaine ($C_{14}H_{22}N_2O$) has a molecular weight of 270.80 and clears from blood in a biexponential fashion; the fast component has a T½ of 7 min, and the slow component a T ½ of 108 min. Lidocaine shows a high first-pass extraction by the liver. About 90% of

Table 3.1.6 Absorbed dose (rads mCi^{-1}) from Tc-99m-sulfur colloid in normal subjects and patients with liver disease [11]

	Normal	Moderate disease	Severe disease
Organ			
Liver	0.34	0.21	0.16
Spleen	0.21	0.28	0.42
Red marrow	0.02	0.04	0.07
Ovaries	0.005	0.008	0.012
Testes	0.001	0.002	0.003
Total body	0.019	0.019	0.019

extracted lidocaine is metabolized into monoethylglycylxylidine, and the remaining 10% is excreted in urine unchanged. Age does not affect the biokinetic behavior of lidocaine.

Based upon its wide clinical application in cardiology and with the knowledge that lidocaine is metabolized primarily in the liver, it was hypothesized that a technetium-99m-labeled lidocaine or its analogues could find potential imaging application in either cardiology or hepatology. Since technetium-99m could not be attached to lidocaine directly, iminodiacetic acid (IDA) was chosen as a bifunctional chelate to carry the ligand (lidocaine) at one end and the radiotracer (Tc-99m) at the other end [6]. Each molecule of labeled Tc-99m-HIDA complex, therefore, consists of two molecules each of the ligand and the chelate and an atom of technetium-99m in the middle (Fig. 3.1.2). When Tc-99m-HIDA was injected into mice and gamma camera imaging began, the investigators were startled not to find any myocardial uptake, but were immensely pleased to see radioactivity first in the hepatocytes and later throughout the biliary system [22]. For lack of any other better terminology, the investigators settled on a new name, Hepatic IminoDiacetic Acid, or HIDA. Thus, the major portion of the name (HIDA) reflects the chelate (IDA) more than it does the ligand (lidocaine), which provides the most critical functional information.

Radiolabeling with technetium-99m does not affect the blood clearance or the hepatic uptake of lidocaine, but it alters the intrahepatic transit. Unlike lidocaine, Tc-99m-HIDA is not metabolized during its transit through the hepatocyte. It is secreted as native Tc-99m-HIDA into the bile canaliculi. This feature is readily demonstrated by re-injection of radiolabeled gallbladder bile intravenously into the same animal where the exact kinetics of the original injection are reproduced. Lidocaine forms a dimer with technetium-99m, which increases the molecular weight from 270.8 for lidocaine to 833 for Tc-99m-HIDA complex (Fig. 3.1.2). Increase in molecular weight enhances hepatocyte uptake and excretion. Labeling with technetium-99m imparts hepatic specificity. Lidocaine labeled with C14 or Tin (Sn)-113m, however, does not show hepatic uptake and excretion; instead, it is excreted mostly through urine [6].

Structure-Function Relationship

The basic configuration of all Tc-99m-HIDA agents is very similar (Fig. 3.1.3). The bifunctional chelate, IDA, attaches to a molecule of lidocaine at one end and to an atom of technetium-99m at the other. Technetium-99m is the radiotracer, and the biological function resides with lidocaine. The biokinetic behavior of the labeled complex can be altered by making substitutions in the benzene ring at positions 2,4,6 (ortho), 4 (para) or 5 (meta) with a methyl, ethyl, isopropyl or isobutyl group. A halogen is attached in the meta position (mebrofenin). More than 30 new compounds were created by making various substitutions at different positions [23, 24, 25]. Six of the compounds have undergone critical clinical trials, and three have been approved for routine use by the United State's Food and Drug Administration.

Hepatic uptake of Tc-99m-HIDA agents varies from a low of 82.5–98.1% [26]. Hepatic uptake of Tc-99m-disofenin is 89% and mebrofenin 98% (Table 3.1.7). The uptake and excretion of Tc-99m-HIDA agents are dependent upon various factors, of which molecular

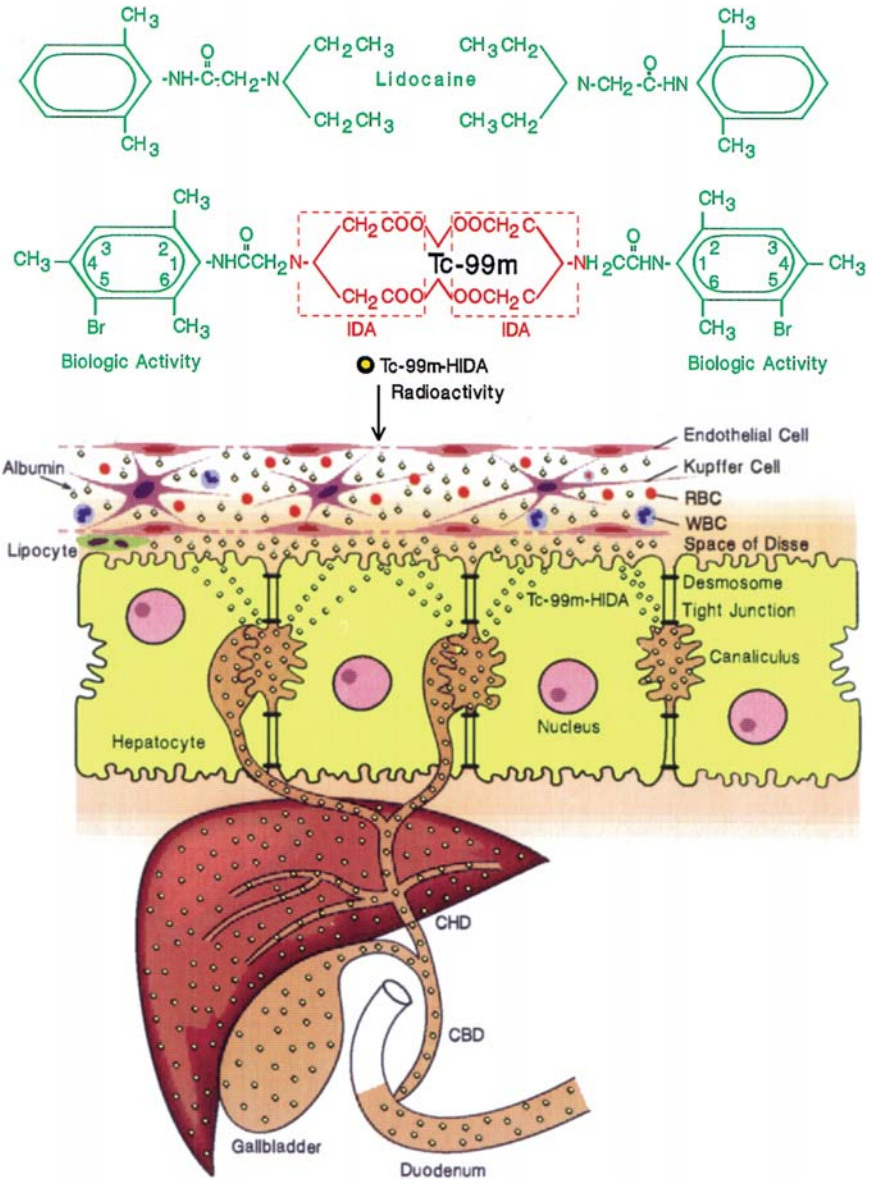

Fig. 3.1.2 Molecular structure and hepatobiliary transit of Tc-99m-HIDA. Lidocaine (*green*) is the ligand with the biologic function, technetium-99m (*black*) is the radiotracer, and iminodiacetic acid (IDA) is the chelate (*red*) that binds them together. A labeled whole complex consists of an atom of Tc-99m, two molecules of lidocaine and two molecules of IDA. Albumin delivers the radiotracer to the space of Disse where the dissociation takes place. Tc-99m HIDA is taken up by the hepatocyte and secreted into bile canaliculi in free form where it mixes with the hepatic bile and serves as an ideal in vivo tracer for imaging of the entire hepatobiliary tree [27]

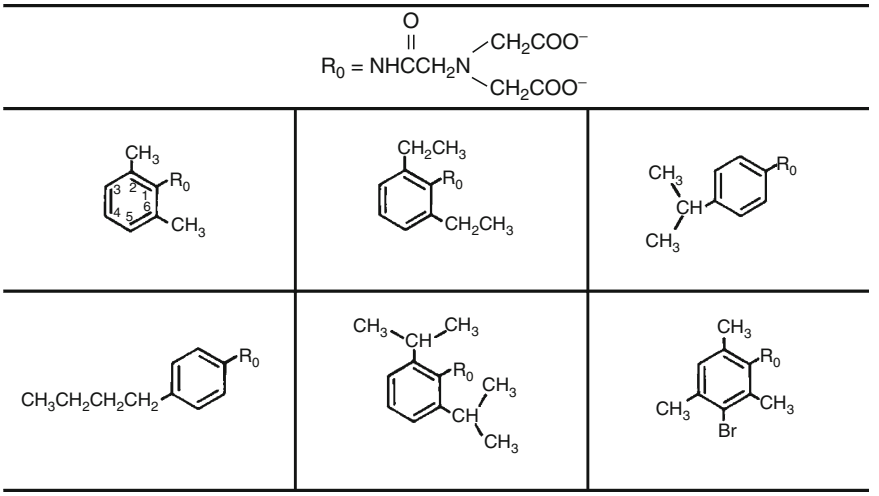

Fig. 3.1.3 Molecular configuration of six Tc-99m HIDA agents. Biological function is altered (varying liver $T_{1/2}$) by making different chemical substitutions at positions 2,4,6 of the benzene ring. Mebrofenin (*TMB*) has a bromine at position 5, which makes it highly resistant to displacement by bilirubin [26]

Table 3.1.7 Biokinetic features of Tc-99m mebrofenin and Tc-99m disofenin

Agent	Liver uptake (% dose)	Urine excretion (% dose)	Liver excretion (T½, min)	Radiation (mrad) to	
				Liver	Gallbladder
Tc-99m-Mebrofenin (Choletec)	98	2.	17	70	410
Tc-99m-Disofenin (Hepatolite)	89	11	19	75	370

structure, weight, lipid solubility and protein binding are important parameters. Radiolabeled complexes with a molecular weight between 300 and 1,000 are preferentially taken up by the hepatocytes and rapidly secreted into bile. An isopropyl substitution at 2 and 6 positions (disofenin) makes it a better agent than a dimethyl or diethyl substitution at the same locations, or an isopropyl substitution at the para position (PIPIDA). A methyl substitution at positions 2, 4, and 6 and a bromine atom at 5 (mebrofenin) result in creating the best agent of all. Tc-99m-mebrofenin shows the highest liver uptake (98%) and strongly resists displacement by a high bilirubin level. Both agents are secreted from the liver rapidly into bile with a mean excretion half time of 17 min with mebrofenin and 19 min with disofenin. The dose not taken up by the liver is excreted through the kidneys. Urinary excretion of mebrofenin is 2% and disofenin 11% of the dose injected.

3

Biokinetics of Tc-99m-HIDA Agents

Biokinetic behavior of Tc-99m-HIDA agents can be divided into six functional phases: (1) blood transport, (2) uptake by the hepatocyte, (3) transit through the hepatocyte and secretion into bile canaliculi, (4) flow through the intrahepatic and extrahepatic ducts, (5) entry into the gallbladder and (6) final discharge into the small intestine [26, 27]. The dose not taken up by the liver is excreted in urine.

Blood Transport

Tc-99m-HIDA agents are transported in blood bound to serum albumin, forming an albumin-Tc-99-HIDA complex [26]. Protein binding enhances hepatic delivery and hepatocyte uptake and decreases renal excretion. The agents clear from the blood at variable rates (Fig. 3.1.4). Hypoalbuminemia decreases hepatic delivery and increases renal excretion. The affinity of Tc-99m-HIDA to bind with albumin is much lower than that of bromsulfalein and bilirubin [28]. A substitution at the para position improves both albumin binding and lipid solubility. Methyl substitution at positions 2, 4 and 6 and a bromine at position 5 (mebrofenin) increase both hepatic delivery and hepatocyte uptake, and markedly reduce renal excretion. A butyl substitution at the para position has a similar effect on the uptake [25]. Albumin-bound Tc-99m-HIDA leaves the sinusoidal space through the fenestrae of the endothelial cells and enters the perisinusoidal space of Disse, a space unique for liver

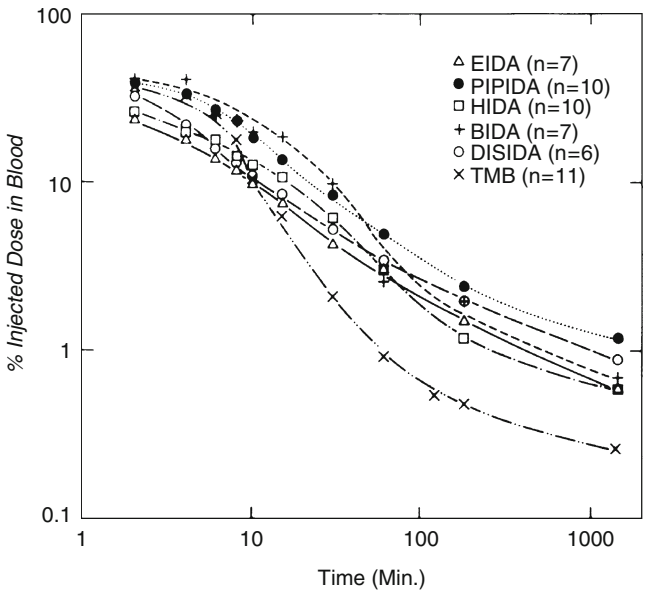

Fig. 3.1.4 Blood clearance of six Tc-99m HIDA agents. Note the fastest blood clearance with mebrofenin, TMB [26]

capillaries. Disassociation between albumin-Tc-99m-HIDA takes place in the space of Disse very close to the basolateral border of the hepatocyte (Fig. 3.1.2). Only Tc-99m-HIDA enters the hepatocyte, leaving albumin behind in the blood. This mechanism is common for most organic anions [28].

Hepatocyte Uptake

The mechanism of uptake of Tc-99m-HIDA by the hepatocyte is similar to those of other organic anions [30]. Liver concentrates three types of organic anions, including bile acids, free fatty acids and non-bile acid cholephils (bromsulfalein, bilirubin, rose bengal, indocyanin green and Tc-99m-HIDA). Non-bile acid cholephils are taken up by the hepatocyte by a mechanism called receptor-mediated endocytosis (RME). RME has been well documented for low density lipoprotein, IgA, insulin, transferrin, asiologlycoprotein and cholesterol [31]. It is believed that Tc-99m-HIDA compounds follow the RME pathway, followed by bilirubin and other organic anions. By subjecting cultured rat hepatocytes to different in vitro experimental conditions, Okuda et al. and Lan et al. have demonstrated three possible pathways for uptake of Tc-99m-HIDA: (1) organic anion pathway probably through RME, (2) bile acid (bile salt) pathway and (3) free fatty acid pathway [28, 32, 33].

Receptor-Mediated Endocytosis

After dissociation from albumin in the space of Disse, Tc-99m-HIDA attaches to its specific receptors through receptor protein (ligandin). These receptors are located along the basolateral border and along the walls of the coated pits, which are mere invaginations of the basolateral membrane into hepatocyte cytosol [31, 34]. The ligand (Tc-99-HIDA) and the receptor protein (ligandin) cluster in the coated pit (Fig. 3.1.5). This collection is one of the primary requirements for RME to progress [34]. After separation from the surface membrane the coated pit forms a coated vesicle, and Tc-99m-HIDA gets internalized within the hepatocyte. After losing the protein covering, the vesicle becomes an endosome. In the case of LDL, IgA, insulin and transferrin, the protein coating the vesicle is clathrin. Co-transport through bile acids and free fatty acids occurs simultaneously with RME.

Despite sharing a common mechanism of uptake, there are a few differences in hepatocyte uptake between Tc-99m-mebrofenin and Tc-99m disofenin. In cultured rat hepatocytes, bilirubin reduces the uptake of disofenin much more profoundly than that of mebrofenin. At 20 μM bilirubin in the culture medium, the hepatocyte uptake of Tc-99m disofenin reduces to 34% from a basal value of 100% without bilirubin in the culture medium. In contrast, the uptake Tc-99m mebrofenin remains at 70% of the basal value under identical experimental conditions. Both disofenin and mebrofenin show a reduction in hepatocyte uptake when bile acids or free fatty acids are added to the culture medium, suggesting the existence of other uptake pathways. These results indicate that Tc-99m-HIDA agents share a common pathway with organic anions (bilirubin), free fatty acid and bile acids. Bromsulfalein (BSP) inhibits uptake by the hepatocyte of Tc-99m disofenin much more profoundly than Tc-99m mebrofenin (Table 3.1.8).

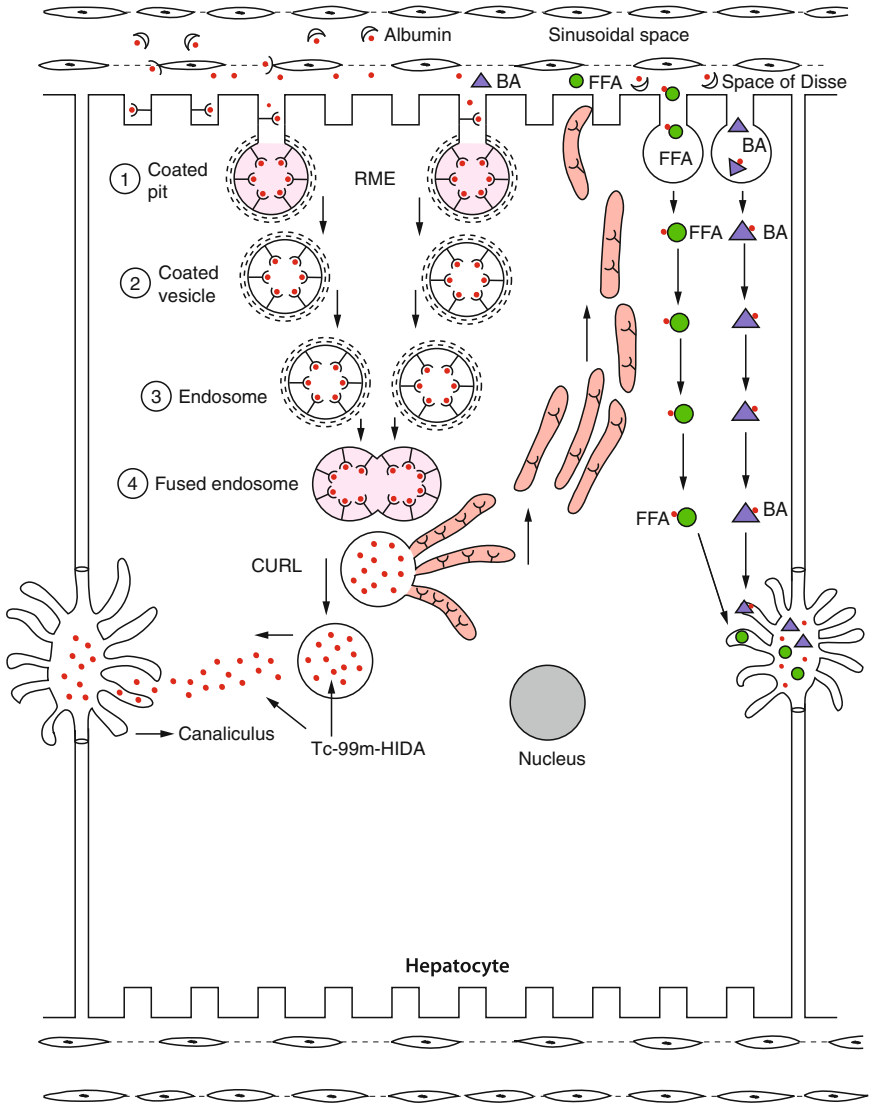

Fig. 3.1.5 Schematic representation of receptor-mediated endocytosis for uptake and excretion of Tc-99m HIDA by the hepatocyte. Primary uptake occurs via receptor-mediated endocytosis (*RME*). After detaching from albumin in the space of Disse, the radiotracer attaches to the ligand in receptors within the coated pits [1], which are invaginations of the basolateral border of the hepatocyte. A coated vesicle [2] is formed when it separates from the surface membrane. The coated vesicle rapidly loses its clathrin coat, forming an endosome [3]. Two endosomes combine together to form a fused endosome [4]. Hydrogen is pumped into the fused intra-vesicular space, initiating uncoupling of the receptor and ligand (*CURL*). Ligand enters the bile canaliculi, and the receptor moves to the surface for recycling. Tc-99m HIDA in addition uses free fatty acid (*FFA*) and bile acid (*BA*) pathways for uptake and excretion in free form into bile canaliculi (modified from Steer [31])

Table 3.1.8 Effect of 20μM of various organic anions on the uptake (%) of Tc-99m disofenin and Tc-99 mebrofenin by cultured rat hepatocytes [32]

Agent	Basal uptake	BSP	Bili	Tauro cholate	Glyco cholate	Cholate	Deoxy cholate	Chenodeoxy cholate
Tc-99m-Disofenin	100	59	34	61	59	66	42	42
Tc-99m-Mebrofenin	100	107	70	69	85	80	62	71

Transit Through the Hepatocyte and Secretion into Bile Canaliculi

Unlike bilirubin and other organic anions, Tc-99m-HIDA agents are secreted into bile canaliculi in their native state, without undergoing any conjugation during their transit through the hepatocyte [6]. The mechanisms by which Tc-99m-HIDA is transported through the hepatocyte and then secreted into the bile canalicular lumen are not clear. The general belief is that the mechanism is similar to those of non-cholephil organic anions, free fatty acids and bile acids. Vesicular transport and receptor-ligandin transport are thought to be involved. After losing the clathrin coat, the vesicle forms an endosome. Two endosomes together form a fused endosome. At this point the ligand (Tc-99m-HIDA) and the receptor (ligandin) separate and start moving in two different directions. The ligand (Tc-99m-HIDA) enters the bile canaliculi, and the ligandin moves to the hepatocyte surface for recycling [35]. Rough endoplasmic reticulum and the Golgi complex are known to synthesize the receptor. After entering the canaliculi, Tc-99m-HIDA mixes thoroughly with the hepatic bile, and from then on it serves as an ideal in vivo tracer for delineation of the entire hepatobiliary tree (Fig. 3.1.2). The curves generated over the liver provide a measure of the rapidity of uptake and excretion of Tc-99m HIDA (Fig. 3.1.6). The dose not taken up by the liver is excreted through urine (Fig. 3.1.7).

Currently, Tc-99m-disofenin and Tc-99m-mebrofenin are the most popular agents (Fig. 3.1.8). Tc-99m mebrofenin, which has bromine at position 5 (meta), clears from the liver much more rapidly than Tc-99m disofenin (Fig. 3.1.9).

Flow Through Intrahepatic and Extrahepatic Ducts

The hepatic bile is radiolabeled instantly, as soon as Tc-99m-HIDA secreted by the hepatocyte enters the bile canaliculi. In vivo bile radiolabeling under total basal conditions allows delineation of the entire intrahepatic and extrahepatic bile ducts. Of the 600 ml total bile produced per day, 450 ml is secreted by the hepatocytes and 150 ml by canalicular cells [36]. The bile within the ducts is radiolabeled as the hepatic bile passes through the ducts.

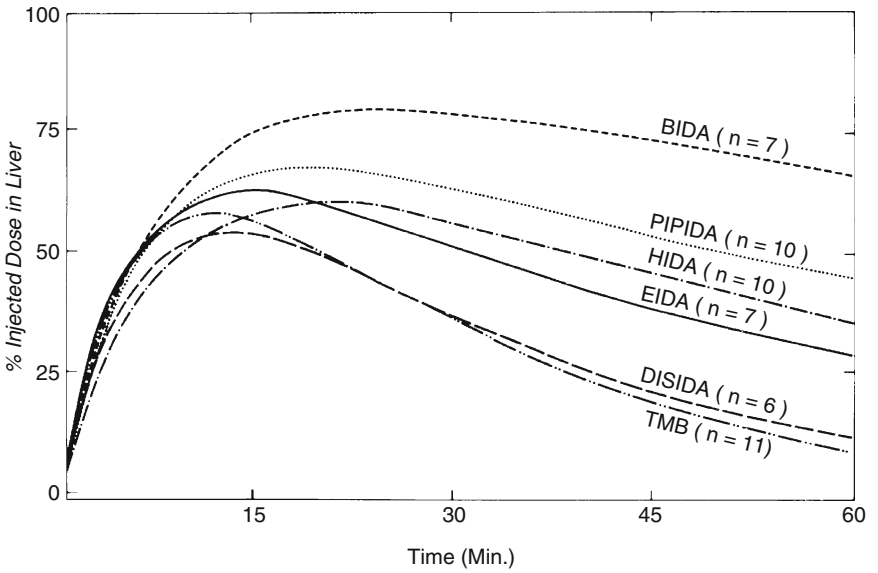

Fig. 3.1.6 Hepatic uptake and excretion of six Tc-99m HIDA agents. Fastest uptake and excretion are noted with disofenin (*DISIDA*) and mebrofenin (TMB)

Gallbladder Storage

About 70% of the hepatic bile secreted during fasting hours enters the gallbladder (0.3 ml min^{-1}), and the rest enters the duodenum directly [37]. A fully filled normal gallbladder can accommodate up to 50 ml of bile. It would, therefore, take approximately 180 min (6 h) for a completely emptied gallbladder to refill to its full capacity. Having the ability to accommodate a constant inflow of 0.3 ml bile min^{-1}, the hepatic bile during fasting is made possible by absorption of an equal volume of water through the gallbladder wall (about 0.3 ml min^{-1}). The gallbladder wall absorbs water, chloride and bicarbonates at a much faster rate than sodium, bile salts and cholesterol from hepatic bile. By this selective absorption, the gallbladder can sequester all of the total body bile salts within it during 10–12 h of fasting. This selective process of solute concentration is called the concentration function of the gallbladder.

Highly concentrated gallbladder bile is discharged into the duodenum upon the arrival of food into the small intestine, where bile salts facilitate digestion and absorption of nutrients into the blood stream. There is a rapid rise in Tc-99m-HIDA counts when radiolabeled hepatic bile enters the gallbladder. Accumulation of a very high specific activity bile in a relatively small volume (50 ml) accounts for the gallbladder being the critical organ in a Tc-99m-HIDA study [38], receiving about 908 mrad mCi^{-1}. The upper large intestine, lower large intestine and small intestine receive decreasing doses (Table 3.1.9). Radiation to the gastrointestinal tract decreases in liver failure when kidneys become the preferential route of excretion for Tc-99m-HIDA.

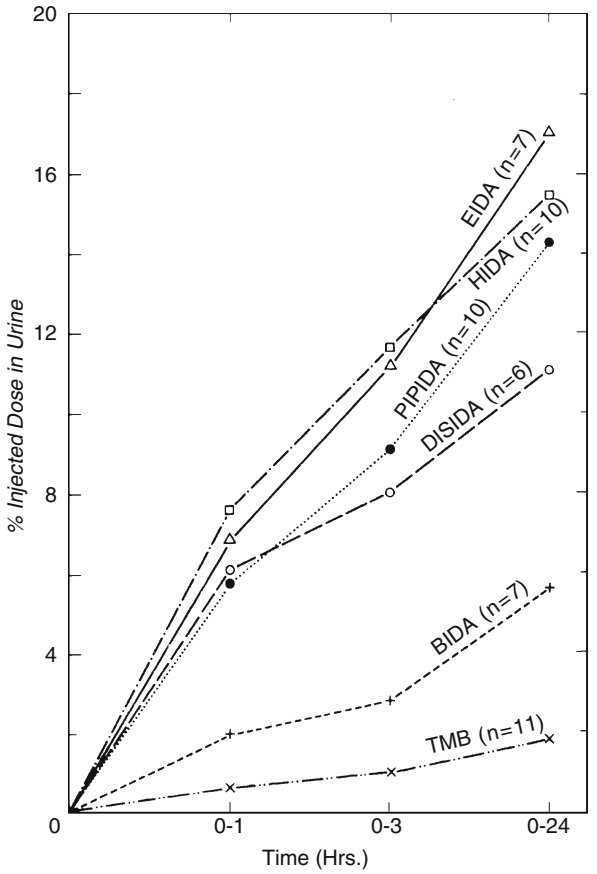

Fig. 3.1.7 Urinary excretion of six Tc-99m HIDA agents. Less than 2% of the injected dose of mebrofenin (*TMB*) is excreted in 24-h urine. Other agents show an increasing amount of urinary excretion [26]

Final Discharge into the Duodenum

When the food leaves the stomach and enters the duodenum, it stimulates CCK-secreting cells in the mucosa of the duodenum and jejunum to release endogenous cholecystokinin into the circulation. It usually takes about 6–26 min (mean 16 min) after a meal for serum CCK levels to rise above the threshold to induce contraction and emptying of the gallbladder [39]. Once the gallbladder contraction is initiated, bile emptying is maintained for 1–2 h post-meal. In addition to initiating gallbladder contraction and emptying, cholecystokinin stimulates water secretion by cholangiocytes lining the bile ducts and hastens bile flow by directly stimulating smooth muscle of the bile ducts [40]. Cholecystokinin also increases intestinal peristalsis and facilitates movement of bile emptied from the gallbladder antegrade towards the jejunum and ileum. By inducing contraction of the pylorus of the stomach, it prevents duodeno-gastric bile reflux.

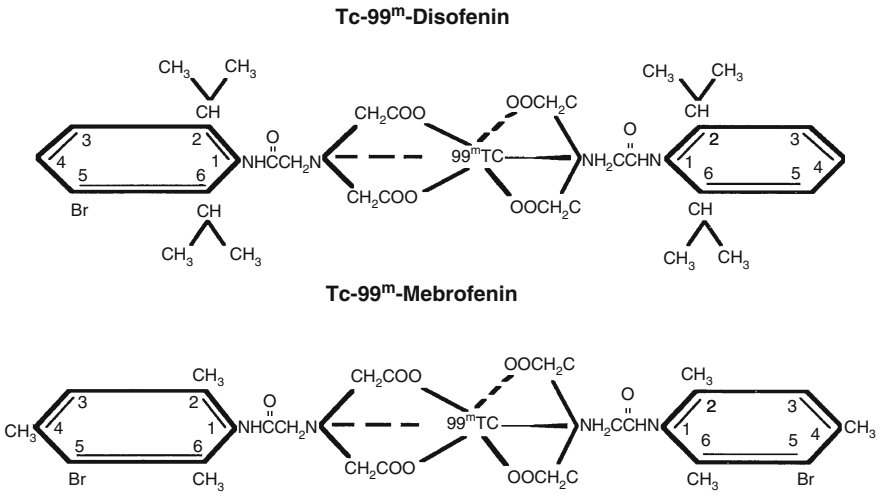

Fig. 3.1.8 Molecular structure of Tc-99m-disofenin and Tc-99m-mebrofenin. An atom of bromine at 5 and three methyl groups at 2, 4, 6 positions in mebrofenin change its biological behavior from that of disofenin with an isopropyl group at 2 and 6 positions

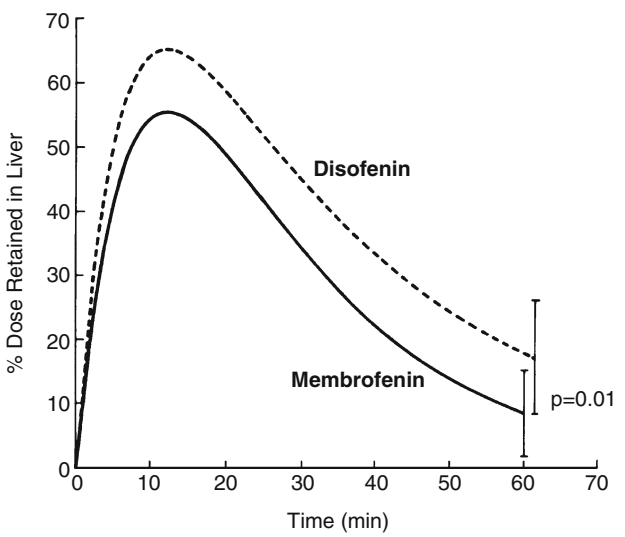

Fig. 3.1.9 Hepatic uptake and excretion of Tc-99m disofenin and Tc-99m mebrofenin. The uptake and excretion by the liver of Tc-99m mebrofenin are significantly faster when compared to Tc-99m disofenin

Table 3.1.9 Radiation-absorbed dose (mrad mCi^{-1}) to various organs from Tc-99m-HIDA in normal subjects and patients with increasing severity of liver disease [38]

Bilirubin level	Normal	Patients with increasing serum bilirubin level			
	<1 mg dl^{-1}	< 1 mg dl^{-1}	1-5 mg dl^{-1}	5-10 mg dl^{-1}	>10 mg dl^{-1}
Organ					
Gallbladder	908	728	617	309	101
Upper colon	302	235	198	100	36
Lower colon	199	154	131	68	27
Small intestine	189	147	125	65	25
Liver	76	91	90	47	18
Ovaries	62	50	43	25	13
Kidneys	43	58	67	105	132
U. Bladder	35	46	53	87	111
Bone marrow	24	21	19	13	9
Spleen	9	8	7	5	3
Testes	4	4	4	4	5
Total body	16	15	14	9	6

Other Tc-99m-Labeled Hepatobiliary Agents

Many Tc-99m-labeled potential hepatobiliary agents have not been approved by the United States Food and Drug Administration for routine clinical use. Some are approved in other countries. These agents include Tc-99m-labeled penicillamine [41, 42], dihydrothiooctic acid [43], tetracycline [44] and pyridoxylidineglutamate [45]. Tc-99m-Pyridoxylidineglutamate has been used extensively in Australia, Japan and other Asian countries [46]. Some of the agents used for imaging of other organs pass through the liver and are secreted into bile, and often they provide information about the hepatobiliary function (Fig. 3.1.10). The myocardial perfusion imaging agent, Tc-99m-sestamibi, is taken up by hepatocytes and secreted into bile, and it provides an opportunity to measure the gallbladder ejection fraction with cholecystokinin in those rare patients where acalculous chronic cholecystitis (cystic duct syndrome) mimics an anginal type of pain.

Technetium-99m-DTPA Galactosyl-Human Serum Albumin

The basolateral and lateral (not canalicular) border of the plasma membrane of the hepatocyte is rich in asialoglycoprotein (ASGP) receptors, which serve as a binding site for Tc-99m DTPA-galactosyl human serum albumin (Tc-99m GSA). These receptors specific for the hepatocytes are not found in any other cells in the body [31]. After an intravenous injection, Tc-99m GSA circulates in the blood, is extracted by the hepatocyte plasma membrane and is transferred to the lysosomes through receptor-mediated endocytosis. Blood disappearance parallels the clearance of indocyanin green, considered a gold

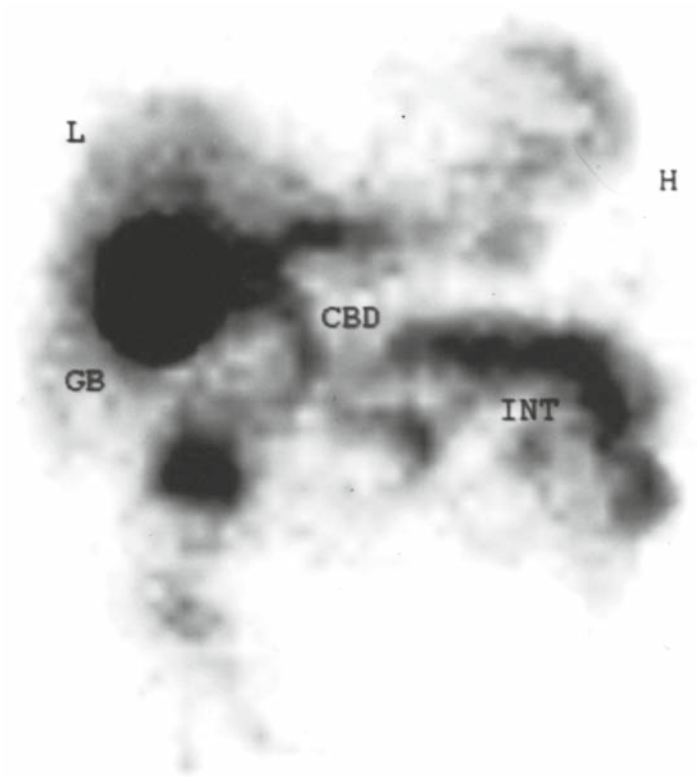

Fig. 3.1.10 Secretion of technetium-99m sestamibi into bile. Myocardial (*H*) perfusion imaging agent shows accumulation in the liver (*L*), bile ducts and gallbladder (*GB*). *CBD* common bile duct, *INT* intestine

standard agent for hepatocyte function [47]. Studies in Japan have shown a great potential for the measurement of the hepatic reserve prior to resection of the liver in patients with hepatocellular carcinoma, cholangiocarcinoma, cirrhosis and metastatic disease. Rapid sequence SPECT imaging allows quantitative measurement of functional reserve and enables prediction of prognosis [48–50].

New SI Units for Measurement of Radiation

The International Commission on Radiation Units and Measurements recommended in 1974 that new SI (system international) units replace old CGS units for all scientific work after 1984. The old and new units of measurement and their relationship are shown in Tables 3.1.10–3.1.12 [51].

Table 3.1.10 Old CGS and new SI units for measurement of radioactivity [51]

Old units curie	New SI units. Becquerel	Disintegrations per second (dps)
Megacurie (MCi)	37 PBq	3.7×10^{16}
Kilocurie (KCi)	37 TBq	3.7×10^{13}
Curie (Ci)	37 GBq	3.7×10^{10}
Millicurie (mCi)	37 MBq	3.7×10^{7}
Microcurie (μCi)	37 kBq	3.7×10^{4}
Nanocurie (nCi)	37 Bq	3.7×10
Picocurie (pCi)	37 mBq	3.7×10^{-2}

Table 3.1.11 Relationship between new Becquerel and old Curie units [51]

1 Becquerel (Bq) = 1 dis sec^{-1} = 27.03×10^{-12} Ci = 27.03 pCi
1 Kilobecquerel (kbq) = 10^3 Bq = 27.03 nCi
1 Megabecquerel (MBq) = 10^6 Bq = 27.03 μCi
1 Gigabecquerel (GBq) = 10^9 Bq = 27.03 mCi

Table 3.1.12 Relationship between old and new SI units for measurement of radiation [51]

Parameter	Old unit	New SI unit	Conversion factor
Radioactivity	Curie (Ci) = 3.7×10^{10} dps	Becquerel (Bq) = 1 dps	1 Ci = 3.7×10^{10} Bq 1 Bq = 2.7×10^{-11} Ci
Radiation exposure	Roentgen (R) = 2.58×10^{-4} C kg^{-1}	Coulomb kg^{-1} C kg^{-1}	1 R = 2.58×10^{-4} C kg^{-1} 1C kg^{-1} = 3.88×10^3 R
Radiation absorbed dose	rad = 100 erg g^{-1}	Gray(Gy) = 1 J kg^{-1}	1 rad = 0.01 Gy 1 Gy = 100 rad
Radiation dose equivalent	rem = QF × rad	Sievert (Sv) = QF × Gy	1 rem = 0.01 Sv 1 Sv = 100 rem

References

1. Sheppard CW, Wells EB, Hahn PF, Goodell JBP. Studies of the distribution of intravenously administered colloidal sol of manganese dioxide and gold in human beings and dogs using radioactive isotopes. J Lab Clin Med 1947;32:274–277
2. Stirret LA, Yuhl ET, Cassen B. Clinical application of hepatic radioactive surveys. Am J Gastroenterol 1954;21:310–317
3. Stirret LA, Yuhl ET, Libby RL. A new technique for diagnosis of carcinoma metastatic to the liver. Surg Gynecol Obstet 1953;96:210–215
4. Taplin GV, Meredith OM Jr, Kade H. Radioactive (I-131 tagged) rose bengal uptake–excretion test for liver function using external gamma ray scintillation counting technique. J Lab Clin Med 1955;45:665–678
5. Harper PV, Lathrop KA, Jimiriez F, Fink R, Gottschalk A. Technetium-99m as a scanning agent. Radiology 1965;85:101–103

6. Loberg MD, Cooper M, Harvey E, Callery P, Faith W. Development of new radiopharmaceuticals based on N-substitution of iminodiacetic acid. J Nucl Med 1976;17:633–638
7. McAfee JG, Subramanian G. Radioactive agents for imaging. In: Freeman LM, Johnson PM (eds) Clinical radionuclide imaging. Grune and Stratton Inc, Orlando, 1984, vol. 1
8. Iya VK, Gopal GS, Chaudhuri SY. Colloidal gold. Preparation and particle size determination by electron microscope. Indian J Chem 1965;3:317–320
9. Dobson EL, Jones HB. The behavior of intravenously injected particulate material; its rate of disappearance from blood as a measure of liver blood flow. Acta Med Scand 1952;273:1–50 (suppl 144)
10. Cloutier RJ, Freeman LM, McAfee JG, McCormick KR, Patton DD, Rosenthal L, Smith EM. MIRD: Dose estimates report number 4. Summary of current radiation dose estimates to humans with various liver conditions from Au-198 colloidal gold. J Nucl Med 1975;16:173–174
11. Atkins HL, Cloutier RJ, Lathrop KA, Freeman LM, McAfee JG, Nelp WB, Patton DD, Smith EM. MIRD: Dose estimates report number 3. Summary of current radiation dose estimates to humans with various liver conditions from Tc-99m sulfur colloid. J Nucl Med 1975;16:108A–108B
12. Metchnikoff E. In Immunite dans les maladies infectieuses. Masson, Paris, 1901
13. von Kupffer C. Uberdie sogenanuten sternzellen der saugentheirer leber. Arch Microsk Anat 1899;26:1
14. Ashoff I. Das reticulo-endotheliale system. Ergebn Inn Med Kinderheilk 1924;26:1
15. Iio M, Wagner HN Jr, Scheffel U, Jabbour B. Studies of the reticulo-endothelial system (RES) 1. Measurement of the phagocytic capacity of the RES in man and dog. J Clin Invest 1963;42:417–416
16. Saba TM. Physiology and physiopathology of the reticuloendothelial system. Arch Intern Med 1970;126:1031–1052
17. Stossel TP. How do phagocytes eat?. Ann Intern Med 1978;89:398–402
18. Kitani K, Taplin GV. Biliary excretion of 99m Tc- albumin microaggregate degradation products (a method for measuring Kupffer cell digestive function)?. J Nucl Med 1972;13:260–265
19. Beckett AH, Boyes RN, Appleton PJ. The metabolism and excretion of lignocaine in man. J Pharm Pharmacol 1966;18:76–81 (suppl)
20. Rowland M, Thomson PD, Guichard A, Melmon KL. Disposition kinetics of lidocaine in normal subjects. Ann N Y Acad Sci 1971;179:383–398
21. Zito RA, Reid PR. Lidocaine kinetics predicted by indocyanin green clearance. New Engl J Med 1978;298:1160–1163
22. Ryan J, Cooper M, Loberg MD, et al. Technetium 99m labeled N-(2,6 dimethylphenyl carbomoylmethyl) iminodiacetic acid(Tc-99m-HIDA). A new radiopharmaceutical for hepatobiliary imaging studies. J Nucl Med 1977;18:997–1004
23. Nunn AD, Loberg MD, Conley RA. A structure-distribution-relationship approach leading to the development of Tc-99m mebrofenin: an improved cholescintigraphic agent. J Nucl Med 1983;24:423–430
24. Wistow BW, Subramanian G, Van Heertum RL, Henderson RW, Gagne GM, Hall RC, McAfee JG. An evaluation of Tc-99m labeled hepatobiliary agents. J Nucl Med 1977;18:455–461
25. Subramanian G, McAfee JG, Henderson R, et al. A new bifunctional chelate for designing Tc-99m labeled radiopharmaceuticals. In: Murry IP, Hoschl R (eds). Proceedings of first Asia and Oceania congress of nuclear medicine, 1976. Sidney, Australia. Pink Panther Printers, pp 144–149
26. Krishnamurthy S, Krishnamurthy GT. Technetium-99m iminodiacetic acid organic anions: review of biokinetics and clinical application in hepatology. Hepatology 1989;9:139–153
27. Krishnamurthy S, Krishnamurthy GT. Evolution of nuclear hepatology as a clinical subspeciality. J Nucl Med Technol 1995;23:35S–45S (suppl)
28. Okada H, Nunes R, Vallabhajosula S, Strashun A, Goldsmith SJ, Berk PD. Studies of the hepatocellular uptake of the hepatobiliary scintiscanning agent Tc-99m-DISIDA. J Hepatol 1986;3:251–259

29. Berk PD, Stremmel W. Hepatocellular uptake of organic anions. In: H Popper, Schaffner F (eds) Progress in liver disease. Grune and Stratton, New York, 1988, pp 125–143, vol. 3
30. Chervu LR, Nunn AD, Loberg MD. Radiopharmaceuticals for hepatobiliary imaging. Semin Nucl Med 1982;12:5–17
31. Streer CJ. Receptor-mediated endocytosis: mechanisms, biologic function and molecular properties. In: Zakim D, Boyer TD (eds) Hepatology, a text book of liver disease. WB Saunders, Philadelphia, 1996, pp 149–214
32. Lan JA, Chervu LR, Johansen KL, Wolkoff AW. Uptake of Technetium-99m Hepatobiliary agents by cultured rat hepatocyte. Gastroenterology 1988;95:1625–1631
33. Roy-Chowdhury J, Jansen PLM. Bilirubin metabolism and its disorders. In: Zakim D, Boyer TD (eds) Hepatology, a text book of liver disease. WB Saunders, Philadelphia, 1996, pp 323–361
34. Goldstein JL, Anderson RG, Brown MS. Coated pits, coated vesicles, and receptor-mediated endocytosis. Nature 1979;279:679–685
35. Pearse BM, Bretscher MS. Membrane recycling by coated vesicles. Ann Rev Biochem 1981;50:85–101
36. Sherlock S, Dooley J. Cholestasis. In: Sherlock S, Dooley J (eds) Diseases of the liver and biliary system. Blackwell Scientific Publication, Boston, 1993, pp 214–235
37. Krishnamurthy GT, Bobba VR, McConnell D, Turner F, Mesgardeh M, Kingston E. Quantitative biliary dynamics: introduction of a new non-invasive scintigraphic technique. J Nucl Med 1983;24:217–223
38. Brown PH, Krishnamurthy GT, Bobba VR, Kingston E. Radiation dose calculation for Tc-99m-HIDA in health and disease. J Nucl Med 1981;22:177–183
39. Bobba VR, Krishnamurthy GT, Kingston E, Turner FE, Brown PH, Langrell K. Gallbladder dynamics induced by a fatty meal in normal subjects and patients with gallstones: concise communication. J Nucl Med 1984;25:21–24
40. Mutt V. Cholecystokinin: isolation, structure, and function. In: Jerzy Glass GB (ed) Gastrointestinal hormones. Raven Press, New York, 1980, pp 169–221
41. Krishnamurthy GT, Tubis M, Endow JS, Blahd WH. Technetium-99m-penicillamine. A new agent for cholescintigraphy. J Nucl Med 1972;13:418 (abstract)
42. Tubis M, Krishnamurthy GT, Endow JS, Blahd WH. 99m Tc-penicillamine, a new cholescintigraphic agent. Comparison with oral cholecystography. J Nucl Med 1972;13:652–654
43. Tonkin AK, DeLand FH. Tc-99m-Dihydrothioctic acid. A new polygonal cell imaging agent. J Nucl Med 1974;15:539
44. Fliegel CP, Dewanjee MK, Holman LB, Davis MA, Treves S. 99mTc-Tetracycline as a kidney and gallbladder imaging agent. Radiology 1974;110:407–412
45. Baker RJ, Bellen JC, Ronai PM. Tc-99m-pyridoxylidineglutamate: a new hepatobiliary radiopharmaceutical. 1. Experimental aspects. J Nucl Med 1975;16:720–727
46. Ronai PM, Baker RJ, Bellen JC, Collins PJ, Lander H. Technetium-99m-pyridoxylidineglutamate: a new hepatobiliary radiopharmaceutical. ll. Clinical aspects. J Nucl Med 1975;16:728–737
47. Hwang E, Taki J, Shuke N, Nakajima K, Kinuya S, Konishi S, Michigishi T, Aburano T, Tonami N. Preoperative assessment of residual hepatic functional reserve using Tc-99m-DTPA-galactosyl human serum albumin dynamic SPECT. 1999;40:1644–1651
48. Sasaki N, Shiomi S, Iwata Y, Nishiguchi S, Kuroki T, Kawabe J, Ochi H. Clinical usefulness of scintigraphy with Tc-99m-galactosyl human serum albumin for prognosis of cirrhosis of the liver 1999;40:1652–1656
49. Uetake M, Koizumi K, Yagawa A, Nogata H, Tezuka T, Kono H, Ozawa T, Kusano T, Miyabukuro M, Hosaka M. Use of Tc-99m DTPA galactosyl human serum albumin to predict postoperative residual liver function. Clin Nucl Med 1999;24:428–434
50. Akaki S, Mitsumori A, Kanazawa S, Togami I, Takeda Y, Hiraki Y. Lobar decrease in 99m-Tc-GSA accumulation in hilar cholangiocarcinoma. J Nucl Med 1999;40:394–398
51. Brown PH. Mathematics and statistics. In: Bernier DR, Christian PE, Langan JK (eds) Nuclear medicine, technology and techniques. Mosby, St Louis, 4th edition, 1997, pp 1–35

3.2 Radiolabeling of Red Blood Cells and Leucocytes

Radiolabeled red blood cells are used in nuclear medicine mainly for the assessment of vascular spaces, measurement of left ventricular volume and ejection fraction, and for localization of bleeding sites. Radiolabeled leucocytes are used primarily for the detection and localization of abscesses and delineation of sites of diffuse or focal infection. Major applications in nuclear hepatology include differentiation of hemangiomas from other focal liver lesions with Tc-99m-labeled red blood cells and differentiation of abscess from other cystic liver lesions with indium-111 oxine or Tc-99m-HMPAO labeled leucocytes.

Red Blood Cell Labeling with Tc-99m

Technetium-99m red blood cells (RBC) are used for blood pool imaging in the separation of vascular malformation (hemangiomas) from other non-vascular liver lesions. Radiolabeling of RBCs with chromium-51 was first accomplished by Gray and Sterling in 1950 for the main purpose of measuring their survival in the diagnosis of hemolytic anemias [1]. Technetium-99m-labeled RBCs are used primarily for blood pool imaging, and survival studies cannot be carried out due to the short physical half life of Tc-99m of only 6 h [2]. Three methods of RBC labeling are available: the in vivo method, in vitro method and combined in vivo and in vitro method. The in vivo method is technically simple, but results in a slightly higher background radiation. The in vitro method, on the other hand, is technically more involved, but gives excellent lesion to non-lesion contrast because of low background radiation.

In Vitro Method (Ultratag Kit made by Mallincrodt, St. Louis, MO)

About 1 ml of patient blood is drawn into a heparinized syringe and added to the mixing vial, which contains 50 μg stannous chloride, 3.7 mg sodium citrate, 5.5 mg dextrose and 0.11 mg sodium chloride. Stannous (2^+) chloride readily crosses the red cell membrane and attaches to the heme component of the hemoglobin molecule, ready to do its job of reducing valence of Tc-99m-pertechnetate from 7^+ to 4^+. About 0.6 ml of 0.1% sodium hypochlorite is added later as an oxidizing agent that converts all excess stannous chloride (2^+) into stannic (4^+) state in plasma, but not inside the red blood cell because of its inability to cross the intact red cell membrane. About 20–30 mCi of 99m-TcO_4 (pertechnetate) is added to the reaction vial. Tc-99m-pertechnetate readily crosses the red cell membrane and attaches to the globin molecule after it gets reduced from 7^+ to 4^+ valence by the waiting stannous (2^+) chloride on the heme fraction of the hemoglobin molecule. Once Tc-99m is reduced from the 7^+ to 4^+ valence state, it does not come out of the hemoglobin molecule. The entry of Tc-99m through the red cell membrane thus becomes one-way traffic. After 15–20 min of gentle incubation at room temperature, most of the Tc-99m is trapped inside the red blood cell [2]. The in vitro method is a very efficient labeling technique and does not necessitate blood centrifugation to remove plasma, because 97% of technetium-99m is associated with the red blood cell and less than 3% remains in plasma. Hemoglobin contains

95% of the total red cell radioactivity, of which 77% is associated with globin and the rest with the heme fraction of the hemoglobin molecule [3].

In Vivo Method

Stannous chloride (10–20 μg kg^{-1}) from a commercial pyrophosphate kit is injected intravenously. Tin (2^+) enters the red cell membrane and attaches to hemoglobin to be ready to act as a reducing agent when Tc-99m-pertechnetate enters the cell. About 30 min later, 20–30 mCi Tc-99m-pertechnetate in saline is injected intravenously. Tc-99m-pertechnetate crosses the red cell membrane, gets reduced by stannous chloride and later binds firmly to hemoglobin.

Combined In Vivo and In Vitro Method

Pre-tinning is accomplished first by intravenous injection of cold stannous pyrophosphate made for bone scanning. Fifteen to 20 min later, about 3–4 ml patient blood is drawn into a 50-ml-volume syringe, and 20–30 mCi Tc-99m-pertechnetate is added to the syringe, shaken gently for 10 min and re-injected through the same catheter. Because of the higher efficiency of labeling and lower background, the in vitro method may be preferred over the in vivo method in the detection of hepatic hemangiomas (blood pool) and gastrointestinal bleeding [4, 5].

Leukocyte Labeling

Leukocytes labeled with either In-111 oxine or Tc-99m-HMPAO are used in nuclear hepatology for the diagnosis of liver abscess, empyema or acute cholecystitis [6, 7].

Indium-111 Oxine

About 50–60 ml of patient blood is drawn into a heparinized syringe, and 10 ml of 0.9% sodium chloride containing 6% hetastarch is added to blood and mixed thoroughly [8]. The mixture is allowed to form sediment for 40 min. After the sedimentation, leukocyte-rich plasma is collected, diluted with saline in a ratio of 2:1 and centrifuged at 150 *g* for 10 min. The leukocyte-rich pellet is washed twice with 10 ml saline and centrifuged each time for 10 min at 150 *g* after washing. Washed cells are then resuspended in 4.5 ml saline. About 0.3–0.5 ml of indium-111 oxine containing 0.4–0.5 mCi (14.8–18.5 MBq) In-111 is added to the reaction vial and incubated gently for 15 min at room temperature. Indium-111 oxine penetrates the leukocyte membrane, and once inside the cell, indium-111 and oxine dissociate. Oxine diffuses out of the cell into the labeling medium, leaving indium-111 behind trapped inside the cell [6]. The suspension is then centrifuged for 8 min at 90 *g*, and the supernatant is discarded and the pellet containing labeled leukocytes is resuspended in platelet-poor plasma. About 6 ml of the suspension containing 0.3–0.4 mCi of In-111 leukocytes is injected intravenously. Indium-111-labeled leucocytes clear from blood with a $T_{1/2}$ of 6 h, which is very close to the value of 7 h for cells labeled with the gold standard P-32, di-isopropylfluorophosphate. After labeling, each leukocyte receives approximately

1,480 rad (14.8 Gy) radiation from Auger electrons of 0.6–25.4 keV energy from In-111. This amount of radiation from its own source does not affect its function [8].

The major advantage of In-111 oxine-labeled leukocytes over Ga-67 citrate or Tc-99m-HMPAO WBCs for imaging abscesses is that the entire abdomen, with the exception of the liver and spleen, remains free of any secreted radioactivity into the bowel [9]. Abdominal infection is diagnosed by taking early images at 2–10 min and repeat images within 30–60 min after injection. Delayed images at 24 h may be needed in some patients. In the case of chest infection, the earliest images that will provide any useful information are taken at 3–4 h after injection. Due to usual margination of leucocytes in the lungs, early chest images are usually not diagnostic [10].

Tc-99m-HMPAO

The blood separation step for leucocyte labeling with Tc-99m HMPAO remains identical to that of labeling with In-111 oxine described above. After separation, leukocytes are resuspended in 20% plasma/ACD solution. About 20–25 mCi of Tc-99m-HMPAO is added to the reaction vial and incubated gently for 10 min at room temperature, washed with plasma and resuspended in plasma and reinjected. The labeling yield is between 50 and 60% with 80% activity bound to granulocytes [11]. The labeled leukocytes clear from blood with a T ½ of 4 h, which is slightly shorter than for In-111-labeled granulocytes. The main advantage of Tc-99m HMPAO is that a much larger dose can be given, yet the total body and organ radiation dose is much less. The agent is easily available at all times of need at a very reasonable cost. The main disadvantage is that free Tc-99m-HMPAO, not bound to leucocytes, is taken up by the hepatocytes and secreted into bile. Intestinal luminal activity interferes with the diagnosis in images taken beyond 30 min after injection. A negative scan rules out abdominal infection. Increasing numbers of studies in recent years have been being done with Tc-99m-HMPHO [11]. Interference from secreted bile radioactivity is avoided by taking abdominal images early, within 10–20 min after injection. The absorbed radiation dose from labeled red blood cells and leucocytes is shown in Table 3.2.1.

Table 3.2.1 Radiation absorbed dose from Tc-99m-labeled RBC and WBC and indium-111-labeled WBC

Organ	Tc-99-m-RBC	Tc-99m-WBC (HMPAO)	In-111 WBC
	rad mCi^{-1} (Gy/37 MBq)	rad mCi^{-1} (Gy/37 MBq)	rads mCi^{-1} (Gy/37 MBq)
Liver	0.07	0.15	5.0
Spleen	0.05	0.22	40.0
Lungs	0.06	–	–
Kidneys	0.05	–	–
Ovaries	–	0.03	0.4
Testes	–	0.19	0.02
Bone marrow	0.03	0.16	4.0
Whole body	0.02	0.03	–

References

1. Gray SJ, Sterling K. The tagging of red blood cells and plasma proteins with radioactive chromium. J Clin Invest 1950;29:1604–1610
2. Srivastava SC, Chervu LR. Radionuclide-labeled red blood cells: current status and future prospects. Semin Nucl Med 1984;14:68–82
3. Srivastava SC, Strau RF. Blood cell labeling with 99mTc: progress and perspectives. Semin Nucl Med 1990;20:41–51
4. Front D, Isreal O, Groshar D, Weininger J. Technetium-99m labeled red blood cell imaging. Semin Nucl Med 1984;14:226–250
5. Birnbaum BA, Weinreb JC, Megibow AT, Sanger JJ, Lubat E, Kanamuller H, Noz ME, Bosniak MA. Definitive diagnosis of hepatic hemangioma: MR imaging VS Tc-99m-labeled red blood cell SPECT. Radiology 1990;176:95–101
6. Thakur ML, Segal AW, Louis L, Welch MJ, Peters TJ. Indium-111-labeled cellular blood components: mechanism of labeling, and intracellular location in human neutrophills. J Nucl Med 1977;18:1022–1026
7. Lantto EH, Lantto TJ, Vorne M. Fast diagnosis of abdominal infections and inflammations with technetium-99m -HMPAO labeled leukocytes. J Nucl Med 1991;32:2029–2034
8. Datz FL. In-111-labeled leukocytes for the detection of infection: current status. Semin Nucl Med 1994;24:92–109
9. Leddin DJ, Paterson WG, DaCosta LR, Dinda PK, Depew WT, Markotich J, McKaigney JP, Groll A, Beck IT. In-111 labeled autologous leukocyte imaging and fecal excretion. Comparison with conventional methods of assessment of inflammatory bowel disease. Dig Dis Sci 1987;32:377–387
10. McAfee JG. Editorial: what is the best method for imaging focal infections? J Nucl Med 1989;31:413–416
11. Allan RA, Sladen GE, Bassingham S, Lazarus C, Clarke SE, Fogelman I. Comparison of simultaneous 99mTc-HMPAO and 111-In oxine labeled white cell scans in the assessment of inflammatory bowel disease. Eur J Nucl Med 1993;20:195–200

3.3 Gallium-67 Citrate

The tumor detection capability of gallium-67 citrate was described first by Edwards and Hays in 1969 [1]. Very soon it was recognized that in addition to the detection of varieties of tumors (lymphomas, hepatomas, malignant melanoma and squamous cell carcinomas), Ga-67 was also taken up in high concentration by infectious lesions and abscesses. Benign conditions, such as pseudonodules of cirrhosis and other non-specific inflammations, do not concentrate the agent [2]. This differential uptake by benign versus malignant lesions and the ability to detect infection led to widespread clinical application of Ga-67 citrate imaging in the 1970s and 1980s, before CT and ultrasound became popular imaging techniques for detection of focal hepatic lesions. Gallium-67 imaging is reemerging primarily for determining therapeutic response to various chemotherapeutic agents in various malignancies.

Table 3.3.1 Radiation absorbed dose from gallium-67 citrate

Organ	mGy/37 MBQ	rads mCi^{-1}
Marrow	18	1.8
Lower colon	8.4	0.84
Spleen	7.0	0.70
Liver	6.3	0.63
Upper colon	5.5	0.55
Kidneys	5.4	0.54
Ovaries	3.0	0.30
Testes	2.5	0.25
Whole body	2.6	0.26

Modified from MIRD pamphlet no. 11, 1975

Pharmacokinetics

Gallium-67 is produced in an accelerator by bombarding zinc target with protons as represented by the equation [^{67}Zn (p, n) ^{67}Ga]. It has a physical half life of 78.3 h and decays by electron capture to stable zinc. It has three principle gamma photons with the mean energy of 93.7 keV (36%), 185 keV (20%) and 300 keV (16.0%). Upon intravenous injection, Ga-67 citrate is transported in blood bound to plasma proteins, mainly transferrin, and to a minor extent to lactoferrin and ferritin. Two different mechanisms are involved with reference to cellular uptake: normal soft tissues concentrate Ga-67 bound to transferrin, whereas tumors concentrate the fraction that is either free or bound loosely to other proteins [3]. In the hepatocytes, Ga-67 uptake is seen mostly in association with lysosomes and mitochondria and to a lesser extent in the cytosol. The nucleus concentrates less than 10% of the total hepatocyte uptake. The exchange of Ga-67 takes place between the lysosomes and the cytosol. After intravenous injection, blood pool activity remains high for up to 24 h [4]. Beyond 48 h, most of Ga-67 is cell bound. About 10% of injected activity is excreted in stool during the first week.

Increased capillary permeability facilitates Ga-67 entry into the site of acute inflammation, abscess or tumor. In the case of an abscess, Ga-67 is found in association with the leukocytes, siderophores and bacteria. Staphyllococcus aurius, *E. coli* and other microorganisms are shown to ingest Ga-67, accounting for high uptake by the abscess [5, 6]

Because of normal uptake by bone, and slow excretion by mucosa into the colon, the bone and lower large bowel receive the largest radiation dose from Ga-67: 18 mGy/37 MBq to bone marrow and 8.4 mGy/37 MBQ to the lower large bowel (Table 3.3.1). Currently, Ga-67 citrate imaging has re-emerged in the evaluation of chemotherapy for lymphomas.

References

1. Edward CL, Hayes RL. Tumor scanning with 67 Ga citrate. J Nucl Med 1969;10:103–105
2. Lomas F, Dibos PE, Wagner HN Jr. Increased specificity of liver scanning with the use of 67-gallium citrate. New Engl J Med 1972;286:1323–1329

3. Tsan MF. Mechanism of gallium-67 accumulation in inflammatory lesions. J Nucl Med 1985;26:88–92
4. Aulbert E, Gebherdt A, Schutz E, Haubold U. Mechanism of gallium-67 accumulation in normal rat liver lysosomes. Nuklearmedizin (Stuttg) 1976;15:185–194
5. Hammersley PA, Taylor DM, Cronshaw S. The mechanism of 67 Ga uptake in animal and human tumors. Eur J Nucl Med 1980;5:411–415
6. Scheffel U, Wagner HN Jr, Klein JL, Tsan MF. Gallium-67 uptake by hepatoma: studies in cell cultures, perfused livers and intact rats. J Nucl Med 1985;26:1438–1444

3.4 Somatostatin Receptor Imaging Agent

Somatostatin is a small peptide found in many normal tissues and in benign and malignant tumors. It was originally thought to regulate primarily the release of growth hormone [1]. Now it is evident that in addition to influencing growth hormone release, somatostatin regulates the release of cyclic neuropeptides and inhibits release of thyrotropin, insulin, glucagon, gastrin, secretin and cholecystokinin [2]. The somatostatin receptors are present in the brain, thyroid, lung, gastrointestinal tract, liver, gallbladder, pancreas, adrenals and activated leukocytes [3]. Two molecular forms of somatostatin have been identified: one consists of 14 (Fig. 3.4.1) and the other 28 amino acids in the molecule. The longer one with 28 amino acids is a dimer formed by the union of two shorter molecules. The serum

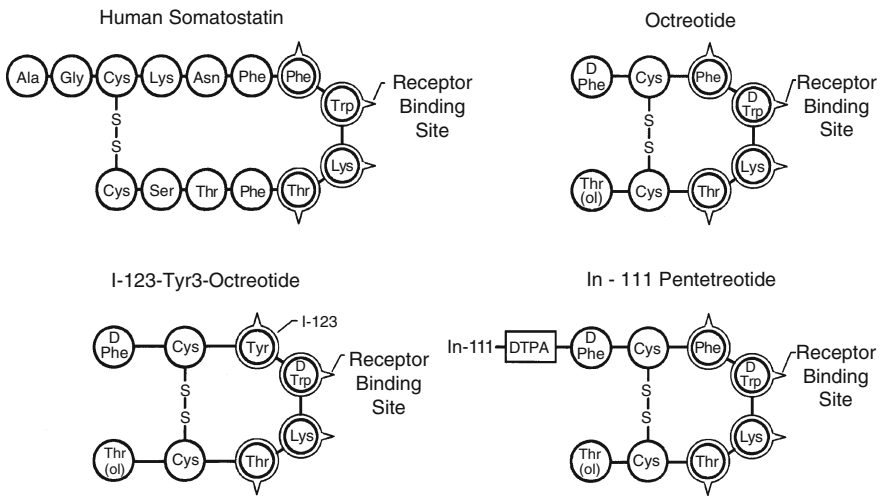

Fig. 3.4.1 Molecular structure of somatostatin and its radiolabeled analogues. Somatostatin consists of 14 amino acids. The receptor-binding sites are located on four sequentially arranged amino acids. In labeled octreotide, radioiodine, I-123, attaches directly to tyrosine (*Tyr*), whereas indium-111 requires DTPA as chelate for its attachment

half life of somatostatin is less than 3 min. Five subtypes of somatostatin receptors (SSTR 1–5) are recognized in the body. Both somatostatin 14 and 28 attach to all five subtypes with equal affinity. Octreotide is an analog of somatostatin with eight amino acids (octapeptide). It binds mainly to somatostatin receptor subtypes 2, 3 and 5, but not to subtypes 1 and 4 [3, 4].

Indium-111 Pentetreotide (OctreoScan)

Radiolabeled octreotide binds to somastostatin receptors on the surface of tumors, enabling their detection [5]. Radiolabeling is achieved with either iodine I-123 or indium-111. When I-123 is chosen, the amino acid tyrosine, a normal component of the molecule, is radiolabeled [6]. In the case of indium-111, a bifunctional chelate, diethylenetriaminepentaacetic acid (DTPA), is required for radiolabeling (Fig. 3.4.1). As a bifunctional chelate, DTPA attaches to indium-111 (radiotracer) with one arm and to the amino acid, D-phenylalanine of somatostatin analogue (ligand), with the other arm. Four amino acids (phenylalanine, tryptophan, lysine and threonine) arranged in a sequence provide the binding site for the radiolabeled analogue [7]. It binds with high affinity to SSTR2 and with lower affinity to SSTR3/5.

Following intravenous administration, In-111 pentetreotide clears from blood rapidly. About 33% of the administered dose remains in circulation at the end of 10 min. Kidneys are the major route of excretion. About 50% of the injected dose is excreted in urine in 6 h, 85% in 24 h and 90% in 48 h. Less than 2% of the dose is excreted in feces in 3 days. Stool radioactivity mostly represents biliary excretion. Kidneys are the target organs for radiation. About 7% of the dose accumulates in the kidneys by 4 h [8]. The recommended dose for scanning is 3 mCi for planar and 6 mCi for SPECT study. Clinical studies usually require a SPECT study necessitating a 6-mCi (222 MBq) dose [9]. Radiation to various organs from a diagnostic dose depends both upon the age and dose. The kidneys, spleen and urinary bladder receive the most radiation [10].

Technetium-99m Depreotide

Tc-99m depreotide is a somatostatin analogue with a molecular formula of $C_{65}H_{95}N_{16}O_{12}S_2$ and structure of R-Tyr-(D-Trp)-Lys-Val-R-(β-Dap)Lys-amide [11]. This agent is not superior to In-111 octreoscan, but due to its higher affinity for SSTR3 may be useful in those patients who show less or no uptake of In-111 octreoscan. In one study, 8 of 25 (32%) patients with negative In-111 octreoscan showed positive uptake with Tc-99m depreotide [12].

References

1. Krulich L, Dhariwal AP, McCann SM. Stimulatory and inhibitory effects of purified hypothalamic extract on growth hormone release from rat pituitary in vitro. Endocrinology 1968;83:783–790
2. Reichlin S. Somatostatin. New Engl J Med 1983;309:1495–1501

3. Reubi JC, Kvols LK, Krenning E, Lamberts SWJ. Distribution of somatostatin receptors in normal and tumor tissue. Metabolism 1990;39:78–81 (suppl 2)
4. Lamberts SWJ, van der Lely AJ, deHerder WW, Hofland LJ. Octreotide. New Engl J Med 1996;334:246–254
5. Krenning EP, Bakker WH, Breeman WAP, Koper JW, Kooji PP, Ausema L, Lameris JS, Reubi JC, Lamberts SWJ. Localization of endocrine-related tumors with radioiodinated analog of somatostatin. Lancet 1989;1:242–244
6. O'Connor ML, Kvols LK, Brown ML, Hung JC, Hayostek RJ, Cho DS, Vetter RJ. Dosimetry and biodistribution of an I-123-labeled somatostatin analog in patients with neuroendocrine tumors. J Nucl Med 1992;33:1613–1619
7. Krenning EP, Bakker WH, Kooji PPM, Breeman WAP, Oei HY, deJong M, Reubi JC, Visser TJ, Bruns C, Kwekkeboom DJ, Reijs AEM, van Hagen PM, Koper JW, Lamberts SWJ. Somatostatin receptor scintigraphy with indium-111 DTPA-D-phe-1-octreotide in man: metabolism, dosimetry and comparison with iodine-123-Tyr-3 Octreotide. J Nucl Med 1992;33:652–658
8. Somatostatin receptor imaging for neuroendocrine tumors. Product monograph. OctreoScan Mallinckrodt Medical Inc., St. Louis, MO, 1994
9. Jamar F, Fiasse R, Leners N, Pauwels S. Somastostatin receptor imaging with Indium-111-pentetreotide in gastroenteropancreatic neuroendocrine tumors: safety, efficacy, and impact on patient management. J Nucl Med 1995;36:542–549
10. Stabin MG, Kooji PPM, Bakker WH, Inoue T, Endo K, Coveney J, deJong R, Minegishi A. Radiation dosimetry for indium-111-pentetreotide. J Nucl Med 1997;38:1919–1922
11. Lebtahi R, LeCloirec J, Houzard C, Daou D, et al. Detection of neuroendocrine tumors: Tc-99m-P829 scintigraphy compared with In-111 pentetreotide scintigraphy. J Nucl Med 2002;43:889–895
12. Shah T, Kulakiene I, Quigley A, Warbey VS, Srirajaskanthan R, et al. The role of Tc-99m-depreotide in the management of neoroendocrine tumours. Nucl Med Commun 2008;29:436–440

3.5 Fluorine18, 2-Flouro-2-deoxy-D-glucose (^{18}F-FDG)

Glucose is the primary source of energy for most living cells in the body, especially for the neurons of the central nervous system. Carbohydrates in the diet are the main source of glucose. Each glucose molecule has 6 carbon (hexose), 6 oxygen and 12 hydrogen atoms and can be shown in the form of either a stick or ring diagram (Fig. 3.5.1). After intravenous administration, glucose diffuses readily out of the intravascular space through the capillary membrane and enters the interstitial space from where it enters cells either through active or passive diffusion. Its uptake is controlled by many transporter proteins on the plasma membrane and uses both sodium-dependent glucose transporter (SGLT) and facilitative sodium-independent glucose transporter pathways [1]. Once inside the cell, glucose is subjected to a ten-step metabolic process (glycolysis) that yields the end product (Fig. 3.5.2). Glucose is converted first into glucose-6-phosphate (G-6-P) by adding a phosphate group to the sixth carbon atom mediated by the enzyme glucokinase (hexokinase). Isomarase enzyme converts it into fructose-6-phosphate, which in turn is converted into fructose 1-6-diphosphate by the addition of another phosphate group at the carbon 1 position.

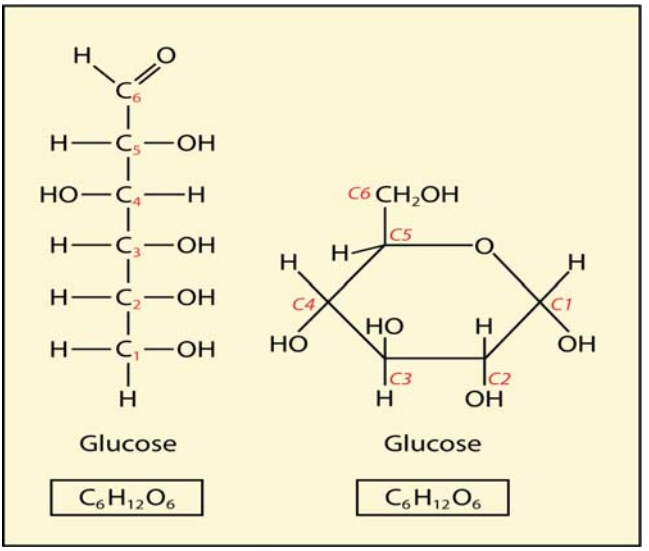

Fig. 3.5.1 Structure. Molecular structure of glucose is shown in stick and ring forms

Through the interaction with other enzymes, pyruvate is released, which may enter into the citric acid cycle or be converted into lactic acid. The final products are water and carbon dioxide. Most of these reactions take place rapidly within the cell. By reversing the metabolic process, glucose is re-synthesized (gluconeogenesis). In the reverse process, G-6-P is converted into glucose by the enzyme glucose-6-phosphatase (G-6-Ptase).

Structure

Removal of one oxygen atom of the hydroxyl group at the second carbon position converts glucose into 2-deoxyglucose (2DG), a glucose analogue (Fig. 3.5.3), which goes through an initial metabolic process similar to that of glucose. By replacing hydrogen with the fluorine (F-18) atom at the second carbon position of 2DG, a new compound, 2-fluoro-2-deoxyglucose (F-18 FDG), is created that behaves quite differently from glucose while going through the rest of the metabolic process [2]. The first metabolic step, however, remains intact, with 2-fluoro-2-deoxyglucose behaving like glucose with the conversion into 2DG-6-P (Fig. 3.5.4). Labeling with fluorine-18 enables the new compound (F18-FDG) for use in positron emission tomography (PET).

Biodistribution

Immediately after intravenous injection, F-18 FDG distributes throughout the body and readily crosses the blood-brain barrier. It diffuses out of the intravascular space into the

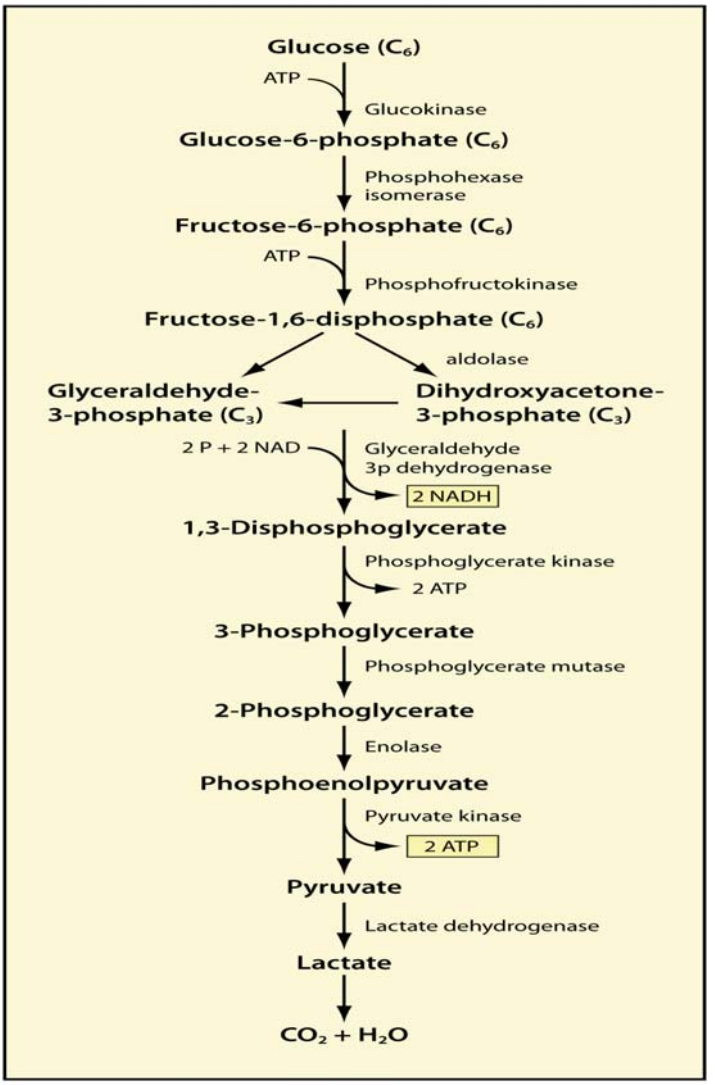

Fig. 3.5.2 Glycolysis. Glucose breaks down into carbon dioxide and water through various intermediary steps (modified from [3])

interstitial space rapidly and enters the cell. Initial entry is directly proportional to organ blood flow. Many glucose transporter proteins on the plasma membrane control its entrance. Sodium-dependent glucose transporter (SGLT) proteins use the Na + K + ATPase pump. The sodium-independent pathway uses facilitative transporter (GLUT) proteins. Of the 13 known GLUT proteins, liver cells have four: GLUT2, GLUT7, GLUT9 and GLUT10 [3, 4]. Although initial uptake reflects organ blood flow, retention depends upon a subsequent

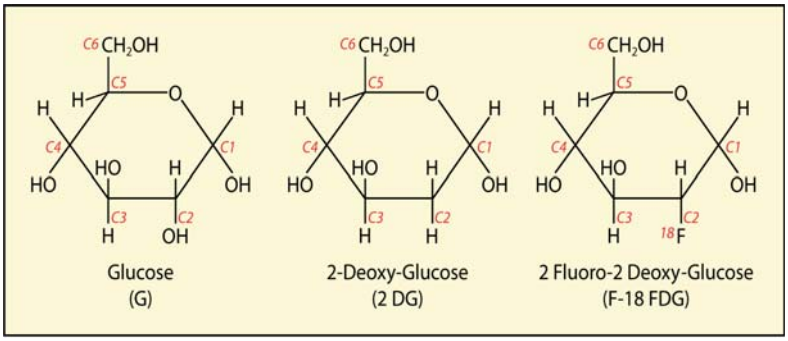

Fig. 3.5.3 Glucose analogues. Removal of oxygen atom from C-2 position of glucose creates 2-deoxyglucose (2DG), which enables labeling with fluorine-18 relatively simple at the C-2 position, resulting in 2-fluoro-2-deoxyglucose (F-18 FDG)

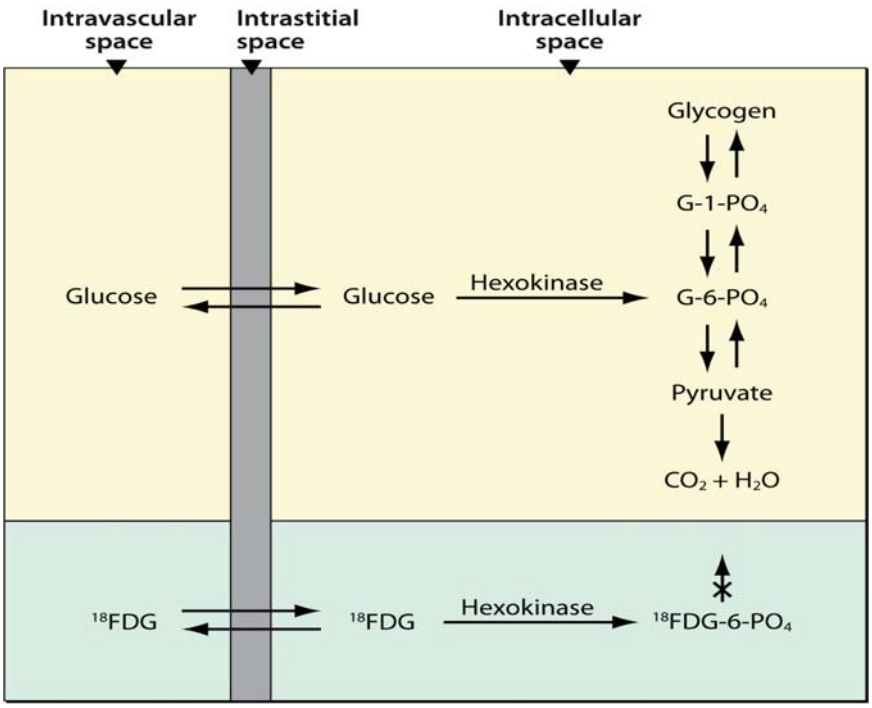

Fig. 3.5.4 Mechanism of glucose and F-18 FDG transfer across the cell. Both leave the intravascular space readily and enter the cell. Through the enzyme hexokinase, both get converted into their respective 6-phosphate form. Unlike glucose, F-18 FDG does not undergo any further metabolic process enabling imaging. Glucose is converted into either glycogen or $CO_2 + H_2O$, depending upon the body's needs

metabolic pathway used by each organ. Organs with high hexokinase content show much higher F-18 FDG uptake than those with low hexokinase activity. The hexokinase content of organs is as follows: brain > heart > kidney > lung > liver [1]. The brain concentrates 6.9%, liver 4.4% and heart 3.3% of the injected dose (Fig. 3.5.5). Organs with high glucose-6-phosphatase enzyme activity show more rapid clearance than those with low enzyme activity. Brain and heart with high hexokinase content show increasing uptake during the first hour, whereas other organs with high G-6-Ptase show declining activity [5]. Increasing uptake by brain and heart is due to rapid conversion of F-18 FDG into F-18 DG-6-P mediated by the enzyme glucokinase (hexokinase). Compared to brain and heart, liver has much less hexokinase activity and more G-6-Ptase activity; both acting together contribute to rapid clearance of F-18 FDG from the liver. In the liver cell, G-6-Ptase converts F-18 FDG-6-P back into F-18 FDG, which diffuses back into blood [1]. Neither F18-FDG nor F-18 FDG-6-P enters the bile. This is evident from the fact that bile ducts and gallbladder are not seen in whole body PET study.

In humans, the brain shows the highest uptake of F-18 FDG, followed by the liver, heart, red bone marrow, etc., as shown in Table 3.5.1. Kidneys excrete 20% of the injected dose in urine in 1 h and 21% in 2 h [5]. The initial uptake continues to increase in the brain and heart during the first hour, whereas it begins to decrease in the liver, kidney, spleen,

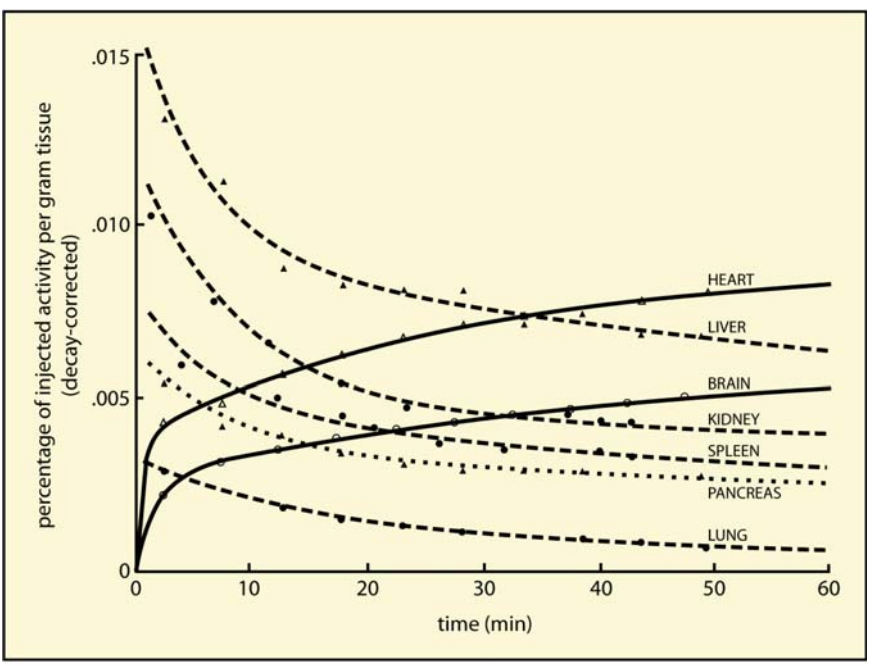

Fig. 3.5.5 Uptake and retention of F-18 FDG by various organs. Brain and heart show continuous uptake for 1 h, whereas other organs begin to show rapid clearance

Table 3.5.1 Organ uptake and radiation dose from F-18 FDG in human organs

Organ	Uptake [5]	Radiation dose [4]	
	(% Injected dose)	(mGy/185 MBq)	(rad 5mCi^{-1})
Brain	6.9	4.81	0.48
Liver	4.4	2.22	0.22
Heart	3.3	12.03	1.20
Red marrow	1.7	2.04	0.20
Kidneys	1.3	3.88	0.39
Lungs	0.9	2.04	0.20
Spleen	0.4	2.22	0.22
Pancreas	0.3	2.22	0.22
Testes	0.04	2.78	0.28
Ovary	0.01	2.78	0.28
Bladder wall	6.3	31.45	3.15
Rest of the body	74.4	–	
Total body	99.95	–	

From Mejia [5]

pancreas and lung (Fig. 3.5.5). Continued uptake by the brain and heart reflects their high hexokinase activity relative to other organs, which begin to show a decrease. Once F-18 FDG is converted into 2DG-6-P, it is trapped inside the cell without much clearance by the heart and brain. The trapping rate is much less in the liver, kidney, spleen, pancreas and lung. Most of the radiotracer cleared from these organs is excreted in urine in its original form as F-18-FDG. Normally, glucose filtered by glomeruli is completely reabsorbed by the tubules. This shows that replacement of one hydroxyl group at the C-2 position in the glucose molecule by one atom of F-18 in FDG changes the biological behavior of the radiotracer to a great extent.

Radiation Dose

On a per organ basis, the urinary bladder wall receives the largest dose (0.091mGy/MBq), followed by the heart, brain, kidneys, liver and other organs, as shown in Table 3.5.1. Dose to the bladder depends upon its initial volume prior to F-18 FDG injection. A completely filled bladder receives much less than an empty bladder [6]. Although a full bladder may receive much less radiation, patients are encouraged to empty prior to imaging to facilitate better visualization of other pelvic organs, especially the ovaries, uterus and pelvic floor lymph nodes.

References

1. Long C. Studies involving enzymatic phosphorylation 1. The hexokinase activity of rat tissue. Biochem J 1952;50:407–415
2. Gallagher BM, Fowler JS, Gutterson NI, MacGregor RR, Wan C, Wolf AP. Metabolic trapping as a principle of radiopharmaceutical design: some factors responsible for the biodistribution of [18F] 2-deoxy-2-fluoro-D-glucose. J Nucl Med 1978;19:1154–1161

3. Oehr P. Transport and metabolism of glucose and FDG. In: Oehr P, Biersack HJ, Coleman RE (eds) PET and PET-CT in onclogy. Springer, Berlin, 2004
4. Oehr P. Radiopharmaceutical production and safety of [18F] FDG. In: Oehr P, Biersack HJ, Coleman RE (eds) PET and PET-CT in onclogy. Springer, Berlin, 2004
5. Mejia AA, Nakamura T, Masatoshi I, Hatazawa J, Masaki M, Watanuki S. Estimation of absorbed doses in humans due to intravenous administration of fluorine-18-fluorodeoxyglucose in PET studies. J Nucl Med 1991;32:699–706
6. Dowd MT, Chen C, Wendel WJ, Faulhaber PJ, Cooper MD. Radiation dose to the bladder wall from 2[18F] fluoro-2-deoxy-D-glucose in adult humans. J Nucl Med 1991;32:707–712

Imaging of Liver and Spleen Morphology 4

In most nuclear medicine departments throughout the world, gamma cameras have completely replaced rectilinear scanners. A large field of view gamma camera with a single or dual head, fitted with a low-energy, parallel hole, all-purpose collimator, is generally chosen for most planar studies using technetium-99m-labeled agents. The main advantage of the dual-head gamma camera is patient convenience, where the data collection time is reduced by one-half as it allows simultaneous anterior and posterior image acquisition. The reduction in imaging time often improves the spatial resolution because of less patient movement during data collection. A triple-head gamma camera, when available, is preferred for SPECT images. The gamma camera image acquisition parameters are identical for both the liver and spleen.

4.1 Imaging with Radiocolloid

Patient Preparation

In general, there is no special patient preparation required for morphology imaging with radiocolloids. This is a distinct advantage over functional imaging with Tc-99m HIDA where the patient preparation requirements are quite stringent. The morphology imaging studies obtained immediately after a full meal may cause image artifacts and obscure the spleen in the anterior view because of photon attenuation by the gastric contents. The posterior and left lateral view images usually clarify this situation.

Radiocolloid imaging introduced in the early 1950s with the use of rectilinear scanners marked the birth of nuclear hepatology. Morphology imaging with radiocolloids remained very popular until the early 1980s, when it was overtaken by CT and ultrasound. Diagnosis of various diseases is made from assessing the changes in image pattern of the organ morphology. A thorough knowledge of normal morphology of the liver and spleen and normal variant patterns is critical to be able to detect disease. This section deals mainly with liver and spleen morphology as seen on a radiocolloid image (Table 4.1.1).

G.T. Krishnamurthy and S. Krishnamurthy, *Nuclear Hepatology,*
DOI 10.1007/978-3-642-00648-7_4, © Springer-Verlag Berlin Heidelberg 2009

4

Table 4.1.1 Data acquisition with Tc-99m-sulfur colloid

Instrument	Single, dual, or a triple head, large field of view gamma camera
Collimator	Low-energy, parallel hole, all purpose collimator
Agent	Technetium-99m-sulfur colloid or Tc-99m-albumin colloid
Dose	Adults, 2–4 mCi for planar images, 4–10 mCi for perfusion or SPECT images. Children, 30-50 μCi Kg^{-1} (minimum 300 μCi)
Spectrometer setting	140 keV photo peak at 15–20% window
Perfusion images	At 1 or 2 s/frame seconds for 60 s
Planar image data collection	500,000–100,000 counts for each of anterior, posterior, and two lateral views. Additional views are obtained as needed. A 5- or 10-cm-long lead marker is placed along the right costal margin to facilitate measurement of liver size and position. The same marker is used for measurement of spleen size using the posterior image
SPECT data collection	
Matrix	64 × 64 word or 128 × 128 word mode. Rotation, clockwise 360°, angle 3–6° for each stop. (360/64 = 6°)
Filters	Depends upon the computer and gamma
Views	Transaxial, coronal, and sagittal

Perfusion images are obtained immediately after the injection of the radiotracer at 1 or 2 s per frame for 60 s using the setup for the planer mode described above and reformatted at 4–8 s/image for clinical interpretation. The planar and SPECT image data are collected 15–30 min after intravenous injection when all of the radiocolloid particles from blood are extracted by the RE cells

Normal Liver

Perfusion

Liver and spleen perfusion images are obtained either in the anterior or posterior view using Tc-99m in any form. The aorta is the first abdominal organ to be seen, followed by the spleen, kidneys, and liver (Fig. 4.1.1). Aorta to spleen transit time is 2–4 s, and aorta to kidney transit time is 3–6 s. Despite the fact that both the hepatic artery and the splenic artery arise from a common celiac artery, there is an apparent delay in the appearance of liver perfusion due to dilution of hepatic artery radioactivity by the cold portal venous blood, as the portal vein receives its radioactivity much later than the splenic artery. The delay in arrival of the portal vein radioactivity is due to a delay in intestinal capillary phase.

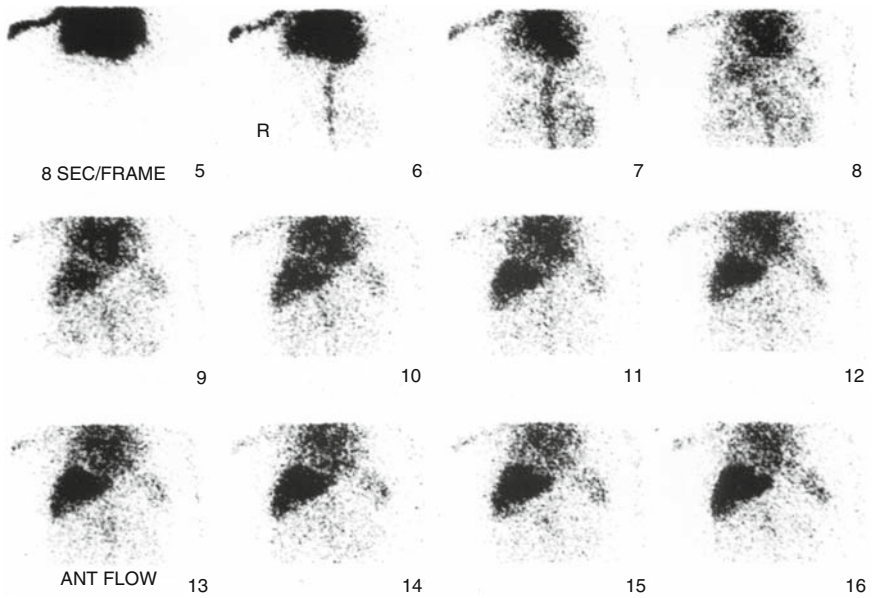

Fig. 4.1.1 Liver perfusion. Anterior perfusion image shows abdominal aorta (frame no. 6), followed by spleen and kidneys (no. 7). Liver appears faintly in the beginning (no. 8), representing hepatic artery perfusion, and becomes clear in late (no. 9) images due to arrival of portal venous blood flow

The liver receives 25% of its blood supply through the hepatic artery and 75% through the portal vein. The liver portal perfusion is clearly seen 10–14 s after the appearance of the abdominal aorta [1].

Shape, Surface, and Borders

There are wide variations in the shape of a normal liver, and most of the variations occur along the superior and inferior margins [2, 3]. The most common shape of a normal liver is that of an approximate triangle consisting of a superior, inferior, and a right lateral border (Fig. 4.1.2). Superior and right lateral borders form a smooth rounded contour at the right upper quadrant. The superior and inferior borders meet at an acute angle at the left tip of the left hepatic lobe. The inferior and right lateral borders meet at various angles. Often the inferior tip of the right hepatic lobe is elongated, forming a Riedel's lobe. The superior border of the liver is "S" shaped, and the contour is influenced by the size of the heart, exit of the hepatic vein, and the elevation of the dome of the right hemi-diaphragm. The shape, which looks like a gendarme's hat, is primarily due to the elevation of the right hemi-diaphragm.

The contour of the inferior border is affected by the fossa for the gallbladder and the entrance of the structures at the porta hepatis. The gallbladder fossa is usually located at the junction of the lateral 1/3 with the medial 2/3 of the inferior border (Fig. 4.1.3).

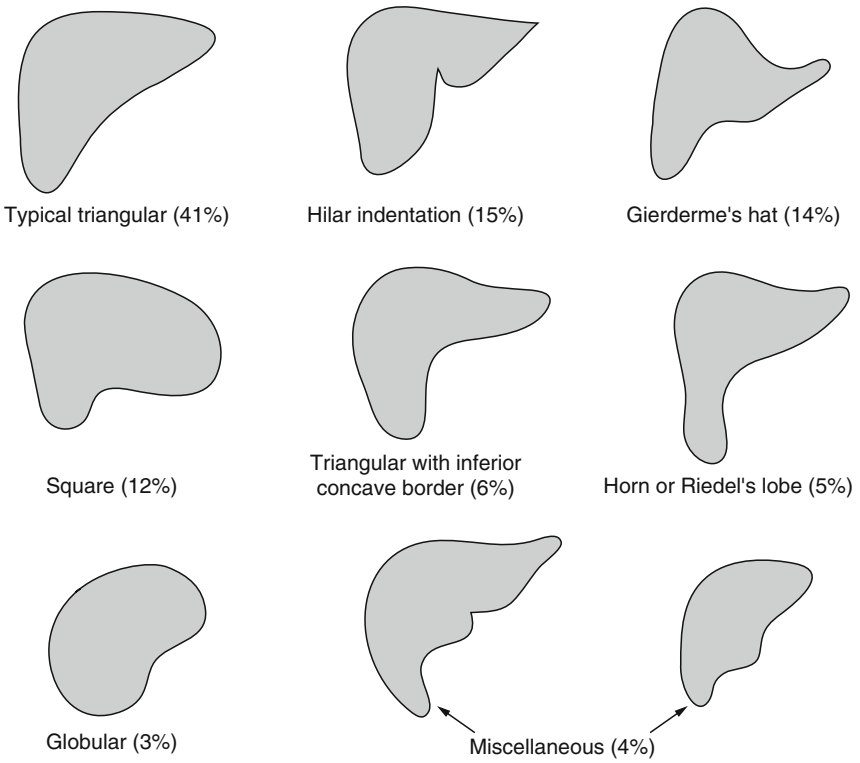

Fig. 4.1.2 Normal variation in liver shape and frequency (%). Triangular shape is the most common type [2–4]

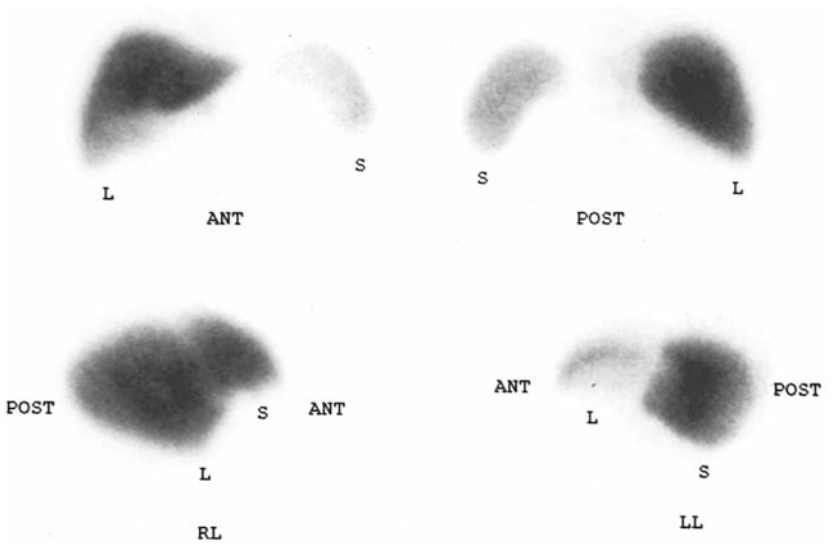

Fig. 4.1.3 Planar image. The liver (*L*) is seen clearly, and the spleen (*s*) faintly in an anterior (*ANT*) view. The spleen may project anterior to the liver in the right lateral (*RL*) view. In the left lateral (*LL*) view, the spleen appears clearly with the left lobe of the liver (*L*) projecting faintly anterior to it

The position of the gallbladder can be located during physical examination by drawing a straight line between the left anterior superior iliac spine and the umbilicus and extending it superiorly to meet the right costal margin. The fundus of the gallbladder corresponds to the point where this line meets the right costal margin. The gallbladder can be located anywhere along the inferior border and may even be intrahepatic. The intrahepatic gallbladder causes a filling defect in a radiocolloid scan and looks like a focal hot spot in a Tc-99m-HIDA study. Alteration in liver shape is usually due to the effect of extrinsic compression. The anterior and right lateral surfaces are smooth in outline, whereas the inferior surface has grooves and fissures for the entrance and exit of vessels and ducts, respectively.

Lobes

The liver is divided into the right and left lobe on the basis of either morphology or physiology. The line of attachment of the falsiform ligament marks the boundary between the morphologic right and left lobe. The division of the liver into physiologic right and left lobes is based on the embryologic development of the bile ducts, hepatic artery, and portal vein. The line of physiological division runs between the fossa for the gallbladder in the front and the deep fissure for the inferior vena cava in the back. The point of entrance of the porta hepatis also indicates the boundary between the physiologic right and left lobes. The line of physiological division (porta hepatis) is situated on the right side of the anatomic line of division (falsiform ligament). Therefore, the physiologic left lobe is much larger than the morphologic left lobe. In the anterior view, the line of attachment of the falciform ligament is shown by a slight decrease in counts because of photon attenuation.

The anterior view usually shows the entire liver and inferior part of the spleen. In the posterior view, the liver appears triangular in shape with a rounded supero-lateral corner. The posterior border in the right lateral view often shows a concave impression because of the right kidney. A wide vertical photopenic area between the right and left lobes is due to absorption of photons by the dense thoracic vertebrae (Fig. 4.1.3). Normally, the uptake of the radiocolloid by the reticulo-endothelial (RE) cells of the vertebral body is seen very faintly. The caudate lobe is situated posteriorly along the superior border, but is not usually seen in the planar posterior image, mainly because of absorption of photons by the vertebrae.

Dimensions of the Normal Liver and Spleen

The size of the liver is usually measured with an anterior view image and the size of the spleen with a posterior view (Fig. 4.1.4). A calibrated radioactive marker placed along the costal margin during data acquisition enables measurement of the organ size. The position of the liver is assessed with reference to the right costal margin. A normal liver is situated above the right costal margin and the normal spleen above the left costal margin. The right lobe of the liver measures 10.0–17.5 cm in the right mid-clavicular line. The maximum vertical height from the superior to inferior border of the right lobe is 10–20 cm The horizontal length from the right lateral border to the tip of the left lobe is 14–24 cm [4, 5]. Because of wide variations in shape at the tips, dimensions that include the tips tend to be

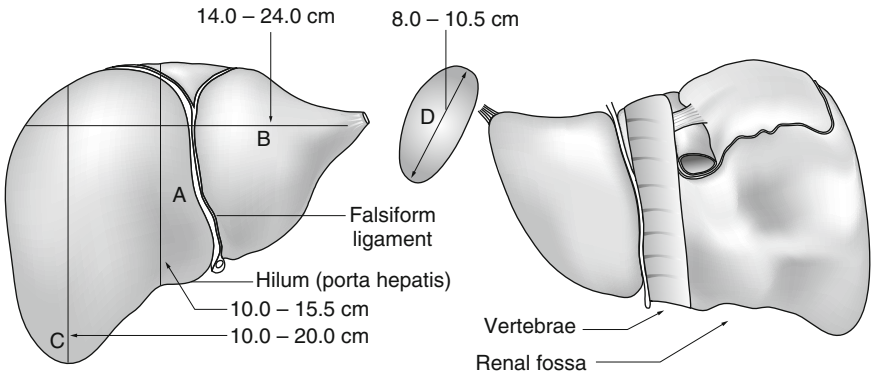

Fig. 4.1.4 Dimensions of the normal liver and spleen. In the anterior view, the right lobe measures 10.0–15.5 cm in the midclavicular line (**a**) and 10.0–20.0 cm from the dome to the inferior tip (c). The horizontal length from right lateral border to the tip of the left lobe ranges from 14.0 to 24.0 cm (**b**). In the posterior view, the upper limit of the normal spleen is 10.5 cm along the posterior oblique axis

less reliable as a measure of overall liver size. The measurement along the right mid-clavicular line serves as a better reference point for estimating true liver size than measurements along other lines. For accurate measurement of spleen size, an oblique line is drawn from the superior to inferior tip using a posterior view image. The upper limit of the normal spleen is about 10.5 cm along this oblique axis [6].

Pattern of Radiocolloid Uptake

A normal liver weighs 1,500–1,800 g and the spleen 150–200 g. The bone marrow is estimated to weigh about 1,500 g [7]. The liver takes up about 90% of radiogold colloid (Au-198) and 85% of Tc-99m-sulfur colloid. The spleen concentrates 3% of Au-198 colloid and 7% of Tc-99m-sulfur colloid. Bone marrow takes up about 7% of Au-198 colloid and 5% of Tc-99m-sulfur colloid (Table 3.1.4). The difference in radiocolloid uptake among these three organs is a function of their overall size and the physico-chemical nature of the radiocolloid particles [8]. The smallest of the particles are preferentially taken up by the bone marrow, medium-size particles by the liver, and the largest particles by the spleen. As the liver disease progresses, there is a shift in radiocolloid uptake from the liver to the

spleen and bone marrow. In moderate severity cirrhosis, radiocolloid uptake by the liver decreases (65–70%), and the uptake by the spleen and bone marrow increases. There is also uptake by lungs and other organs. In advanced cirrhosis, liver uptake may be as low as 30–35%. The spleen and bone marrow continue to show an increase in uptake of radiocolloid up to as high as 25–30% of the dose by each organ. The remaining 10–12% of the injected radiocolloid dose is taken up by activated RE cells in lungs and other organs.

Spleen and Bone Marrow Uptake

In the posterior view, the intensity of radiocolloid uptake by a normal spleen is usually equal to that of the normal liver [9]. In cirrhosis, the intensity of splenic uptake increases in direct proportion to the degree of portal hypertension (Fig. 4.1.5). In advanced cirrhosis,

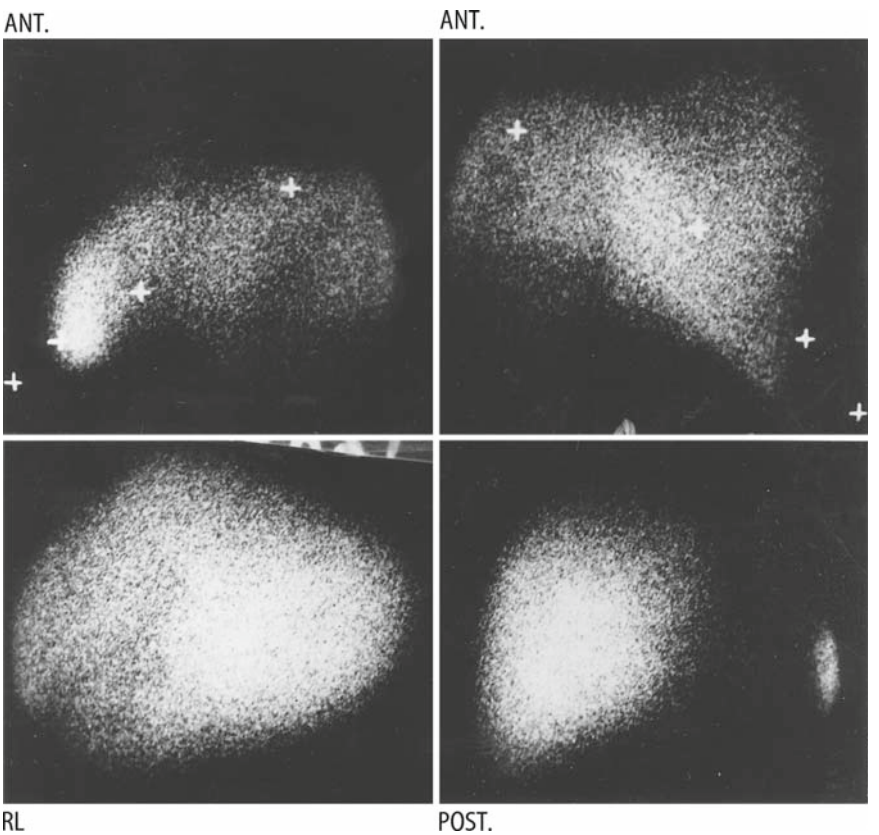

Fig. 4.1.5 Situs inversus. In the anterior (*ANT*) view, the spleen is located on the right and liver on the left side of the body. In the right lateral (*RL*) view, the spleen is superimposed at the posteroinferior part of the liver. Posterior (*POST*) view shows liver on the left and spleen on the right, separated by a photon-deficient column because of absorption by the vertebral bodies

the intensity of spleen and bone marrow uptake often exceeds that of the liver. Often, the intensity of thoracic and lumbar vertebral body radiocolloid uptake by the RE cells may match that of Tc-99m-MDP uptake by the bone mineral matrix. Decreased radiocolloid uptake by the spleen is also abnormal and often is noticed in patients with Hodgkin's disease, reticulum cell sarcoma, poorly differentiated lymphocytic lymphoma, mucosis fungoidis, or other types of lymphomas. In polycythemia rubra vera, the normal spleen/liver ratio is maintained despite an enormous increase in the size of the spleen.

The liver moves 1–3 cm up and down with each respiration. The size of the liver, therefore, may falsely appear large if the patient takes deep breaths during scanning. When the liver enlarges and extends below the right costal margin, the radiocolloid uptake in the liver tissue extending below the right costal margin may appear greater than the tissue uptake behind the costal margin. This apparent effect is due to attenuation of photons by the ribs, and the right breast exaggerates the difference in women. The effect of extrinsic compression on the liver is ascertained by taking one image during deep inspiration and another during deep expiration. An intrinsic liver defect will not change its position, whereas a defect due to extrinsic compression moves with respiration [10]. Decreased radiocolloid uptake by the liver and increased uptake by the spleen, lungs, and other soft tissues are indicators of poor prognosis [11, 12]. Fatty infiltration of the liver causes irregular uptake of radiocolloid and accumulation of xenon-133 during a V/Q study obtained for the diagnosis of pulmonary embolism.

Appearance of the Normal Liver and Spleen on SPECT Images

Increased spatial resolution and high lesion to non-lesion contrast on single photon emission computed tomography (SPECT) show some of the normal structures much more prominently than in a planar image. Often such normal structures are misinterpreted as cold lesions in a radiocolloid scan or as hot lesions on a blood pool or Tc-99m-HIDA study. The right and left branches of the portal vein, hepatic artery, and bile ducts pass through the middle of the liver in the opposite direction, 180° apart (Fig. 4.1.6). The coronal, sagittal, and transaxial slices passing through these structures may depict these normal structures as cold or hot lesions depending on the radiotracer used for the study. A cold lesion on a radiocolloid scan that fills in with Tc-99m RBC suggests a vessel or a hemangioma. A cold lesion that fills in with Tc-99m-HIDA suggests a biliary origin (choledochal cyst). In the sagittal slice passing through the middle of the right lobe, the right portal vein may appear as a curvilinear defect in the radiocolloid scan. Sagittal slices over the lateral aspect of the right lobe show a linear defect that is usually due to the posterior branch of the right portal vein. The anterior branch of the right portal vein is slightly smaller and is not always evident on sagittal slices. These anatomical variants may not be evident in the planar images due to overlying or underlying liver tissue. The right and left portal veins and the right posterior segmental vein are 1.5–2 cm in diameter, large enough to be seen on the SPECT images as defects (Fig. 4.1.6). The medial and lateral segmental veins of the left lobe are too small to cause a defect [13]. Two or three of the most anterior coronal slices may show only the left lobe, confirming its more anterior location. Lower transaxial slices show the gallbladder fossa as a pear-shaped defect along the anterior margin.

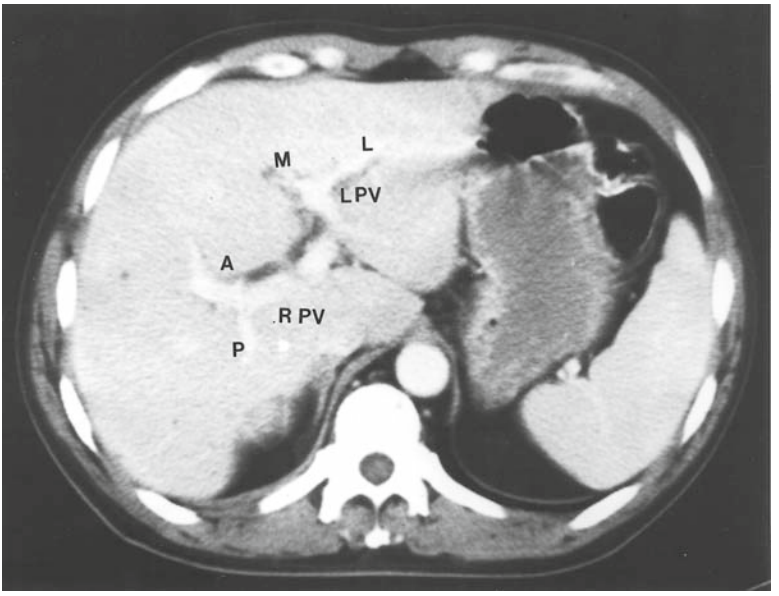

Fig. 4.1.6 Portal vein. Transaxial CT with contrast shows division of the portal vein in the middle of the liver into right portal vein (*RPV*) and left portal vein (*LPV*). LPV divides into medial (*M*) and lateral (*L*), and RPV into anterior (*A*) and posterior (*P*) segmental branches

Abnormal Liver

Hepatomegaly

A general response of the liver to any injury is one of diffuse enlargement. Hepatomegaly usually disappears when the offending agent is removed. Metabolic diseases in children are generally associated with hepatomegaly (Table 4.1.2). Most normal-size livers do not extend below the right costal margin. In patients with chronic obstructive lung disease, the liver may be pushed downwards to be palpable below the right costal margin. It is important to establish if a clinically palpable liver is due to displacement or enlargement.

The space-occupying lesions of the liver can be divided into four categories: (1) marginal lesions, (2) intrahepatic solitary focal lesions, (3) intrahepatic multiple focal lesions, and (4) intrahepatic diffuse lesions (Table 4.1.3).

Marginal Lesions

Most marginal lesions are caused by compression of the liver margin by adjoining normal organs or lesions arising from them. A normal right kidney placed high in the posterior

Table 4.1.2 Causes of hepatomegaly

Common causes	Uncommon causes	Rare causes
(1) Hepatitis	(1) Hepatoma	(1) Glycogen storage disease
(2) Fatty infiltration	(2) Hemochromatosis	(2) Gaucher's disease
(3) Cirrhosis	(3) Granuloma	(3) Cystic fibrosis
(4) Metastatic tumors	(4) Drug-induced hepatitis	(4) Galactosemia
(5) Congestive heart failure	(5) Wilson's disease	(5) Kwashiorkor
(6) Leukemia	(6) Infections	(6) Budd-Chiari syndrome
(7) Lymphoma	(7) Hemangioendothelioma	(7) Amyloidosis
(8) Abscess	(8) Polycystic disease	(8) Gangliosidosis
(9) Biliary obstruction	(9) Cholangiocarcinoma	

Table 4.1.3 Space-occupying lesions of the liver

Marginal lesions	Intraparenchymal lesions		
Compression by adjacent organs	Single focal	Multiple focal	Diffuse
Right kidney (hypernephroma)	Hepatoma	Metastasis	Hepatitis
Enlarged gallbladder	Abscess	Polycystic disease	Cirrhosis
Pancreatic Ca, Pseudocyst	Adenoma	Fatty infiltration	Fatty infiltration
Intracapsular hematoma	Hemangioma	Hemangioma	Wilson's disease
Choledochal cyst	FNH	--------	Lymphoma
Colon mass in hepatic flexure	Metastasis	Multiple mets	Chemotoxins
Right costal margin	Simple cyst	Multicystic disease	Hemochromatosis
Prominent portahepatis	Hydatid cyst	Hydatid cyst	Sclerosing cholangitis
Ascites	Infarction	Amoebic abscess	Biliary cirrhosis
Right breast	Intrahepatic GB	–	–
Enlarged heart	Pseudo tumor	–	–
Bile leak into GB fossa	–	–	

FNH = Focal nodular hyperplasia

abdomen or a mass arising from it (hypernephroma) may cause a defect along the posterior border of the right lobe of the liver. Such lesions are seen as a focal defect in the posterior planar view or as a concave posterior border in the planar right lateral view. In a SPECT image, it may appear as a round defect in the posterior slices of the coronal view and in the mid and lower slices of the transaxial views. A fully filled gallbladder may cause a cold defect in a radiocolloid scan along the inferior border in the anterior planar image. The gallbladder fossa appears as a pear-shaped defect along the anterior border in the right lateral planar image. A large choledochal cyst arising from the common bile duct may compress the middle of the inferior liver margin, causing a cold defect near the porta hepatis in a radiocolloid scan.

A normal stomach after a full meal or a mass arising from the stomach or pancreas (pseudocyst, cancer) may cause a defect along the inferior border of the left lobe. Depressed

right lateral ribs or a hematoma following an auto accident may cause a defect along the lateral surface of the right lobe. A lesion arising from the hepatic flexure of the colon may cause compression along the inferior liver margin of the right lobe. Post-traumatic subcapsular hematomas cause defects along any surface depending upon the point of impact, but most tend to occur along the right lateral or the anterior surface [14]. A large pendulous right breast or breast prosthesis causes a concave defect along the superior border that may be misinterpreted as a filling defect or as hypoconcentration of radiocolloid. Breast artifact is corrected by taking a repeat image after lifting the pendulous breast or removing the prosthesis (Fig. 4.1.7). An enlarged heart because of congestive heart failure or cardiomyopathy causes an impression along the superior margin at the junction of the right and left lobes.

Marginal lesions of the spleen are seen mostly along the medial (hilum) or the lateral surface. Lateral surface lesions are mostly hematomas secondary to trauma due to auto accidents. Medial surface lesions are due to a large pancreatic pseudocyst, choledochal cyst, or a postprandial fluid-filled stomach. Most post-traumatic hematomas along the lateral surface resolve in 3–4 weeks [14].

Intrahepatic Solitary Focal Lesions

These are the most common type of liver lesions seen when scintigraphy is obtained early in the course of liver disease. They tend to be associated with normal or mildly abnormal liver function tests. Most focal liver lesions appear to be round. Infarction appears wedge shaped, and radiation necrosis causes a characteristic appearance (quadrangular) depending upon radiation port. A thorough knowledge of the mode of clinical presentation, clinical findings, and changes in liver function tests are necessary to arrive at an etiological diagnosis. This is true for all types of liver imaging procedures, including radiocolloid

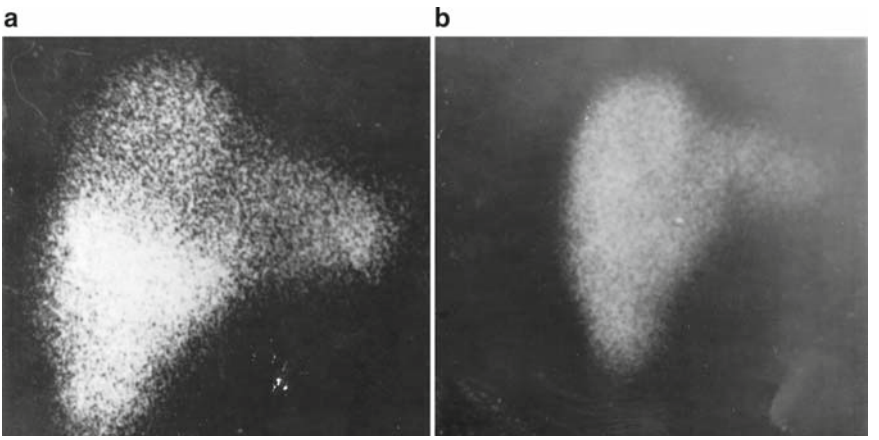

Fig. 4.1.7 Liver artifact. A large defect over the superior part of the right lobe caused by a breast prosthesis (**a**) disappears in the repeat image after its removal (**b**)

4

scan, computerized tomography, ultrasound, and magnetic resonance imaging. No single imaging test or even a combination of imaging tests is capable of making an etiological diagnosis all of the time [15–18].

Intrahepatic Multiple Focal Lesions

Multiple metastases, polycystic or multicystic liver disease, and fatty infiltration are examples of multiple intrahepatic focal lesions. Multiple metastatic lesions are the most common (Fig. 4.1.8). In a patient with a known primary cancer elsewhere, multiple liver lesions are considered secondary until proven otherwise. Polycystic liver disease is associated with cysts in the kidney, spleen, and other organs and has an autosomal dominance pattern of inheritance. Fatty infiltration may cause focal or diffuse defects. On ultrasound, fatty infiltration appears as a hypoechoic mass with angulation and interdigitating margins. [19]. Liver with fatty infiltration shows xenon-133 retention after a lung ventilation study obtained to rule out pulmonary embolism. Xenon-133 retention by the liver is specific for fatty infiltration [20].

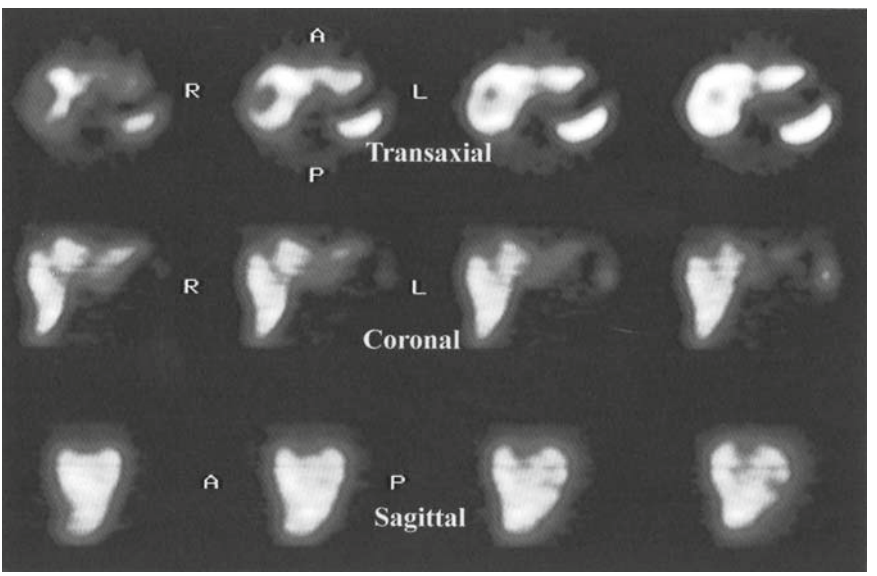

Fig. 4.1.8 Multiple metastatic liver disease. Transaxial, coronal, and sagittal SPECT images with radiocolloid show multiple intrahepatic metastasis from colon cancer (courtesy of Dr. Kumaresan, Hyderabad)

Intrahepatic Multiple Diffuse Lesions

Alcoholic hepatitis, viral hepatitis, and cirrhosis are the most common causes followed by other rare diseases, such as hemochromatosis, Wilson's disease, primary biliary cirrhosis, primary sclerosing cholangitis, and drugs (chemotherapy) or toxin-induced hepatitis. Many of these diseases are associated with a changing image pattern, depending upon the phase of parenchymal liver disease. Viral and alcoholic hepatitis often heal completely when the offending agent is removed completely. Defects due to chemotherapy usually disappear after the completion of the course. The role of radiocolloid imaging in the detection of liver lesions has diminished recently and has been replaced by CT and ultrasound, which have better spatial resolution and provide additional information about structural changes in organs around the liver [21]. Radiocolloid imaging is now requested mostly to clarify an abnormality already seen with the CT or ultrasound study to confirm whether the lesion is hepatic in origin. The posterior view image shows all three organs that take up radiocolloid, the liver, spleen, and bone marrow, in the thoracic and lumbar vertebral bodies and provides information related to their relative function. Bone marrow replacement by a tumor causes a "cold" defect in the vertebra in a radiocolloid image and a "hot" lesion in a Tc-99m MDP at the corresponding site (Fig. 4.1.9).

Relative Merits of the Diagnostic Tests

The accuracy of positive predictive and negative predictive values is similar for CT, ultrasound, and radiocolloid scan. The sensitivity of CT and radiocolloid scan is similar, but slightly low for ultrasound (Table 4.1.4). Any one of the three imaging modalities is

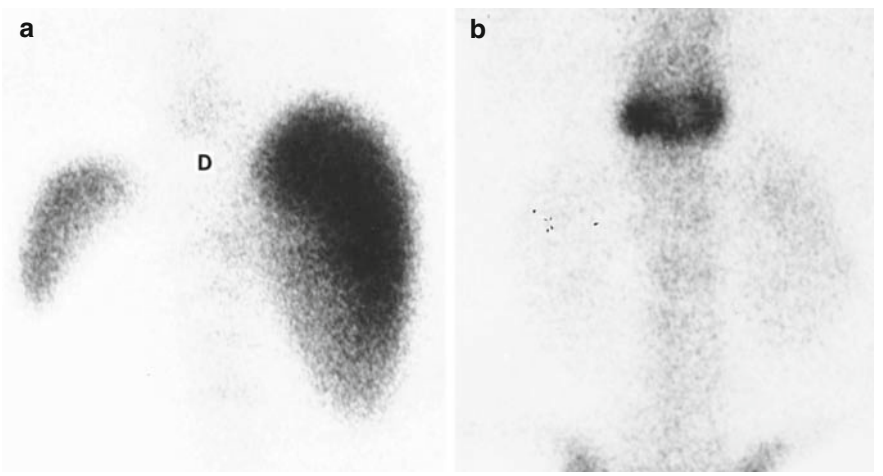

Fig. 4.1.9 Discordant Tc-99m colloid and Tc-99m MDP uptake by a vertebra. A metastatic tumor in T-12 vertebra causes a "cold" defect (*D*) on the radiocolloid image **(a)** and a "hot" lesion on Tc-99m MDP bone scan **(b)**

Table 4.1.4 Sensitivity, specificity, accuracy, positive predictive and negative predictive value of radiocolloid scan (RN), CT, and ultrasound (US) studies in the detection of space-occupying lesions of the liver

No. of patients	Sensitivity			Specificity			+ Predictive value			− Predictive value			Ref.
	RN	CT	US	RN	CT	US	RN	CT	US	RN	CT	US	
1,438	86	75	75	79	91	82	82	90	81	83	77	76	[15]
122	86	93	82	83	88	85	83	83	76	86	86	78	[16]
80	79	76	61	81	89	94	74	83	87	84	84	77	[17]
1,640	84	81	73	81	89	87	80	85	81	84	82	77	

capable of detecting a solitary liver lesion, but the choice of one over another depends upon local expertise, availability, reproducibility, and cost [22]. Because CT and ultrasound studies provide additional information about nearby organs, they have become clinically popular and have almost completely replaced radiocolloid scans for liver imaging today. Once a lesion is detected by one imaging modality, incremental information from the second or third imaging test is not substantial enough to justify obtaining more than one morphologic imaging procedure. This factor is observed more critically by insurance companies and other third party payers than by physicians and patients. The information obtained from a combination of one morphological and one physiological imaging may be better for patient management than the information gathered from a combination of two or more morphological imaging procedures.

Biochemical tests specific for a disease may offer clues in arriving at an etiological diagnosis from an imaging procedure. Most hepatomas are associated with a rise in serum alpha-fetoprotein, and the tumor size correlates with serum levels [23]. However, a slight rise in serum alpha-fetoproteins levels is often seen in viral hepatitis, post-necrotic cirrhosis, chronic active hepatitis, drugs, and a variety of other liver diseases. Hepatomas may cause diffuse irregular radiocolloid uptake or present as a solitary or multiple focal liver lesion [24].

References

1. DeNardo GL, Stadalnik RC, DeNardo SJ, Raventos A. Hepatic scintiangiographic patterns. Radiology 1974;111:135–141
2. Quinn JL lll. Nuclear medicine in gastroenterology. Hospital practice 1972, pp 115–122
3. McAfee JG, Ause RG, Wagner HN Jr. Diagnostic value of scintillation scanning of the liver. Follow-up of 1,000 studies. Arch Intern Med 1965;116:95–110
4. Mould RF. An investigation of the variations in normal liver shape. Br J Radiol 1972;45: 586–590
5. Rosenfield AT, Schneider PB. Rapid evaluation of hepatic size on radioisotope scan. J Nucl Med 1974;15:237–240
6. Siegel RM, Becker DV, Hurley JR. Evaluation of spleen size during routine liver imaging with Tc-99m and the scintillation camera. J Nucl Med 1970;11:689–692
7. MIRD. Summary of current radiation dose estimates to humans with various liver conditions from Tc-99m-sulfur colloid. J Nucl Med 1975;16:108A–108B

8. MIRD. Dose estimate report no. 4. Summary of current radiation dose estimate to humans with various liver conditions from Au-198 colloid. J Nucl Med 1975;16:173–174
9. Bekerman C, Gottschalk A. Diagnostic significance of the relative uptake of liver compared with spleen in 99m-Tc-sulfur colloid scintiphotography. J Nucl Med 1971;12:237–240
10. Oppenheim BE, Hoffer PB, Gottschalk A. The use of inspiration-expiration scintiphotos to determine the intrinsic or extrinsic nature of liver defects. J Nucl Med 1972;13:554–556
11. Keyes JW Jr, Wilson GA, Quinones JD. An evaluation of lung uptake of colloid during liver imaging. J Nucl Med 1973;14:687–691
12 Ahmad M, Witztum KF, Fletcher JW, Hendershott LR, Klos D, George EA, Donati RM. Xenon-133 accumulation in hepatic steatosis. J Nucl Med 1977;18:881–885
13. Pettigrew RI, Witztum KF, Perkins GC, Johnson ML, Burks RN, Verba JW, Halpern SE. Single photon emission computed tomography of the liver: Normal vascular intrahepatic structures. Radiology 1984;150:219–223
14. Froelich JW, Simone JF, McKussick KA, Winzelberg GC, Strauss HW. Radionuclide imaging and ultrasound in liver/spleen trauma: a prospective comparison. Radiology 1982;145:457–461
15. McClees EC, Gedgaudas-McClees RK. Screening for diffuse and focal liver disease: the case for hepatic scintigraphy. JCU J Clin Ultrasound 1984;12:75–81
16. Anderson PO, Adams DF, McNeil BJ, Sanders R, Siegelman SS, Finberg HJ, Hessel SJ, Abrams HL. Computed tomography, ultrasound, and scintigraphy of the liver in patients with colon or breast carcinoma: a prospective comparison. Radiology 1983;149:225–230
17. Kemeny MM, Sugarbaker PH, Smith TJ, Edwards BK, Shawker T, Vermess M, Jones AE. A prospective analysis of laboratory tests and imaging studies to detect hepatic lesions. Ann Surg 1982;195:163–167
18. Brendel AJ, Leccia F, Drouillard J, San Galli F, Eresue J, Wynchank S, Barat JL, Ducassou D. Single photon emission computed tomography (SPECT), planar scintigraphy, and transmission computed tomography: a comparison of accuracy in diagnosing focal hepatic disease. Radiology 1984;153:527–532
19. Quinn SF, Gosink BB. Characteristic sonographic signs of hepatic fatty infiltration. AJR Am J Roentgenol 1985;145:753–755
20. Patel S, Sandler CM, Rauschkolb EN, McConnell BJ. Xe-133 uptake in focal hepatic fat accumulation: CT correlation. AJR Am J Roentgenol 1982;138:541–544
21. Krishnamurthy S, Krishnamurthy GT. Evolution of nuclear hepatology. J Nucl Med Tech 1995;23:35S–45S
22. McGarrity TJ, Samuels T, Wilson FA. An analysis of imaging studies and liver function tests to detect hepatic neoplasia. Dig Dis Sci 1987;32:1113–1117
23. Tonami N, Aburano T, Hisada K. Comparison of alpha 1 fetoprotein radioimmunoassay method and liver scanning for detecting primary hepatic cell carcinoma. Cancer 1975;36:466–470
24. Bloomer JR, Walman TA, McIntire KR, Klastskin G. Alpha-fetoprotein in non-neoplastic hepatic disorders. JAMA 1975;233:38–41

4.2 Adenoma and Focal Nodular Hyperplasia

Adenoma and focal nodular hyperplasia (FNH) are relatively rare solitary tumors of women in their reproductive years and show a close association with the use of oral contraceptives [1]. The tumors remain mostly asymptomatic (Fig. 4.2.1). They are discovered incidentally during abdominal CT and ultrasound examinations obtained for some other medical indication. These tumors may suddenly become symptomatic and present with

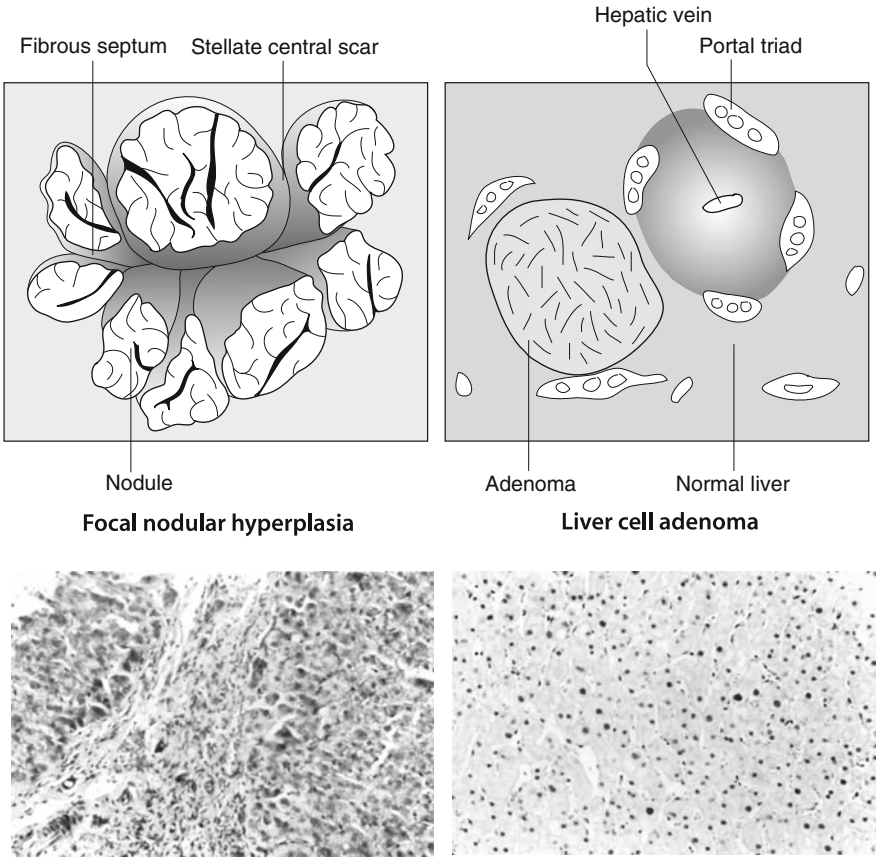

Fig. 4.2.1 A schematic diagram (*top*) of focal nodular hyperplasia and liver cell adenoma. Focal nodular hyperplasia consists of radiating dense fibrous tissue with all types of liver cells, but without any capsule. Histology (*bottom*, *left*) shows the hepatocytes, Kupffer cells, and fibrous tissue with formation of small nodules. Adenoma (*bottom*, *right*) consists of a capsule with monotonous sheets of hepatocytes without any Kupffer cells or fibrous tissue (courtesy of Dr. Ted Pinkert)

acute onset of abdominal pain, hemorrhage, and hypotension [2]. Adenoma bleeds more frequently than focal nodular hyperplasia. One study reported bleeding incidence at presentation of 4 in 27 patients with adenoma and none of 23 patients with focal nodular hyperplasia [3]. They may extend beyond the liver border in some patients and become clinically palpable on routine examination. Liver function tests are usually normal in both tumors.

Both tumors appear as non-specific space-occupying lesions in a radiocolloid scan, ultrasound, MRI, or CT examination. Arteriography, contrast CT, or blood pool imaging may show hypervascularity in FNH. Adenoma, on the contrary, usually shows no hypervascularity. But these morphologic and arteriographic characteristics are not distinct enough to separate FNH reliably from adenoma (Table 4.2.1) or from other space-occupying lesions of the liver listed in Table 4.1.2.

Adenoma

Adenoma is a well-encapsulated, round, solitary lesion, varying in size from 8 to 15 cm. It consists of sheets of hepatocytes without any bile ducts or fibrous septa (Fig. 4.2.1). Kupffer cells are either completely absent or markedly decreased in number. Few of those Kupffer cells that are present lack phagocytic capacity and hence the nodule appears as "cold" in a radiocolloid scan [4]. The hepatocytes are able to concentrate Tc-99m-HIDA, but cannot secrete into bile because of the lack of bile ducts [5]. About 80% of adenomas show mixed echogenecity on the ultrasound examination, and about 86% appear as a hypodense mass on non-contrast CT examination [4]. The most consistent pattern of hepatic adenoma on a multimodality imaging is one of a well-circumscribed solitary mass lesion on CT or US with no uptake on a radiocolloid scintigraphy. Atypical forms with functioning Kupffer cells are rare [6]. Some adenomas may show a nodule-in-nodule pattern on CT and MRI and are indistinguishable from hepatocellular carcinoma. Adenomas may be separated from carcinomas by depicting its functional characteristics. Lack of Ga-67 citrate uptake (in contrast to hepatocellular carcinoma) and no radiocolloid uptake, as well as late uptake with no excretion of Tc-99m HIDA, may distinguish adenoma from hepatoma and FNH and other types of focal liver tumors [7].

Focal Nodular Hyperplasia

In contrast to hepatic adenoma, which consists mostly of sheets of hepatocytes, focal nodular hyperplasia (FNH) usually contains almost all of the cellular components of a normal liver, including the hepatocytes, Kupffer cells, bile ducts, and other supporting cells. There is a central area of fibrosis with radiating fibrous connective tissue that divides the nodule into several smaller sections of varying size, mimicking the pattern seen with pseudonodules of cirrhosis [8]. A capsule is absent, a clear distinction from adenoma

Table 4.2.1 Characteristic features of hepatic adenoma and focal nodular hyperplasia

Parameter	Adenoma	Focal nodular hyperplasia
Age	30–40 years	30–40 years
Female:male ratio	30:0	10:1
Oral contraceptive association	+++	++
Well-defined capsule	Present	Absent
Bile ducts	Absent	Decreased and narrowed
Fibrosis	Absent	Present
Hypervascularity	++	++++
Hepatocyte number (in lesion)	Normal or increase	Normal or decrease
Kupffer cells	Absent or decrease	Normal or decrease
Radiocolloid uptake	Absent	Normal or decrease
Tc-99m-HIDA uptake	Increase or normal	Normal
Tc-99m-HIDA excretion	Absent	Slow
Tc-99m-NGA receptors	not known	Increase or normal

HIDA = Hepatic iminodiacetic acid, *NGA* = galactosyl neoglyco-albumin

(Fig. 4.2.1). Bile ducts show proliferation with narrow lumens impeding bile flow through them. The hepatocytes show a clear to dark cytoplasm with sparse bile canaliculi [2]. Most FNHs are found just beneath the liver surface, and some are pedunculated. The size of the lesions varies from 1 to 15 cm. Malignant transformation is uncommon. About 90% of FNH are hypervascular, and the rest are hypovascular on the angiogram. On the ultrasound examination, 50% are hyperechoic, 40% hypoechoic, and 10% show a mixed pattern [9, 10].

Scintigraphic Features

Both focal nodular hyperplasia and a regenerating nodule of cirrhosis contain Kupffer cells. Most of the other focal liver lesions (adenoma, hemangioma, primary and metastatic liver lesions) do not contain any Kupffer cells, or those few Kupffer cells that are present lack phagocytic function. A normal radiocolloid uptake pattern is seen in 64% of FNH, and the remaining 34% show decreased uptake [11]. A characteristic scintigraphic feature of FNH includes a hypervascularity seen on contrast CT (Fig. 4.2.2a). About 76% of them showed hypervascularity in a perfusion study with Tc-99m-HIDA (Fig. 4.2.2b). Early phase functional images (within 10 min) show Tc-99m-HIDA uptake by the nodule equal to that of the adjoining normal liver (Fig. 4.2.2c). Late phase images (after 45 min) show slow clearance by the nodule and a normal clearance from adjoining normal liver. At 60 min, the radioactivity retained by FNH is about twice as much as the normal liver and hence appears as “a hot nodule” on the late image (Fig. 4.2.2 d and e). Mean excretion half time of 18 min for the normal liver increases to 40 min for FNH, explaining the reason for the appearance of a hot lesion [11]. The slow excretion is due to narrowing of the cholangioles draining the FNH. The time of appearance of the hot nodule is a function of both how rapidly the radiotracer is cleared from the normal liver and how slowly it is cleared from the nodule. The nodule is usually seen clearly between 18 and 60 min after injection of Tc-99m-HIDA. Routine inclusion of the perfusion phase as an integral part of hepatobiliary imaging enhances the nodule detectability by showing its hypervascularity. The radiocolloid image depicts the lesion as “cold” (Fig. 4.2.2f). The overall detectability of FNH is 92% with Tc-99m-mebrofenin cholescintigraphy, 84% with CT, and 84% with MRI [10] (Fig. 4.2.3).

Surface Receptors

The hepatocytes of FNH show an increase in the number of surface receptors for Tc-99m-galactosyl-human serum albumin much more intensely than the adjoining normal liver parenchyma. In a study comprising 12 patients with focal nodular hyperplasia, 9 with hepatocellular carcinoma, and 3 patients with metastatic liver cancer, the authors were able to distinguish FNH from primary and metastatic liver lesions by calculating a nodule/normal liver ratio obtained with Tc-99m- neoglycoalbumin. Eight of 12 patients with FNH showed an increase in ratio, and the remaining 4 showed an uptake equal to that of the adjoining normal liver tissue. The nodule/normal liver mean ratio was 1.7 ± 0.3 in patients

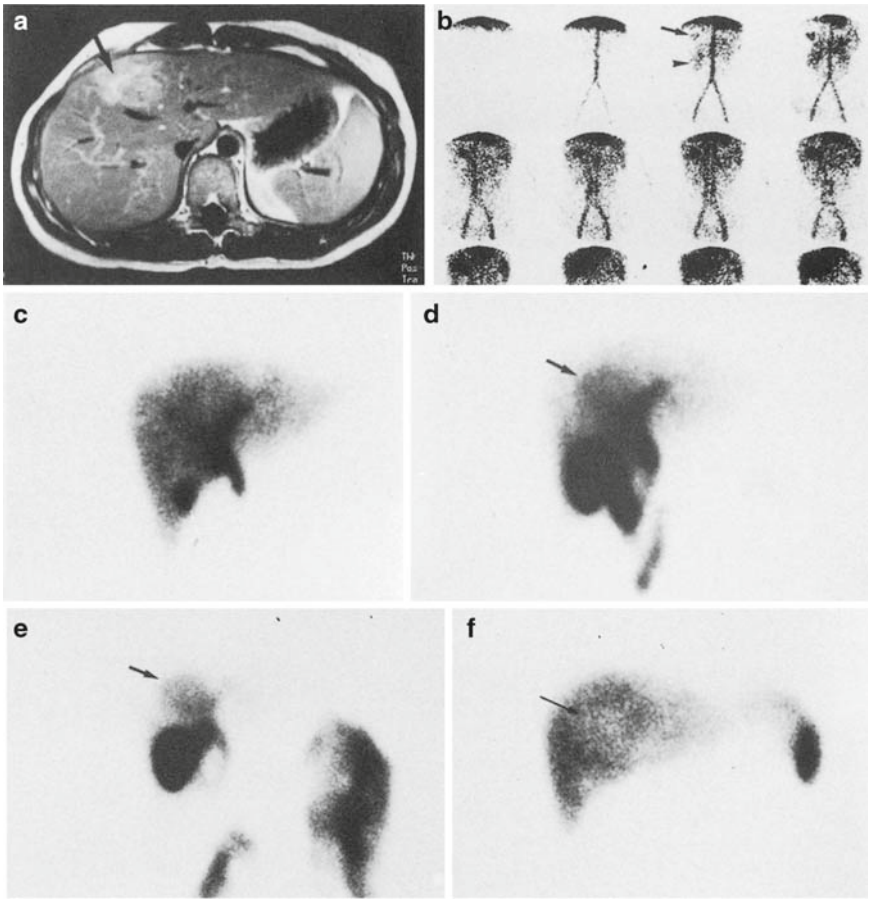

Fig. 4.2.2 Functional characteristics of focal nodular hyperplasia. It is hypervascular as seen on a contrast CT (**a**) and perfusion study with Tc-99m-HIDA (**b**). Early images show normal uptake (**c**), and late images at 45 min (**d**) and 60 min (**e**) show retention of Tc-99m HIDA (**e**). The lesion appears as "cold" on a radiocolloid image (**f**). (Reproduced with permission from the publisher, [11])

with FNH and 0.4 ± 0.2 in patients with primary and metastatic cancer, enabling clear separation of benign from malignant liver lesions [12]. Multimodality imaging with tumor-seeking agents like Ga-67 citrate and Tl-201 chloride, combined with Tc-99m phytate (colloid) and a hepatobiliary agent (Tc-99m-pyridoxyl-5-methyl tryptophan), often aids in separating benign from malignant hepatic lesions [13, 14].

Treatment

A flexible treatment approach is recommended, and asymptomatic patients are managed conservatively [15]. Some nodules regress spontaneously on discontinuation of oral

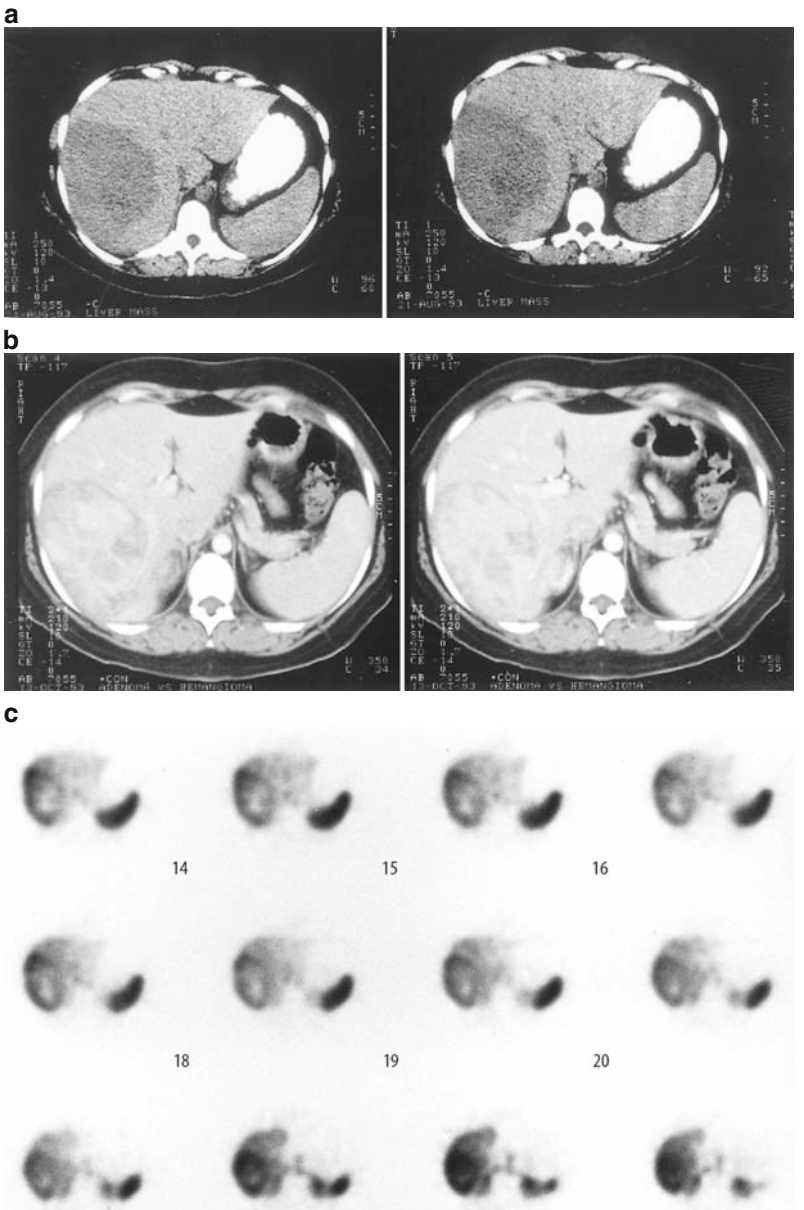

Fig. 4.2.3 (**a**–**c**) Blood pool features. A large focal nodular hyperplasia in the posterior right lobe appears as hypodense on a CT scan without contrast (**a**) and as non-uniform hyperdense lesion with the contrast agent (**b**). Blood pool imaging with autologous Tc-99m RBCs shows a non-filling center (**c**)

contraceptives [16]. Surgical resection is preferred when the nodule grows rapidly in size or becomes acutely symptomatic. Because both hepatic adenoma and FNH occur more frequently in young women during their child-bearing years and are often detected serendipitously on US or CT, done for unrelated reasons, proper management requires clear differentiation of adenoma from FNH before deciding on a specific form of therapy [17, 18]. Biopsy is not mandatory.

Adenomatosis (multiple small adenomas) is a distinct entity and behaves much differently from adenoma and focal nodular hyperplasia in terms of its clinical presentation. Adenomatosis occurs in both sexes, shows no association with oral contraceptives, and is associated with elevation of serum alkaline phosphatase and gamma glutamyl transpeptidase. Hemorrhage is uncommon, and it requires no specific form of therapy [19].

References

1. Baum JK, Holtz F, Brookstein JJ, et al. Possible association between benign hepatoma and oral contraceptives. Lancet 1973;2:926–929
2. Stauffer JQ, Lapinski MW, Donold DJ, Myers TK. Focal nodular hyperplasia of the liver and intrahepatic hemorrhage in young women on oral contraceptives. Ann Intern Med 1975;83:301–306
3. Mathieu D, Bruneton JN, Drouillard J, Pointreau CC, Vasile N. Hepatic adenoma and focal nodular hyperplasia: Dynamic CT study. Radiology 1986;160:53–58
4. Welsh TJ, Sheedy PF, Johnson CM, Stephen D, Charboneau JW, Brown ML, May GR, Adson MA, McGill DB. Focal nodular hyperplasia and hepatic adenoma: comparison of angiography, CT, US, and scintigraphy. Radiology 1985;156:593–595
5. Drane WE, Krasicky GA, Johnson DA, Radionuclide imaging of primary tumors and tumor like conditions of the liver. Clin Nucl Med 1987;12:569–582
6. Lubbers RP, Ros PR, Goodman ZD, Ishak KG. Accumulation of technetium-99m sulfur colloid by hepatocellular adenoma: scintigraphic pathologic correlation. Am J Roentgenol 1987;148:1105–1108
7. Kume N, Suga K, Nishigauchi K, Shimizu K, Matsunaga N. Characterization of hepatic adenoma with atypical appearance on CT and MRI by radionuclide imaging. Clin Nucl Med 1997:22;825–831
8. Knowles DM, Wolff M. Focal nodular hyperplasia of the liver, a clinicopathologic study and review of the literature. Human Pathol 1976;7:533–545
9. Biersack HJ, Thelen M, Torres JF, Lackner K, Winkler CG. Focal nodular hyperplasia of the liver as established by Tc-99m-sulfur colloid and HIDA scintigraphy. Radiology 1980;137:187–190
10. Rogers JV, Mack LA, Freeny PC, Johnson ML, Sones PJ. Hepatic focal nodular hyperplasia: angiography, CT, sonography, and scintigraphy. Am J Roentgenol 1981;137:983–990
11. Boulahdour H, Cherque D, Charlotte F, Rahmouni A, Dhumeaux D, Zafrani E, Meignan M. The hot spot hepatobiliary scan in focal nodular hyperplasia. J Nucl Med 1993;34:2105–2110
12. Kurtaran A, Muller C, Novacek G, Kaserer K, Mentes M, Raderer M, Pidlich J, Eibenberger K, Angelberger P, Virgolini I. Distinction between hepatic focal nodular hyperplasia and malignant liver lesions using technetium-99m-galactosyl-neoglycoalbumin. J Nucl Med 1997;38:1912–1915
13. Bernard EJ, Nicholls W, Howman-Giles R, Kan A, Stevens M. Tl-201 positive, Ga-67 negative hepatoblastoma: a case report of a 12-year-old boy. Clin Nucl Med 1997:22;835–837
14. Shuke N, Yoshikawa D, Saito Y, Sato J, Ishikawa Y, Yoshida H, Kino S, Miyokawa N, Aburano T. Focal nodular hyperplasia of the liver. Scintigraphic demonstration using three imaging agents. Clin Nucl Med 1999;24:451–453

15. Pain JA, Gimson AE, Williams R, Howard ER. Focal nodular hyperplasia of the liver: results of treatment and options in management. Gut 1991;32:524–527
16. Ross D, Pina J, Mirza M, Galvan A, Ponce L. Regression of focal nodular hyperplasia after discontinuation of oral contraceptives. Ann Intern Med 1976;85:203–204
17. Sandler MA, Petrocelli RD, Marks DS, Lopez R. Ultrasonic features and radionuclide correlation in liver cell adenoma and focal nodular hyperplasia. Radiology 1980;135:393–397
18. Sherlock S, Dooley J. Diseases of the liver and biliary system. Blackwell Science, Malden, MA, 1997, 10th edn, pp 337–369
19. Flejou J Barge J, Menu Y, Degott C, Bismuth H, Potet F, Benhamou J. Liver adenomatosis. An entity distinct from liver adenoma? Gastroenterology 1985;89:1132–1138

4.3 Hemangioma

Hemangiomas are the most common liver lesions, accounting for nearly 5–7% of all benign tumors [1]. They are congenital vascular malformations at birth that increase in size with the growth of the liver. Hemangiomas affect both sexes and occur at all ages, but manifest clinical symptoms usually in the 3rd–5th decades of life. They are relatively more common in women than in men, with a ratio of 4:1–6:1 [2]. They are more frequent in multiparous women and increase in size during pregnancy and after administration of estrogens [3].

Histopathology

Cavernous hemangioma is usually a solitary lesion consisting of multiple vascular channels, lined by a single layer of flat endothelial cells, and supported by an intervening fibrous tissue. They vary in size from few millimeters to several centimeters, some as large as 20–30 cm in size. Hemangiomas larger than 4 cm are referred to as giant cavernous hemangiomas. Most are sessile without a capsule and are located deep inside the superior part of the liver. Occasionally, a pedunculated lesion may be seen well separated from the main liver mass. Hemangiomas consist of a large blood pool, but show a decreased blood flow (ml gm^{-1} min^{-1}) through the lesion when compared to the adjoining normal liver tissue [4].

Clinical Presentation

Most hemangiomas are asymptomatic. In the past they were usually discovered at autopsy [2]. Today hemangiomas are discovered serendipitously while performing an ultrasound or CT scan of the abdomen, often when these imaging studies are obtained for assessment of other abdominal organs [5]. Large hemangiomas may cause abdominal pain because of compression of the adjoining organs or thrombosis within the lesion. Acute onset of severe abdominal pain may indicate hemorrhage.

Diagnosis

Most hemangiomas are discovered today during their asymptomatic phase with the ultrasound or CT as space-occupying lesions of the liver. The real challenge, therefore, is not one of discovery, but that of differentiation from other types of liver lesions, such as adenoma, focal nodular hyperplasia, primary or metastatic tumors. Blood pool imaging with Tc-99m RBC, contrast CT, MRI, and contrast angiography have been used for diagnosis [6–9]. Imaging with Tc-99m-labeled autologous red blood cells carries the highest specificity and is considered the diagnostic modality of choice for confirmation of hemangiomas [10].

Blood Pool Scintigraphy

Patient red blood cells are labeled with Tc-99m using an in-vitro method as described in detail in Chap 3.2. A rapid sequence perfusion study is obtained after injecting 15–30 mCi of autologous Tc-99m RBC (or Tc-99m pertechnetate for in vivo method) by collecting data at one frame/2 s for 60 s. Planar blood pool images in the anterior, posterior, and two lateral views are obtained after the perfusion study. Delayed images are obtained at 30 or 60 min by collecting at least 1 million counts per image. When not seen clearly in planar images by 60 min, SPECT imaging study is obtained between 1 and 2 h. The SPECT data are collected over a 360° rotation by obtaining 64 frames at 30 s/frame using a 64 × 64 × 8 matrix. After appropriate correction for camera nonuniformity and center of rotation deviation, the projections are reconstructed with the vendor-specific filtered back-projection algorithm. Transaxial, coronal, and sagittal slices are obtained with known pixel size to be able to measure size accurately. Images are recorded on 8 × 10-inch X-ray film.

Scintigraphic Features

A normal study (Fig. 4.3.1) clearly shows a blood pool in the abdominal aorta, inferior vena cava, two kidneys, liver, and spleen. Generally, the inferior vena cava is seen much more prominently than the aorta. The heart is the hottest organ in the chest, and the spleen is the brightest organ in the abdomen in the posterior view.

Hemangiomas typically show a decreased perfusion followed by delayed filling, reflecting their basic pathophysiology. Despite an enormous increase in the blood pool, blood flow (ml gm^{-1} min^{-1}) is generally reduced relative to surrounding normal liver tissue. Due to reduction in blood flow, mixing of radiolabeled RBC with the unlabeled RBC within the hemangioma occurs slowly over several minutes or hours, depending upon the size of the hemangioma. Very large hemangiomas are often missed when sufficient time is not allowed for complete mixing or equilibration, prior to acquisition of SPECT data. Giant hemangiomas are delineated better in delayed SPECT images obtained 2–4 h after injection of the labeled red blood cells.

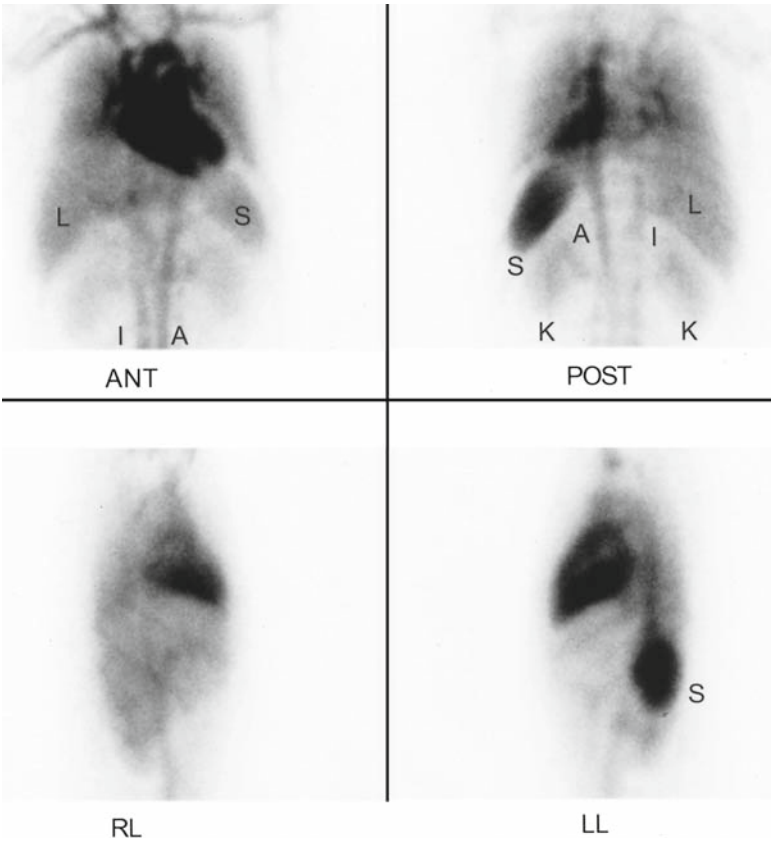

Fig. 4.3.1 Normal abdominal blood pool. Anterior (*ANT*) and posterior (*POST*) planar images show inferior vena cava (*I*), aorta (*A*), liver (*L*), spleen (*S*), and two kidneys (*K*). Liver appears faint in the right lateral (*RL*) view and spleen appears bright in the left lateral (*LL*) view

Small hemangiomas at the peripheral part of the liver equilibrate early and are seen faintly on planar blood pool images and become very clear on the SPECT images (Fig. 4.3.2). Complete equilibration with unlabeled RBC takes a much longer time as the size of the hemangioma increases. They manifest varied characteristics on the ultrasound and CT image. Many appear as hypodense on CT without contrast and become isodense (Fig. 4.3.3) or hyper-dense after the contrast. Some fill in only partially and others not at all. These varied features make it difficult to distinguish hemangioma from other benign and malignant liver lesions from a CT scan.

Giant hemangiomas often involve one complete segment or lobe of the liver (Fig. 4.3.4). Rapid sequence perfusion study shows markedly decreased blood flow, followed by delayed equilibration. Some may equilibrate only partially even at the end of 3–4 h and

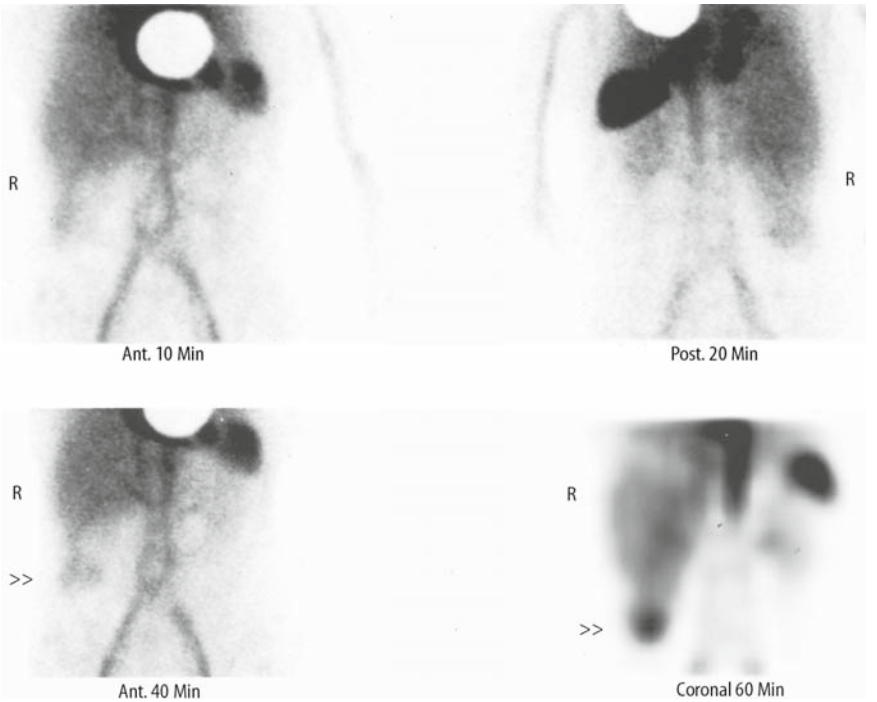

Fig. 4.3.2 Solitary hemangioma. Planar images at 10, 20, and 40 min show blood pool at the tip of the right lobe equal to that of the rest of the liver. Coronal SPECT image at 60 min clearly shows increased blood pool at the tip, establishing hemangioma

may require images at 18–24 h. Biopsy of such large lesions is a high risk procedure and should be avoided.

The sensitivity and accuracy of an imaging test depend very much on the size of the hemangioma. For lesions larger than 2 cm, the sensitivity and accuracy of Tc-99m RBC perfusion and SPECT blood pool imaging varies from 89 to 92% and 89 to 94%, respectively. For similarly sized lesions, MRI sensitivity varies from 85 to 100% and accuracy from 81 to 100% [10]. For lesions less than 2 cm, scintigraphic sensitivity is 58% and accuracy 60%, and MRI carries a sensitivity of 83% and accuracy of 84% (Table 4.3.1). As MRI often fails to differentiate hemangioma from hypervascular neoplasm or focal nodular hyperplasia, blood pool imaging with SPECT is considered as the method of choice for confirmation of hemangioma [6, 10]. Angiography is necessary only in those patients who do not show a blood pool pattern typical for hemangioma. Needle biopsy is avoided in most patients unless the lesion is small and the diagnosis is not confirmed from blood pool imaging. MRI with contrast may be

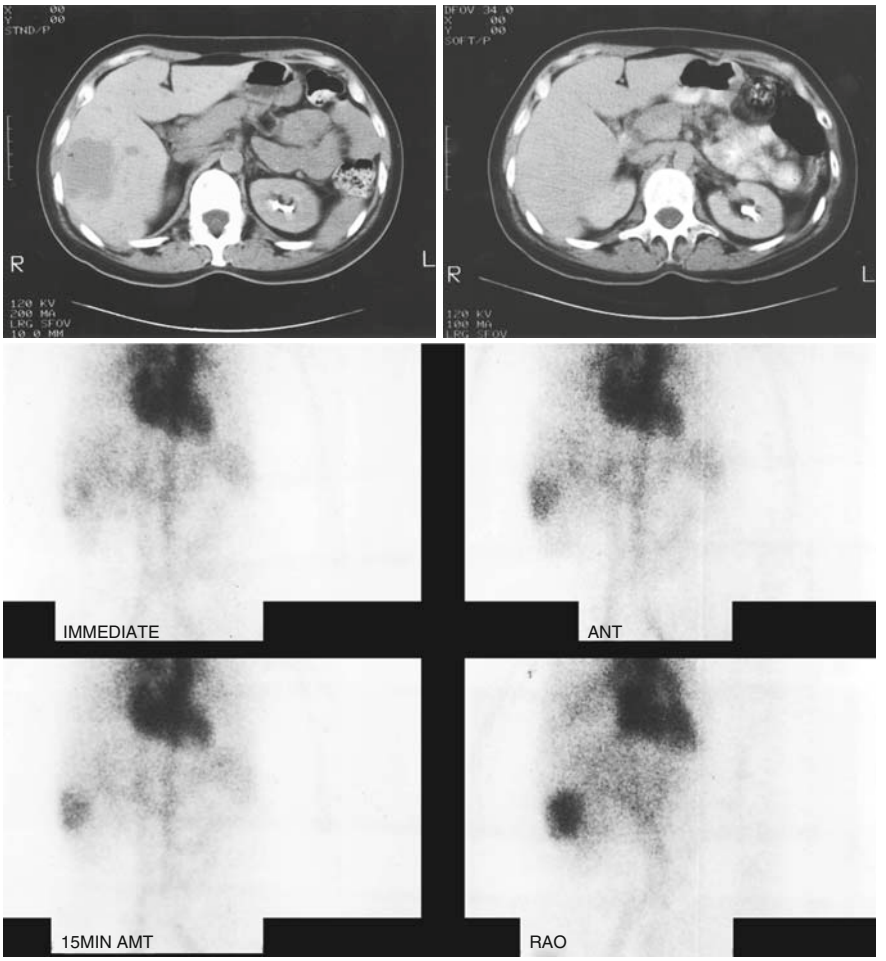

Fig. 4.3.3 Variable pattern hemangioma. A CT without contrast (*upper left*) shows a hypodense lesion in the right lobe that becomes isodense (*upper right*) after injection of the radiocontrast agent. Immediate planar Tc-99m RBC blood pool scintigraphy shows hemangioma faintly, which becomes much clearer at 5 and 15 min and in the right anterior oblique (*RAO*) view

preferred over angiography and needle biopsy for small lesions not seen on the blood pool study [10].

About 90% of hemangiomas are single, found in both hepatic lobes, and in the right lobe nine times more frequently than the left (Table 4.3.2). Most are situated along the superior margin of both lobes [11]. Multiple hemangiomas may involve both lobes at different locations (Fig. 4.3.5). The typical pattern of a "cold" lesion on blood flow and a delayed filling

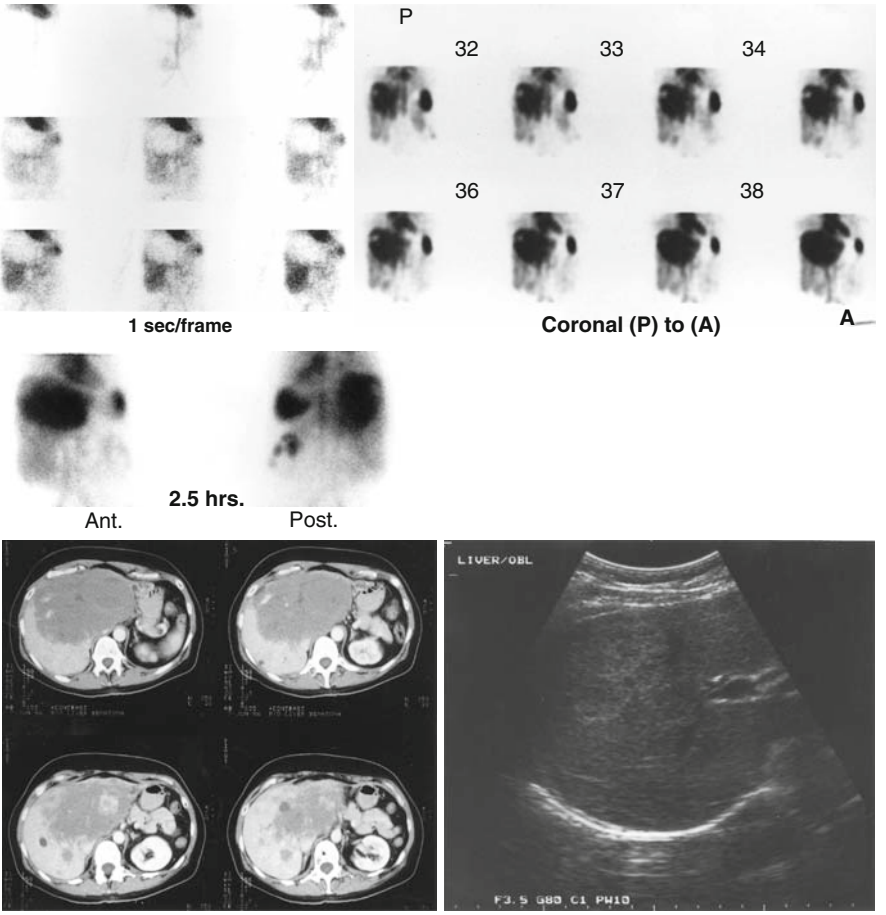

Fig. 4.3.4 Giant cavernous hemangioma. A perfusion scintigraphy (*upper left*) shows no blood flow through a giant hemangioma involving the superior part of the right lobe and the medial left lobe in a patient with breast cancer. Coronal view SPECT at 60 min shows hemangioma with a small supero-lateral region not yet equilibrated (*upper right*). An anterior (*ANT*) and posterior (*POST*) planar image at 2.5 h shows complete filling in of the hemangioma (*middle left*). A CT with contrast (*lower left*) shows a variable blood pool within the hemangioma and an ultrasound study (*lower right*) shows mixed hyper- and hypoechoic regions (courtesy of Dr. Ronald Hagelman, Tucson, AZ)

(hot) on the blood pool image is found in 66% of the hemangiomas. Others show atypical patterns of early incomplete and delayed complete filling. For lesions between 1 and 2 cm, SPECT increases sensitivity by 11% over planar images. On ultrasound examination, 59% appear as hyperechoic, 11% hypoechoic, and 30% show a mixed pattern.

Treatment

No treatment is required for most patients without symptoms. Lobectomy or segmentectomy is recommended for patients with recent onset of pain or with a rapidly expanding lesion [12, 13].

Table 4.3.1 Comparison of Tc-99m red blood cell SPECT and MR imaging in the diagnosis of hepatic hemangioma [10]

	Hemangioma size in cm (n = 64)		
	1.0–1.9 (n = 24)	2.0–2.9 (n = 13)	3.0–13.0 (n = 27)
SPECT			
No. positive (n = 50)	14	12	24
No. negative (n = 14)	10	1	3
Sensitivity (%)	58	92	89
Accuracy (%)	60	94	89
MR imaging			
No. positive (n = 58)	20	11	27
No. negative (n = 6)	4	2	0
Sensitivity (%)	83	85	100
Accuracy (%)	84	81	100

Table 4.3.2 Features of 130 hemangiomas [11]

Feature	Number (%)
Distribution	
Single	116 (89)
Multiple	14 (11)
Right lobe	118 (91)
Subdiaphragmatic	103 (87)
Left lobe	12 (9)
Superficial	109 (84)
Deep	21 (16)
Posterior	83 (64)
Anterior	47(36)
Scintigraphic features	
Typical filling pattern	86 (66)
Atypical filling pattern	44 (34)
Ultrasound features	
Hyperechoic	76 (59)
Hypoechoic	14 (11)
Mixed pattern	39 (30)

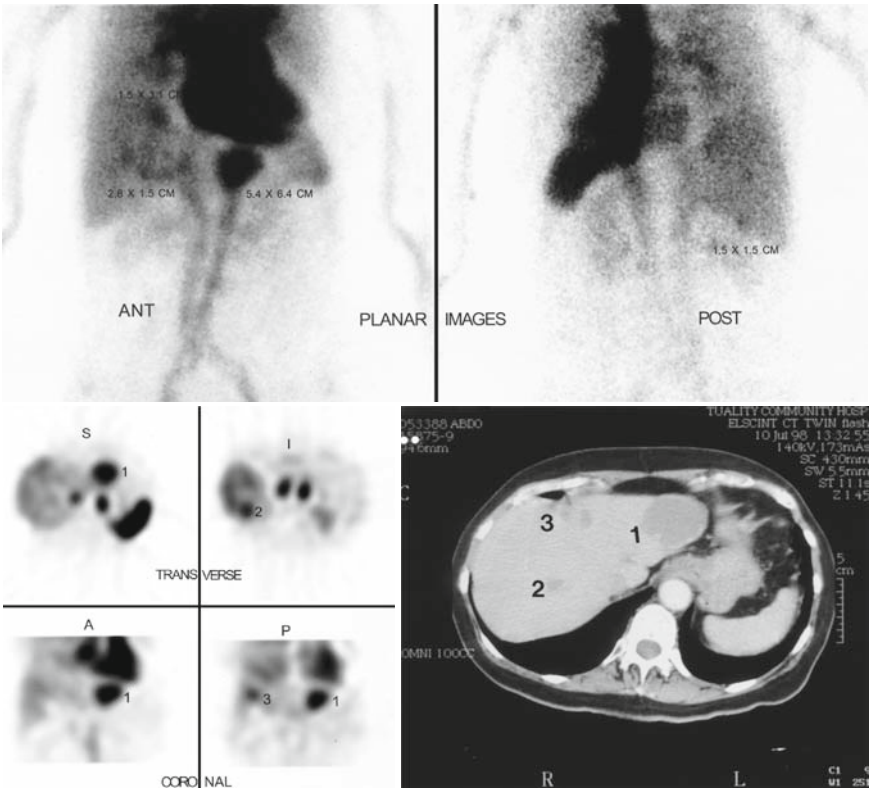

Fig. 4.3.5 Multiple hemangiomas. Anterior (*ANT*) and posterior (*POST*) view planar images (*top*) show three hemangiomas of variable sizes. Superior (*S*) and inferior (*I*) cut transverse SPECT images (*left bottom*) show one hemangioma in the left lobe (*no. 1*) and another in the posterior part of the right lobe (*no. 2*). Anterior (*A*) and posterior (*P*) coronal slices confirm no. 1 lesion, and the posterior slice shows an additional (*no. 3*) hemangioma. A CT with contrast agent shows three hypodense lesions. Only lesion no. 1 shows slight enhancement at the periphery

References

1. Ishak KG, Rabin L. Benign tumors of the liver. Med Clin North Am 1975;59:995–1013
2. Edmondson HA. Tumors of the liver and intrahepatic bile ducts. In: Atlas of tumor pathology. Section VII, Fascicle 25. Washington DC, Armed Forces Institute of Pathology, 1958, p 113
3. Kew MC. Tumors of the liver. In: Zakim D, Boyer TD (eds) Hepatology. A textbook of liver disease. WB Saunders, Philadelphia, 1996, p 1513

4. Taylor RD, Anderson PM, Winston MA, Blahd WH. Diagnosis of hepatic hemangioma using multiple radionuclide and ultrasound technique. J Nucl Med 1976;17:362–364
5. Sherlock S, Dooley J. Hepatic tumors. In: Diseases of the liver and biliary system.10th edn, Blackwell Science, Malden, MA 1997
6. Rabinowitz SA, McKusick KA, Strauss HW. Tc-99m red blood cell scintigraphy in evaluating focal liver lesions. AJR Am J Roentgenol 1984;143:63–68
7. Brodsky RI, Friedman AC, Maurer AH, Radecki PD, Caroline DF. Hepatic cavernous hemangioma: diagnosis with Tc-99m-labeled red cells and single photon emission CT. AJR Am J Roentgenol 1987;148:125–129
8. Bree RL, Schwab RE, Glazer GM, Fink-Bennett D. The varied appearance of hepatic hemangioma with sonography, computed tomography, magnetic resonance imaging and scintigraphy. RadioGraphics 1987;7:1153–1175
9. Whitney WS, Herfkens RJ, Jeffrey RB, McDonnell CH, Li KCP, Van Dalsem WJ, Low RN, Francis IR, Dabatin JF, Glazer GM. Dynamic breath-hold multiplanar spoiled gradient-recalled MR imaging with gadolinium enhancement for differentiating hepatic hemangiomas from malignancies at 1.5 T. Radiology 1993;189:863–870
10. Birnbaum BA, Weinreb JC, Megibow AJ, Sanger JJ, Lubat E, Kanamuller H, Noz ME, Bosniak MA. Observations on the growth of renal neoplasms. Radiology 1990;176:95–101
11. El-Desouki M, Mohamadiyeh M, Al-Rashed R, Othman S, Al-Mofleh. Features of hepatic hemangioma on planar and SPECT Tc-99m-labeled red blood cell scintigraphy. Clin Nucl Med 1999,24:583–589
12. Belli L, DeCarlis L, Beati C, et al. Surgical treatment of symptomatic giant hemangiomas of the liver. Surg Gyn Obstet 1992;174:474–478
13. Sinanan MN, Marchioro T. Management of cavernous hemangioma of the liver. Am J Surg 1989;157:519–522

4.4 Somatostatin Receptor Scintigraphy

Somatostatin Source

Somatostatin belongs to a multigene family peptide and is synthesized, stored, and released by many cells in the body [1]. Upon release from cells, somatostatin acts as an autocrine, paracrine, and endocrine hormone. Two forms of somatostatin are identified: one with 14 (Chap. 3, Fig. 3.4.1) and the other with 28 amino acids. The larger form is a dimer formed by the union of two shorter molecules, attached at the N-terminal end [2, 3]. The cells secreting somatostatin are distributed throughout the body. High concentration of somatostatin is found in the anterior pituitary, thyroid, lungs, liver, spleen, gastrointestinal tract, pancreas, kidneys, adrenal medulla, and paraganglions of the nervous system. Somatostatin-secreting cells were once called APUD (amine precursor uptake decarboxylation) cells and now have been renamed neuroendocrine cells [4].

Action of Somatostatin

In contrast to most hormones, which generally have a stimulatory effect on their target cells in the body, somatostatin has predominantly an inhibitory effect on its target cells. It is

a short peptide with a serum half life of less than 3 min. It inhibits secretion of: (1) growth hormone and thyrotropin from the anterior pituitary gland; (2) insulin, glucagon, and exocrine secretion from the pancreas; (3) gastrin, vasoactive intestinal polypeptide (VIP), secretin, and cholecystokinin from the gastrointestinal tract, and (4) hormones secreted by tumors arising from various organs (Table 4.4.1). By its ability to inhibit the production and release of the hormone, somatostatin either reduces or totally abolishes the hormonal effect on the target cells and often reduces the size of the primary and metastatic tumors. Other physiological actions of somatostatin include reduction of hepatic blood flow, inhibition of gallbladder contraction and bile emptying, and inhibition of gastrointestinal motility. It increases absorption of water and electrolytes from the intestine [5].

Somatostatin Receptors

Five subtypes of somatostatin receptors have been recognized [5]. Each subtype has its own chromosome location and manifests a different level of affinity for somatostatin uptake (Table 4.4.2). Normal organs that are seen faintly on a indium-111 pentetreotide (OctreoScan) scan include the lungs, anterior pituitary, and G-I tract, and the organs that are seen intensely include the thyroid, liver, and spleen (Fig. 4.4.1). Neuroendocrine

Table 4.4.1 Somatostatin receptor-positive tumors

Gastrinoma	Carcinoid
Insulinoma	Medullary thyroid cancer
Glucagonoma	Pituitary adenoma
Small cell lung cancer	Neuroblastoma
VIPoma	Paraganglioma
Cholangiocarcinoma	Meningioma
Pheochromacytoma	Motilinoma

Table 4.4.2 Characteristics of human somatostatin receptor subtypes [5]

Character	Subtype 1	Subtype 2	Subtype 3	Subtype 4	Subtype 5
Chromosome no.	14	17	22	20	16
G protein binding	+	+	+	+	+
Receptor affinity to:					
Somatostatin-14	+++	+++	++	++++	+++
Octretide	±	+++	++	±	++
Vapreotide	±	++	+	+	+++
Lantreotide	±	++	+	+	++++
Distribution in normal organs	Brain, lungs, stomach, jejunum, kidneys, liver, pancreas	Brain, kidneys, bile ducts	Brain, pancreas	Brain, lungs	Brain, heart, adrenals, pituitary, small-intestine, skeletal muscle

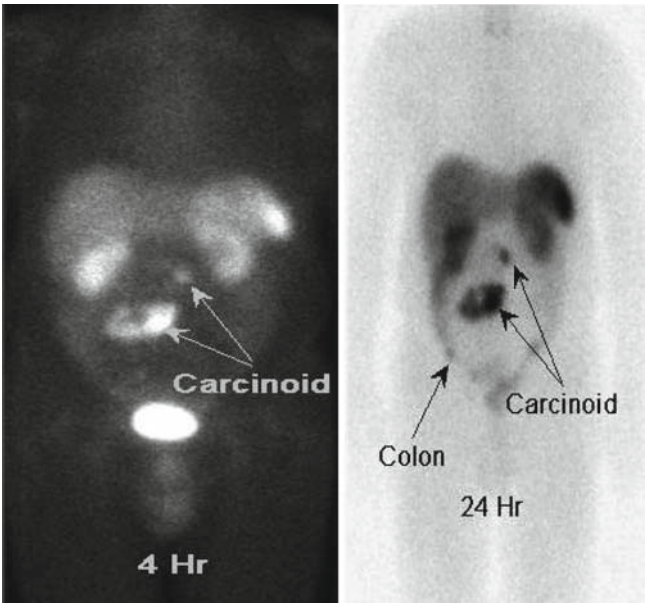

Fig. 4.4.1 Two foci of carcinoid tumor seen with In-111 OctreoScan. Both lesions seen in the 4-h image become much crisper in the 24-h image. Colon seen at 24 h represents bile and often makes it difficult to separate from the tumor

tumors with the heaviest concentration of somatostatin receptors and visible on In-lll pentetreotide (OctreoScan) scans are shown in Table 4.4.3.

Octreotide

Somatostatin with a serum half life of less than 3 min is unsuitable for diagnostic or therapeutic application. This problem is solved by making molecular substitution of its basic structure and creating somatostatin analogues of longer serum half life. The first successful synthetic compound was octreotide with eight amino acids. It behaves much like the parent hormone with 14 or 28 amino acids in inhibiting somatostatin secretion by the tumor. The serum half life of octreotide is about 2 h after a subcutaneous administration. In order to accomplish both the task of binding to the receptors and at the same time carry its physiological action, all somatostatin analogues must retain the basic loop structure and four receptor-binding amino acids, phenylalanine (Phe), tryptophan (Trp), lysine (Lys), and threonine (Thr). Octreotide differs from somatostatin in not only having only eight amino acids, but also by carrying D-Phe in place of -Phe. Vapreotide (RC-160) and lanreotide (BIM-23014) are newer synthetic analogues of somatostatin used in the treatment of somatostatin receptor-positive tumors [5].

Table 4.4.3 Somatostatin receptor positivity by in-vivo scintigraphy and in-vitro autoradiography [12]

Tumor type	In-vivo scintigraphy (%)	In-vitro autoradiography (%)
Meningioma	100	98
Paraganglioma	100	92
Small cell lung cancer	100	57
Hodgkin's disease	98	100
Carcinoid	95	88
Gastrinoma	93	100
Unclassified APUDoma	89	100
Neuroblastoma	89	65
Pheochromacytoma	87	73
Non-Hodgkin's lymphoma	83	87
Non-functioning pituitary adenoma	75	55
Pituitary GH producing tumor	70	98
Medullary thyroid cancer	69	38
Breast cancer	68	46
Insulinoma	46	67
Sarcoidosis	100	100
Tuberculosis	100	100
Rheumatoid arthritis	100	86

Radiolabeling of Octreotide

Octreotide was radiolabeled first with radioiodine I-123. The loop structure and three of the four receptor-binding amino acids were retained; the fourth receptor binding amino acid, phenylalanine, was replaced by tyrosine to enable easy radioiodination [6, 7]. The radiolabeling technique was cumbersome and the cost of production and delivery very high due to the short physical half life of I-123 (13 h). Because of these drawbacks, imaging did not become very popular clinically. Replacement of radioiodine I-123 with indium-lll appeared logical and was readily accomplished (Chap. 3, Fig. 3.4.1).

Indium-111 Pentetreotide (OctreoScan)

A bifunctional chelate, diethylenetriaminepentaacetic acid (DTPA), attaches to the ligand (octreotide) at one end and to the radiotracer indium-111 at the other end [8]. The loop structure and the four receptor-binding amino acids, Phe, D-Trp (in place of Trp), Lys, and Thr, are retained. To facilitate firm chelation with DTPA, Phe is replaced by D-Phe [9]. Following intravenous injection, In-111 pentetreotide (OctreoScan) distributes rapidly in the extravascular space with only 33% of the dose remaining in the intravascular pool at the end of 10 min and less than 1% at the end of 20 h. About 50% of the dose is excreted

in urine in 6 h, 85% in 24 h, and more than 90% in 72 h. A very small amount is secreted into bile, which is excreted in the stool, with about 2% of the dose in 72-h stool (Fig. 4.4.1). The biokinetics of In-lll pentetreotide differ slightly from those of C-14 octreotide. In rats, most of C-14 octreotide enters the liver to be excreted in bile [9], whereas most of In-lll pentetreotide enters the kidney to be excreted in urine [9, 10]. The usual scan dose of In-lll pentetreotide is 3–6 mCi bound to 10 μgm of the peptide. The biological half time of In-111 pentetreotide is about 6 h [9]. Soon after injection, most of In-111 is attached to the receptors on the surface of the cell. After about 6 h, 50% of the cell radioactivity gets internalized. Auto radiographic studies show that In-111 inside the cell remains with the cytoplasm and the nucleus of cultured cells from carcinoid and glucagonoma [11]. This feature indicates a therapeutic potential for In-lll pentetreotide.

OctreoScan Imaging Protocol

For patient preparation, discontinue therapy with somatostatin analogues for 24–48 h before injection and throughout imaging. Hydrate the patient with 16–24 oz of liquids just before and after the dose. For image acquisition, see Table 4.4.4.

Somatostatin Receptor-Positive Tumors

Successful detection of hepatic and extrahepatic somatostatin receptor positive tumors with In-lll OctreoScan depends upon several factors, including tumor size, histology, location, and receptor subtype within the tumor (Fig. 4.4.2). A clear distinction must be made between tumor somatostatin receptor content versus tumor positivity with In-lll OctreoScan.

Table 4.4.4 OctreoScan imaging protocol

Agent	In-lll pentetreotide
Dose	3 mCi for planar and 6 mCi for SPECT images
Route	Intravenous
Imaging time	4 and 24 h. Repeat at 48 or 72 h if necessary. SPECT images are taken at 4 h
Bowel preparation	Laxatives (Bisacodyl, fleet enema) before scan
Image acquisition parameters	
Gamma camera	Large field of view camera
Collimator	Medium energy parallel-hole collimator
Spectrometer settings	One set over 172 keV and the other over 245 keV energy with 20% window
Matrix	64 × 64 or 128 × 128 word matrix
Counts per image	300,000 for head and neck or 10-min image Chest and abdomen, each 500,000 counts or 10 min per view
SPECT protocol	
Matrix	64 × 64 or 128 × 128 matrix, 360° rotation, with 4 or 6°, 60–90 stops
Filter	Hemming or Wiener

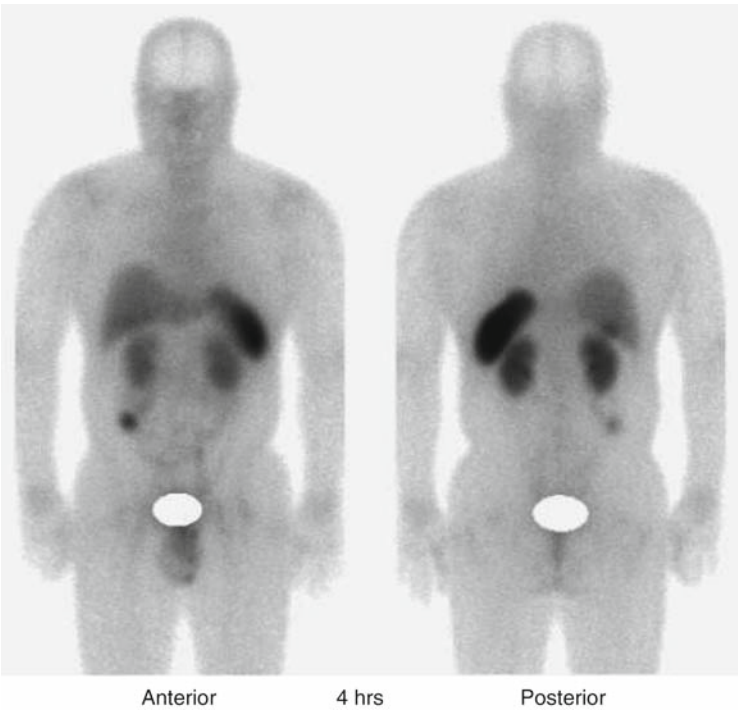

Fig. 4.4.2 Somatostatin receptor-positive neuroendocrine tumor with liver metastasis. Metastatic lesion in the liver is seen better in the posterior than in the anterior view. Note normal bowel activity with focal collection in the cecum mimicking a carcinoid lesion. Normal uptake is seen in the kidneys, liver, spleen, and genitalia

Tumors may have differing concentrations of receptor subtypes with varying affinity levels for somatostatin-14 or somatostatin-28 vs. In-lll pentetreotide (Table 4.4.2). Octreotide has a relatively higher affinity for receptor subtypes 2, 3, and 5 than for subtypes 1 and 4. Since In-lll pentetreotide differs in structure slightly from that of octreotide, it could have a slightly different affinity for tumor uptake than octreotide and may explain lower or higher rate of scintigraphic tumor detection rate in clinical studies.

Overall detection and localization of somatostatin receptor-positive tumors with In-lll pentetreotide scintigraphy alone vary from 98 to 100% for Hodgkin's disease, meningioma, lung cancer, and paraganglioma, 90–95% for gastrinoma and carcinoid, and 80–89% for pheochromacytoma and neuroblastoma [12]. The detection and localization of metastatic gastrinoma in the liver are 92% by In-lll pentetreotide scintigraphy alone compared to a sensitivity of 83% by multimodality imaging with ultrasound, CT, MRI, and contrast angiogram [13]. Overall, in-vivo scintigraphy shows an excellent correlation with in-vitro autoradiography, but wide variations are seen in a few specific types of tumors (Table 4.4.3). In vivo scintigraphy with In-lll pentetreotide often may show results much

better than those predicted from in vitro autoradiographic studies, suggesting a role for factors other than somatostatin receptor binding alone. Such findings are commonly seen in the case of carcinoid, small cell lung cancer, paraganglioma, neuroblastoma, pheochromacytoma, and medullary thyroid cancer. In the case of insulinoma, growth hormone-producing pituitary adenoma, and unclassified APUDomas, scintigraphy may detect lesions less often than predicted from autoradiographic results. Both planar and SPECT images are obtained early at 3–4 h when the likelihood of bowel activity due to bile is less (Fig. 4.2.1). Segmented bowel activity can mimic focal tumor, and SPECT images taken at a later time (beyond 4 h) may not be able to separate the two.

Several factors, both technical and physiological, contribute towards false-positive results, which occur in one in ten patients with Zollinger-Ellison syndrome [14]. High specificity of In-111 somatostatin receptor scintigraphy can be achieved by reducing false-positive results through clear understanding of the disease and circumstances that cause false-positive scans. An intrahepatic gallbladder may mimic hepatic metastasis by accumulating the radiotracer secreted into bile. An improvement in specificity aids in the proper management of patients. Planar images may identify only a few of the intrahepatic lesions, whereas SPECT may identify many more intrahepatic lesions (Fig. 4.2.3).

Radiation Dosimetry

Following intravenous injection, In-111 OctreoScan is distributed diffusely throughout the body. Good hydration and frequent urination reduce the radiation dose to the organs [15]. A dose of 3 mCi In-lll pentetreotide is sufficient for planar imaging, and a dose of 6 mCi is required for a SPECT study. SPECT imaging has now become a routine standard for achieving the best sensitivity and specificity of the test. SPECT of the chest, abdomen, and pelvis are obtained routinely. Kidneys are the critical organs receiving the largest dose, followed by the spleen, urinary bladder, and liver [16]. The radiation to the kidneys from a 6-mCi (222-MBq) dose is 11.4 rad (115.44 mGy). The effective dose equivalent is 2.28 rem 6 mCi (22.2 mSv 222^{-1} MBq). Internalization of In-lll into the cytoplasm and nucleus of the cells from carcinoid and glucagonoma from In-lll pentetreotide raises the therapeutic potential for In-lll [11].

Somatostatin receptor status of the tumor may have great impact on clinical diagnosis and management, especially in the selection of the type of therapy. Documentation of somatostatin receptor positivity can reduce the number and necessity of other diagnostic imaging tests. It is suggested that somatostatin receptor scintigraphy be used as the imaging modality of first choice in the case of gastrinoma because of its cost-effectiveness and also for its impact on patient management [17, 18]. Somatostatin receptor-positive tumors have been successfully treated medically with a combination of octreotide and prednisone [19]. Although somatostatin has been labeled with technetium-99m, it has not gained widespread clinical acceptance [20].

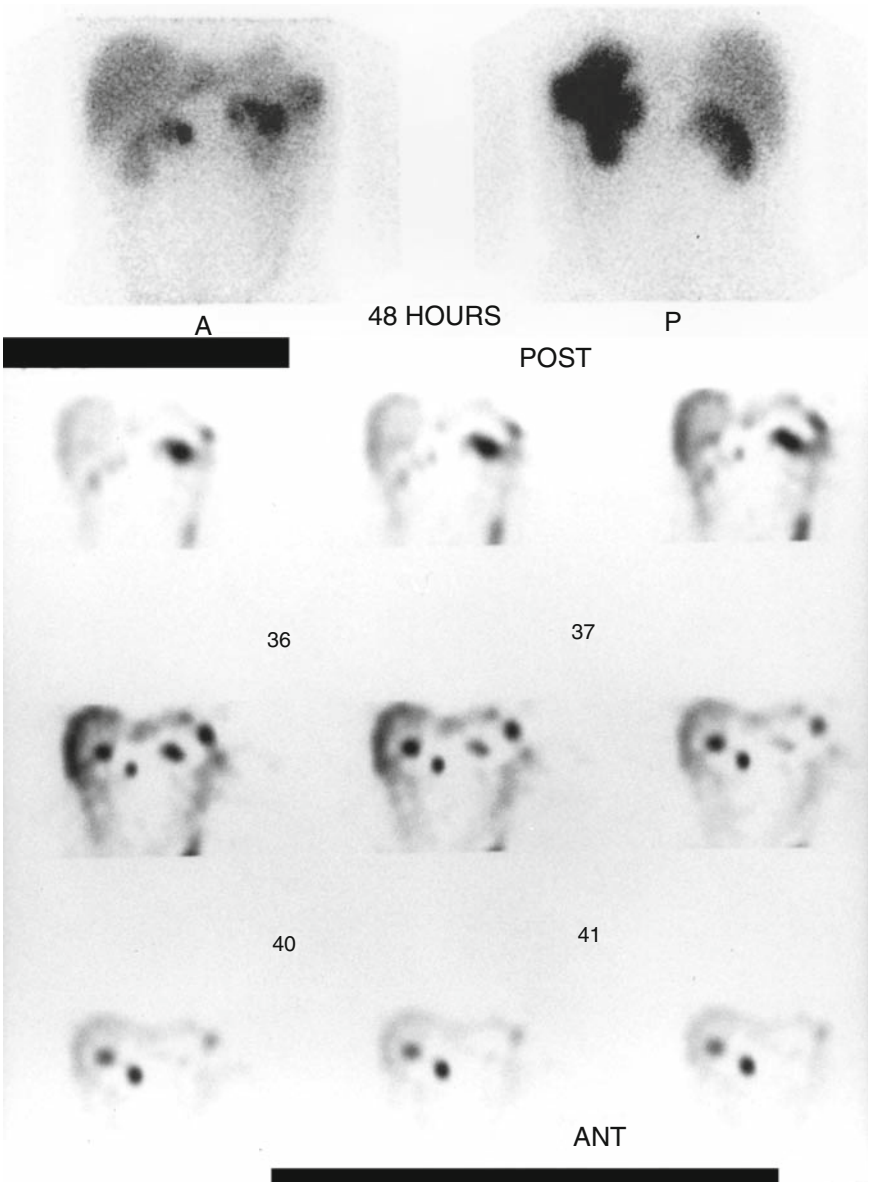

Fig. 4.4.3 Metastatic gastrinoma. Planar images (*top*) in the anterior and posterior view show lesions in parapancreatic and paragastric lymph nodes. Normal activity is seen in the kidneys and spleen. Coronal view SPECT images show (*bottom*) multiple intrahepatic lesions in the liver, not shown by planar images (*Post* = posterior; *Ant* anterior slices)

References

1. Krulich L, Dhariwal APS, McCann SM. Stimulatory and inhibitory effects of purified hypothalamic extracts on growth hormone release from rat pituitary in-vitro. Endocrinology 1968;83:783–790
2. Reichlin S. Somatostatin, part 1. N Engl J Med 1983;309:1495–1501
3. Reichlin S. Somatostatin, part 2. N Engl J Med 1983;309:1556–1563
4. Reubi JC, Kvols L, Krenning E, Lamberts SWJ. Distribution of somatostatin receptors in normal and tumor mice. Metabolism 1990;39:78–81
5. Lamberts SWJ, Vanderlely A, De Herder WW, Hofland LJ. Octreotide. N Engl J Med 1996;334:246–254
6. Krenning EP, Bakker WH, Breeman WAP et al. Localization of endocrine- related tumors with radioiodinated analogue of somatostatin. Lancet 1989;1:242–244
7. Kvols LK, Brown ML, O'Connor MK et al. Evaluation of a radiolabeled somatostatin analogue (I-123 octreotide) in the detection and localization of carcinoid and islet cell tumors. Radiology 1993;187:129–133
8. Krenning EP, Bakker WH, Kooiji PPM et al. Somatostatin receptor scintigraphy with indium-lll DTPA-D-Phe-1-octreotide in man. Metabolism, dosimetry, and comparisons with iodine-123-Tyr-3-octreotide. J Nucl Med 1992;33:652–658
9. Somatostatin receptor imaging for neuroendocrine tumors. Product monograph. OctreoScan. Mallincrodt Medical Inc. Mallincrodt Nuclear Medicine Division, St. Louis, MO, 1994
10. Krenning EP, Kwekkeboom DJ, Bakker WH, et al. Somatostatin receptor scintigraphy with (In-lll -DTPA-D-Phe-1) and (I-123-Tyr-3)-octreotide: the Rotterdam experience with more than 1,000 patients. Eur J Nucl Med 1993;20:716–731
11. Andersson P, Forssel-Aronsson E, Johanson V, Wangberg B, Nilsson O, Fjalling M, Ahlman H. Internalization of indium-lll into human neuroendocrine tumor cells after incubation with indium-lll-D-Phe-1-octreotide. J Nucl Med 1996;37:2002–2006
12. Krenning EP, Kwekkeboom DJ, Pauwels S, Kvols K, Reubi JC. Somatostatin receptor scintigraphy. In: Freeman LM (ed). Nuclear medicine annual 1995. Raven Press Ltd, New York, 1995, pp 1–50
13. Gibril F, Reynolds JC, Doppman JL, Chen CC, Venzon DJ, Tremanini B, Weber HC, Stewart CA, Jensen RT. Somatostatin receptor scintigraphy: its sensitivity compared with that of other imaging methods in detecting primary and metastatic gastrinoma. A prospective study. Ann Intern Med 1996;125:26–34
14. Gibril F, Reynolds JC, Chen CC, Yu F, Goebel SU, Serrano J, Doppman JL, Jensen RT. Specificity of somatostatin receptor scintigraphy: a prospective study and effects of false-positive localization on management in patients with gastrinomas. J Nucl Med 1999;40539:553
15. Yamada T, Niinuma K, Lemaire M, Terasaki T, Sugiyama Y. Mechanism of the tissue distribution and biliary excretion of the cyclic peptide octreotide. J Pharmacol Expt Ther 1996;279:1357–1364
16. Stabin MG, Kooji PPM, Bakker WH, Inoue T, Endo K, Coveney J, deJong R, Minegishi A. Radiation dosimetry for indium-111-pentetreotide. J Nucl Med 1997;38:1919–1922
17. Termanini B, Gibril F, Reynolds JC, Doppman JL, Chen CC, Stewart CA, Sutliff VE, Jensen RT. Value of somatostatin receptor scintigraphy: A prospective study in gastrinoma of its effects on clinical management. Gastroenterology 1997;112:335–347
18. Jamar F, Fiasse R, Laners N, Pauwels S. Somatostatin receptor imaging with indium-lll-pentetreotide in gastroenteropancreatic neuroendocrine tumors: Safety, efficacy and impact on patient management. J Nucl Med 1995;36:542–549

19. Palmieri G, Lastoria S, Colao A, Vergara E, Varrella P, Biondi E, Selleri C, Catalano L, Lombardi G, Bianco AR, Salvatore M. Successful treatment of a patient with a thymoma and pure red-cell aplasia with octreotide and prednisone. N Engl J Med 1997;336:263–265
20. Vallabhajosula S, Moyer BR, Lister-James J, McBride BJ, Lipszyc H, Lee H, Bastidas D, Dean RT. Preclinical evaluation of technetium-99m-labeled somatostatin receptor-binding peptides. J Nucl Med 1996;37:1016–1022

Imaging and Quantification of Hepatobiliary Function

5

5.1 Hepatobiliary Imaging

The liver is one of the most frequently imaged organs in the body, using ultrasound, CT, MRI, or scintigraphy. The first three imaging techniques depend upon morphological changes to detect disease, whereas scintigraphy uses both morphological and physiological changes to discover liver pathology. Since physiological changes usually precede morphological alterations by several weeks or months, there is great potential for early diagnosis by scintigraphy, well before irreversible functional changes take place. Once very popular, imaging with radiocolloids now has been almost completely replaced by quantitative hepatobiliary functional imaging with Tc-99m HIDA [1].

Functional studies are obtained with the protocol outlined in Table 5.1.1, by using any one of several Tc-99m-HIDA agents that delineates the entire hepatobiliary tree as it travels from the hepatocyte to enter the duodenum (Chap. 3). Time of appearance of various normal biliary structures depends upon many factors, of which the tonus of the sphincter of Oddi plays the major role[2]. Following intravenous injection of Tc-99m-disofenin or Tc-99m-mebrofenin, the liver peak uptake is reached within 10 min, and the common bile duct is seen by 20 min. Both the gallbladder and small intestine are seen within 30 min in the great majority of patients (Table 5.1.2). Some patients show a reciprocal relationship between the time of appearance of the gallbladder and small intestine, with the intestine appearing late when the gallbladder appears early and vice-versa. Normally about 50% of gallbladders are seen within 15 min, 90% within 30 min, and 95% within 50 min. In the remaining 5%, gallbladders appear between 50 and 60 min after injection of the radiotracer [3].

Identification of Lobes, Segments, and Areas from Tc-99m-HIDA Images

Physiologically, the liver is divided into three lobes (including the caudate lobe), four segments, and eight areas (Fig. 5.1.1). The right lobe is divided into anterior and posterior segments, and the left lobe into medial and lateral segments. The right and left branches of the portal vein travel through the middle of the liver in opposite directions and divide the liver into superior and inferior areas. The right and left lobe each consists of four areas. The caudate lobe is situated along the superior margin of the posterior surface and is considered an independent lobe because of its unique blood supply. Its veins drain blood directly into the inferior vena cava.

G.T. Krishnamurthy and S. Krishnamurthy, *Nuclear Hepatology,*
DOI 10.1007/978-3-642-00648-7_5, © Springer-Verlag Berlin Heidelberg 2009

Table 5.1.1 Hepatobiliary imaging protocol

Patient preparation	Patient should fast overnight (6–10 h optimal), minimum 4 h and maximum 24 h. Routine pre-emptying of the gallbladder with cholecystokinin is unnecessary and should be avoided. Pre-emptying may be needed only when the patient is fasting for longer than 24 h or on parenteral nutrition. When a pre-emptying protocol is used, one should wait for 60 min after CCK-8 to begin hepatic phase imaging with Tc-99m-HIDA
Agent	Tc-99m-mebrofenin or Tc-99m-disofenin
Dose	2–4 mCi for serum bilirubin less than 2 mg% 5–8 mCi for serum bilirubin 3–10 mg% 10 mCi for serum bilirubin greater than 11 mg%
Children	200 μCi kg^{-1} (minimum 1 mCi)
Position	Supine
Camera	Large field of view dual-head gamma camera
Collimator	Low energy, all purpose, parallel hole
Window	20% at 140 keV photopeak
Matrix	128 × 128 × 16
Computer data acquisition	Data acquisition is separated into two parts: (1) Hepatic phase and (2) gallbladder phase
Hepatic phase	Obtain 1 frame 2 s^{-1} for 30 frames (first minute) and 1 frame per min for 59 min (total 60 min). Obtain a right lateral view when gallbladder appearance is not certain at 60 min
Gallbladder phase	1 frame per min for 30 min (61–90 min) Beginning at 5 min, CCK-8 is infused at a dose rate of 3 ng kg^{-1} min^{-1} for 10 min through an infusion pump

Table 5.1.2 Time of appearance of normal common bile duct, gallbladder, and small intestine

Appearance of the common bile duct within 20 min		100%
Appearance of the gallbladder:	within 15 min	50%
	within 30 min	90%
	within 50 min	95%
	within 60 min	100%
Appearance of the small intestine within 60 min		80%

Division of the liver into physiologic right and left lobes is currently preferred over anatomic division because it serves as a useful boundary line during surgical resection of the liver. The lobes, segments, and areas are identified on an anterior, right lateral, and posterior view image, much like identifying the lobes and segments of a lung from a perfusion scan. Obstruction of a segment or an area bile duct is seen as bile stasis over the corresponding region, similar to identifying a lack of perfusion of a lobe or segment in a lung scan due to pulmonary embolism. The numbers shown in Fig. 5.1.1 are adopted from Table 1.1.1 of Chap. 1, as developed by different authors over the years. Healy and Schroy suggested a directional nomenclature after careful dissection of nearly 100 cadaver livers [4].

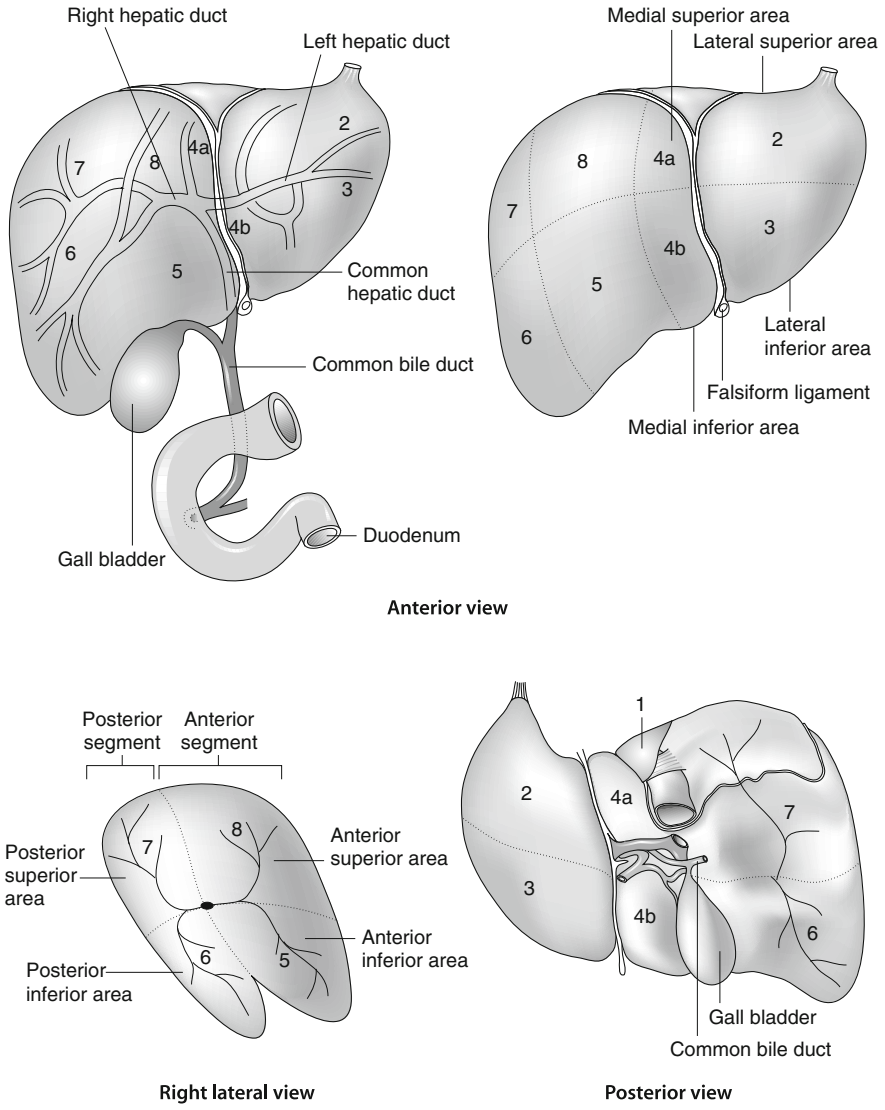

Fig. 5.1.1 Biliary anatomy. The bile ducts from the medial (*nos. 4a, 4b*) and lateral (*nos. 2, 3*) segments of the left lobe unite to form the left hepatic duct (*LHD*) and are seen separately in an anterior image. The ducts from the anterior (*nos. 5, 8*) and posterior (*nos. 6, 7*) segments of the right lobe join to form the right hepatic duct (*RHD*), and a right lateral view is required to separate them and their branches. RHD and LHD unite to form the common hepatic duct, which in turn forms the common bile duct after joining with the cystic duct from the gallbladder. The caudate lobe in the posterior view is usually obscured by photon attenuation by vertebral bodies

The medial segment of the physiologic left lobe (4a, 4b) forms a part of the right lobe when the liver is divided morphologically into right and left lobes on the basis of the attachment of the falciform ligament. The caudate lobe (no. 1) is posterior in location, but usually not seen on a posterior view image due to attenuation of photons by the vertebrae. The inferior area of the medial segment of the physiologic left lobe (4b) is often referred to as the quadrate lobe.

There are many variations in the manner in which the segmental ducts unite to form lobar ducts. The right hepatic duct is formed by the union of its anterior and posterior segmental ducts and the left hepatic duct by the union of its medial and lateral segmental ducts in 72% of the patients. The posterior segmental duct from the right lobe joins the left hepatic duct directly in 22% of patients. In the remaining 6%, the anterior segmental duct from the right lobe joins with the left hepatic duct directly [4]. It is very rare for the bile from either the medial or lateral segmental duct of the left lobe to drain directly into one of the segmental ducts of the right lobe (Fig. 1.1.4, Chap. 1).

The distal 0.5–1.5 cm of the right and left hepatic ducts, and the entire common hepatic and common bile ducts are outside of the liver parenchyma (extrahepatic), although they may appear as intrahepatic in an anterior view Tc-99m-HIDA study. This apparent depiction is due to extension of the inferior liver border in front of these ducts. The common hepatic duct usually measures about 2-7 cm, and the common bile duct is about 7-17 cm in length. The total length of the common duct (common hepatic plus common bile ducts) from its origin at the union of the right and left hepatic ducts to its termination into the duodenum varies from 10 to 20 cm. On a Tc-99m-HIDA image, however, total length of the common duct measures about 6.6 ± 1.3 cm [3]. This foreshortening is caused by the position of the gamma camera (placed anteriorly) and its relationship with the direction of the common hepatic and common bile duct.

Duct Asymmetry

Asymmetry in appearance of the right and left hepatic duct is common on cholescintigraphy. Normally, the left hepatic duct appears much more prominent than the right in 55% of the subjects; the right hepatic duct is more prominent than the left in 13%, and both ducts appear as equal in 10% of the subjects (Table 5.1.3). In the remaining 22% of the subjects, neither duct is seen because of rapid bile flow through a lax sphincter of Oddi [3]. Several reasons are offered for duct asymmetry, including: (1) a more anterior location of the left liver lobe than the right, (2) a more anterior location of the left hepatic duct in comparison to the right

Table 5.1.3 Variations in the appearance the normal right and left hepatic ducts

Left hepatic duct more prominent than right hepatic duct	55%
Right hepatic duct more prominent than the left hepatic duct	13%
Right hepatic duct = left hepatic duct	10%
Neither duct seen clearly	22%

hepatic duct, (3) a variant bile flow pattern where either the posterior or the anterior segmental duct from the right lobe drains bile directly into the left hepatic duct, (4) an undivided portion of the left hepatic duct is twice as long as the right duct and hence prone to tortuosity, impeding bile flow through it, and (5) a short right hepatic duct that lies in direct line with the common hepatic duct offers less impedance to bile flow through it. A slower bile flow allows relatively more counts to accumulate in the image to manifest as an apparent prominence.

Hepatobiliary studies are usually carried out 4–10 h after the fast, which establishes the basal state. Fasting less than 4 h or more than 24 h is avoided. Cholecystokinin reaches its lowest serum level during fasting, promoting maximum increase in the tonus of the sphincter of Oddi and maximum relaxation of the smooth muscle of the gallbladder wall. Acting together, both of these factors promote rapid filling of the gallbladder to its normal volume of 50 ml. The liver normally secretes about 600 ml bile per day (0.4 ml min^{-1}) continuously, of which about 70% (0.3 ml min^{-1}) enters the gallbladder, and the remaining 30% (0.1 ml min^{-1}) enters the duodenum directly during fasting [5, 6]. A fully filled gallbladder is still able to accommodate this constant inflow of hepatic bile (0.3 ml min^{-1}) by absorbing an equal volume of water through the wall. The lateral intercellular spaces between the columnar epithelial calls are kept widely open during fasting, allowing free passage of water from the gallbladder lumen into the interstitium. Fasting for less than 4 h results in either non-visualization or low Tc-99m-HIDA counts within the gallbladder because of the preferential flow of bile directly into the duodenum through a lax sphincter of Oddi.

Effect of Food Intake on Uptake and Excretion of Tc-99m-HIDA

Physiological changes that take place soon after a meal affect some of the functional parameters obtained with Tc-99m-HIDA study and should be taken into account during data interpretation. In the immediate postprandial state, time to peak hepatic uptake of Tc-99m-HIDA decreases compared to studies performed after 6–10 h of fasting (Fig. 5.1.2). These changes are attributed to an increase in postprandial liver blood flow and faster extraction of Tc-99m-HIDA by the liver [7]. The radiotracer also clears from the liver parenchyma much more rapidly in the immediate post-prandial state, which is attributed to an increase in ductal bile flow induced by endogenous release of secretin, cholecystokinin, and other gastrointestinal hormones. Faster uptake combined with rapid liver clearance shifts the peak of the hepatic curve to an earlier time. The gallbladder does not fill in because of its contraction induced by post prandial release of endogenous cholecystokinin. When the gallbladder is the organ of interest for study, it is essential to maximize hepatic bile entry into it by fasting for at least 8–10 h, when both the absorption of water through the wall and the tonus of the sphincter of Oddi are at their peak [8]. Longer duration of fasting provides much better counting statistics because of preferential entry of Tc-99m HIDA mixed hepatic bile into the gallbladder [9]. Fasting longer than 24 h has an adverse effect on gallbladder filling because of the formation of bile sludge, which decreases water absorption through the wall.

Quantification of Liver Function

Besides providing an excellent morphology of the entire hepatobiliary system, imaging with Tc-99m-HIDA enables simultaneous quantification of liver and gallbladder function

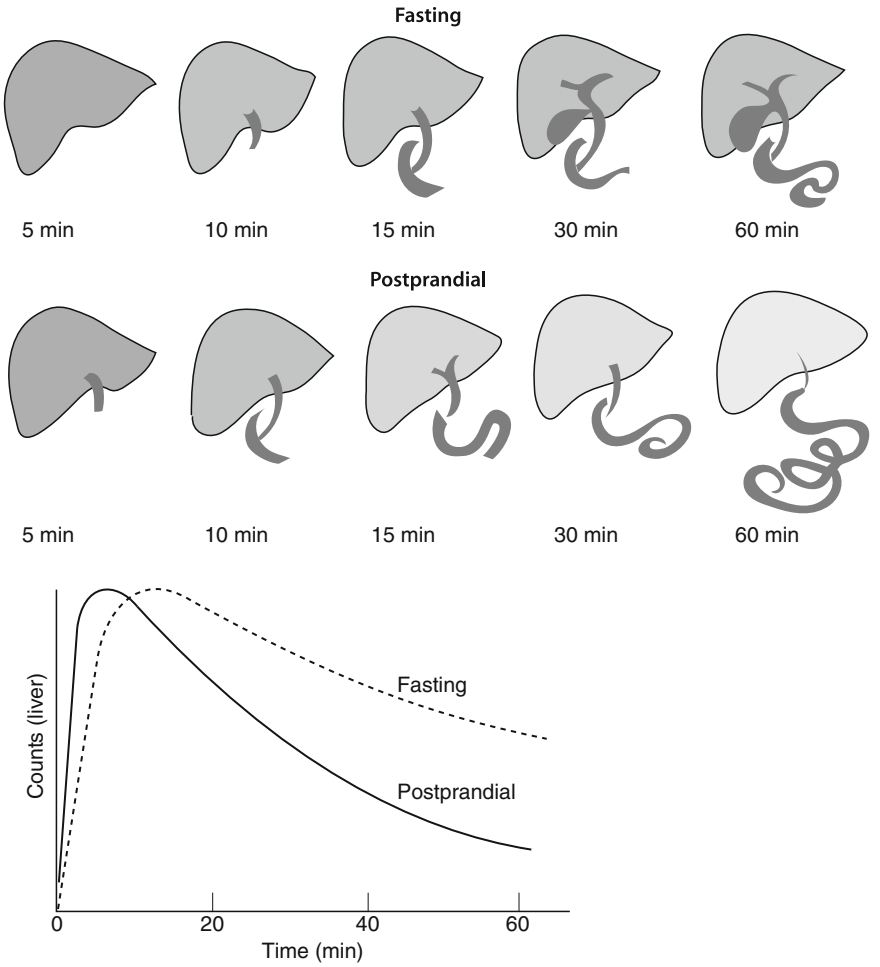

Fig. 5.1.2 Effect of feeding on the kinetics of Tc-99m-HIDA: In the fasting state (*top*), increased tonus of the sphincter of Oddi diverts more of the hepatic bile into the gallbladder than intestine. There is residual radioactivity in the liver at 60 min. In the post-prandial state (*bottom*), there is more rapid hepatic uptake and excretion, shifting the peak of the curve to an earlier time, and very little residual radioactivity remains in the liver beyond 15 min. The gallbladder does not fill in because of a lax sphincter

as an integral part of imaging. Traditionally, the liver function is monitored by obtaining the serum level of various substances produced by the liver, including albumin, bilirubin, alkaline phosphatase, and transaminase. Serum levels are indirect indicators of liver function and are influenced by the status of the cardiac and renal function, and hence may not reflect accurately the hepatocyte function in the presence of heart or kidney failure. Measurement of radioactivity emitted from the liver serves as a direct indicator of the physiological status of the hepatocyte, which is unaffected by renal function [10]. The biokinetic pathway

of Tc-99m-HIDA involves several steps before its elimination from the liver into the small intestine (Chap. 3.1). Quantification of function allows differentiation of hepatocyte from biliary disease. New FDA-approved software called Krishnamurthy Hepato-Biliary Software (KHBS) is now available for quantification of liver and gallbladder function and can be loaded onto a PC. It has seven main components for analysis: Hep-function, HEP-segments, HEP-static, GB-function, GB-segments, GB-static, and HPS (hepatopulmonary syndrome). Setup block allows entering local parameters and the option to edit images. GB-phase parameters are entered for CCK-8 and fatty meal stimulation (Fig. 5.1.3). Hepatic extraction fraction and excretion half time are two of the functional parameters measured routinely as an integral part of hepatobiliary imaging [1]. Hepatic extraction fraction measures the integrity of the basolateral border, and excretion halftime reflects intracellular transit from the basolateral border to the canalicular border, secretion into canaliculi, and flow through the small and large bile ducts.

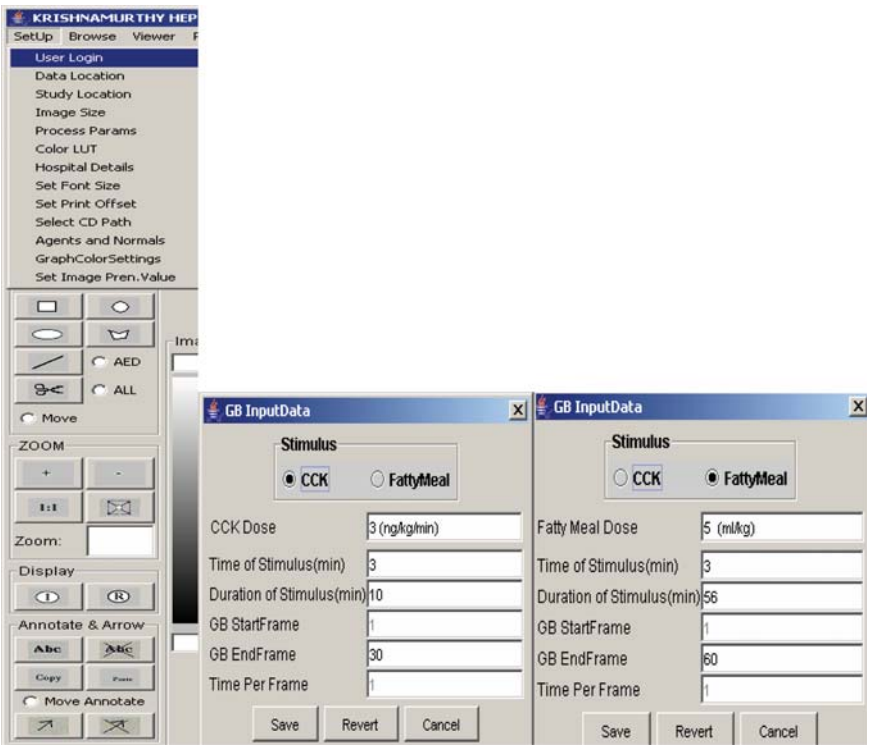

Fig. 5.1.3 Setup and GB-input data for KHBS. Activation of the setup block provides the option to enter desired parameters pertaining to local need. User login, data location (or study location), image size, color option, hospital details, font size, agents, and normals, etc., are entered into the SetUp menu once for permanent storage. Images can be resized with magnification or minimizing buttons. Annotation and move option are available for image editing for report or for power point presentation. Gallbladder parameters are changed depending upon CCK-8 or fatty meal stimulus

5

Hepatic Extraction Fraction (HEF)

Studies are acquired as the patient lies in the supine position underneath a large field of view dual-head gamma camera, and the data are collected as described in Table 5.1.1. Both Hep-phase and gallbladder-phase data are transferred from the gamma camera terminal to the PC where KHBS is located. By activating the browse button, data location is identified, and both phase image data of a patient are uploaded onto KHBS. Report block at the top creates desired images for interpretation. The perfusion, HEP-phase, GB-phase, and multiple image presentation formats are changed to meet local preference. The perfusion part of the study is analyzed subjectively using 30 frames of the first minute data. HEP-function block at the top of the screen is then activated. The software sums up the first 30-frame perfusion data, labels it as frame one, and uses the remaining 59 min frames (total 89 frames) for assessment of the liver function. When interrupted data are acquired, instead of continuous data, the HEP-static format is activated for image presentation.

After activating the HEF-function block at the top, seven regions of interest (ROI) are drawn, one each over the heart, background (spleen), right lobe, left lobe, gallbladder, stomach, and intestine, as shown at the bottom of the screen (Fig. 5.1.4). Each ROI consists of at least 50–75 pixels. Heart and background regions are usually drawn on the first minute frame. The heart ROI may include one or both ventricles. Background is drawn over the spleen. Raw data curve from each ROI is displayed instantly after completion of the ROI. Often intestinal activity may overlay the spleen region in later images and give a false background. Normally, the spleen curve parallels the heart curve when there is no intestinal overlap. A different background region is chosen if there is intestinal overlap of the spleen. The liver ROIs include only the parenchyma of the superior right lobe and left lobe, and are usually drawn on the 10- to 20-min frames when ducts become visible. Care is taken to avoid inclusion of heart or bile ducts with the liver ROI. Superior and right lateral liver margins, and gallbladder, which move in and out of the ROI during deep inspiration or upon coughing, are excluded from the liver ROIs. The spleen, which appears clearly in the first minute summed frame, disappears in the later frames. Stomach, gallbladder, and intestinal ROIs are usually drawn on the last (60-min) frame. After selecting all ROIs, the entire 60-min study is reviewed in cine mode to ensure separation of the regions of interest. Regions of interest are altered if there is superimposition by other structures. After checking all seven ROIs for accuracy, the HEP-function result block is activated to obtain the result (Fig. 5.1.5).

The software first smoothes the liver curves and then subjects them to deconvolution. The liver true response curve is deconvoluted from the input (heart) and output (liver) curve using Fourier transformation. Since the hepatic curve represents the sum of counts from the hepatocyte and hepatic blood pool, the deconvolution corrects for hepatic blood pool [11]. A smoothed decreasing long tail in the shape of one-half of a cosine wave is appended to the end of the input and output curves. This long tail avoids errors due to abrupt data termination at 30 min. The append begins at the 30th frame and falls to zero at the 128th added frame, giving approximately six times the duration of acquisition [12]. Duration of such a length is a minimum required to avoid artifacts in the deconvolution process. The formula for the appended tail in frame i of the heart or liver curve is given by:

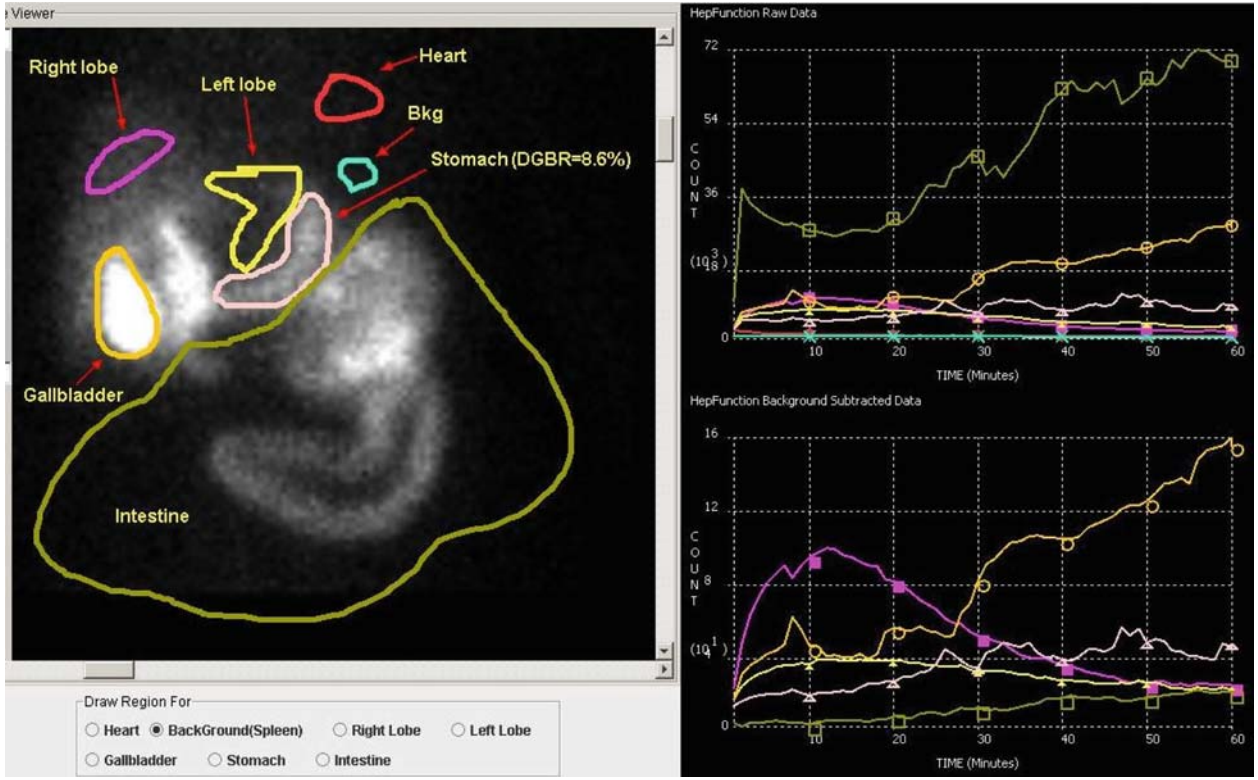

Fig. 5.1.4 Hepatic phase ROIs. Heart and background (*Bkg*) regions of interest are chosen on the first-minute frame. Right and left lobe ROIs are drawn over the liver parenchyma in 10-20-min frame by excluding bile ducts. Gallbladder, stomach, and intestinal ROIs are drawn on the last 60-min frame. *Curves* on the *right* represent the *same color* ROIs on the *left*

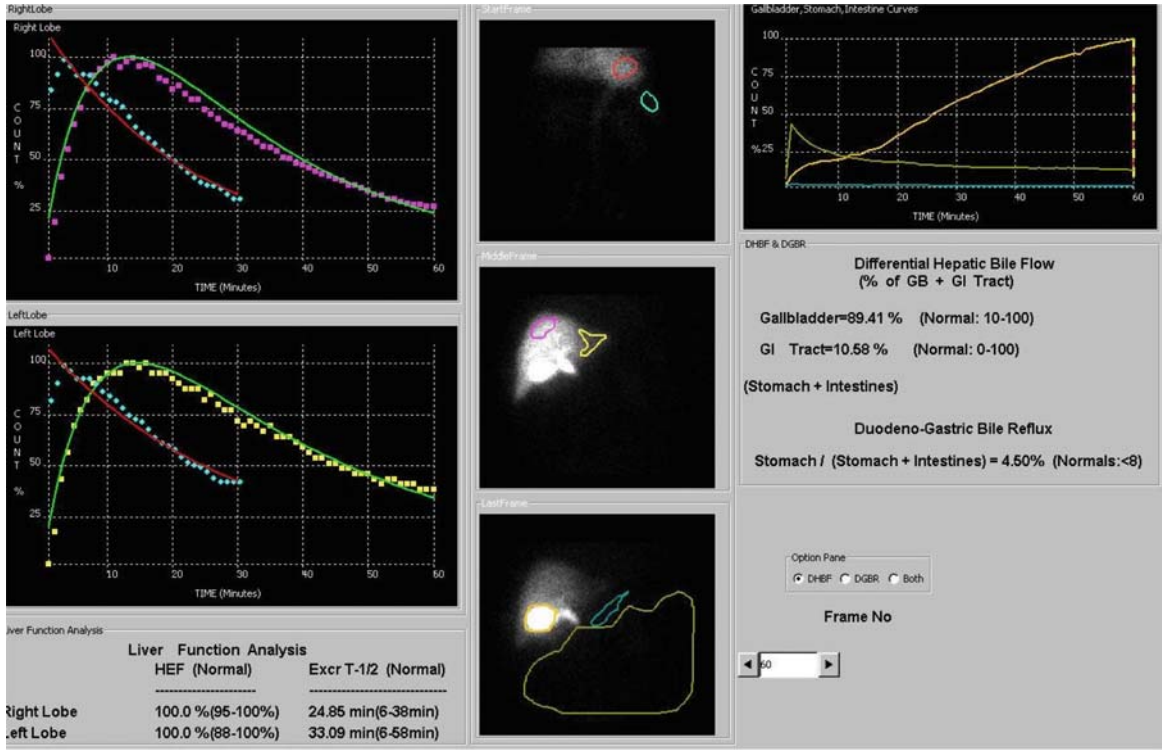

Fig. 5.1.5 Results of Hep-phase: Hepatic extraction is calculated by deconvolutional analysis using the heart for the input and liver for the output function. The excretion half time is measured by non-linear least-square fit using spleen as the background. Excretion *T1/2* is slightly longer for the left than the right liver lobe (statistically not significant). Basal differential hepatic bile flow and DGBR values are shown on the *right*. *Middle panel* shows the ROIs for each structure to check for accuracy

$$\text{Tail} = 0.5 \times \text{AMP} \times (\text{Cos}[\pi \times (\text{i} - 30)(128 - 30)] + 1)$$

where $i = 30–128$, and AMP is the heart or liver curve value (counts per pixel) at frame 30.

The hepatic extraction fraction (HEF) is the ratio of the Y intercept of the exponential fit to the maximum data point in the liver response curve. The exponential fit is by linear least square, working in reverse from 30 min to the first frame, which visually departs significantly from the exponential fit. HEF is calculated by the following equation.

$$\text{Hepatic Extraction Fraction}\,(\text{HEF}) = \frac{\text{Y intercept exponential fit liver response curve}}{\text{Y-MAX data value liver response curve}}$$

The deconvolutional technique separates hepatocyte counts from the hepatic blood pool counts. A deconvoluted liver curve, therefore, represents a hypothetical true response as though Tc-99m HIDA was injected directly into the hepatic artery or portal vein [11, 12]. The normal hepatic extraction fraction with Tc-99m-mebrofenin and Tc-99m-disofenin varies from 92% to 100%. The extraction fraction decreases as the hepatocyte function decreases. Functional changes show good correlation with Child's classification (Table 5.1.4) of the severity of liver disease [13].

Hepatic Excretion Half Time

After the uptake, Tc-99m-HIDA is secreted by the hepatocytes in its native state into bile canaliculi, where it mixes thoroughly with the canalicular bile. Secretion of radioactive bile into canaliculi serves as the direct in vivo, non-invasive method of radiolabeling hepatic bile, without altering basal liver physiology. After mixing with the canalicular bile, Tc-99m- HIDA follows the path taken by the hepatic bile. Excretion half time is a measure of how fast the radiotracer is secreted by the hepatocyte into bile canaliculi and how rapidly it flows through the intrahepatic bile ducts to enter the common hepatic duct and common bile duct before entering the gallbladder and duodenum. Measurement of excretion half time uses the liver and spleen ROI (Fig. 5.1.4). Since both the liver and spleen receive their arterial blood supply from a common source, the celiac artery, the spleen

Table 5.1.4 Child's classification of liver disease

Clinical and laboratory findings	Child's class		
	A	B	C
Ascites	None	Controlled	Uncontrolled
Neurological Findings	None	Minimal	Advanced
Nutrition	Excellent	Good	Poor
Bilirubin (mg%)	<2.0	2.0–3.0	>3.0
Albumin (gm%)	>3.5	3.0–3.5	<3.0

serves as the most appropriate organ for subtraction of the blood background. The background subtracted liver curve is modeled by an uptake and excretion compartment and is given by the following equation [12].

$$L(t) = k(e^{-0.693t/TE} - e^{0.693t/TU}),$$

where L(t) = background corrected liver counts/pixel at time *t*,

k = a constant of the model, *TE* = excretion effective T ½, and *TU* = uptake effective T½.

Although the hepatic phase data are collected for 60 min, calculation of HEF uses only the first 30-min data, whereas excretion $T_{1/2}$ uses all 60-min data points. Patient values are shown along with normal range (Fig. 5.1.5). Although in most patients with normal liver function, both HEF and $T_{1/2}$ excretion can be obtained by collecting total data only for 45 min, in patients with moderate to severe liver disease (serum bilirubin levels above 5 mg%), it is necessary to collect data for a minimum of 60 min to obtain a reliable excretion half time [13]. Normal T ½ excretion values obtained with KHBS using Tc-99m mebrofenin range from 6 to 38 min for the right lobe and from 6 to 58 min for the left lobe (Fig. 5.1.5). A longer excretion $T_{1/2}$ value of the left lobe is due to influence of bile within the left hepatic duct, which is more superficial than the right hepatic duct. Both HEF and $T_{1/2}$ excretion values are highly reproducible, both within and between institutions, and among different technologists [14]. HEF values remain within a normal range in early biliary disease, but decrease in hepatocellular disease. When the liver disease is severe and progressive, the HEF value begins to decrease, and excretion half time increases in both hepatocyte and biliary disease [15]. Both parameters provide a reliable measure of the severity of hepatobiliary diseases, irrespective of the etiology (Fig. 5.1.6).

Effect of Bile Duct Obstruction on Liver Function

In the case of hyperacute or acute total obstruction of the common bile duct, HEF values remain within a normal range for 4–5 days, as long as the serum bilirubin level remains below 8 mg% (Fig. 5.1.6A). HEF begins to decrease when obstruction persists and the serum bilirubin level rises above 8 mg% [16]. Excretion half time, on the other hand, increases from the very beginning (Fig. 5.1.6B). Prolongation of the excretion half time in biliary obstruction is due to bile stasis within the canaliculi and intrahepatic bile ducts. In congenital biliary atresia, a condition resulting from extrahepatic bile duct obstruction, HEF remains high for about 2 months after birth and then begins to decrease if the obstruction is not relieved [17, 18]. Excretion half time and HEF show an inverse relationship; as the HEF decreases, excretion half time increases, and vice-versa (Fig. 5.1.6C). High serum bilirubin levels decrease HEF by two mechanisms: first, it displaces Tc-99m-HIDA from its carrier protein, albumin, and second, bilirubin competes with Tc-99m-HIDA for the hepatocyte uptake by receptor mediated endocytosis.

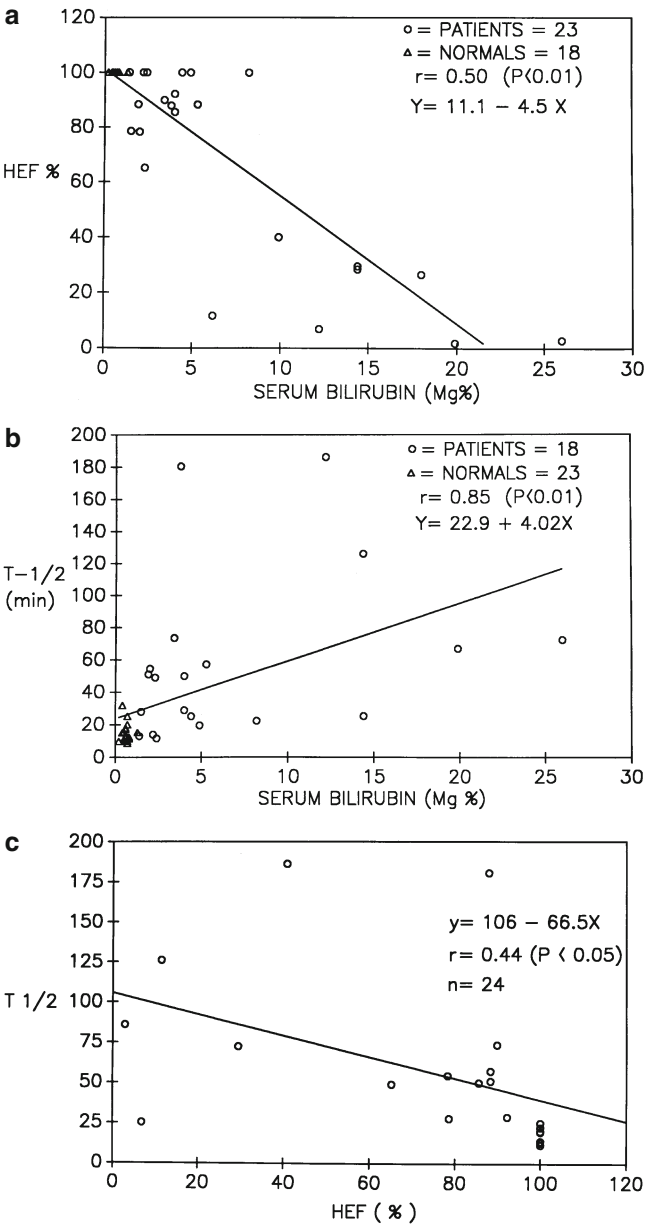

Fig. 5.1.6 Relationship between hepatic extraction fraction (*HEF*) and excretion half time in health and disease. HEF remains near normal level in early disease and begins to decrease as bilirubin increases (**a**). Excretion half time increases from the very beginning and raises further as serum bilirubin value increases (**b**). HEF and excretion half times show an inverse relationship (**c**)

Basal Differential Hepatic Bile Flow

This parameter is obtained as a part of HEP-phase data analysis as shown in Figs. 5.1.3 and 5.1.4. After leaving the liver, the hepatic bile in the basal state enters the gallbladder and duodenum, with volume depending upon the tonus of the sphincter of Oddi. Normal gallbladders are usually visualized within 60 min, and 10-100% of the hepatic bile enters the gallbladder. In about 20% of normal subjects, all of the hepatic bile enters the gallbladder and none the intestine, so that intestinal bile entry at 60 min remains at 0%. Intestinal bile entry, therefore, normally ranges from 0 to 100%. Longer duration of fasting increases the sphincter tone and diverts more of the hepatic bile to enter the gallbladder than intestine. Total bile produced during 60 min of hepatic phase imaging is obtained by adding gallbladder and intestinal counts at 60 min. Percent of the hepatic bile entering the gallbladder is obtained by the following formula.

$$\text{Hepatic bile flow into gallbladder } (\%) = \frac{\text{Gallbladder total counts at 60 min} \times 100}{\text{Gallbladder total counts at 60 min} + \text{Intestinal total counts at 60 min}}$$

$$= \frac{49{,}700 \times 100}{49{,}700 + 50{,}300} = 49.7\%.$$

$$\text{Hepatic bile flow into Intestine } (\%) = \frac{\text{Intestinal total counts at 60 min} \times 100}{\text{Gallbladder total counts at 60 min} + \text{Intestinal total counts at 60 min}}$$

$$= \frac{50{,}300 \times 100}{49{,}700 + 50{,}300} = 50.3\%$$

Basal Duodeno-Gastric Bile Reflux (Basal-DGBR)

This parameter is obtained as a part of HEP-phase data analysis as shown in Figs. 5.1.4 and 5.1.5. Bile entering the duodenum during fasting flows forward to enter the jejunum. Normally, there is no bile reflux into the stomach. The stomach ROI is selected carefully by avoiding inclusion of the left lobe of the liver or duodenal loop in the stomach ROI, both of which will result in a falsely high DGBR. Normal DGBR values up to 8% represent mostly background activity. The DGBR value should be ignored when there is no visible bile entry into the intestine. A high DGBR value in such cases represents only the background activity in the stomach and intestine. DGBR values are checked with the images to confirm bile reflux. DGBR values higher than 8% are usually associated with visible bile reflux into the stomach (Fig. 5.1.5)

The DGBR value is obtained by dividing total stomach counts at 60 min by the sum of stomach and intestinal counts at 60 min.

$$\text{DGBR}(\%) = \frac{\text{Stomach counts at 60 min} \times 100}{\text{Stomach counts} + \text{Intestinal counts at 60 min}}$$

Both differential hepatic bile flow and basal DGBR values are shown on the right side of the Hep-function result along with normal values (Fig. 5.1.5). Three figures in the middle show the ROIs for each region to enable the physician to check for accuracy. Since radiolabeled bile has to enter the duodenum to have any reflux into the stomach, all DGBR values are ignored when there is no bile entry into the intestine. Occasionally, DGBR may empty in the middle of data acquisition; in such an instance, the peak reflux value is obtained by changing the frame number as shown in the option block at the bottom (Fig. 5.1.5).

Quantification of Gallbladder Function

A normal gallbladder measures about 50 ml in volume and requires 3–4 h to fill to its full capacity after complete emptying. Since the gallbladder is already filled to its full capacity after 4–6 h of fasting, two mechanisms are responsible for accommodating a constant inflow of 0.3 ml min^{-1} of the hepatic bile: (1) absorption of water through the gallbladder wall and (2) an increase in tonus of the sphincter of Oddi. During fasting, the epithelium of the gallbladder wall absorbs water from the lumen through widely opened lateral intercellular spaces between the columnar cells of the mucosa. Bile salts, bile pigments, cholesterol, and other bile constituents are not absorbed. This process of selective absorption of water resulting in a higher concentration of solutes is called the concentration function of the gallbladder [8]. After an overnight fast, the mean pressure within the sphincter of Oddi is 15 mmHg, 12 mmHg in the common bile duct, and 10 mmHg inside the gallbladder. Because of the pressure difference at various levels, hepatic bile follows the path of the least resistance and enters the gallbladder.

Bile from the common hepatic duct enters the gallbladder in a step-wise fashion and corresponds to the phasic waves passing through the sphincter of Oddi [19]. Radioactive hepatic bile first enters the gallbladder along its central long axis and moves slowly laterally towards the wall [20]. After entering the central long axis, radiolabeled bile usually takes at least 30 more minutes to reach the wall (Fig. 5.1.7). One should wait till the entire gallbladder bile is radiolabeled before embarking on measurement of its emptying. For example, when a gallbladder appears first at 45 min of the hepatic phase imaging, the measurement of the ejection fraction should start at 75 min (45 + 30 = 75 min) to allow sufficient time for radiolabeling of the entire gallbladder bile. After completion of 60 min of HEP-phase data collection, in such an instance, the patient is made to wait for an additional 15 min before starting GB-phase imaging with cCK-8. The ejection fraction value would be falsely high if partially radiolabeled gallbladder bile were measured.

Gallbladder Ejection Fraction

Measurement of gallbladder emptying is clinically popular primarily due to the availability of a simple, non-invasive, and reliable quantitative diagnostic test. In the past, gallbladder emptying was measured with oral cholecystogram by applying a technique called the sum of the

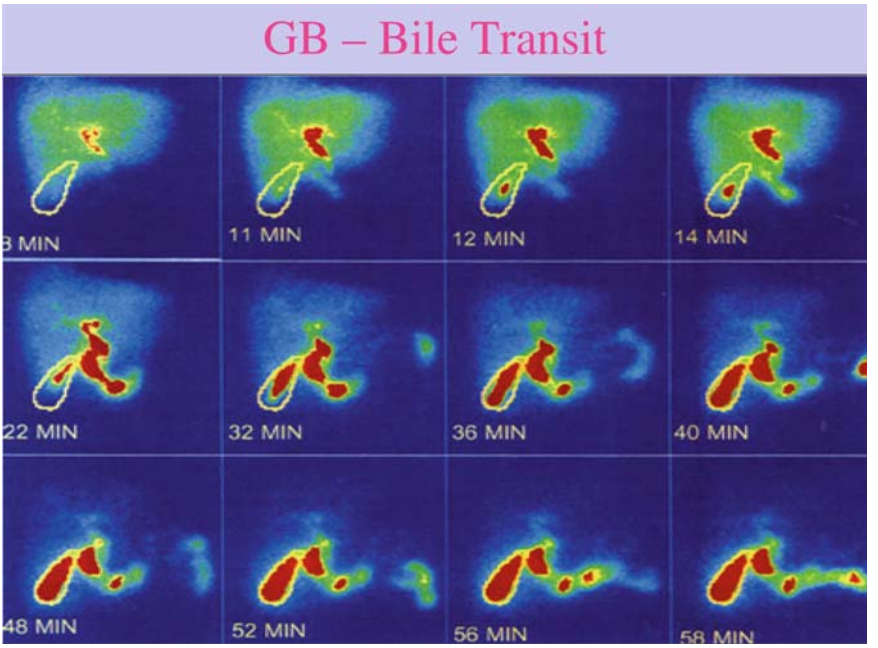

Fig. 5.1.7 Filling of the gallbladder: Gallbladder fills from inside out. Radiolabeled bile first enters the gallbladder at 12 min along its central long axis and moves laterally to reach the wall at 48 min, taking a total of 36 min. One must wait for all of the gallbladder bile to be radiolabeled before embarking on study emptying. Partially radiolabeled gallbladder bile may result in overestimation of its ejection fraction

cylinder method, which was introduced in 1949 by De Silva [21]. On the oral cholecystogram, the gallbladder image is divided into series of small cylinders, and the volume of each cylinder is computed by applying a mathematical formula for the volume of a cylinder. By summing the volume of all cylinders, gallbladder total volume is obtained. A slightly modified version of sum of the cylinder method has been adopted for measuring the gallbladder volume with the ultrasound [22]. Both oral cholecystogram and ultrasound are geometric techniques and are based on the assumption that the gallbladder is a cylinder before, during, and after contraction. It is frequently seen that the gallbladder is not a cylinder before contraction, and it often changes its shape during and after contraction. A count-based, non-geometric technique overcomes these shortcomings [23]. Cholescintigraphy with Tc-99m-HIDA is a non-geometric method and enables precise measurement of both the ejection fraction and ejection rate. The scintigraphic method uses Tc-99m HIDA counts to represent bile volume as there is a direct linear relationship between bile volume and counts within the gallbladder (Fig. 5.1.8).

Data Collection

The gallbladder phase data are acquired using the protocol outlined in Table 5.1.1 at 1 frame per minute for 30 min when CCK-8 is used as the stimulus for contraction. The data are collected

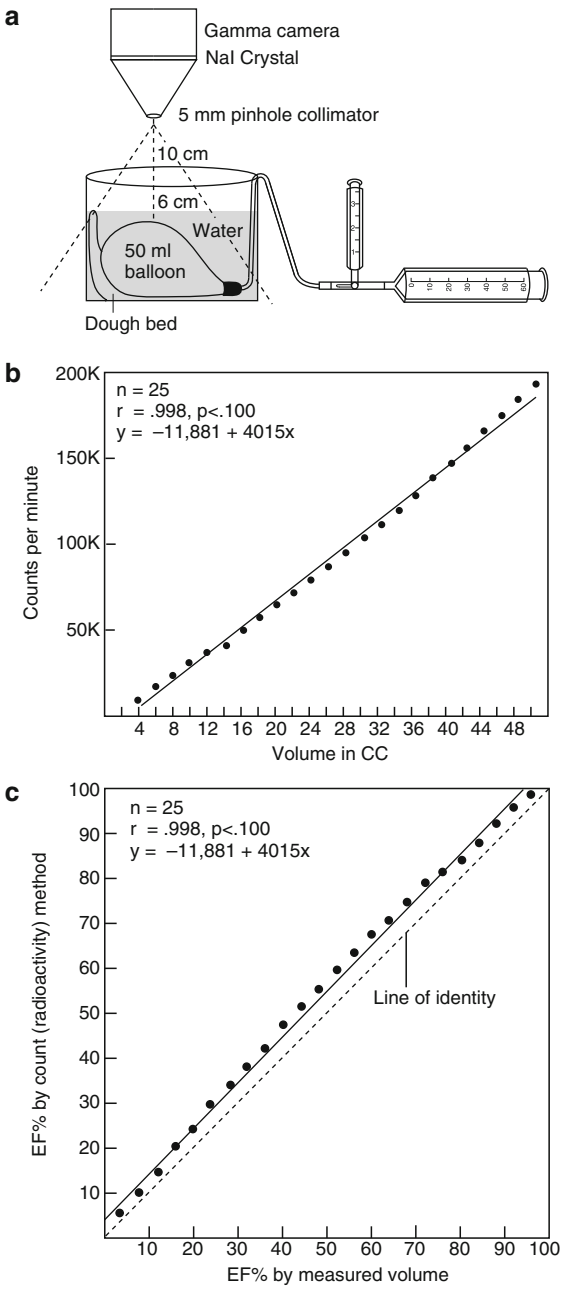

Fig. 5.1.7 Gallbladder bile volume and Tc-99m HIDA count relationship. A rubber balloon filled with 50 ml water and Tc-99m representing the gallbladder is placed inside a container placed underneath a gamma camera. One milliliter of water is removed at a time through the syringe, and counts are taken with the gamma camera after each withdrawal (**a**). Counts show a linear relationship with the bile volume (**b**). Ejection fraction measured by volume and Tc-99m-HIDA count methods show a perfect linear (**c**) relationship [23]

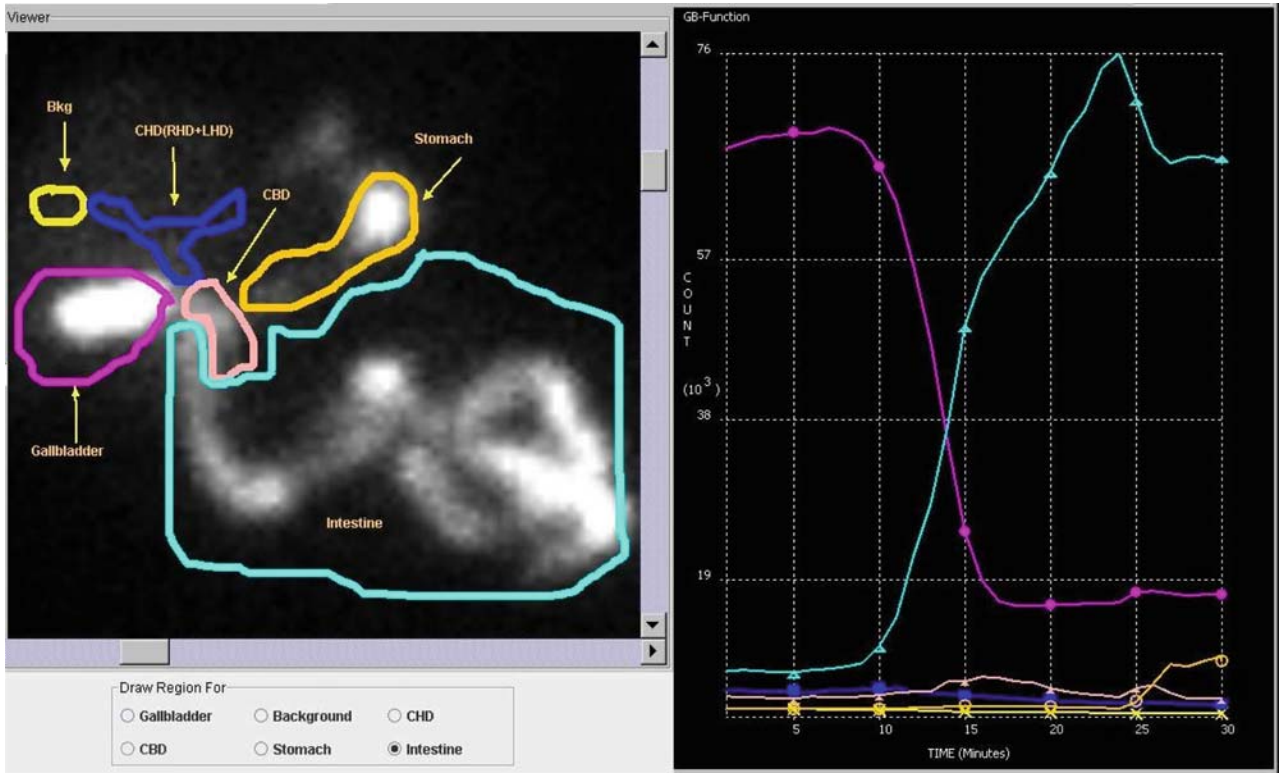

Fig. 5.1.8 Gallbladder phase ROIs: Gallbladder, bkg, CHD, and CBD ROIs are drawn usually on the first-minute frame, stomach, and intestinal ROIs on the last-minute frame. Curves on the *right* represent the counts from *regions of the same color*

for a minimum of 60 min, preferably 60–120 min, when a fatty meal is used as the stimulus to induce gallbladder contraction. A magnification factor of 1.2–2.4 may be used during data acquisition. The gamma camera angle is changed to a degree that maximally separates the CBD from the gallbladder and the duodenum [9]. Infusion of CCK-8 is begun at 3 min at a dose rate of 3 ng kg^{-1} min^{-1} and infused for 10 min through an infusion pump. The first 5 min counts prior to CCK-8 infusion represent the basal volume of the gallbladder.

Dose Rate and Duration of Cholecystokinin Infusion

In the United States, a fragment of the hormone cholecystokinin is available for clinical use as CCK-8 (Kinevac). In Europe and other countries, the entire molecule with 33 or 39 amino acids is made available. The hormone is prepared according to the manufacturer's instructions in the package insert (Kinevac, Sincalide, Bracco Diagnostics, Princeton NJ). Volume is adjusted with saline to achieve the desired dose rate and duration of infusion. Selection of a proper dose and dose rate within the physiologic range is critical for accurate results. Duration of the infusion is a matter of personal preference. We routinely use a dose rate of 3 ng kg^{-1} min^{-1} and infuse for a total duration of 10 min through an infusion pump. Before the test begins, the patient is given instructions to raise the hand as soon as the symptoms begin and to raise the hand again when symptoms abate. The patient is asked to grade pain intensity as mild, moderate, or severe. The technologist notes down the time of onset, total duration, and intensity of pain on a work sheet for interpretation.

Effect of Non-Physiologic Dose of Cholecystokinin

The package insert (Sincalide, Kinevac by Bracco Diagnostics, Princeton, NJ) suggests a CCK-8 dose of 0.02 µg kg^{-1} (20 ng kg^{-1}) infused over 30 or 60 s. This dose rate was originally developed in 1970s with the use of oral cholecystogram, and studies since have demonstrated that this dose rate is too large for cholescintigraphy and often produces a falsely low ejection fraction in 20–26% of normal subjects [24–28]. A change in dose rate and/or duration of infusion produces different values for the gallbladder ejection fraction (Table 5.1.5). Ideally, one should establish local values when the technique chosen is different from the published literature [29].

Table 5.1.5 Effect of dose and duration of CCK-8 infusion on gallbladder ejection fraction (mean ± S.E)

CCK-8 dose rate (ref)	Duration of CCK-8 infusion		
	3 min	30 min	60 min
0.5 ng kg^{-1} min^{-1} [27]	–	79.3% ± 6.9%	91.3% ± 5.3%
3.3 ng kg^{-1} min^{-1} [23] (10 ng kg^{-1} 3 min^{-1})	59.4% ± 4.0%	–	–
5.0 ng kg^{-1} min^{-1}[27]	–	82.4% ± 6.7%	94.0% ± 5.1%

5

Calculation of Gallbladder Ejection Fraction

After uploading the gallbladder phase data onto KHBS, the gallbladder function button at the top is activated. Six ROIs are drawn: gallbladder, background, common hepatic duct (CHD), common bile duct (CBD), stomach, and intestine (Fig. 5.1.8). The background ROI is drawn over the liver, superior and lateral to the gallbladder. The CHD region includes both the right hepatic duct and left hepatic ducts in the form of a letter *T* or *Y*. The gallbladder, background, CHD, and CBD regions are drawn using the first frame. Stomach and intestinal ROIs are drawn on the last frame. Net gallbladder counts are obtained after subtraction of the background counts and corrected for decay [9]. Region of interest over the CHD enables identification of possible bile reflux in the presence of critical obstruction of the common bile duct. The software also calculates post-CCK-8 duodeno-gasrtic bile reflux (Fig. 5.1.9).

$$\text{Gallbladder ejection fraction(GBEF)}\,(\%) = \frac{\text{GB Peak counts} - \text{First minimum GB counts (B)}}{\text{GB Peak counts}} \times 100$$

$$\text{GBEF} = \frac{A - B}{A} \times 100$$

Latent period (LP) = Time from beginning of CCK – 8 infusion to beginning of gallbladder emptying
Ejection period (EP) = Time from beginning of gallbladder emptying to the first minimum counts
Normal values for 10 min infusion of 3ng / kg / min of CCK – 8
Ejection rate (ER) = % Ejection fraction / Ejection period
= % / minute
Normal values for 10 min infusion of 3ng / kg / min of CCK – 8
Latent period (LP)
Ejection period (EP) = 7–19 min
Ejection period (EF) ≥ 50%
Ejection rate (ER) ≥ 3.5% / min

Post-CCK-8 duodeno-gastric bile reflux is calculated by dividing stomach counts by the sum of stomach and intestinal counts. Normally cholecystokinin acts on the gallbladder, promoting its contraction and emptying. It acts on the pylorus sphincter of the stomach and prevents bile reflux. Occasionally, one may find a large amount of DGBR with CCK-8 that may explain a patient's symptoms.

Ejection Fraction with Fatty Meal Stimulation

Fatty meal stimulates the release of endogenous cholecystokinin from the endocrine cells lining the mucosa of the duodenum, jejunum, and upper ileum. It may take as long as 6–26 min after a meal for the endogenous CCK level to rise above the serum threshold to initiate gallbladder contraction and emptying. Once the gallbladder begins to empty, it continues

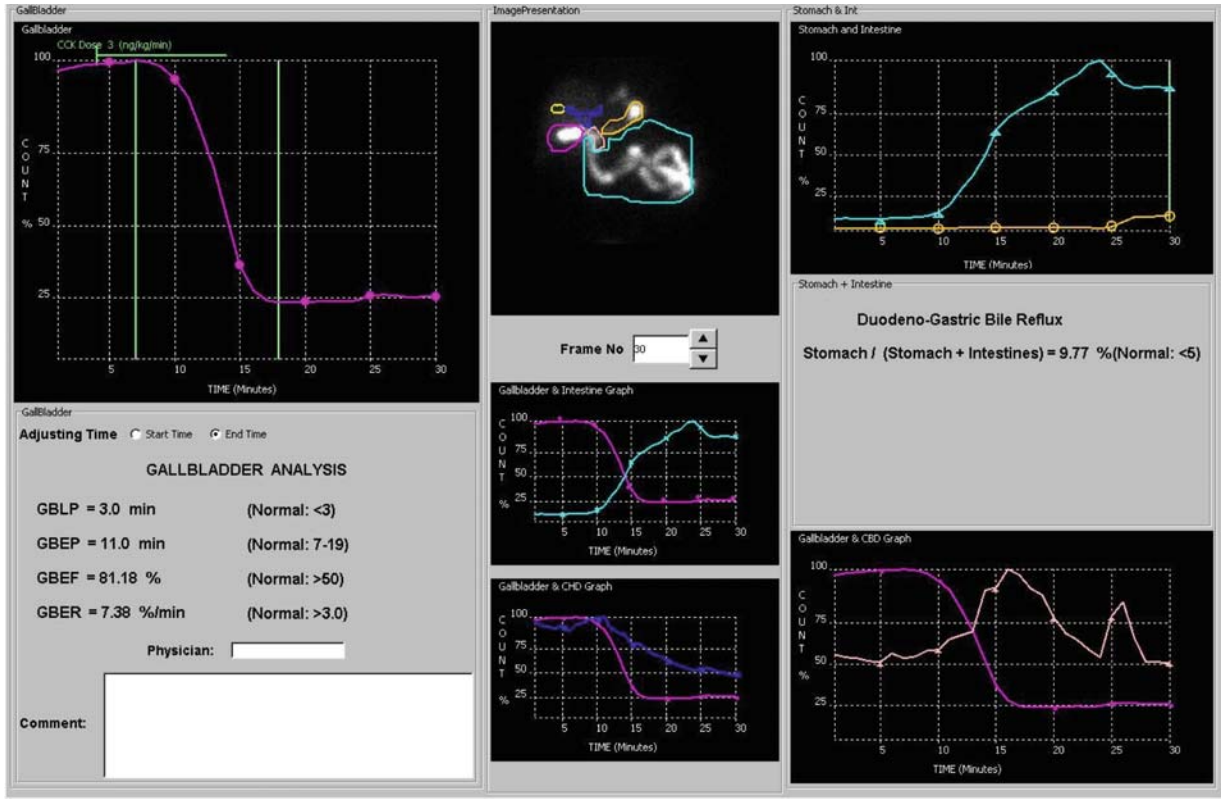

Fig. 5.1.9 GB-phase results. Occasionally gallbladder counts may increase just before it begins to empty (*first vertical bar*). First minimum counts represent the end of gallbladder emptying (*second vertical bar*). Ejection fraction (*EF*) is calculated by dividing counts emptied between *two vertical bars* by counts at the *first vertical bar*. Time between two vertical bars is the ejection period (*EP*). Ejection rate (*ER*) is calculated by dividing % EF by EP. Post-CCK DGBR is obtained by dividing stomach counts by the sum of stomach and intestinal counts

5

ejection for 1–3 h post-meal. The duration of data collection with the fatty meal, therefore, should be for a minimum of 60 min, preferably for 120 min. The data are collected at 1 frame per min for 60 or 120 min (Fig. 5.1.10). A standardized test meal (8 oz 70 kg^{-1} body weight) of known nutritional contents and caloric value is ingested at 5 min, such that a baseline count prior to the meal represents basal gallbladder volume [30, 31]. Mean (± SD) ejection fraction for 1 h fatty meal stimulation study is 50% ± 20%. Individual values can be as low as 32%. In the same group of normal subjects, 10 min infusion of 3 ng kg^{-1} min^{-1} of CCK-8 produces a mean EF of 70% ± 17% [32]. In the USA, the nutritional value of Half and Half (H & H) milk varies from city to city (Table 5.1.6). One must standardize the technique and establish local normal values.

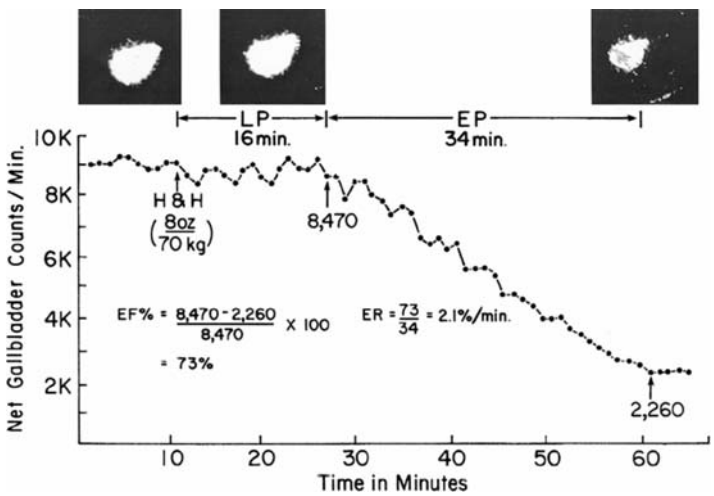

Fig. 5.1.10 Gallbladder emptying with fatty meal stimulation: Meal is ingested at 10 min. There is a latent period of 16 min before the gallbladder begins to empty. Ejection fraction is 73%, ejection period of 34 min, and an ejection rate 2.1% per min [31]

Table 5.1.6 Variations in nutritional contents and total calories of Half-and-Half milk in six US cities [33]

Nutrient content per 30 ml	Portland, OR (Alpenrose)	New York, NY (America choice)	Detroit, MI (CFBerger)	Jackson, MS (Dairy fresh)	Los Angeles, CA (Altadena)	Miami, FL (McArthur dairy)
Total fat (g)	3.0	3.0	3.0	3.5	3.0	3.0
Cholesterol (mg)	10.0	15.0	10.0	15.0	15.0	15.0
Carbohydrate (g)	1.0	1.0	1.0	1.0	1.0	1.0
Protein (g)	1.0	1.0	1.0	1.0	1.0	1.0
Sodium (mg)	10.0	20.0	10.0	20.0	15.0	15.0
Total calories (30 ml)	40.0	40.0	35.0	40.0	40.0	40.0

Data Analysis

Software is adapted for measurement of the ejection fraction with fatty meal. Two regions of interest, one over the gallbladder and the other over the liver as background, are drawn. Due to the slow rate of bile emptying, CBD and CHD are not well delineated with the fatty meal stimulation. The value of the gallbladder ejection fraction with a fatty meal is reported with a reference to its total duration of measurement, i.e., at 60 min or 120 min, post-meal. Both a 30-min continuous infusion of CCK-8 or a 60-min post fatty meal appear to produce a mean ejection fraction of about 80% (Table 5.1.7). The latent period (the time from meal ingestion to beginning of gallbladder emptying) is variable depending upon the time for release of endogenous CCK [28]. A delay in gastric emptying may also cause late release of cholecystokinin. Since there are no CCK-secreting cells in the esophagus and stomach [33], hormone-induced gallbladder emptying does not begin until food reaches the duodenum. The gallbladder ejection fraction is low in patients with gallstones and diabetes [34]. Obese diabetics have a much more pronounced reduction in EF compared to non-obese diabetic patients [35]. A cephalic phase emptying because of cholinergic nerve stimulation, independent of hormonal action may induce gallbladder emptying [36]. A comparison of fatty meal stimulation with cholecystokinin in the same group of normal subjects showed wide variation in the ejection fraction [32]. The fatty meal ejection fraction at the end of 1 h ranges from 23 to 91% (mean 54%), whereas a 10-min infusion of CCK-8 in the same group of normal subjects produces values ranging from 37 to 91% (mean 76%). ROI over the stomach region enables calculation of duodeno-gastric bile reflux.

Gallbladder Segmentation

Often a septa or fold can divide the gallbladder chamber into two separate compartments, proximal and distal (Fig. 5.1.11). Ultrasound studies usually show the length, thickness, and position of the septa inside the gallbladder. Carefully done histopathological examination (Fig. 5.1.12) confirms the folds. Recognition of such compartments is essential during hepatic phase imaging as the two compartments may show a different degree of filling and emptying. Radiolabeled hepatic bile enters the proximal compartment first, followed 5–10 min later by entry into the distal compartment. Two compartments are easy to recognize with cholescintigraphy in the early images as the radiolabeled bile enters the gallbladder (Fig. 5.1.13). It becomes much more difficult to recognize it in late images as bile radioactivity equilibrates in both compartments. For calculation of the gallbladder segmental function, GB-Seg block at the top is activated, and the patient data are loaded. One ROI is drawn around the entire gallbladder and another between the two compartments (Fig. 5.1.14). The program calculates the

Table 5.1.7 Effect of type of meal and duration of emptying on gallbladder ejection fraction (%)

Meal type	Meal volume	(Mean ± SE)		
		Duration from meal ingestion		
		30 min	60 min	120 min
Half & Half [28]	8 oz 70 kg^{-1}	–	64.4 ± 6.7%	–
Lipomul [27]	15 ml	49.8 ± 5.2%	71.7 ± 3.6%	77.8 ± 2.0%

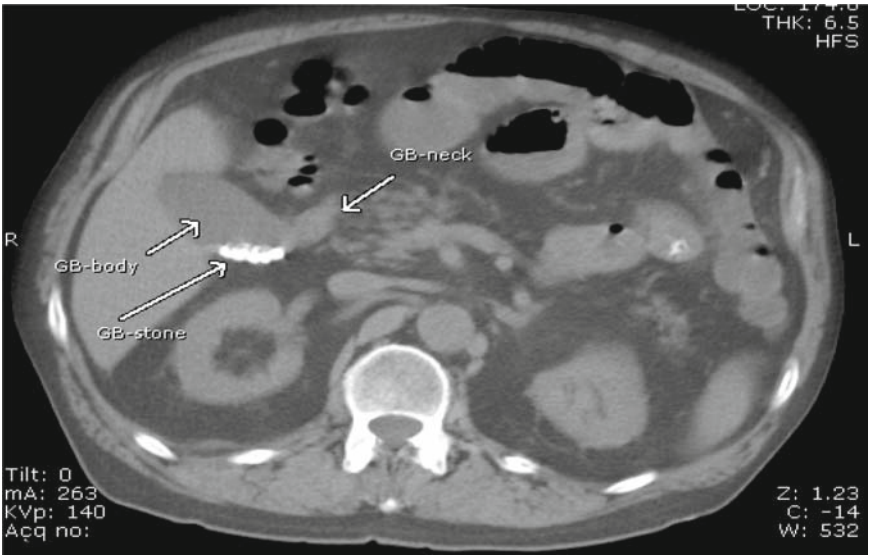

Fig. 5.1.11 Gallbladder segmentation. CT scan shows a constriction near the neck dividing the gallbladder into proximal (*GB-neck*) and distal (*GB-body*) compartments. Gallstones are layered in the distal compartment

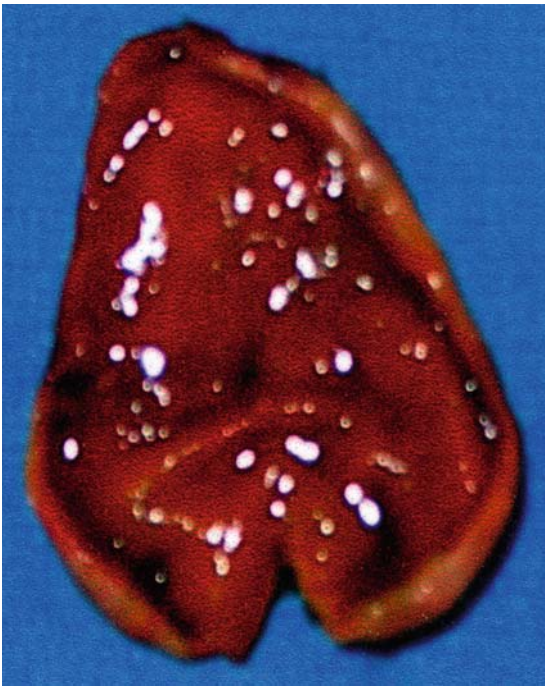

Fig. 5.1.12 Gallbladder fold or septa. A transverse fold divides the gallbladder into proximal and distal compartments. This fold acts in vivo as a barrier between two segments and reduces bile emptying from the distal segment

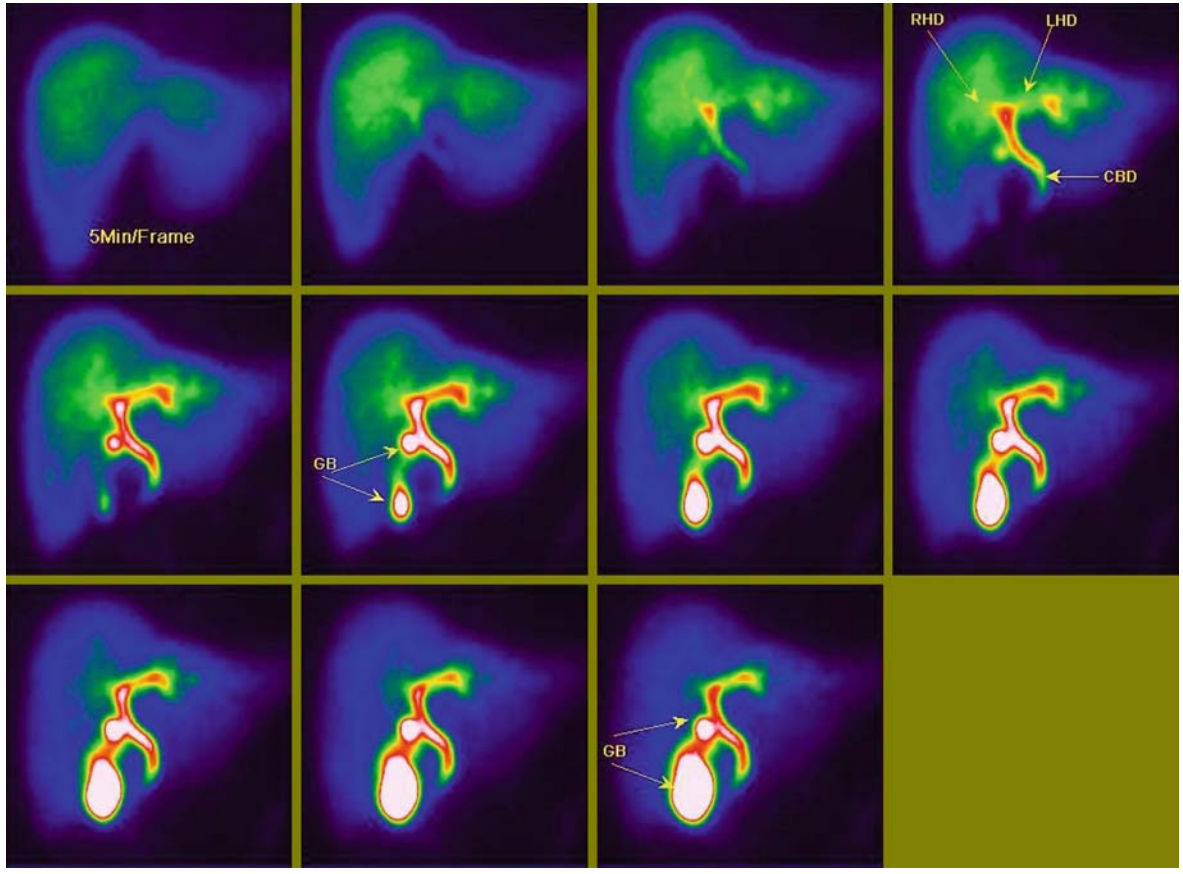

Fig. 5.1.13 Filling of a segmental gallbladder (*GB*). The proximal segment appears first at 20 min (*top row right*), and distal segment begins to appear at 25 min (*middle row left*). Left hepatic duct (*LHD*) is seen much more prominently than the right hepatic duct (*RHD*). The distal segment is much larger in size than the proximal segment (*bottom row right*)

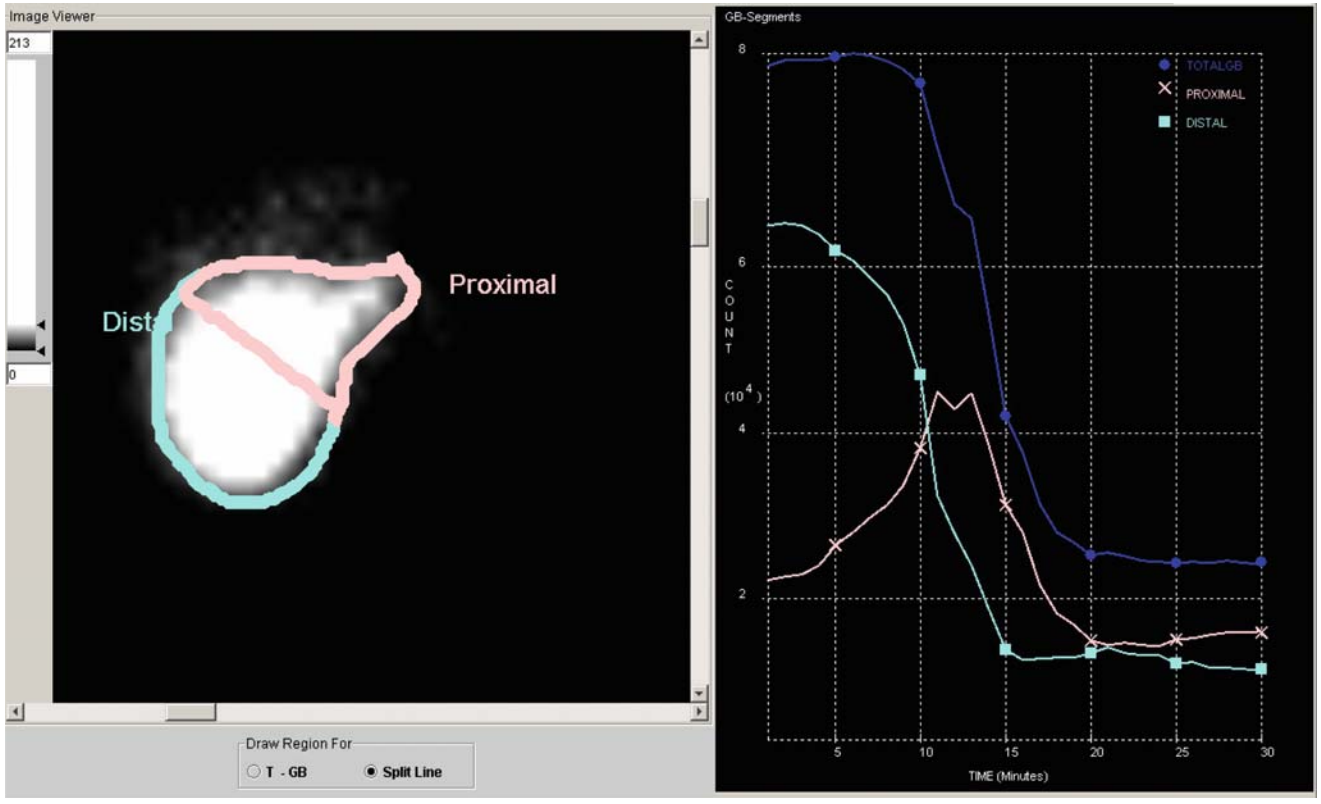

Fig. 5.1.14 Regions of interest for gallbladder segmentation. One region is drawn around the entire gallbladder and the other over the septum that divides it into proximal and distal compartments. Counts and curves from the proximal and distal compartment and total gallbladder are displayed

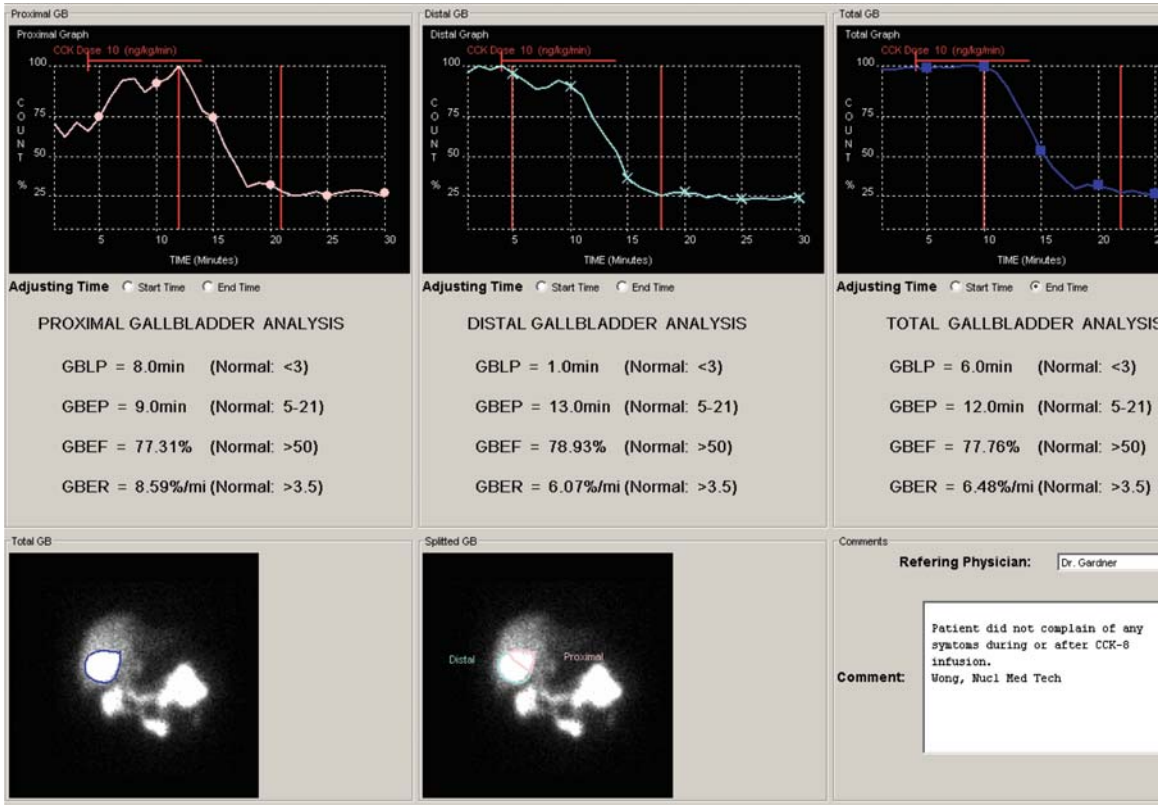

Fig. 5.1.15 Results of gallbladder segmentation. By drawing one region of interest around the entire gallbladder and another over the fold or septum (*bottom*), the software calculates the ejection fraction for each compartment separately along with the gallbladder total ejection fraction (*top*)

total EF and EF for each compartment separately (Fig. 5.1.15). The distal compartment usually empties poorly because of septa acting as a one-way valve. Because these findings are new and not well appreciated, ultrasonographers should mention the presence of the septa or fold in their ultrasound report of the gallbladder to draw the attention of clinicians who may then request a Tc-99m HIDA study for further evaluation of abdominal pain [37].

References

1. Krishnamuthy S, Krishnamurthy GT. Technetium-99m iminodiacetic acid organic anions: review of biokinetics and clinical application in hepatology. Hepatology 1989;9:139–153
2. Bobba VR, Krishnamurthy GT, Kingston E, Brown PH, Eklem M, Turner FE. Comparison of biokinetics and biliary imaging parameters of four Tc-99m iminodiacetic acid derivatives in normal subjects. Clin Nucl Med 1983;8:70–75
3. Williams W, Krishnamurthy GT, Brar HS, Bobba VR. Scintigraphic variations of normal biliary physiology. J Nucl Med 1984;25:160–165
4. Healey JE, Schroy PC. Anatomy of the biliary ducts within the human liver. Analysis of the prevailing pattern of branchings and the major variations of the biliary ducts. Arch Surg 1953;66:599–616
5. Sherlock S, Dooley. Diseases of the liver and biliary system, 10th edn Blackwell Science, Malden, MA, 1997, pp 217–237
6. Krishnamurthy GT, Bobba VR, McConnell D, Turner FE, Mesgarzadeh M, Kingston E. Quantitative biliary dynamics: introduction of a new non-invasive scintigraphic technique. J Nucl Med 1983;24:217–223
7. Klingensmith WC III, Spitzer CM, Fritzberg AR, Kuni CC. The normal fasting and postprandial diisopropyl-IDA Tc-99m hepatobiliary study. Radiology 1981;141:771–776
8. Wheeler HO. Concentrating function of the gallbladder. Am J Med 1971;51:588–595
9. Krishnamurthy S, Krishnamurthy GT. Evolution of nuclear hepatology as a clinical subspeciality. J Nucl Med Technol 1995;23:35S–44S
10. Krishnamurthy GT, Krishnamurthy S. Cholescintigraphic measurement of liver function: how is it different from other methods? Eur J Nucl Med Mol Imaging 2006;33:11203–1106
11. Tagge EP, Campbell DA Jr, Reichle R, Averill DR Jr, Merion RM, Dafoe DC, Turcotte JG, Juni JE. Quantitative scintigraphy with deconvolutional analysis for the dynamic measurement of hepatic function. J Surg Res 1987;42:605–612
12 Brown PH, Juni JE, Lieberman DA, Krishnamurthy GT. Hepatocyte versus biliary disease: a distinction by deconvolutional analysis of technetium-99m IDA time-activity curves. J Nucl Med 1988;29:623–630
13. Doo E, Krishnamurthy GT, Eklem MJ, Gilbert S, Brown PH. Quantification of hepatobiliary function as an integral part of imaging with technetium-99m-mebrofenin in health and disease. J Nucl Med 1991;32:48–57
14. Spackman J, Bartlett ME, Ryals L, et al. Reproducibility of technetium-99m-mebrofenin hepatic functional parameters obtained with a semiautomatic software. J Nucl Med Technol 1991;19:228–231
15. Krishnamurthy GT, Krishnamurthy S. Nuclear hepatology. A textbook of hepatobiliary diseases. Springer, Berlin, 2000
16. Juni JE, Reichle R. Measurement of hepatocellular function with deconvolutional analysis: application in the differential diagnosis of acute jaundice. Radiology 1990;177:171–175
17. Howan-Giles R, Moase A, Gaskin K, Uren R. Hepatobiliary scintigraphy in a pediatric population: Determination of hepatic extraction fraction by deconvolution analysis. J Nucl Med 1993;34:214–221
18. Howman-Giles R, Uren R, Bernard E, Dorney S. Hepatobiliary scintigraphy in infancy. J Nucl Med 1998;39:311–319

19. van der Linden W, Kempi V. Filling of the gallbladder as studied by computer-assisted Tc-99m-HIDA scintigraphy: concise communication. J Nucl Med 1984;25:292–298
20. Krishnamurthy GT, Krishnamurthy S. Hepatic bile entry and transit within the gallbladder lumen: a new quantitative cholescintigraphic technique for measurement of its concentration function. J Nucl Med 2002;43:901–908
21. deSilva GS. A simple method for computing the volume of the human gallbladder. Radiology 1949;52:94–102
22. Everson GT, Braverman DZ, Johnson ML, Kern F Jr. A critical evaluation of real-time ultrasonography for the study of gallbladder volume and contraction. Gastroenterology 1980;79:40–46
23. Krishnamurthy GT, Bobba VR, Kingston E. Radionuclide ejection fraction: a technique for quantitative analysis of motor function of the human gallbladder. Gastroenterology 1981;80:482–490
24. Krishnamurthy S, Krishnamurthy GT. Biliary dyskinesia: role of the sphincter of Oddi, gallbladder and cholecystokinin. J Nucl Med 1997;38:1824–1830
25. Krishnamurthy S, Krishnamurthy GT. Cholecystokinin and morphine pharmacological intervention during Tc-99m-HIDA cholescintigraphy: a rational approach. Semin Nucl Med 1996;26:16–24
26. Krishnamurthy GT, Bobba VR, Kingston E. Optimization of octapeptide of cholecystokinin (OP-CCK) dose for gallbladder emptying. In: Raynaud C (ed) Proceedings of the third world congress of nuclear medicine and biology, Paris, France. Pergamon Press, New York, 1982, pp 2244–2247
27. Ziessman HA, Fahey FH, Hixson DJ. Calculation of a gallbladder fraction: advantage of continuous sincalide infusion over the three-minute infusion method. J Nucl Med 1992;33:537–541
28. Toftdahl DB, Hojgaard L, Winkler K. Dynamic cholescintigraphy: induction and description of gallbladder emptying. J Nucl Med 1996;37:261–266
29. Krishnamurthy S, Krishnamurthy GT. Gallbladder ejection fraction: a decade of progress and future promise (editorial). J Nucl Med 1992,32:542–544
30. Fisher RS, Rock E, Levine G, Malmud L. Effects of somatostatin on gallbladder emptying. Gastroenterology 1987;92:885–890
31. Bobba VR, Krishnamurthy GT, Kingston E, Turner FE, Brown PH, Langrell K. Gallbladder dynamics induced by a fatty meal in normal subjects and patients with gallstones: concise communication. J Nucl Med 1984;25:21–24
32. Krishnamurthy GT, Brown PH. Comparison of fatty meal and intravenous cholecystokinin infusion for gallbladder ejection fraction. J Nucl Med 2002;43:1603–1610
33. Sjolund K, Sanden G, Hakanson R, Sundler F. Endocrine cells in human intestine: an immunocytochemical study. Gastroenterology 1983;85:1120–1130
34. Fisher RS, Stelzer F, Rock F, Malmud LS. Abnormal gallbladder emptying in patients with gallstones. Dig Dis Sci 1982;27:1019–1024
35. Shreiner DP, Sarva RP, Van Thiel D, Yingvorapant N. Gallbladder function in diabetic patients. J Nucl Med 1986;27:357–360
36. Hopman WPM, Jansen JBM, Rosenbusch G, Lamers CB. Cephalic stimulation of gallbladder contraction in humans: role of cholecystokinin and the cholinergic system. Digestion 1987;38:197–203
37. Krishnamurthy GT, Krishnamurthy S, Milleson T, Brown PH, Urstadt DS. Segmentation of the gallbladder: effect on bile entry and exit and its clinical relevance in a patient with abdominal pain. Nucl Med Commun 2007;28:109–115

5.2 Measurement of Hepatic Arterial vs. Portal Venous Blood Flow

The liver has a dual blood supply through the hepatic artery and portal vein. The hepatic artery supplies about 400 ml of arterial blood per min at 100–120 mmHg systolic blood pressure. Thus, approximately 25% of the total liver blood supply comes via the hepatic artery

and the remaining 75% through the portal vein. After injection into a peripheral vein, the radiotracer arriving via the portal vein takes 7–10 s more to reach the liver than the radiotracer arriving via the hepatic artery. This delay via the portal vein is primarily due to the time taken for the radiotracer to traverse the intestinal veins and portal vein.

The hepatic arterial versus portal venous blood supply to the liver is measured using a first-pass curve obtained with any radiotracer that passes through the liver [1]. Technetium-99m pertechnetate, Tc-99m-DTPA, and Tc-99m-MDP have been used. These tracers that merely pass through, but are not retained by the liver do not allow any additional liver imaging. The agents that both pass through and are retained by the liver (Tc-99m S-colloid or Tc-99m HIDA) allow follow-up imaging of the liver. Immediately upon an antecubital vein injection, the radiotracer mixes thoroughly with blood in the ventricles before its arrival at the liver. The quantity of the radiotracer reaching the liver is directly proportional to the volume of blood supplied to the liver. The differential blood flow to the liver, via the hepatic artery versus portal vein, is calculated by two methods. One method is based on analysis of the slope of the uptake and washout [2], and the other method employs the area under the curve by deconvolutional analysis [3].

Data Collection

A fasting patient is positioned supine underneath a large field of view gamma camera fitted with a low-energy, all-purpose, parallel-hole collimator. The position of the gamma camera in either the anterior or posterior view is adjusted to make sure that it covers the lower part of the lungs, entire liver, spleen, and kidneys. A simultaneous anterior and posterior perfusion can be obtained with a dual-head gamma camera (Fig. 5.2.1A, B). About 10–15 mCi (370–555 MBq) of Tc-99m-labeled agent is injected intravenously as a rapid bolus followed by a 30-ml saline flush. Data are collected on 64-by-64 word mode matrix at 1 frame per 0.5 s for 100 s [2]. Data acquisition is begun just before the injection of the radiotracer. The first 30 frames are summed to form a composite image on which four regions of interest are drawn: (1) liver (mid part of the right lobe excluding the right kidney and aorta), (2) lower right lung, (3) spleen, and (4) cross talk region between the right lung and the liver (Fig. 5.2.2). The left kidney is substituted for the spleen in patients with splenectomy.

Slope Method

Time-activity curves are generated over all four regions as outlined above (Fig. 5.2.3A). The cross-talk curve from the region between the right lung and liver (Fig. 5.2.3B) is scaled to the same height as the early part of the liver curve (before the arrival of the liver arterial phase, usually between 0 and 20 s) and subtracted from the liver and spleen curve to generate the corrected liver and spleen curves (Fig. 5.2.3C). Corrected liver and spleen curves are displayed separately (Fig. 5.2.3D, E). Three time points are identified on the corrected time-activity curve. The initial arrival of radioactivity at the liver is denoted by Ta, which corresponds to the beginning of the hepatic arterial phase. Because the hepatic and splenic arteries have a common origin from the celiac artery, the time of peak activity on the spleen curve (Sp) is considered the end of the arterial phase and beginning of the portal venous phase, and corresponds to time, Tp, on the liver curve (Fig. 5.2.3D).

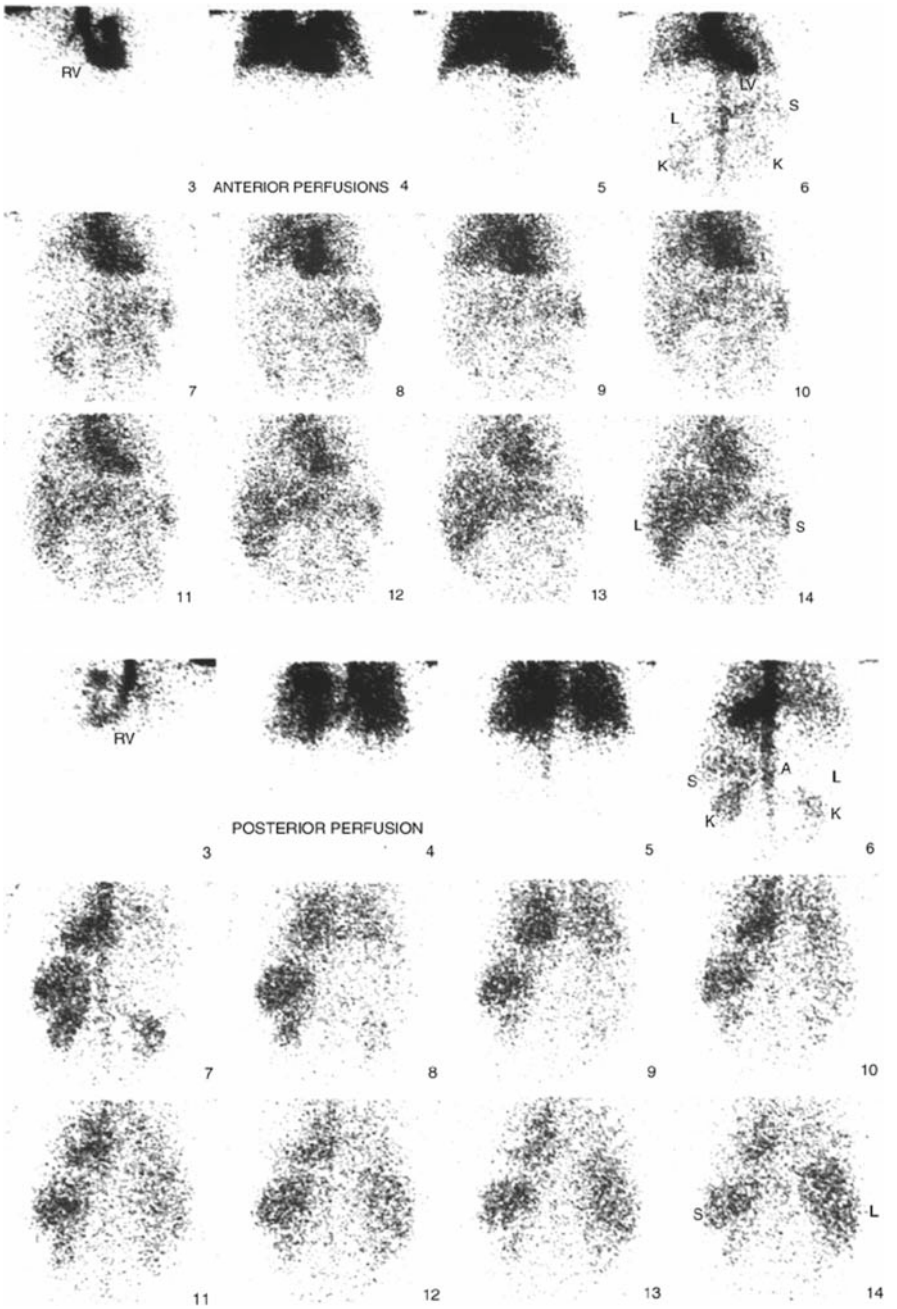

Fig. 5.2.1 Liver perfusion study. Anterior (*top*) and posterior (*bottom*) view liver perfusion study obtained with 5 mCi Tc-99m-HIDA shows the passage of radiotracer serially through the right ventricle (*RV*), left ventricle (*LV*), abdominal aorta (*A*), spleen (*S*), kidneys (*K*), and liver. Left lobe perfusion is seen better in the *anterior view*, and the perfusion of the spleen and kidneys is seen better in the *posterior view*

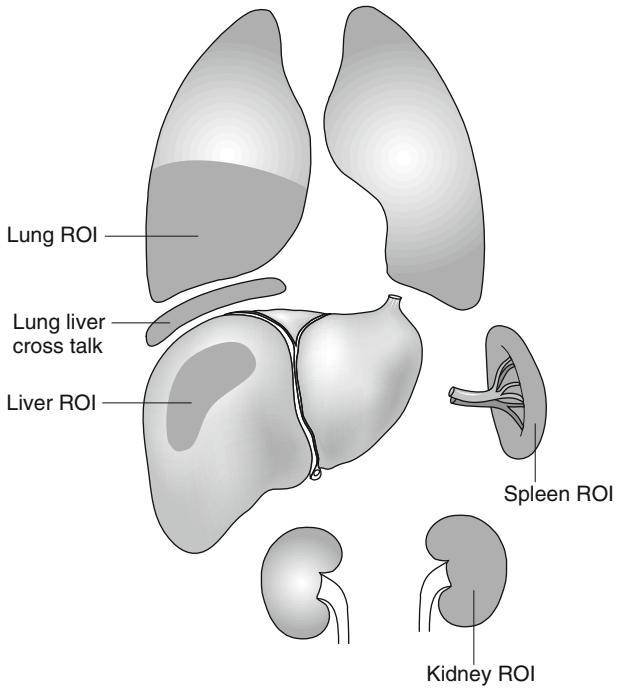

Fig. 5.2.2 Regions of interest. Regions of interest (*ROI*) are drawn over the middle of the liver, right lower lung, spleen, left kidney, and cross-talk region between liver and right lung. ROIs should exclude liver margins and aorta

Normally, there is 7 ± 2-s delay between the arrival of the hepatic arterial and portal venous blood supply to the liver. The slope of the arterial phase, La, is measured from Ta to Ta + 7 s, and the slope of the portal venous phase, Lp, is measured from Tp to Tp + 7 s. Total counts are integrated, and percent arterial blood flow to the liver is measured using the following formula from a linear fit to the curve [2].

$$\text{Percent arterial liver blood flow} = \text{La} / (\text{La} + \text{LP}) \times 100$$

La = slope of the hepatic arterial phase; Lp = slope of portal venous phase.

To correct for the fraction of hepatic arterial component still present during the portal venous phase in the liver curve, the slope of the splenic curve is used with the following modification. The ratio of Sa/Sp of the splenic curve is assumed to represent the fraction of the arterial flow present during the portal venous phase of the liver curve [2].

$$\text{Correct portal slope (Lp correct)} = \text{Lp} - \text{La (Sp / Sa)}$$

$$\text{Percent arterial liver blood flow} = \text{La} / [\text{La} + \text{Lpcorrect}] \times 100$$

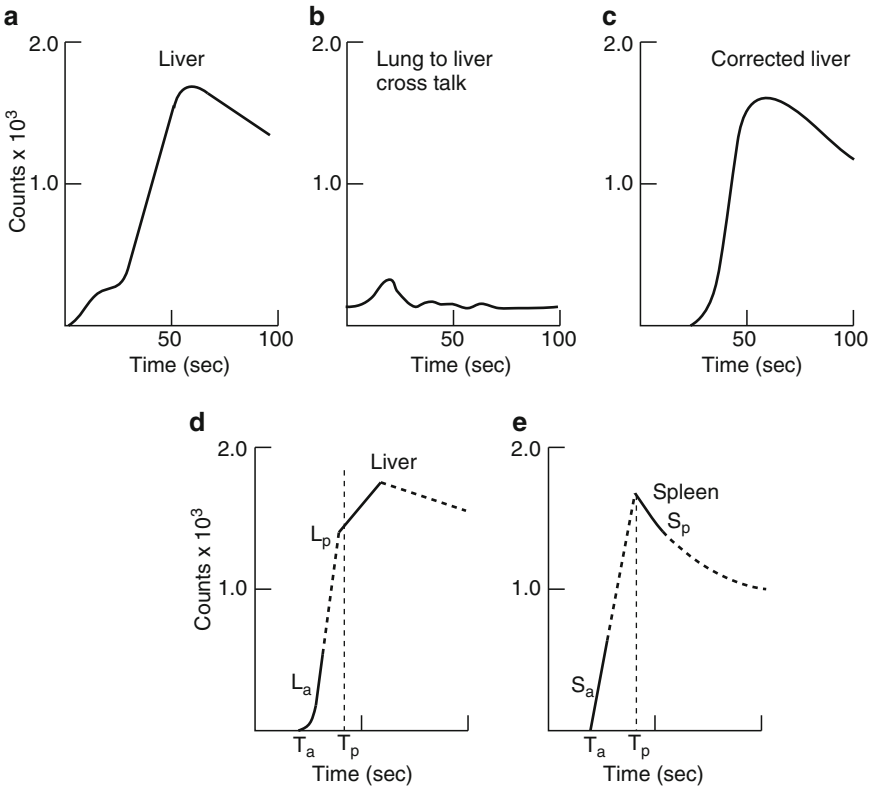

Fig. 5.2.3 Hepatic arterial vs. portal venous blood flow by the slope method. Time-activity curves are generated over the liver (**a**) and cross-talk region between the lung and liver (**b**). Both curves are scaled to the same height, and the corrected liver curve (**c**) is obtained after subtracting the cross-talk counts. The onset of the arterial (*Ta*) and portal venous (*Tp*) phases are noted on the corrected liver curve (**d**). *La* and *Lp* represent the slope of the arterial and portal venous phases measured over 7 s from *Ta* and *Tp*, respectively. Spleen curve (**e**) shows the onset of arterial (*Ta*) and peak arterial flow (*Tp*); *Sa* and *Sp* represent the slopes of the curve in a manner similar to *La* and *Lp* [2, 4]

Area Method

This method uses the deconvolutional analysis [2, 4]. Like the slope method, it is dependent upon the temporal separation between the arrival of the hepatic arterial and portal venous blood to the liver. It takes into account the role of recirculation of the injected radiotracer. Data acquisition is identical to the slope method described above (Fig. 5.2.1). Using a large of field of view gamma camera, computer data are collected on a 64 × 64 word matrix at one frame per 0.5 s for 100 s. The data collection is started just before injection of 10–15 mCi (555–740 MBq) of the radiotracer. On the first 30-frame composite image, regions of interest are drawn, and time/activity curves are generated over: (1) liver, mid right lobe excluding the right kidney and aorta, (2) lower right lung, (3) spleen, and (4) cross-talk region between the right lung and liver (Fig. 5.2.2). The cross-talk curve is scaled to the

same height as the initial part of the liver curve (before the arrival of the radiotracer to the liver) and subtracted from the liver and spleen curve to generate the corrected liver and spleen curve (Fig. 5.2.4A). Liver and spleen curves are deconvoluted with the lung curve using the modified Fourier transformation technique (Fig. 5.2.4B). The curve is expanded from 200 to 1,024 data points by addition of an exponentially decreasing tail that eliminates artifacts because of a sharp cutoff at the end of data termination. An assumption is made that the spleen blood flow pattern is similar to that of the hepatic artery. The spleen curve is used to approximate hepatic arterial blood flow. The spleen curve is multiplied by a constant so that the up-slope superimposes over the early part of the liver curve (Fig. 5.2.4C). The liver and modified spleen curves are integrated to give the areas under the curve, A_L and A_s, respectively

$$\text{Arterial liver blood flow (\%Ha)} = \text{As} / \text{AL} \times 100$$

$$\text{Portal venous blood (\%)} = 100 - \%\text{Ha}$$

Both the slope and area methods are found clinically useful and have been validated in experimental animals [5]. The slope method technically is much simpler, but carries wider variability between studies. The area method using the deconvolutional analysis provides the best separation between normal patients and those with increasing severity of liver disease. The arterial-to-venous ratio increases as the severity of liver disease increases from Child's class A to C (Table 5.1.3). In cirrhosis, low pressure (7–10 mmHg) portal venous blood flow is affected much earlier than high pressure (100–120 mmHg) hepatic arterial blood flow. Portal venous blood flow decreases as the portal venous pressure raises (Fig. 5.2.5). Measurement of the hepatic arterial vs. portal venous blood flow is found useful in the diagnosis of hepatic vein thrombosis and also in following patients treated for portal hypertension [4].

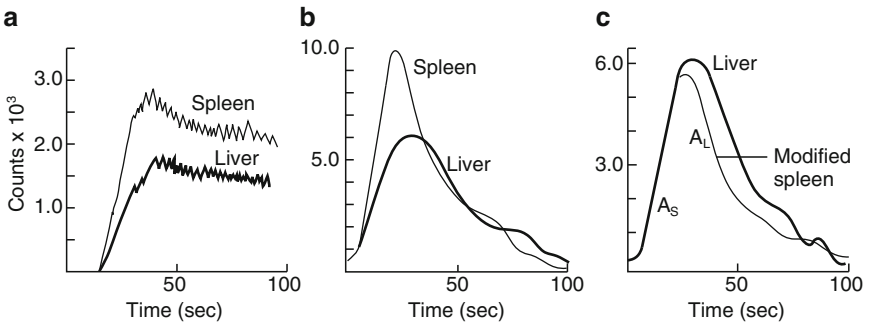

Fig. 5.2.4 Hepatic arterial vs. portal venous blood flow by the area method. Corrected spleen and liver curves are obtained first (**a**) after subtracting the background counts from the lung to liver cross-talk region and then subjected to deconvolutional analysis (**b**). Magnitude of the spleen curve is modified so that its upslope matches with that of the liver (**c**). A_s and A_L represent the area under the modified spleen and liver curves, respectively

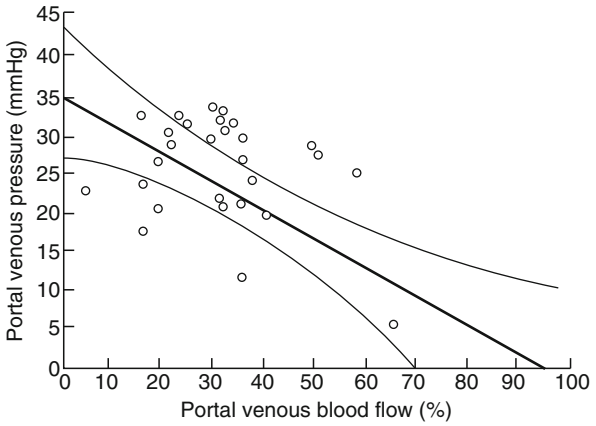

Fig. 5.2.5 Relationship between portal venous blood flow vs. portal venous pressure. There is an inverse relationship between the two; as the portal venous pressure increases, the portal venous blood flow decreases [7]

The final shape of the liver and spleen curve depends upon whether or not the chosen agent is retained by these organs. Technetium-99m sulfur colloid, which is retained by both organs, and Tc-99m-HIDA, which is retained only by the liver but not by the spleen, produce curves whose shape is different from each other and also from those agents (Tc-99m labeled MDP, albumin, or pertechnetate) not retained by either organ. The choice of the agent does not usually affect the values of arterial vs. venous blood flow, because the first-pass study is independent of the biokinetic behavior of the radiotracer [5].

Normal median portal venous blood flow is 78% and the median hepatic artery flow 22%. The median portal venous blood flow decreased to 68% in mild liver disease and remains below 49% in severe liver disease. The median portal venous blood flow falls below 4% in patients with portal vein thrombosis. Scintigraphic technique is shown to be 90% sensitive and 100% specific in patients with portal vein thrombosis when portal blood flow falls below 20% [4]. Perfusion changes and indices of hepatic arterial blood flow in patients with cirrhosis can be measured by comparing them to the renal or splenic arterial peak, thus avoiding the influence of portal venous reduction on the hepatic arterial peak [6]. Calculation of the hepatic arterial-to-portal venous ratio provides a non-invasive method to evaluate objectively the benefits of transjugular intrahepatic portosystemic shunt (TIPS) therapy. In a study involving 28 patients, the mean (SD) portal venous pressure of 25.5 ± 4.6 mmHg before TIPS decreased to 18.5 ± 3.9 mmHg after TIPS. The portal venous blood flow of 29.2 ± 11.1% before then increased to 38.2 ± 13.4% after TIPS, indicating its therapeutic benefits. Portal venous flow shows an inverse relationship with the portal venous pressure; portal venous blood flow decreases as the portal venous pressure increases. The relationship between portal venous flow and pressure tends to normalize after a successful TIPS procedure [7, 8].

References

1. Sarper R, Tarcan YA. An improved method of estimating the portal venous fraction of total hepatic blood flow from computerized radionuclide angiography. Radiology 1983;147:559–562
2. O'Connor MK, MacMathuna P, Keeling PWN. Hepatic arterial and portal venous components of liver blood flow: a dynamic scintigraphic study. J Nucl Med 1988;29:466–472
3. Biersack HJ, Torres J, Thelen M, Monzon O, Winkler C. Determination of liver and spleen perfusion by quantitative sequential scintigraphy: results in normal subjects and in patients with portal hypertension. Clin Nucl Med 1981;6:218–220
4. McMathuna P, O'Connor MK, Weir DG, Keeling PWN. Non-invasive diagnosis of portal vein occlusion by radionuclide angiography. Gut 1992;33:1671–1674
5. O'Connor MK, Krom RF, Carton EG, Sanchez-Urdazpal L, Juni JE, Ferguson DM, Wiesner RF. Ratio of hepatic arterial-to-portal venous blood flow-validation of radionuclide techniques in an animal model. J Nucl Med 1992;33:239–245
6. Koranda P, Myslivecek M, Erban J, Seidlova V, Husak V. Hepatic perfusion changes in patients with cirrhosis. Indices of hepatic arterial blood flow. Clin Nucl Med 1999;24:507–510
7. Menzel J, Schober O, Reimer P, Domschke W. Scintigraphic evaluation of hepatic blood flow after intrahepatic portosystemic shunt (TIPS). Eur J Nucl Med 1997;24:635–641
8. Ganger DR, Klapman JB, McDonald V, Matolon JA, Kaur S, Rosenblate H, Kave R, Saker M, Jensen DM. Transjugular intrahepatic portosystemic shunt (TIPS) for Budd-Chiary syndrome and portal vein thrombosis. Am J Gastroenterol 1999;94:603–608

5.3 Hepatopulmonary Syndrome

The functional relationship between the liver and lung originally recognized in 1935 is now called hepatopulmonary syndrome (HPS). The syndrome consists of a triad of: (1) liver disease, (2) increased alveolar-arterial oxygen gradient, and (3) intrapulmonary vasodilatation [1, 2].

Clinical Presentation

Patients usually present with a combination of symptoms indicative of both liver and lung disease: esophageal varices, gastrointestinal bleeding, spider nevi, ascites, and splenomegaly, indicative of liver disease, and dyspnea, clubbing, platypnea, and orthodeoxia, indicative of lung disease [3, 4]. Platypnea is dyspnea in an upright position, which is relieved by assuming a supine position [5]. Orthodeoxia is arterial deoxygenation, exaggerated in the upright position and relieved by recumbency. Platypnea and orthodeoxia, which were found only in a small percentage of patients with cirrhosis (5%), are much more frequent and severe in intensity in patients with HPS, often reaching as high as 88–100% [6]. Spider nevi of the palms and around the umbilicus are considered the cutaneous markers of HPS [7]. As the liver reaches its end stage, the patients develop ascites, generalized edema, pleural effusion, and interstitial fluid accumulation in the lungs. Chest X-ray changes consist of either finely diffuse spidery infiltrates or focal arteriovenous malformations [8].

Pathophysiology

Arterial deoxygenation due to an intrapulmonary shunt is the hallmark of HPS. Pulmonary artery pressure remains normal or slightly low [6]. Severe hypoxemia (PaO_2 <60 mmHg), in the absence of primary lung disease, in combination with liver disease clinically should raise the suspicion of HPS. The pulmonary capillaries, which normally measure 8–15 μm, dilate up to 100 μm in diameter, often forming spider nevi on the pleural surface [9]. Radiolabeled macroaggregates of albumin (MAA) of 15–150 μm in diameter normally get trapped almost completely within the pulmonary capillary bed after intravenous injection. These radiolabeled Tc-99m MAA particles readily pass through the dilated pulmonary capillaries in patients with HPS and enter the systemic circulation to be trapped in normal size capillaries of the brain, liver, kidney, and other organs, in proportion to their blood supply [10, 11, 12]. Normally less than 6% of Tc-99m-MAA particles bypass the lung to lodge in other organs [11, 13]. It is theorized that the liver in HPS either produces vasodilators or is incapable of inactivating vasodilators produced elsewhere. Incriminated vasodilators include prostaglandins, vasoactive intestinal polypeptide, calcitonin, glucagon, nitric oxide, and atrial natriuretic factor, etc. [6].

Diagnosis

Arterial blood gases are obtained to document hypoxemia (Table 5.3.1). Contrast 2D echocardiography (2D echo) with indocyanin green or agitated saline is the most preferred initial diagnostic imaging procedure [14, 15]. Saline agitation creates microbubbles of 60–90-μm size, which opacify the right heart chambers within one to three cardiac cycles after injection into an antecubital vein. The left heart chambers are not opacified due to filtration of all bubbles by the normal lung capillaries [16]. The bubbles pass through dilated intrapulmonary capillaries in HPS to enter the pulmonary veins and left heart chambers. A confirmatory

Table 5.3.1 Diagnostic workup for hepatopulmonary syndrome (modified from [18])

Cirrhosis with hypoxemia		
	Chest X-ray	
	Normal	Abnormal (treat, if hypoxemia persists)
Contrast echo (EC) and pulmonary function tests (PFTs)		
(−) CE and normal PET	(+) CE and normal	(+) CE and abnormal
	PFT's	PFT's
↓	↓	↓
No HPS	**HPS**	Tc-99m MAA Scan
		Shunt >6% / Shunt <6%
		↓ / ↓
		HPS / **No HPS**

diagnosis of HPS requires documentation of arterial hypoxemia (PaO_2 less than 70 mmHg), normal pulmonary function tests, typical chest X-ray findings, and opacification of left heart chambers in the absence of a right-to-left cardiac shunt. Right-to-left cardiac shunt is suggested on a 2D echo when both right and left ventricular chambers are opacified simultaneously, within one to three cardiac cycles after intravenous injection of agitated saline [17].

Scintigraphic Quantification

A mild form of HPS is found in as many as 4–17% of patients with varieties of chronic liver diseases [18]. Despite being very sensitive, 2D echo lacks the specificity and ability to quantify the degree of shunt. A perfusion scintigraphy supplements 2D echo by providing both quantification and specificity for a definitive diagnosis of HPS.

Procedure

The patient is made to sit upright for 5 min to maximize the degree of intrapulmonary shunt. Macroaggregates of Tc-99m-albumin particles are prepared carefully as per instructions provided in the package insert. A drop of the prepared material is fed into a hemocytometer chamber and examined under the light microscope to ascertain that at least 90% of the particles are in the 15–90-μm size range. A radiochromatogram is obtained to confirm that there is better than 90% radiolabeling. About 2–3 mCi Tc-99m-MAA is injected into an antecubital vein while the patient is seated. After injection, the patient is made to lay supine. A large field of view dual-head gamma camera, fitted with a low-energy, all purpose, parallel-hole collimator, is positioned laterally on each side, or in front and behind the head. The spectrometer is set for 140-keV photon peak energy with a 20% symmetrical window. The camera heads are positioned above the shoulders to avoid counts below the neck. The counts are taken for a preset time of 5 min with each head and recorded on a 64 × 64 computer matrix. After taking 5-min head counts, the detectors are moved over to the chest to the anterior and posterior position. Preset 5-min counts are taken again in the anterior and posterior view simultaneously and recorded on a 64 × 64 computer matrix.

Data Analysis

On the lateral or anterior and posterior views of the head, regions of interest are drawn to cover the entire brain, excluding the scalp and superior sagittal sinus when they are visible. On the anterior and posterior view chest images, regions of interest are drawn to cover both lungs. Care is taken to avoid the liver or kidneys in the lung ROI (Fig. 5.3.1). Geometric mean counts are calculated using the following formula:

$$\text{Geometric mean brain counts (GMBC)} = \sqrt{\text{right lateral or anterior view brain counts} \times \text{left lateral or posterior view brain counts}}$$

$$= \sqrt{1022 \times 1262} = 1{,}135$$

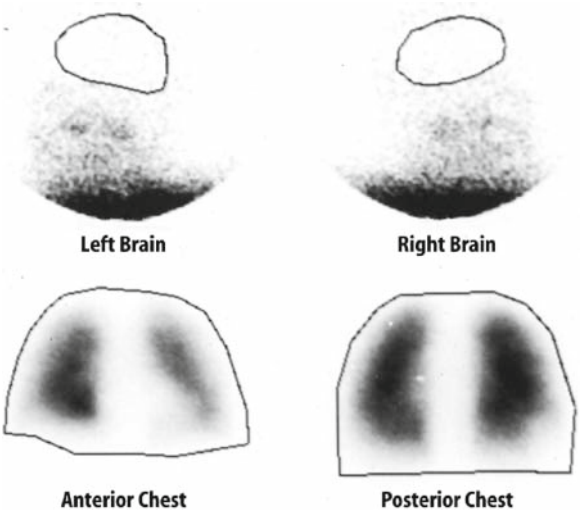

Fig. 5.3.1 Quantification of hepatopulmonary shunt: Regions of interest are drawn over the brain in two lateral views of the head and over the lungs in the anterior and posterior views of the chest. Total counts in 5 min are noted in each view. The geometric mean counts are obtained by using the equation given in the text. Hepatopulmonary shunt ratio is obtained by dividing brain counts by the sum of brain and lung counts

$$\begin{aligned}&\text{Geometric mean lung counts } (\text{GMBC})\\&= \sqrt{\text{anterior view lung counts} \times \text{posterior view lung counts.}}\\&= \sqrt{637{,}417 \times 970{,}115} = 786{,}363\end{aligned}$$

An assumption is made that about 13% of the cardiac output is delivered to the brain [19]. By applying this correction factor, the hepatopulmonary shunt is calculated by the following equation:

$$\begin{aligned}\text{Hepatopulmonary shunt } (\text{HPS}) &= \frac{\frac{\text{GMBC}(\text{Brain})}{0.13}}{\frac{\text{GMBC}(\text{Brain})}{0.13} + \text{GMLC}(\text{Lung})}\\&= \frac{1{,}135 / 0.13}{1{,}135 / 0.13 + 786{,}363}\\&= 8730 / 795{,}093 = 0.02 = 2\%\end{aligned}$$

In normal subjects and in patients with intrinsic lung disease or with cirrhosis but without shunt, the hepatopulmonary shunt ratio varies from 3 to 6% [11, 17]. A value higher than 6% is considered indicative of HPS [17, 18]. Patients with Child's class A, B, or C liver

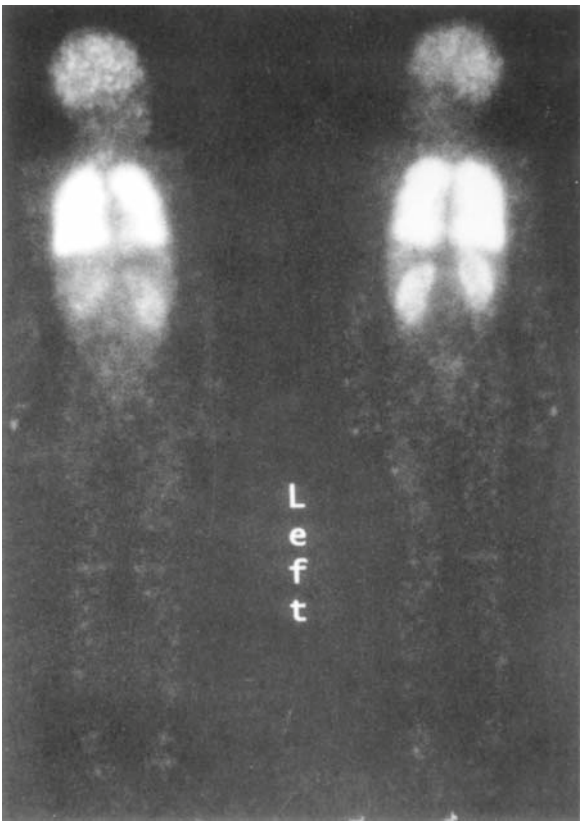

Fig. 5.3.2 Hepatopulmonary shunt. An 8-year-old boy waiting for liver transplantation has 37% right-to-left shunt due to intrapulmonary vasodilatation. In addition to brain, kidneys and liver are seen in a Tc-99m MAA scan [20]

disease without HPS generally show values below 5%. The mean shunt value is 30 ± 4% in patients with hepatopulmonary syndrome. A shunt value of 37% was found in an 8-year-old child (Fig. 5.3.2) waiting for liver transplantation [20].

Standardization

The technique of measuring hepatopulmonary shunt is very simple, and often there may be room for complacency. It is necessary to check rigidly for Tc-99m-MAA particle size and percent labeling. Greater than 90% of the particles should be between 15 and 90 μm in size, and labeling efficiency better than 90%. A preparation not meeting these two requirements is discarded. Injection of too many small particles (below 15 μm) overestimates the degree of the shunt, and the shunt is underestimated when too many particles are much larger than 90 μm in size.

Treatment

Treatment is medical in early liver failure and surgical for end-stage liver disease. Medically, the patients are treated with indomethacin [21], almitrine bismesylate [22], octreotide, or other drugs [6]. Surgical treatment involves liver transplantation for end-stage liver disease. Liver transplantation, once listed as a clear contraindication, is now considered an optimal therapy for HPS and is shown to improve both liver and pulmonary functions [23]. In the Cleveland Clinic study, the mean ratio of 18.7% in HPS patients decreased to 4.5% after liver transplantation with marked improvement of pulmonary blood gases [24].

References

1. Snell AM. The effect of chronic disease of the liver on composition and physiochemical properties of blood: changes in the serum proteins; reduction in the oxygen saturation of the arterial blood. Ann Intern Med 1935;9:690–711
2. Kennedy TC, Knudson RJ. Exercise aggravated hypoxemia and orthodeoxia in cirrhosis. Chest 1977;72:305–309
3. Krowka MJ, Cortese DA. Hepatopulmonary syndrome: an evolving perspective in the era of liver transplantation. Hepatology 1990;11:138–142
4. Robin ED, Laman D, Horn BR, Theodore J. Platypnea related to orthodeoxia caused by true vascular lung shunts. N Engl J Med 1976;294:941–943
5. Altman M, Robin ED. Platypnea (diffuse zone 1 phenomenon?) N Engl J Med 1969;281:1347–1348
6. Lange PA, Stoller JK. The hepatopulmonary syndrome. Ann Intern Med 1995;122:521–529
7. Sherlock S. Liver-lung interface. Semin Respir Med 1988;9:247–253
8. Krawka MJ, Dickson ER, Cortese DA. Hepatopulmonary syndrome. Clinical observation and lack of therapeutic response to somatostatin analogue. Chest 1993;104:515–521
9. Berthalot P, Walker JG, Sherlock S, Reid L. Arterial changes in the lungs in cirrhosis of the liver-lung spider nevi. N Engl J Med 1966;274:291–298
10. Genovesi MG, Tierney DF, Taplin GV, Eisenberg H. An intravenous radionuclide method to evaluate hypoxemia caused by abnormal alveolar vessels. Limitation of conventional technique. Am Rev Respir Dis 1976;114:59–65
11. Wolfe JD, Tashkin DP, Holly FE, Brachman MB, Genovesi MG. Hypoxemia of cirrhosis: detection of abnormal small pulmonary vascular channels by a quantitative radionuclide method. Am J Med 1977;63:746–754
12. Gates GF, Orme HW, Dore EK. Cardiac shunt assessment in children with macroaggragated albumin technetium-99m. Radiology 1974;112:649–653
13. Robin ED, Horn B, Goris ML, Theodore J, Kessel AV, Mazoub J, et al. Detection, quantitation, and pathophysiology of lung spiders. Trans Assoc Am Physicians 1975;88:202–216
14. Hind CR, Wong CM. Detection of pulmonary arteriovenous fistulas in patients with cirrhosis by contrast 2D echocardiography. Gut 1981;22:1042–1045
15. Shub C, Tajik AJ, Seward JB, Dines DE. Detecting intrapulmonary right-to-left shunt with contrast echocardiography. Observation in patients with diffuse pulmonary arteriovenous fistulas. Mayo Clin Proc 1976;51:81–84
16. Krowka MJ, Tajik AJ, Dickson ER, Wiesner RH, Cortese Da. Intrapulmonary vascular disorders (IPVD) in liver transplant candidates. Screening by two-dimensional contrast-enhanced echocardiography. Chest 1990;97:1165–1170
17. Abrams GA, Jaffe CC, Hoffer PB, Binder HJ, Fallon MB. Diagnostic utility of contrast echocardiography and lung perfusion scan in patients with hepatopulmonary syndrome. Gastroenterology 1995;109:1283–1288

18. Abrams GA, Nanda NC, Dubovsky EV, Krowka MJ, Fallon MB. Use of macroaggregated albumin lung perfusion scan to diagnose hepatopulmonary syndrome: a new approach. Gastroenterology 1998;114:305–310
19. Wade OL, Bishop JM. Cardiac output and regional blood flow. Blackwell Scientific, Oxford, England, 1962
20. Murakami JW, Rosenbaum DM. Right-to-left pulmonary shunting in pediatric hepatopulmonary syndrome. Clin Nucl Med 1999;24:897
21. Andrivet P, Cadranel J, Housset B, Harigault R, Harf A, Anot S. Mechanism of impaired arterial oxygenation in patient liver cirrhosis and severe respiratory insufficiency. Effect of indomethacin. Chest 1993;103:500–507
22. Krowka MJ, Cortese DA. Severe hypoxemia associated with liver disease. Mayo Clin experience and the experimental use of almitrine bismesylate. Mayo Clin Proc 1987;62:164–173
23. Scott VL, Dodson F, Kang Y. The hepatopulmonary syndrome. Surg Clin North Am 1999; 79:23–41
24. Lange PA, Vogt DA, Carey WB, Stroller JK. Prevalence and reversibility of hepatopulmonary syndrome following liver transplantation. Am Rev Respir Dis 1993;147:540A (abstract)

5.4 Duodenogastric Bile Reflux

Gastrointestinal peristalsis begins at the gastric pacemaker located near the gastro-esophageal junction and travels antegrade towards the gastric fundus, body, and pylorus, and progresses further along the small and large intestine. Peristaltic waves move the gastrointestinal intraluminal contents in an antegrade fashion. Duodenal contents are thus prevented from entering the stomach by the dual action of the antegrade peristalsis and contraction of pyloric sphincter [1]. Patients with atrophic gastritis, gastric ulcer, and esophagitis are often found to have bile in the stomach (duodeno-gastric bile reflux) raising an etiological relationship between dyspepsia and bile reflux [2].

Detection of bile by chemical analysis in the gastric juice aspirated through a nasogastric tube has been used over the years as a test for duodeno-gastric bile reflux. Chemical analysis is not only cumbersome, but also the insertion of the naso-gastric tube itself may cause duodeno-gastric bile reflux (DGBR). Counting or imaging of radiolabeled bile in the stomach makes the test technically much simpler and avoids the necessity of chemical analysis and intubation [3]. Gamma camera imaging makes the test readily acceptable, enables detection, provides quantification of the degree of duodeno-gastric (D-G) bile reflux, and avoids the necessity of gastric juice aspiration through the N-G tube in both children and adults [4].

Rationale

After its secretion by the liver, the hepatic bile enters the gallbladder or duodenum, or both. During fasting, about 70% of the hepatic bile enters the gallbladder, and the remaining 30% enters the duodenum directly [5]. Facilitated by the peristaltic waves, bile entering the duodenum moves forward with the rest of the duodenal contents received from the stomach.

Since only the amount of bile entering the duodenum is available for reflux into the stomach, a technique that enables quantitative measurement of bile entry into the duodenum will be ideal for measuring bile flow forward into the jejunum or backward into the stomach (D-G reflux). Bile entering the gastrointestinal tract is quantified by selecting two regions of interest: one over the stomach and another over intestinal tract (excluding liver, gallbladder, and bile ducts). Duodeno-gastric bile reflux is calculated by dividing total stomach counts by total counts in the stomach and intestine. The technique allows measurement of D-G bile reflux both during fasting and after administration of cholecystokinin or after feeding.

Data Collection and Analysis

Hepatic phase imaging data are used for calculation of D-G bile reflux during fasting, and gallbladder phase imaging data for calculation of post-cholecystokinin or post-prandial D-G bile reflux. Data are collected as outlined in Table 5.1.1. By 60-min post-injection, most of Tc-99m HIDA clears from the liver, leaving the nearby gastric region free of interference by cross-talk counts from the left lobe of the liver (Fig. 5.4.1). All 60-min data are

Table 5.4.1 Bile flow into stomach vs. small intestine in 20 normal subjects

No.	Subject	Total stomach counts	Total intestinal counts	% Stomach	% Intestine
1	HC	93,729	3,830,883	2.3	97.7
2	H	71,380	3,012,831	2.3	97.7
3	CC	36,521	2,684,925	1.3	98.7
4	E	51,226	1,483,318	3.3	97.3
5	EJ	103,127	3,651,893	2.7	97,3
6	GE	43,555	1,091,999	3.8.	96.2
7	AP	67,967	2.661,020	2.5	97.5
8	B	42,169	1,309127	3.1	96.9
9	BB	85,603	2,063,219	3.9	96.1
10	WD	20,095	616,171	3.2	96.8
11	HR	40,526	1,169,047	3.3	96.4
12	LC	23,421	3,343,890	0.7	99.3
13	KD	19,204	731,084	2.5	97.5
14	KJ	15,746	2,107,383	0.7	99.3
15	KC	26,342	2,259,335	1.1	99.9
16	MV	16,093	459,163	3.4	96.6
17	MK	20,084	1,299,986	1.5	98.5
18	NL	27,480	680,653	3.8	96.2
19	O	28,626	1,847,370	1.5	98.5
20	PJ	24,585	1,545,024	1.6	98.4
			Mean ± SD	2.4 ± 1.05	97.6 ± 1.05
			S.E	0.23	0.23

Note: No background subtraction was made from either the stomach or intestine

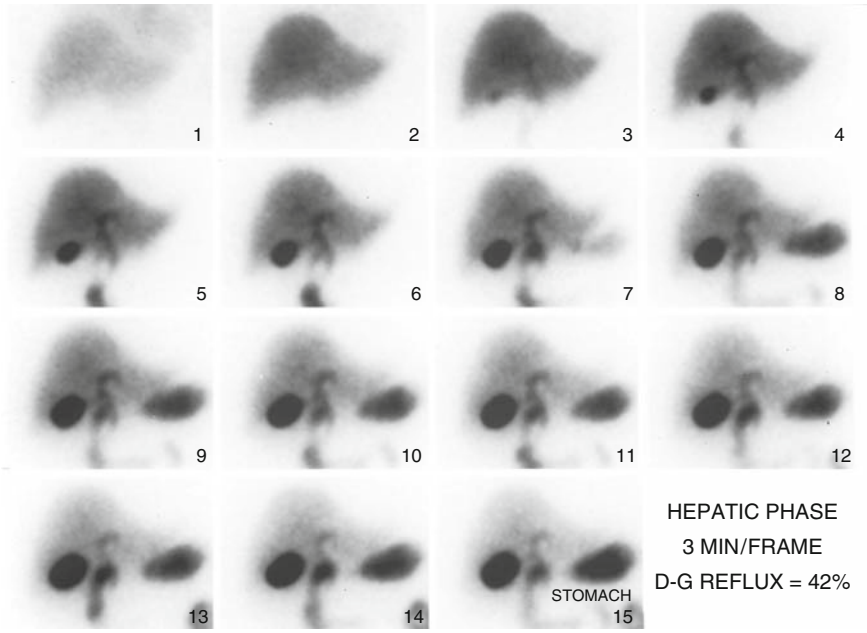

Fig. 5.4.1 Basal duodeno-gastric bile reflux. Duodeno-gastric bile reflux is rare in normal subjects. Reflux in this patient occurs early (*frame no. 7*) and continues throughout. It is calculated as a part of Hep-phase data analysis

carefully reviewed in a cine display for any overlap of intestinal radioactivity onto gastric ROI [6]. A frame between 50 and 60 min (usually the 60-min frame) that does not contain any superimposition of intestinal loops onto the gastric bed is chosen for selection of gastric and intestinal ROIs. Gastric ROI includes the traditional gastric bed, below the left lobe of liver and to the left side of the distal common bile duct, and extending laterally up to the splenic bed. The intestinal ROI includes the rest of the upper abdomen, excluding the liver, gallbladder, and common bile duct. The urinary bladder is excluded from intestinal ROI (Fig. 5.4.2). Time/activity curves are generated from both ROIs. By 60-min post-injection, most of radioactivity clears from the cardiac blood pool and kidneys. Sometimes the D-G reflux may occur early and empty in the late hepatic phase imaging. In such circumstances the frame with the peak D-G reflux is chosen for ROI selection. The counts are corrected for physical decay.

$$\begin{aligned}&\text{Duodeno-gastric bile reflux (\%)}\\&= \frac{\text{Total counts in gastric ROI} \times 100}{\text{Total counts in gastric ROI} + \text{Total counts in intestinal ROI}}\\&= \frac{54{,}173 \times 100}{54{,}173 + 74{,}066}\\&= 42\%\end{aligned}$$

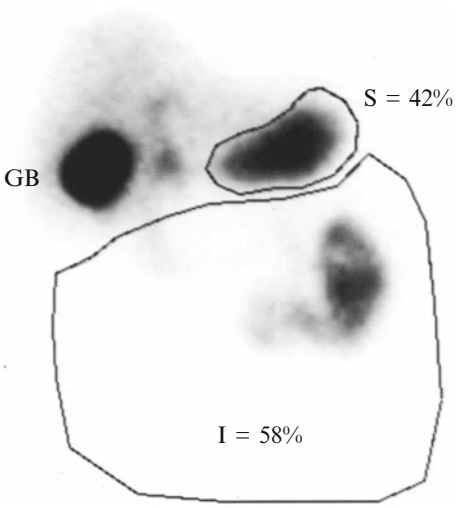

Fig. 5.4.2 Post-CCK-8 duodeno-gastric bile reflux. It is calculated as an integral part of GB-phase data analysis. The gastric ROI (*S*) is drawn below the left lobe of the liver, on the left side of the distal common bile duct extending laterally to the splenic region. The intestinal ROI (*I*) encompasses the rest of the abdomen. Basal D-G bile reflux of 42% (Fig. 5.4.1) increased to 58% with CCK-8

Bile reflux after CCK-8 is similarly calculated using data obtained during the gallbladder phase. Cholecystokinin normally induces the contraction and emptying of the gallbladder, stimulates contraction of the pyloric sphincter, and simultaneously increases small intestinal peristalsis, facilitating rapid antegrade bile movement through the small bowel. Contraction of the pyloric sphincter normally prevents D-G bile reflux. Post-CCK images are checked in the cine display to ascertain that there is no movement of bile radioactivity beyond the field of view of the gamma camera. If there is, then the gamma camera position is adjusted to include all bile regions, and an additional view over the lower abdomen is taken. Cine display of all frames is essential to ascertain that no intestinal loop is encroaching upon the gastric region, and when found, such frames are excluded for ROI selection [7]. Often there is no D-G bile reflux during fasting; rather, it occurs only after CCK-8 (Fig. 5.4.3).

Bile Reflux in Health and Disease

The data shown in Table 5.4.1 were collected in 22 patients without gallstones who were referred for measurement of the gallbladder ejection fraction. They did not have any symptoms of gastric dyspepsia. Mean D-G reflux in these subjects was 2.4% (95% CI = 0.4–4.4%). D-G reflux during fasting or after CCK-8 administration is rare and usually does not exceed 5%. When significant reflux is found, it suggests bile gastritis may be responsible for patient symptoms. Prokinetic agents are often prescribed for patients with large volume D-G reflux.

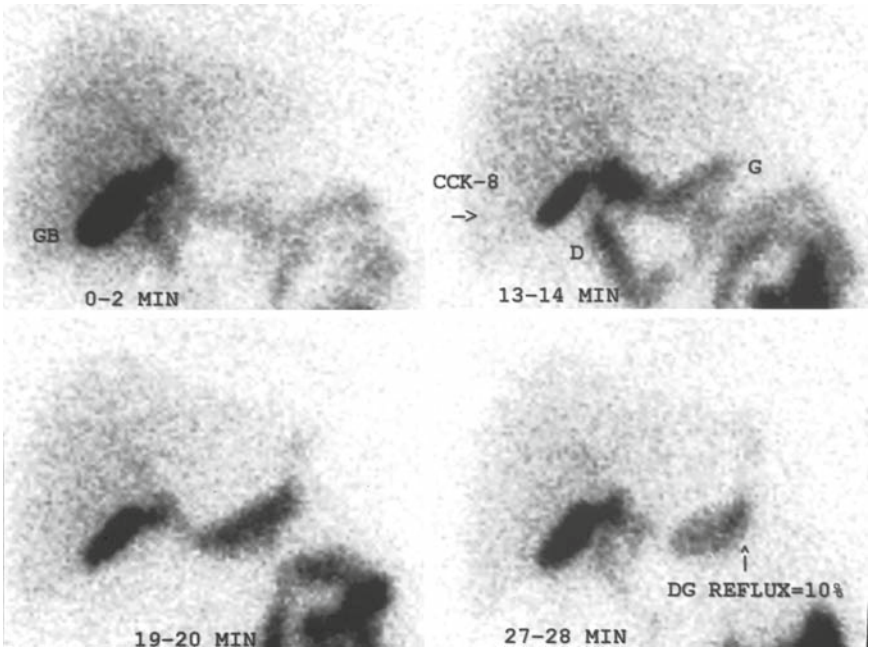

Fig. 5.4.3 Duodeno-gastric bile reflux only after CCK-8. There is no basal D-G bile reflux (0–2 min). Bile reflux of 10% occurs after CCK-8 administration (*G stomach*)

References

1. Fisher RS, Cohen S. Physiological characteristics of the human pyloric sphincter. Gastroenterology 1973;64:67–75
2. Capper WM, Airth GR, Kilby JO. A test for pyloric regurgitation. Lancet 1966;2:621–623
3. Rokkjaer M, Marqversen J, Kraglund K, Peterson J. Quantitative determination of pyloric regurgitation in response to intraduodenal bolus injection. Scand J Gastroenterol 1977;12: 827–832
4. Nicolai JJ, Silberbusch J, vanRoon F, Schopman W, Berg JWO. A simple method for quantification of biliary reflux. Scand J Gastroenterol 1980;15:775–780
5. Krishnamurthy GT, Bobba VR, McConnell D, Turner FE, Mesgarzadeh M, Kingston E. Quantitative biliary dynamics: introduction of a new non-invasive scintigraphic technique. J Nucl Med 1983;24:217–223
6. Sorgi M, Causer D, Wolverson RL, Mosimann F, Tulley N, Ghosh SK, Donovan IA, Alexander-Williams J, Harding LK. Quantification and the elimination of errors in bile reflux tests using a gamma camera. Scand J Gastroenterol 1984;19:33–35
7. Thomas WEG, Jackson PC, Cooper MJ, Davies ER. The problems associated with scintigraphic assessment of duodenogastric reflux. Scand J Gastroenterol 1984;19 (suppl 92): 36–40

5.5 Imaging and Quantification of Hepatocyte Asialoglycoprotein Receptors with Tc-99m Galactosyl Human Serum Albumin

Hepatocyte plasma membrane is rich in asialoglycoprotein (ASGP) receptors, which are not found in any other cell in the body. The receptor is located along the basolateral and lateral domain, but not along the canalicular domain [1]. Technetium-99m-DTPA-galactosyl-human-serum albumin (Tc-99m GSA) binds to these receptors, and the amount bound varies inversely with the severity of liver disease [2–4]. It is not taken up by the spleen and like radiocolloid is not secreted into bile. ASGP receptor concentration on the membrane reflects the functional integrity of the hepatocyte accurately, much like indocyanin green, cholinesterase, serum albumin, and hepaplastin [3]. The quantity of Tc-99m GSA uptake correlates well with blood clearance of indocyanin green (Fig. 5.5.1). Technetium-99 GSA uptake decreases in patients with varieties of liver diseases including chronic hepatitis, cirrhosis, cholangiocarcinoma, hepatocellular cancer, metastasis, fulminant hepatic failure, and space-occupying benign lesions of the liver [2–4].

Almost all of the injected radiotracer clears from the blood and is taken up exclusively by the liver normally within 15 min. Several parameters have been developed to express the hepatocyte function, the most common one being the extraction index at 15 min. It represents the percentage of the integral of the cumulative counts in the liver for 1 min between 15 and 16 min to the total dose [2].

Data Collection and Analysis

After 4–6 h of fasting, with the patient in supine position, a gamma camera (single, double, or a triple head) fitted with a low-energy, high-resolution, parallel-hole collimator is positioned anterior to the liver. Sequential anterior planar images (128 × 128) at 1 frame per 30 s

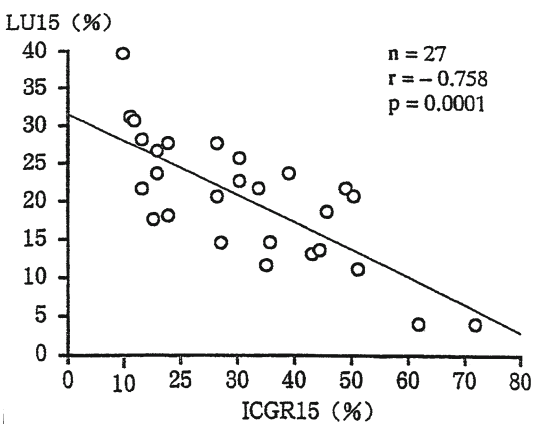

Fig. 5.5.1 Correlation between Tc-99m-GSA uptake (*LU15*, %) and indocyanin green blood retention. There is a good inverse relationship between Tc-99m GSA uptake by the liver with plasma clearance of indocyanin green at 15 min [2]

for 20 min are obtained immediately after a bolus injection of 5 mCi Tc-99m GSA (185 MBq) into the antecubital vein. Immediately after the planar images, SPECT data are acquired on a 128 × 128 × 16-matrix computer for 64 stops at 10 s per stop at a 5.6° interval [2]. The spectrometer is set for 140 keV at a 20% window. Liver uptake at 15 min is calculated by using the following formula.

$$\text{Liver uptake at 15min (LU15)} = \frac{\int_{15}^{16} C(t)\,dt \times 100\%}{\text{Total injected dose}}$$

Whole liver counts and residual liver counts are obtained by measuring organ volume from SPECT images. Whole organ volume is determined by detecting the edge for each slice and then adding all of the slices. The volume of each lobe is obtained by selecting the gallbladder fossa -inferior vena cava plane (plane of Sérégé-Cantele), which divides the liver into physiologic right and left lobes, or by referring to the CT or MRI references [2]. After obtaining the volume, each lobe is divided into its physiologic segments: the right lobe into the anterior and posterior segments, and the left lobe into the medial and lateral segments [2–4]. The ratio of the counts in each lobe to the whole liver counts provides LU15 for the lobe.

Residual count ratio (RCR) is determined by the following formula.

$$\text{RCR} = \text{RC} / \text{WC}$$

where RC = residual liver count from SPECT images (counts from region of the liver left not to be resected), and WC = whole liver count calculated from SPECT images.

$$\text{Index of residual liver function (RLU15)} = \text{LU15} \times \text{RCR}$$

Some authors express uptake as hepatic GSA clearance using the Patlak plot method and generate functional images of clearance (Ku). This method is powerful, but some may raise an issue with the chosen terminology “clearance” for an agent that does not clear from the liver [3, 4]. The uptake shows an excellent correlation with indocyanin green plasma clearance. Estimation of predicted postoperative residual function after resection of the liver for hepatocellular carcinoma, cholangiocarcinoma, and metastatic liver tumors shows good correlation with postoperative liver function (Fig. 5.5.2). This functional parameter may be ideal for predicting end-stage liver disease and timing of liver transplantation.

References

1. Steer CJ. Receptor-mediated endocytosis: mechanisms, biologic function, and molecular properties. In: Zakim D, Boyer TD (eds) Hepatology. A textbook of liver disease. WB Saunders, Philadelphia, 1996, pp 149–214
2. Uetake M, Koizumi K, Yagawa A, Nogata H, Tezuka T, Kono H, Ozawa T, Kusano T, Miyaburuko M, Hosaka M. Use of Tc-99m DTPA galactosyl human serum albumin to predict postoperative residual liver function. Clin Nucl Med 1999;24:428–434

3. Hwang E, Taki J, Shuke N, Nakajima K, Kinuya S, Konishi S, Michigishi T, Aburano T, Tonami N. Preoperative assessment of residual hepatic functional reserve using Tc-99m-DTPA-galactosyl-humen-serum albumin dynamic SPECT. J Nucl Med 1999;40:1644–1651
4. Sasaki N, Shiomi S, Iwata Y, Nishiguchi S, Kuroki T, Kawabe J, Oci H. Clinical usefulness of scintigraphy with Tc-99m-galactosyl-human serum albumin for prognosis of cirrhosis of the liver. J Nucl Med 1999;1652–1656

Gallbladder, Sphincter of Oddi, Cholecystokinin, and Opioid Relation

6

The bile, essential for digestion and absorption of nutrients, is secreted by the liver continuously, stored in the gallbladder during fasting, and discharged into the duodenum intermittently after each meal. The bile salts, which are an important component of bile, promote efficient digestion and absorption of essential nutrients from the intestine. The gallbladder has a unique mechanism to sequester almost all of the bile salts during fasting and release them into the duodenum after the arrival of food. Food stimulates the release of endogenous cholecystokinin into circulation from the endocrine cells lining the mucosa of the duodenum, jejunum, and upper ileum. Cholecystokinin (CCK) acts on its receptors located in the smooth muscle and initiates the contraction and emptying of concentrated bile from the gallbladder; it simultaneously relaxes the sphincter of Oddi to allow smooth passage of bile into the duodenum. During the evolutionary process it appears as though nature has placed these three organs very close to each other anatomically to obtain the maximum efficiency of the biological system (Fig. 6.1.1).

6.1 Effect of Cholecystokinin on the Gallbladder and Sphincter of Oddi

Cholecystokinin

A hormone being responsible for contraction and emptying of the gallbladder was proposed first by Ivy and Oldberg in 1928 [1]. A year later, Ivy and associates identified the hormone and named it "cholecystokinin" (from the Greek: chole = bile, cysto = sac, kinin = move; move the bile sac) because of its primary motor effect on gallbladder contraction [2].

Source

Cholecystokinin is found in various organs of the body, including the gastrointestinal, endocrine, genitourinary, and nervous systems [3]. The highest concentration is found in the upper intestinal tract, cerebral cortex, and anterior pituitary gland [4, 5]. In the gastrointestinal tract, the cells secreting cholecystokinin are distributed primarily in the mucosa of the duodenum, jejunum, and upper ileum (Fig. 6.1.2). There are about 40 million (1.3 million cm^{-1}) CCK-secreting cells in the duodenum, 80 million (0.55 million cm^{-1}) in

G.T. Krishnamurthy and S. Krishnamurthy, *Nuclear Hepatology,*
DOI 10.1007/978-3-642-00648-7_6, © Springer-Verlag Berlin Heidelberg 2009

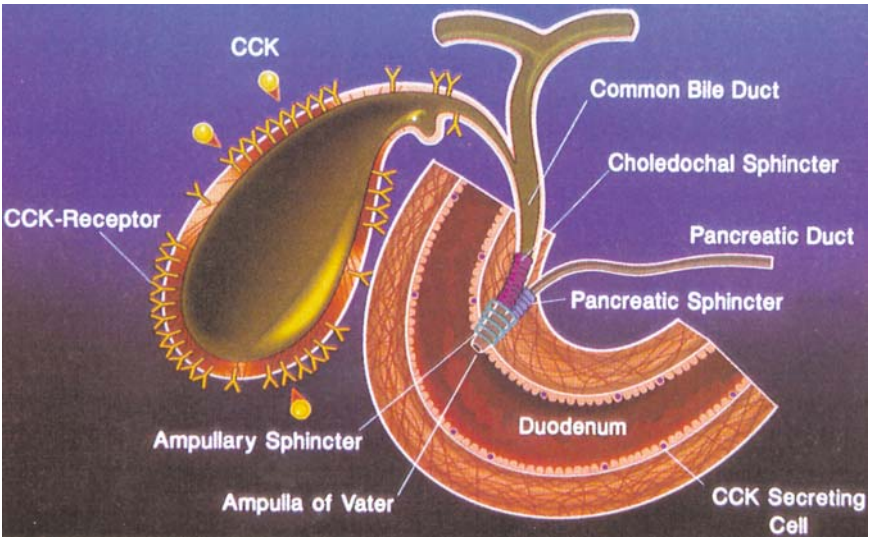

Fig. 6.1.1 The relationship among the sphincter of Oddi, gallbladder, and cholecystokinin. The sphincter of Oddi consists of three components: choledochal sphincter, pancreatic sphincter, and ampullary sphincter. Gallbladder wall contains mainly stimulatory (contraction) and the sphincter of Oddi inhibitory (relaxation) receptors for cholecystokinin. CCK-secreting endocrine cells are distributed densely in the mucosa of the duodenum [44]

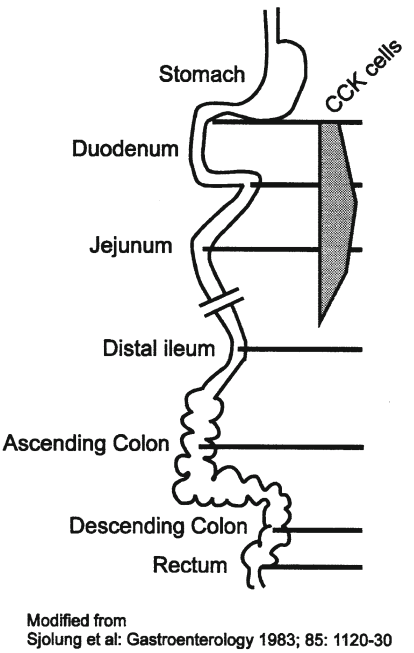

Fig. 6.1.2 Distribution of cholecystokinin and fibroblast growth factor-secreting cells in the alimentary canal. The cholecystokinin-secreting cells are concentrated mainly in the duodenum, jejunum, and proximal ileum. There are no CCK-secreting cells in the esophagus, stomach, and intestinal tract beyond the proximal ileum [4]. Fibroblast growth factor stimulating cells are distributed mainly in the terminal ileum

the jejunum, and about 5 million cells in the entire ileum [4]. There are no CCK-secreting cells in the esophagus, stomach, distal ileum, colon, and rectum. The cerebellum and posterior pituitary gland do not contain any CCK-secreting cells. Two types of hormone-secreting cells are found in the intestinal mucosa: open endocrine cells and closed endocrine cells. Open endocrine cells are tall and flask shaped with microvilli along the free border, which enable direct contact with the digested nutrients passing through the intestinal lumen. Closed endocrine cells are basket shaped without any microvilli and do not reach the mucosal surface and hence have no direct contact with the nutrients passing through the intestinal lumen [6].

Structure

At least five molecular forms of cholecystokinin have been identified. All five are linear-chain polypeptides, each with a varying number of amino acids in its molecule [3, 7]. The longer hormones with 33–58 amino acids can be cleaved at different locations to yield hormones of shorter molecular length. The component that retains the carboxyl terminal tetrapeptide exhibits most of the biological function of the parent molecule (Fig. 6.1.3). Component I with more than 40 and component II with 33–39 amino acids in the molecule are the most abundant forms. ComponentdIII contains 12, component IV has eight (octapeptide or CCK-8), and component V consists of four amino acids. Component V with four amino acids is the shortest biologically active form.

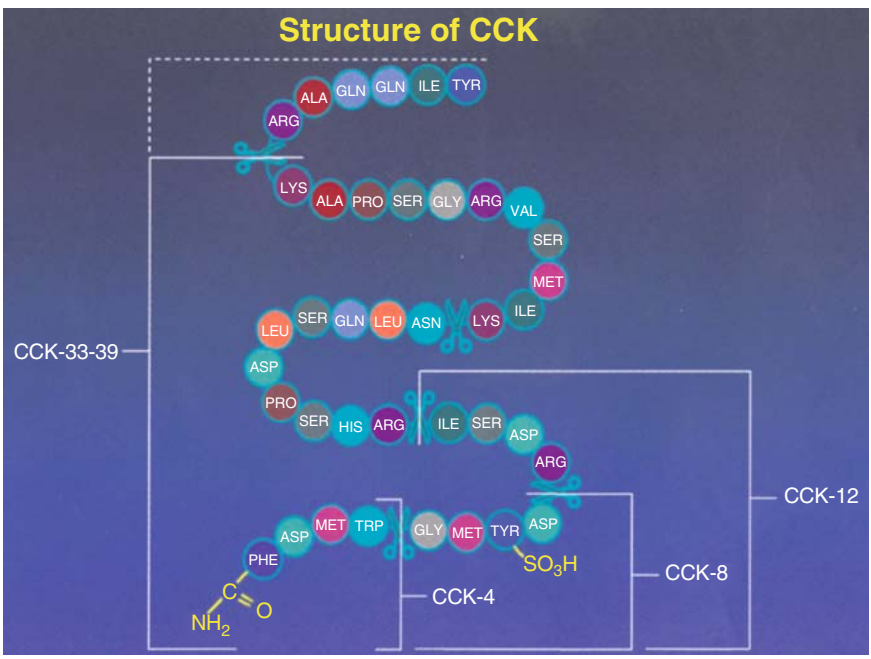

Fig. 6.1.3 Molecular structure of cholecystokinin. It consists of 33–39 amino acids that can be cleaved (scissors) at several locations to produce shorter fragments. Amino terminal tetrapeptide (CCK-4) is necessary for biological actions of the fragments [44]

Hormone CCK-8 has been synthesized and is available for clinical use as Sincalide (Kinevac). The terminal amino acid, phenylalanine, is amidated, and the seventh amino acid, tyrosine, is sulfated. Sulfation of the amino acid tyrosine is essential for retention of the biological potency of the hormone. To be biologically active, each component must possess the carboxy terminal tetrapeptide. When the amino acids are numbered serially beginning at the carboxyl terminal ($CO\text{-}NH_2$) end, the hormonal fragments are called CCK-4, CCK-8, CCK-12, CCK-33, CCK-39, etc. The molecular weight of CCK-8 is 1,143. Because of its shorter length and lesser mass, CCK-8, on a molar basis, is four to five times biologically more potent than CCK-33. All five components of CCK are found in the small intestinal mucosa and the central nervous system. Currently, it is believed that each component is secreted, in-vivo, by a specific group of CCK-secreting cells. The concentration of larger components (CCK-33, CCK-39) is higher in the central nervous system and the gastrointestinal tract, whereas the concentration of smaller components (CCK-8) is higher in the anterior pituitary gland [5].

Cerulein

Other peptides with a carboxyl terminal tetrapeptide identical to that of CCK also possess a cholecystokinetic effect. Gastrin and cerulein are two such peptides with an identical carboxy terminal tetrapeptide, and both exhibit a cholecystokinetic effect. Cerulein, isolated first from the skin of an Australian frog, is not found in humans. It closely resembles the CCK-8 structure and consists of ten amino acids (decapeptide), two more than CCK-8. The seventh amino acid, tyrosine, is sulfated. The sixth amino acid is threonine in cerulein, and methionine in CCK-8 (Fig. 6.1.4). Biologically, cerulein is ten times more potent than CCK-33 on a molar basis, and 47 times more potent on the basis of its net weight. The molecular weight is 1,352 [8].

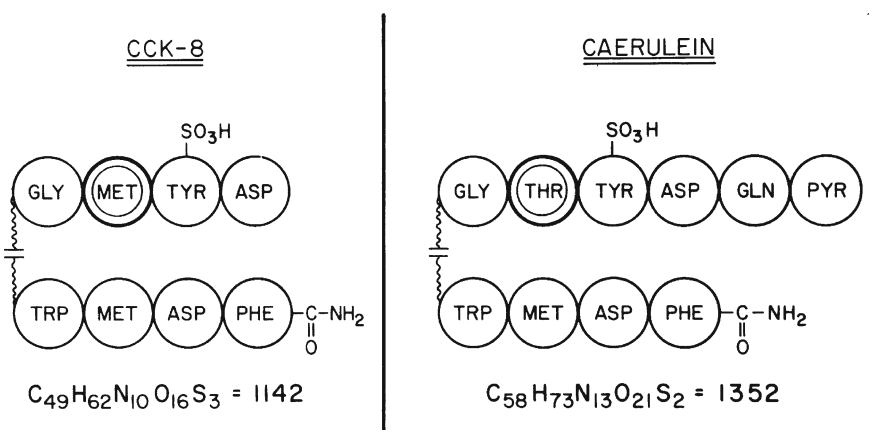

Fig. 6.1.4 Structure of CCK-8 and cerulein. Both contain an identical N-terminal tetrapeptide. The sixth amino acid is methionine in CCK-8 and threonin in cerulein. Both are sulfated on the seventh amino acid, tyrosine. Cerulein has two amino acids (decapeptide) more than CCK-8. Molecular weight of CCK-8 = 1,142 and cerulein = 1,352 [32]

Release of CCK

Cholecystokinin is released into circulation soon after the arrival of food into the duodenum. Fat is the most potent stimulant of all nutrients. Serum CCK level begins to rise 8–10 min after a meal and reaches the peak level by 30–60 min [9, 10]. The serum level remains above the basal level for 2–4 h post- meal, depending upon the nature of food ingested. The serum half life of CCK is 2.5 min [11].

Receptors

Cholecystokinin acts through two types of receptors, CCK-A (CCK-1) and CCK-B (CCK-2). CCK-A receptors are distributed predominantly in the smooth muscle of the gut and a few areas of the brain, and CCK-B receptors are distributed mainly in the brain. The gallbladder contains mostly CCK-A and the pancreas mostly CCK-B type receptors [12, 13]. These receptors are located on the surface of the cell and provide easy access to cholecystokinin. Cholecystokinin binds to CCK-A receptors in the gallbladder smooth muscle and initiates its contraction and bile emptying immediately. By binding to CCK-B type receptors, cholecystokinin stimulates pancreatic enzyme and bicarbonate secretion. CCK-B receptors manifest an inhibitory effect on the motility of the distal colon and pylorus of the stomach, acting via nitric oxide pathway [14]. Both cholecystokinin and leptin influence eating by acting on the brain as inhibitory hormones [15]. In humans, plasma cholecystokinin levels are associated with satiety [16]. Cholecystokinin antagonists (loxiglumide, devazepide, and TP-680) either block or reverse its actions by competitively binding to CCK receptors. These antagonists increase appetite, food intake, and weight gain in animals by blocking CCK brain receptors [17, 18].

Actions of CCK

The stimulation of gallbladder contraction and subsequent bile emptying is one of the most important and the best known actions of cholecystokinin. Cholecystokinin simultaneously relaxes the sphincter of Oddi and facilitates smooth passage of bile through it into the duodenum [19]. Cholecystokinin also exhibits other biological actions listed in Table 6.1.1. It increases both the volume and flow of hepatic bile by increasing water secretion by bile canaliculi and bile ducts. For a short time, it was thought that a separate hormone (pancreozymin), different from CCK, acted on the pancreas to increase its enzyme and bicarbonate secretion [20]. It is now well recognized that a single hormone, cholecystokinin, is responsible for both actions: induction of gallbladder contraction and stimulation of pancreatic enzyme secretion [21]. In the pancreas, both cholecystokinin and secretin bind to the same receptor and increase enzyme and bicarbonate secretion [22]. Cholecystokinin increases intestinal peristalsis and promotes antegrade flow of bile and nutrients through the lumen. By inducing contraction of the pyloric sphincter, CCK prevents duodeno-gastric bile reflux.

Cholecystokinin binds to stimulatory CCK-A receptors in the gallbladder smooth muscle and initiates its contraction [13]. Simultaneously, it binds to inhibitory receptors in the

Table 6.1.1 Actions of cholecystokinin

(1)	Contracts and empties the gallbladder
(2)	Increases pancreatic enzyme and bicarbonate secretion
(3)	Relaxes the sphincter of Oddi and lower esophageal junction
(4)	Increases secretion of insulin, glucagon, and somatostatin by Islet cells
(5)	Contracts the pyloric sphincter, preventing duodeno-gastric bile reflux
(6)	Increases hepatic bile secretion
(7)	Increases intestinal peristalsis
(8)	Increases intestinal blood flow
(9)	Suppresses appetite
(10)	Relaxation of lower esophageal sphincter.
(11)	Protection of gastric mucosa through release of somatostatin
(12)	Decreases systolic blood pressure

sphincter of Oddi smooth muscle and promotes its dilatation. These combined, but paradoxical, actions promote smooth passage of bile from the gallbladder into the duodenum [23]. CCK-A receptor-rich smooth muscle is distributed mostly in the fundus and body of the gallbladder. Very few receptors are found in the smooth muscle of the neck and the cystic duct. When serum CCK level rises above the threshold, the fundus contracts first, followed by the body. The relaxation of the sphincter of Oddi occurs at the same time, allowing smooth passage of bile through it [24, 25].

Cholecystokinin and cerulein both act on the same receptors [26–29]. The cystic duct smooth muscle, which has only a few CCK receptors, does not usually contract, because its threshold for contraction is set at a much higher level than the threshold for contraction of the smooth muscle in the body and fundus. When a large bolus dose of CCK-8 is injected, however, the cystic duct often contracts and prevents gallbladder emptying [30]. In chronic acalculous chronic cholecystitis (cystic duct syndrome), not only is there a decrease in the total number of CCK receptors in the body and fundus, but also the cystic duct smooth muscle threshold is lowered, allowing contraction of the body, fundus, and cystic duct, all at the same time, resulting in non-emptying of the gallbladder [31].

Due to the low serum concentration of cholecystokinin during fasting, most CCK receptors in the smooth muscle are free, facilitating maximum relaxation of the gallbladder wall and a maximum increase in the tonus of the sphincter of Oddi. Both of these factors acting together promote preferential hepatic bile entry into the gallbladder during fasting. Upon CCK release post-meal, these receptors get saturated, initiating contraction of the gallbladder (stimulatory receptors) with simultaneous relaxation (inhibitory receptors) of the sphincter of Oddi. The degree of gallbladder bile emptying (ejection fraction) correlates directly with the total number of CCK receptors in the gallbladder smooth muscle [32].

Dose Response

The degree of gallbladder emptying is dependent both upon the dose rate and duration of infusion of cholecystokinin or cerulein [33]. The higher the dose is, the greater the degree

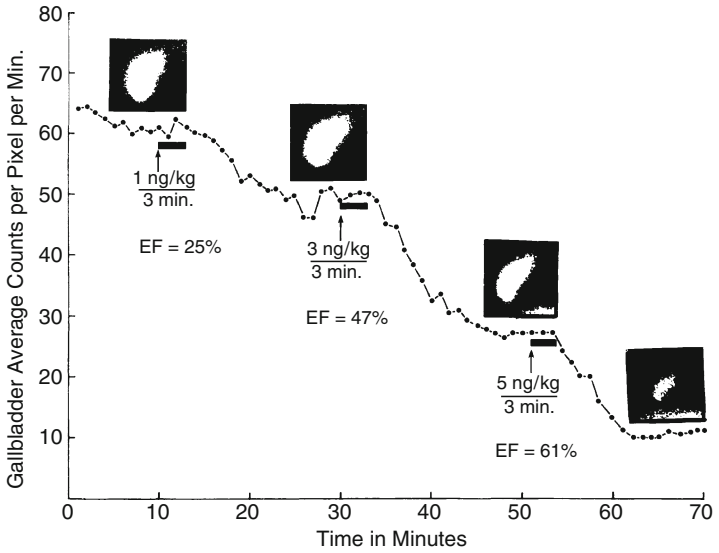

Fig. 6.1.5 Dose response curve. The gallbladder ejection fraction increases as the dose of ceruletide (or CCK-8) increases [32]

of emptying, as long as the administered dose is within the physiological range (Fig. 6.1.5). The threshold for the beginning of gallbladder contraction and emptying lies between 0.5 and 1.0 ng kg min^{-1} of CCK-8 or cerulein. Peak emptying is noted between 3 and 5 ng kg min^{-1} dose [34, 35]. A further increase in CCK-8 dose actually decreases gallbladder emptying. An infusion of 0.02 μg kg^{-1} (20 ng kg^{-1}) or 0.04 μg kg^{-1} (40 ng kg^{-1}) over a 3-min period results in an ejection fraction that is much lower than that obtained with 0.01μg kg^{-1} over 3 min (Fig. 6.1.6). The CCK-8 doses listed in Table 6.1.2 are shown to be within the physiological range and promote smooth contraction and emptying of the gallbladder. For an identical dose, dose rate, and duration, it appears that ceruletide may be more potent than CCK-8. For a 3-min infusion of 5 ng kg^{-1}, the gallbladder mean ejection fraction is 61% with ceruletide and 38% with CCK-8 (Fig. 6.1.6).

Effect of a Large Dose of CCK-8

The dose required during quantitative cholescintigraphy, in general, is found to be much lower than the hormonal dose recommended in the package insert (Kinevac) by the vendor. The package insert dose originally was meant for oral cholecystogram or for stimulating pancreatic enzyme secretion [33]. The recommended dose in the package insert (0.02 μg kg^{-1} or 20 ng kg^{-1}) often produces abdominal pain and low ejection fraction (Fig. 6.1.7) when used in control subjects [34–35]. A low ejection fraction response obtained with a larger dose of CCK-8 is attributed to reaching the cystic duct smooth muscle threshold for contraction, with the resultant effect of non-emptying of the gallbladder [36–37].

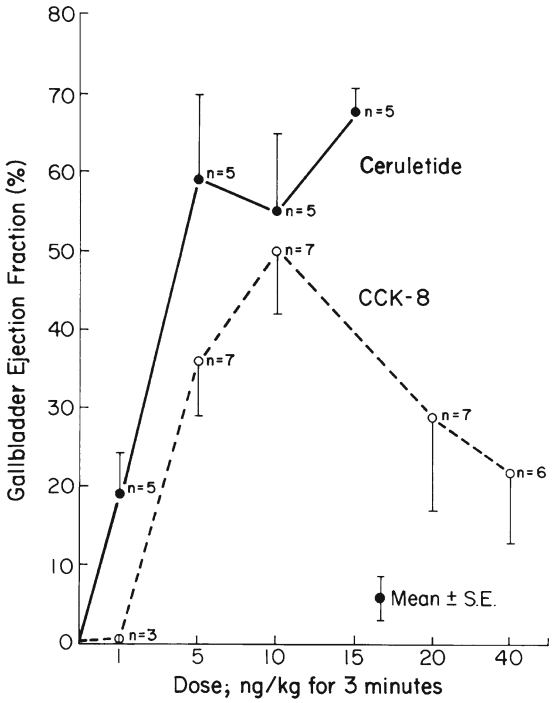

Fig. 6.1.6 Effect of non-physiologic CCK-8 or ceruletide dose on gallbladder emptying. After the peak response at 5 ng kg^{-1} 3 min for ceruletide and 10 ng kg^{-1} 3 min for CCK-8, the gallbladder ejection fraction begins to decrease for any further increase in dose [31]

Table 6.1.2 Cholecystokinin-33 (CCK-33), octa-peptide of cholecystokinin (CCK-8), and ceruletide dose for measurement of gallbladder ejection fraction

Hormone (Ref)	Route	Dose rate	Trade name	Manufacturer	GBEF (%)
CCK-33 (PI)	IV	1 IDU/kg/min	CCK-33/Kabi	Pharmacia Laboratory, Piscataway, NJ	–
CCK-8 [31]	IV	10 ng kg^{-1} 3 min	Kinevac	Bracco Diagnostics, Princeton, NJ	>35%
Ceruletide [32]	IV	5 ng kg^{-1} 3 min	Tymtran	Adria Laboratory, Columbus, OH	>40%
Ceruletide (PI)	I M	300 ng kg^{-1}	Tymtran	Adria Laboratory Columbus, OH	–

IDU = Ivy dog unit, PI = package insert

Cholecystokinin dual action of antegrade intestinal peristalsis and simultaneous contraction of the pyloric sphincter normally produces forward bile flow through the intestinal lumen and prevents duodenal-gastric bile reflux [38–40].

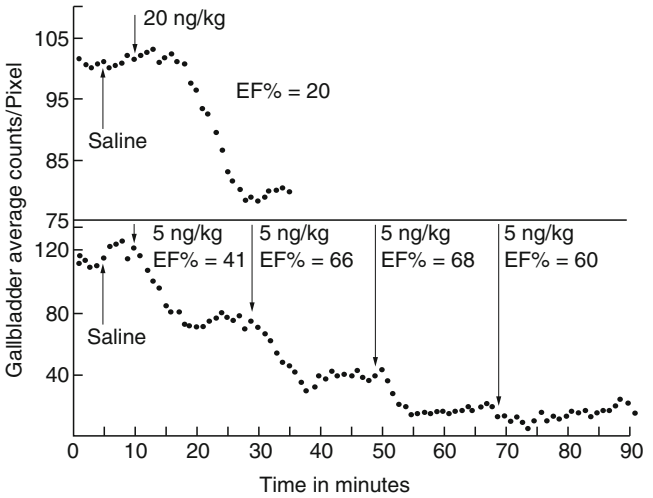

Fig. 6.1.7 Effect of sequential CCK-8 doses on gallbladder emptying. A 5 ng kg^{-1} 3 min CCK-8 dose given sequentially four times on a single occasion, with 30 min between doses, produces similar ejection fractions. Note that a 20 ng kg^{-1} 3-min CCK-8 dose given on a different day produces a lower ejection fraction [38]

Sequential CCK Doses

The gallbladder ejection fraction remains constant for a fixed dose of cholecystokinin or ceruletide, given on two separate occasions (Fig. 6.1.7). A second identical dose of CCK-8 or ceruletide given 20–30 min after the first dose produces an ejection fraction similar to that of the first dose. There is neither a potentiation nor inhibition effect from the first dose when a period of 20–30 min is allowed between doses. A short serum half life of 2.5 min does not seem to leave any significant residual CCK activity from the first dose to influence the effect of the second dose [41, 42]. This unique feature enables cholescintigraphy to study the effect of various drugs on the sphincter of Oddi and the gallbladder after a single dose of Tc-99 m-HIDA. The dose of CCK-8 (Kinevac, Bracco Laboratory, Princeton, NJ) and ceruletide (Tymtran, Adria Lab, Columbus, OH) is measured in microgram units, and cholecystokinin-33 (CCK™, Pharmacia Laboratory, Piscataway, NJ) in Ivy dog units. One Ivy dog unit is defined as the amount of CCK-33, when injected intravenously over 10–15 s, that raises the pressure within the gallbladder by 1 cm of H_2O [43].

Sphincter of Oddi

Rugero Oddi in 1887 first proposed the sphincter mechanism at the distal end of the common bile duct that today bears his name [44]. The existence of the sphincter remained controversial for many years, when Boyden in 1937 put an end to the controversy by showing both macroscopic and microscopic details of the sphincter in both animals and humans [45, 46].

Structure and Function

The human sphincter of Oddi is about 10–15 mm in length, situated within the muscular layer of the media of the duodenum (Fig. 6.1.1). It consists of three distinct segments: (1) sphincter choledochus, (2) sphincter pancreaticus, and (3) ampullary sphincter. The choledochal sphincter covers the distal end of the intraduodenal part of the common bile duct before it joins with the pancreatic duct (duct of Wirsung). The pancreatic sphincter is located at the distal end of the pancreatic duct. The ampullary sphincter covers the distal end of both ducts after they unite to form a single common channel that opens into the duodenal lumen at an elevation called the ampulla of Vater [46]. The term "sphincter of Oddi" refers to all three sphincters.

The main function of the sphincter of Oddi is regulation of bile flow through it and prevention of the reflux of duodenal contents into the common bile duct and pancreatic duct. Internally, it prevents bile reflux into the pancreatic duct and reflux of pancreatic enzymes into the common bile duct. In the majority of humans (86%), the distal common bile duct and the distal pancreatic duct join together, forming a common channel of 10–12 mm length that opens into the duodenum at the papilla of Vater. In 6% of patients, the two ducts join together just before opening into the duodenum with a common channel. In the remaining 8% of patients, the two ducts open separately into the duodenal lumen at the ampulla of Vater [46]. The sphincter consists of a circular and a longitudinal layer of muscle. In humans, the entire sphincter is located within the duodenal wall, and the wall has to be cut opened to expose the sphincter of Oddi for clinical and experimental studies. In American and the Australian opossums, however, the entire sphincter is situated outside of the duodenal wall, making it easy to study its function, without any need to cut open the duodenal wall.

Sphincter Pressure

The basal pressure within the sphincter Oddi is 15–18 mmHg and rises with the arrival of periodic phasic waves. Phasic waves occur at an average of 4 waves/min, and each wave lasts for 10–15 s (Fig. 6.1.8). During the passage of a phasic wave, the pressure within the sphincter of Oddi rises sharply, reaching a peak amplitude as high as 90–140 mmHg [47, 48]. Normally, 80% of phasic waves progress antegrade (towards the duodenum), 9% retrograde (towards the liver), and 13% occur simultaneously (Table 6.1.3) at the proximal, middle, and distal segments of the sphincter. The wave normally begins proximally and travels distally within the sphincter. The sphincter of Oddi basal pressure, phasic wave frequency, and direction of propagation remain unchanged after cholecystectomy. Wide variations in normal sphincter of Oddi pressures reported in the literature are often due to technical differences among the studies and should be taken into account when comparing results of one study with the other. Pressure changes within the sphincter of Oddi remain constant between repeat studies when a standardized technique is applied [49].

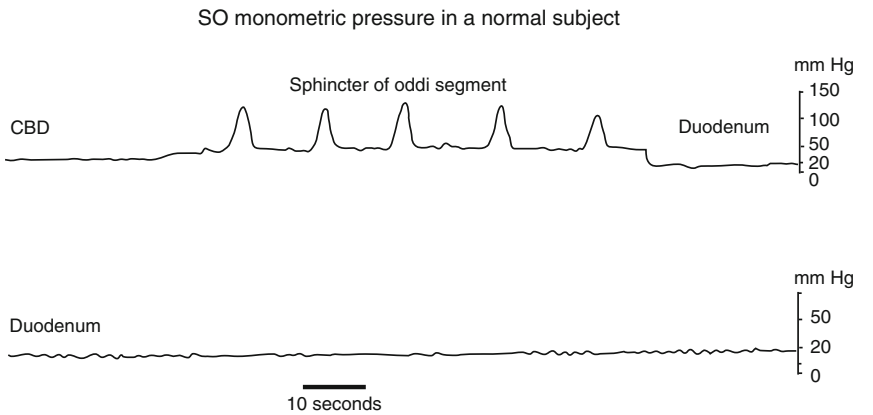

Fig. 6.1.8 Manometric pressure changes in the common bile duct (*CBD*) and sphincter of Oddi. Sphincter of Oddi basal pressure of 15 mmHg raises to as high as 100–150 mmHg at the peak of a phasic wave. Pressure within common bile duct remains at 15–20 mmHg [46]

Table 6.1.3 Pressure and wave frequency, sequence, and amplitude changes in a normal sphincter of Oddi [48]

Parameter	Median	Range
Basal pressure (mmHg)	15	5–35
Wave amplitude (mmHg)	135	95–195
Wave frequency (no/min)	4	2–6
Wave sequence (%):		
Antegrade	80	12–100
Simultaneous	13	0–50
Retrograde	9	0–50

Action of Cholecystokinin on the Sphincter of Oddi

Cholecystokinin acts on the sphincter of Oddi smooth muscle and immediately abolishes the phasic wave activity (Fig. 6.1.9). The hormone reduces the sphincter of Oddi wave amplitude and pressure from a peak 130–140 mmHg to less than 10 mmHg pressure and reduces the wave frequency from four to less than one. Abolition of waves and reduction in wave amplitude decrease the pressure inside and simultaneously promote dilatation of the sphincter orifice [50, 51]. Reduction in wave amplitude and frequency reaches the nadir within 2–4 min after a single bolus injection of CCK-8, and the basal state is reestablished after 8–10 min, reflecting the effect of a short serum half life (2.5 min) of the hormone [11]. The effect on the sphincter is maintained throughout the duration of infusion

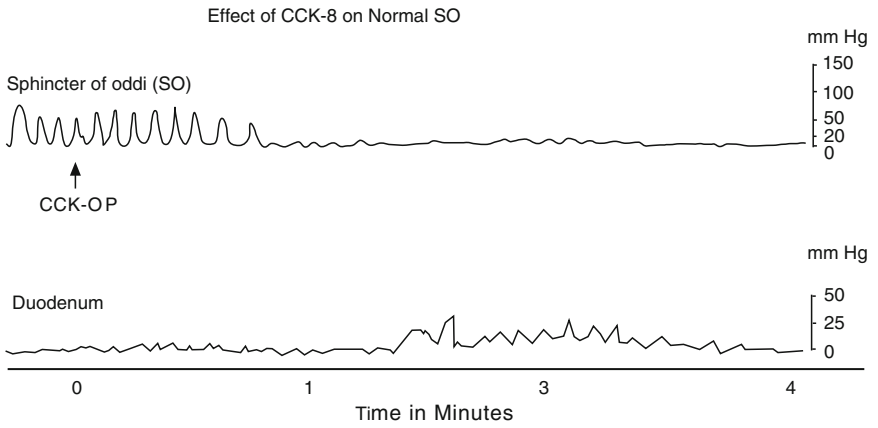

Fig. 6.1.9 Action of CCK-8 on normal sphincter of Oddi. CCK-8 abolishes the phasic waves in the sphincter of Oddi and increases the number of waves and pressure in the duodenum [46]

of the hormone. The sphincter remains open for 2–3 h post-meal because of the longer duration of endogenous CCK release.

Gallbladder

The main function of the gallbladder is to store and concentrate (bile salts) bile during fasting and discharge into the duodenum soon after the arrival of food from the stomach. A normal gallbladder holds up to 50 ml and empties almost completely following a fatty meal. Since bile salts are very essential for efficient digestion and absorption of nutrients, the gallbladder sequesters almost all of them by selectively absorbing water and electrolytes through the wall during fasting. Absorption of water takes place through widely open lateral intercellular spaces between columnar epithelial cells lining the mucosa. Although several hormones, including cholecystokinin, are known to act on gallbladder contraction and emptying, until recently not much was known about its filling. A new hormone called fibroblast growth factor (FGF19) in the portal blood that facilitates gallbladder relaxation and filling was identified recently [52]. After discharge into the duodenum, bile salts travel through the jejunum and ileum, helping the digestion and absorption of nutrients. After absorption in the terminal ileum, bile salts activate nuclear farnesoid X receptor (FXR), which stimulates the production and release of FGF19 (Fig. 6.2.2). Acting through cyclic adenosine monophosphate (cAMP), FGF19 promotes gallbladder relaxation, increases its volume, and facilitates filling [53].

Reduction in gallbladder ejection fraction in patients with biliary dyskinesia is attributed to either a decrease in the total number of receptors in the body and fundus or a decrease in the threshold for contraction of the CCK receptors in the neck and cystic duct or both [54, 55]. Because of this phenomenon, it is essential to keep the CCK-8 dose within the physiological range during quantitative cholescintigraphy in the diagnosis of biliary dyskinesia. Cholecystokinin antagonists like loxiglumide, devazepide, and TP-680

decrease gallbladder emptying by competitively occupying the CCK-A receptor in the gallbladder smooth muscle. Animals given CCK antagonists show a reduction in gallbladder emptying and an increase in appetite and weight gain [14, 15]. Cholecystokinin protects gastric mucosal integrity through the release of somatostatin, and it relaxes the lower esophageal sphincter through activation of CCK-A receptors at the distal end of the esophagus [56, 57]. Controversy about its action on the pancreas, whether acting on the pancreatic acinar cells directly or acting indirectly through the vagus nerve (cholinergic), seems to have been settled in recent studies by using freshly prepared normal human pancreatic cells. At physiologic concentration, cholecystokinin in humans stimulates enzyme secretion by pancreatic acinar cells directly through calcium signaling and mitochondrial activation. Blockade by atropine and tetrodotoxin does not inhibit the direct action [58]. After a century of trials, some feel that a judgment can now be made about the direct action of cholecystokinin on the pancreatic acinar cells [59].

References

1. Ivy AC, Oldberg E. A hormone mechanism for gallbladder contraction and evacuation. Am J Physiol 1928;86:599–613
2. Ivy AC, Kloster Gl, Lueth HC, Drewyer GE. On the preparation of "cholecystokinin." Am J Physiol 1929;91:336–344
3. Rehfeld JF. Four basic characteristics of the gastrin-cholecystokinin system. Am J Physiol 1981;240:G255–G266
4. Sjolund K, Sanden G, Hakanson R, Sundler F. Endocrine cells in human intestine: an immunocytochemical study. Gastroenterology 1983;85:1120–1130
5. Rehfeld JF, Lindholm J, Andersen BN, Bardram L, Cantor P, Fenger M, Ludecke DK. Pituitary tumors containing cholecystokinin. N Engl J Med 1987;316:1244–1247
6. Wilding PPH, Ghatei MA, Bloom SR. Hormones of the gastrointestinal tract. In: DeGroot LJ (ed) Endocrinology. WB Saunders, Philadelphia, 1995, vol. 3, pp 2870–2894
7. Elyseelein VE, Reeve JR Jr, Shively JE, Hawke D, Walsh JH. Partial structure of a large canine cholecystokinin (CCK58): amino acid sequence. Peptides 1982;3:687–691
8. Basso N, Bagarani M, Materia A, Gizzonio D, DePaolis C, Praga C, Speranza V. Effect of caerulein in patients with biliary colic. Gastroenterology 1985;89:605–609
9. Low-Beer TS, Harvey RF, Davies ER, Read AF. Abnormalities of serum cholecystokinin and gallbladder emptying in celiac disease. N Engl J Med 1975;292:961–963
10. Wiener I, Inoue K, Fagan CJ, Lilja P, Watson LC, Thompson JC. Release of cholecystokinin in man: correlation of blood levels with gallbladder contraction. Ann Surg 1981;194:321–327
11. Thompson JC, Fender HR, Ramus NI, Villar HV, Rayford PL. Cholecystokinin metabolism in man and dogs. Ann Surg 1975;182:496–504
12. Wank SA, Pisegna JR, deWeerth A. Brain and gastrointestinal cholecystokinin receptor family: structure and functional expression. Proc Natl Acad Sci 1992;89:8691–8695
13. Tang C, Biemond I, Lamers CB. Cholecystokinin receptors in human pancreas and gallbladder muscle: a comparative study. Gastroenterology 1996;111:1621–1626
14. Fornai M, Colucci R, Antonioli L, Crema F, et al. Cholecystokinin CCK-2 receptors mediate the peptide's inhibitory actions on the contractile activity of human distal colon via the nitric oxide pathway. Brit J Pharmacology 2007;151:1246–1253
15. Wright M, Woodrow G, O'Brien S, Armstrong E, et al. Cholecystokinin and leptin: their influence upon the eating behaviour and nutrient intake of dialysis patients. Nephrol Dial Transplant 2004;19:133–140

16. Burton-Freeman B, Davis PA, Schneeman BO. Plasma cholecystokinin is associated with subjective measures of satiety in women. Am J Clin Nutrition 2002;76:659–667
17. Hewson G, Leighton GE, Hill RG, Hughes J. The cholecystokinin receptor antagonist L364,718 increases food intake in the rat by attenuation of the action of endogenous cholecystokinin. Br J Pharmacol 1988;93:79–84
18. Tachibana I, Kanagawa K, Yamamoto Y, Otsuki M. Pharmacological profile of a new serine derivative cholecystokinin receptor antagonist TP-680 on pancreatic, biliary and gastric function. J Pharmacol Exp Ther 1996;279:1404–1412
19. Mutt V. Cholecystokinin: Isolation, structure, and function. In: Glass GBJ (ed) Gastrointestinal hormones. Raven, New York, 1980, pp 169–221
20. Harper AA, Raper HS. Pancreozymin, a stimulant of the secretion of pancreatic enzymes in extracts of the small intestine. J Physiology 1943;103:115–125
21. Jorpes E, Mutt V. Cholecystokinin and pancreozymin, one single hormone? Acta Physiol Scand 1966;66:196–202
22. Grossman MI. Gastrin, Cholecystokinin and secretin act on one receptor (hypothesis). Lancet 1970;1(7656):1088–1089
23. Behar J, Biancani P. Pharmacologic characterization of excitatory and inhibitory cholecystokinin receptors of the cat gallbladder and sphincter of Oddi. Gastroenterology 1987;92:764–770
24. Ivy AC, Drewyer GE, Orndoff BH. The effects of cholecystokinin on the human gallbladder. Endocrinology 1930;14:343–348
25. Steigerwalt RW, Goldfine ID, Williams JA. Characterization of cholecystokinin receptors on bovine gallbladder membranes. Am J Physiol 1984;247:G709–G714
26. Behar J, Biancani P. Effects of cholecystokinin and the octapeptide of cholecystokinin on the feline sphincter of Oddi and gallbladder. Mechanisms of action. J Clin Invest 1980;66:1231–1239
27. Sarles JC, Bidart JM, Devaux MA, Echinard C, Castagnini A. Action of cholecystokinin and caerulein on the rabbit sphincter of Oddi. Digestion 1976;14:415–423
28. Wetzner SM, Vincent ME, Robbins AH. Ceruletide-assisted cholecystography: a clinical assessment. Radiology 1979;131:23–26
29. Hedner P, Rorsman G. On the mechanism of action for the effect of cholecystokinin on the choledochoduodenal junction in the cat. Acta Physiol Scand 1969;76:248–254
30. Courtney DF, Clanachan AS, Scott GW. Cholecystokinin constricts the canine cystic duct. Gastroenterology 1983;85:1154–1159
31. Torsoli A, Romarino ML, Alessandrini A. Motility of the biliary tract. Rendic R Gastroenterol 1970;2:67
32. Upp JR Jr, Nealon WH, Singh P, Fagan CJ, Jonas AS, Greeley GH Jr, Thompson JC. Correlation of cholecystokinin receptors with gallbladder contractility in patients with gallstones. Ann Surg 1987;205:641–648
33. Sturdevant RA, Stern DH, Resin H, Isenberg JI. Effect of graded doses of octapeptide of cholecystokinin on gallbladder size in man. Gastroenterology 1973;64:452–456
34. Krishnamurthy GT, Bobba VR, Kingston E. Optimization of octapeptide of cholecystokinin (OP-CCK) dose for gallbladder emptying. In: Raynaud C (ed) Proceedings of the III World Congress of Nuclear Medicine and Biology. Paris, France. Pergamon Press, 1982, pp 2244–2247
35. Krishnamurthy GT, Turner FE, Mangham D, Bobba VR, White SA, Langrell K. Ceruletide intravenous dose-response study by a simplified scintigraphic technique. AJR Am J Roentgenol 1985;144:733–737
36. Krishnamurthy S, Krishnamurthy GT. Gallbladder ejection fraction: a decade of progress and future promise (editorial). J Nucl Med 1991;32:542–544
37. Zeissman HA, Fahey FH, Hixson DJ. Calculation of a gallbladder ejection fraction: advantage of continuous sincalide infusion over the three-minute infusion method. J Nucl Med 1992; 33:537–541

38. Toftdahl DB, Hojgaard L, Winkler K. Dynamic cholescintigraphy: induction and description of gallbladder emptying. J Nucl Med 1996;37:261–266
39. Valenzuela JE, Defilippi C. Inhibition of gastric emptying in humans by secretin, the octapeptide of cholecystokinin, and intraduodenal fat. Gastroenterology 1981;81:898–902
40. Fraser R, Fone D, Horowitz M, Dent J. Cholecystokinin octapeptide stimulates phasic and tonic pyloric motility in healthy humans. Gut 1993;34:33–37
41. Krishnamurthy GT, Bobba VR, Kingston E, Turner FE. Measurement of gallbladder emptying sequentially using a single dose of 99mTc-labeled hepatobiliary agent. Gastroenterology 1982;83:773–776
42. Sostre S, Canto MI, Kalloo AN. Gallbladder response to a second dose of cholecystokinin during the same imaging study. Eur J Nucl Med 1992;19:964–965
43. Torsoli A, Romarino ML, Colagrande C, Demaio G. Experiments with cholecystokinin. Acta Radiologica 1961;55:193–206
44. Oddi R. D'une disposition a sphincter speciale del'ouverture du canal cholique. Arch Ital Biol 1887;8:317–322
45. Boyden EA. The sphincter of Oddi in man and certain representative mammals. Surgery 1937;1:25–37
46. Boyden EA. The anatomy of the choledochoduodenal junction in man. Surg Gynecol Obstet 1957;104:641–652
47. Geenen JE, Hogan WJ, Dodds WJ, Stewart ET, Arndorfer RC. Intraluminal pressure recording from the human sphincter of Oddi. Gastroenterology 1980;78:317–324
48. Carr-Locke DL, Gregg JA. Endoscopic manometry of pancreatic and biliary sphincter zones in man. Basal results in healthy volunteers. Dig Dis Sci 1981;26:7–15
49. Thune A, Scicchitano J, Roberts-Thomson IC, Toouli J. Reproducibility of endoscopic sphincter of Oddi manometry. Dig Dis Sci 1991;36:1401–1405
50. Toouli J, Roberts-Thompson C, Dent J, Lee J. Manometric disorders in patients with suspected sphincter of Oddi dysfunction. Gastroenterology 1985;88:1243–1250
51. Toouli J, Hogan WJ, Geenen JE, Dodds WJ, Arndorfer RC. Action of cholecystokinin-octapeptide on sphincter of Oddi basal pressure and phasic wave activity in humans. Surgery 1982;92:497–503
52. Choi M, Moschetta A, Bookout AL, Peng L, Umetani M, Holstrom SR, et al. Identification of a hormonal basis for gallbladder filling. Nat Med 2006;12:1253–1255
53. Portincasa P, DiCaula A, Wang HH, Palasciano G, van Erpecum KJ, Moschetta A, Wang DQH. Coordinate regulation of gallbladder motor function in the gut-liver axis. Hepatology 2008;47:2112–2126
54. Hogan WJ, Geenen JE. Biliary dyskinesia. Endoscopy 1988;20:179–183
55. Krishnamurthy S, Krishnamurthy GT. Biliary dyskinesia: role of the sphincter of Oddi, gallbladder, and cholecystokinin. J Nucl Med 1997;38:1824–1830
56. Konturek JW, Hengst K, Konturek SJ, Sito E, Stachura J, Domschke W. Physiological role of cholecystokinin in gastroprotection in humans. Am J Gastroenterol 1998;93:2385–2390
57. Boeckxstaens GE, Hirsch DP, Fakhry N, Holloway RH, D'Amato M, Tytgat GNJ. Involvement of cholecystokinin-A receptors in transient lower esophageal sphincter relaxations triggered by gastric distension. Am J Gastroenterol 1998, 93:1823–1828
58. Murphy JA, Criddle DN, Sherwood M, Chvanov M, Mukherjee R, McLaughlin E, Booth D, et al. Direct activation of cytosolic Ca2 + signaling and enzyme secretion by cholecystokinin in human pancreatic acinar cells. Gastroenterology 2008;135:632–641
59. Saluja A, Longsdon C, Garg P. Direct versus indirect action of cholecystokinin on human pancreatic acinar cells: is it time for a judgment after a century of trial? Gastroenterology 2008;135:357–360

6.2 Opioids

Opioids are the mainstay in the management of moderate to severe intensity pain of diverse etiology. They are the drugs of first choice for the treatment of postoperative pain. Opioids are often mixed with other pain medications, including many non-steroidal anti-inflammatory drugs, such as aspirin acetaminophen, and neproxin. Opioids raise the pressure in the sphincter of Oddi by acting on its smooth muscle and thus interfere with cholecystokinin- or fatty meal-stimulated gallbladder ejection fractions. The action of many opioids on the sphincter lasts much longer than their serum half-life would indicate, suggesting that the metabolites may also possess a constrictive action on the sphincter of Oddi. The interaction between the opioids and the sphincter of Oddi calls for their careful scrutiny during quantitative cholescintigraphy.

History of Opioids

"Opioid" is a generic name that refers to both natural and synthetic compounds with a morphine-like action. They are derived from the opium plant, which in Greek means juice. The juice comes from the capsule of the unripe seed of *Papaver Somniferum*. The milky juice from the seed is dried and made into opium powder, which contains more than 20 alkaloids. Serturner first isolated a pure substance from this powder in 1806, which produced somnolence first, followed by a dream state. He called it morphine after the Greek god of dreams, Morpheus. Codeine was isolated from opium powder in 1832 and papaverine in 1848 [1]. The analgesic action of all opioids is graded with reference to morphine, which serves as the gold standard for pain control. Table 6.2.1 shows different opioids available for pain control and their effect on the sphincter of Oddi.

Biokinetics of Morphine

Morphine consists of an OH group at positions 3 and 6 and a CH_3 group at 17 (Fig. 6.2.1). Other opioids differ structurally from morphine by having different chemical substitutions at positions 3, 6, and 17. Morphine is administered by oral, subcutaneous, intramuscular, or intravenous routes. Many dermal patches are now available for long-term continuous application. Intravenous injections are preferred for hospital patients, especially during the immediate postoperative period. Upon intravenous injection, morphine distributes in an initial volume of 71.8 l kg^{-1} and clears from plasma with biexponential components: component I with a half time of 0.16 h and component II with a half time of 2.5 h (Table 6.2.2). Morphine is metabolized in the liver and converted into morphine glucuronide, which clears from plasma much more slowly than the parent molecule. About 60% of injected morphine is excreted in urine in 24 h, and 73% in 3 days. The excretion rate does not change in patients with cirrhosis of the liver [2].

Table 6.2.1 Effect of opioids on the sphincter of Oddi. The drugs are grouped under four major categories into marked, moderate, mild, or no effect based on the extent of sphincter of Oddi pressure rise

Generic name	Proprietary name
Marked rise in sphincter pressure	
Morphine	Morphine
Levorphanol	Dromoran
Meperidine (methadone)	Demerol
Moderate rise in sphincter pressure	
Dextromoramide	Palfium
Diacetyl morphine	Heroin
Codeine	Codeine
Fentanyl	Sublimaze
Butorphanol	Stadol
Nalbuphine	Nubain
Hydrocodone	Hycodon
Oxycodone	Roxicodone
Propoxyphene	Darvon
Bupremorphine	Buprenex
Mild rise in sphincter pressure	
Dextropropoxyphene HCl	Doloxene
Pentazocine	Talwin
Phenazocine	Norphen
Phenoperidine	Peridine
No effect on the sphincter	
Hydroxyzine	Hydroxyzine

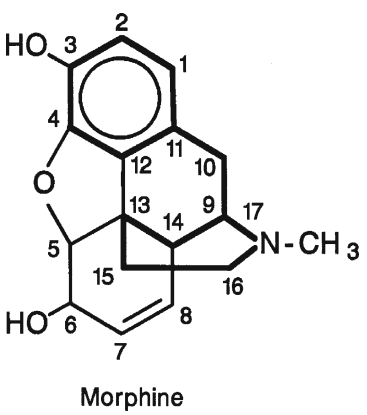

Fig. 6.2.1 Structure of morphine. Note OH group at positions 3 and 6 and CH_3 at position 17. The structure of other opioids differs mainly in having different chemical substitution at these positions

Dose

A minimum of 0.04 mg kg^{-1} of intravenous morphine is recommended during Tc-99 m-HIDA cholescintigraphy [3]. Intravenous doses as large as 15 mg are well tolerated [4]. In adults, a total intravenous dose of 3–4 mg of morphine sulfate is usually adequate

for confirmation of acute cholecystitis with cholescintigraphy. Liver extracts 60–80% of morphine on first pass and converts rapidly into a glucuronide form. Because of high extraction and rapid metabolism in the liver, oral morphine is not as effective as an intravenous dose.

Action of Morphine on the Sphincter of Oddi

Morphine acts on the sphincter of Oddi within 2–3 min after an intravenous injection, and increases the sphincter basal wave frequency from 4 to 10–12 min^{-1} and the wave amplitude from 70 mmHg to 136 mmHg (Fig. 6.2.2). The common bile duct basal pressure increases from 10 mmHg to 29 mmHg [4]. Low doses increase only the rate and amplitude, whereas higher doses increase basal pressure as well [5]. During a Tc-99 m-HIDA study, most gallbladders with a patent cystic duct are visualized within 5–15 min after an intravenous dose of morphine. The effect of morphine on the sphincter of Oddi is mediated by all types of opioid receptors. Naloxone and atropine slightly modify, but do not completely abolish the effect of morphine on the sphincter.

Morphine is the most potent of all opioids. The effect of other opioids on the sphincter of Oddi is a function of their structural configuration (Table 6.2.2). The effect of levorphonol, dextromoramide, and meperidine on the sphincter of Oddi is equivalent to that of morphine [6, 7]. Fentanyl, nolbuphine, hydrocodon, propoxyphene, and bupremorphine show a moderate spasmodic effect on the sphincter. Pentazocine, phenozocine, and phenoperidine show a mild effect, and hydroxyzine has no effect on the sphincter of Oddi [8].

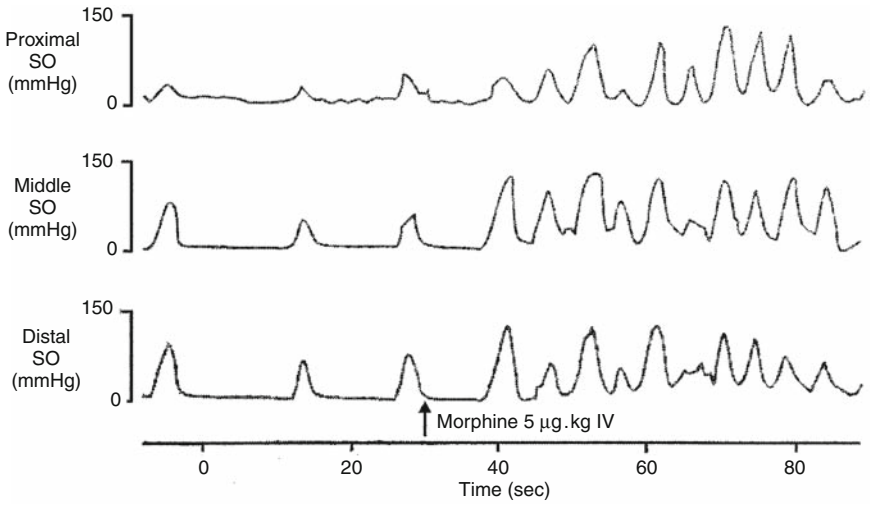

Fig. 6.2.2 Effect of morphine on the sphincter of Oddi. Morphine increases both the number and the amplitude of wave pressure throughout the sphincter of Oddi and forces hepatic bile entry into the gallbladder when the cystic duct is patent [4]

Table 6.2.2 Pharmacokinetics of morphine [2]

Initial volume of distribution (l kg^{-1})	71.8 ± 65.2
Clearance half time of the fast component (h)	0.16 ± 0.1
Clearance half time of the slow component (h)	2.5 ± 1.5
Plasma protein binding (%)	19.8 ± 6.1
Urinary excretion in 72 h (% dose)	72.9 ± 10.0

Screening for Opioid Intake

Quantitative cholescintigraphy is frequently used in the diagnosis of biliary dyskinesia, which consists of two disease entities: cystic duct syndrome (CDS) or chronic acalculous cholecystitis (CAC) and sphincter of Oddi spasm (SOS). The most consistent quantitative functional abnormality in patients with biliary dyskinesia is a reduction in gallbladder ejection fraction in the case of cystic duct syndrome and bile reflux into the hepatic duct followed by a rapid refilling of the gallbladder in the case of sphincter of Oddi spasm [9]. Because of the spasmodic effect on the sphincter of Oddi, it is critical to ensure that the patient is not on any opioids prior to performing a quantitative cholescintigraphy [10]. This issue becomes even more complex in outpatients where many patients are unaware that a non-steroidal anti-inflammatory drug they take for various indications (arthritis, headache, peptic ulcer, or primary or metastatic cancer) may also contain an opioid. This problem is relatively easy to recognize in hospitalized patients by careful review of charts for a list of current medications.

As only about 60–75% of the administered dose of morphine is excreted in 24–72 h urine, a safe rule is to allow a minimum of 24 h for inpatients and 48 h for outpatients to be off of opioids before performing a quantitative cholescintigraphy for the diagnosis of biliary dyskinesia [2]. If the ejection fraction is within normal range in a patient who has received an opioid, then there is no need to repeat the test. The test should be repeated if the ejection fraction is low and the patient has received an opioid within the last 48 h. The ejection fraction measured after discontinuation of an opioid for longer than 48 h often shows a dramatic increase in value when compared to the value before discontinuation (Fig. 6.2.3).

Morphine or Cholecystokinin: One, Neither, or Both?

Varieties of protocols are used in the performance of a Tc-99 m HIDA study. The clinical indication for a Tc-99 m-HIDA study is established first in order to determine when to give or not to give morphine or cholecystokinin [11, 12]. In patients with suspected acute cholecystitis, giving morphine before or during cholescintigraphy is appropriate. When the gallbladder is not seen in the clinical setting of acute cholecystitis, giving morphine at 60 min reduces the total time required for final diagnosis. In a patient with suspected biliary dyskinesia, however, it is inappropriate to give morphine or cholecystokinin prior to cholescintigraphy. In suspected biliary dyskinesia, it is better to wait and take delayed

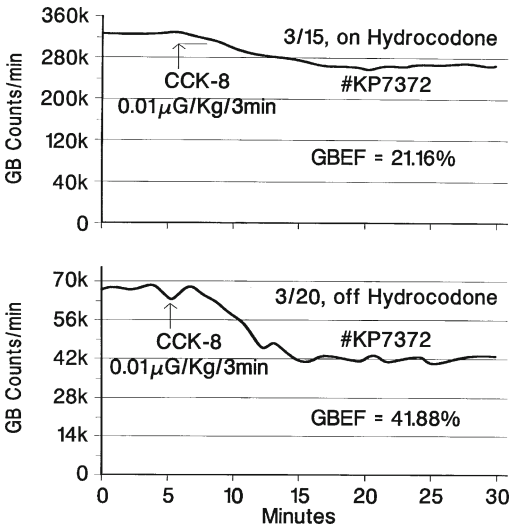

Fig. 6.2.3 Effect of CCK-8 on gallbladder ejection fraction with and without opioids. Note an ejection fraction of 21.16% while on hydrocodone and a value of 41.88% while off of hydrocodone

images at 2–4 h than to give morphine at 60 min after injection of Tc-99 m-HIDA. If the gallbladder fills late without morphine, then cholecystokinin is given to measure the gallbladder ejection fraction to rule out biliary dyskinesia. Poor emptying of the gallbladder is a characteristic feature of biliary dyskinesia. The gallbladder also empties poorly in patients given an opioid (Fig. 6.2.3). Questions often arise about whether one should measure the ejection fraction with CCK when the gallbladder appears after morphine administration. In some patients given morphine, the gallbladder empties normally with CCK and thus excludes biliary dyskinesia [13]. Once the gallbladder ejection fraction reduces below the normal value, it never regains its normal function unless the reduction was due to prior opioid administration. Dual studies have confirmed that the ejection fraction is highly reproducible in both normal subjects and patients with biliary dyskinesia [14].

References

1. Jaffe JH, Martin WR. Opioid analgesics and antagonists. In: Gilman AG, Rall TW, Niles AJ, Taylor P (eds) Goodman and Gilman's: The pharmacological basis of therapeutics, 8th edn. Pergamon, New York, 1990, pp 485–521
2. Patwardhan RV, Johnson RF, Hoyumpa A Jr, Sheehan JJ, Desmond PV, Wilkinson GR, Branch RA, Schenker S. Normal metabolism of morphine in cirrhosis. Gastroenterology 1981;81:1006–1011
3. Choy D, Shi EC, McLean RG, Hoschl R, Murray IPC, Ham JM. Cholescintigraphy in acute cholecystitis: use of intravenous morphine. Radiology 1984;151:203–207
4. Helm JF, Venu RP, Geenen JE, Hogan WJ, Dodds WJ, Toouli J, Arndorfer RC. Effects of morphine on the human sphincter of Oddi. Gut 1988;29:1402–1407
5. Venu R, Toouli J, Geenen JE, Hogan WJ, Helm J, Dodds WJ, Arndorfer RC. Effect of morphine on motor activity of the human sphincter of Oddi. Gastroenterology 1982;84:1342 (Abstract)

6. Jones RM, Fiddian-Green R, Knight PR. Narcotic induced choledochoduodenal sphincter spasm reversed by glucagon. Anesth Analg 1980;59:946–947
7. Hopton DS, Torrance HB. Action of various new analgesic drugs on the human common bile duct. Gut 1967;8:296–300
8. Chessick KC, Black S, Hoye SJ. Spasm and operative cholangiography. Arch Surg 1975; 110:53–57
9. Krishnamurthy S, Krishnamurthy GT. Biliary dyskinesia: role of the sphincter of Oddi, gallbladder, and cholecystokinin. J Nucl Med 1997;38:1824–1830
10. Joehl RJ, Koch KL, Nahrwold DL. Opioid drugs cause bile duct obstruction during hepatobiliary scans. Am J Surg 1984;147:134–138
11. Westlake PJ, Hershfield NB, Kelly JK, Kloiber R, Lui R, Sutherland LR, Shaffer EA. Chronic right upper quadrant pain without gallstones: does HIDA scan predict outcome after cholecystectomy? Am J Gastroenterol 1990;85:986–990
12. Krishnamurthy S, Krishnamurthy GT. Cholecystokinin and morphine pharmacological intervention during 99mTc-HIDA cholescintigraphy: a rational approach. Semin Nucl Med 1996;26:16–24
13. Achong DM, Oates E. Normal gallbladder ejection fraction after morphine augmentation. Clin Nucl Med 1999;24:837–841
14. Krishnamurthy GT, Krishnamurthy S, Brown PH. Constancy and variability of gallbladder ejection fraction: impact on diagnosis and therapy. J Nucl Med 2004;45:1872–1877

Intrahepatic Cholestasis 7

Cholestasis is retention of bile within the hepatobiliary system resulting in an accumulation of bile products in the body fluids. It is divided into intrahepatic and extrahepatic types, depending upon the location of the pathology. Intrahepatic cholestasis is defined traditionally as bile retention within the hepatocytes, bile canaliculi, cholangioles, small or large bile ducts down to and including the proximal two thirds of the right hepatic and left hepatic ducts. Extrahepatic cholestasis is bile stasis due to a pathology located at the distal third of the right hepatic and left hepatic ducts and beyond, down to and including the sphincter of Oddi. The previous classification into obstructive and non-obstructive jaundice is no longer popular clinically [1].

Bile secretion: Formation of bile is an osmotic pressure-dependent uptake and secretory process that occurs along the basolateral and canalicular domains of the hepatocyte, respectively. Of a total of approximately 600 ml of bile produced by the liver per day, 450 ml is secreted by the hepatocytes and the remaining 150 ml by cells lining the bile canaliculi and bile ducts (Chap. 2, Fig. 1). About 50% of bile secreted by the hepatocytes (225 ml) is bile acid dependent, and the remaining 50% (225 ml) is independent of bile acid secretion. The uptake of bile acids, non-bile acid organic anions, cations, and other solutes by the hepatocytes from blood in the space of Disse occurs along the basolateral border. Of the several mechanisms utilized for the solute uptake, Na^+-K^+ ATPase pump, Na^+-BS^- (bile salt) co-transport, sodium–hydrogen exchange, Na-HCO_3^- symporter, and organic anion endocytosis play the major roles [2]. Bile salts (taurocholate) are the most important and abundant solutes in bile. Transport of bile salts from blood into hepatocytes is mediated by the sodium-taurocholate co-transporter (NTCP) system [3]. ATPase of the basolateral border regulates the extracellular and intracellular ion concentration gradient [4].

7.1 Imaging with Tc-99m HIDA

Active transport of solutes across the canalicular membrane is the rate-limiting step in the amount of bile produced per day. The tight junction between the two adjacent hepatocytes is functionally leaky (a leaky tight junction) and allows passage of water and electrolytes from blood into the canalicular lumen. The canalicular lumen situated between two adjacent hepatocytes is about 0.75 μm in diameter, and the wall contains microvilli of 500–1,000 nm

G.T. Krishnamurthy and S. Krishnamurthy, *Nuclear Hepatology,*
DOI 10.1007/978-3-642-00648-7_7, © Springer-Verlag Berlin Heidelberg 2009

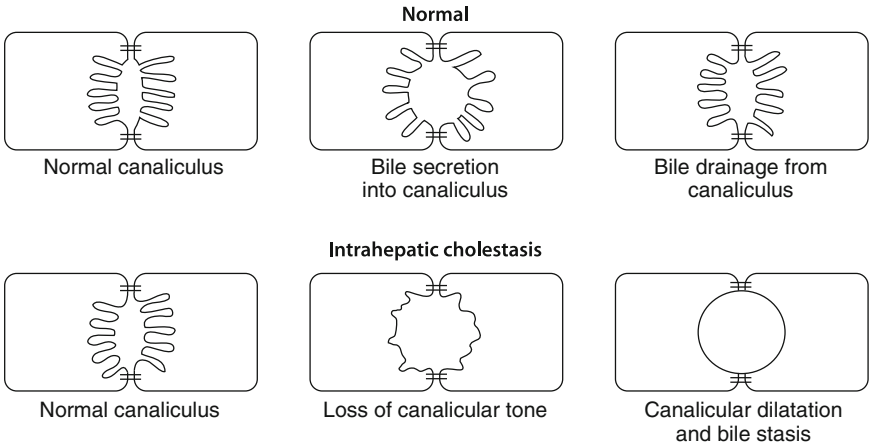

Fig. 7.1.1 Pathogenesis of intrahepatic cholestasis. Normal canaliculi and microvilli contract and propel bile forwards. Infections, drugs, and other toxins cause bile stasis by inactivating contractile function of the bile canaliculi and microvilli

in length and 100 nm in diameter. The canaliculi and their microvilli contract and propel bile towards larger bile ducts. Secretion of large lipophilic cations (anticancer drugs, calcium-channel blockers, cyclosporin A, and other drugs) is mediated by a transporter protein called multidrug-resistance-1 P-glycoprotein (MDR1). Secretion of phosphatidylcholine is facilitated by another protein called multidrug-resistance-3 P-glycoprotein, called MDR3. Transport of organic anions, including bromosulphalein, glucuronides, and possibly Tc-99m HIDA, across the canalicular membrane is attributed to multidrug resistance protein 2 (MRP2). Endotoxin lipopolysaccharide induces cholestasis by an early retrieval followed by down-regulation of MRP2, which moves from the canalicular membrane to the interior of the cell [5]. Inhibition of contraction of the canalicular wall and microvilli results in atony and dilatation of the canaliculi, leading to intrahepatic cholestasis (Fig. 7.1.1). Tc-99m-HIDA is secreted into canalicular bile in free form, without undergoing any biotransformation during its intracellular transit. This free status can be confirmed by reinjecting Tc-99m-HIDA-labeled gallbladder bile intravenously into the same animal, reproducing the original biokinetic parameters [6]. Reduction in uptake and slow transit through the hepatocytes, and collection in the dilated canaliculi produced a low hepatic extraction fraction and prolongation of excretion half-time in a Tc-99m HIDA study.

Etiology of Intrahepatic Cholestasis

Three types of injury are recognized as being responsible for cholestasis: (1) direct injury, (2) immunologic, and (3) cholestatic. These injuries are caused by microorganisms, poisons, drugs, and metabolic, granulomatous, veno-occlusive, ischemic, and other diseases (Fig. 7.1.2). The injury may involve the endoplasmic reticulum, lysosomes, mitochondria of the hepatocytes or the canalicular cells. In the case of drugs, the injury may be caused directly by the offending agent or by one of its metabolic products [7].

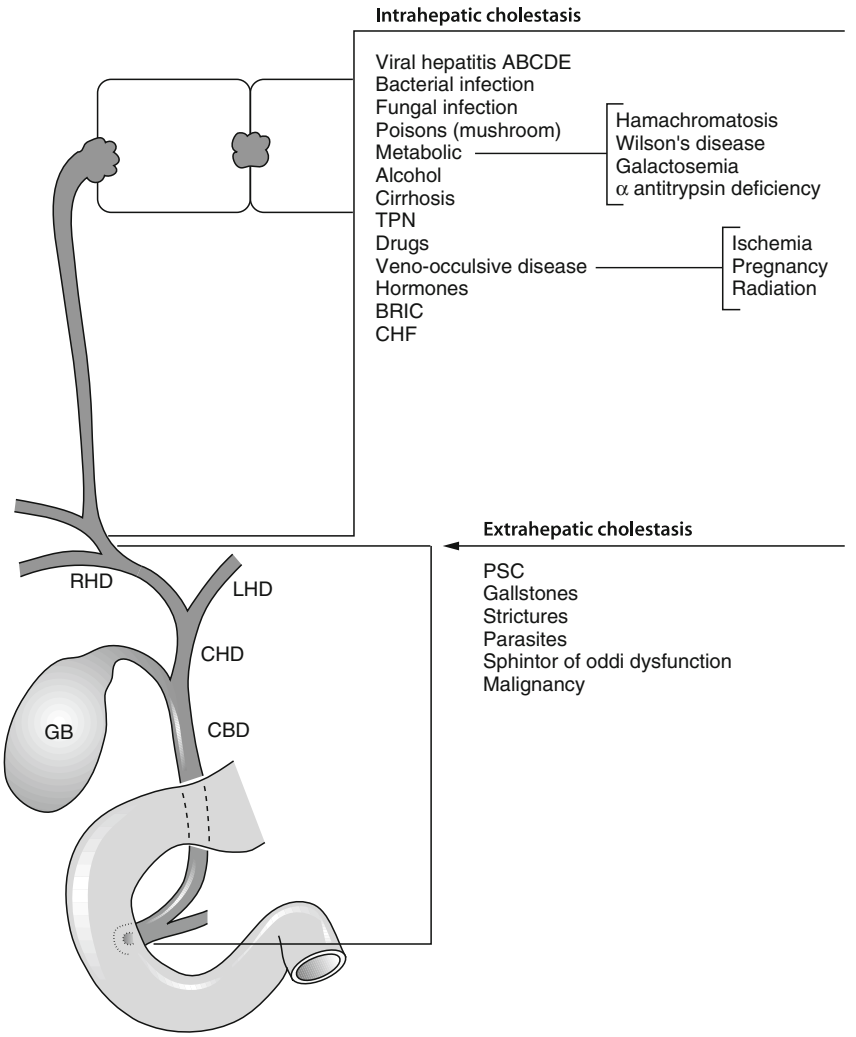

Fig. 7.1.2 Location of intrahepatic vs. extrahepatic cholestasis. Intrahepatic cholestasis occurs between the hepatocyte and the proximal right hepatic and left hepatic ducts. Pathology of the extrahepatic cholestasis lies between the proximal right hepatic and left hepatic ducts and the sphincter of Oddi

Viral Hepatitis

All types of viral hepatitis (A, B, C, D, E, and G) cause intrahepatic cholestasis, and all produce an identical image pattern. The diagnosis is usually made by getting a detailed clinical history and by obtaining a serum hepatitis profile. Bacterial and fungal infections and toxins (mushroom poisoning) also cause intrahepatic cholestasis primarily by affecting the hepatocytes and cholangioles. The bile secretion rate is reduced, hence bile ducts and the gallbladder appear late in a Tc-99m HIDA study (Fig. 7.1.3).

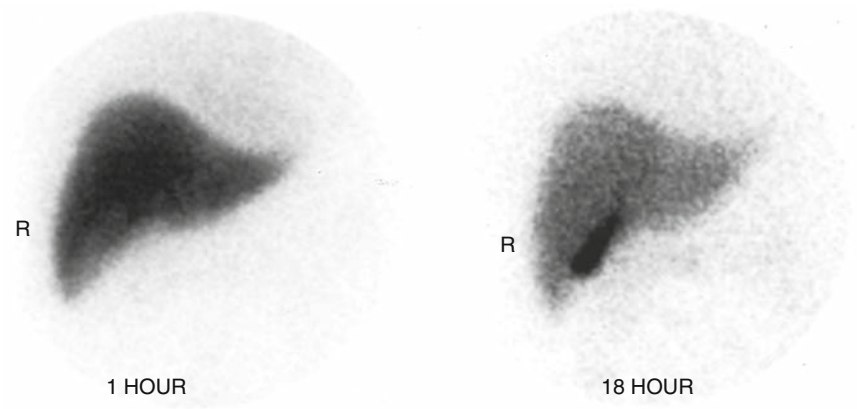

Fig. 7.1.3 Hepatitis A. Diffuse radiotracer retention with no bile secretion for 1 h in a patient with hepatitis A. Gallbladder is seen at 18 h, and the intestinal activity has moved away from the field of view of the gamma camera

Drugs

Drugs are the most common cause of intrahepatic cholestasis, which is classified into two major types [8]: (1) hypersensitive (exudative) and (2) canalicular. The hypersensitive type is characterized by fever, anorexia, marked eosinophilia, and increased levels of serum cholesterol and alkaline phosphatase. The canalicular type is characterized by intense pruritus, associated with a normal eosinophil count and serum alkaline phosphatase level [9]. Sulfonamides, quinidine, and allopurinol are incriminated in the hypersensitivity type of intrahepatic cholestasis. Sex hormones, phenothiazines, antibiotics, (erythromycin), and nitrofurantoin are common causes of the canalicular type of intrahepatic cholestasis. The drug or one of its metabolite secreted into bile canaliculi interferes with canalicular contraction, causing intrahepatic cholestasis [10].

It is estimated that about 2% of hospitalized patients in the USA suffer from some form of intrahepatic cholestasis related to a prescription drug. Up to 1% of patients receiving chlorpromazine develop intrahepatic cholestasis [9]. Various drugs that cause intrahepatic cholestasis are listed in Table 7.1.1. Most of the drugs react with cytochrome p450 and undergo conjugation with glucuronic acid, sulfate, amino acids, or glutathione prior to elimination from the body. The cytochrome p450 system is under genetic control and produces cytotoxic effects mainly through formation of electrophiles and free radicals [11, 12]. A detailed drug history aids in identifying the offending agent responsible for intrahepatic cholestasis. A cholescintigraphic image pattern remains non-specific in intrahepatic cholestasis [13].

Metabolic Causes

Hemochromatosis due to iron overload, Wilson's disease due to copper overload, and fatty infiltration and deficiency of several enzymes are known metabolic causes of intrahepatic cholestasis [14, 15].

Table 7.1.1 Localization of drug-induced intrahepatic cholestasis [9]

Hepatocyte (A)	Canaliculus (B)	Hepatocyte and canaliculus (A + B)	Ducts (C)
Carbon tetrachloride	Estrogens	Phenytoin	Benoxyprofen
Halothane	Testosterone	Quinidine	Ascending cholangitis
Chloroform	Phenothiazine	Allopurinol	Floxuridine
Amiodarone	Erythromycin	Butazolidine	–
Methyldopa	Nitrofurantoin	Thiobendozole	–
Isoniazide	Azathioprine	Furasemide	–
Ketoconazol	Cyclosporin A	Sulfonamide	–
Acetaminophen	Tranquillizers	–	–
Rifampin	Antipsychotic agents	–	–
Indomethacin	–	–	–
Tetracycline	–	–	–
Valproic acid			
Flexin			
Novobiocin			
Cocaine			
Flutamide			

Alcoholic Hepatitis

Alcohol is metabolized primarily in the liver and converted into acetaldehyde through the enzyme alcohol dehydrogenase. Acetaldehyde in turn is converted into acetate by the enzyme aldehyde dehydrogenase. Each gram of alcohol produces seven calories of energy. Most of the liver injury from alcohol occurs primarily due to its metabolite, acetaldehyde, whose accumulation exerts a toxic effect on the plasma membrane, tubulin, and other cytoskeletons of the hepatocyte [16]. When alcohol intake continues for many years, other toxic effects are manifested in the form of fatty infiltration, fibrosis, and ultimately cirrhosis of the liver and portal hypertension.

Primary Biliary Cirrhosis (PBC)

It is a disease of unknown etiology and affects primarily the canaliculi, cholangioles, and small bile ducts. Clinically, PBC presents with pruritus and malaise accompanied by elevation of serum liver enzymes and lipoproteins. It is more common in middle-aged women than men. Serum anti-mitochondrial antibody is found in almost 100% of the patients [17]. Both planar and SPECT cholescintigraphy with Tc-99m-HIDA shows diffuse parenchymal retention with uniform prolongation of excretion half time from all regions of the liver. The extrahepatic biliary tree remains normal, a common feature for all intrahepatic cholestasis. Cholescintigraphic features enable differentiation of PBC from primary sclerosing cholangitis, where the parenchymal retention is non-uniform [18]. The gallbladder remains normal in size, but shows a reduction of CCK-8 stimulated ejection fraction. In a middle-aged woman

with a positive serum antimitochondrial antibody who clinically presents with pruritus and malaise, a Tc-99m-HIDA study is confirmatory for PBC if it shows a diffuse prolongation of excretion half time and no obstruction of the extrahepatic biliary tree. A normal extrahepatic biliary tree may even preclude the need for a contrast cholangiogram to exclude primary sclerosing cholangitis, which PBC often clinically mimics [18]. Characteristic cholescintigraphic features of primary sclerosing cholangitis and primary biliary cirrhosis enable differentiation between two relatively rare conditions [18, 19].

Benign Recurrent Intrahepatic Cholestasis (BRIC)

BRIC is a rare disorder affecting patients in their 30s and is often found in several members of the same family. Intense pruritus with elevation of liver enzymes, accompanied by spontaneous recovery, is its characteristic feature. The extrahepatic biliary tree is normal [20]. There are no identifiable serum markers for BRIC. The hepatocytes are unable to get rid of bile acids and other organic anions from the body [21]. Uptake of Tc-99m-HIDA by the hepatocyte is normal, but secretion into bile is delayed or absent, resulting in nondelineation of the entire biliary system, often mimicking total acute common bile duct obstruction. The image pattern appears much like a radiocolloid scan without the spleen.

Total Parenteral Nutrition (TPN)

The major liver enzyme abnormalities in patients with TPN are elevation of gamma glutamyl transferase, ALT, and alkaline phosphatase. Peak enzyme elevation occurs 1–4 weeks after initiation of TPN. Early pathological changes include fatty infiltration in adults and intrahepatic cholestasis in children. When TPN is continued for many years, fibrosis and cirrhosis set in [22]. Uptake of Tc-99m-HIDA by the hepatocyte is maintained, but secretion is markedly delayed or even absent, mimicking total CBD obstruction. The gallbladder is often non-visualized [23].

Ischemic Hepatitis

This condition is often due to an acute reversible hypotension or cardiac failure. Following the ischemic episode there is a rapid rise in aspartate amino transferase and lactic dehydrogenase, and mild elevation of bilirubin and glucose. Liver enzyme abnormality returns to normal, usually within 8–10 days [24]. Functional abnormalities tend to be much more severe in intrahepatic cholestasis than in patients with early partial obstruction of the common bile duct [25].

Acute Cholangitis

Acute cholangitis clinically presents as a Charcot triad, which consists of fever with chills, jaundice, and abdominal pain, as described originally by Charcot in 1877 [26].

Obstruction of the common bile duct first initiates the process and then sustains acute cholangitis. Obstruction leads to bacterial overgrowth and reflux of infected bile from the liver into the blood stream. Up to 90% of patients may remain asymptomatic when the obstruction of the common bile duct is not critical or complete [27, 28]. Charcot triad sets in mostly when the obstruction becomes complete. Both gram-positive and gram-negative organisms are found with equal frequency. Serum bilirubin rises above 5 mg% in more than 50% of the patients. Leucocytosis is frequent (63%), and elevation of serum amylase occurs in 30% of the patients [29]. Elevation of serum bilirubin above 5 mg% is a common feature of acute cholangitis, but not of acute cholecystitis (Table 7.1.2).

In the past, choledocholithiasis and postoperative stricture were the most common causes of acute cholangitis. In series reported prior to 1980, stone or postoperative stricture accounted for almost 90% of acute cholangitis; now they account for only 26%. Instrumentation (ERCP) of the biliary tract is now the most common cause of acute cholangitis (35%), indicating a shift in the etiology of acute cholangitis in more recent years [29].

Scintigraphic Features of Intrahepatic Cholestasis

Injury to the hepatocyte, bile canaliculi, and small bile ducts produces a nonspecific image pattern in a Tc-99m-HIDA study. Location of the exact site of injury among these three cannot be made from the images. An etiologic diagnosis, therefore, requires a thorough knowledge of clinical presentation, liver function tests, and a serum viral profile for hepatitis. The diseases that combine the features of both intrahepatic and extrahepatic cholestasis (e.g., sclerosing cholangitis) have a very characteristic image presentation and often enable an etiologic diagnosis [18, 19].

Table 7.1.2 Clinical and laboratory findings in acute cholangitis vs. acute cholecystitis [29]

Parameter	Acute cholangitis	Acute cholecystitis
Clinical features:		
Mean age (years)	60	50
Male:female	1:1	3:2
Fever (%)	90	90
Chills (%)	75	50
Jaundice (%)	95	30
RUQ pain (%)	80	95
RUQ tenderness (%)	80	95
Laboratory findings:		
WBC >10,000 (%)	70	70
WBC >20,000 (%)	10	5
Bilirubin >1.5 mg (%)	95	30
Bilirubin >5.0 mg (%)	55	5
Elevation of alkaline phosphatase (%)	90	40
Increase in SGOT and SGPT (%)	95	50
Increase in serum amylase (%)	35	15

The dose of Tc-99m-HIDA for imaging is increased to 5 and 10 mCi to compensate for a decrease in hepatocyte uptake secondary to a high serum bilirubin, which competes with Tc-99m-HIDA. The hepatic extraction fraction decreases and excretion half time increases in direct proportion to an elevation of serum bilirubin (Fig. 7.1.4). Delayed images at 4 or 24 h are necessary to show intestinal activity, which establishes patency of the bile duct. In a patient who presents clinically with a Charcot triad, nonvisualization of the gallbladder with features of intrahepatic cholestasis in a TC-99m-HIDA study suggests acute cholangitis (Fig. 7.1.5).

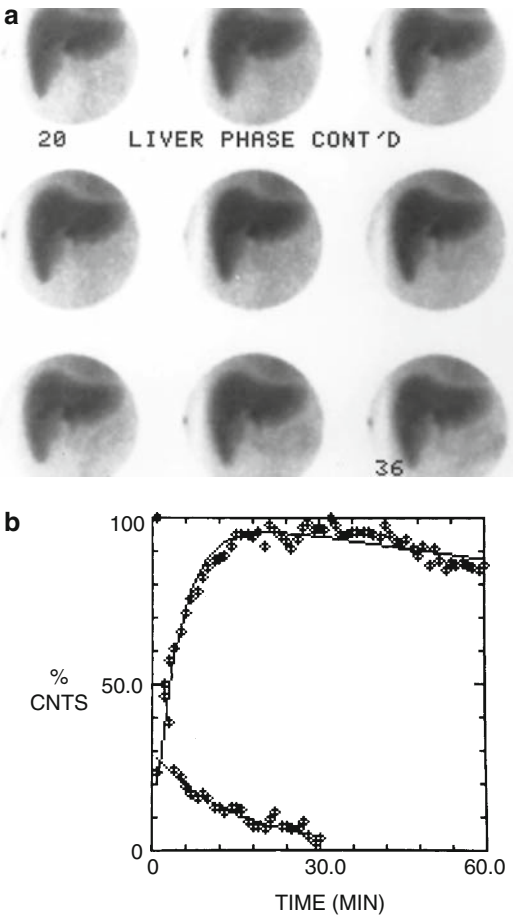

Fig. 7.1.4 Cholescintigraphic features of intrahepatic cholestasis. Hepatocytes show decreased extraction and delayed excretion of Tc-99m-HIDA. Images are shown between 20 and 36 min (**a**). Hepatic extraction is only 28% (normal, 92–100%), and $T_{1/2}$ excretion is 278 min (normal, 11-33 min) (**b**)

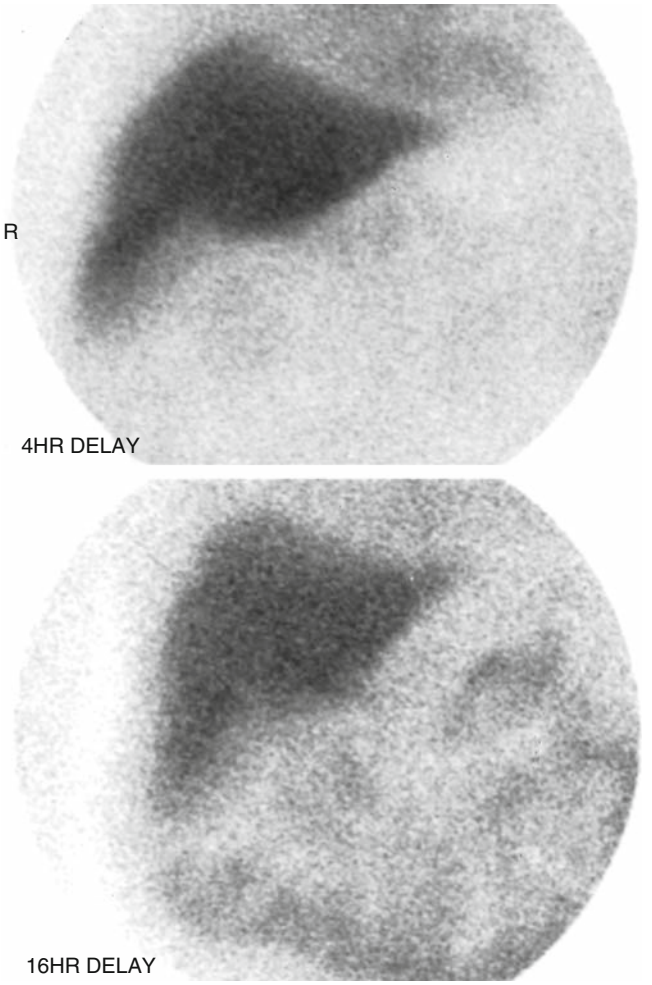

Fig. 7.1.5 Acute cholangitis secondary to acute cholecystitis. The gallbladder is non-visualized due to obstruction of the cystic duct, and there is diffuse retention at 4 and 16 h. Common bile duct is patent and allows bile entry into small intestine

References

1. Sherlock S, Dooley J (1997) Cholestasis. In: Diseases of the liver and biliary system, 10th edn. Blackwell Science Inc, Malden, MA, pp 217–237
2. Trauner M, Meier PJ, Boyer JL. Molecular pathogenesis of cholestasis. N Eng J Med 1998;339:1217–1227
3. Hagenbuch B, Meier PJ. Sinusoidal (basolateral) bile salt uptake system of hepatocytes. Semin Liver Dis 1996;16:129–136

4. Sellinger M, Barrett C, Malle P, Gordon ER, Boyer JL. Cryptic Na+, K(+) -ATPase activity in rat liver canalicular plasma membrane: evidence for its basolateral origin. Hepatology 1990;11:223–229
5. Kubitz R, Wettstein M, Warskulat U, Haussinger D. Regulation of the multidrug resistance protein 2 in the rat liver by lipopolysaccharide and dexamethasone. Gastroenterology 1999;116:401–410
6. Loberg MD, Cooper M, Harvey E, Callery P, Faith W. Development of new radiopharmaceuticals based on N-substitution of iminodiacetic acid. J Nucl Med 1976;17:633–638
7. Sherlock S. Patterns of hepatic injury in man. Lancet 1982;1(8275):782–786
8. Lee WM. Drug-induced hepatotoxicity. N Engl J Med 1995;333:1118–1128
9. Sherlock S, Dooley J (1997) Drugs and the liver. In: Diseases of the liver and biliary system, 10th edn. Blackwell Science Inc, Malden, MA, pp 337–369
10. Corcoran GB, Racz WJ, Smith CV, Mitchell JR. Effects of N-acetylcysteine on acetaminophen covalent binding and hepatic necrosis in mice. J Pharmacology Exp Ther 1985;232:864–872
11. Smith CV, Hughes H, Mitchell JR. Free radicals in-vivo. Covalent binding to lipids. Mol Pharmacol 1984;26:112–116
12. Seeff LB, Cuccherini BA, Zimmerman HJ, Adler E, Benjamin SB. Acetaminophen hepatotoxicity in alcoholics. Ann Intern Med 1986;104:399–404
13. Lieberman DA, Krishnamurthy GT. Intrahepatic versus extrahepatic cholestasis. Discrimination with biliary scintigraphy combined with ultrasound. Gastroenterology 1986;90:734–743
14. Powell LW, Halliday JW, Cowlishaw JL. Relationship between serum ferritin and total body iron stores in idiopathic hemochromatosis. Gut 1978;19:538–542
15. Bearn AG. Wilson's disease. An inborn error of metabolism with multiple manifestations. Am J Med 1957;22:747–753
16. Lauterburg BH, Bilzer H. Mechanisms of acetaldehyde hepatotoxicity. J Hepatol 1988;7: 384–390
17. Walker JG, Doniach D, Roitt IM, Sherlock S. Serological tests in diagnosis of primary biliary cirrhosis. Lancet 1965;1:827–831
18. Keeffe EB, Lieberman DA, Krishnamurthy S, Krishnamurthy GT, Gilbert SA. Primary biliary cirrhosis: Tc-99m-HIDA planar and SPECT scanning. Radiology 1988;166:143–148
19. Rodman CA, Keeffe EB, Lieberman DA, Krishnamurthy S, Krishnamurthy GT, Gilbert SA, Eklem MJ. Diagnosis of sclerosing cholangitis with Tc-99m-labeled iminodiacetic acid planar and single photon emission computed tomographic scintigraphy. Gastroenterology 1987;92: 777–785
20. Lesser PB. Benign familial recurrent intrahepatic cholestasis. Am J Dig Dis 1973;18:259–264
21. Minuk GY, Shaffer EA. Benign recurrent intrahepatic cholestasis. Evidence for an intrinsic abnormality in hepatocyte secretion. Gastroenterology 1987;93:1187–1193
22. Quigley EM, Marsh MN, Shaffer JL, Markin RS. Hepatobiliary complications of total parenteral nutrition. Gastroenterology 1993;104:286–301
23. Shuman WP, Gibbs P, Rudd TG, Mack LA. PIPIDA scintigraphy for cholecystitis: False-positives in alcoholism and total parenteral nutrition. Rm J Roentgenol 1982;138:1–5
24. Gitlin N, Serio KM. Ischemic hepatitis: Widening horizons. Am J Gastroenterol 1992;87:831–836
25. Lima J, Brown R, Krishnamurthy S, Krishnamurthy GT. Reliability of quantitative Tc-99m-mebrofenin scintigraphy (QMS) in the diagnosis of intrahepatic cholestasis(IHC). J Nucl Med 1991;32:976–977
26. Charcot JM: Lecons sur les maladies du foie des voies biliaires at des veins. Paris Faculte' de medecine. Recueilleies et publices. Bournelle et Senestre, 1877
27. Flemma RJ, Flint LM, Osterhout S. Bacteriologic studies of biliary tract infection. Ann Surg 1967;166:563–572
28. Pitt HA, Postier RG, Cameron JL. Biliary bacteria: significance and alterations after antibiotic therapy. Arch Surg 1982;117:445–450
29. Pitt HA, Cameron JL. Acute cholangitis. In: Way LW, Pelligrini CA, eds. Surgery of the gallbladder and bile ducts. WB Saunders, Philadelphia, 1987, pp 295–313

7.2 Imaging with Tc-99m Galactosyl Human Serum Albumin

Identification of unique asialoglycoprotein (ASGP) receptors on the plasma membrane of the hepatocyte [1] and introduction of technetium-99m-DTPA-galactosyl-human-serum albumin (Tc-99m GSA), which binds to it, allow non-invasive functional imaging and quantification. Asialoglycoprotein receptor concentration on the plasma membrane is an indicator of the functional integrity of the hepatocyte. The quantity of Tc-99m GSA uptake correlates inversely with blood retention of indocyanin green [2]. Liver uptake of Tc-99 GSA decreases in patients with chronic hepatitis, cirrhosis, cholangiocarcinoma, hepatocellular cancer, metastasis, fulminant hepatic failure, and space-occupying benign lesions of the liver [2–5].

Data collection and analysis: Most of the clinical studies reported in the literature are from Japan, and the agent is not available in most other countries, including the United States. Functional imaging and quantification require standardization to keep the variables to a minimum. Patient fasting, which is not necessary during imaging with Tc-99m-S-colloid, is very essential for imaging with Tc-99m GSA, because the uptake may be variable due to postprandial hyperperfusion of the GI tract. After 4–6 h of fasting, the patient is positioned supine underneath a gamma camera (single, double, or a triple head) fitted with a low-energy, high-resolution, parallel-hole collimator that is positioned anterior to the liver. Sequential anterior planar images (128 × 128) at one frame per 30 s for 20 min are obtained immediately after a bolus injection of 5 mCi Tc-99m GSA (185 MBq) into the antecubital vein. Immediately after the planar images, SPECT data are acquired on a 128 × 128 × 16 computer matrix for 64 stops at 10 s per stop at 5.6° intervals [2]. The spectrometer is set for 140 keV at a 20% window. The liver uptake index at 15 min is calculated as described in Chap. 5.

Some authors express uptake as hepatic GSA clearance using the Patlak plot method and generate functional images of clearance [3, 4]. The receptor index decreases in patients with chronic hepatitis and cirrhosis (Fig. 7.2.1). Since the cells other than the hepatocytes

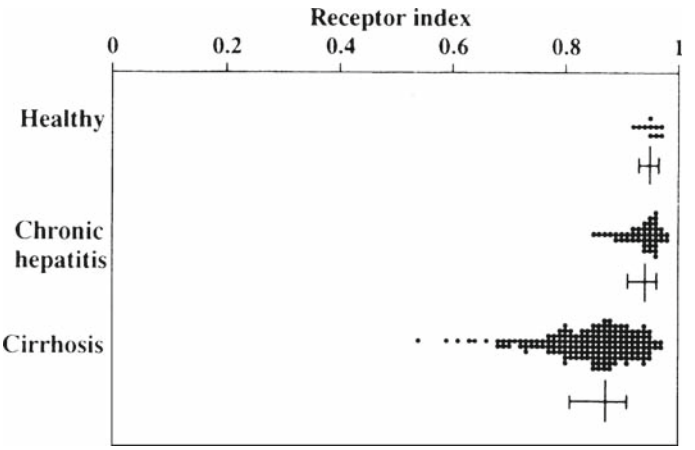

Fig. 7.2.1 Relationship between Tc-99m GSA receptor index and liver disease. Normal hepatocytes rich in ASGP receptors show high index. Reduction of Tc-99m GSA receptor index occurs in patients with chronic hepatitis and cirrhosis of liver [4]. *GSA* galactosyl human serum albumin

do not take up any Tc-99m GSA, preoperative imaging allows accurate measurement and prediction of residual liver function postoperatively after resection of hepatocellular carcinoma, cholangiocarcinoma, and metastatic liver tumors (Fig. 7.2.2). It is not known at this

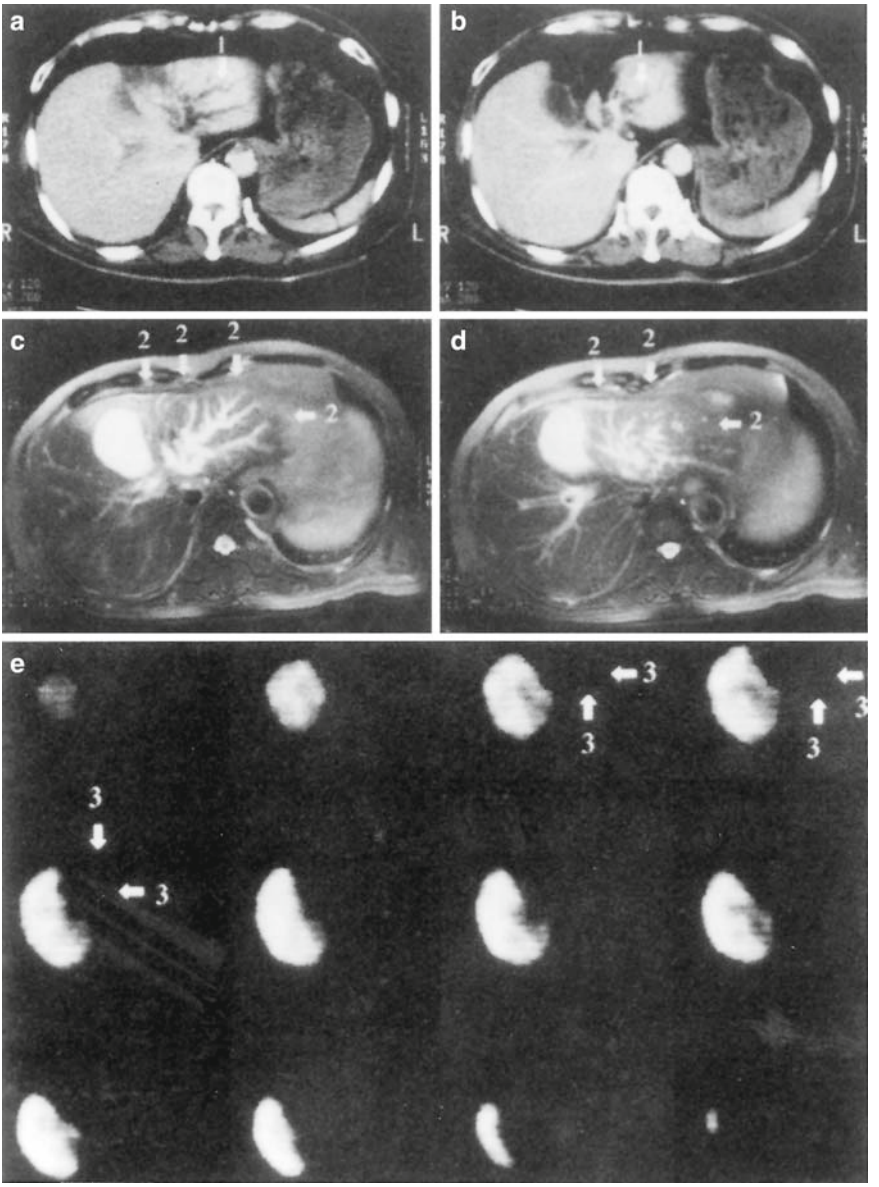

Fig. 7.2.2 Absence of Tc-99m GSA uptake by tumors. CT with contrast shows dilatation of bile ducts in the left lobe (**a**, **b**, *arrow*) of a patient with cholangiocarcinoma. T2-weighted MR shows hyper-intensity of left lobe bile ducts (**c**, **d**, *arrow*). Liver SPECT shows no uptake of Tc-99m GSA (**e**) by the left lobe of. *GSA* galactosyl human serum albumin [3]

time if this functional parameter can serve as an ideal marker for end-stage liver disease and timing of liver transplantation.

References

1. Steer CJ. Receptor-mediated endocytosis: mechanisms, biologic function, and molecular properties. In: Zakim D, Boyer TD (eds) Hepatology. A textbook of liver disease. WB Saunders, Philadelphia, 1996, pp 149–214
2. Uetake M, Koizumi K, Yagawa A, Nogata H, Tezuka T, Kono H, Ozawa T, Kusano T, Miyaburuko M, Hosaka M. Use of Tc-99m DTPA galactosyl human serum albumin to predict postoperative residual liver function. Clin Nucl Med 1999;24:428–434
3. Hwang E, Taki J, Shuke N, Nakajima K, Kinuya S, Konishi S, Michigishi T, Aburano T, Tonami N. Preoperative assessment of residual hepatic functional reserve using Tc-99m-DTPA-galactosyl-human-serum albumin dynamic SPECT. J Nucl Med 1999;40:1644–1651
4. Sasaki N, Shiomi S, Iwata Y, Nishiguchi S, Kuroki T, Kawabe J, Ochi H. Clinical usefulness of scintigraphy with Tc-99m-galactosyl-human serum albumin for prognosis of cirrhosis of the liver. J Nucl Med 1999;10:1652–1656
5. Koizumi K, Monzawa S, Shindo C, Hosaka M. Primary hepatic amyloidosis well delineated by Tc-99m DTPA galactosyl HSA liver SPECT. Clin Nucl Med 1999;24:271–273

Extrahepatic Cholestasis 8

Extrahepatic cholestasis is the retention of bile products within the body secondary to a pathology located outside of the liver parenchyma, usually beyond the middle third of the right and left hepatic ducts, including the common hepatic and common bile ducts. Causes of extrahepatic cholestasis can be divided into four major categories depending upon the exact site of location of the pathologic process: (1) intraluminal, (2) wall thickening, (3) extrinsic compression, and (4) combined intrahepatic and extrahepatic causes (Table 8.1.1). The mode of clinical presentation depends very much upon the duration, degree of obstruction, and exact site of pathology.

Normally, the biliary structures appear in a sequential pattern on a Tc-99m HIDA study; the right and left hepatic ducts appear first, followed by the common hepatic duct, gallbladder, common bile duct, and duodenum. Quantitative parameters show the normal hepatic extraction fraction and excretion half-time (Fig. 8.1.1). Ducts proximal to the right and left hepatic ducts are not usually seen clearly. They become prominent only when there is obstruction to bile flow distally.

8.1 Intraluminal Causes

Clinical Presentation

Intraluminal obstruction is usually caused by gallstones, inspissated bile, parasites, blood clots, or pedunculated tumors arising from the wall (Table 8.1.1). The onset of signs and symptoms depends upon the degree and duration of obstruction. A patient with acute complete obstruction of the common bile duct usually presents with sudden onset of epigastric or right upper quadrant pain, which often radiates to the chest, shoulder, or interscapular region in the back. When complete obstruction persists for longer than 3 days, acute cholangitis may set in with onset of clinical Charcot triad, which consists of fever with chills, jaundice, and biliary colic. The time for the serum liver function tests to become abnormal after the onset of obstruction depends upon the presence or absence of the gallbladder; in the absence of the gallbladder, the liver function tests become abnormal within 4–6 h, whereas they may take as long as 48–72 h with an intact gallbladder. In presence of the gallbladder, the liver function tests become abnormal much earlier when the level of

G.T. Krishnamurthy and S. Krishnamurthy, *Nuclear Hepatology,*
DOI 10.1007/978-3-642-00648-7_8, © Springer-Verlag Berlin Heidelberg 2009

Table 8.1.1 Causes of extrahepatic cholestasis

(1) Intraluminal causes
(a) Gallstones (choledocholithiasis)
(b) Hemobilia (blood clots)
(c) Parasites (round worm)
(d) Inspissated bile or concretions
(e) Miscellaneous causes
Tumor emboli
Papilloma
Adenomyoma
Fibroma
Cystedenoma
(2) Wall thickening
(a) Benign (stricture)
(b) Malignant (cholangiocarcinoma)
(3) Combined intrahepatic and extrahepatic cholestasis
Sclerosing cholangitis
(4) Extrinsic compression

obstruction lies proximal to the junction of the cystic duct with the common hepatic duct than when the obstruction lies distal to their junction. Patients with partial bile duct obstruction usually make a benign clinical presentation.

Choledocholithiasis

Formation of gallstones is initiated with secretion of lithogenic bile, which is the first indication of a breakdown of normal mechanisms responsible for keeping bile solutes in solution [1]. The majority of gallstones are composed of cholesterol, and few consist of bile pigments. The stone may form de novo within the common bile duct (primary stone), or it may originate in the gallbladder or liver and then move down into the common bile duct (secondary stone). About 85–90% of all stones are secondary, and the rest are primary. Secondary stones are more common in western China, Hong Kong, and other Asian countries. In certain ethnic groups, as much as 50% of the CBD stones are primary [2].

Pathophysiology of Bile Duct Obstruction

The pathophysiologic changes that follow bile duct obstruction depend upon several factors, of which the mode of onset (sudden vs. gradual) and severity (partial vs. complete) are the most important. Much of our knowledge about post-obstructive pathophysiologic changes is derived from ligation of the common bile duct in experimental animals. Following complete ligation of the common bile duct in the rat, the serum alkaline phosphatase and alanine aminotransferase (ALT) levels begin to rise rapidly within 5 h, reach peak levels by 20 h, and later begin to decline to reach a steady state by 4 days. Serum bilirubin begins to rise by 5 h, reaches peak levels by 4 days, and then begins to decline to reach a new steady state level, which is often set at a much lower level than the

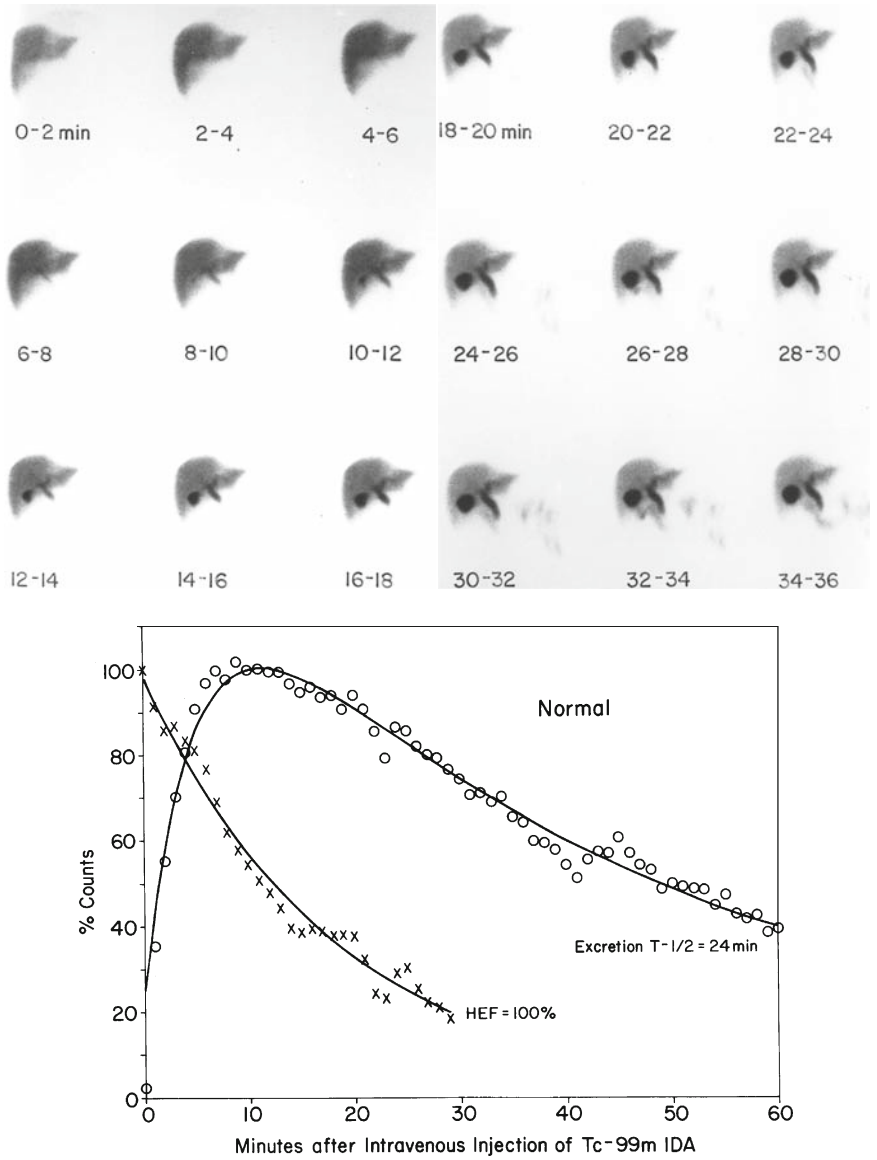

Fig. 8.1.1 Normal cholescintigraphy. Liver shows excellent uptake and excretion of Tc-99 HIDA. The right hepatic duct and left hepatic ducts, common hepatic duct, and gallbladder are seen early (*top left*), followed by the common bile duct and duodenum (*top right*). Hepatic extraction fraction (*HEF*) and excretion values are normal (*bottom*)

peak. The serum alkaline phosphatase level begins to rise and reach peak levels much earlier than the serum bilirubin level. The number of bile canaliculi doubles in 5 h and then begins to decrease after 4 days. The hepatocytes shrink in size and reach a steady state by 2 days.

Post-obstructive shrinkage of the hepatocytes and swelling of bile canaliculi together lead to a bile leak into the blood stream [3]. Bile flow decreases to 65% of the basal value when the pressure within the ducts exceeds 16–17 cm of water, and the bile secretion ceases completely when the pressure rises above 20–30 cm of water [4, 5].

In piglets, the serum levels of aspartate aminotransferase (AST), ALT, alkaline phosphatase, total bilirubin, and direct bilirubin more than double by 24 h after ligation of the common bile duct. Elevation of bile duct pressure occurs much faster than the dilatation of the common bile duct. Common bile duct pressure rises from a basal 7.2 cm H_2O to 19.0 cm H_2O, whereas the duct diameter increases from a basal 5.6 mm to 9.8 mm, and the bile concentration of ciprofloxacin reduces to one-seventh of the original concentration, emphasizing the importance of pressure changes on the rate of secretion of bile and bile components [6].

In dogs, liver function tests may remain normal for up to 3 h, but become abnormal by 24 h following the complete ligation of the common bile duct. The hepatocyte uptake and secretion into bile of Tc-99m-HIDA continue for up to 3 h post-ligation, enabling cholescintigraphic delineation of the gallbladder and hepatobiliary tree, proximal to the site of obstruction. The hepatobiliary tree often simulates features seen in a physiologically tight sphincter of Oddi, where all of the hepatic bile may be diverted into the gallbladder, and none enters the duodenum. By 24 h, the hepatocytes continue to concentrate Tc-99m-HIDA, but are unable to secrete it into bile, which results in total non-visualization of the entire biliary tree [7]. Scintigraphy then appears much like a radiocolloid liver scan without the spleen.

Cholescintigraphic Features of Total Obstruction of the Common Bile Duct

The cholescintigraphic features merely reflect the pathophysiological changes that follow obstruction of the common bile duct as described above. The normal mean secretory pressure of the hepatocytes in humans is about 35 cm of water, the mean pressure within the gallbladder is 10 cm, in the common bile duct (CBD) is 12 cm, and in the sphincter of Oddi is 15 cm of water [8]. Bile secretion continues at a normal rate as long as all these normal pressure differentials are maintained. Bile secretion begins to decrease when CBD pressure begins to rise, and the secretion ceases completely when CBD pressure equals or exceeds the secretory pressure of the hepatocytes [9]. Normally about 30% of the hepatic bile that enters the duodenum during fasting enables cholescintigraphic visualization of the small intestine within 60 min in about 80% of the subjects. In the remaining 20% of normal subjects, the duodenum is not seen due to entry of all of the hepatic bile into the gallbladder [10–12]. The flow of the entire hepatic bile into the gallbladder and none into the duodenum during fasting in normal subjects is simply a reflection of an increase in the tonus of the sphincter of Oddi.

After 6–8 h of fasting, a normal gallbladder is usually filled to its full capacity of 50 ml, and its ability to accommodate a constant inflow of hepatic bile (about 0.3 ml min^{-1}) is due to absorption of an equal volume of water through the wall. When only the gallbladder is seen by 60 min, but not the duodenum, the reasons for non-visualization may include a physiologically tight sphincter of Oddi or a complete obstruction of the common bile duct. After CCK-8 infusion, the gallbladder contracts and empties bile normally into the duodenum in the case of a physiologically tight sphincter of Oddi [10], but no bile enters the duodenum in the case of complete obstruction of the CBD [13, 14].

Bile Duct Obstruction for Less than 48 Hours (Hyper Acute)

A gallstone dislodged from either the gallbladder or intrahepatic ducts or an acute edematous acute pancreatitis is the most common cause of acute complete obstruction of the CBD. A dislodged gallstone usually gets trapped just above or within the sphincter of Oddi, the narrowest part of the CBD. The time interval between the onset of acute CBD obstruction and cessation of hepatic bile secretion is variable, depending upon the level (below or above the entrance of the cystic duct into the common hepatic duct), degree (complete or partial), and presence or absence of the gallbladder. Following acute complete obstruction of the CBD, the liver continues to secrete bile slowly for 24–48 h. The uptake of Tc-99m-HIDA remains relatively high (Fig. 8.1.2a), but the secretion slows, resulting in delayed visualization of biliary structures (Fig. 8.1.2b, c). The gallbladder and bile

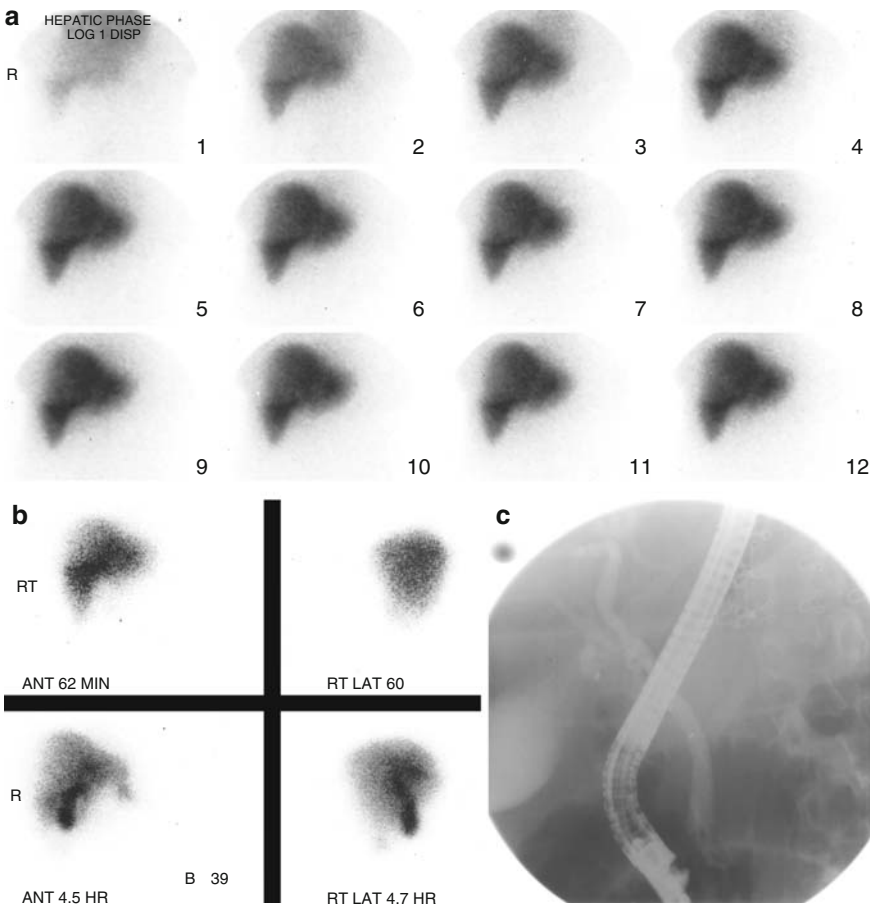

Fig. 8.1.2 Hyperacute CBD obstruction (less than 48 h). Obstruction of less than 48 h shows excellent uptake of Tc-99m-HIDA by the hepatocytes. Bile secretion is delayed (**a**). The gallbladder is seen at 4.5 h (**b**). Cholangiogram confirms obstruction due to stone at distal end of non-dilated CBD (**c**)

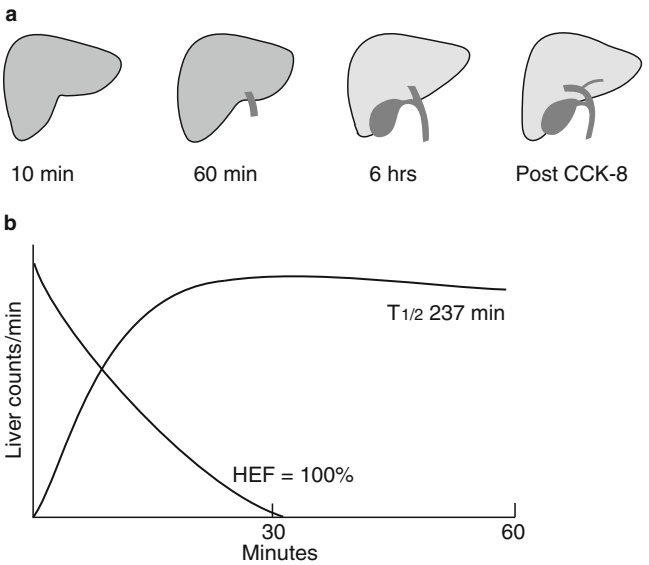

Fig. 8.1.3 Effect of acute complete duct obstruction on functional parameters. In acute obstruction, hepatic extraction fraction (*HEF*) remains normal, but excretion half-time increases. Gallbladder appears late and fills more after CCK-8. There no bile entry into the duodenum

ducts (proximal to the level of obstruction) are seen, but not the duodenum. Quantitative parameters show a normal hepatic extraction fraction and prolongation of the excretion half-time (Fig. 8.1.3). Administration of CCK-8 increases bile secretion and flow by the intrahepatic bile ducts and forces the hepatic bile to enter the gallbladder; also, there is no bile entry into the duodenum. Due to high pressure in the common bile duct, the gallbladder fails to empty in response to CCK-8 infusion. Some patients show an immediate bile flow into the gallbladder, while others may take a few more minutes after CCK-8 (Fig. 8.1.4). Filling of the gallbladder in response to CCK-8 is a physiological paradox and confirmatory feature for acute total obstruction of the common bile duct. The only other condition that shows a similar feature is spasm of the sphincter of Oddi (Chap. 10).

Obstruction for More than 48 Hours

Extraction of Tc-99m-HIDA by the hepatocytes is maintained at a relatively high level, but the secretion into bile ceases completely. Cholescintigraphy obtained after 48 h of obstruction, therefore, shows good liver uptake without delineation of any of the biliary structures (Fig. 8.1.5a). Hepatic extraction fraction values in the range of 50–85% are common between 2 and 5 days, and the values fall below 50% when total obstruction persists for more than 5 days (Fig. 8.1.5b). Cholescintigraphic images and quantitative parameters accurately reflect histopathological changes of bile duct obstruction as described above in experimental animals. In the rat, for example, a mean HEF value of 97% before bile duct ligation falls to 70% by 2 h and 16% by 48 h after complete ligation of the common bile duct.

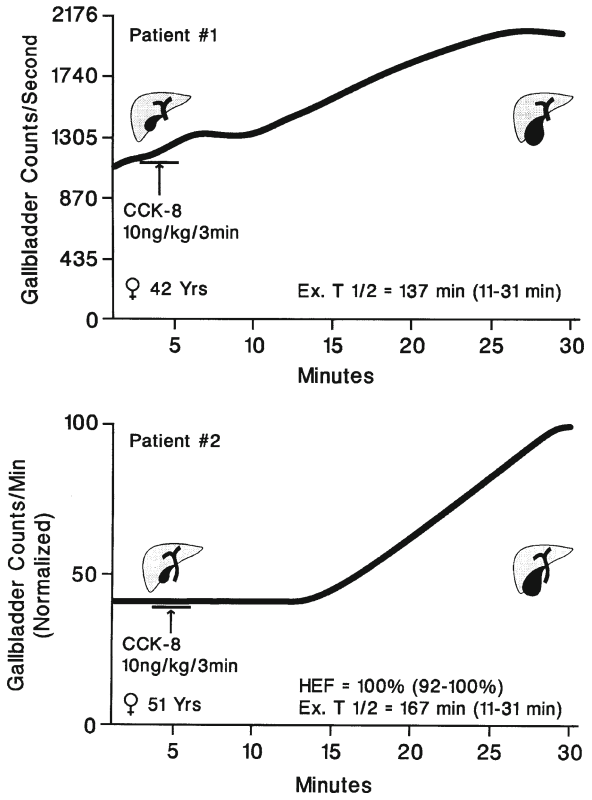

Fig. 8.1.4 Paradoxical filling of the gallbladder. Cholecystokinin administration in patients with hyperacute complete CBD obstruction increases bile secretion by intrahepatic ducts and forces the hepatic bile to enter the gallbladder, instead of eliciting its emptying. In patient no. 1, gallbladder fills in immediately, and it takes few more minutes to fill in patient no. 2. Gallbladder size and counts increase after CCK-8

Long-standing CBD obstruction ultimately compromises hepatocyte functioning and results in a low HEF value [15–17].

Both bilirubin and Tc-99m-HIDA share a common organic anion receptor-mediated endocytosis for uptake by the hepatocyte. When serum levels are high, bilirubin occupies most of the available receptor sites and blocks the uptake of Tc-99m-HIDA by the hepatocytes and produces a low HEF value. Technetium-99m mebrofenin competes with bilirubin for hepatocyte uptake much better than Tc-99m-labeled diisopropyl IDA (DISIDA), diethyl IDA, para-isopropyl-IDA (PIPIDA), or para-butyl IDA. The reciprocal relationship between Tc-99m-HIDA uptake and serum bilirubin level is well documented in both animal and human studies [17, 18]. In a patient with acute onset of biliary pain, a HEF value above 65% combined with cessation of bile secretion (non-visualization of the bile ducts and gallbladder) is a reliable indicator of a pure biliary disease (complete CBD obstruction), whereas an HEF value below 50% under similar circumstances indicates accompanying severe hepatocellular damage [19, 20].

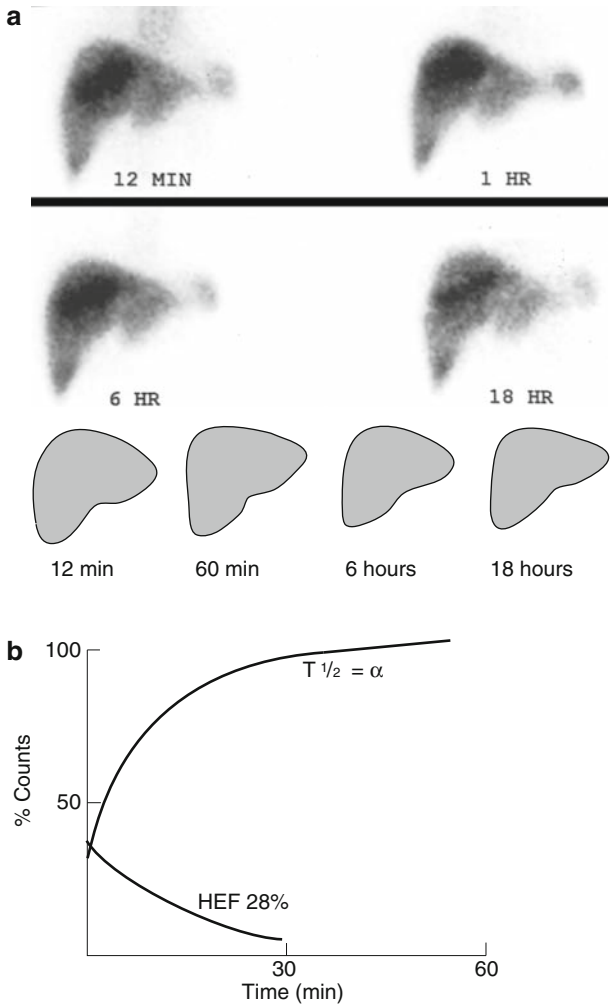

Fig. 8.1.5 Complete obstruction of the duct for more than 48 h. There is uptake by the hepatocytes, but no secretion of the radiotracer into bile. The entire biliary tree and the small intestine are nonvisualized for up to18 h (*top*). Hepatic extraction fraction (*HEF*) is reduced to 28% and excretion half-time shows infinity (*bottom*)

Partial Obstruction

Patients with a partial bile duct obstruction usually present with mid-abdominal or right upper quadrant pain. Elevation of serum alkaline phosphatase or gamma glutamyl transferase is the earliest biochemical abnormality. Cholescintigraphic features of partial CBD obstruction include normal hepatic extraction fraction, bile stasis in ducts proximal to obstruction, and prolongation of excretion half-time values (Fig. 8.1.6a). Intestinal activity may be seen within 60 min or delayed slightly in a few of the patients. Diagnosis of

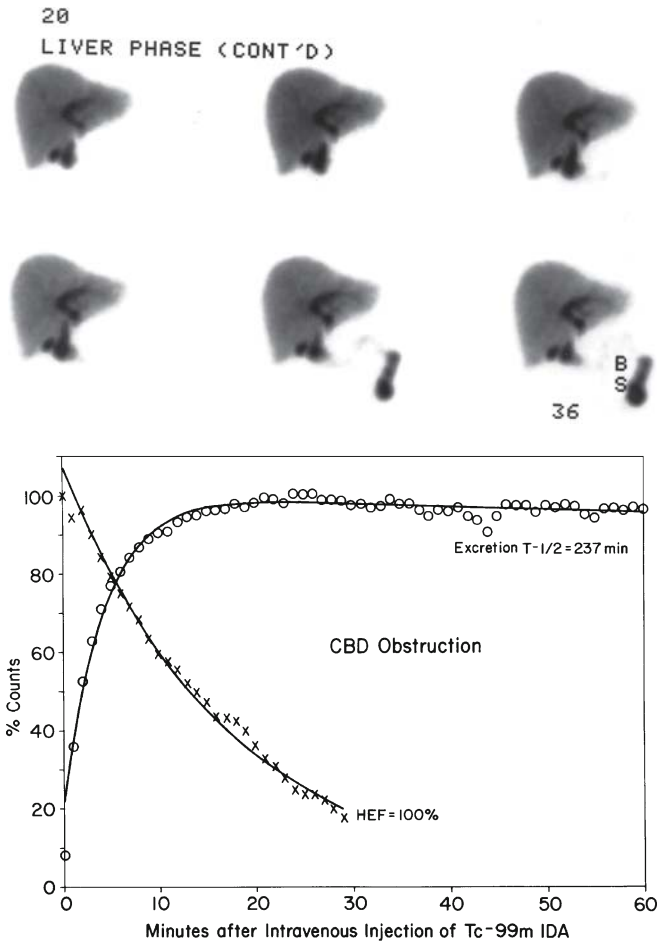

Fig. 8.1.6 Partial obstruction of the common bile duct. The uptake of the radiotracer remains normal, but the excretion is slowed. Common bile duct is poorly visualized. There is bile pooling in the intrahepatic ducts. The gallbladder and small intestine are seen (*top*). Hepatic extraction fraction (*HEF*) remains normal, but the excretion half-time increases to 237 min (*bottom*)

obstruction of the common bile duct can neither be excluded nor confirmed solely on the basis of the appearance or non-appearance of the duodenum, respectively.

Quantitative parameters indicate the severity of the disease, and an etiological diagnosis (biliary vs. hepatocellular) is usually made in combination with the image pattern. A mean HEF value of 94% was obtained in 14 patients with isolated partial CBD obstruction and a value of 96% in 13 patients with sclerosing cholangitis. In contrast, 14 patients with cirrhosis had a mean HEF of 60%. Hepatic extraction values below 30% are more common in patients with Child class C than class A and B cirrhosis [20]. Complete CBD obstruction of longer than 5-day duration, however, compromises hepatocyte function and lowers HEF values to levels seen in patients with cirrhosis [15]. Excretion half-time values begin to

increase immediately after the onset of CBD obstruction and reach values as high as 200–300 min (Fig. 8.1.6b). Many patients with critical obstruction may show only an up-slope to the curve with T1/2 value of infinity [15, 20]. Cholescintigraphic features of partial CBD obstruction are non-specific, and an etiological diagnosis (stone vs. stricture) can be made only in a few of the patients based solely on an image pattern. A gallstone lodged in the CBD may cause a filling defect with a convex superior border enabling an etiological diagnosis in a few of the patients [21].

Functional Recovery Pattern

The liver recovers its function rapidly after relief of CBD obstruction. Generally, serum bilirubin values decline much more rapidly than serum alkaline phosphatase levels, a feature that is the reverse of what takes place during the onset of obstruction [3]. Serum bilirubin levels decline by 50% of the preoperative value within 2 days, reach 25% by 1 week, and 10% by 3 weeks (Fig. 8.1.7). By 10 days after the relief of obstruction, the serum bilirubin level declines to 25%, whereas the alkaline phosphatase level may decline to only 60% of the preoperative value [9].

Hemobilia

This is a unique name that combines both Greek (*haima*, meaning blood) and Latin (*bilis*, meaning bile) to convey the exact meaning of the pathologic process: a mixture of blood and bile. Blunt and penetrating liver trauma is the most common cause, followed by iatrogenic factors secondary to instrumentation or surgery on or around the biliary tract. Liver biopsy, endoscopic retrograde cholangiopancreatography (ERCP), or transhepatic cholangiography is the most common iatrogenic cause [22]. Gunshot injury is becoming a more common cause in recent years because of the rapid rise in gun-related crimes. Penetrating injury may rupture an artery or a vein and the accompanying bile duct, establishing a direct communication between blood and bile.

Parasites

Obstruction of the common bile duct due to parasites is usually caused by migration of the round worm (*Ascaris Lumbricoids*) through the sphincter of Oddi. A female round worm is about 25–35 cm in length and 3–6 mm in diameter. A male worm is slightly smaller in size, measuring 15–30 in length and 2–4 mm in diameter. The upper small intestine is the usual habitat, and often live worms are passed in the stool. When the worm migrates into the common bile duct, the usual symptoms of bile duct obstruction (right upper quadrant pain, vomiting, fever, and jaundice) occur. A history of passing the parasites in the stool is the most helpful diagnostic clue. Ova are found on the microscopic examination of the stool specimen [23].

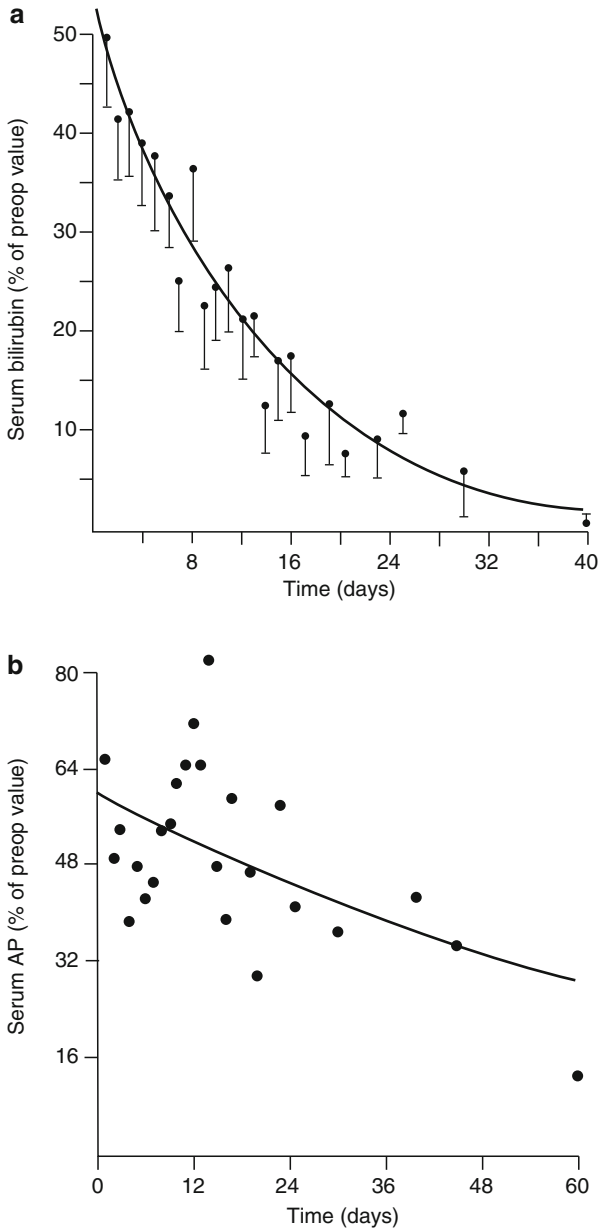

Fig. 8.1.7 Recovery of liver function. After relief of bile duct obstruction, bilirubin level declines much more rapidly than serum alkaline phosphatase. Serum bilirubin declines to 50% of preoperative value in 2 days, to 25% value by 1 week, and to less than 10% by 3 weeks. Alkaline phosphatase level, however, remains above 50% of the preoperation value at the end of 1 week [8]

The appearance of a "bull's eye" sign in an ultrasound study of the common bile duct suggests a round worm, especially in countries with a high prevalence of ascariasis [24].

Miscellaneous Causes

Tumor emboli from cholangiocarcinoma (near the bifurcation), foreign bodies, inspissated bile, papilloma, adenomyoma, fibroma, cystedenoma, and giant cell tumors are some of the rare causes of intraluminal obstruction [25].

Segmental Biliary Obstruction

An intraluminal segmental or lobar bile duct obstruction produces a characteristic scintigraphic pattern. Obstruction due to a gallstone is more common in China, Hong Kong, and other Far Eastern countries than in the western hemisphere [26]. The scintigraphic pattern depends upon whether the obstruction is partial or complete. In the case of a partial segmental bile duct obstruction, the uptake and excretion of Tc-99m-HIDA by the hepatocytes into hepatic bile continues manifesting a bile pool within the duct, proximal to the level of obstruction [27]. A focal retention is seen over the involved segment, while the rest of the normal liver clears most of its radioactivity in the images obtained between 45 and 60 min after injection [28]. In the right lobe, where the segmental ducts are positioned anterior and posterior, a right lateral view is necessary to identify the obstructed duct. In the case of the left lobe, where the segmental ducts are positioned medial and lateral, an anterior view image alone will suffice to identify the obstructed duct. When the segmental or area duct obstruction is complete and persists for a longer duration, uptake of Tc-99m-HIDA decrease or ceases completely, resulting in a filling defect.

Measurement of Duct Size on Cholescintigraphy

Measurement of actual duct size from the cholescintigraphic images is prone to inaccuracy due the effect of specific activity, scatter, and pooling of radiolabeled bile within the biliary system. An in-vitro experiment (Fig. 8.1.8) clearly illustrates the effect of changing of the dose or intensity of image settings on duct size. A 4-mm internal diameter tube is measured in different sizes when the dose and/or intensity settings are changed. High specific activity hepatic bile in a normal subject or bile pooling within the duct in a patient with distal bile obstruction increases the photon scatter, depicting the duct as though it is dilated when in actuality it is not. Ultrasound is far superior for measurement of ductal dilatation. Cholescintigraphy supplements contrast cholangiopancreatography (ERCP) when it fails to identify the intrahepatic segmental duct obstruction primarily because of lack of retrograde flow of the contrast [26, 29]. Magnetic resonance cholangiopancreatography (MRCP) is an emerging new technology that may eventually replace ERCP in some patients with obstruction of the extrahepatic biliary tree. Magnetic resonance does not require any contrast agent to visualize the bile ducts, but depends upon ductal dilatation to be able to detect the level of obstruction [30, 31].

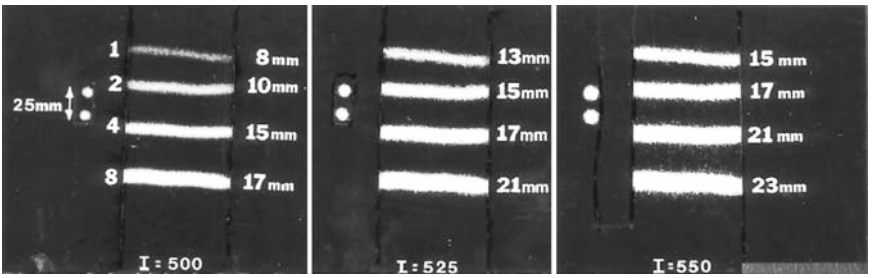

Fig. 8.1.8 Effect of bile pooling on duct size. Measurement of duct size from cholescintigraphy is subject to error due to the effect of the scatter and image intensity (*I*). Numbers 1–4 denote increase in radioactivity. A 4-mm internal diameter tube appears at various sizes depending upon activity and intensity (*I*) settings

References

1. Admirand WH, Small DM. The physiological basis of cholesterol gallstone formation in man. J Clin Invest 1968;47:1043–1052
2. Madden J. Common duct stones. Their origin and surgical management. Surg Clin North Am 1973;53:1095–1113
3. Vital A, Bioulac-Sage P, Iron A, Balabaud C. Morphologic structure of bile canaliculi after bile duct ligation in the rat. A time-course study. Arch Pathol Lab Medicine 1982;106:464–467
4. Accatino L, Contreras A, Fernandez S, Quintana C. The effect of complete biliary obstruction on bile flow and bile acid secretion: post-cholestatic choleresis in the rat. J Lab Clin Med 1979;93:706–717
5. Johnson G, Sundman L. Bile and dry matter output at elevated liver secretion pressure. Acta Clin Scand 1964;128:153
6. Chen C, Shiesh S, Wu M, Lin X. The effect of bile duct obstruction on the biliary secretion of ciprofloxacin in piglets. Am J Gastroenterol 1999;94:2408–2411
7. Klingensmith WC III, Whitney WP, Spitzer VM, Klintmalm GB, Koep LM, Kuni CC. Effect of complete biliary-tract obstruction on serial hepatobiliary imaging in an experimental model: concise communication. J Nucl Med 1981;22:866–868
8. Oster MJ, Csendes A, Funch-Jensen P, Skjoldborg H. Intra-operative pressure measurements of the choledocho-duodenal junction, common bile duct, cystico-choledochal junction, and gallbladder in humans. Surg Gynecol Obstet 1980;150:385–389
9. Pelligrini CA. Pathophysiology of biliary obstruction. In: Way LW, Pelligrini CA (eds). The surgery of the gallbladder and bile ducts. Philadelphia, WB Saunders, 1987, pp 103–117
10. Williams W, Krishnamurthy GT, Brar HS, Bobba VR. Scintigraphic variations of normal biliary physiology. J Nucl Med 1984;25:160–165
11. Krishnamurthy GT, Bobba VR, McConnell D, Turner F, Mesgarzadeh M, Kingston E. Quantitative biliary dynamics: introduction of a new non-invasive scintigraphic technique. J Nucl Med 1983;24:217–223
12. Doo E, Krishnamurthy GT, Eklem MJ, Gilbert S, Brown PH. Quantification of hepatobiliary function as an integral part of imaging with technetium-99m-mebrofenin in health and disease. J Nucl Med 1991;32:48–57
13. Blue PW. Hyperacute complete common bile duct obstruction demonstrated with Tc-99m-IDA cholescintigraphy. Nucl Med Commun 1985;6:275–279

14. Lee AW, Ram MD, Shin WJ, Murphy K. Technetium-99m BIDA biliary scintigraphy in the evaluation of the jaundiced patient. J Nucl Med 1986;27:1407–1412
15. Juni JE, Reichle R. Measurement of hepatocellular function with deconvolutional analysis: application in the differential diagnosis of acute jaundice. Radiology 1990;177:171–175
16. Lima J, Shankaran H, Krishnamurthy GT, et al. Evaluation of hepatocyte function following acute common bile duct obstruction (ACBDO) by Tc-99m-mebrofenin scintigraphy in rats. Eur J Nucl Med 1992;19:687 (abstract)
17. Lima J. Quantificaçáo em hepatologia nuclear. Thesis submitted to the University of Coimbra as partial fulfillment for a doctoral degree. University of Coimbra, Portugal, 1997
18. Krishnamurthy S, Krishnamurthy GT. Technetium-99m-iminodiacetic acid organic anion: Review of biokinetics and clinical application in hepatology. Hepatology 1989;9:139–153
19. Lecklitner ML, Austin AR, Benedetto AR, Growcock GW. Positive predictive value of cholescintigraphy in common bile duct obstruction. J Nucl Med 1986;27:1403–1406
20. Brown PH, Juni JE, Lieberman DA, Krishnamurthy GT. Hepatocyte versus biliary disease: a distinction by deconvolutional analysis of technetium-99m-IDA time-activity curve. J Nucl Med 1988;29:623–630
21. Krishnamurthy GT, Lieberman DA, Brar HS. Detection, localization and quantitation of degree of common bile duct obstruction by scintigraphy. J Nucl Med 1985;26:726–735
22. Sandblom P. Hemobilia. In: Way LW, Pelligrini CA (eds). Surgery of the gallbladder and bile ducts. Philadelphia, WB Saunders, 1987, pp 643–654
23. Louw JH, Rode H. Ascariasis. In: Way LW, Pelligrini CA (eds). Surgery of the gallbladder and bile duct. Philadelphia, WB Saunders, 1987, pp 539–555
24. Cremin BJ. Ultrasonic diagnosis of biliary ascariasis, “a bull’s eye in the triple O.” Br J Radiol 1982;55:683–684
25. Sherlock S, Dooley J. Diseases of the liver and biliary system. Blackwell Science, Inc. Malden, MA, 10th edn, 1997, pp 641–649
26. Yeh SH, Liu OK, Huang MJ. Sequential scintigraphy with technetium-99m-pyridoxylideneglutamate in the detection of intrahepatic lithiasis: concise communication. J Nucl Med 1980;21:17–21
27. Zeman RK, Gold JA, Gluck L, Caride VJ, Burrell M, Hoffer PB. Tc-99m-HIDA scintigraphy in segmental biliary obstruction. J Nucl Med 1981;22:456–458
28. Gupta S, Owshalimpur D, Cohen G, Margules R, Herrera N. Scintigraphic detection of segmental bile-duct obstruction. J Nucl Med 1982;23:890–891
29. Gibney RG, Cooperberg PL, Scudamore CH, Nagy AG. Segmental biliary obstruction: false-negative diagnosis with direct cholangiography without US guidance. Radiology 1987;164:27–30
30. Lee MG, Lee HJ, Kim MH, Kang EM, Kim YH, Lee SG, Kim PN, Ha HK Auh YH. Extrahepatic biliary diseases: 3D MR cholangiopancreatography compared with endoscopic retrograde cholangiopancreatography. Radiology 1997;202:663–669
31. Asselah T, Ernst O, Sergent G, L’herminé C, Paris JC. Caroli’s disease: a magnetic resonance cholangiopancreatography diagnosis. Am J Gastroenterology 1998;93:109–110

8.2 Wall Thickening

Wall thickening occurs gradually over weeks or months before causing impediments to bile flow because of narrowing of the lumen. Wall thickening may be caused by a benign or malignant cause.

Table 8.2.1 Causes of benign stricture of the bile duct

(1) Open cholecystectomy
(2) Laparoscopic cholecystectomy
(3) Migrating stones
(4) Ischemia
(5) Hepatic intra-arterial chemotherapy
(6) Radiation
(7) Infection
(8) Chronic pancreatitis
(9) Liver transplantation
(10) Blunt or penetrating trauma

Benign Causes

Stricture

Many conditions that cause benign stricture are listed in Table 8.2.1. Wall injury that leads to benign stricture occurs more commonly following a diagnostic or therapeutic instrumentation of the biliary tree. Most strictures occur at the middle of the common hepatic duct, which lies directly across the point of ligation of the cystic duct during an open or laparoscopic cholecystectomy [1]. Laparoscopic cholecystectomy, which has almost replaced open surgical cholecystectomy, is the most common cause of benign stricture [2]. Small gallstones migrating from either the gallbladder or liver may temporarily lodge in the common bile duct and cause constant irritation and subsequent stricture formation. Ischemia [3], infusion of chemotherapy agents [4], infection, radiation [5], chronic pancreatitis [6], and liver transplantation [7] are other well-established causes of benign stricture.

Pathophysiology

The pathophysiological changes that follow a benign stricture are quite different from those that occur after an intraluminal obstruction. In contrast to an intraluminal obstruction, which occurs suddenly, stricture formation takes months or years after the initiating injury. Post-transplant CBD stricture occurs at or just above the anastomotic site in 10–20% of patients with liver transplantation. Duct ischemia prior to transplantation is responsible for the stricture [7]. The cause of benign stricture in non-transplant patients often remains unknown.

Clinical Features

The clinical presentation of benign stricture often remains vague for many weeks or months because of its slow progression. Intermittent upper abdominal pain is the most common presenting symptom. Elevation of serum alkaline phosphatase or transaminase is

8

the earliest liver function abnormality, followed by elevation of serum bilirubin, especially when the stricture becomes critical with dilatation of the bile duct.

Cholescintigraphic Diagnosis

Early in the course of benign stricture, the uptake (HEF) and excretion of Tc-99m-HIDA by the hepatocytes are maintained within normal range, but the bile flow through the stricture is reduced (Fig. 8.2.1a). The reduction in bile flow leads to bile stasis within the intrahepatic ducts with delineation of the segmental and area ducts (Fig. 8.2.1b). There is an increase in excretion half-time, which serves as a quantitative measure of the degree of obstruction (Fig. 8.2.1c). The delay in gallbladder filling may indicate an increase in its intraluminal pressure. The distal common bile duct initially shows a smooth tapering towards the stricture, but this appearance changes when the duct above the stricture dilates (Fig 8.2.1d).

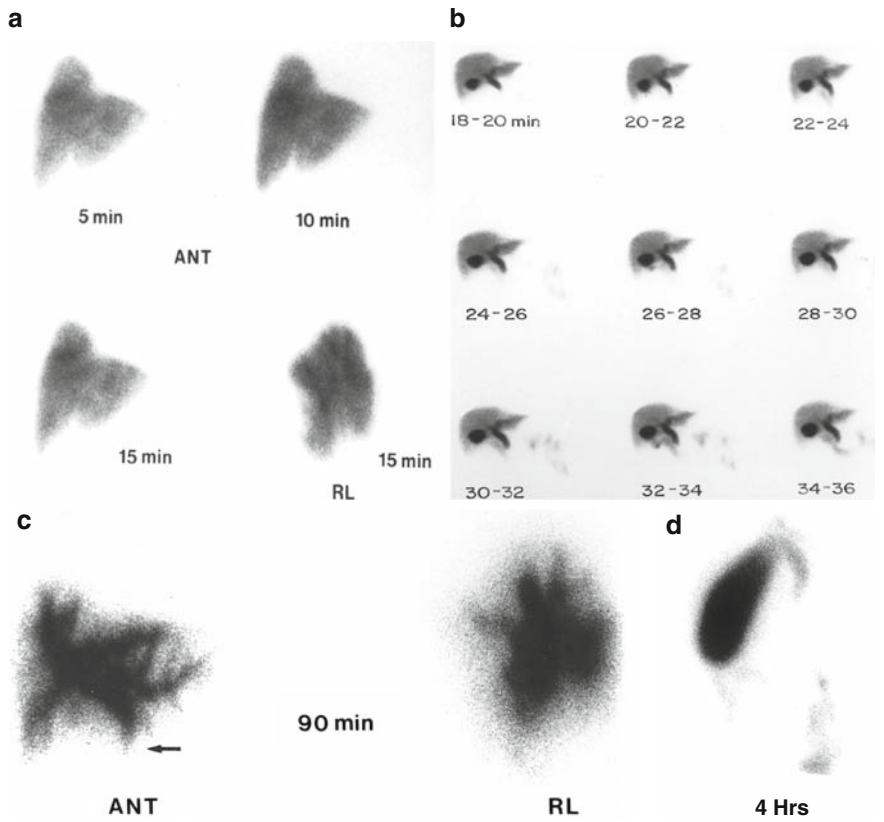

Fig. 8.2.1 Early benign stricture. Liver shows excellent uptake, but slightly delayed secretion of Tc-99m HIDA into bile (**a**). Later, there is intense bile pooling within the intrahepatic ducts (**b, c**). Common bile duct and the gallbladder appear late, indicating high pressure within them. There is smooth tapering of the CBD towards the stricture (**d**)

The stricture of the common bile duct diverts most of the hepatic bile to enter the gallbladder, and very little bile enters the duodenum [8]. The hepatic extraction fraction remains high in early stricture, but begins to fall when the obstruction becomes severe and persists for a longer duration [9].

Low extraction fraction with complete cessation of bile secretion occurs in critical stenosis with serum bilirubin levels above 10 mg% (Fig. 8.2.2.).

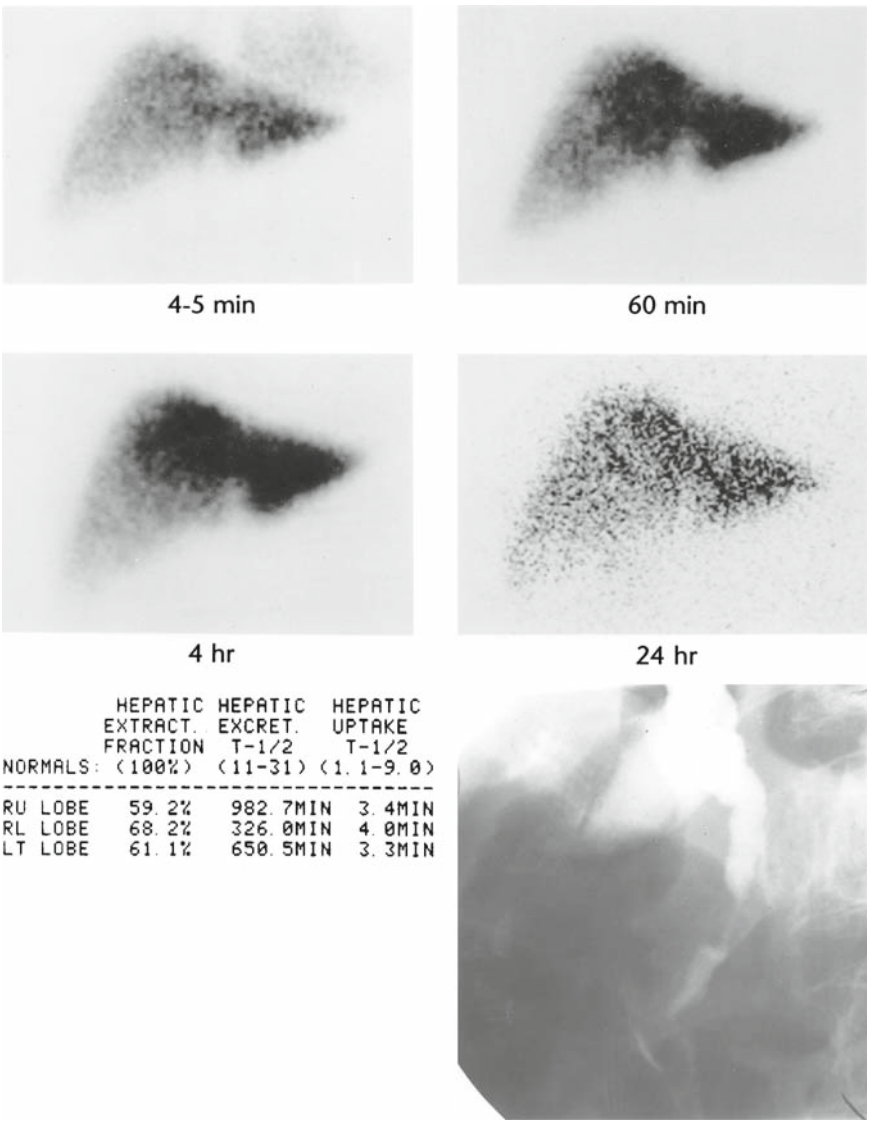

Fig. 8.2.2 CBD critical stricture. Bile secretion ceases and the bile ducts, gallbladder, and intestine are not seen even at 24 h (*top*). The hepatic extraction decreases and excretion T1/2 increases (*bottom left*). Cholangiogram confirms critical stenosis of the common bile duct (*bottom right*)

Ultrasound is used frequently for the diagnosis, and its accuracy depends very much upon the presence or absence of ductal dilatation [10]. A normal common bile duct usually measures up to 10 mm in diameter, and the ultrasound is unable to detect the stricture when the dust size remains within the normal range (Fig. 8.2.3). Ultrasound accuracy, however, increases when the diameter of the common bile duct exceeds 10 mm, serum bilirubin level raise above 10 mg%, and jaundice persists for longer than a week [11]. Dilatation of the extrahepatic ducts occurs much earlier than dilatation of the intrahepatic ducts, as dictated by the law of Laplace, which states that the stress is directly proportional to the internal diameter of the tubing [12]. Because of their larger internal diameter, the extrahepatic ducts sustain more stress and dilate much earlier than the intrahepatic ducts, which are much smaller in size.

Stricture impedes bile flow and reduces gallbladder emptying in response to CCK-8 infusion. There may be prolongation of the latent period with a reduction in gallbladder ejection fraction [8]. The bile emptied from the gallbladder may reflux into the common

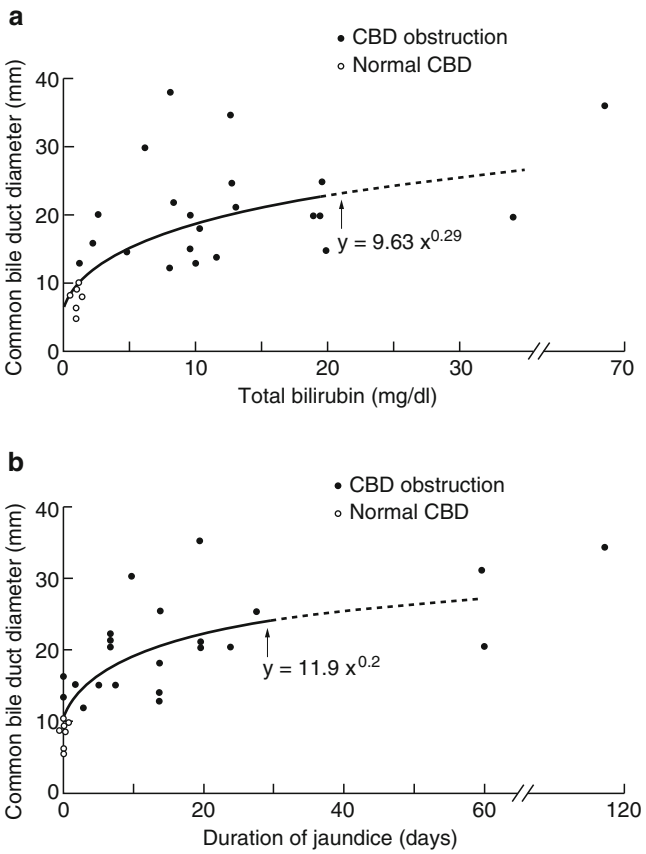

Fig. 8.2.3 Relationship of common bile duct size with serum bilirubin and duration of jaundice. There is usually no dilatation of the common bile duct (*CBD*) with bilirubin levels below 5 mg%; dilatation occurs when serum bilirubin rises above 10 mg%; dilatation is variable between 5 and 10 mg% (**a**). Diameter of the CBD increases (**b**) as the duration of jaundice increases [11]

hepatic duct and right and left hepatic ducts, instead of flowing forward into the duodenum. Bile reflux into the common hepatic and right and left hepatic duct is one of a reliable signs of obstruction and is referred to as Krishnamurthy-Bobba sign [13, 14]. Refluxed bile reenters the gallbladder immediately after cessation of CCK-8 infusion, and the gallbladder curve often shows a rapid refilling. In patients with right upper quadrant pain, mild elevation of serum alkaline phosphatase, and normal bilirubin, cholescintigraphy maintains a much higher sensitivity for the detection of obstruction than ultrasound. Ultrasound, however, becomes a preferred modality for diagnosis in cases with high serum bilirubin and dilatation of ducts [11, 15, 16].

In normal subjects, the mean time of appearance of the common bile duct is 16 min, of the gallbladder 20 min, and of the duodenum 24 min. The gallbladder ejection fraction of 35% or higher is obtained in response to a 3-min infusion of 10 ngm kg^{-1} (3.3 ngm min^{-1} for 3 min) of CCK-8. The latent period is less than 3 min, and the ejection period is between 8 and 12 min. The curve over the common bile duct may show a peak corresponding to the second half of the gallbladder ejection period. The common hepatic duct curve usually does not show any peak as the bile emptied from the gallbladder flows antegrade through the sphincter of Oddi and enters the duodenum [17–19]. Because of forward bile entry into the duodenum, there is no rapid refilling of the gallbladder.

During quantitative cholescintigraphy, patients with bile duct obstruction often experience a mild to moderate degree of abdominal pain because of either contraction of the gallbladder or distension of the common bile duct. Pain is experienced mostly during the gallbladder ejection period. Pain experienced after completion of the gallbladder ejection is considered non-biliary in origin. Since cholecystokinin increases intestinal peristalsis, late onset abdominal pain (after the gallbladder ejection period) is considered to indicate pain of intestinal origin due to increased peristalsis. A precise documentation of the temporal relationship between the onset of pain and the phase of gallbladder emptying is essential for defining the exact origin of abdominal pain [20, 21].

Cholescintigraphic Accuracy of Biliary Obstruction

Of a total of 214 patients with well-documented biliary obstruction (Table 8.2.2), cholescintigraphy accurately detected obstruction in 200 patients, for a sensitivity of 93% [12, 19, 22–28]. Differentiation between functional vs. anatomic obstruction is made by using either amyl nitrite or a calcium channel blocker, nifedapine. These drugs, which relieve functional but not anatomic obstruction, promote smooth passage of bile only in case of a functional obstruction [29, 30]. The quantitative cholescintigraphic parameters are technically simple to measure, reliable, and easily reproducible within and between individuals and among institutions [31, 32]. Simultaneous quantification provides an objective parameter that may alter patient management strategy as to the timing of therapy and also allows later testing for whether or not the chosen therapy has achieved its intended goals. In most patients, nuclear hepatology studies supplement morphological imaging studies; however, in patients where functional alterations precede morphological changes, one may have to depend mostly on the findings of cholescintigraphy [33]. An etiological diagnosis of biliary obstruction, whether it is intraluminal, wall thickening, or extrinsic compression,

Table 8.2.2 Sensitivity of Tc-99m-HIDA cholescintigraphy in the detection of biliary obstruction

Author (ref.)	Number of patients with biliary obstruction	Obstruction identified with cholescintigraphy
Zeman [22]	60	59
Krishnamurthy [19]	14	13
Lecklitner [24]	25	23
Lieberman [26]	19	14
Darweesh [23]	15	10
Brown [12]	14	14
Juni [25]	10	10
Lieberman [27]	13	13
Lee [28]	44	44
Total	214	200 (93%)

often cannot be made from cholescintigraphy alone. An ultrasound, CT ERCP, or MRCP is required for an etiological diagnosis. An ERCP may be ideal for confirmation of an intraluminal obstruction, ultrasound for wall thickening, and CT for an extrinsic compression.

Malignant Causes

Cholangiocarcinoma

Cholangiocarcinoma is the most common malignancy of the biliary system, causing wall thickening and obstruction to bile flow. Incidence of cholangiocarcinoma appears to have been rising in recent years, which is partly related to the higher frequency of its detection by using more sophisticated diagnostic methods [34]. Cholangiocarcinoma occurs more commonly in the 6th decade of life and affects men more frequently than women in the ratio of 1.2:1. The proximal common hepatic duct or one or both of its bifurcating branches are the most common locations [35]. About 58% of cholangiocarcinomas occur in the proximal third, 17% in the middle third, 18% in the distal third, and the remaining 7% are distributed diffusely throughout the common hepatic and common bile duct (Fig. 8.2.4). The site and frequency of occurrence of cholangiocarcinoma has changed in the more recent reports, probably reflecting early diagnosis by non-invasive imaging methods and early confirmation by cholangiopancreatography [36, 37].

Clinical Presentation

Presenting symptoms and signs include weight loss, jaundice, and pruritus. Serum bilirubin levels may fluctuate, but the general trend is one of sustained increase. Patients usually seek medical attention late in the course of the disease, many after the onset of jaundice. By this time there is dilatation of the bile duct proximal to the site of cancer, and it is readily detected on ultrasound or CT examination [38]. Bismuth classifies cholangiocarcinoma

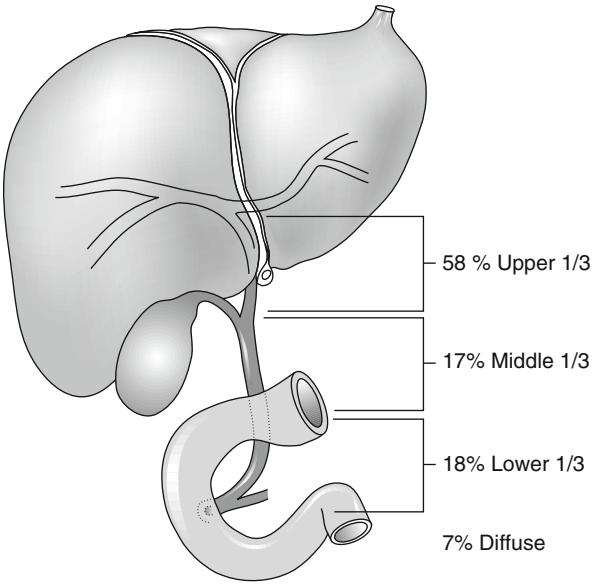

Fig. 8.2.4 Location of cholangiocarcinoma. Most occur in the common hepatic duct at its bifurcation [37]

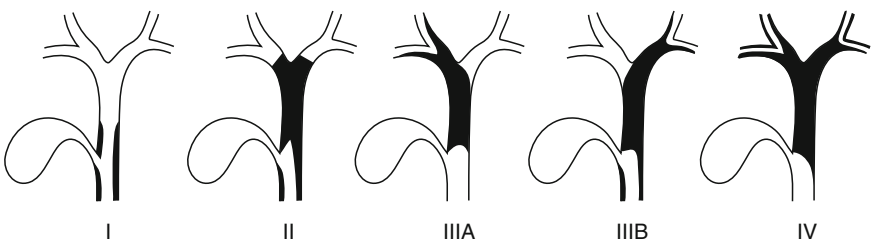

Fig. 8.2.5 Staging of cholangiocarcinoma. In stage I, only the common duct is involved; both the right hepatic duct (*RHD*) and left hepatic duct (*LHD*) are free of cancer. In stage II, both the proximal hepatic duct and distal RHD and LHD are involved. Stage III involves the common hepatic duct along with either the right hepatic duct (*IIIA*) or the left hepatic duct (*IIIB*). In stage IV, entire extrahepatic biliary tree is involved, including both the right and left hepatic ducts along with their segmental branches

into four types based on its location and extent (Fig. 8.2.5). Type I involves the common bile duct or the distal common hepatic duct. The proximal common hepatic duct and the right hepatic and left hepatic ducts are free of cancer. In type II, the carcinoma extends up to the level of the junction of the right and left hepatic ducts, but the proximal part of both the right and left hepatic ducts are free of cancer. In type III, the cancer involves either the right hepatic (IIIa) or the left hepatic duct (IIIb). One of the lobar ducts is free of cancer. Type IV extends to both the right and left hepatic ducts and their segmental branches, and the cancer is unresectable [39].

Carcinoma of the Ampulla of Vater

Of the 18% of the cholangiocarcinoma arising from the distal third of the common bile duct (Fig. 8.2.5), 75% are less than 4 mm from the ampulla of Vater [36]. The clinical presentation of the peri-ampullary cholangiocarcinoma is distinctly different from those arising from the common hepatic duct and its bifurcation. Periampullary carcinoma presents more often as painless jaundice. Courvoisier first made the observation in 1890 that a palpable, painless gallbladder in a patient with jaundice has either a periampullary or a pancreatic cancer [40]. Periampullary cholangiocarcinoma accounts for less than 1–3% of obstructive jaundice. The common age group is between 55 and 65 years, with equal prevalence between men and women. There is frequent association with primary sclerosing cholangitis [41].

About 50% of patients with cholangiocarcinoma already have intra-abdominal and intrahepatic metastases at the time of their first presentation to a clinician [42]. Obstruction manifests as two types of image pattern on Tc-99m-HIDA study, depending upon the degree (partial vs. complete obstruction) and duration of obstruction. Early segmental duct partial obstruction may show a normal or slightly reduced Tc-99m-HIDA uptake with bile stasis proximal to obstruction [43]. Complete obstruction, however, shows marked reduction or no uptake at all in the region affected by the tumor [44]. Involvement of the left hepatic duct, for example, may show no uptake at all over the entire left lobe.

Most patients with cholangiocarcinoma present late, after the onset of jaundice, when hyperbilirubinemia and ductal dilatation are evident. A typical pattern consists of bile pooling in the duct proximal to the site of obstruction and increased liver to duodenal transit time, often as long as 24 h. Multimodality imaging, including ultrasonography, cholescintigraphy, CT, ERCP, and MRCP, are complementary imaging modalities [45]. Biopsy is required prior to deciding on a definitive therapeutic strategy.

Stent Patency

Placement of a palliative endo-prosthesis to relieve bile duct obstruction due to malignancy is now a standard treatment [46]. Endo-prosthesis relieves the obstruction promptly and establishes bile flow immediately. The plastic stents tend to occlude prematurely or move ferred, and they function much better and for a longer period of time than the plastic variety [47, 48]. The stent patency is easily documented with Tc-99m-HIDA cholescintigraphy.

Surgery is recommended for early stages. Some prefer surgery even for tumors located proximally at the bifurcation (Klatskin tumor). Pylorus-preserving partial pancreatoduodenectomy or the Kausch-Whipple resection is the preferred surgical procedure [49, 50]. Insertion of an endo-prosthesis is now a popular therapeutic option, especially in the terminal stage. Migration, infection, and occlusion are frequent complications of the endo-prosthesis. Recent progress in stent design and improvements in stent insertion techniques have contributed towards longer duration of stent function, for up to 3–4 months. Occluded stents are easily replaced, and it is currently not a one-time procedure [51].

Refrences

1. Andren-Sandberg A, Alinder G, Bengmark S. Accidental lesions of the common bile duct at cholecystectomy. Pre- and perioperative factors of importance. Ann Surg 1985;201:328–332
2. The Southern Surgeons' Club. A prospective analysis of 1,518 laparoscopic cholecystectomies. N Engl J Med 1991;324:1073–1078
3. Terblanche J, Allison HF, Northover JM. An ischemic basis for biliary strictures. Surgery 1983;94:52–57
4. Mueller PR, van Sonnenberg E, Ferrucci JT Jr, et al. Biliary stricture dilatation: multicenter review of clinical management in 73 patients. Radiology 1986;160:17–22
5. Martenson JA Jr, Gunderson LL, Buskirk SJ, et al. Hepatic duct stricture after radical radiation therapy for biliary cancer: recurrence or fibrosis? Mayo Clin Proc 1986;61:530–536
6. Itoh H, Shimono R, Hamamoto K. Evaluation of common bile duct stenosis in chronic pancreatitis using cholescintigraphy. Eur J Nucl Med 1988;14:137–140
7. Ward EM, Kiely MJ, Maus TP, Wiesner RH, Kron RA. Hilar biliary strictures after liver transplantation: cholangiography and percutaneous treatment. Radiology 1990;177:259–263
8. Krishnamurthy GT, Bobba VR, McConnell D, Turner F, Mesgarzadeh M, Kingston E. Quantitative biliary dynamics: introduction of a new non-invasive scintigraphic technique. J Nucl Med 1983;24:217–223
9. Brown PH, Juni JE, Lieberman DA, Krishnamurthy GT. Hepatocyte vs. biliary disease: a distinction by deconvolutional analysis of technetium-99m-HIDA time-activity curve. J Nucl Med 1988;29:623–630
10. Honickman SP, Mueller PR, Wittenberg J, et al. Ultrasound in obstructive jaundice: prospective evaluation of site and cause. Radiology 1983;147:511–515
11. Lapis JL, Orlando RC, Mittlesteadt CA, Staab EV. Ultrasonography in the diagnosis of obstructive jaundice. Ann Intern Med 1978;89:61–63
12. Compton RA. Bursting forces within the human body. Radiology 1973;107:77–80
13. Itoh H, Murase K, Hamamoto K. Reflux sign in cholescintigraphy after administration of a gallbladder contracting agent. J Nucl Med 1989;30:1192–1197
14. Brar HS. Scintigraphic cholecystokinin-induced bile reflux named as Krishnamurthy-Bobba sign. J Nucl Med 1990;31:248–249
15. Cooperberg PL, Burhenne HJ. Real-time ultrasonography. Diagnostic technique of choice in calculous gallbladder disease. N Engl J Med 1980;302:1277–1279
16. Laing FC, Jeffrey RB Jr. Choledocholithiasis and cystic duct obstruction: difficult ultrasonographic diagnosis. Radiology 1983;146:475–479
17. Krishnamurthy S, Krishnamurthy GT. Quantitative assessment of hepatobiliary diseases with Tc-99m-HIDA scintigraphy. In: Freeman LM, Weissman HS (eds). Nuclear medicine. Annual Raven Press, New York, 1988, pp 309–330
18. Doo E, Krishnamurthy GT, Eklem MJ, Gilbert S, Brown PH. Quantification of hepatobiliary function as an integral part of imaging with technetium-99m-mebrofenin in health and disease. J Nucl Med 1991;32:48–57
19. Krishnamuthy GT, Lieberman DA, Brar HS. Detection, localization, and quantitation of degree of common bile duct obstruction by scintigraphy. J Nucl Med 1985;26:726–735
20. Krishnamurthy S, Krishnamurthy GT. Biliary dyskinesia: role of the sphincter of Oddi, gallbladder and cholecystokinin. J Nucl Med 1997;38:1824–1830
21. Krishnamurthy S, Krishnamurthy GT. Evolution of nuclear hepatology as a clinical entity. J Nucl Med Technol 1995;23(suppl):35S–45S
22. Zeman RK, Lee C, Jaffe MH, Burrell MI. Hepatobiliary scintigraphy and sonography in early biliary obstruction. Radiology 1984;153:793–798

23. Darweesh RMR, Dodds WJ, Hogan WJ, et al. Efficacy of quantitative hepatobiliary scintigraphy and fatty meal sonography for evaluating patients with suspected partial common bile duct obstruction. Gastroenterology 1988;94:779–786
24. Lecklitner ML, Austin AR, Benedetto AR, Growcock GW. Positive predictive value of cholescintigraphy in common bile duct obstruction. J Nucl Med 1986;27:1403–1406
25. Juni JE, Reichle R. Measurement of hepatocellular function with deconvolutional analysis: Application in the differential diagnosis of acute jaundice. Radiology 1990;177:171–175
26. Lieberman DA, Krishnamurthy GT. Intrahepatic vs extrahepatic cholestasis. Discrimination with biliary scintigraphy combined with ultrasound. Gastroenterology 1986;90:734–743
27. Lieberman DA, Brown PH, Krishnamurthy GT. Improved scintigraphic assessment of severe cholestasis with the hepatic extraction fraction. Dig Dis Sci 1990;35:1385–1390
28. Lee AW, Ram MD, Shih WJ, Murphy K. Technetium-99m-BIDA biliary scintigraphy in the evaluation of the jaundiced patient. J Nucl Med 1986;27:1407–1412
29. Madacsy L, Velosy B, Lonovics J, Csernay L. Differentiation between organic stenosis and functional dyskinesia of the sphincter of Oddi with amyl nitrite-augmented quantitative hepatobiliary scintigraphy. Eur J Nucl Med 1994;21;203–208
30. Bhatnagar A. Nifedipine interventional cholescintigraphy: a new method for assessing sphincter of Oddi? Indian J Nucl Med 1997;12:93–96
31. Gilbert SA, Brown PH, Krishnamurthy GT. Quantitative nuclear hepatology. J Nucl Med Technol 1987;15:38–43
32. Spackman J, Bartlett ME, Ryals L, et al. Reproducibility of technetium-99m-mebrofenin hepatic functional parameters obtained with semiautomatic software. J Nucl Med Technol 1991;19:228–231
33. Krishnamurthy S, Krishnamurthy GT. Functional imaging in nuclear hepatology. Indian J Nucl Med 1997;12:216–232
34. Tomkins RK, Saunders KD, Roslyn JJ, Longmire WP Jr. Changing patterns in diagnosis and management of bile duct cancer. Ann Surg 1990;211:614–620
35. Klatskin G. Adenocarcinoma of the hepatic duct at its bifurcation within the porta hepatic. An unusual tumor with distinctive clinical and pathologic features. Am J Med 1965;38:24
36. Wise L, Pizzimbono C, Dehner LP. Periampullary cancer. A clinicopathologic study of 62 patients. Am J Surg 1976;131:141–148
37. Sherlock S, Dooley J. Diseases of the liver and biliary system, 10th edn, Blackwell Science, Malden, MA, 1997, pp 641–649
38. Reiman TH, Balfe D, Weyman PJ. Suprapancreatic biliary obstruction: CT evaluation. Radiology 1987;163:49–56
39. Bismuth H, Nakache R, Diamond R. Management strategies in resection for hilar cholangiocarcinoma. Ann Surg 1992;215:31–38
40. Courvoisier LG. Kasuistisch-statistiche Beitrage zur Pathologie und Chirurgie der Gallenwege. Leipzig FCV, Vogel, 1890
41. DeGroen PC, Gores GJ, LaRusso NF, Gunderson LL, Nagorney DM. Biliary tract cancers. N Engl J Med 1999;341:1368–1378
42. Burke EC, Jarnagin WR, Hochwald SN, Pisters PWT, Fong Y, Blungart LH. Hilar cholangiocarcinoma. Pattern of spread, the importance of hepatic resection for curative operation, and a pre-surgical staging system. Ann Surg. 1998;228:385–394
43. Zeman RK, Gold JA, Gluck L, Caride VJ, Burrell M, Hoffer PB. Tc-99m-HIDA scintigraphy in segmental biliary obstruction. J Nucl Med 1981;22:456–458
44. Gupta S, Owshalimpur D, Cohen G, Margules R, Herrera N. Scintigraphic detection of segmental bile-duct obstruction. J Nucl Med 1982;23:890–891
45. Zeman RK, Lee C, Stahl RS, Cahow CE, Viscomi GN, Neumann RD, Gold JA, Burrell MI. Ultrasonography and hepatobiliary scintigraphy in the assessment of biliary-enteric anastomoses. Radiology 1982;145:109–115

46. Mueller RR, Ferrucci JT Jr, Teplick SK, van Sonnenberg E, Haskin PH, Butch RJ, Papanicolaou N. Biliary stent endoprosthesis: analysis of complications in 113 patients. Radiology 1985;156:637–639
47. Mathieson JR, McLoughlin RE, Cooperberg PL, Prystai CC, Stordy SN, MacFarlane JK, Schmidt N. Malignant obstruction of the common bile duct: long-term results of Gianturco-Rosch metal stents used as initial treatment. Radiology 1994;192:663–667
48. Boguth L, Tatalovic S, Antonucci F, Heer M, Susler H, Zollikofer CL. Malignant biliary obstruction: clinical and histopathologic correlation after treatment with self-expanding metal prostheses. Radiology 1994;192:669–674
49. Beger HG, Treitschke F, Gansauge F, Harada N, Hiki N, Mattfeldt T. Tumor of the ampulla of Vater. Experience with local or radical resection in 171 consecutively treated patients. Arch Surg 1999;134:526–532
50. Launois B, Terblanche J, Lakehal M, Catheline JM, Bardaxoglou E, Landen S, Campion JP, Sutherland F, Meunier B. Proximal bile duct cancer: high resectability rate and 5 year survival. Ann Surg 1999;230:266–275
51. Lee MJ, Mueller PR, Saini S, Morrison MC, Brink JA, Hahn PF. Occlusion of biliary endoprosthesis: presentation and management. Radiology 1990;176:531–534

8.3 Combined Intrahepatic and Extrahepatic Cholestasis (Sclerosing Cholangitis)

By involving both intrahepatic and extrahepatic ducts sequentially, or simultaneously, sclerosing cholangitis is a typical example of a disease that combines features of both intrahepatic and extrahepatic cholestasis. Sclerosing cholangitis (SC) is a slowly progressive disease of unknown etiology characterized by chronic inflammation, fibrosis, and narrowing of both intrahepatic and extrahepatic ducts at multiple levels [1]. Several contributing factors have been identified (Table 8.3.1). Multiple strictures with normal duct in between give the characteristic beaded appearance on the contrast cholangiogram.

Table 8.3.1 Cholescitigraphic features of primary sclerosing cholangitis, isolated common bile duct obstruction, and primary biliary cirrhosis

Parameter	Primary sclerosing cholangitis	Isolated common bile duct obstruction	Primary biliary cirrhosis
Level of CBD obstruction	Proximal	Distal	None
Number of obstructions	Multiple	Single	None
Beading of the ducts	Common	Rare	None
Bile pooling proximal to obstruction	Uncommon	Very common	Uncommon
Cystic duct obstruction	Common	Rare	Rare
Liver clearance half time	Marked increase	Moderate increase	marked increase
Regional variations in clearance half time	Wide variation from region to region	Uniform increase from all regions	Uniform increase from all regions.

The term "primary" is used when all other possible causes of cholangitis have been excluded. Cholangitis associated with choledocholithiasis, biliary tract surgery, carcinoma, chemotherapy, or acquired immunodeficiency syndrome (AIDS) is called secondary sclerosing cholangitis. Only after exclusion of these secondary causes is the term primary applied.

Primary Sclerosing Cholangitis

Primary sclerosing cholangitis usually affects patients in their 40s, and men more often (75%) than women [2]. An association with inflammatory bowel disease is found in 75% of the patients [3, 4]. The clinical onset is insidious, with fatigue, pruritus, and malaise. Biochemical changes are characterized by moderate elevation of serum alkaline phosphatase and mild elevation of alanine amino transferase. Elevation of serum bilirubin is a late event. Urinary copper excretion is increased [3]. Unlike primary biliary cirrhosis, there is no specific serological marker for primary sclerosing cholangitis.

Pathophysiology

Histologically, four stages are identified. Stage I represents the initial degenerative changes in the duct-lining epithelial cells and infiltration by lymphocytes and neutrophils. Stage II is characterized by peri-portal necrosis, stage III consists of portal to portal fibrous septa and disappearance of bile ducts, and stage IV represents the end stage with cirrhosis and onion skin appearance on biopsy, a characteristic histological finding. The cholangiogram shows a typical beaded appearance of the extrahepatic ducts. Both intrahepatic and extrahepatic ducts are involved, but the contrast cholangiogram is often incapable of detecting the involvement of the intrahepatic ducts [5]. In 100 patients with primary sclerosing cholangitis, 87% had involvement of both intrahepatic and extrahepatic ducts, 11% had involvement of only the intrahepatic ducts, and 2% had involvement of only the extrahepatic ducts [4].

The disease progresses slowly over 10-15 years before reaching the stage of cirrhosis, portal hypertension, liver failure, and death. The median survival is 12 years [5]. The course of the disease is reversible during stage I, may be reversible in stage II, but is irreversible at stages III and IV. The following criteria are required for the diagnosis: (1) alkaline phosphatase increased by more than 1.5 times the normal amount for at least 6 months and (2) multiple strictures or beading of the ducts on the cholangiogram. Characteristic planar and SPECT images on Tc-99m-HIDA study may be included as one of the required criteria [6].

Secondary Sclerosing Cholangitis

Secondary sclerosing cholangitis follows an identifiable cause, such as surgery on the biliary tract, choledocholithiasis, intra-arterial infusions of chemotherapeutic agents [8],

cholangiocarcinoma [9], acquired immunodeficiency syndrome [10], and congenital biliary abnormalities. The diagnosis of primary sclerosing cholangitis is made only after excluding all of the above causes. Inflammatory bowel disease (ulcerative colitis or Crohn's disease) is now considered an accompaniment of primary sclerosing cholangitis, and when found either before or in association with cholangitis, the condition is still labeled primary sclerosing cholangitis. The scintigraphic findings of secondary sclerosing cholangitis have not been studied as thoroughly as primary sclerosing cholangitis. The ERCP findings of secondary sclerosing cholangitis are indistinguishable from those of the primary sclerosing cholangitis.

Cholescintigraphic Diagnosis

Cholescintigraphic planar images are obtained for 60 min with 3–5 mCi of Tc-99m-HIDA. SPECT images are obtained between 60–90 min [6, 11]. Early planar images (within 10 min) show patchy uptake by the liver (Fig. 8.3.1). Late images show a typical pattern of beading of the right hepatic, left hepatic, common hepatic, or common bile ducts, depending upon the extent of the disease (Fig. 8.3.1). The hepatic extraction fraction remains within the normal range early in the course of the disease and begins to decrease in advanced stages [6, 11]. The excretion half time increases from the very beginning. Due to multiple duct involvement at various levels, the excretion half time varies widely from region to region, often reaching values as high as six to seven times the normal value. The gallbladder is often not visualized due to obstruction of the cystic duct (Table 8.3.1).

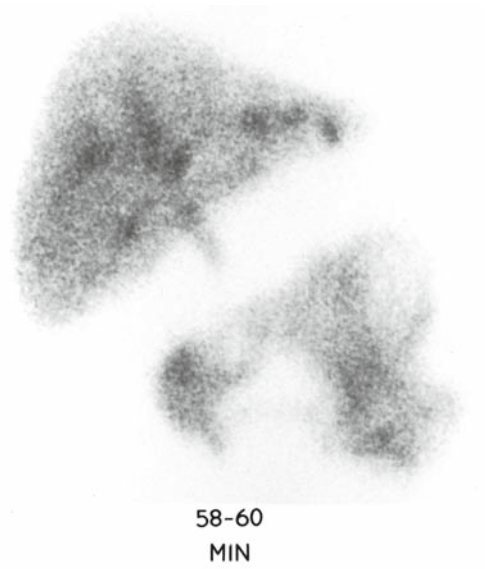

Fig. 8.3.1 Sclerosing cholangitis. Planar image shows beading of right hepatic, left hepatic duct, common hepatic and common bile ducts. Gallbladder is not seen due to obstruction of the cystic duct

SPECT images show characteristic features of varying parenchymal retention among the different regions. Liver parenchyma with normal bile ducts shows rapid clearance, while the parenchyma drained by obstructed bile ducts shows retention, giving the characteristic scintigraphic images (Fig. 8.3.2). The involvement and extent of cholangitis as indicated by cholescintigraphy may be more critical and much larger than the disease shown on the contrast cholangiogram. This underestimation of severity and extent by the cholangiogram is due to the inability of the contrast to enter most of the intrahepatic ducts. Several features characteristic of primary sclerosing cholangitis that help to differentiate it from primary biliary cirrhosis and isolated common bile duct obstruction are shown in Table 8.3.1. Magnetic resonance cholangiopancreatography is an emerging new technique that is capable of demonstrating involvement of both intrahepatic and extrahepatic ducts [12, 13].

Therapy

The medical therapy for primary sclerosing cholangitis includes such drugs as D-penicillamine, cyclosporine, methotrexate, corticosteroids, azathioprine, colchicine, or cholesteramine. Antibiotics are prescribed when there is superimposed infection [5]. Endoscopic stenting is shown to be safe and effective, and it works for several years until end-stage liver disease sets in [14]. Liver transplantation is recommended for end-stage liver disease when medical therapy fails.

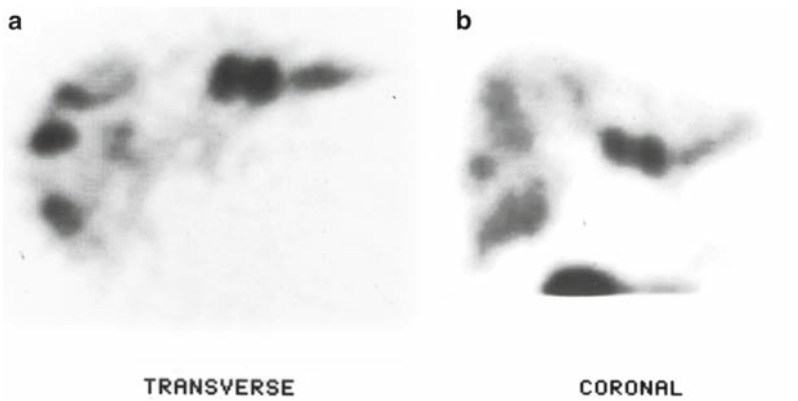

Fig. 8.3.2 SPECT in sclerosing cholangitis. Transaxial (**a**) and coronal (**b**) slices, obtained between 60–90 min, show multiple areas of focal parenchymal retention over the involved ducts along with regions of complete clearance from ducts not affected

References

1. LaRusso NF, Wiesner RH, Ludwig J, MacCarty RL. Current concepts. Primary sclerosing cholangitis. N Eng J Med 1984;310:899–903
2. Wiesner RH, Grambsch PM, Dickson ER, Ludwig J, MacCarty RL, Hunter EB, Fleming TR, Fisher LD, Beaver SJ, LaRusso NF. Primary sclerosing cholangitis: natural history, prognostic factors, and survival analysis. Hepatology 1989;10:430–436
3. Gross JB Jr, Ludwig J, Wiesner RH, McCall JT, LaRusso NF. Abnormalities in tests of copper metabolism in primary sclerosing cholangitis. Gastroenterology 1985;89:272–278
4. Lee YM, Kaplan MM. Primary sclerosing cholangitis. N Eng J Med 1995;332:924–933
5. Wiesner RH. Current concepts in primary sclerosing cholangitis. Mayo Clin Proc 1994; 69:969–982
6. Rodman CA, Keeffe EB, Lieberman DA, Krishnamurthy S, Krishnamurthy GT, Gilbert S, Eklem MJ. Diagnosis of sclerosing cholangitis with technetium 99m-labeled iminodiacetic acid planar and single photon emission computed tomographic scintigraphy. Gastroenterology 1987;92:777–785
7. Ament AE, Bick RJ, Miraldi FD, Haaga JR, Wiedenmann SD. Sclerosing cholangitis: cholescintigraphy with Tc-99m-labeled DISIDA. Radiology 1984;151:197–201
8. Pien EH, Zeman RK, Benjamin SB, Barth KH, Jaffe MH, Choyke PL, Clark LR, Paushter DM. Iatrogenic sclerosing cholangitis following hepatic arterial chemotherapy infusion. Radiology 1985;156:329–330
9. Shea WJ Jr, Demas BE, Goldberg HI, Hohn DC, Ferrell LD, Kerlan RK. Sclerosing cholangitis associated with hepatic arterial FUDR chemotherapy: radiographic-histologic correlation. AJR Am J Roentgenol 1986;146:717–721
10. MacCarty RL, LaRusso NF, May GR, Bender CE, Wiesner RH, King JE, Coffey RJ. Cholangiocarcinoma complicating primary sclerosing cholangitis: cholangiographic appearances. Radiology 1985;156:43–46
11. Dolmatch BL, Laing FC, Federle MP, Jeffrey RB, Cello J. AIDS- related cholangitis: radiographic findings in nine patients. Radiology 1987;163:313–316
12. Lee MG, Lee HJ, Kim MH, Kang EM, Kim YH, Lee SG, Kim PN, Ha NK, Auh YH. Extrahepatic biliary diseases: 3D MR cholangiopancreatography compared with endoscopic retrograde cholangiopancreatography. Radiology 1997;202:663–669
13. Asselah T, Ernst O, Sergent G, L'herminé C, Paris J. Caroli's disease: a magnetic resonance cholangiopancreatography diagnosis. Am J Gastroenterol 1998;93:109–110
14. Ponsioen CY, Lam K, van Milligen de Wit AWM, Huibregtse K, Tytgat GNJ. Four years experience with short-term stenting in primary sclerosing cholangitis. Am J Gastroenterol 1999;94:2403–2407

8.4 Extrinsic Compression

Extrinsic compression of the bile duct can occur at any point along their course from the small intrahepatic duct to the termination of the common bile duct (Table 8.4.1). Compression due to an enlarged lymph node occurs more frequently at the porta hepatis

Table 8.4.1 Causes of bile duct obstruction due to extrinsic compression

(1) Peri-ductal lymph node enlargement
(2) Carcinoma of head of the pancreas
(3) Chronic pancreatitis
(4) Acute edematous pancreatitis
(5) Annular pancreas
(6) Duodenal diverticula
(7) Pseudocyst of the pancreas.
(8) Mirizzi syndrome

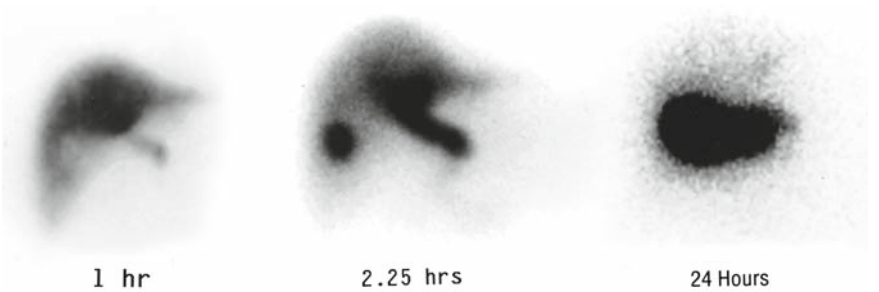

Fig. 8.4.1 Extrinsic compression. Common bile duct obstruction because of extrinsic compression by cancer of the head of the pancreas. Uptake is excellent (*left*). Distal common bile duct ends abruptly (*middle*), and the gallbladder is seen late (*middle*) and does not empty even at 24 h (*right*)

where there are many lymph nodes. Lymphosarcoma, reticulum cell sarcoma, and Hodgkin's disease account for the majority of such obstructions [1]. Acute edematous pancreatitis is a frequent cause. Carcinoma of the stomach, pancreas, and gallbladder may invade the bile duct directly, whereas cancer of other distant organs spreads via a hematogenous route [2]. Chronic pancreatitis, which causes obstruction due to thickening of the intraduodenal portion of the duct wall, may also cause obstruction by an extrinsic compression due to fibrosis around the distal common bile duct [3]. Duodenal diverticulae are found along the medial duodenal wall, very close to the ampulla of Vater, in about 2% of patients undergoing barium meal examination [4]. On rare occasions, the ampulla of Vater may be found within the diverticulum. Acute cholecystitis and acute pancreatitis often co-exist and cause non-visualization of the gallbladder during a Tc-99m-HIDA study [5, 6]. Non-visualization of the gallbladder in a patient with a marked elevation of serum lipase or amylase may indicate acute biliary pancreatitis. Elevation of serum lipase and amylase aids in differentiating pancreatitis from acute cholecystitis. Cancer of the head of the pancreas is a well-recognized cause of extrinsic compression (Fig 8.4.1).

Mirizzi Syndrome

This is a rare type of common bile duct obstruction resulting from extrinsic compression from a large gallstone impaction in the Hartmann's pouch or at the neck of the gallbladder. Patients with Mirizzi syndrome usually have a long cystic duct that runs parallel to the common hepatic duct before joining it to form the common bile duct [7, 8]. Two types of Mirizzi syndrome are described. Type I Mirizzi syndrome consists of extrinsic compression of the common hepatic duct by the stone in the gallbladder neck or in Hartmann's pouch. In type II Mirizzi syndrome, the stone erodes into the common hepatic duct forming a cholecystocholedochal fistula. Recent studies have shown a role for non-invasive diagnosis with MR imaging [9]. Laparoscopic cholecystectomy is the preferred initial approach in uncomplicated cases, and open cholecystectomy is recommended when anomalies exist around the Callot triangle [10].

References

1. Leuitan R, Diamond HD, Craver LF. Jaundice in Hodgkin's disease. Am J Med 1961;30:99
2. Popp JW Jr, Schapiro RH, Warshaw AL. Extrahepatic biliary obstruction by metastatic breast carcinoma. Ann Intern Med 1979;91:568–571
3. Itoh H, Shimono R, Hamamoto K. Evaluation of common bile duct stenosis in chronic pancreatitis using cholescintigraphy. Eur J Nucl Med 1988;14:137–140
4. McSherry CK, Glenn F. Biliary tract obstruction and duodenal diverticula. Surg Gynecol Obstet 1970;130:829–836
5. Serafini AN, Al-Sheikh W, Barkin JS, Hourani M, Sfakiankis G, Clarke LP, Ashkar FS. Biliary scintigraphy in acute pancreatitis. Radiology 1982;144:591–595
6. Ali A, Turner DA, Fordham EW. Tc-99m-IDA cholescintigraphy in acute pancreatitis: concise communication. J Nucl Med 1982;23:867–869
7. Mirizzi PL. Sindrome del conducto hepatico. J Int Chir 1948;8:731–733 (from Chap. 9)
8. Montefusco P, Spicer N, Geiss AC. Another facet of Mirizzi's syndrome. Arch Surg 1983;118:1221–1223
9. Kim PN, Outwater EK, Mitchel DG. Mirizzi syndrome: evaluation by MR imaging. Am J Gastroenterol 1999;94:2546–2550
10. Sare M, Gürer S, Taskin V, Aladag M, Hilmioglu F, Gürel M. Mirizzi syndrome: choice of surgical procedure in the laparoscopic era. Surg Laparosc Endosc 1998;8:63–67

Diseases of the Gallbladder

9

Liver and gallbladder diseases are two of the most common digestive system problems around the world [1]. In the United States, there are about 20.5 million people with gallbladder disease, with an estimated annual cost for medical care of more than 6.4 billion dollars [2]. Gallstones account for the majority of gallbladder problems. Women are affected two to three times as frequently as men [3]. Race, heredity, gender, age, and obesity are some of the important known risk factors for gallstones (Table 9.1.1). Between the ages 60 and 74, the prevalence of gallbladder disease is as high as 25.3% in men and 33.1%% in women (Table 9.1.2), and it is relatively more common among the Mexican Americans (Table 9.1.3). The highest rate among the Americans is found in the Pima Indians of Arizona [4]. By the teenage years, as many as 10–13% of Pima Indian girls develop lithogenic bile, and by 35–44 years, about 71% develop gallstones. Almost 90% of Pima Indian women over the age of 65 develop gallbladder disease, and the prevalence is much higher than in Pima Indian men. Such a high prevalence is also found in Mestizo Hispanics of Chile and the high-altitude rural population of Peru [5, 6]. The incidence of gallbladder disease varies from country to country; the Italians [7], British [8], Scottish [9], and Swedish [10] people have a much higher rate than people from other parts of Europe.

Natural history of gallstones: Most gallstones initially remain asymptomatic. The frequency of pain developing in an asymptomatic gallstone patient is 10 ± 3% at end of 5 years, 15 ± 4% at 10 years, and 18.4 ± 4% at 15 years (Fig. 9.1.1), which remains unchanged at 20 years [11]. Asymptomatic gallstone patients develop biliary pain (become symptomatic) at an average rate of 2% per year [12, 13]. The frequency of gallstone formation and onset of biliary pain both increase during pregnancy because of elevation of serum estrogens, which induce bile stasis, crystallization, and stone growth within the gallbladder. Gallstones form seven times more frequently in obese women than in non-obese women of comparable age [10]. Stones form more frequently in patients with increased body mass index and less physical activity than in lean people who maintain vigorous physical activity [14]. Stones smaller than 10 mm in size tend to pass through the cystic duct and common bile duct spontaneously during or after delivery [15].

Composition of gallstones: Gallstones are generally classified into two main types: cholesterol and pigment stones [16–18]. The color of the mucosal surface of the gallbladder depends on the nature of the gallstone composition (Fig. 9.1.2). Cholesterol stones are the

G.T. Krishnamurthy and S. Krishnamurthy, *Nuclear Hepatology*,
DOI 10.1007/978-3-642-00648-7_9, © Springer-Verlag Berlin Heidelberg 2009

Table 9.1.1 Risk factors for gallstones

(1) Heredity
(2) Obesity
(3) Gender
(4) Diabetes
(5) Age
(6) Low socioeconomic status
(7) Parity
(8) Pregnancy
(9) Drugs, e.g., somatostatin analogues (octreotide)

Table 9.1.2 Prevalence of gallstones and gallbladder disease in men and women in the United States [2]

	Gallstones		Gallbladder disease	
Age (years)	Men (%)	Women (%)	Men (%)	Women (%)
20–29	1.3	4.4	1.3	6.5
30–39	1.1	5.2	1.9	10.2
40–49	5.9	8.2	7.3	15.7
50–59	7.3	11.9	11.7	25.0
60–74	17.2	16.4	25.8	33.1
Mean	5.5	8.6	7.9	16.6

Table 9.1.3 Effect of gender and ethnicity on the prevalence of gallstones and gallbladder disease in the United States [2]

Gender, ethnicity	Gallstones	Gallbladder disease
Men		
Whites (non-Hispanics)	5.8	8.6
Blacks (non-Hispanics)	3.9	5.3
Mexican Americans	6.1	8.9
Women		
Whites (non-Hispanics)	8.6	16.6
Blacks (non-Hispanics)	7.9	13.9
Mexican Americans	12.8	26.7

most common, are soft in consistency, and consist of layers of cholesterol alternating with mucin and glycoproteins (Fig. 9.1.3). Although cholesterol is insoluble in water, it is kept in solution in bile by the formation of micelles, which are composed of cholesterol, bile salts, and phospholipids (lecithin). As the bile cholesterol concentration increases, a large

Fig. 9.1.1 Natural history of asymptomatic gallstones. Cumulative probability of onset of biliary pain in patients with asymptomatic gallstones increases with time: 10 ± 3%, 15 ± 4%, 18 ± 4%, and 18 ± 4%, at the end of 5,10, 15, and 20 years, respectively [11]

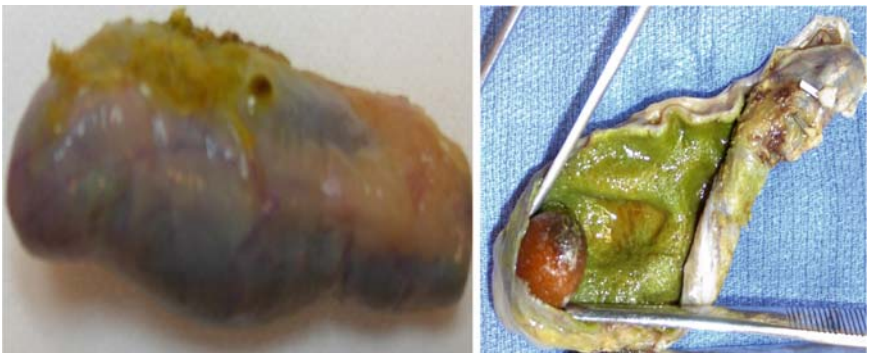

Fig. 9.1.2 Gallbladder color. Combination of light-colored cholesterol and dark-colored pigment crystals and stones may cast different hues on the surface (*left*) and inside of a gallbladder (*right*)

number of multilayered vesicles and crystals are formed, which aggregate and grow into large stones [19, 20]. Pigment stones are more common in patients with cirrhosis or chronic hemolytic anemia. They are black or brown in color, hard in consistency, and contain bilirubin or calcium salts [21]. Stones formed within the common bile duct usually belong to the pigment type. The great majority of gallstones (65–70%) seen on a plain abdominal X-ray are pigment stones [22].

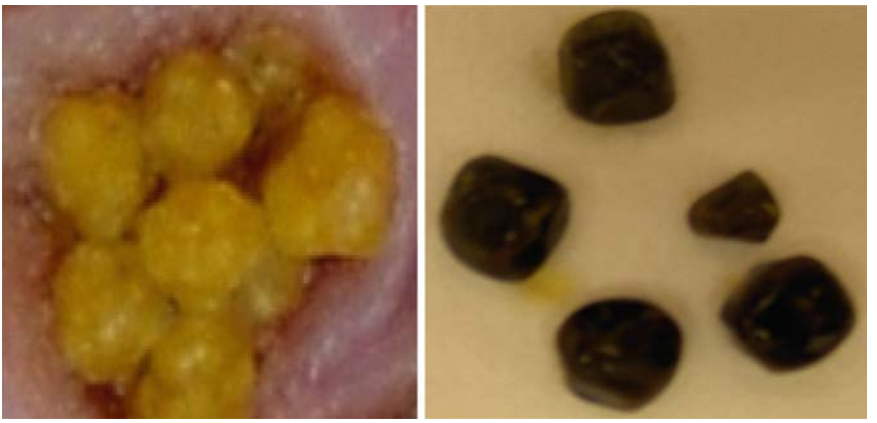

Fig. 9.1.3 Gallstone color. Cholesterol stones (*left*) are yellowish and soft, and pigment stones (*right*) are dark in color and hard in consistency. Pigment stones have multiple facets

9.1 Chronic Calculous Cholecystitis

Clinical Presentation

Patients with chronic calculous cholecystitis usually present with mild- to moderate-intensity upper abdominal pain without fever or leucocytosis. They ignore pain in the beginning and seek medical aid only when pain becomes intolerable. Pain usually begins 15–30 min after a meal, and this time interval roughly corresponds to the time taken for the serum endogenous cholecystokinin level to rise above the threshold to induce gallbladder contraction and emptying. The site of origin and direction of propagation of biliary pain are variable. The most common location is the epigastrium or the right hypochondrium (Fig. 9.1.4). The pain beginning in the right lower quadrant may mimic an acute appendicitis, or that beginning on the left side of the abdomen may simulate gastritis or diverticulitis. The pain may radiate to the chest and shoulder, mimicking an anginal attack. The pain deep in the abdomen and radiating to the interscapular region may simulate an attack of acute pancreatitis [23]. The pain following dinner usually reaches its peak intensity at midnight [24]. Biliary pain is attributed to distension of the gallbladder or common bile duct wall when they contract against obstruction to bile flow. Pain intensity correlates directly with the degree of wall distension [25]. Stones lying free within the gallbladder lumen do not cause pain. Pain is intermittent, with weeks or months of pain-free intervals between attacks. In a given patient, however, the pain frequency, duration, and intensity remain constant despite wide variations among patients [26].

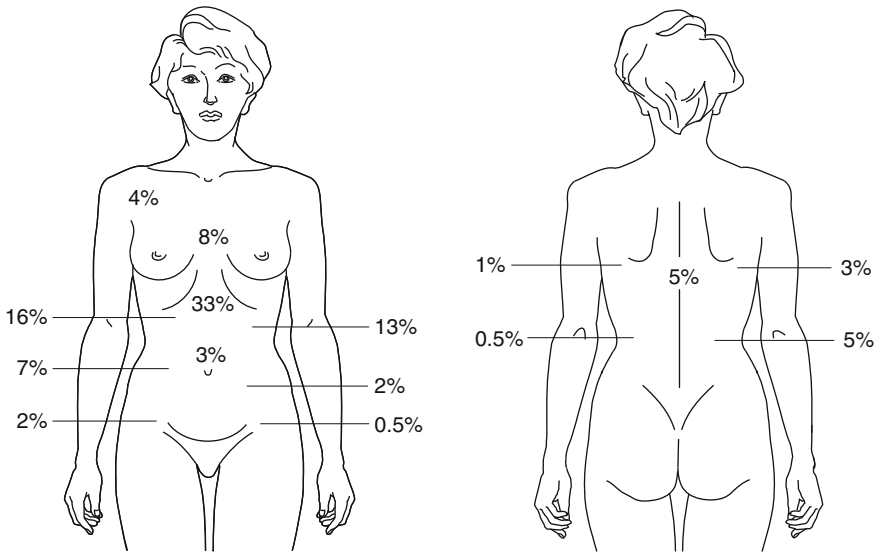

Fig. 9.1.4 Location and propagation of biliary pain. Epigastrium is the most common location, followed by the right hypochondrium. The pain may radiate to the chest and shoulder, mimicking an anginal attack, or to the back, mimicking pancreatitis. Radiation to the lower quadrants of the abdomen may mimic appendicitis or diverticulitis [22]

Biliary Pain Pathway

The liver and biliary tract receive both somatic and autonomic (sympathetic and parasympathetic) nerve supply. The somatic supply is provided through the thoracic intercostal nerves from spinal segments T8, 9, and 10, which supply the parietal peritoneum. The phrenic nerve (cervical third and fourth segments) supplies the diaphragm and the underlying parietal peritoneum and the gallbladder. Pain originating from the gallbladder, bile ducts, and peritoneum is also carried centrally (afferent) through the branches of the right phrenic nerve. The axons from the sympathetic preganglionic neurons located in thoracic spinal segments T7 to T10 travel along the ventral root and the corresponding sympathetic ganglion to reach the celiac ganglion via the greater and lesser splanchnic nerves. Postganglionic sympathetic fibers from the celiac ganglion supply the liver and the biliary tree (Fig.1.1.7, Chap. 1). Biliary tract pain is carried centrally through these afferent sympathetic fibers. Afferent nerve fibers originating from the corresponding somatotomes and dermatomes join the liver and biliary tract afferent fibers in the spinal cord and serve as a common channel for referred pain. Afferent fibers cross the midline to enter the opposite spino-thalamic tract before reaching the thalamus where pain is processed and sent to higher centers in the cortex.

The parasympathetic nerve supply is via the right and left vagal nerves, which originate in the medulla. After entering the abdomen, vagal fibers pass through the posterior and

anterior hepatic plexus before entering the liver, bile ducts, and gallbladder. The parasympathetic branches to the gallbladder and intrahepatic ducts come mainly from the left (anterior) vagus, and branches to the extrahepatic bile ducts and the sphincter of Oddi arrive mainly from the right (posterior) vagus. The parasympathetic system supplies the efferent nerve fibers and controls motor function of the gallbladder, bile ducts, and sphincter of Oddi. Pain from the gallbladder and common bile duct is referred to the epigastrium, right hypochondrium, right shoulder, or anterior chest (Fig. 9.1.4).

Histopathologic Features

The gallbladder of patients with chronic cholecystitis is often small in size and consists of thickening, fibrosis, and microcalcification of the wall. A single large stone or multiple small stones are common (Fig. 9.1.2). Bile is usually clear, but when it is viscous and contains debris, it settles at the bottom of the fundus of the gallbladder as sludge. The wall shows chronic inflammation and infiltration with lymphocytes, without any hemorrhage or necrosis, which are features of acute cholecystitis. The mucous membrane shows ulceration and scarring. Fibrosis and wall thickening reduce absorption of water through the wall, which accounted for delayed visualization or non-visualization of the gallbladder in the days of oral cholecystogram. Yet most of such non-visualized gallbladders in oral cholecystograms were seen in a Tc-99m-HIDA study, because the entry of even a single drop of high specific activity hepatic bile enables visualization of the gallbladder in a cholescintigram.

Diagnosis of Cholelithiasis

Ultrasonography is the diagnostic procedure of choice for detection of gallstones. The gallstones are hyperechoic and produce an acoustic shadow beyond the wall (Fig. 9.1.5). A confirmatory diagnosis of cholelithiasis by ultrasound requires demonstration of stone movement with gravity by taking gallbladder images at several different angles [27]. Often a calcified polyp may mimic a gallstone by casting an acoustic shadow, but it does not move with change of patient position. The stones are readily demonstrated in a fully filled gallbladder, but are often missed when the gallbladder is contracted and small in size, incompletely filled with bile, or completely filled with stones. Small stones mixed with sludge settle at the fundus and may fail to produce an acoustic shadow. Bile sludge is a thick, echo-dense fluid containing mucin, protein, calcium bilirubinate granules, and cholesterol monohydrate crystals [28, 29]. Bile sludge produces an irregular dense echo pattern within the gallbladder and does not produce an acoustic shadow (Fig. 9.1.6). Sludge formation increases after prolonged fasting or parenteral nutrition, and it usually clears after a fatty meal. Sludge formed during pregnancy disappears after delivery [15]. The sludge may collect at the dependent part of the gallbladder in a layered fashion and simulate settlement of the contrast agent (Fig. 9.1.7). About 15% of gallstones contain enough calcium to be seen on a plain abdominal X-ray film or on a CT scan [30].

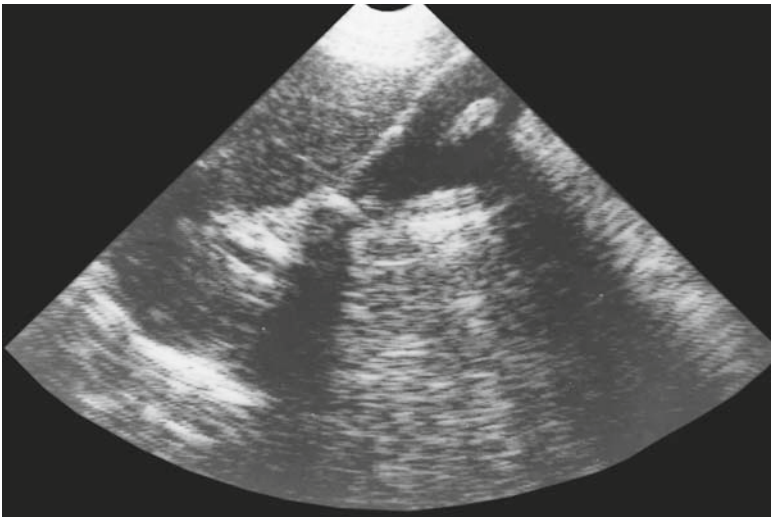

Fig. 9.1.5 Detection of gallstone with the ultrasound. Typically, the gallstone appears as hyperechoic within an acoustic shadow beyond the wall. Note one stone in the neck and another in the body of the gallbladder

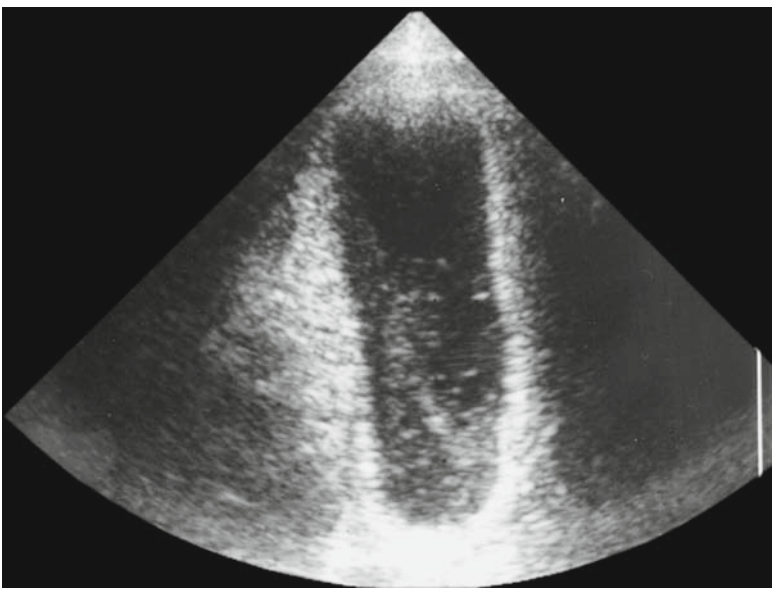

Fig. 9.1.6 Bile sludge. On the ultrasound study the sludge appears as an irregular echo-dense mass without an acoustic shadow. Also note thickening of the wall

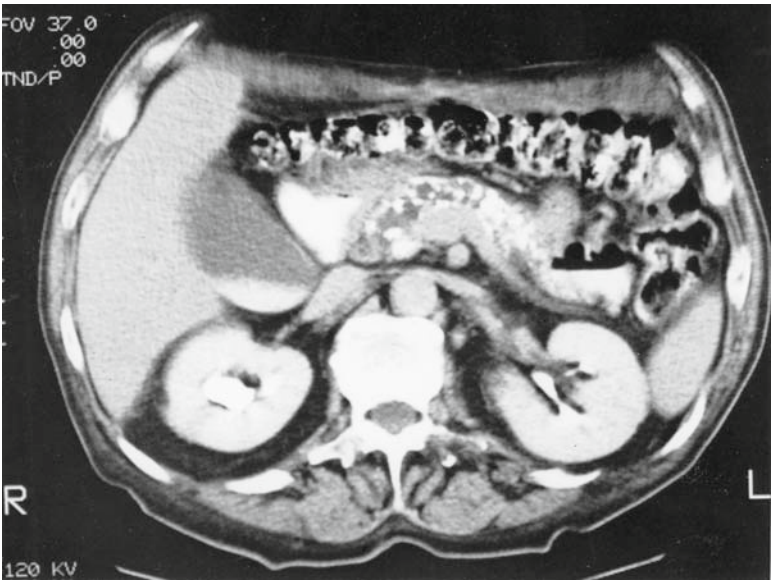

Fig. 9.1.7 Layering of radiocontrast. High-density radiocontrast agent settles at the dependent part of the gallbladder and appears as a separate layer from bile

Bile Aspiration

When standard imaging procedures fail to show gallstones, duodenal bile aspiration is performed to demonstrate cholesterol crystals, the forerunner of gallstones. After positioning the tip of an orally passed tube in the second part of the duodenum, CCK-8 is infused intravenously to induce contraction and emptying of the gallbladder. The bile emptied from the gallbladder into the duodenum is aspirated through the naso-duodenal tube and examined under the microscope for stones or subjected to biochemical analysis [31]. The test is relatively invasive and expensive and used mostly for research purposes when all other simple methods fail to demonstrate gallstones.

Quantitative Cholescintigraphy

Cholescintigraphy is used for measuring gallbladder motor function (ejection fraction) and for differentiating symptomatic from asymptomatic gallstones by closely monitoring the temporal relationship between the onset of pain and the phase of gallbladder emptying. A geometric technique for measurement of gallbladder volume by using an oral cholecystogram was first introduced in 1948 by deSilva [32]. A slightly modified method was adopted for volume measurement with the ultrasound [33]. Both oral cholecystogram and ultrasound are geometric methods and require that the gallbladder is of a particular shape (pear) before contraction and that it maintains that shape during and after contraction. It is widely recognized

that the gallbladder has many different shapes when it is full and that it changes its shape to different forms during and after its contraction.

To overcome the theoretical disadvantages of a geometric technique, a counts-based, non-geometric cholescintigraphic method was introduced in 1981 [34]. The cholescintigraphic method does not require that the gallbladder be of a particular shape. Counts originating from the gallbladder accurately represent the bile volume (see Fig. 5.1.4, Chap. 5). Emptying is expressed as an ejection fraction by dividing counts emptied by the total counts before emptying. The technique is highly reproducible either with ingesting a fatty meal or after intravenous administration of cholecystokinin [35, 36]. The short serum half life (2.5 min) of cholecystokinin enables measurement of serial ejection fractions by administering two to four sequential doses of CCK-8 on a single occasion [37]. Such techniques enable the study of the effect of various drugs on the gallbladder or on the sphincter of Oddi function (Fig. 6.1.5, Chap. 6).

Cholescintigraphy is usually obtained 6–10 h after fasting (minimum 4 h) to ensure a maximum tightness of the sphincter of Oddi and maximum relaxation of the gallbladder. In patients with serum bilirubin less than 2 mg%, a dose of 2–3 mCi (74–111 MBq) of HIDA will suffice. Larger doses are required in patients with hyperbilirubinemia. During the first 60 min of data collection (hepatic phase imaging), a relatively larger fraction of the hepatic bile enters the gallbladder in both normal subjects and patients with gallstones. A gallbladder count rate of more than 35,000 min^{-1} by 30 min and more than 70,000 min^{-1} by 45 min^{-1} is usual with a 5-mCi dose of Tc-99m-HIDA (Table 9.1.4). A gallbladder that appears early (within 10–15 min) shows a much higher count rate at 60 min (Fig. 9.1.8) than a gallbladder that visualizes late (between 30 and 60 min). In those 5–10% of the patients in whom the gallbladder appears late (after 50 min), it is necessary to wait 90 min to ensure adequate counts within the gallbladder. Variations in the time of appearance and rate of filling of the gallbladder are common and should be taken into account before proceeding with quantitative cholescintigraphy [38].

Fatty Meal Stimulation

Gallbladder emptying is under both nervous and hormonal control [39]. Nervous control is exerted via the cholinergic (vagus) and adrenergic nervous system. Gallbladder emptying in response to a sham feeding occurs via the cholinergic nerve stimulation and can be blocked completely with atropine or after vagotomy [40]. Gallbladder emptying after a

Table 9.1.4 Gallbladder counts following intravenous injection of 5 mCi Tc-99-HIDA in normal subjects and patients with gallstones [34]

Time	Normal subject (n = 15)	Gallstone patients (n = 15)
15 min	5,100 ± 70	4,200 ± 60
30 min	40,600 ± 520	38,700 ± 490
45 min	75,200 ± 680	70,800 ± 630
60 min	72,000 ±620	78,100 ± 710

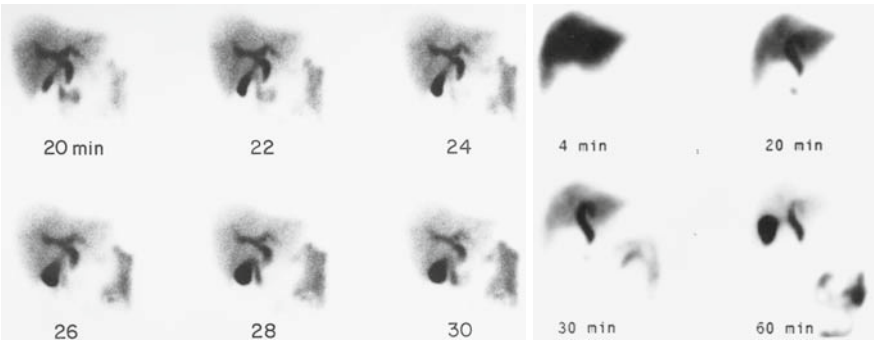

Fig. 9.1.8 Normal cholescintigram. Gallbladder, intrahepatic and extrahepatic bile ducts, and duodenum all appear within 30 min in one patient (*left*), whereas the gallbladder appears by 60 min in another patient (*right*). Distal common bile duct has a convex left margin, and the first part of the duodenum stays closer to the gallbladder

meal, however, occurs predominantly through the release of endogenous cholecystokinin (hormonal control), while the nervous control plays a minor role.

It can take 10–20 min after a meal for the serum CCK level to rise above a threshold to induce contraction and emptying of the gallbladder. The mean latent period (time from fatty meal ingestion to the beginning of gallbladder emptying) is 15.5 min. Post-prandial serum CCK levels stay above the threshold for 2–3 h post-meal [41, 42], and the gallbladder emptying is maintained as long as the serum CCK levels remain above the threshold for contraction (Fig. 9.1.9).

Effect of Nutrients on Gallbladder Emptying

The degree of gallbladder emptying post-meal is dependent upon various factors, including the quality, quantity, total calorie intake, and the proportion of proteins, fats, and carbohydrates in the meal. A mean ejection fraction of 82% has been reported with a liquid meal consisting of 300 ml meritene, 15 ml lipomul with 36 g carbohydrates, 29 g of fats, and 10 g of proteins, and an ejection fraction of 64% with half-and-half milk [40, 43]. These results clearly show that one must strictly follow the investigator's protocol, while adopting values reported in the literature, or must establish local values if a different type of meal is used.

Causes of Gallbladder Low Ejection Fraction

Many conditions associated with a gallbladder low ejection fraction are listed in Table 9.1.5. A decrease in emptying is attributed to various factors, including wall fibrosis, a decrease in the total number of CCK receptors in the gallbladder wall, or inactivation of

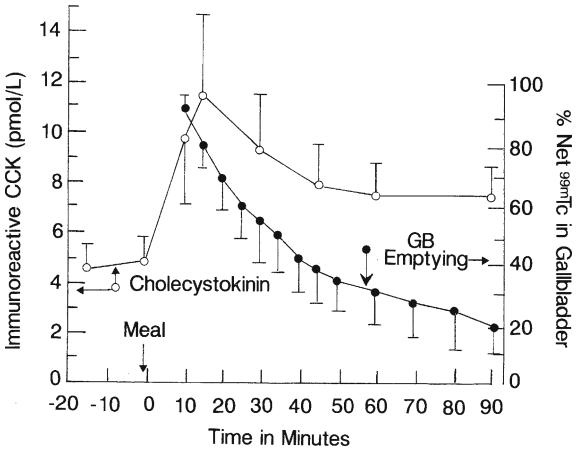

Fig. 9.1.9 Relationship between serum cholecystokinin (*CCK*) level and gallbladder emptying. Serum CCK level begins to rise soon after a meal, peaks by 10–30 min, and the level is maintained above the threshold for contraction for more than 90 min. Gallbladder maintains its emptying as long as the post-prandial serum CCK level remains above the threshold for contraction (modified from [41])

Table 9.1.5 Causes of gallbladder low ejection fraction

(1) Cystic duct syndrome (chronic acalculous cholecystitis)
(2) Diabetes
(3) Chronic calculous cholecystitis
(4) Obesity
(5) Common bile duct obstruction
(6) Sphincter of Oddi spasm
(7) Opiates
(8) Somatostatin analogues (octreotide)
(9) Anticholinergic drugs (atropine)
(10) Congenital anomalies (septum, bilobed, etc.)

cholecystokinin by anti-cholecystokinin peptides in the serum [44]. The total number of CCK receptors in the gallbladder smooth muscle shows a direct correlation with the degree of emptying; the higher the receptor number, the greater is the ejection fraction, and vice versa [41]. Although a decrease in gallbladder emptying is a common feature of patients with cholelithiasis, a normal or even an exaggerated emptying has been reported in a few selected patients with cholelithiasis [45].

A delay in the appearance of the gallbladder or low ejection fraction in response to CCK stimulation indicates a functional abnormality [46, 47]. The efficiency with which the wall absorbs water, sodium, and other electrolytes from the lumen is a reflection of the concentration function of the gallbladder and determines the time of appearance of the

gallbladder in a Tc-99m-HIDA study. It has been argued in the past whether the abnormal concentration and contraction functions of the gallbladder precede or follow the development of the gallstones. Most of the conditions associated with a decrease in gallbladder emptying are also associated with a higher incidence of gallstones (Table 9.1.5). Patients with ulcerative colitis, for example, show a lower gallbladder ejection fraction and a higher incidence of gallstones when compared to a control group [48]. Treatment with octreotide, a somatostatin analogue, which decreases gallbladder emptying, also increases the incidence of cholelithiasis and cholecystitis [49]. Octreotide decreases gallbladder emptying by interfering with the release of both acetylcholine (cholinergic stimulation) and cholecystokinin (hormonal stimulation), and also by directly blocking the effect of cholecystokinin on the gallbladder wall [50]. The recent literature, therefore, appears to support the hypothesis that the functional abnormalities precede the development of gallstones by months or years.

Some of the investigators suggest using ultrasound for measurement of both the gallbladder volume and emptying, and claim that it can substitute cholescintigraphy for measurement of emptying [51]. Ultrasound emptying measurements are subject to error due to change of shape, shift of axis, and other technical artifacts introduced during contraction and emptying of the gallbladder. Combining the geometric ultrasound technique for measurement of the resting volume (after making necessary volume correction) and non-geometric cholescintigraphy for measurement of gallbladder emptying overcomes many of the theoretical limitations of a geometric method. Combination offers the best features of both techniques for evaluation of gallbladder morphology and function [52].

References

1. Williams R. Global challenges in liver disease. Hepatology 2006;44:521–526
2. Sandler RS, Everhart JE, Donowitz M, Adams E, Cronin K, Goodman C, Gemmen E, Shah S, Avdic A, Rubin R. The burden of selected digestive diseases in the United States. Gastroenterology 2002;122:1500–1511
3. Everhart JE, Khare M, Hill M, Maurer KR. Prevalence and ethnic differences in gallbladder disease in the United States. Gastroenterology 1999;117:632–639
4. Sampliner RE, Bennett PH, Comess LJ, Rose FA, Burch TA. Gallbladder disease in Pima indians. Demonstration of high prevalence and early onset by cholecystography. N Engl J Med 1979;283:1358–1364
5. Miquel JF, Covarrubias M, Villaroel L, Mingrone G, Greco AV, Puglielli L, Carvallo P, Marshall G, Del Pino G, Nervi F. Genetic epidemiology of cholesterol cholelithiasis among Chilean Hispanics, Amerindians, and Maoris. Gastroenterology 1998;115:937–946
6. Moro PL, Checkley W, Gilman RH, Lescano G, Bonilla JJ, Silva B, Garcia HH. Gallstone disease in high-altitude Peruvian rural population. Am J Gastroenterol 1999;94:153–158
7. Rome Group for the Epidemiology and Prevention of Cholelithiasis (GREPO). Prevalence of gallstone disease in an Italian adult female population. Am J Epidemiol 1984;119:796–805
8. Godrey PJ, Bates J, Harrison M, King MB, Padley NR. Gallstones and mortality: a study of all gallstone related deaths in a single health district. Gut 1984;25:1029–1033
9. Layde PM, Vessey MP, Yeates D. Risk factors for gall-bladder disease: a cohort study of young women attending family planning clinics. J Epidemiol Community Health 1082;36:274–278

10. Lindstrom CG. Frequency of gallstone disease in a well-defined Swedish population. A prospective necropsy study in Malmo. Scand J Gastroenterol 1977;12:341–346
11. Gracie WA, Ransohoff DF. The natural history of silent gallstones: the innocent gallstone is not a myth. N Engl J Med 1982;307:798–800
12. McSherry CK, Ferstenberg H, Calhoun WF, Lahman E, Virshup M. The natural history of diagnosed gallstone disease in symptomatic and asymptomatic patients. Ann Surg 1985;202:59–63
13. Thistle JL, Cleary PA, Lachin JM, Hersh T. The natural history of cholelithiasis: the National Co-operative Gallstone Study. Ann Intern Med 1984;101:171–175
14. Williams PT. Independent effects of cardiorespiratory fitness, vigorous physical activity, and body mass index on clinical gallbladder disease risk. Am J Gastroenterol 2008;103: 2239–2247
15. Valdivieso V, Covarrubias C, Siegel F, Cruz F. Pregnancy and cholelithiasis: pathogenesis and natural course of gallstones diagnosed in early puerperium. Hepatology 1993;17:1–4
16. Donovan JM, Carey MC. Physical-chemical basis of gallstone formation. Gastroenterol Clin North Am 1991;20:47–66
17. Holzbach RJ, Busch N. Nucleation and growth of cholesterol crystals. Kinetic determinates in supersaturated native bile. Gastroenterol Clin North Am 1991;20:67–84
18. LaMont JT, Smith BF, Moore JRL. Role of gallbladder mucin in pathophysiology of gallstones. Hepatology 1984;4(Suppl):51S–56S
19. Admirand WH, Small DM. The physicochemical basis of cholesterol gallstone formation in man. J Clin Invest 1968;47:1043–1052
20. Somjen GJ, Gilat T. Contribution of vesicular and micellar carriers to cholesterol transport in human bile. J Lipid Res 1985;26:699–704
21. Johnston DE, Kaplan MM. Pathogenesis and treatment of gallstones. N Engl J Med 1993;328:412–421
22. Trotman BW, Petrella EJ, Soloway RD, Sanchez HM, Morris TA 3d, Miller WT. Evaluation of radiographic lucency or opaqueness of gallstones as a means of identifying cholesterol or pigment stones. Correlation of lucency or opaqueness with calcium and mineral. Gastroenterology 1975;68:1563–1566
23. Gunn A, Kiddie N. Some clinical observations on patients with gallstones. Lancet 1972;2: 239–241
24. Rigas B, Torosis J, McDougall CJ, Vener KT, Spiro HM. The circadian rhythm of biliary colic. J Clin Gastroenterol 1990;12:409–414
25. Sullivan FJ, Eaton SB Jr, Ferrucci JT Jr, Dreyfuss JR, Sloan RW. Cholangiographic manifestations of acute biliary colic. N Engl J Med 1973;288:33–35
26. Doran FS. The sites to which pain is referred from the common bile duct in man and its implications for the theory of referred pain. Br J Surg 1967;54:599–606
27. Cooperberg PL, Burhenne HJ. Real time ultrasonography. Diagnostic technique of choice in calculous gallbladder disease. N Engl J Med 1980;302:1277–1279
28. Ko CW, Sekijima JH, Lee SP. Biliary sludge. Ann Intern Med 1999;130:301–311
29. Portincasa P, van Erpecum KJ, Jansen A, Renooij W, Gadellaa M, van Berge-Henegouwen GP. Behavior of various cholesterol crystals in bile from patients with gallstones. Hepatology 1996;23:738–748
30. Berk RN, Ferrucci JT Jr, Fordtran JS, Cooperberg PL, Weissmann HS. The radiological diagnosis of gallbladder disease. An imaging symposium. Radiology 1981;141:49–56
31. Delchier JC, Benfredj P, Preaux AM, Mentreau JM, Dhumeaux D. The usefulness of microscopic bile examination in patients with suspected microlithiasis: a prospective evaluation. Hepatology 1986;6:118–122
32. deSilva GS. A simple method for computing the volume of the human gallbladder. Radiology 1949;52:94–102

33. Everson GT, Braverman DZ, Johnson MA, Kern F Jr. A critical evaluation of real time ultrasonography for the studies of gallbladder volume and contraction. Gastroenterology 1980;69:40–46
34. Krishnamurthy GT, Bobba VR, Kingston E. Radionuclide ejection fraction: a technique for quantitative analysis of motor function of the human gallbladder. Gastroenterology 1981;80:482–490
35. Fisher RS, Stelzer F, Rock E, Malmud LS. Abnormal gallbladder emptying in patients with gallstones. Dig Dis Sci 1982;27:1019–1024
36. Krishnamurthy GT, Bobba VR, Kingston E, Turner F. Measurement of gallbladder emptying sequentially using a single dose of 99mTc-labeled hepatobiliary agent. Gastroenterology 1982;83:773–776
37. Krishnamurthy GT, Bobba VR, Langrell K. The gallbladder emptying response to sequential exogenous and endogenous cholecystokinin. Nucl Med Commun 1984;5:27–33
38. Williams W, Krishnamurthy GT, Brar HS, Bobba VR. Scintigraphic variations of normal biliary physiology. J Nucl Med 1984;25:160–165
39. Hopman WPM, Jansen JBMJ, Rosenbusch G, Lamers CBHW. Cephalic stimulation of gallbladder contraction in humans: role of cholecystokinin and the cholinergic system. Digestion 1987;38:197–203
40. Fisher RS, Rock E, Malmud LS. Gallbladder emptying response to sham feeding in humans. Gastroenterology 1986;90:1854–1857
41. Upp JR Jr, Nealon WH, Singh P, Fagan CJ, Jonas AS, Greeley GH Jr, Thompson JC. Correlation of cholecystokinin receptors with gallbladder contractility in patients with gallstones. Ann Surg 1987;205:641–648
42. Vezina WC, McAlister VC, Wall WJ, Engel CJ, Grant DR, Ghent CN, Hutton LC, King ME, Chey WY. Normal fasting volume and postprandial emptying of the denervated gallbladder in liver transplant recipients. Gastroenterology 1994;107:847–853
43. Bobba VR, Krishnamurthy GT, Kingston E, Turner FE, Brown PH, Langrell K. Gallbladder dynamics induced by fatty meal in normal subjects and patients with gallstones: concise communication. J Nucl Med 1984;25:21–24
44. Sarles H, Hags G, Lanier R, Demol P, Bataille D. Present status of the anticholecystokinin hormone. Digestion 1979;19:73–76
45. Northfield TC, Kupfer RM, Maudgal DP, Zenter-Munro PL, Meller ST, Garvie NW, McCready R. Gallbladder sensitivity to cholecystokinin in patients with gallstones. Br Med J 1980;280:143–144
46. Krishnamurthy S, Krishnamurthy GT. Evolution of nuclear hepatology as a clinical subspeciality. J Nucl Med Technol 1995;23:35S–45S
47. Nahrwold DL, Rose RC, Ward SP. Abnormalities in gallbladder morphology and function in patients with cholelithiasis. Ann Surg 1976;184:415–421
48. Damiao AO, Sipahi AM, Vezozzo DP, Goncalves PL, Habr-Gama A, Teixeira MG, Fukushima JT, Laudanna AA. Effects of colectomy on gallbladder motility in patients with ulcerative colitis. Dig Dis Sci 1997;42:259–264
49. Trendle MC, Moertel CG, Kvols LK. Incidence and mortality of cholethiasis in patients receiving chronic octreotide for metastatic carcinoid and malignant islet cell tumors. Cancer 1997;79:830–834
50. Fisher RS, Rock E, Levin G, Malmud L. Effects of somatostatin on gallbladder emptying. Gastroenterology 1987;92:885–890
51. Pallotta N, Corazziari E, Scopinaro F, Bonino R, Schillaci O, Vignoni A, Mangano M, Torsoli AT. Noninvasive estimate of bile flux through the gallbladder in humans. Am J Gastroenterol 1998;93:1877–1885
52. Krishnamurthy GT, Krishnamurthy S. Hazards of formulating new theories about gallbladder (GB) function based on ultrasound volume data. Am J Gastroenterol 1999;94:1703–1705

9.2 Chronic Acalculous Cholecystitis

Chronic acalculous cholecystitis (CAC), also known as cystic duct spasm or cystic duct syndrome, is one of two diseases that come under the broad category of 'biliary dyskinesia,' the other one being spasm of the sphincter of Oddi (Chap. 10). Biliary dyskinesia is a purely functional abnormality without an easily identifiable morphologic abnormality. The term cystic duct syndrome merely indicates the major site of functional abnormality. The syndrome was first described by Cozzolino et al. in 1961, but did not receive much clinical recognition until a reliable and easily reproducible diagnostic procedure became available for measurement of the gallbladder ejection fraction [1].

Clinical Presentation

Patients with chronic acalculous cholecystitis usually present with symptoms very similar to those with chronic calculous cholecystitis. Intermittent mild to moderate intensity right upper quadrant or epigastric pain is the most common presenting symptom. Pain begins 30–60 min after a meal and is often associated with nausea and vomiting. Post-prandial pain after dinner reaches its peak intensity at midnight. Women in their 30s and 40s are affected three to four times more frequently than men of similar age. The physical examination, liver function tests, blood counts, and serum amylase and lipase levels are normal. Gallbladder morphology remains normal, and no gallstones are found within the gallbladder.

Histopathologic Features

Histopathologic abnormalities are confined mostly to the cystic duct. There is kinking and narrowing of the cystic duct lumen due to thickening and fibrosis of the wall [2]. Adhesion and angulation of the infundibulum are common. The connection of the cystic duct with the common hepatic duct normally shows wide variations (Fig. 9.2.1). About 50% of

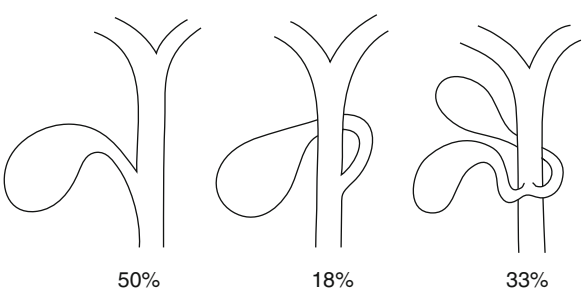

Fig. 9.2.1 Variations in the union of the cystic duct with the common hepatic duct. The cystic duct usually joins the common hepatic duct at 45° angle along its right margin (50%). It may pass behind the common hepatic duct before joining it on the left side (18%). A spiral cystic duct joins in front in 33% of the patients [3]

cystic ducts join with the common hepatic duct along its right margin at a 45 degree angle, 18% pass behind the common hepatic duct before joining it along its left margin, and the remaining 32% show a spiral form before joining the common hepatic duct either in front or behind [3]. Microscopic examination of the cystic duct shows infiltration with chronic inflammatory cells, concentric thickening, and fibrosis of the media and adventitia with narrowing of the duct lumen (Fig. 9.2.2).

Functional Abnormality

The major abnormality pertains to the concentration and contraction functions of the gallbladder. Bile aspirated from the duodenum in patients with CAC shows a lower concentration of bile salts and phospholipids than in normal subjects [4]. Hepatic bile enters the gallbladder slowly through the narrowed cystic duct. Although the gallbladder may appear within 30 min in a Tc-99m-HIDA study (Fig. 9.2.3), a delayed appearance (after 40 min) is more common (Fig. 9.2.4). Some of the gallbladders may take as long as 2–3 h for their appearance. Late appearance is attributed to delayed and decreased entry of hepatic bile into the gallbladder primarily due to slow absorption of water and electrolytes through the wall. Gallbladder low ejection fraction in response to intravenous cholecystokinin or after a fatty meal ingestion is the characteristic feature. Low ejection fraction is due to a combination of several factors, of which wall fibrosis, a decrease in the total number of CCK receptors in the gallbladder wall, and a decrease in the cystic duct threshold for CCK are considered very important contributing factors (Fig. 9.2.5). A decrease in the cystic duct threshold with a paradoxical contraction is attributed to an activation of inhibitory CCK receptors, which induce contraction of the cystic duct instead of normal relaxation [5, 6].

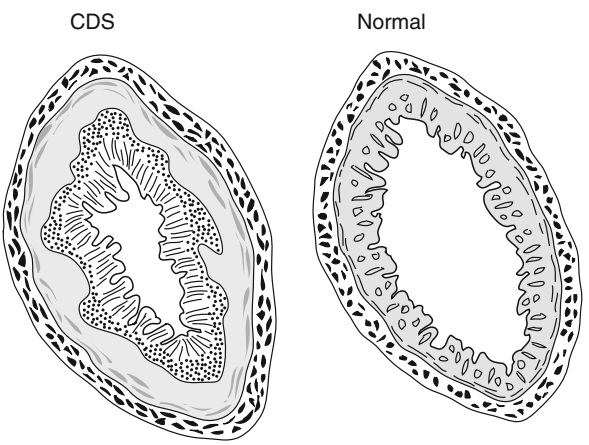

Fig. 9.2.2 Cystic duct histopathology in normal subjects and patients with cystic duct syndrome (*CDS*). Normal cystic duct wall shows thin mucosa, muscular layer, and adventitia. All three layers show inflammation and concentric thickening with narrowing of the lumen in CDS

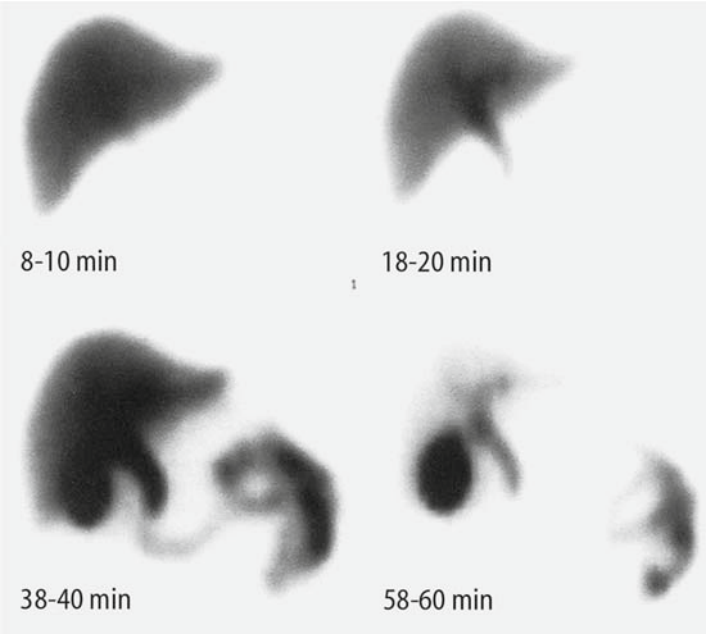

Fig. 9.2.3 Normal bile formation and flow. Bile flow into the gallbladder may remain normal in some of the patients with cystic duct syndrome. The gallbladder, intrahepatic ducts, extrahepatic ducts, and small intestine are seen within 40 min. Radioactivity clears almost completely from the liver and enters the gallbladder at 60 min

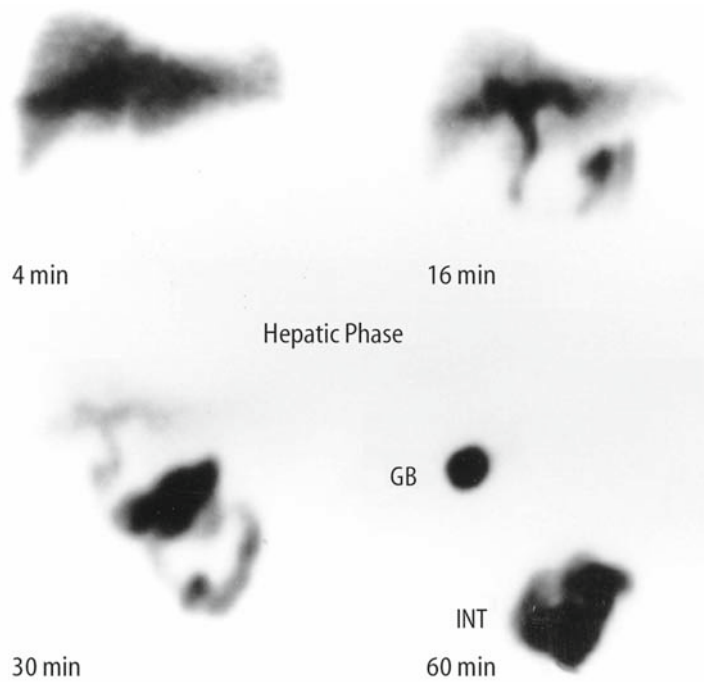

Fig. 9.2.4 Delayed gallbladder appearance. Gallbladder that does not appear by 30 min fills in by 60 min with fewer counts than normal. Intrahepatic and extrahepatic ducts are normal

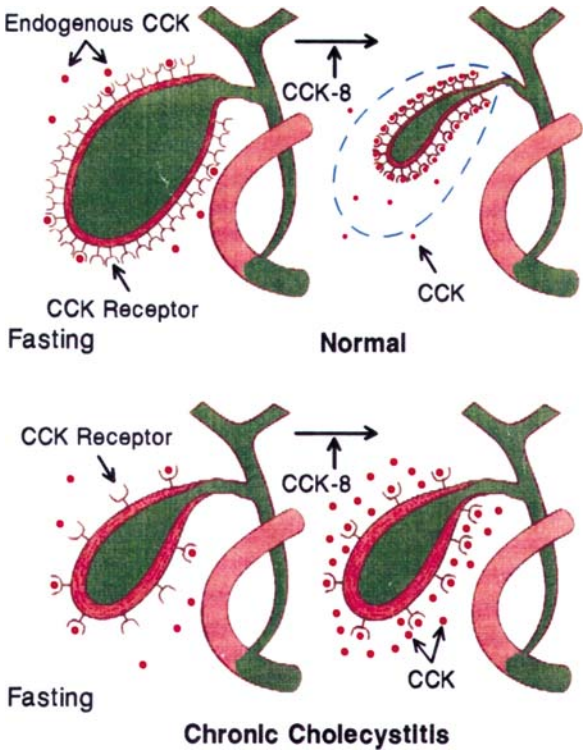

Fig. 9.2.5 Gallbladder cholecystokinin (*CCK*) receptors in health and disease. A normal gallbladder rich with CCK receptors produces almost complete emptying, while the gallbladder with chronic cholecystitis elicits poor emptying because of paucity of CCK receptors

A decrease in the smooth muscle threshold for CCK induces cystic duct contraction before the contraction of the fundus and body, with subsequent non-emptying of the gallbladder [7]. Unable to empty bile against a spasmodic cystic duct, the gallbladder contracts and assumes many different shapes, with globular being the most common form. Usually there is no bile reflux into the common hepatic duct or to the right and left hepatic ducts [8].

During fasting, the serum endogenous cholecystokinin reaches its lowest level, which promotes the maximum increase in the tone of the sphincter of Oddi and maximum relaxation of the gallbladder wall. An increase in sphincter tone raises the sphincter of Oddi mean basal pressure to 15 cmH_2O. The common bile duct and the gallbladder pressure are maintained at 12 cmH_2O and 10 cmH_2O, respectively. The pressure differences at these three levels promote preferential entry of the hepatic bile into the gallbladder as the bile seeks the path of the least resistance. During cholescintigraphy, Tc-99m-HIDA simply follows the path taken by the hepatic bile [8].

After 4–6 h of fasting, a normal gallbladder is completely filled to its maximum capacity of 50 ml, but it continues to receive hepatic bile at the rate of 0.3 min. A completely filled

gallbladder is able to accommodate an additional 0.3 ml of hepatic bile per minute simply by absorbing an equal volume of water through the wall. Absorption of water takes place along the lateral intercellular channels situated between the columnar cells of the mucosa (see Fig. 2.5, Chap. 2). These lateral intercellular channels are open widely during fasting when the gallbladder is completely relaxed, but they close tightly when the gallbladder contracts after a meal. These two factors, an increase in sphincter tone and absorption of water through the wall, are the primary mechanisms by which the gallbladder sequesters most bile salts during fasting. The process by which the gallbladder concentrates bile salts during fasting by selective absorption of water and electrolytes through the wall is called the concentration function of the gallbladder [9]. The concentration function can be measured quantitatively and non-invasively with cholescintigraphy using Tc-99m HIDA as described in Chap 2.

Measurement of Gallbladder Ejection Fraction

Imaging Procedure

The patient preparation and data acquisition and analysis are monitored carefully. The patient fasts for a minimum of 4 h, preferably for 8–10 h. Detailed drug history is taken to ensure that the patient is not currently taking any medications that act either on the gallbladder or sphincter of Oddi. Opioids, calcium channel blockers, nitrates, sympathetic and parasympathetic agonists or antagonists, and other drugs that are known to act on the gallbladder or the sphincter of Oddi are withdrawn for a day or two before scheduling the patient for measurement of the gallbladder ejection fraction.

The data are collected with the large field of view gamma camera interfaced to an online computer in two separate phases: the hepatic phase between 0 and 60 min and gallbladder phase between 61 and 90 min. The hepatic phase data are collected on a 64 × 64 matrix as one frame per minute for 60 min, following intravenous injection of 2–3 mCi of Tc-99m-HIDA. After ascertaining the adequacy of counts within the gallbladder (Table 9.1.4), the gallbladder phase data are acquired. When the gallbladder appears late and does not contain adequate counts at the end of 60 min, a second dose of Tc-99m-HIDA is given at 60 min, and the gallbladder phase data collection is delayed for an additional 30–60 min. This delay ensures adequate counts within the gallbladder for measurement of the ejection fraction. Images are carefully scrutinized in cine display to check for superimposition of structures over one another, especially the superimposition of the gallbladder and duodenal radioactivity. In the supine position, the gallbladder fundus lies anteriorly and the neck posteriorly. Small gallstones often gravitate to the dependent posterior part and settle in the neck, blocking bile entry into the gallbladder. Changing the patient position to a right lateral decubitus position or asking the patient to walk for few minutes usually dislodges the stones from the neck and allows bile entry into the gallbladder. A septum at the neck may allow filling of the proximal segment and delay entry of radiolabeled bile into the distal segment (Fig. 9.2.6).

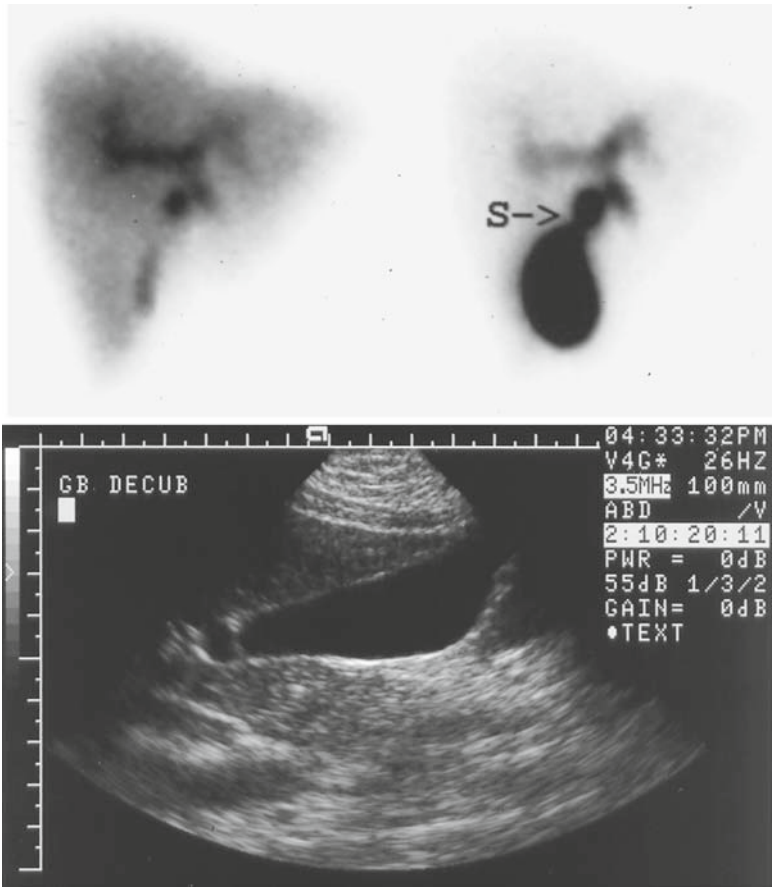

Fig. 9.2.6 Septa at the neck (*S*). Bile enters the small proximal segment at the neck first (*left*) followed by delayed filling of the body and fundus (*right*) forming the distal segment (*A*). Ultrasound shows septa at the neck

Gallbladder Phase Data Acquisition and Analysis

This data collection usually occurs between 61 and 90 min after Tc-99m-HIDA injection, unless there is a delay in filling of the gallbladder [10–12]. If there is a superimposition of structures during the hepatic phase data collection, the gamma camera angle is changed to the position that maximally separates the gallbladder from the common bile duct and the duodenum. When the gallbladder and duodenum are superimposed, drinking a glass of water moves the duodenal radioactivity away from the gallbladder region of interest [13]. The data are collected at one frame per minute for 30 min. Beginning at 3 min, 3 ng $kg^{-1}min^{-1}$ of cholecystokinin-8 (sincalide, Bracco Diagnostics Inc., Princeton, NJ) is infused over 10 min through an infusion pump [8, 14].

Before the test begins, the patient is instructed to raise a hand when pain is experienced and raise the hand again when pain is relieved. The time of onset and relief of pain are noted on the gallbladder time/activity curve to critically establish the temporal relationship between pain and the phase of gallbladder emptying. Biliary pain typically occurs during the gallbladder ejection period. Pain experienced after the ejection period is considered non-biliary in origin [8]. Saline may be infused as a placebo prior to cholecystokinin infusion. The gallbladder ejection fraction depends upon various factors, including the dose, dose rate, and the duration of infusion of sincalide. These variables are controlled strictly to obtain a consistent result. The gallbladder ejection fraction is calculated using the counts before and after emptying [14, 15]. The normal gallbladder ejection fraction is 35% and higher when 3 ng kg^{-1} min^{-1} CCK-8 is infused over 3 min, and 50% and higher when the identical dose rate is infused over 10 min. Large bolus doses of sincalide produce a non-physiological response and should be avoided.

Contraction and emptying of the gallbladder are initiated when sincalide binds to its receptors located in the smooth muscle, which are distributed irregularly in the wall (Fig. 9.2.7). The smooth muscle is much thicker in the fundus and neck than in the body and cystic duct. Cholecystokinin receptors located in the smooth muscle of the

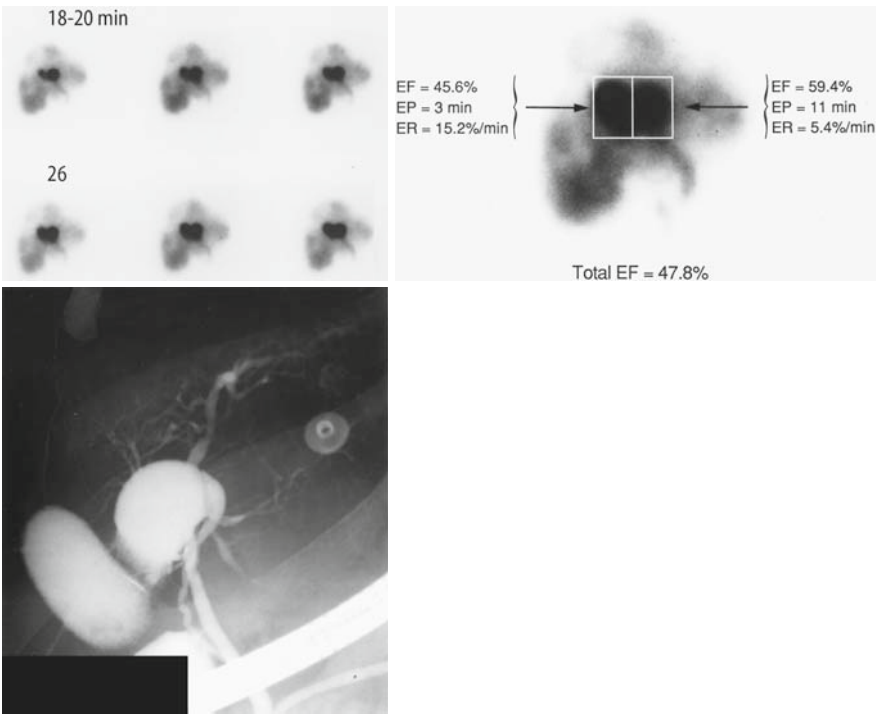

Fig. 9.2.7 Valentine gallbladder. A bi-lobed gallbladder high in position fills with bile (*top left*). Each segment empties at different rate in response to CCK-8 infusion, with a total ejection fraction of 47.5% (*top right*). Cholangiogram (*bottom*) shows the septa in between two segments [18]

body, fundus, and cystic duct show varied thresholds for contraction. In dogs, for example, the smooth muscle in the cystic duct shows a much higher threshold (is less sensitive) than the smooth muscle in the fundus [5]. The cystic duct, therefore, does not contract when the fundus and body contract in response to a physiologic dose of sincalide. A dose rate within a physiologic range causes smooth, sustained, and coordinated contraction and emptying of the gallbladder.

Sincalide Dose

A low ejection fraction is often obtained in normal subjects when a large, non-physiologic dose rate of sincalide is given rapidly. In the package insert, the manufacturer of sincalide (Bracco Laboratory, Princeton, NJ) recommends a dose of 0.02 μg kg^{-1} (20 ng kg^{-1}) given in 30–60 s. The recommended dose in the package insert for sincalide originally was developed for an oral cholecystogram or for stimulation of pancreatic enzyme secretion. This dose rate is too large for cholescintigraphy and often causes a low ejection fraction in normal subjects and should be avoided [7, 16, 17]. An optimal dose rate for cholescintigraphy is 3.0 ng kg^{-1} min^{-1} infused over 3 or 10 min. This dose rate (3 ng kg^{-1} min^{-1}) is much lower than the dose recommended in the package insert. Currently, we have standardized the sincalide dose as 3 ng kg^{-1} min^{-1} for 10 min and consider GBEF of 50% or greater as normal. We hope that others will follow this procedure in total such that it becomes a universal standard. Local normal values should be established when a different sincalide dose rate or duration of infusion is chosen.

Congenital Abnormalities of the Gallbladder

Congenital folds or septa often cause abnormalities in filling and emptying of the gallbladder [18]. An intrahepatic gallbladder may cause a filling defect in the liver in the early images (within 10 min) that fills later with radiolabeled bile and may not empty normally in response to CCK because of adhesion of its wall to the liver parenchyma. Often a gallbladder is divided into two segments of equal or unequal size (Valentine gallbladder) by a fold, and each segment may fill differently and empty at different rates in response to sincalide (Fig. 9.2.7). An epithelial fold or septa near the neck creates a pouch-like compartment (Hartmann pouch) where gallstones may lodge and delay or prevent bile entry into the distal compartment (Fig. 9.2.8). Septa in the middle of the gallbladder may allow normal filling of the proximal segment but delay the filling of the distal segment for 10–15 min. In such instances, only the proximal segment may empty bile normally, while the distal segment is prevented from emptying by the septa, which acts as a one-way valve (Fig. 9.2.9). Imaging at a shorter frame rate (one frame/minute) enables easy recognition of such morphologic variations [19, 20]. Failure to recognize such morphologic abnormalities may provide false functional information. The distal segment, which fills late, may empty bile poorly, while the proximal segment shows a normal ejection fraction. Poor emptying of the distal segment may promote formation of gallstones. When the shape of the gallbladder in the anterior view mimics the duodenal loop, a right lateral view helps to

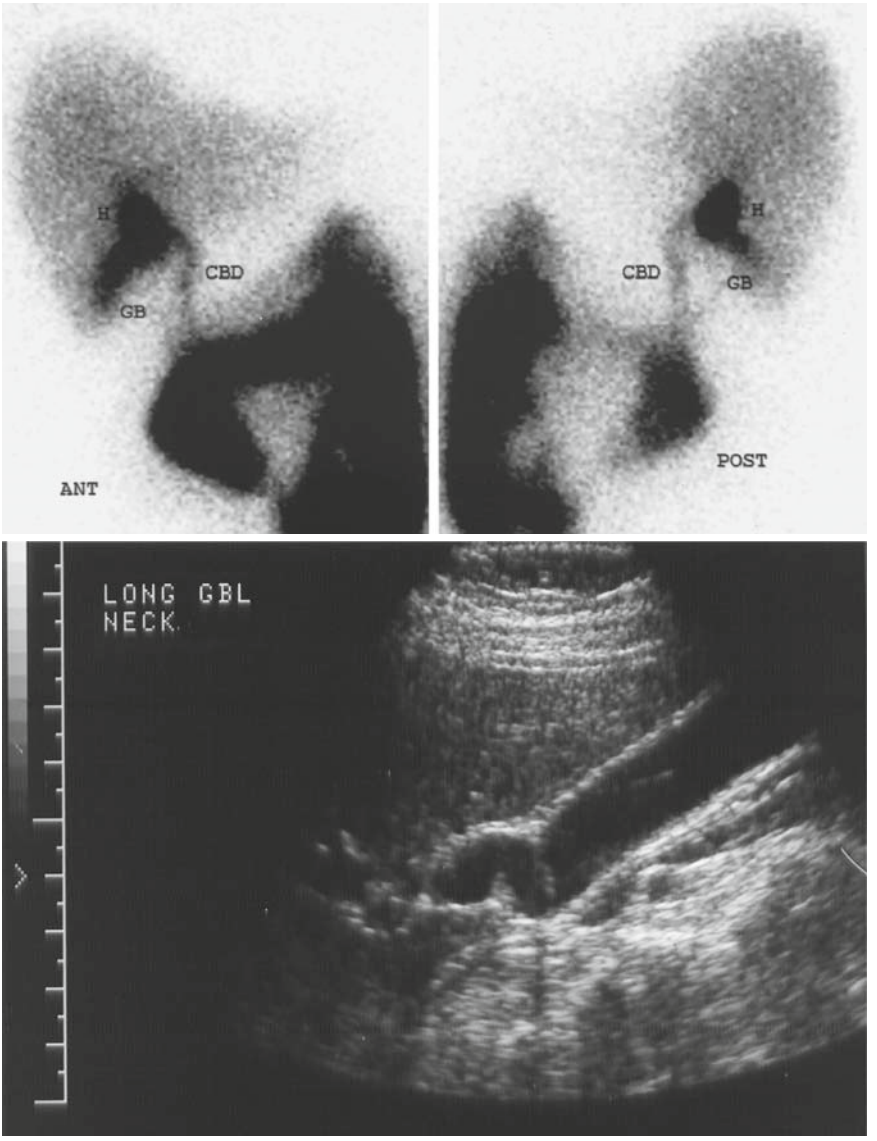

Fig. 9.2.8 Hartmann pouch. Anterior (*Ant*) and posterior (*Post*) view cholescintigrams (*top*) show a pouch (*H*) at the neck (Hartmann pouch) of the gallbladder (*GB*). An ultrasound of the gallbladder (*bottom*) confirms the pouch at the neck

separate them (Fig. 9.2.10). The gallbladder projects at the middle of the anterior liver border, while the common bile duct remains posterior in location. Cholescintigraphy usually does not show gallstones as a filling defect within the gallbladder due to mixing of

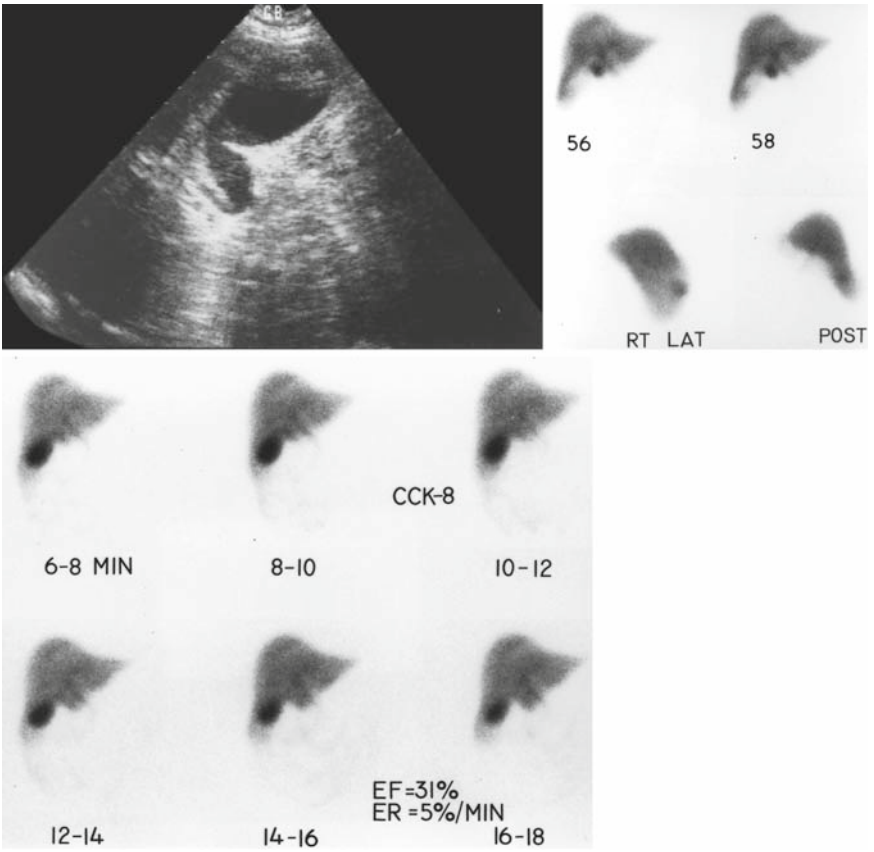

Fig. 9.2.9 Septa in the body of the gallbladder. An ultrasound study shows a prominent septa in the body (*top left*).The proximal segment fills in by 58 min (*top right*), whereas the distal segment takes 3 h to fill in the cholescintigram (*bottom*). After CCK-8, mostly the proximal segment empties, with a total ejection fraction of 31%

Tc-99m-HIDA with gallbladder bile. A large gallstone, however, may occasionally become visible within the gallbladder when most of the bile empties in response to CCK-8 (Fig. 9.2.11).

Irritable Bowel

At the end of the hepatic phase imaging (60 min), most of the bile entering the duodenum moves and collects at the ligament of Trietz, jejunum, and proximal ileum. In a patient with irritable bowel syndrome, the bile moves much more rapidly through the small and large bowel, resulting in the visualization of the distal ileum and proximal colon. Administration of CCK-8 during the gallbladder phase in such patients increases the intestinal peristalsis and moves the bile much further away, resulting in the delineation of the

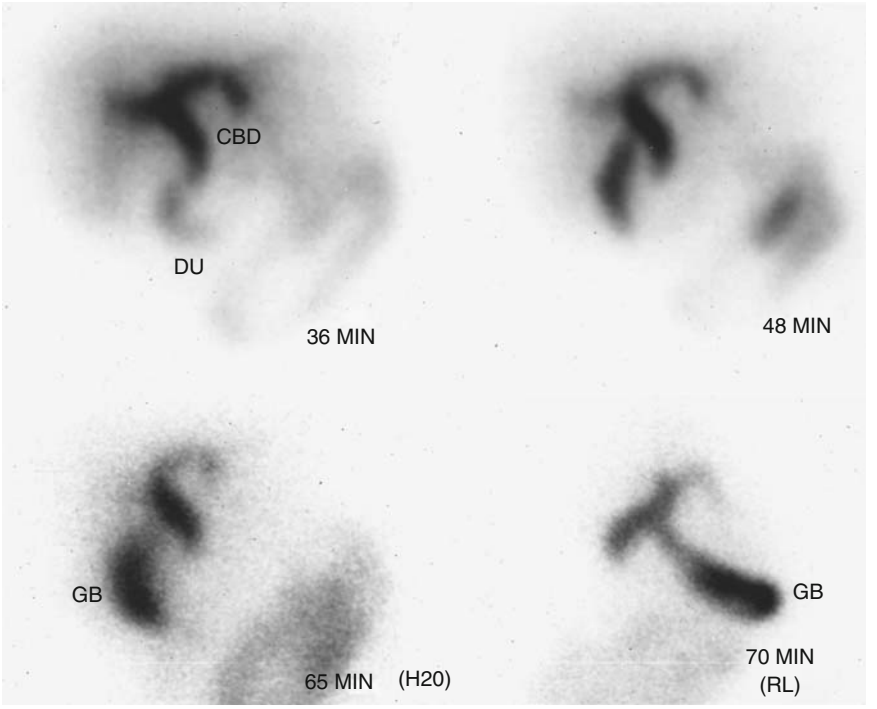

Fig. 9.2.10 Curved gallbladder. A comma-shaped gallbladder (*GB*) may mimic first part of the duodenum (*DU*). A right lateral view (*RL*) helps to visualize the long axis of the gallbladder and relationship with the common bile duct (*CBD*)

entire ascending, transverse, and descending colon. This recognition of colon appearance is essential in separating the biliary from bowel pain (Fig. 9.2.12).

Therapeutic Response to Cholecystectomy

Laparoscopic or open cholecystectomy is the most appropriate therapy for cystic duct syndrome (Table 9.2.1). Of a total of 320 patients with cystic duct syndrome who underwent cholecystectomy solely on the basis of a low ejection fraction, 287 patients (90%) had relief of pain [21–27]. Histopathological examination showed evidence of gallbladder or cystic duct disease in 285 patients (89%). Such a high therapeutic success rate, however, is not universal. One report showed pain relief in only 69% of patients with the cystic duct syndrome [28]. Recent studies have identified *Helicobacter* DNA in both bile and the gallbladder wall of patients with chronic cholecystitis, raising the possibilities of an infection as a forerunner of chronic cholecystitis and of antibiotics having a role in the treatment [29, 30]. These therapeutic options may add new dimensions to the role of quantitative functional imaging in the diagnosis and management of patients with various types of gallbladder disease [31].

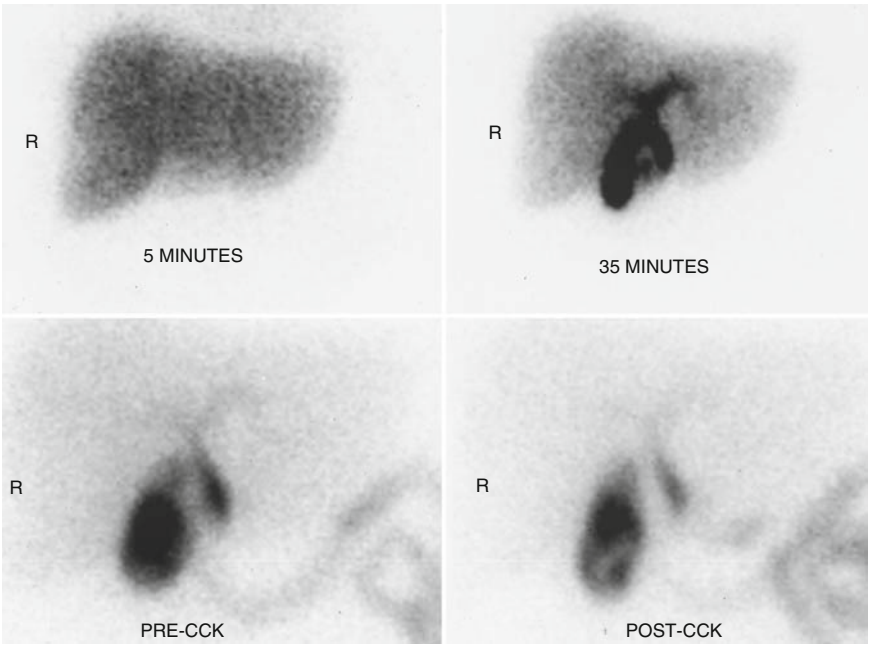

Fig. 9.2.11 Gallstone within the gallbladder. Radiolabeled hepatic bile enters the gallbladder (35 min), surrounds the gallstones, and obscures it (*pre-CCK*). The stones become obvious as a filling defect only after CCK-8-induced gallbladder emptying

Table 9.2.1 Cholescintigraphic, histopathologic, and post-cholecystectomy results in patients with cystic duct syndrome (chronic acalculous cholecystitis)

Authors [Ref]	No. of patients with pain and low EF (cholecystectomy)	No. of abnormal histopathology of the gallbladder	No. of patients with post-cholecystectomy relief of pain
Pickelman et al. [20]	19	11	18
Fink-Bennet et al. [21]	124	115	105
Zack et al. [22]	59	54	56
Misra et al. [23]	67	60	58
Halverson et al. [24]	12	10	10
Sorenson et al. [25]	11	11	11
Kleiger et al. [26]	28	26	27
Total	320	287 (90%)	285 (89%)

Standardization of Technique

In the literature, many different values have been reported for the post CCK-8 gallbladder ejection fraction. This wide variation is primarily due to differences in methodology.

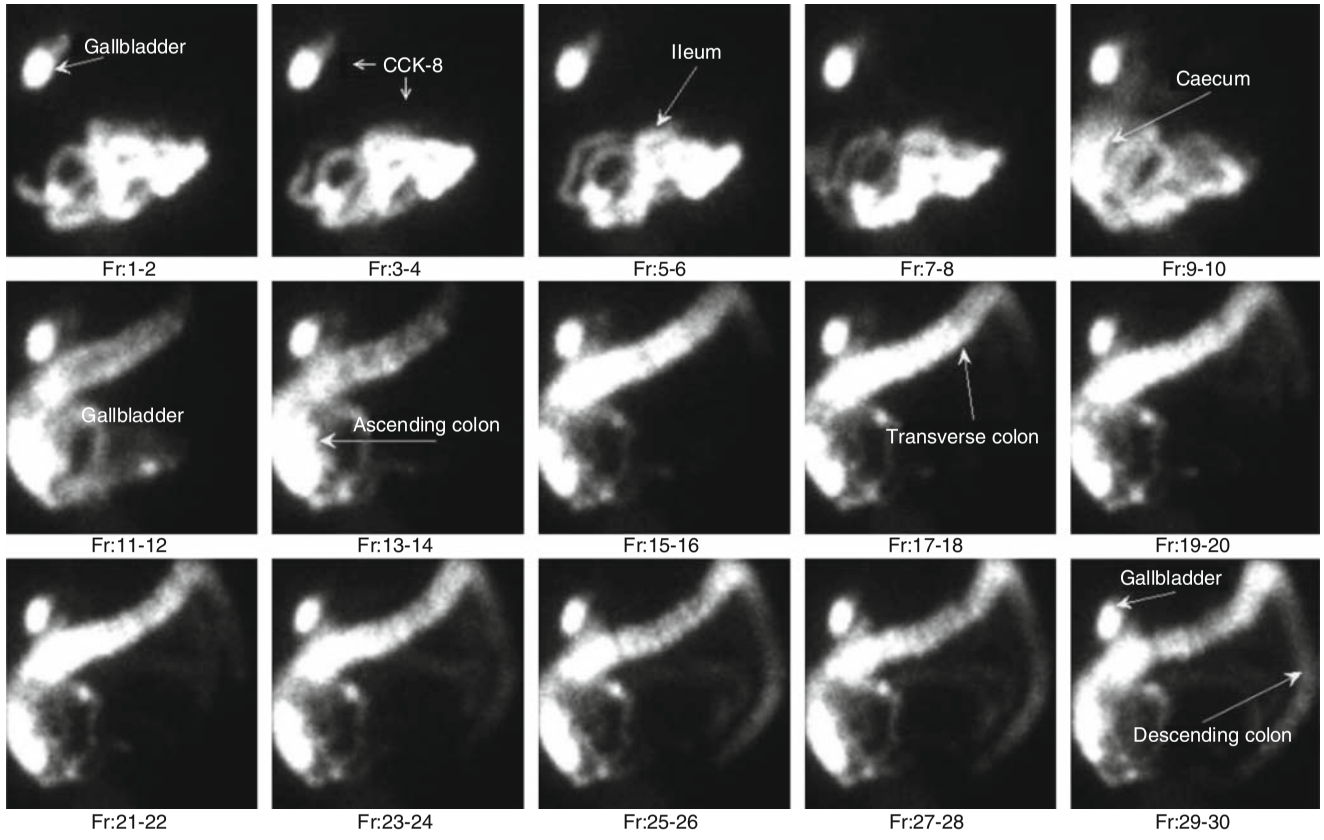

Fig. 9.2.12 Irritable bowel. Bile transit is hastened by CCK-8 infusion. The bile emptied from the gallbladder after CCK-8 mixes with rest of the intestinal bile and moves rapidly through the ascending (*AC*), transverse (*TC*), and descending colon

Variations in the dose, dose rate, and duration of infusion of CCK-8 influence the gallbladder ejection fraction. Unlike the left ventricular ejection fraction, which is controlled solely by the ventricle itself through its pace maker, the gallbladder ejection fraction can be controlled to any desired level simply by controlling the dose, dose rate, and duration of infusion of CCK-8.

The gallbladder contracts and empties bile as long as the serum cholecystokinin level is maintained above the threshold level. After cessation of CCK-8 infusion, the gallbladder emptying continues for an additional 8–12 min and then stops. The emptying resumes upon CCK-8 reinfusion. One can obtain as many as two to four sequential gallbladder ejection fractions following a single dose of Tc-99m-HIDA [14]. The CCK-8 contractile receptors in the cystic duct usually do not respond when the hormonal dose is within the physiologic limit. Large, non-physiologic doses, however, induce cystic duct contraction with subsequent non-emptying of a normal gallbladder [17]. The physiologic dose rate of cck-8 ranges from 1 to 4 ng kg^{-1} min^{-1}. A steady-state serum cholecystokinin level can be achieved for 1–2 h by continuously infusing doses as low as 0.3 ng kg^{-1} min^{-1}. A basal serum cholecystokinin level of less than 1 pmol l^{-1} raises to above 4 pmol l^{-1} by 10 min, reaches a peak level of 6.5 pmol l^{-1} by 30 min, and a steady-state level between 5 and 6 pmol l^{-1} can be maintained for as long as 70 min^{-1} by a constant infusion [16]. Infusion of a smaller dose over a longer period of time simulates postprandial CCK release and is much more effective than infusion of a larger dose as a bolus [7, 17].

References

1. Cozzolino HJ, Goldstein F, Greening RR, Wirts CW. The cystic duct syndrome. JAMA 1963;185:920–924
2. Goldstein F, Grunt R, Margulies M. Cholecystokinin cholecystography in the differential diagnosis of acalculous gallbladder disease. Am J Dig Dis 1974;19:835–849
3. Shaw MJ, Dorsher PJ, Vennes JA. Cystic duct anatomy: an endoscopic perspective. Am J Gastroenterology 1993;88:2102–2106
4. Venkataramani A, Strong RM, Anderson DS, Gilmore IT, Stokes K, Hoffman AF. Abnormal duodenal bile composition in patients with acalculous chronic cholecystitis. Am J Gastroenterol 1998;93:434–441
5. Upp JR Jr, Nealon WH, Singh P, Fagan CJ, Jonas AS, Greeley GH Jr, Thompson JC. Correlation of cholecystokinin receptors with gallbladder contractility in patients with gallstones. Ann Surg 1987;205:641–648
6. Courtney DF, Clanachan AS, Scott GW. Cholecystokinin constricts the canine cystic duct. Gastroenterology 1983;85:1154–1159
7. Krishnamurthy GT, Bobba VR, Kingston E. Optimization of octapeptide of cholecystokinin (OP-CCK) dose for gallbladder emptying. In: Raynaud C (ed). Proceedings of the Third World Congress of Nuclear Medicine and Biology. Paris, Pergamon Press, 1982, pp 2244–2247
8. Krishnamurthy S, Krishnamurthy GT. Biliary dyskinesia: role of the sphincter of Oddi, gallbladder, and cholecystokinin. J Nucl Med 1997;38:1824–1830
9. Wheeler HO. Concentrating function of the gallbladder. Am J Med 1971;51:588–595
10. Krishnamurthy GT, Krishnamurthy S. Hepatic bile entry into and transit pattern within the gallbladder lumen: a new quantitative cholescintigraphic technique for measurement of its concentration function. J Nucl Med 2002;43:901–908

11. Balon HR, Fink-Bennett DM, Brill DR, Fig LM, Freitas JE, Krishnamurthy GT, Klingensmith WC 3rd, Royal HD. Procedure guideline for hepatobiliary scintigraphy. J Nucl Med 1997;38:1654–1657
12. Krishnamurthy S, Krishnamurthy GT. Evolution of nuclear hepatology as a clinical speciality. J Nucl Med Technology 1995;24(Suppl):35S–45S
13. Keller IA, Weissman HS, Kaplun LL, freeman LM. The use of water ingestion to distinguish the gallbladder and duodenum on cholescintigraphy. Radiology 1984;152:811–813
14. Krishnamurthy GT, Bobba VR, Kingston E. Radionuclide ejection fraction: a technique for quantitative analysis of motor function of the human gallbladder. Gastroenterology 1981;80:482–490
15. Krishnamurthy GT, Bobba VR, Kingston E, Turner F. Measurement of gallbladder emptying sequentially using a single dose of Tc-99m-labeled hepatobiliary agent. Gastroenterology 1982;83:773–776
16. Toftdahl DB, Hojgaard L, Winkler K. Dynamic cholescintigraphy: induction and description of gallbladder emptying. J Nucl Med 1996;37:261–266
17. Krishnamurthy S, Krishnamurthy GT. Gallbladder ejection fraction: a decade of progress and future promise (editorial). J Nucl Med 1992;33:542–543
18. Gad MA, Krishnamurthy GT, Glowniak JV. Identification and differentiation of congenital gallbladder abnormality by quantitative Tc-99m HIDA cholescintigraphy. J Nucl Med 1992;33:431–434
19. Kramer EL, Rumancik WM, Harkavy L, Tiu S, Banner HJ, Sanger JJ. Hepatobiliary scintigraphy of the compartmentalized gallbladder. Am J Roentgenol (AJR) 1985;145:1205–1206
20. Krishnamurthy GT, Krishnamurthy S, Milleson T, Brown PH, Urstad DS. Segmentation of the gallbladder: effect on bile entry and exit and its clinical relevance in a patient with abdominal pain. Nucl Med Commun 2007;28:109–115
21. Pickelman J, Peiss RL, Henkin R, Salo B, Nagel P. The role of sincalide cholescintigraphy in the evaluation of patients with acalculous gallbladder disease. Arch Surg 1985;120:693–697
22. Fink-Bennett D, DeRidder P, Kolozsi WZ, Gordon R, Jaros R. Cholecystokinin cholescintigraphy: detection of abnormal gallbladder motor function in patients with chronic acalculous gallbladder disease. J Nucl Med 1991;32:1695–1699
23. Zech ER, Simmons LB, Kendrick RR, Soballe PW, Olcese JA, Goff WB 2d, Lawrence DPl, DeWeese RA. Cholecystokinin enhanced hepatobiliary scanning with ejection fraction calculation as an indicator of disease of the gallbladder. Surg Gynecol Obstet 1991;172:21–24
24. Misra DC Jr, Blossom GB, Fink-Bennett D, Glover JL. Results of surgical therapy for biliary dyskinesia. Arch Surg 1991;126:957–960
25. Halverson JD, Garner BA, Siegel BA, Alexander R, Edmundowicz SA, Campbell W, Miller JE. The use of hepatobiliary scintigraphy in patients with acalculous biliary disease. Arch Intern Med 1992;152:1305–1307
26. Sorenson MK, Francher S, Lang NP, Eidt JF, Broadwater JR. Abnormal gallbladder nuclear ejection fraction predicts success of cholecystectomy in patients with biliary dyskinesia. Am J Surg 1993;166:672–675
27. Klieger PS, O'Mara RE. The clinical utility of quantitative cholescintigraphy: the significance of gallbladder dysfunction. Clin Nucl Med 1998;23:278–282
28. Westlake PJ, Hershfield NB, Kelly JK, Kloiber R, Liu R, Sutherland LR, Shaffer EA. Chronic right upper quadrant pain without gallstones: does HIDA scan predict outcome after cholecystectomy? Am J Gastroenterol 1990;85:986–990
29. Fox JG, Dewhirst FE, Shen Z, Feng Y, Taylor NS, Paster BJ, Ericson RL, Lau CN, Correa P, Araya JC, Roa I. Hepatic Helicobacter species identified in bile and gallbladder tissue from Chileans with chronic cholecystitis. Gastroenterology 1998;114:755–763
30. Blaser MJ. Helicobacters and biliary tract disease. Gastroenterology 1998;114:840–841
31. Krishnamurthy S, Krishnamurthy GT. Functional imaging in nuclear hepatology. Indian J Nucl Med 1997;12:216–232

9.3 Acute Cholecystitis

Acute cholecystitis is one of the common abdominal emergencies that require immediate diagnosis and therapy. It usually presents with right upper quadrant pain, fever, and leucocytosis. Since gallstones are found in nearly 10% of all Americans, a mere association between gallstone and abdominal pain with fever cannot be equated with a diagnosis of acute cholecystitis [1, 2]. The great majority of gallstones remains silent, and only about 15–20% ever become symptomatic [3]. About 85–90% of acute cholecystitis associated with gallstones is called acute calculous cholecystitis, and the remaining 10–15% without gallstones is called acute acalculous cholecystitis [4].

Clinical Presentation

Acute cholecystitis clinically presents as right upper quadrant or epigastric pain and fever, mimicking other abdominal and lower thoracic acute emergencies (Table 9.3.1). Pain may radiate to the right shoulder, mediastinum, or lower anterior chest, mimicking an acute myocardial infarction [5]. The pain radiation to the right lower quadrant may mimic an acute appendicitis or that radiating to the left lower quadrant may mimic an acute diverticulitis. Pain is due to distension of the inflamed gallbladder wall. On deep inspiration when the liver moves downwards, the fundus of the gallbladder extends below the right costal margin and is felt as a soft mass during deep palpation. When the palpating finger touches the inflamed gallbladder wall, the patient experiences pain and abruptly stops breathing. This is called Murphy's sign.

Acute cholecystitis is three to four times more common in women than men, and the incidence increases with age. The clinical presentation of a calculous or an acalculous acute cholecystitis is very similar. A combination of fever with chills, right upper quadrant abdominal tenderness, and clinical jaundice is called Charcot triad. The triad is found more frequently when acute cholecystitis occurs in association with obstruction of the common bile duct. The place of maximum tenderness over the gallbladder fundus corresponds to the point where a line drawn between the left superior iliac spine and umbilicus meets the right costal margin when the line is extended upwards (Fig 9.3.1). This point also

Table 9.3.1 Differential diagnosis of acute cholecystitis

(1) Acute pancreatitis
(2) Acute hepatitis
(3) Gastritis
(4) Acute appendicitis
(5) Acute cholangitis
(6) Acute nephritis
(7) Angina or acute myocardial infarction
(8) Pleurisy
(9) Right lower lobe pneumonia
(10) Acute diverticulitis

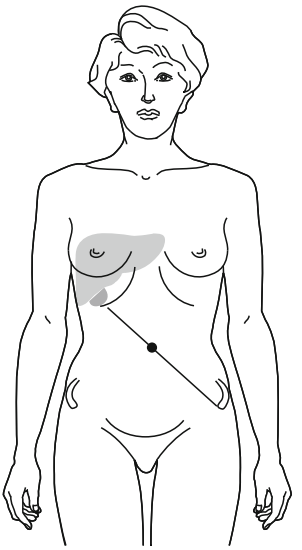

Fig. 9.3.1 Clinical location of the gallbladder fundus and Murphy's sign. A *straight line* drawn between the left anterior superior iliac spine and the umbilicus points to the fundus of the gallbladder when extended upwards to meet the right costal margin. This is also the point of Murphy's sign

corresponds to the intersection of the lateral border of the right rectus abdominus muscle with the right ninth costal cartilage. Murphy's sign is readily elicited by deep palpation at this point. Clinical presentation of acute cholecystitis is variable and mimics varieties of other abdominal diseases, and hence, clinical diagnosis alone is not reliable to plan for a definitive therapy. The accuracy of clinical diagnosis alone ranges from 45 to 77% [6].

Acute cholecystitis is usually accompanied by leucocytosis; about 75% of patients have more than 10,000 white cells dl^{-1}. Liver function tests usually remain normal, especially when the patients present early in the course of the disease. A few of the patients who present late may show a mild elevation of serum alkaline phosphatase and transaminase. An elevation of serum bilirubin indicates a complicated acute cholecystitis, such as acute cholangitis or obstruction of the common bile duct.

Pathophysiology

Macroscopic appearance of the gallbladder wall as seen directly by the surgeon just prior to cholecystectomy may reflect the true pathology much more accurately than the histopathological changes seen under the microscope after laparoscopic cholecystectomy. The microscopic findings after laparoscopic cholecystectomy may show changes secondary to tissue damage sustained during surgical manipulation and not necessarily the changes because of acute cholecystitis.

The histopathologic changes are divided into six evolving stages: (1) edema, (2) congestion, (3) focal necrosis, (4) suppuration, (5) gangrene, and (6) perforation. Edema is the earliest change initiated by infection or a gallstone impaction in the cystic duct or in Hartman's pouch. Edema leads to obstruction of the cystic duct and distension of the

gallbladder [7]. When the gallbladder distends, the stone may get dislodged and fall back into the lumen, and the pathologic changes initiated by the stone may then subside completely with spontaneous recovery. When inflammation and edema of the cystic duct continue, a full blown picture of acute cholecystitis sets in, and edema extends to involve the rest of the gallbladder wall. Either wall edema or stone or a combination of both is the most common cause of obstruction of the cystic duct, which prevents entry of hepatic bile into the gallbladder, resulting in its non-visualization in a Tc-99m-HIDA study [8]. Acute inflammation increases the vascularity of the gallbladder wall and infiltration with inflammatory cells: neutrophils and monocytes during the acute phase and lymphocytes as it enters the subacute phase. Edema and infiltration with inflammatory cells produce thickening of the gallbladder wall, which is seen with ultrasonography [9].

As the focal necrosis progresses and becomes more diffuse, it may lead to the development of suppuration and abscess formation. Inflammation from the superior gallbladder wall, which lies in direct contact with the liver, often spreads to the adjoining liver tissue and causes edema and pericholecystic fluid collection, manifesting a "rim sign" of acute cholecystitis on cholescintigraphy [10]. When the necrosis becomes diffuse, the pain receptors often lose their sensation and produce a negative Murphy's sign. A negative Murphy's sign, therefore, is an ominous feature and calls for an immediate therapeutic intervention. Necrosis leads to ulceration and occasional perforation and bile leak. Due to its faraway location from the entrance of the cystic artery, the fundus is more vulnerable to ischemic necrosis, rupture, and bile leak than the body and neck. When the diagnosis and treatment of acute cholecystitis are delayed, the incidence of perforation and bile peritonitis increases to as high as 12% [11].

Cholescintigraphic Approach

The patient should fast for a minimum of 4 h, preferably for 8–10 h, but not more than 24 h. Serum endogenous cholecystokinin reaches its lowest level during fasting, which promotes a maximum increase in the tone of the sphincter of Oddi and maximum relaxation of the gallbladder wall. A wide basal pressure difference between these two structures during fasting promotes preferential bile entry into the gallbladder when the cystic duct is patent, and Tc-99m-HIDA simply follows the path taken by the hepatic bile [12, 13].

Hepatic Phase Imaging

With the patient in the supine position, a large field of view dual-head gamma camera fitted with a low-energy all-purpose collimator is positioned anteriorly and posteriorly over the upper abdomen to cover the entire liver. In patients with a normal bilirubin level, a dose of 2–3 mCi (74–111 MBq) Tc-99m-HIDA is injected intravenously, and the data are acquired at 1 frame/minute for 60 min. Hypervascularity of the acutely inflamed gallbladder wall can be demonstrated by obtaining a radionuclide perfusion study by collecting the first minute data at 1 frame per 2 s [14]. A higher dose (3–6 mCi or 111–222 MBq) is needed when a perfusion study is desired. After completion of 60 min data collection, the images

are viewed in cine mode display and reformatted at 2 frames/image and recorded on X-ray film for interpretation.

Delayed Imaging vs. Morphine Administration

Two options are available when the gallbladder is not seen by 60 min (during hepatic phase imaging) in a patient with clinically suspected acute cholecystitis. One option is to choose a delayed imaging protocol by obtaining images at 3–4 h after injection of Tc-99m HIDA, some times even at 24 h. The other option is to administer morphine (0.04 mg kg^{-1}) intravenously at 60 min and take images immediately for an additional 30 min (total imaging time 90 min). In both cases, a second dose of Tc-99m-HIDA (1–3 mCi) is administered if the radiotracer from the first dose clears almost completely from the liver by 60 min.

The diagnostic sensitivity, specificity, and accuracy of cholescintigraphy using the delayed imaging protocol vary from 92 to 100% [15–20]. A mean sensitivity of 97%, specificity of 96%, and accuracy of 97% have been reported from a total of 1,426 patients from six reports (Table 9.3.2). The major disadvantage of the delayed imaging protocol is that it simply delays the diagnosis and hence the therapy.

Morphine Dose

The most popular imaging protocol for suspected acute cholecystitis is to administer morphine intravenously at 60 min if the gallbladder is not seen by then. Morphine acts immediately on the sphincter of Oddi and raises the sphincter pressure by increasing the frequency and amplitude of phasic waves [21]. The usual dose of morphine is 0.04 mg kg^{-1}, infused intravenously over 1 min. A standard 70-kg weight patient would require a minimum total dose of 2.8 mg. Since morphine sulfate for intravenous use is packaged in a 2-mg unit dose, it is convenient to dispense a 4-, 6-, or 8-mg dose for adults. When the cystic duct is patent, morphine increases the sphincter of Oddi pressure and forces the hepatic bile entry the gallbladder [22–30]. Hepatic bile does not enter the gallbladder, despite

Table 9.3.2 Sensitivity, specificity, and accuracy of Tc-99m –HIDA cholescintigraphy in the diagnosis of acute cholecystitis by using a delayed imaging protocol (without using morphine)

Authors (Ref.)	No. of patients	Sensitivity (%)	Specificity (%)	Accuracy (%)
Fonseca et al. [15]	113	100	100	100
Freitas et al. [16]	186	97	87	94
Matolo et al. [17]	619	92	97	95
Mauro et al. [18]	95	100	94	96
Szlabick et al. [19]	117	100	98	99
Weissman et al. [20]	296	95	99	98
Total	1,426	97%	96%	97%

morphine, if the cystic duct is obstructed, as is the case in patients with acute cholecystitis. A sensitivity of 96% and a specificity of 94% have been shown with the morphine protocol (Table 9.3.3). The major advantage of intravenous morphine is that it enables an early diagnosis, usually within 90 min, allowing the referring physician to plan for an appropriate therapy strategy immediately. The disadvantage of intravenous morphine is its central sedation. Caution is exercised while giving morphine to outpatients, and the patient is instructed not to drive for at least 8–10 h after receiving morphine.

Scintigraphic Features of Acute Cholecystitis

Obstruction of the cystic duct is the salient pathophysiologic feature of acute cholecystitis (Fig. 9.3.2A). The most common cause of cystic duct obstruction is edema of the wall [7, 8]. Gallstones, which may initiate inflammation, often fall back into the lumen when the gallbladder distends, but the edema continues. A diagnostic test that establishes the status of the cystic duct (patency or obstruction), therefore, carries a much higher sensitivity and specificity than other morphology imaging modalities that only show gallstones, wall thickening, or pericholecystic fluid collection as indicators of acute cholecystitis (Fig. 9.3.2B). Documentation of the cystic obstruction in an appropriate clinical setting confirms the diagnosis of acute cholecystitis with a high degree of certainty [31]. Hypervascularity of an acutely inflamed gallbladder wall is seen in 72% of patients with acute cholecystitis and can be shown by including a Tc-99m-HIDA perfusion study as a part of the imaging protocol. Hypervascularity of the wall correlates with the severity of acute cholecystitis [14, 32].

Pericholecystic Hepatic Retention of Tc-99m-HIDA or "Rim Sign"

An acute inflammation along the superior gallbladder wall often spreads to the adjoining liver parenchyma, causing focal hepatitis where pericholecystitic hepatocytes show a

Table 9.3.3 Sensitivity and specificity of Tc-99m HIDA cholescintigraphy in the diagnosis of acute cholecystitis with morphine augmentation

Authors (Ref.)	Sensitivity	Specificity
Choy et al. [22]	23/24 (96%)	35/35 (100%)
Kim et al. [23]	11/11 (100%)	18/18 (100%)
Keslar et al. [24]	19/19 (100%)	12/12 (100%)
Mehta et al. [25]	18/18 (100%)	13/13 (100%)
Vasquez et al. [26]	10/10 (100%)	22/26 (85%)
Fig et al. [27]	12/12 (100%)	14/17 (96%)
Kistler et al. [28]	13/14 (93%)	14/18 (78%)
Fink-Bennett et al. [29]	35/36 (97%)	115/117 (98%)
Kim et al. [30]	24/28 (86%)	15/17 (88%)
Total	165/172 (96%)	258/273 (94%)

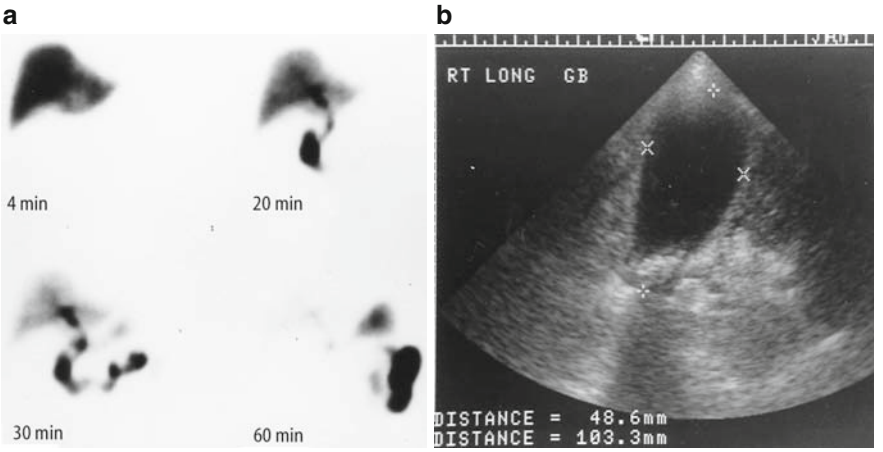

Fig. 9.3.2 Acute cholecystitis. Cholescintigraphic non-visualization of the gallbladder due to obstruction of the cystic duct is the most characteristic feature. Liver shows normal uptake excretion and the bile enters the duodenum (**a**). Ultrasound shows gallstones in the neck and thickening of the gallbladder wall (**b**)

normal pattern of uptake, but a delayed excretion of Tc-99m-HIDA relative to the hepatocytes far away from the gallbladder, manifesting a thin strip of increased radioactivity along the gallbladder fossa in the late images (Fig. 9.3.3A). This is called a "rim sign" [33]. The spread of infection from the gallbladder wall into the adjacent liver tissue takes place via a special set of bile ducts called the "aberrant ducts of Luschka" [34]. These aberrant ducts connect the pericholecystic hepatocytes with the adventia of the gallbladder wall where they end blindly (Fig. 9.3.3B). An increase in intraluminal pressure because of inflammation produces pseudo-diverticulum in the gallbladder wall. Microorganisms from the superior gallbladder wall travel along these aberrant channels and pseudo-diverticulum and infect the hepatocytes and Kupffer cells of liver parenchyma.

On histopathological examination, the liver tissue from the rim sign region shows edema, sinusoidal congestion, hyperplasia of Kupffer cells, and obliteration of the canalicular lumen, impeding bile flow from the rim sign region [35]. Rim sign is found in 34–60% of patients with acute cholecystitis. Despite a strong positive predictive value, the rim sign alone does not carry a high enough specificity for acute cholecystitis to terminate cholescintigraphy at 60 min when the gallbladder is not seen. Morphine augmentation is necessary to increase the sensitivity, specificity, and overall diagnostic certainty (Table 9.3.3) before planning for a definitive therapeutic strategy [36]. Gangrene, abscess, and perforation of the gallbladder wall with bile leak are some of the complications of acute cholecystitis [37, 38]. Among patients with a definite rim sign, the frequency of complication is often as high as 45%. A gangrenous acute cholecystitis on the ultrasound study shows an edematous wall with thick sludge or pus within the gallbladder (Fig. 9.3.4).

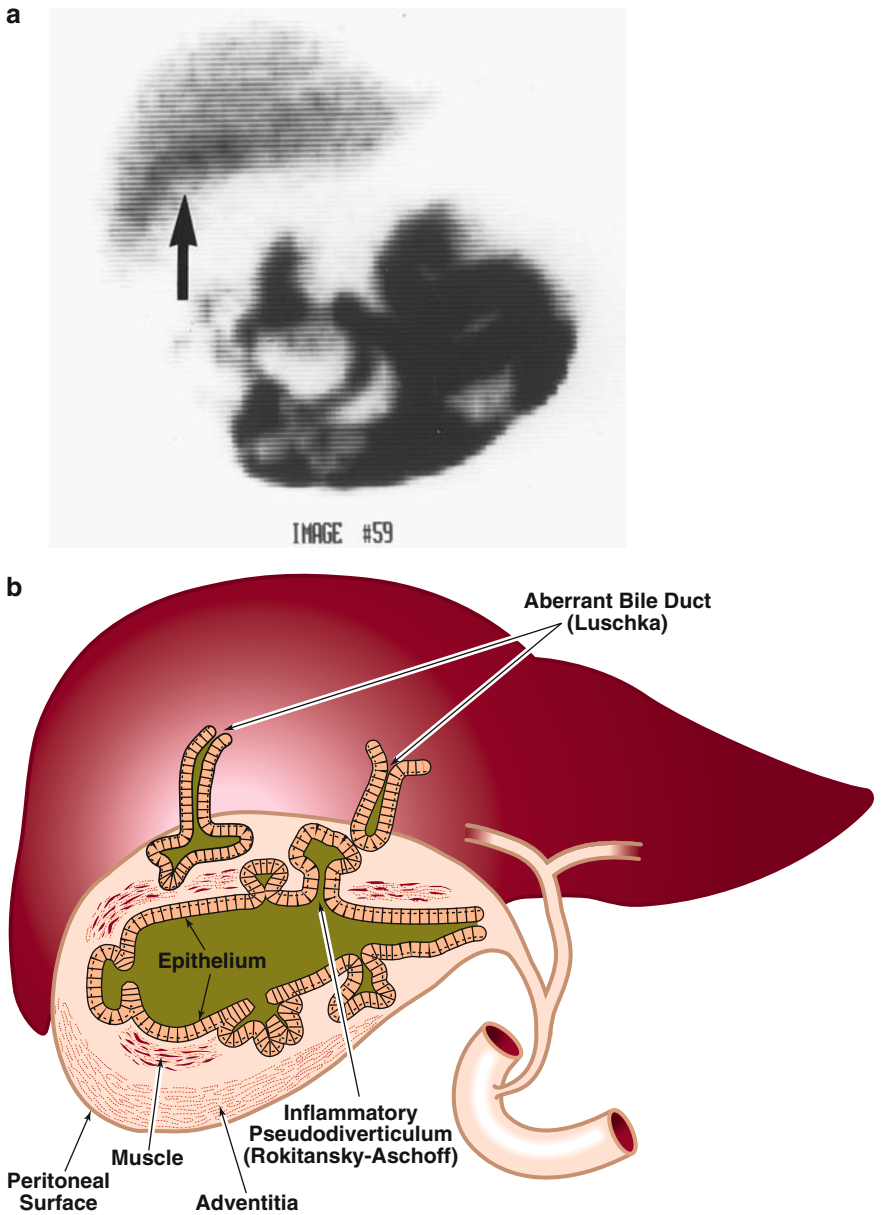

Fig. 9.3.3 Rim sign of acute cholecystitis. Hepatocytes adjacent to the superior gallbladder wall show normal uptake, but a delayed excretion of Tc-99m-HIDA, resulting in a thin rim of increased radioactivity (*arrow*) along the gallbladder fossa (**a**). The gallbladder infection spreads to the liver via the aberrant bile ducts (Luschka) and inflammatory pseudo diverticulum (**b**), which end blindly in the adventia of the gallbladder wall [34]

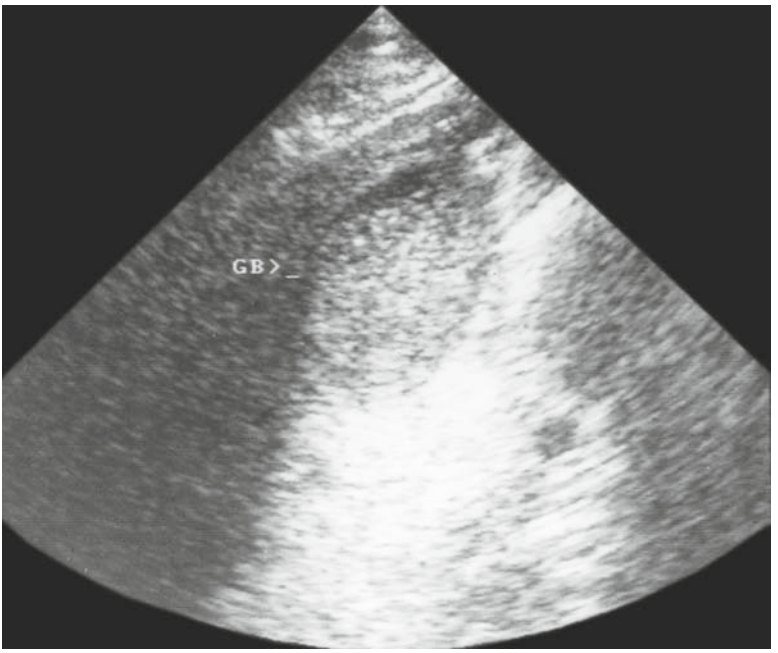

Fig. 9.3.4 Gangrenous acute cholecystitis. Ultrasound shows edematous gallbladder wall, and the lumen contains hyper-echoic pus or bile sludge

Gallbladder Pre-Emptying with CCK

Some advocate intravenous cholecystokinin with the notion that pre-emptying, prior to cholescintigraphy, facilitates rapid gallbladder filling when the cystic duct is patent. Administration of cholecystokinin prior to cholescintigraphy is counterproductive physiologically as it creates conditions that are just the opposite of what is required for diversion of hepatic bile into the gallbladder. By stimulating contraction of the gallbladder and relaxation of the sphincter of Oddi, cholecystokinin promotes free bile flow directly into the duodenum (Chap. 6). Comparison of studies with and without CCK-8 pre-emptying shows a much lower specificity for studies obtained with a CCK-8 pre-emptying protocol. The specificity of cholescintigraphy without CCK-8 pre-emptying is 94%, in contrast to 81% with a CCK-8 pre-emptying protocol. Pre-emptying with CCK-8, however, does not alter the sensitivity (94%) of cholescintigraphy [39]. In a study of 86 patients using a CCK-8 pre-emptying protocol, the gallbladder did not visualize by 60 min in 43 patients. In 18 of these 43 patients, the gallbladder filled in only after the use of intravenous morphine, indicating the necessity of maximizing the tonus of the sphincter of Oddi prior to cholescintigraphy [40]. Pre-emptying is appropriate in patients on hyperalimentation or those who have waited for longer than 24 h (Fig. 9.3.5).

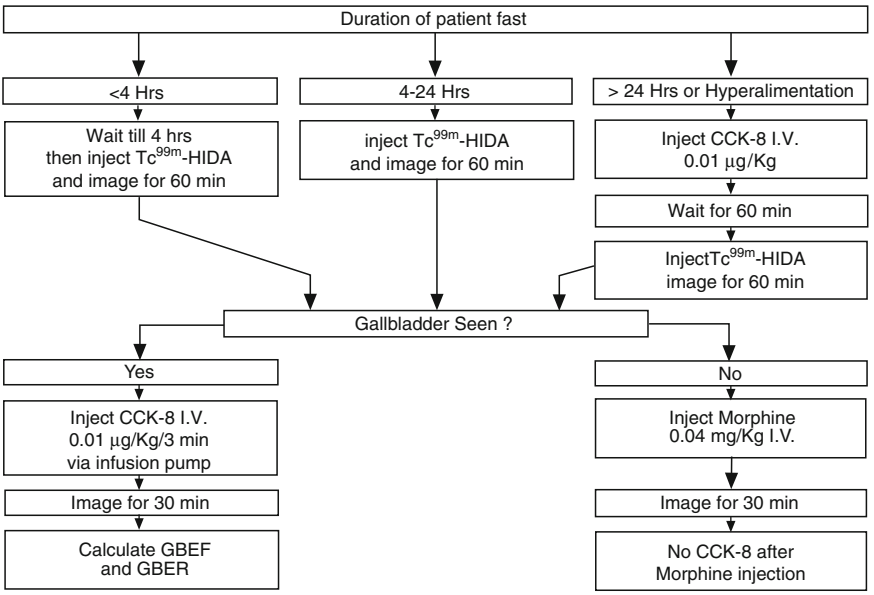

Fig. 9.3.5 Protocol for Tc-99m-HIDA study. Four-hour fasting is the minimum, 8–10 h is ideal, and more than 24 h fasting should be avoided. Morphine or CCK-8 use depends upon the clinical situation at hand

The decision as to when to use morphine vs. cholecystokinin is dependent upon the clinical challenge at hand. Administration of morphine is appropriate in a clinical setting of acute cholecystitis, and its use is inappropriate in a clinical setting of biliary dyskinesia. Administration of cholecystokinin, on the other hand, is appropriate in a clinical setting of biliary dyskinesia, but not in patients with acute cholecystitis [39]. Rarely, there is a need to use both agents sequentially in a given patient [41, 42].

Cholangitis

The superior gallbladder wall not covered by the peritoneum lies directly against the inferior surface of the liver (the bare area). The aberrant ducts of Luschka and inflammatory pseudo-diverticulum serve as the shortest and most direct route for spreading infection from the gallbladder wall to the biliary canaliculi and hepatocytes (Fig. 9.3.3B). The microorganisms responsible for acute cholecystitis travel along these aberrant ducts and cause acute cholangitis. Clinically acute cholangitis is suggested by the onset of the Charcot triad of fever and chills accompanied by gallbladder tenderness and jaundice in the absence of obstruction of the common bile duct. The characteristic features of a combined acute cholecystitis and acute cholangitis on cholescintigraphy include non-visualization of the gallbladder (despite morphine), delayed clearance of Tc-99m-HIDA from the entire liver (intrahepatic cholestasis), leucocytosis, right upper quadrant pain, fever, and

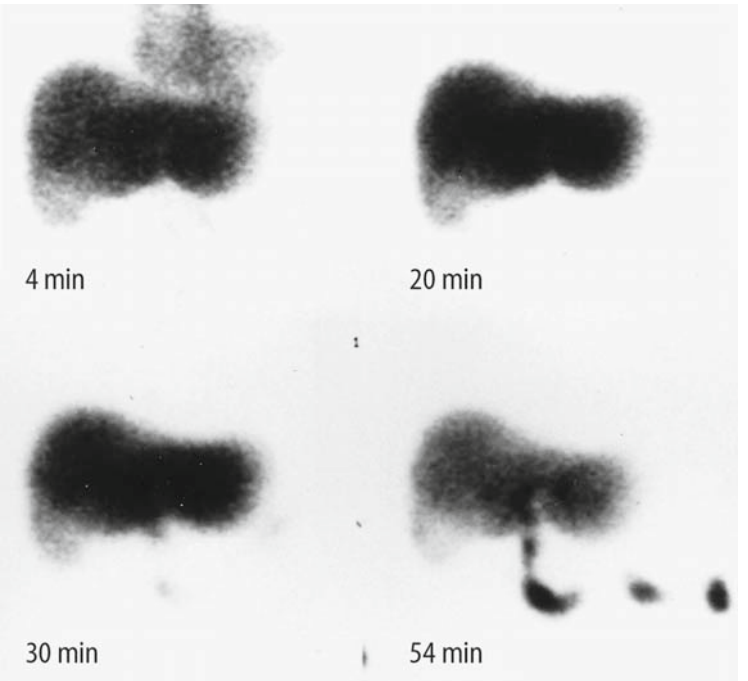

Fig. 9.3.6 Acute cholecystitis and acute cholangitis. The gallbladder is non-visualized, and there is diffuse retention of Tc-99m HIDA by the liver parenchyma. Rim sign is absent, and bile enters the duodenum

jaundice (Fig 9.3.6). Rim sign is typically absent due to diffuse retention of Tc-99m-HIDA by the liver, not just by the pericholecystic hepatocytes.

Differential Diagnosis of Acute Cholecystitis

Many diseases are to be considered in the differential diagnosis in any patient who presents clinically with abdominal pain, fever, and leucocytosis (Table 9.3.1). Pain due to a right renal stone is colicky in nature and very severe in intensity when compared to pain of acute cholecystitis, which tends to be of moderate intensity. A renal stone often causes hematuria as it passes through the ureter. The pain due to viral hepatitis is mild in intensity and is accompanied by abnormal liver function tests. The viral hepatitis profile confirms the diagnosis. Acute pancreatitis and acute cholecystitis often coexist. Non-visualization of the gallbladder in association with a rise in serum amylase or lipase indicates the co-existence of acute cholecystitis and acute pancreatitis [43, 44]. A peptic ulcer may cause epigastric pain mimicking cholecystitis. Infection with *Helicobacter pylori* is now the most common cause of peptic ulcer. These bacteria produce the enzyme urease that splits C-14 labeled urea in the stomach and liberates C-14-labeled carbon dioxide, which is eliminated in the expired breath. A positive C-14 urea breath test confirms active *H. pylori* infection.

Gallbladder pain radiation upwards into the chest and shoulder may mimic an anginal pain. An abnormal electrocardiogram, elevation of cardiac enzymes, or abnormal Tc-99m pyrophosphate myocardial image helps confirm a cardiac origin of acute pain. A thorough clinical evaluation along with the measurement of an appropriate biochemical profile aids the primary care physician in requesting the most appropriate imaging test to either confirm or rule out each diagnostic possibility.

Comparison of Cholescintigraphy and Ultrasound

Immediately after the introduction of Tc-99m-HIDA agents in 1976 and up until 1984, most cholescintigraphic studies were carried out with the first-generation agents using a delayed imaging protocol, which often delayed diagnosis, sometimes for up to 24 h. The diagnostic time interval using the current generation Tc-99m-HIDA agents is now reduced to less than 90 min by administering morphine intravenously at 60 min when the gallbladder is not seen in a patient with suspected acute cholecystitis. A meta-analysis of 2,466 patients from 30 reports revealed cholescintigraphy as the test of choice for acute cholecystitis and ultrasound for cholelithiasis [45]. For acute cholecystitis, the cholescintigraphic sensitivity is 97% (95% confidence interval, 0.96–0.98) and specificity 90% (95% confidence interval, 0.86–0.95). Morphine administration shortens the diagnostic time interval, but does not alter the sensitivity or specificity when compared to delayed imaging protocols (Tables 9.3.2 and 9.3.3). Adjusted sensitivity of ultrasound for acute cholecystitis is 88% (95% confidence interval, 0.74–1.0) and specificity 80% (95% confidence interval, 0.62–0.98). Adjusted sensitivity for detection of cholelithiasis with the ultrasound is 84% (95% confidence limit, 0.76–0.92) and adjusted specificity is 99% (95% confidence interval, 0.97–1.0). Since the salient pathophysiology of acute cholecystitis is cystic duct obstruction, cholescintigraphy, which establishes the status of the cystic duct (patency or obstruction), is much more reliable than ultrasound or CT, both of which depend upon wall thickening as an indicator of acute cholecystitis.

Application of Baye's Analysis

Clinical diagnosis is often a probability estimate based on the frequency of the disease in the study population. Because it is impossible to study the entire population, the estimates are made from studies comprising a limited number of samples from the population at risk. After the clinical examination, a clinician makes a rough estimate of the disease probability (pre-test probably) based on the frequency of that disease found in that particular population. Imaging tests are requested either to confirm the clinical diagnosis or rule out the disease from consideration with a high degree of certainty. The clinicians feel more comfortable to proceed with a definitive therapeutic strategy after confirmation of acute cholecystitis by an imaging procedure. When the clinical diagnosis is not confirmed by the imaging test, then the clinicians have the option of accepting the results of the imaging test as final or ignore it completely and obtain additional diagnostic tests.

Most imaging procedures are interpreted subjectively, and they provide a dichotomous result in the form of either the disease being present or absent. The probability of a disease being present or absent after an imaging test (post-test probability) depends upon various factors, including the sensitivity, specificity, false-positive, and false-negative ratio of the test, and the prevalence of the disease in the study population. Probabilities are assessed by applying Bayesian analysis [46, 47]. After conducting a thorough clinical evaluation and obtaining a basic biochemical profile, the clinician arrives at a tentative clinical diagnosis and then chooses one of the diagnostic imaging tests for confirmation. In the case of acute cholecystitis, Tc-99m-HIDA cholescintigraphy and ultrasound are two of the most common imaging options, and the clinician may decide to choose either one or both for confirmation.

Target Disease

	Target disease	
Test Result	Present	Absent
Positive	a	b
Negative	c	d

<<Probability of acute cholecystitis when the imaging test is positive or negative is given by the following formulas.

$$\text{Probability of acute cholecystitis when the testispositive (abnormal)} = \frac{\left[\begin{array}{c}\text{Sensitivity} \times \text{Prevalence of acute}\\ \text{cholecystitis in the study population}\end{array}\right]}{\left[\begin{array}{l}\text{Sensitivity} \times \text{Prevalence}\\ \text{of acute cholecystitis}\\ \text{in the study population}\end{array}\right] + \left[\begin{array}{l}\text{Falsepositive}\\ \text{fraction} \times \text{Prevalence of no acute}\\ \text{cholecystitis in the study}\\ \text{population}\end{array}\right]}$$

$$\text{Probability of acute cholecystitis when the testis negative (normal)} = \frac{\left[\begin{array}{c}\text{False-negative fraction} \times \text{Prevalence of acute cholecystitis in the}\\ \text{study population}\end{array}\right]}{\left[\begin{array}{l}\text{False-negativefraction} \times \text{prevalence}\\ \text{of acute cholecystitis}\\ \text{in the study population}\end{array}\right] + \left[\begin{array}{l}\text{Specificity} \times\\ \text{Prevalence of no}\\ \text{acute cholecystitis in}\\ \text{the study population}\end{array}\right]}$$

Pre-test probability (prevalence): The proportion of patients who have the target disease, as determined before the test is carried out = a + c/a + b + c + d.

Post-test probability: The proportion of patients with the target disease with a positive test.

Likelihood ratio (LR): It is the ratio of the probability of a test result among the patients with the target disease to the probability of the same test result among patients who do not have the target disease.

The likelihood ratio for a positive test = sensitivity/1-specificity.

The likelihood ratio for a negative test = 1–sensitivity/specificity

After knowing the pre-test (clinical evaluation) and post-test (after an imaging procedure) probability, the clinicians can calculate the Bayes factor or likelihood ratio of the target disease prior to subjecting the patient to a definitive therapy. The Bayes factor is considered more objective and can substitute for a *p* value of a null hypothesis [48, 49]. By referring to the nomogram (Fig 9.3.7), the post-test likelihood ratio is obtained directly without need for an actual calculation [50, 51]. The likelihood ratio corresponds to the

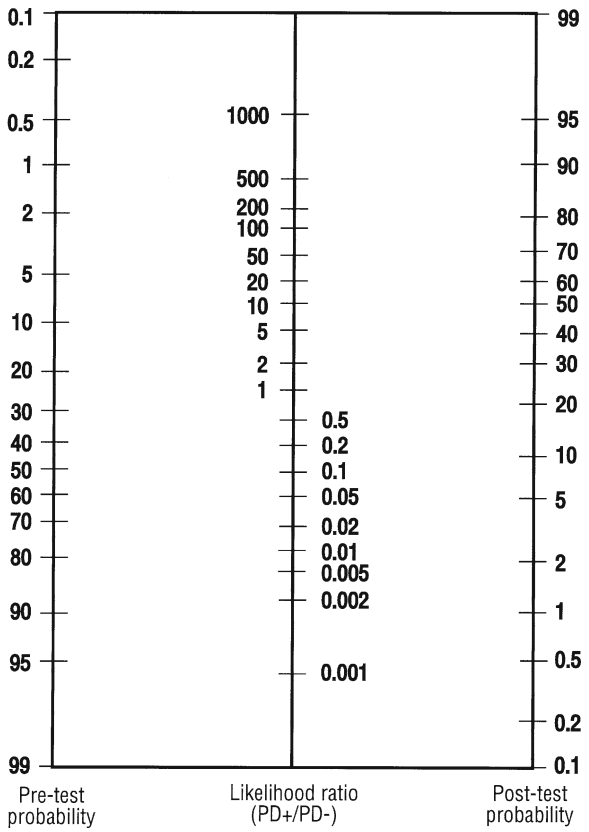

Fig. 9.3.7 Nomogram for likelihood ratio. A *line* drawn between the pre-test (clinical diagnosis) and post-test (after imaging test) probability intersects the *line* in the middle and indicates the likelihood ratio [51]

point where a straight line drawn between the pre-test probability and post-test probability intersects the likelihood ratio line in the middle. Let us assume that in a patient with right upper quadrant pain and fever, the pre-test probability of acute cholecystitis (after the clinical examination) is 20%. If the gallbladder is not visualized in a Tc-99m-HIDA study (97% sensitivity), the likelihood ratio of acute cholecystitis is approximately 200. The cost effectiveness of a positive (GB not seen) Tc-99m HIDA test is greater when the pre-test probably is lower, and the cost effectiveness decreases as the pre-test probably increases to a very high level.

The discriminating power of a test is the difference in post-test probability between a positive (gallbladder not seen) and a negative test (gallbladder seen) for acute cholecystitis [31]. The wider the difference between positive and negative tests, the greater is the discriminating power (Fig. 9.3.8). Cholescintigraphy, which establishes the patency or obstruction of the cystic duct (the basic pathology of acute cholecystitis), provides a much better discriminating power than ultrasound. Ultrasound, which detects gallstones and thickness of the gallbladder wall but does not establish the status of the cystic duct, therefore, provides a much lower discriminating power for acute cholecystitis (Fig. 9.3.9). The discriminating power of a test works at its best when the prevalence of disease in the study population is around 50%. The discriminating power decreases precipitously when the prevalence is below 20% or above 80% [31].

Application of Baysian analysis requires the establishment of true sensitivity and specificity of an imaging test. The ultimate diagnosis of acute cholecystitis, however, is based upon the histopathological criteria chosen by the pathologist. Some pathologists are satisfied with the mere presence of transmural inflammation of the gallbladder wall, while others insist upon the presence of hemorrhage and necrosis before assigning the definitive diagnosis of acute cholecystitis. The best combination of sensitivity and specificity for cholescintigraphy is obtained when the presence of any one of the above two histological criteria is chosen as the basis for the diagnosis of acute cholecystitis [52]. Under an appropriate clinical setting, most clinicians are satisfied with the cholescintigraphic documentation of cystic duct obstruction as sufficient evidence for the diagnosis of acute cholecystitis in planning for a definitive therapy.

Acute Acalculous Cholecystitis

Clinically, it presents very similarly to acute calculous cholecystitis, but has few unique clinical features of its own. The patients are usually much older and have additional risk factors, such as a recent surgery, crush injury, burns, sepsis, or hyperalimentation. About 10–15% of all acute cholecystitis belongs to the acalculous variety. The incidence of acute acalculous cholecystitis appears to be increasing recently, which may be attributed to increased clinical awareness and sensitivity of the diagnostic tests [53]. The morbidity and mortality of acute acalculous cholecystitis are much higher than in acute calculous cholecystitis. As obstruction of the cystic duct is common for both conditions, the diagnostic sensitivity of cholescintigraphy is similar for both calculous and acalculous acute cholecystitis [54, 55]. Edema (and not the stone) as the primary cause of cystic duct obstruction is easy to appreciate in the case of acute acalculous cholecystitis, as there are no gallstones associated with it.

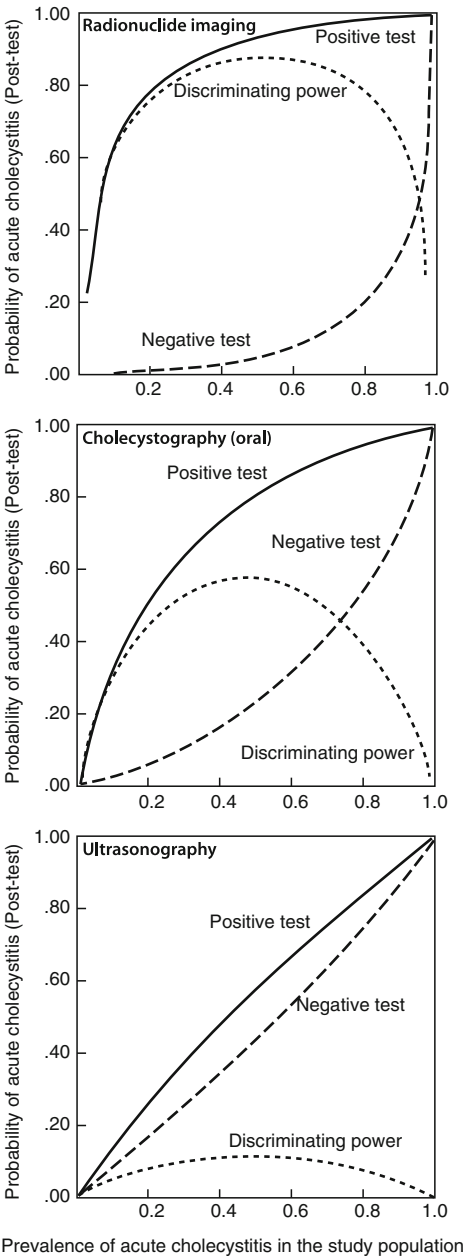

Fig. 9.3.8 Relative merits of imaging tests for acute cholecystitis. Radionuclide imaging (cholescintigraphy) and oral cholecy-stogram, which establish the status of the cystic duct, show a wider difference between a positive (cystic duct not patent) and negative test (cystic duct patent) when compared to ultrasound, which shows only gallstones and wall thickening

Gallbladder Cancer

Gallbladder cancer is a relatively rare, but highly lethal disease. In the United States, about 7,100 new cases per year are found, and 3,500 deaths are attributed to it annually [56]. There are no specific symptoms that draw special attention, and the majority of cancers are

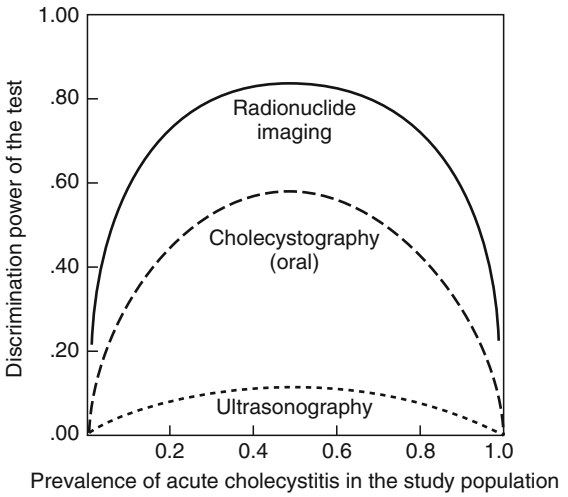

Fig. 9.3.9 Discriminating power. The difference between a positive (gallbladder not seen) and a negative test (gallbladder seen) probability is the discriminating power of the diagnostic test. A positive cholescintigraphy and oral cholecystography in an appropriate clinical setting confirm acute cholecystitis. A negative test (gallbladder seen) rules out acute cholecystitis. Ultrasound shows the least discriminating power for acute cholecystitis [31]

advanced at the time of diagnosis. Many are discovered incidentally during microscopic examination of the gallbladder specimen submitted after a routine cholecystectomy for a benign cause (gallstone). Adenocarcinomas account for 80–95% cases, and the rest include squamous cell and undifferentiated or anaplastic type. Cholecystectomy is the initial therapy, but prognosis is poor [57]. The role of chemotherapy and/or radiation therapy is not well established.

References

1. Ingelfinger FJ. Digestive diseases as a national problem. Gallstones. Gastroenterology 1968;55:102–104
2. Friedman GD, Kannel WB, Dawber TR. The epidemiology of gallbladder disease: observations in the Framingham Study. J Chronic Dis 1966;19:273–292
3. Gracie WA, Ransohoff DF. The natural history of silent gallstones: the innocent gallstone is not a myth. N Engl J Med 1982;307:798–800
4. Pelligrini CA, Way LW. Acute cholecystitis. In: Way LW, Pelligrini CA (eds). Surgery of the gallbladder and bile ducts. WB Saunders, Philadelphia, 1987, pp 251–264
5. Ryan ET, Pak PH, DeSanctis RW. Myocardial infarction mimicked by acute cholecystitis. Ann Intern Med 1992;116:218–220
6. Freitas JE, Fink-Bennet DM, Thrall JH, Resinger WW, Calderon HC, Mirkes SH, Shah PK. Efficacy of hepatobiliary imaging of acute abdominal pain: concise communication. J Nucl Med 1980;21:919–924
7. Schein CJ. Acute cholecystitis. Harper and Row, New York, 1972
8. Eikman EA, Cameron JL, Colman M, Natarajan TK, Dugal P, Wagner HN, Jr. A test for patency of the cystic duct in acute cholecystitis. Ann Intern Med 1975;82:318–322

9. Handler SJ. Ultrasound of gallbladder wall thickening and its relation to cholecystitis. AJR Am J Roentgenol 1979;132:581–585
10. Brachman MB, Tanasescu DE, Ramanna L, Waxman AD. Acute gangrenous cholecystitis: radionuclide diagnosis. Radiology 1984;151:209–211
11. Ranson JHC. Perforation of the gallbladder. In: Way LW, Pelligrini CA (eds). Surgery of the gallbladder and bile ducts. WB Saunders, Philadelphia, 1987, pp 265–273
12. Krishnamurthy S, Krishnamurthy GT. Evolution of nuclear hepatology as a clinical subspeciality. J Nucl Med Technol 1995;23(Suppl):35S–45S
13. Wheeler HO. Concentrating function of the gallbladder. Am J Med 1971;51:588–595
14. Colletti PM, Ralls PW, Siegel ME, Halls JM. Acute cholecystitis: diagnosis with radionuclide angiography. Radiology 1987;163:615–618
15. Fonseca C, Greenberg D, Rosenthall L, Arzoumanian A. Assessment of the utility of gallbladder imaging with 99m-Tc-IDA. Clin Nucl Med 1978,3:437–441
16. Freitas JE, Gulati MD. Rapid evaluation of acute abdominal pain by hepatobiliary scanning. JAMA 1980;244:1585–1587
17. Matolo NM, Stadalnik RC, Dixon SM. Value and limitations of scanning of the biliary tract. Surg Gynecol Obstet 1980;150:521–524
18. Mauro MA, McCartney WH, Melmud JR. Hepatobiliary scanning with 99m-Tc-PIPIDA in acute cholecystitis. Radiology 1982;142:193–197
19. Szlabick RE, Catto JA, Fink-Bennett D, Ventura V. Hepatobiliary scanning in the diagnosis of acute cholecystitis. Arch Surg 1980;115:540–544
20. Weissmann HS, Badia J, Sugarman LA, Kluger L, Rosenblatt R, Freeman LM. Spectrum of 99m-Tc-IDA cholescintigraphic patterns in acute cholecystitis. Radiology 1981;138:167–175
21. Helm JF, Venu RP, Geenen JE, Hogan WJ, Dodd WJ, Toouli J, Arndorfer RC. Effects of morphine on the human sphincter of Oddi. Gut 1988;29:1402–1407
22. Choy D, Shi EC, McLean RG, Hoschl R, Murray IP, Ham JM. Cholescintigraphy in acute cholecystitis: use of intravenous morphine. Radiology 1984;151:203–207
23. Kim EE, Pjura G, Lowry P, Nguyen M, Pollack M. Morphine-augmented cholescintigraphy in the diagnosis of acute cholecystitis. AJR Am J Roentgenol 1986;147:1177–1179
24. Keslar PJ, Turbiner EH. Hepatobiliary imaging and the use of intravenous morphine. Clin Nucl Med 1987;12:592–596
25. Mehta A, Alazraki N. The effectiveness of morphine in expediting the radionuclide diagnosis of acute cholecystitis. J Nucl Med 1987;28:596 (abstract)
26. Vasquez TE, Greenspan G, Evans DG, Halpern SE, Ashburn WL. Clinical efficacy of intravenous morphine administration in hepatobiliary imaging for acute cholecystitis. Clin Nucl Med 1988;13:4–6
27. Fig LM, Stewart RE, Wahl RL, Shapiro B. Potential pitfalls in the use of morphine hepatobiliary scintigraphy. J Nucl Med 1989;30:850 (abstract)
28. Fink-Bennett D, Balon H, Robbins T, Tsai D. Morphine-augmented cholescintigraphy: its efficacy in detecting acute cholecystitis. J Nucl Med 1989;30:850 (abstract)
29. Kistler AM, Ziessman HA, Gooch D, Bitterman P. Morphine-augmented cholescintigraphy in acute cholecystitis. A satisfactory alternative to delayed imaging. Clin Nucl Med 1991;16:404–406
30. Kim CK, Tse KK, Juweid M, Mozley PD, Woda A, Alavi A. Cholescintigraphy in the diagnosis of acute cholecystitis: morphine augmentation is superior to delayed imaging. J Nucl Med 1993;34:1866–1870
31. Krishnamurthy GT. Acute cholecystitis: the diagnostic role for current imaging tests. West J Med 1982;137:87–94
32. Moncada R, Cordoso M, Danley R, Rodriguez J, et al. Acute cholecystitis: 137 patients studied by infusion tomography of the gallbladder. AJR Am J Roentgenol 1977;129:583–585
33. Bushnell DL, Perlman SB, Wilson MA, Polcyn RE. The rim sign: association with acute cholecystitis. J Nucl Med 1986;27:353–356

34. Netter FH. The CIBA collection of medical illustration, vol. 3. Digestive system, part 111. Liver, biliary tract and pancreas. CIBA Pharmaceutical Co., Summit, NJ, 1964, pp 1–31
35. Meekin GK, Ziessman HA, Klappenbach RS. Prognostic value and pathophysiologic significance of the rim sign in cholescintigraphy. J Nucl Med 1987;28:1679–1682
36. Oates E, Selland DG, Chin CT, Achong DM. Gallbladder nonvisualization with pericholecystic rim sign: morphine-augmentation optimizes diagnosis of acute cholecystitis. J Nucl Med 1996;37:267–269
37. Smith R, Rosen JM, Gallow LN, Anderson PO. Pericholecystic hepatic activity in cholescintigraphy. Radiology 1985;156:797–800
38. Swayne LC, Ginsberg HN. Diagnosis of acute cholecystitis by cholescintigraphy: significance of pericholecystic hepatic uptake. AJR Am J Roentgenol 1989;152:1211–1213
39. Krishnamurthy S, Krishnamurthy GT. Cholecystokinin and morphine pharmacological intervention during 99m-Tc-HIDA cholescintigraphy: a rational approach. Semin Nucl Med 1996;26:16–24
40. Chen CC, Holder LE, Maunoury C, Drachenberg CI. Morphine augmentation increases gallbladder visualization in patients pretreated with cholecystokinin. J Nucl Med 1997;38: 644–647
41. Kim CK. Pharmacological intervention for the diagnosis of acute cholecystitis: cholecystokinin pretreatment or morphine, or both? J Nucl Med 1997;38:647–649
42. Krishnamurthy S, Krishnamurthy GT. Evolution of nuclear hepatology as a clinical speciality. J Nucl Med Technology 1995;24(Suppl):35S–45S
43. Serafini AN, Al-Sheikh W, Barkin JS, Hourani M, Sfakiankis G, Clarke LP, Ashkar FS. Biliary scintigraphy in acute pancreatitis. Radiology 1982;144:591–595
44. Ali A, Turner DA, Fordham EW. Tc-99m-IDA cholescintigraphy in acute pancreatitis: concise communication. J Nucl Med 1982;23:867–869
45. Shea JA, Berlin JA, Escarce JJ, Clarke JR, Kinosian BP, Cabana MD, Tsai WW, Horangic N, Malet PF, Schwartz S, Williams SV. Revised estimates of diagnostic test sensitivity and specificity in suspected biliary tract disease. Arch Intern Med 1994;154:2573–2581
46. Hamilton GW, Trobaugh GB, Ritchie JL, et al. Myocardial imaging with thallium-201: an analysis of clinical usefulness based on Bayes' theorem. Semin Nucl Med 1976;17:439–448
47. McNeil BJ, Adelstein SJ. Determining the value of diagnostic and screening tests. J Nucl Med 1976;17:439–448
48. Goodman SN. Toward evidence-based medical statistics. 1: The p value fallacy. Ann Intern Med 1999;130:995–1004
49. Goodman SN. Toward evidence-based medical statistics. 2: The Bayes factor. Ann Intern Med 1999;130:1005–1013
50. Fagan TJ. Nomogram for Bayes's theorem. N Engl J Med 1975;293:257
51. Glossary. Terms used in therapeutics. ACP Journal Club 1998;129:A–21
52. Freitas JE, Coleman RE, Nagle CE, Bree RL, Krewer KD. Gross MD. Influence of scan and pathologic criteria on the specificity of cholescintigraphy: concise communication. J Nucl Med 1983;24:876–879
53. Frazee RC, Nagorney DM, Mucha P, Jr. Acute acalculous cholecystitis. Mayo Clinic Proc 1989;64:163–167
54. Swayne LC. Acute acalculous cholecystitis: sensitivity in detection using technetium-99m iminodiacetic acid cholescintigraphy. Radiology 1986;160:33–38
55. Weissmann HS, Burkowitz D, Fox MS, Gliedman ML, Rosenblatt R, Sugarman LA, Freeman LM. The role of technetium 99m iminodiacetic (IDA) cholescintigraphy in acute acalculous cholecystitis. Radiology 1983;146: 177–180
56. Jemal A, Siegel R, Ward E, et al. Cancer statistics, 2007. CA Cancer J Clin 2007;57:43–66
57. Gourgiotis S, Kocher HM, Solaini L, Yarollahi A, Tsiambas E, Salemis NS. Gallbladder cancer (review). Am J Surg 2008;196:252–264

9.4 Management of Gallbladder Disease

Cholecystectomy is the treatment of choice for most diseases of the gallbladder. The very first cholecystectomy was performed in 1882 by a German surgeon, Langenbach [1]. Today as many as 600,000 cholecystectomies are performed annually in the United States with either laparoscopic or open cholecystectomy. Open cholecystectomy carries a mortality rate ranging from 0 to 2.4% and morbidity ranging from 4.1 to 14.7%. The incidence of bile duct injury varies from 0.06 to 0.45% [2]. Laparoscopic cholecystectomy, which has now almost replaced open cholecystectomy, carries a similar rate of mortality, but a slightly lower morbidity (1.6–12%) than open cholecystectomy [3]. Laparoscopic cholecystectomy in the beginning was restricted mostly to symptomatic cholelithiasis, but now it is performed for varieties of gallbladder diseases, including acute cholecystitis, gangrenous cholecystitis, hydrops, and empyema, etc. [4]. The young as well as the old patients tolerate the laparoscopic cholecystectomy procedure well, and the hospital stay is much shorter than with an open cholecystectomy [5]. Administration of prophylactic antibiotics does not seem to affect the rate of wound infection in case of elective laparoscopic cholecystectomy [6]. Laparoscopic cholecystectomy for symptomatic gallstone disease during pregnancy is considered safe both for the mother and fetus, and is preferred over conservative management for all trimesters [7].

Complications

The complications of acute cholecystitis can occur either before or after treatment. The complications of delayed or untreated acute cholecystitis include acute cholangitis, gallbladder perforation, and bile leak. Post-operative complications include bile leak, cholangitis, infection, and stricture formation. Bile fistula occurs as a chronic complication.

Perforation of the Gallbladder

Perforation of the gallbladder is rare and is found in 10% of patients undergoing open cholecystectomy for acute gangrenous cholecystitis [8]. The bile may leak into a small closed space or leak freely into the peritoneum, causing bile peritonitis. Localized leak is the most common type and accounts for 50% of all perforations (Fig. 9.4.1). Most of the localized leaks and those that form fistula remain undiagnosed as they usually do not produce symptoms. Free perforation with bile peritonitis presents with the most disabling symptoms and is responsible for many deaths if not treated immediately. Most perforations into the subhepatic space are walled off and manifest very few symptoms. Perforation near the neck or Hartmann pouch may form a biloma and compress the common bile duct externally, manifesting a Mirizzi syndrome.

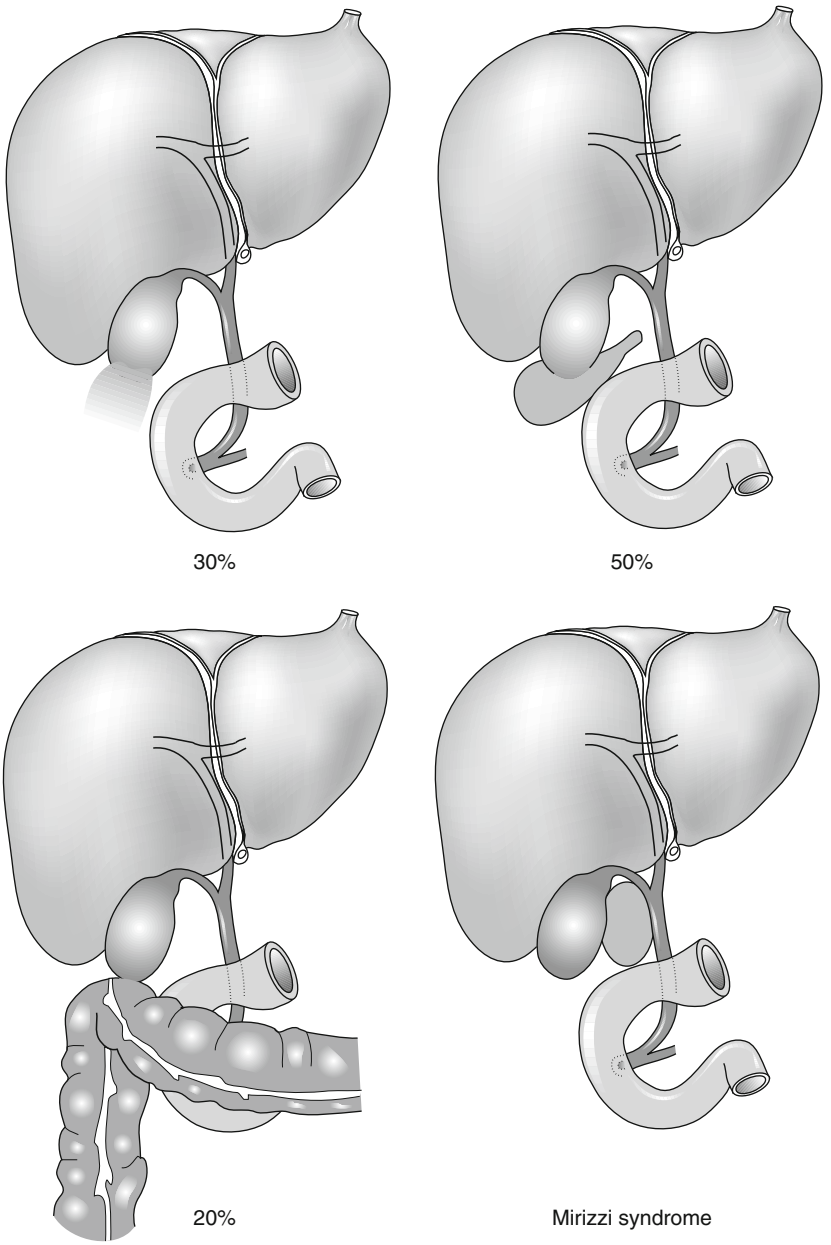

Fig. 9.4.1 Types of gallbladder perforation. Subhepatic bed is the most common site, followed by leak into free peritoneum and colon. Perforation near the neck and Hartmann pouch may form a biloma and compress the common bile duct extrinsically, manifesting a Mirizzi syndrome [7]

9

Bile Leak

The most common complication of laparoscopic cholecystectomy is bile leak through an unligated cystic duct or from an injury to the common hepatic or common bile duct (Fig. 9.4.2). Leak is best defined as bile collection in an unanticipated location or in an anticipated location at an unanticipated time. The common hepatic duct, which lies directly in front of the tip of the laparoscopic instrument, sustains injury more frequently than other bile ducts. The incidence of bile duct injury from laparoscopic cholecystectomy is twice as frequent as from open cholecystectomy. The consequence of bile leak depends upon its volume and location. A small volume subhepatic bile leak (Fig. 9.4.2A) or large volume bile leak into the stomach (Fig. 9.4.2B) causes few of the symptoms. Large volume hepatic subcapsular leak (Fig. 9.4.2C) or leak into the peritoneal cavity (Fig. 9.4.2D) requires treatment. Since the leak prefers the path of least resistance, major bile ducts often are not visualized beyond the point of the leak (Fig. 9.4.2).

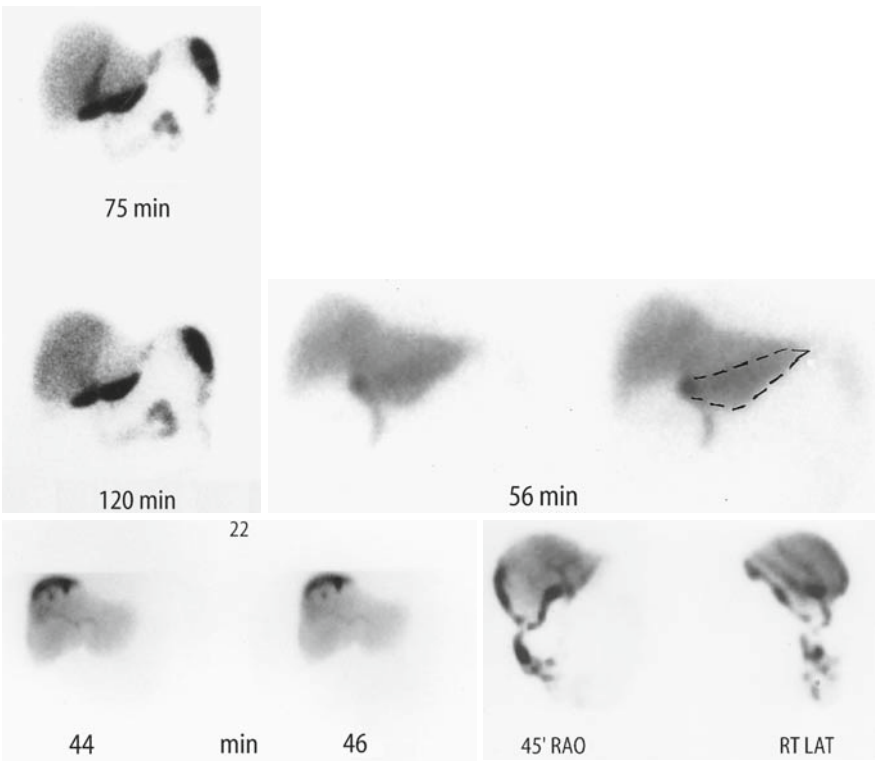

Fig. 9.4.2 Locations of bile leak. Bile may leak into subhepatic space (*top left*), stomach (*top right*), right subdiaphragmatic (*bottom left*), or peritoneal space (*bottom right*)

Treatment of Bile Leak

Small volume bile leaks close spontaneously if the tonus of the sphincter of Oddi is maintained at its minimum by treating patients with antispasmodics (Fig. 9.4.3). Use of opioids is avoided. Large volume bile leaks may require sphincterotomy. Sphincterotomy creates the path of least resistance for hepatic bile and promotes closure of the leak (Fig. 9.4.4A, B). Often the leak from the common hepatic or common bile duct may require stents or surgical repair. Malignant strictures usually require stents [9].

Bile Duct Stricture

The frequency of postoperative bile duct stricture is much higher after laparoscopic than after open cholecystectomy (Table 9.4.1). Most postoperative strictures occur in the proximal one half of the common hepatic duct, often involving its bifurcation into right and left hepatic ducts. Strictures near the bifurcation are treated with Hepp-Couinaud hepaticojejunostomy using the left hepatic duct [10]. Lately, the design of laparoscopic instruments has improved, and it is now possible to perform cholecystectomy safely with needles as small as 3 mm in diameter [11]. Postoperative strictures commonly occur at the site of ductal injury and are classified into four grades depending upon its location from the bifurcation into left hepatic with right hepatic duct [12]. Grade I strictures are more than 2 cm, grade II less than 2 cm from the union, grade III are at or just below the union, and grade IV at the site of union. Well-designed prospective studies have shown that immediate cholecystectomy is much more cost-effective than delayed elective cholecystectomy [13–16].

Postoperative subhepatic fluid collection is common and is noted in as many as 25% of the patients following an open cholecystectomy [17], but only about 30–45% of this subhepatic fluid collection is due to bile leak [18]. Bile fistulae as a consequence of acute and

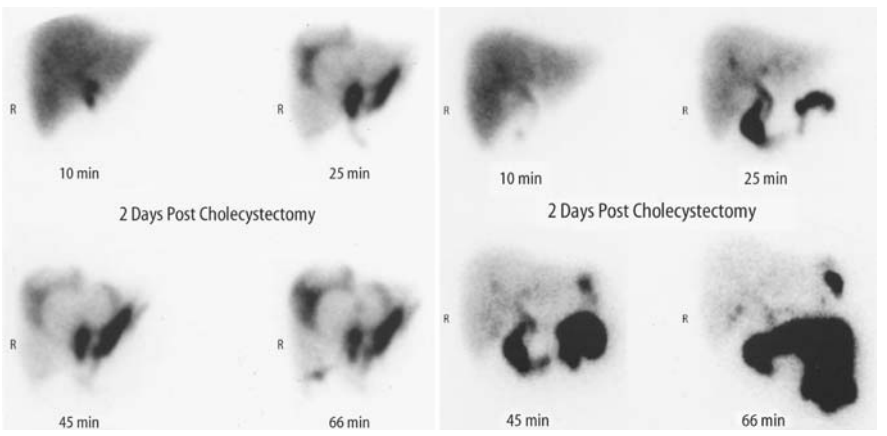

Fig. 9.4.3 Spontaneous closure of bile leak. Bile leak into the lateral aspect of the right lobe 2 days after cholecystectomy (*left*) stops spontaneously after 12 days (*right*). Narcotics that constrict the sphincter of Oddi were discontinued during this time period

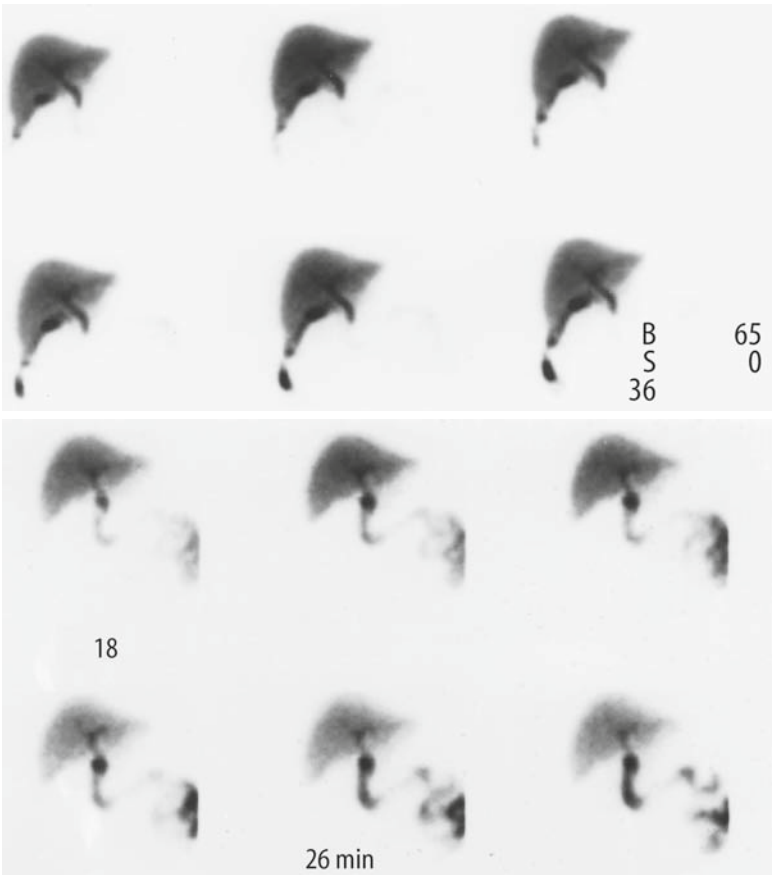

Fig. 9.4.4 Closure of bile leak after sphincterotomy. A large volume bile leak through an unligated cystic duct (*top*) required sphincterotomy for its stoppage (*bottom*)

Table 9.4.1 Complications of open vs. laparoscopic cholecystectomy [3]

Complication	Open cholecystectomy (%)	Laparoscopic cholecystectomy (%)
CBD injury	0.1	0.2
Bile leak	0.8	5.6
Pancreatitis	1.0	1.1
Jaundice	1.2	1.0
Atelectasis	10.0	5.4
Ileus	12.0	5.3
Urinary retention	17.4	6.5

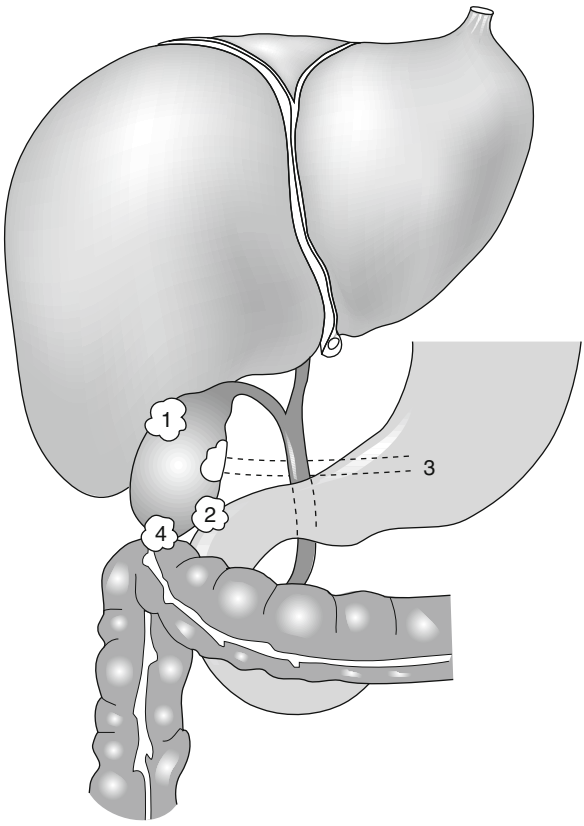

Fig. 9.4.5 Common sites of biliary fistula. Fistulas occur as a complication of either acute or chronic cholecystitis. Most of them remain asymptomatic

chronic complications occur in the subhepatic space, duodenum, stomach, or hepatic flexure of the colon (Fig. 9.4.5).

Prophylactic Cholecystectomy

Patients with asymptomatic gallstones or diabetes mellitus usually show a decrease in gallbladder emptying, but generally do not require cholecystectomy when either disease exists alone [19, 20]. However, patients with a combination of asymptomatic gallstones and diabetes mellitus develop acute cholecystitis and its complications 2.2 times more frequently than with either disease alone. Based upon such findings, prophylactic cholecystectomy is recommended for asymptomatic gallstone patients with diabetes mellitus [21]. Prophylactic cholecystectomy is also recommended for patients undergoing cardiac

transplantation, but not for those undergoing renal transplantation [22, 23]. Newer therapy in the form of oral dissolution, contact dissolution, and extracorporeal biliary lithotripsy has been used less and less frequently in recent years [24]. Some of the preventive measures are known to reduce the incidence of gallstones and accompanying complications. A 30-min exercise five times a week reduces symptomatic gallstones by 34% in men [25], and recreational physical activity (jogging, running, bicycling) reduces the incidence of symptomatic gallstones and cholecystectomy significantly in women [26].

References

1. Langenbuch CJA. Ein Fall von extirpation der Gallenblase wegen chronischer Cholelithiasis. Heilung Berl Klin Wochenscher 1882:19;725–727
2. Deziel DJ. Complications of cholecystectomy. Incidence, clinical manifestations, and diagnosis. Surg Clin North Am 1994;74:809–823
3. Shea JA, Berlin JA, Bachwich DR, Staroscik RN, Malet PF, McGuckin M, Schwartz JS, Escarce JJ. Indications for and outcomes of cholecystectomy: a comparison of the pre- and postlaparoscopic eras. Ann Surg 1998;227:343–350
4. Eldar S, Sabo E, Nash E, Abrahamson J, Matter I. Laparoscopic cholecystectomy for the various types of gallbladder inflammation. A prospective trial. Surg Laparoscopy Endoscopy 1998;8:200–207
5. Lujan JA, Sanchez-Bueno F, Parrilla P, Robles R, Torralba JA, Gonzales-Costea R. Laparoscopic vs. open cholecystectomy in patients aged 65 and older. Surg Laparoscopy Endoscopy 1998;8:208–210
6. Higgins A, London J, Charland S, Ratzer E, clark J, Haun W, Maher P. Prophylactic antibiotics for elective laparoscopic cholecystectomy. Arch Surg 1999;134:611–614
7. Date RS, Kaushal M, Ramesh A. A review of the management of gallstone disease and its complications in pregnancy. Am J Surg 2008;196:599–608
8. Ranson JHC. Perforation of the gallbladder. In: Way LW, Pelligrini CA (eds). Surgery of the gallbladder and bile ducts. WB Saunders, Philadelphia, 1987, pp 265–273
9. Way LW, Biliary stricture. In: Way LW, Pelligrini CA (eds). Surgery of the gallbladder and bile ducts. WB Saunders, Philadelphia, 1987, pp 419–429
10. Murr MM, Gigot J, Nagorney DM, Harmsen WS, Ilstrup DM, Farnell MB. Long-term results of biliary reconstruction after laparoscopic bile duct injuries. Arch Surg 1999;134:604–610
11. Cheah WK, Goh P, Gagner M, So J. Needlescopic retrograde cholecystectomy. Surg Laparoscopy Endoscopy 1998;8:237–238
12. Martin RF, Rossi RL. Bile duct injuries. Spectrum, mechanisms of injury, and their prevention. Surg Clin North Am 1994;74:781–803
13. MacArthur P, Cuschieri A, Sell RA, Shields R. Controlled clinical trial comparing early with interval cholecystectomy for acute cholecystitis. Br J Surg 1975;62:850–852
14. Fowkes FG, Gunn AA. The management of acute cholecystitis and its hospital cost. Br J Surg 1980;67:613–617
15. Lo CM, Liu CL, Fan ST, Lai EC, Wong J. Prospective randomized study of early versus delayed laparoscopic cholecystectomy for acute cholecystitis. Ann Surg 1998;227:461–467
16. Hunter JG. Acute cholecystitis revisited: get it while it's hot. Ann Surg 1998;227:468–469
17. Elboim CM, Goldman L, Hann L. Significance of post-cholecystectomy subhepatic fluid collection. Ann Surg 1983;198:137–141
18. Gilsdorf TR, Phillips M, McLeod MK, Gregg RO. Radionuclide evaluation of bile leakage and the use of subhepatic drains after cholecystectomy. Am J Surg 1986;156:259–262

19. Shreiner DP, Sarva RP, Van Thiel D, Yingvorapant N. Gallbladder function in diabetic patients. J Nucl Med 1986;27:357–360
20. Fisher RS, Stelzer F, Rock E, Malmud LS. Abnormal gallbladder emptying in patients with gallstones. Dig Dis Sci 1982;27:1019–1024
21. Ransohoff DF, Miller GL, Forsythe SB, Hermann RE. Outcome of acute cholecystitis in patients with diabetes mellitus. Ann Intern Med 1987;106:829–832
22. Menegaux F, Dorent R, Tabbi D, Pavie A, Chigot J, Gandjbakhch I. Biliary surgery after heart transplantation. Am J Surg 1998;175:320–321
23. Melvin WS, Meier DJ, Elkhammas EA, Bumgardner GL, Davies EA, Henry ML, Pelletier R, Ferguson RM. Prophylactic cholecystectomy is not indicated following renal transplantation. Am J Surg 1998;175:317–319
24. Johnston DE, Kaplan MM. Pathogenesis and treatment of gallstones. N Engl J Med 1993;328:412–421
25. Leitzmann MF, Giovannucci EL, Rimm EB, Stampfer MJ, Spiegelman D, Wing AL, Willett WC. The relation of physical activity to risk for symptomatic gallstone disease in men. Ann Intern Med 1998;128:417–425
26. Leitzmann MF, Rimm EB, Willet WC, Spiegelman D, Grodstein F, Stampfer MJ, Colditz GA, Giovannucci E. Recreational physical activity and the risk of cholecystectomy in women. N Engl J Med 1999;341:777–784

Biliary Dyskinesia

10

Biliary dyskinesia consists primarily of two disease entities, the sphincter of Oddi spasm (SOS) and cystic duct spasm (CDS). In the past when its pathophysiology was not clearly understood, cystic duct spasm was called cystic duct syndrome. These two entities are anatomically separate, but physiologically connected by an abnormal functional response to cholecystokinin. The sphincter of Oddi spasm is located within the sphincter at the distal end of the common bile duct, whereas the cystic duct spasm is confined mostly to the cystic duct of the gallbladder [1, 2]. In the literature, sphincter of Oddi spasm is also known by such names as papillary stenosis or bile duct dyskinesia, and cystic duct spasm as chronic acalculous cholecystitis. Both the sphincter of Oddi and gallbladder contain receptors for cholecystokinin, which is released endogenously into circulation from the intestinal mucosa upon entry of food into the duodenum [3, 4]. By binding to CCK-A type receptors, cholecystokinin normally stimulates the contraction of the gallbladder with simultaneous relaxation of the sphincter of Oddi. The cystic duct, which also contains CCK receptors, normally does not respond, because its serum threshold for contraction is set at a much higher level than the threshold for contraction of the fundus and body of the gallbladder [5]. Controversy over the real existence of the entity of biliary dyskinesia prevailed for many years [6]. Manometric studies, however, have helped to understand the basic sphincter mechanism and the action of cholecystokinin on it in both health (Chap. 6) and disease, especially in patients with SOS (Table 10.1.1). Both quantitative cholescintigraphy and biliary manometry have contributed to clear understanding of the bile secretion and flow mechanisms and the pathophysiological changes associated with biliary dyskinesia [7–9].

Pathophysiology

A normal sphincter of Oddi exhibits an average of six to seven contractions per minute with a wave amplitude of 113 mmHg. The mean pressure in the sphincter of Oddi is about 15.0 mmHg, and 9.0 mmHg in the common bile duct. About 54% of the contraction waves progress antegrade, 18% retrograde, and 28% occur simultaneously in the proximal, middle, and caudal segment of the sphincter (Table 10.1.1). Administration of cholecystokinin abolishes the contraction waves and relaxes the sphincter of Oddi immediately, and promotes smooth passage of bile emptied from the gallbladder into the duodenum

G.T. Krishnamurthy and S. Krishnamurthy, *Nuclear Hepatology*,
DOI 10.1007/978-3-642-00648-7_10, © Springer-Verlag Berlin Heidelberg 2009

(Fig. 10.1.1). Sphincter of Oddi spasm is characterized manometrically by an increase in basal pressure of the sphincter to 37 mmHg, and the common bile duct to 17 mmHg. The total number of basal contractions increases to 17 min^{-1}, and the number of retrograde contraction increases to 41% (Fig. 10.1.2A). In the case of SOS, usually dormant contractile receptors in the sphincter become activated. These activated receptors paradoxically induce contraction of the sphincter in response to cholecystokinin [10, 11]. Cholecystokinin administration increases both the number of waves and the number of retrograde waves per minute (Fig. 10.1.2B). Because of this paradoxical response (contraction) of the sphincter, the bile either fails to empty from the gallbladder or the emptied bile refluxes into the common hepatic duct and right and left hepatic ducts, and reenters the gallbladder soon after cessation of CCK-8 infusion [12].

Table 10.1.1 Biliary pressure profile in asymptomatic control subjects and patients with sphincter of Oddi spasm [9]

Structure	Control subjects ($n = 9$)	SOS patients ($n = 10$)	P value
CBD pressure (mmHg)	8.6 + 1.02 (6–13)	17.0 + 1.25 (12–22)	0.001
Sp. Oddi pressure (mmHg)	14.9 + 0.99 (11–21)	36.9 + 5.44 (20–70)	0.005
Phasic contractions:			
Amplitude (mmHg)	113.0 + 8.6 (95–125)	109.5 + 9.3 (85–160)	0.37
Frequency (per min)	6.89 + 0.20	7.56 + 0.41	0.46
Direction of propagation:			
Antegrade	54% + 6%	29% + 7%	0.04
Simultaneous	28% + 4%	0% + 3%	0.34
Retrograde	18% + 6%	41% + 9%	0.01

Values are mean + SE. Ranges within parentheses. Adopted from Meshkinpour et al. [9]

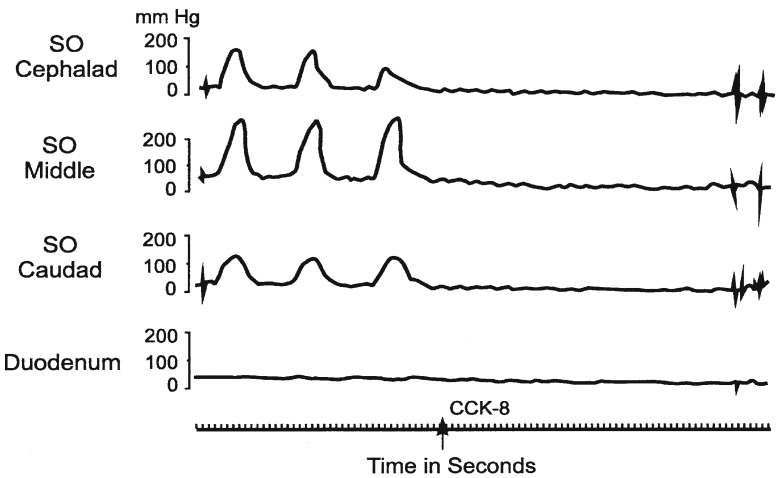

Fig. 10.1.1 Action of CCK-8 on normal sphincter of Oddi. Normal contraction waves are abolished immediately after CCK-8 administration, which facilitates dilatation of the sphincter for smooth passage of bile through it [11]

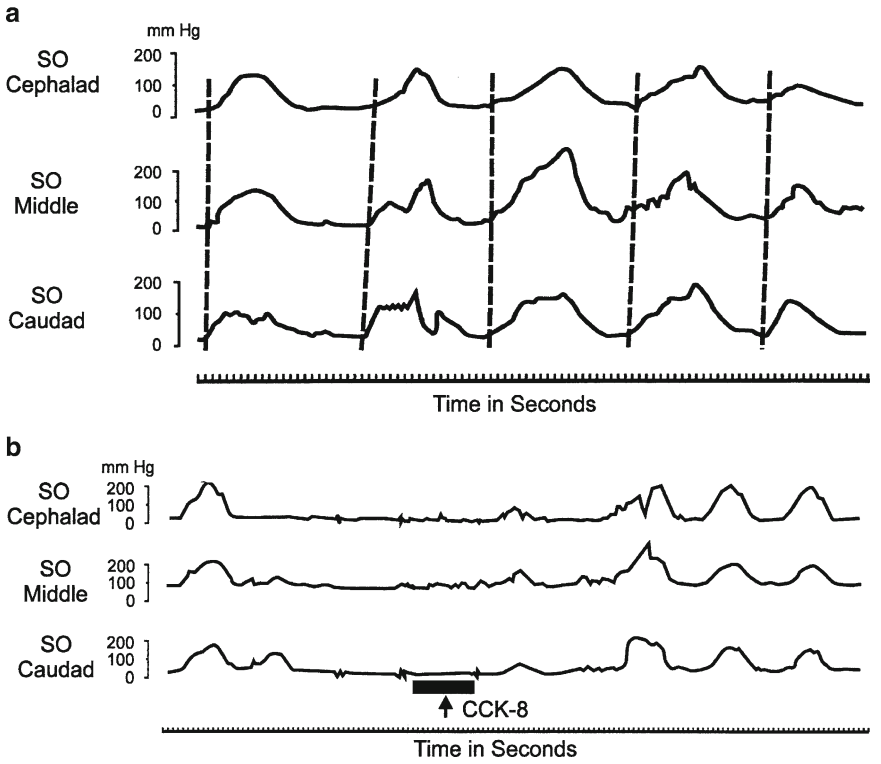

Fig. 10.1.2 a, b Propagation of contraction waves and effect of CCK-8 on the sphincter in SOS. Contraction begins first at the caudal end and travels retrograde towards the middle and cephalic end of the sphincter (*top*). Administration of CCK-8 paradoxically increases the number of retrograde contractions (*bottom*), resulting in closure of the sphincter [11]

Cystic duct spasm is often associated with kinking, fibrosis, and thickening of the wall with narrowing of the of the cystic duct lumen [13]. Hepatic bile enters the gallbladder slowly, but cannot get out readily in response to cholecystokinin (Chap. 9.2). Due to a decrease in the total number of CCK receptors, there is poor contraction and emptying of the gallbladder, post-meal [14, 15]. The threshold of the cystic duct contraction receptors is presumably lowered, which results in its contraction when cholecystokinin is released.

Clinical Presentation

Biliary dyskinesia patients are mostly women in their 3rd or 4th decades of life, and present with post-prandial right upper quadrant or epigastric pain. Pain usually begins 30 min after a meal and reaches its peak intensity 2–3 h later. Liver function tests and blood counts remain within normal range. The gallbladder and intrahepatic and extrahepatic bile ducts are morphologically normal, and gallstones are usually absent on the ultrasound examination. Because of these normal biochemical and morphologic findings, the diagnosis of

biliary dyskinesia is frequently delayed for months or years, and patients often go from physician to physician seeking relief from post-prandial abdominal pain.

Cholescintigraphic Diagnosis

Although biliary manometry is considered the gold standard, it is invasive, expensive, and not readily availability in many community hospitals. Cholescintigraphy provides a non-invasive and less expensive alternative. Imaging and quantitative analysis are carried out by acquiring data in two separate phases: the hepatic phase and gallbladder phase. Patients are studied after 4–6 h of fasting. Detailed clinical and drug history is taken to exclude the intake of opioids, smooth muscle relaxants, calcium channel blockers, or other drugs that act either on the sphincter of Oddi or gallbladder. In hypertensive patients, calcium channel blockers are discontinued for 2–3 days prior to the test. With the patient in the supine position, a large field of view dual-head gamma camera fitted with a low-energy, all-purpose, parallel-hole collimator is positioned anteriorly and posteriorly, and 3–5 mCi Tc-99m HIDA is injected intravenously. The data are acquired on the computer at one frame/minute for 60 min [16–19]. Hepatic phase images usually appear normal (Fig. 10.1.3, top) unless the disease is far advanced, in which case there may be bile stasis in the extrahepatic ducts and delay in entry of bile into the duodenum. If the gallbladder is not seen by 60 min, delayed images are obtained at 3–4 h after injection of a second dose of Tc-99m HIDA. Injection of opioids to induce contraction of the sphincter of Oddi to fill the gallbladder is avoided.

Gallbladder Phase Imaging

The data are acquired with the gamma camera. Hepatic phase images are carefully scrutinized for superimposition of duodenal or common bile duct radioactivity over the gallbladder. If there is any superimposition, the gamma camera angle is altered to separate the gallbladder from other structures. Often this may require changing the gamma camera angle by 10–15° to the left or right anterior oblique position (Fig. 10.1.3, bottom). Most of the time, no such angulation is required. The data are collected at one frame/minute for 30 min, (between 61–90 min) after injection of Tc-99m HIDA. Cholecystokinin at a dose of 3 ng kg^{-1} min^{-1} is infused intravenously for 10 min beginning at 65 min after HIDA injection The patient's symptoms (nausea, abdominal cramps, and/or pain) are monitored carefully, and their time of onset, severity, and time of relief are noted on the data sheet or gallbladder time/activity curve. ROIs are drawn over the gallbladder, liver (background), common hepatic ducts including the right hepatic and left hepatic ducts, common bile duct, stomach, and intestine (Fig. 10.1.4), and gallbladder ejection fraction, ejection period, ejection rate, and duodenogastric bile reflux are obtained (Fig. 10.1.5). The gallbladder, common hepatic duct (including the right and left hepatic ducts), common bile duct, and stomach and their corresponding curves are scrutinized carefully. Sphincter of Oddi spasm is differentiated from cystic duct spasm (Fig. 10.1.6) by careful analysis of both the image pattern and quantitative functional parameters [12, 13]. In most cases, the gallbladder ejection fraction remains normal. In many patients, the post-CCK-8 paradoxical refilling volume exceeds the basal volume by showing much higher counts after refilling than basal counts before

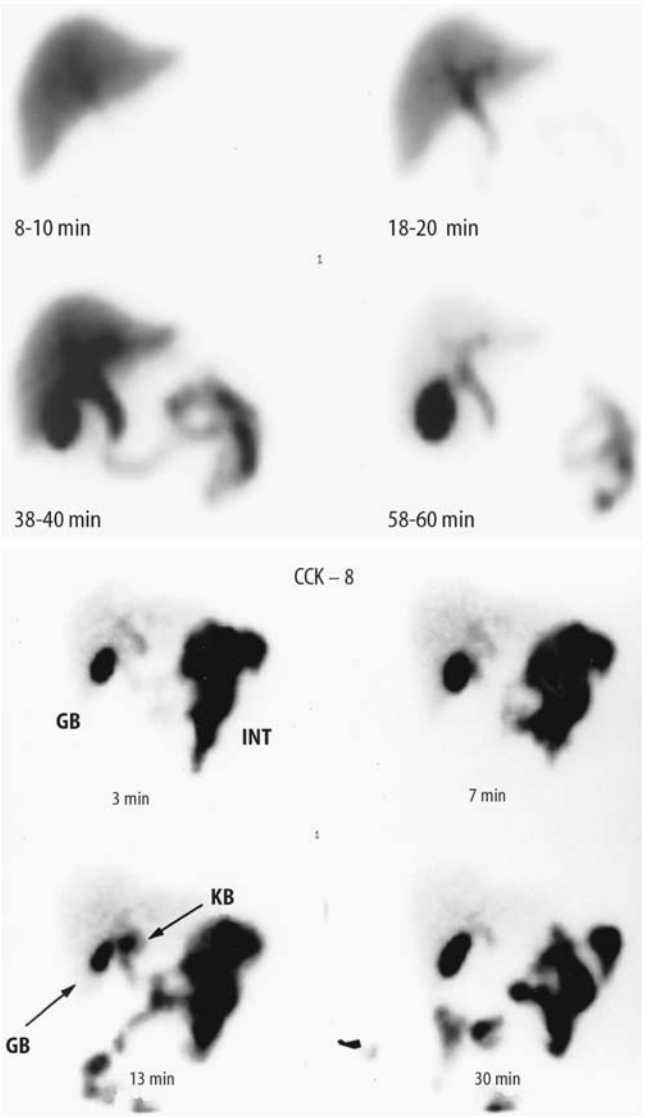

Fig. 10.1.3 Cholescintigraphy in SOS. The uptake and excretion of 99mTc-HIDA are normal with delineation of the gallbladder and entire biliary tree. Bile enters the small intestine normally (*top*). After CCK-8 infusion, the gallbladder contracts and empties bile, which refluxes into the common hepatic duct (*KB*). Refluxed bile reenters the gallbladder immediately after cessation of CCK-8 infusion with an increase in size of the gallbladder (*bottom*)

hormone injection (Fig. 10.1.7). A true paradoxical filling recurs with the second dose of CCK-8 (Fig. 10.1.8) and must be differentiated from pseudo-paradoxical filling that may occur due to superimposition of intestinal activity on the gallbladder region of interest (Fig. 10.1.9).

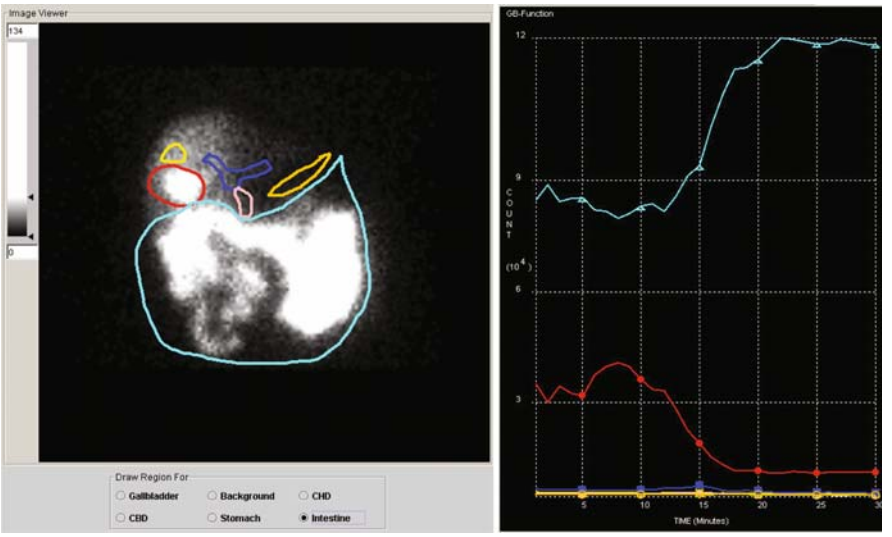

Fig. 10.1.4 Regions of interest for gallbladder phase study. One ROI is drawn over each of the gallbladder, liver (*background*), common hepatic duct, including right hepatic and left hepatic ducts, common bile duct, stomach, and intestine. *Raw curves* on the *right* represent the region of the same color

Sphincter of Oddi Spasm

Cholescintigraphic findings vary depending upon the presence or absence of the native gallbladder. There is usually no bile pooling within the intrahepatic ducts in SOS, a feature distinctly different from those with stricture of the common bile duct [17]. Several types of functional abnormalities have been shown by different authors, depending upon the method of data collection and analysis [20, 21]. Shaffer et al. measured the hepatobiliary peak uptake time and calculated the percent excretion at 45, 60, and 90 min. Cholecystokinin at a dose of 0.02 units kg^{-1} min^{-1} was infused slowly between 60 and 90 min. The region of interest included both the liver and bile ducts. In 22 subjects with previous cholecystectomy with no current symptoms (control), the hepatobiliary mean peak time was 9.8 ± 0.7 min. Percent excretion at 45, 60, and 90 min was 50.6 + 3.6, 66.3 + 2.8, and 84.7 + 1.3, respectively. The emptying rate between 0 and 60 min, and 60-90 min (after CCK) was 1.46 + 0.07 min^{-1} and 0.73 + 0.6 min^{-1}, respectively. In nine patients with post-cholecystectomy SOS, the mean peak time was increased to 23 min, and percent excretion at 45 and 60 min was decreased to 20 and 39, respectively. The emptying rate between 0 and 60 min was 1.05 + 0.13 min^{-1} and increased to 1.12 + 0.19 min^{-1} after CCK infusion between 60 and 90 min [21]. Others have shown prolongation of the hepatic hilum to duodenal transit time [22, 23]. Most of the functional parameters improved after papillotomy (Fig. 10.1.10).

The hepatic phase images appear normal in most patients with early SOS (Fig. 10.1.3), and the gallbladder shows a normal ejection fraction. Cholescintigraphy in SOS is characterized by reflux of gallbladder bile into the common hepatic and right and left hepatic ducts with re-entry of refluxed bile into the gallbladder immediately after cessation of

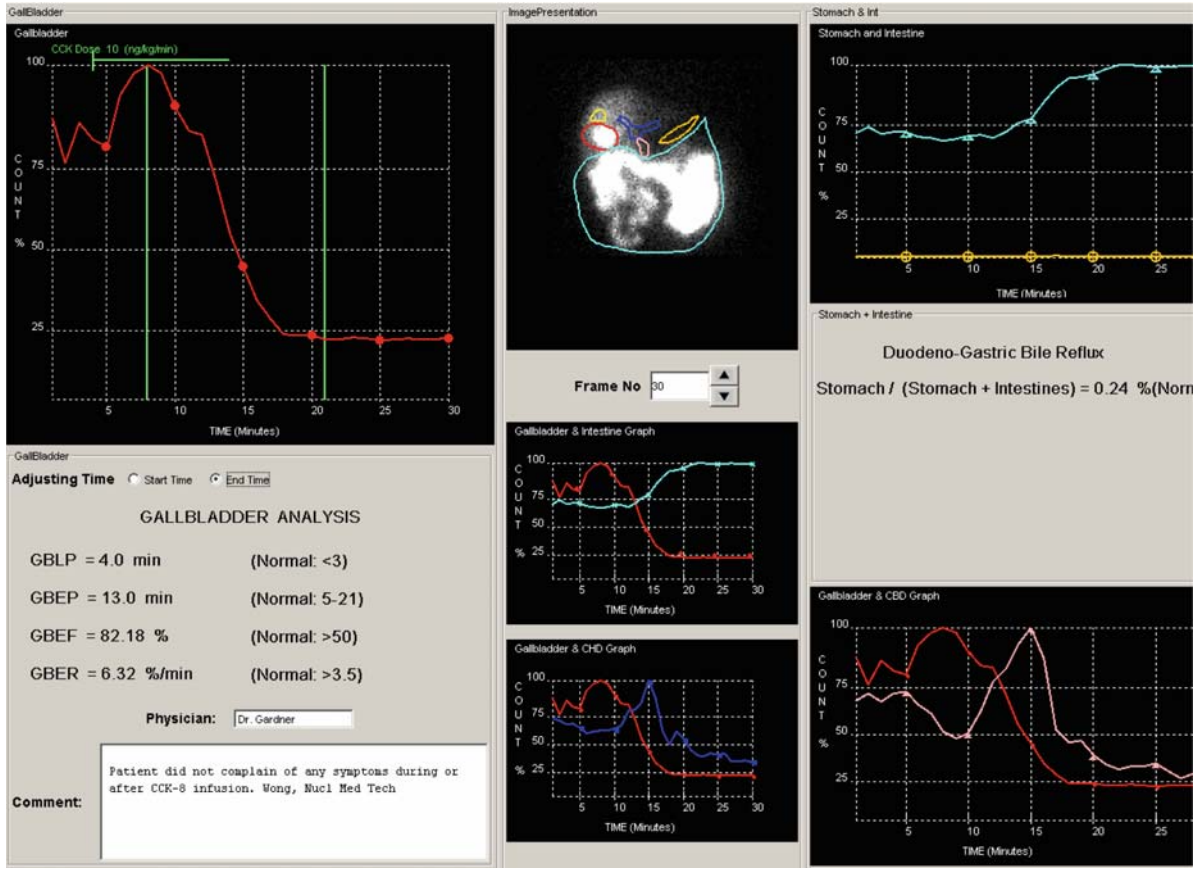

Fig. 10.1.5 Gallbladder phase results. The length of *horizontal bar* at the *top* represents the duration of CCK-8 infusion. The software calculates the results automatically after the ROIs are drawn. *Two vertical bars* denote the beginning and end of gallbladder emptying. The operator makes adjustments if automatically calculated results do not agree with the expected results

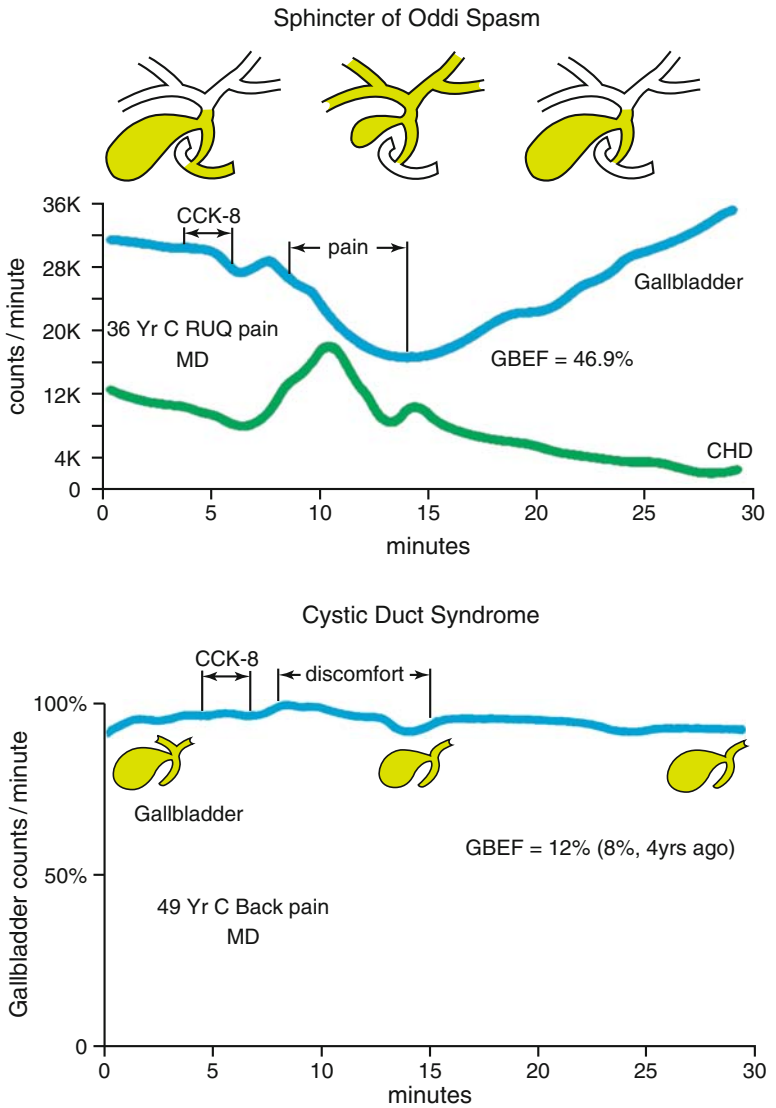

Fig. 10.1.6 Biliary dynamics in biliary dyskinesia. In the case of sphincter of Oddi spasm, the gallbladder contracts and empties bile, which refluxes into the common hepatic and intrahepatic ducts. Most of the refluxed bile reenters the gallbladder (*top*). In patients with cystic duct syndrome, the gallbladder empties poorly, and no refilling occurs (*bottom*). Pain or discomfort occurs mostly during the gallbladder ejection period [12]

CCK-8 infusion. The curve shows rapid refilling of the gallbladder almost to its original volume, often even exceeding the original volume because of stimulation and expulsion of hepatic bile by cholecystokinin. Intrahepatic and extrahepatic bile ducts can accommodate almost all of 40–50 ml of bile emptied from the gallbladder without being dilated. Common hepatic duct bile reflux also occurs in patients with stenosis of the common bile duct and

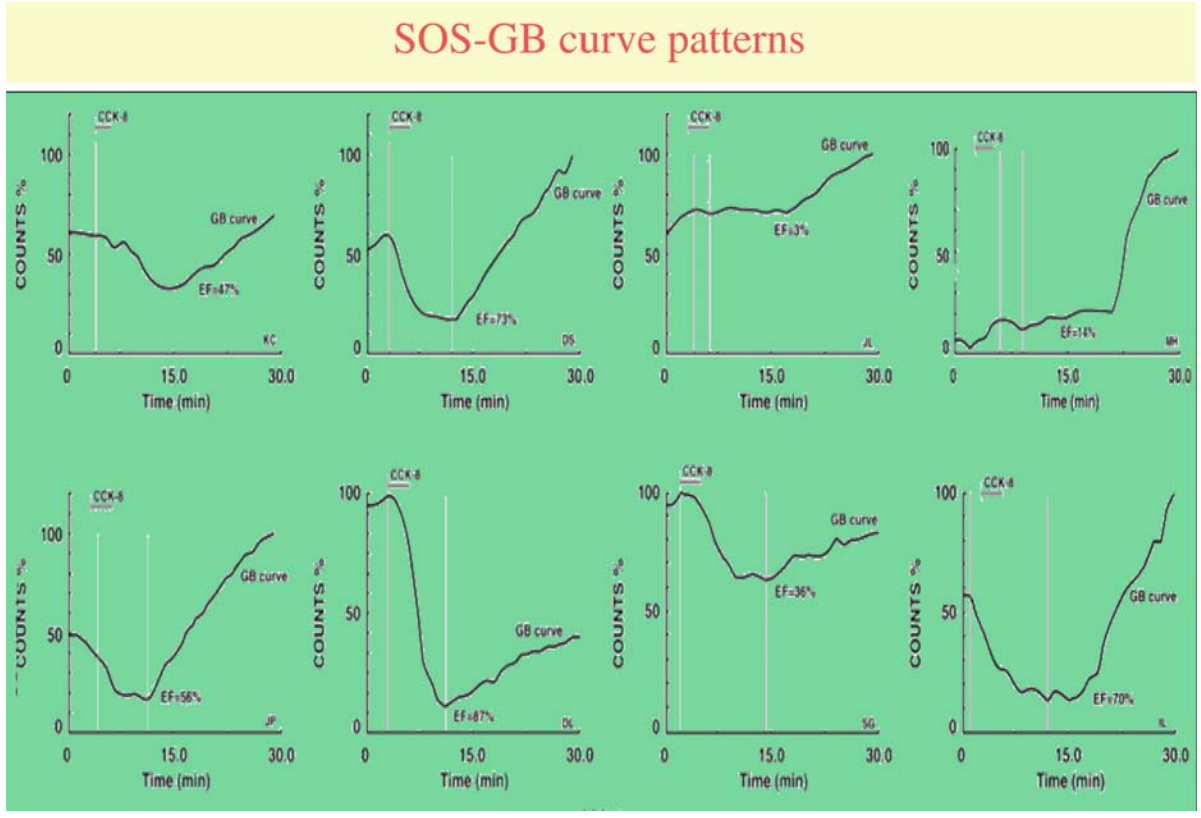

Fig. 10.1.7 Types of post-CCK-8 paradoxical filling curve patterns seen in patients with sphincter of Oddi spasm. Most gallbladders show normal ejection fraction followed by different patterns of refilling. Many gallbladders show much larger bile volume after refilling than the basal volume as shown by overshooting of the refilling curve [18]

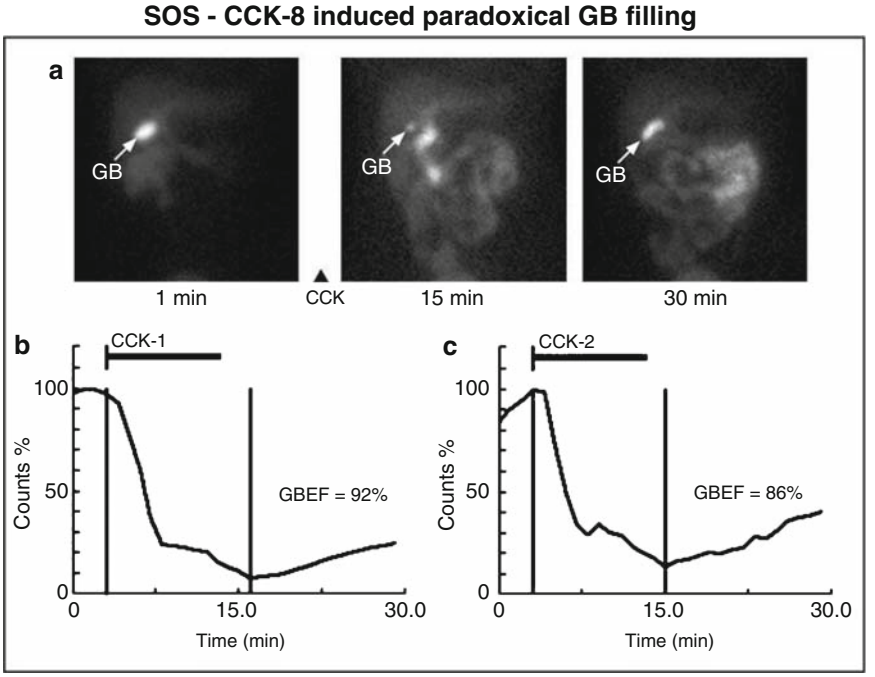

Fig. 10.1.8 True paradoxical filling with CCK-8 given twice. In both cases, the gallbladder empties normally (EF 92% and 86%), followed by paradoxical filling

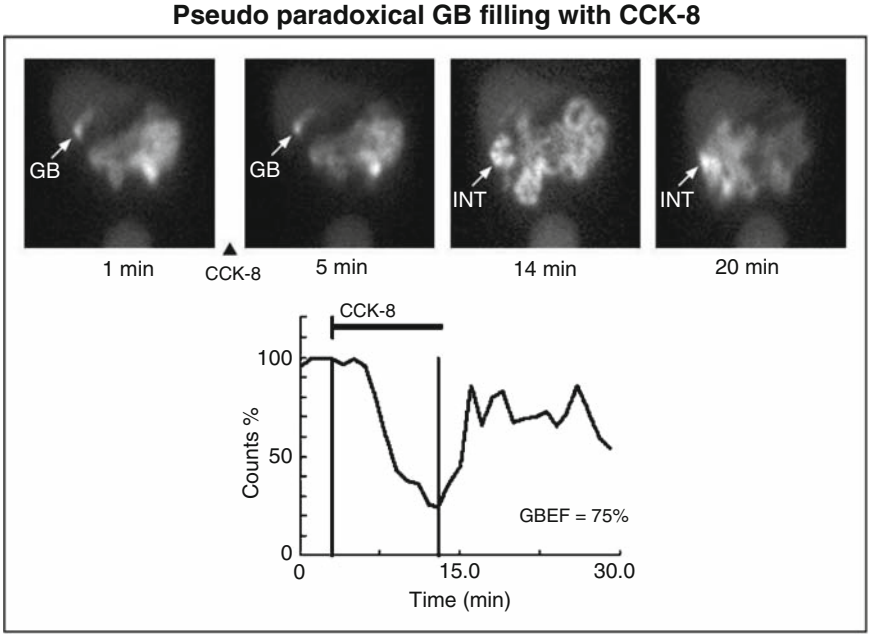

Fig. 10.1.9 An apparent paradoxical filling after normal emptying (EF75%) of the gallbladder (*GB*) due to superimposition of intestinal (*INT*) activity

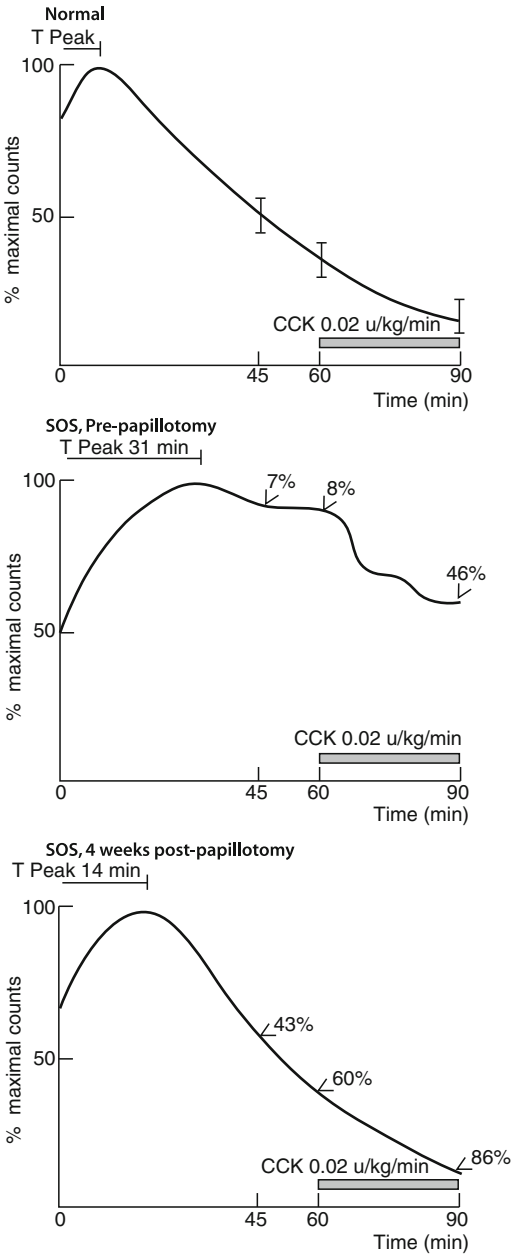

Fig. 10.1.10 Hepatic bile clearance in SOS. Normally, peak uptake of 99mTc-HIDA occurs within 10 min and 66% is excreted within 60 min. CCK enhances excretion. In patients with SOS, the peak is delayed and 60-min excretion is decreased. CCK administration has only a partial effect before papillotomy. Both uptake and excretion improve after papillotomy [21]

is referred to as the Krishnamurthy-Bobba sign [24]. When patients complain of pain during the gallbladder dynamic phase, the pain duration usually corresponds to the gallbladder ejection period. Not every patient with biliary dyskinesia, however, complains of pain at the time of the study. The extrahepatic ducts may appear early and persist for a longer duration of time, resulting in a marked delay in peak hepatic uptake in advanced cases [22, 25].

Sphincter of Oddi spasm is differentiated from anatomic stricture of the common bile duct by assessing both the image pattern and quantitative curve analysis after a pharmacologic intervention. Amyl nitrite, nitric oxide, and nifedipine relieve the spasm and dilate the sphincter, promoting rapid bile flow through it in patients with SOS, but not in those with an anatomic stricture (Fig. 10.1.11) of the common bile duct [26-28]. Sensitivity of cholescintigraphy in SOS varies from 70 to 90% [29].

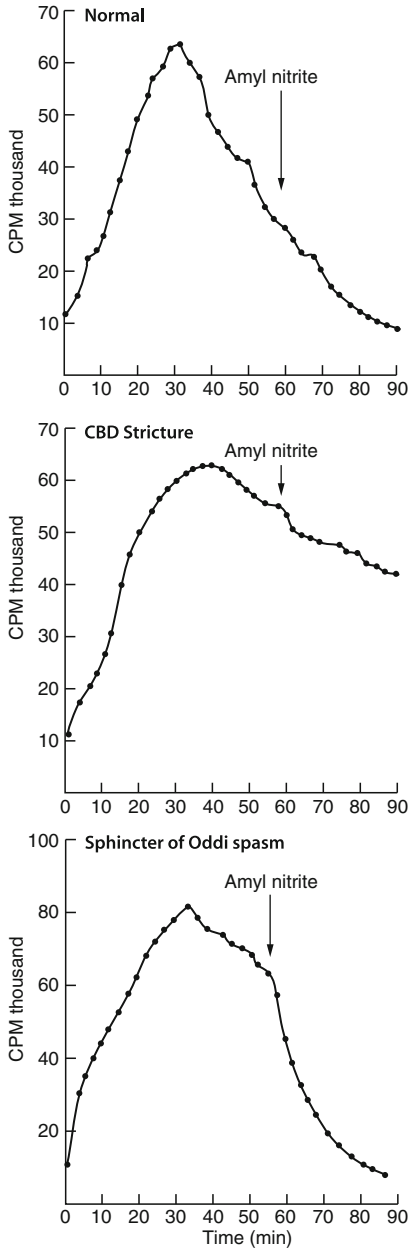

Fig. 10.1.11 Cholescintigraphic differentiation of SOS from CBD stricture. The normal common bile duct time/activity curve shows an early peak with rapid decline before and after amyl nitrite (*top*). The peak is delayed in both stricture and SOS. Following amyl nitrite, there is a rapid decline in patients with SOS (*bottom*), but not with stricture (*middle*) [26]

Cystic Duct Spasm

This spasm is often characterized by a slow filling of the gallbladder during the hepatic phase with poor emptying response to cholecystokinin in the gallbladder phase. Although most of the gallbladders appear within 60 min after injection of Tc-99m HIDA, some are delayed for 3–4 h. Reduction in the gallbladder ejection fraction with CCK-8 is the salient feature. Many patients, but not all, experience mild- to moderate-intensity abdominal pain during the gallbladder ejection period. The gallbladder curve appears flat in patients with ejection fractions below 15%, and it is often difficult to note the exact time of the onset and end of gallbladder emptying (Fig. 10.1.4B). There is usually no bile reflux into the intrahepatic or extrahepatic ducts, and the gallbladder curve does not show refilling after cessation of CCK-8 infusion [12, 18]. The direction of the latter half of the curve is assessed carefully to make sure that there is no refilling of the gallbladder, which would suggest SOS. A large, non-physiological CCK-8 dose when given as a rapid intravenous bolus often produces a low ejection fraction and abdominal pain in many of the normal subjects, mimicking cystic duct syndrome. This effect is attributed to exceeding the cystic duct threshold for contraction and should be avoided.

Differentiation of SOS from CDS

The differentiation is critical for appropriate patient management because cholecystectomy is the preferred treatment for CDS and antispasmodics or sphincterotomy for SOS. Cholecystectomy for SOS is inappropriate and may make the patient's condition get worse by taking away its low pressure reservoir function [30]. Both conditions are relatively more common in women than men. Proper attention is given during patient preparation, data collection, and analysis. The hepatic phase imaging data appear similar in both conditions, and there is bile entry into the duodenum in early cases. Only during the gallbladder phase is a difference seen between SOS and CDS. Cholecystokinin-induced bile reflux into the common hepatic duct and paradoxical refilling of the gallbladder are typical for SOS. In the authors' experience, another condition that may cause such a paradoxical filling is hyperacute (within 48 h) complete obstruction of the common bile duct (Chap. 8). Cholecystokinin stimulates bile secretion by cholangiocytes lining the intrahepatic bile ducts and expels bile from the liver by inducing contraction of the bile ducts. The hepatic bile is forced to enter the gallbladder in the presence of complete obstruction of the common bile duct. Other features of hyperacute CBD obstruction include its acute clinical presentation, abnormal liver function tests, and no bile entry into the duodenum during the hepatic phase. On rare occasions, superimposition of jejunal or ileal loop activity over the gallbladder region may cause false elevation of the gallbladder curve, which is readily recognized with the cine display of the gallbladder phase data. Patients with CDS do not exhibit paradoxical filling of the gallbladder, and there is no bile reflux into the intrahepatic ducts (Fig. 10.1.12).

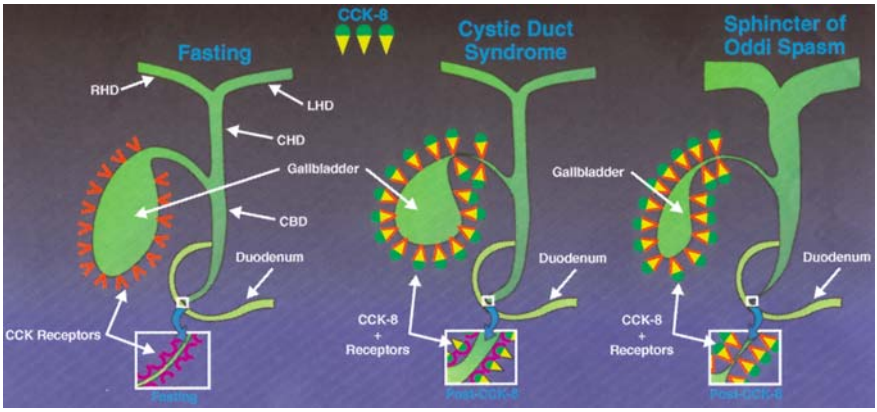

Fig. 10.1.12 Differentiation of CDS from SOS. Cholecystokin (*CCK*) receptors on the gallbladder smooth mucle remain free in the fasting state (*left*). In cystic duct syndrome (*middle*), the gallbladder empties poorly in response to CCK-8 infusion because of a decrease in the total number of CCK receptors in the gallbladder body and fundus and activation of contractile receptors in the cystic duct. In the case of the sphincter of Oddi spasm (*right*), the sphincter contracts because of activation of the contractile receptors, and the bile emptied from the gallbladder refluxes into the common hepatic and intrahepatic ducts, later reentering the gallbladder (CCK-induced paradoxical filling of the gallbladder) after cessation of CCK-8 infusion [12]

Treatment

Treatment for SOS is different from that of CDS. A normal sphincter of Oddi function is modulated by local generation of nitric oxide [27]. Medical treatment with nitrites, nitrates, calcium channel blockers (nifedipine), and other smooth muscle relaxants has been shown to relieve the spasm and dilate the sphincter in patients with SOS [28]. Endoscopic sphincterotomy is reserved for those patients who fail to respond to medical therapy. Sphincterotomy is invasive, expensive, and carries a high rate of procedural complications. The overall endoscopic sphincterotomy complication rate in 2,347 patients in a multicenter study from 17 institutions in the United States was 9.8%. The complication rate is much higher (21.7%) in patients with sphincter of Oddi dysfunction [31]. Acute pancreatitis (5.4%) and hemorrhage (2.0%) account for the great majority of complications from endoscopic sphincterotomy. Special training and frequent experience in doing large numbers of patient procedures reduce complication rates [32]. Sphincteroplasty through an endoscopic balloon dilatation is effective in patients with bile duct stones [33]. However, its role in sphincter of Oddi spasm has not been studied critically in a large number of patients. Cholecystectomy is a relative contraindication in SOS. An intact gallbladder acts as a reservoir and accommodates bile that fails to pass through the sphincter in patients with SOS. Cholecystectomy takes away this reservoir function, and the symptoms persist or may even get worse, manifesting a post-cholecystectomy syndrome [30, 34].

Cholecystectomy

This is the treatment of choice for CDS. Due to its low morbidity and low mortality, laparoscopic cholecystectomy has become more popular and has replaced open cholecystectomy as the preferred therapy [35]. Of a total of 320 patients with CDS who underwent cholecystectomy solely on the basis of a gallbladder low ejection fraction, 90% had relief of abdominal pain [36–42]. Histopathological examinations showed microscopic changes of disease in the gallbladder wall or cystic duct in 90% of patients (Chap. 9.2). Abdominal pain is known to persist in about 20% of patients undergoing cholecystectomy for various reasons [43], and the majority of these patients may have SOS. Clinically, SOS is divided into three types. Only type I responds to endoscopic sphincterotomy, and types II and III have a varied response. Type III is considered as duodenal visceral hyperalgesia, and the pain may not originate from the biliary tree at all [44]. Sphincterotomy is more effective than placebo in patients with sphincter pressure greater than 40 mmHg than in those without pressure elevation [45].

Post-cholecystectomy Syndrome

This can now be considered an iatrogenic disease exaggerated by an inappropriate therapy (cholecystectomy) for patients with SOS. Removal of the gallbladder, which serves as a low pressure reservoir by accommodating hepatic bile, exaggerates the symptoms in patients with SOS. This syndrome can now be studied non-invasively by combining magnetic resonance cholangiopancreatography (MRCP) with quantitative cholescintigraphy. Rubini and Dimonte reported five patients with post-cholecystectomy syndrome and showed dilatation of the common hepatic and common bile ducts in four and cystic duct remnant in three (two remnants with gallstones) on MRCP. Cholescintigraphy showed bile pooling in both intrahepatic and extrahepatic ducts, with no bile entry into the duodenum at 60 min in all five patients. Bile did not enter the duodenum for another 60 min after a high-fat meal. Both peak hepatic uptake time and excretion half time were increased. The hepatic extraction fraction stayed above 80%, suggesting primarily a biliary disease. All four patients who underwent endoscopic sphincterotomy responded well with relief of symptoms [46].

Pitfalls

Cholescintigraphy plays an important role in the evaluation of patients with biliary dyskinesia. Clear understanding of the mechanism of bile secretion and flow and factors that alter bile flow is important in arriving at a proper diagnosis. Functional imaging and measurement of parameters quantitatively require appropriate patient preparation and attention to technical details during data acquisition and analysis. Unlike the left ventricle, whose ejection fraction remains constant, the gallbladder ejection fraction can be controlled to any desired level simply by controlling the dose, dose rate, and duration of infusion of

cholecystokinin. Cholecystokinin is available in two different molecular forms: an intact molecule with 33 amino acids (CCK-33) and a fragment with 8 amino acids (CCK-8 or sincalide). The dose recommended in the package insert of Kinevac (Bracco Diagnostic Inc., Princeton, N.J.) is found to be too large and often elicits a non-physiologic response during cholescintigraphy [47–49]. The dose should be reduced for cholescintigraphy (Chap. 6). When cholecystokinin is not available, the test is standardized using a fatty-meal stimulation, where the total calorie, fat, carbohydrate, and protein contents are controlled strictly for the chosen meal. Use of opioids for pain control is quite common in both inpatients and outpatients, and their use reduces the gallbladder ejection fraction. The gallbladder ejection fraction returns to normal after the discontinuation of opioids (Fig. 10.1.13). A commitment to high technical quality control, test standardization, and direct interaction with the patient before, during, and after the procedure produces the best clinical outcome [50].

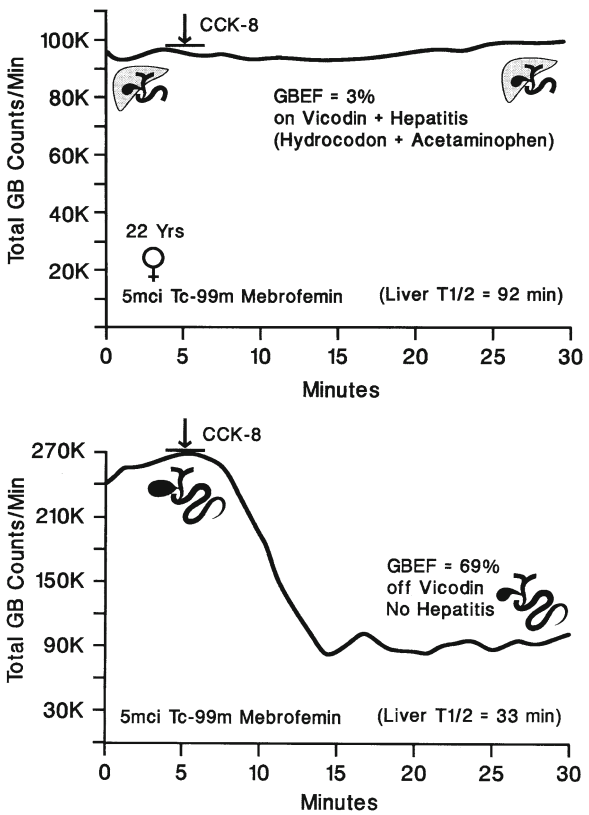

Fig. 10.1.13 Effect of opioids on gallbladder ejection fraction. A patient on vicodin for pain during viral hepatitis A shows slow clearance of the radiotracer from the liver ($T_{1/2}$ = 92 min) and an ejection fraction of only 3% (*top*). Both the clearance and ejection fraction return to normal after discontinuation of vicodin and recovery from hepatics (*bottom*)

References

1. Oddi R. D'une disposition a sphincter specille del'ouverture du canal cholidoque. Arch Ital Biol 1887;8:317–322
2. Cozzolino HJ, Goldstein F, Greening RR. The cystic duct syndrome. JAMA 1963;185: 920–924
3. Ivy AC, Oldberg E. A hormone mechanism of gallbladder contraction and evacuation. Am J Physiology 1928;86:599–613
4. Sjolund K, Sanden G, Hakanson R, Sundler F. Endocrine cells in human intestine: an immunocytochemical study. Gastroenterology 1983;85:1120–1130
5. Courtney DF, Clanachan AS, Scott GW. Cholecystokinin constricts the canine cystic duct. Gastroenterology 1983;85:1154–1159
6. Steinberg WM. Sphincter of Oddi dysfunction: a clinical controversy. Gastroenterology 1988;95:1409–1415
7. Geenen JE, Hogan WJ, Dodds WJ, Stewart ET, Arndorfer RC. Intraluminal pressure recording from the human sphincter of Oddi. Gastroenterology 1980;78:317–324
8. Thune A, Scicchitano J, Thompson IR, Toouli J. Reproducibility of endoscopic sphincter of Oddi manometry. Dig Dis Sci 1991;36:1401–1405
9. Meshkinpour H, Mollot M, Eckerling GB. Bookman. Bile duct dyskinesia. Clinical and manometric study. Gastroenterology 1984;87:759–762
10. Hogan WJ, Geenen JE. Biliary dyskinesia: Endoscopy 1988;20:179–183
11. Toouli J, Roberts-Thompson IC, Dent J, Lee J. Manometric disorders in patients with suspected sphincter of Oddi dysfunction. Gastroenterology 1985;88:1243–1250
12. Krishnamurthy S, Krishnamuthy GT. Biliary dyskinesia: role of the sphincter of Oddi, gallbladder, and cholecystokinin. J Nucl Med 1997;38:1824–1830
13. Goldstein F, Grunt R, Margulies M. Cholecystokinin cholescintigraphy in the differential diagnosis of acalculous gallbladder disease. Dig Dis 1974;19:835–849
14. Upp JR, Nealon WH, Singh P, Fagan CJ, Jonas AS, Greeley GH, Thompson JC. Correlation of cholecystokinin receptor with gallbladder contractility in patients with gallstones. Ann Surg 1987;205:641–648
15. Steigerwalt RW, Goldfine ID, Williams JA. Characterization of cholecystokinin receptors on bovine gallbladder membranes. Am J Physiol 1984;247:G709–G714
16. Krishnamurthy GT, Bobba VR, McConnell D, et al. Quantitative biliary dynamics: introduction of a new noninvasive scintigraphic technique. J Nucl Med 1983;24:217–223
17. Krishnamurthy S, Krishnamurthy GT. Evolution of nuclear hepatology as a clinical subspeciality. J Nucl Med Technol 1995;23:35S–45S
18. Krishnamurthy GT, Krishnamurthy S, Watson RD. Characterization of basal hepatic bile flow and the effects of intravenous cholecystokinin on the liver, sphincter, and gallbladder in patients with sphincter of Oddi spasm. Eur J Nucl Med Mol Imaging 2004;31:85–93
19. Krishnamurthy GT, Krishnamurthy S. Diagnosis of sphincter of Oddi spasm with quantitative cholescintigraphy. Indian J Nucl Med 2004;19:75–80
20. Cicala M, Scopinaro F, Corzziari E, Viscardi A, Habib FI, Torsoli A. Quantitative cholescintigraphy in the assessment of choledochoduodenal bile flow. Gastroenterology 1991;100:1106–1113
21. Shaffer EA, Hershfield NB, Logan K, Kloiber R. Cholescintigraphic detection of functional obstruction of the sphincter of Oddi. Effect of papillotomy. Gastroenterology 1986;90:728–733
22. Fullarton GM, Hilditch T, Campbell A, Murray WR. Clinical and scintigraphic assessment of the role of endoscopic sphincterotomy in the treatment of sphincter of Oddi dysfunction. Gut 1990;31:231–235
23. Drane WE, Johnson DA. Sincalide-augmented quantitative hepatobiliary scintigraphy(QHBS): Definition of normal parameters and preliminary relation between QHBS and sphincter of

Oddi(SO) manometry in patients suspected of having SO dysfunction. J Nucl Med 1990;31:1462–1468
24. Brar HS. Scintigraphic cholecystokinin-induced bile reflux named as Krishnamurthy-Bobba sign. J Nucl Med 1990;31:248
25. Sostre S, Kalloo AN, Spiegler EJ, Camargo EE, Wagner HN Jr. A noninvasive test of sphincter of Oddi dysfunction in post-cholecystectomy patients: The scintigraphic score. J Nucl Med 1992;33:1216–1222
26. Madacsy L, Velosy B, Lonovics J, Csernay L. Differentiation between organic and functional dyskinesia of the sphincter of Oddi with amyl nitrite-augmented quantitative hepatobiliary scintigraphy, Eur J Nucl Med 1994;21:203–208
27. Mourelle M, Guarner F, Moncada S, Malagelada JR. The arginine/nitric oxide pathway modulates sphincter of Oddi motor activity in guinea pigs and rabbits. Gastroenterology 1993;105:1299–1305
28. Bhatnagar A. Nifedifine interventional cholescintigraphy: a new method for assessing sphincter of Oddi? Indian J Nucl Med 1997;12:93–96
29. Dodds WJ, Thakur S, Collier RD. Quantitative hepatobiliary scintigraphy (editorial). J Nucl Med 1990;31:1468–1469
30. Tanaka M, Ikeda S, Nakayama F. Change in bile duct pressure response after cholecystectomy: loss of gallbladder as a pressure reservoir. Gastroenterology 1984;87:1154–1159
31. Freeman ML, Nelson DB. Sherman S, Haber GB, Herman ME, Dorsher PJ, Moore JP, Fennerty B, Ryan ME, Shaw MJ, Lande JD, Pheley AM. Complications of endoscopic biliary sphincterotomy. N Engl J Med 1996;335:909–918
32. Huibregtse K. Complications of endoscopic sphincterotomy and their prevention. N Engl J Med 1996;335:961–962
33. Mathuna PM, White P, Clarke E, Merriman R, Lennon JR, Crowe J. Endoscopic balloon sphincteroplasty (papillary dilatation) for bile duct stones: efficacy, safety, and follow-up in 100 patients. Gastrointest Endosc 1995;42:468–474
34. Gregg JA, Clark G, Barr C, McCartney A, Milano A, Volcjak C. Postcholecystectomy syndrome and its association with ampullary stenosis. Am J Surg 1980;139:374–378
35. Frassinelli P, Werner M, Reed III JF, Scagliotti C. Surgical Laparoscopy & Endoscopy 1998;8:30–34
36. Pickelman J, Peiss RL, Henkin R, Salo B, Nagel P. The role of sincalide cholescintigraphy in the evaluation of patients with acalculous gallbladder disease. Arch Surg 1985;120:693–697
37. Fink-Bennet D, DeRidder P, Kolozsi WZ, Gordon R, Jaros R. Cholecystokinin cholescintigraphy: Detection of abnormal gallbladder motor function in patients with chronic acalculous gallbladder disease. J Nucl Med 1991;32:1695–1699
38. Zech ER, Simmons LB, Kendrick RR, et al. Cholecystokinin enhanced hepatobiliary scanning with ejection fraction calculation as an indicator of disease of the gallbladder. Surg Gynecol Obstet 1991;172:21–24
39. Misra DC, Blossom GB, Fink-Bennet D, et al. Results of surgical therapy for biliary dyskinesia. Arch Surg 1991;126:957–960
40. Halverson JD, Garner BA, Siegel BA, et al. The use of hepatobiliary scintigraphy in patients with acalculous biliary disease. Arch Intern Med 1992;152:1305–1309
41. Sorenson MK, Francher S, Lang NP, Eidt JF, Broadwater JR. Abnormal gallbladder nuclear ejection fraction predicts success of cholecystectomy in patients with biliary dyskinesia. Am J Surg 1993;166:672–675
42. Kleiger PS, O'Mara RE. The clinical utility of quantitative cholescintigraphy: the significance of gallbladder dysfunction. Clin Nucl Med 1998;23:278–282
43. Black NA, Thompson E, Sanderson CFB, ECHSS group. Symptoms and health status before and 6 weeks after open cholecystectomy: a European cohort study. Gut 1994;35:1301–1305
44. Desautels SG, Slivka A, hutson WR, chun A, Mitrani C, DiLorenzo C, Wald A. Postcholecystectomy pain syndrome: pathophysiology of abdominal pain in sphincter of Oddi type III. Gastroenterology 1999;116:900–905

45. Craig AG, Toouli J. Sphincterotomy for biliary sphincter of Oddi dysfunction. Cochrane databse of systematic reviews 2001, issue 1, art. no.:CD001509. DOI:10.1002/14651858.CD001509
46. Rubini G, Dmonte M. Postcholecystectomy syndrome. Evaluation by biliary cholescintigraphy and MR cholangiopancreatography. Clin Nucl Med 1999;24:784–789
47. Krishnamurthy GT, Bobba VR, Kingston E. Optimization of octapeptide of cholecystokinin (OP-CCK) dose for gallbladder emptying. In: Raynaud C, (ed) Proceedings of the third world congress of nuclear medicine and biology. Paris, France: Pergamon Press; 1982, pp 2224–2247
48. Toftdahl DB, Hojgaard L, Winkler K. Dynamic cholescintigraphy: Induction and description of gallbladder emptying. J Nucl Med 1996;37:261–266
49. Ziessman HA, Fahey FH, Hixon DJ. Calculation of a gallbladder ejection fraction: advantage of continuous Sincalide infusion over the 3-minute infusion method. J Nucl Med 1992;33:537–541
50. Krishnamurthy S, Krishnamurthy GT. Gallbladder ejection fraction: a decade of progress and future promise (editorial). J Nucl Med 1992;32;542–544

Pediatric Nuclear Hepatology 11

The liver and biliary system develops from a bi-lobed (cephalic and caudal) endodermal bud that sprouts along the ventral surface of the distal end of the foregut at its junction with the midgut. The cephalic bud divides into two branches, which later form the right and left lobes of the liver. The caudal bud gives rise to biliary tract and the gallbladder (Fig. 1.1.1, Chap. 1). The biliary tract starts first as a patent tubular structure, but turns into a solid core during early intrauterine life through the proliferation of epithelial cells. After recanalization of the solid core by 12–14 weeks, bile secretion begins and flows into the small intestine. Most of the congenital abnormalities of the biliary tract are due to either failure of recanalization of the ducts (biliary atresia) or faulty recanalization with cystic dilatation of intrahepatic (Caroli's disease) and extrahepatic ducts (choledochal cyst).

Physiologic jaundice occurs in 65% of near- or full-term infants, and usually clears within few weeks after birth. Persistent uncomplicated long-term hyperbilirubinemia is a concern, and past studies suggested some link with neurological sequelae, such as mental retardation, autism, and cerebral palsy. The effects of uncomplicated high serum bilirubin levels have been addressed well in more recent studies. In a Canadian study involving 56,019 near- or full-term infants with serum bilirubin levels greater than 20 mg%, no evidence of bilirubin toxicity (kernicterus, gaze palsy) was found, lessening the anxiety over uncomplicated hyperbilirubinemia [1]. There is also no increased risk of autism due to hyperbilirubinemia [2]. However, persistent hyperbilirubinemia beyond 2 weeks should raise concern for several other possibilities (Table 11.1.1), some requiring immediate intervention, while others may be managed by careful follow-up without a specific therapy. Neonatal hepatitis and congenital biliary atresia are two of the diseases that account for the great majority of persistent jaundice beyond 2 weeks in a neonate.

11.1 Congenital Biliary Atresia vs. Neonatal Hepatitis

Congenital biliary atresia (CBA) is a progressive, sclerosing, inflammatory disease, primarily affecting the extrahepatic bile duct from the region of the portahepatis to its termination in the duodenum. It is estimated to affect 1 in 12,000 live births [3]. Untreated, the disease progresses relentlessly, leading to biliary cirrhosis and death. Hepatoportoenterostomy (Kasai procedure) is the definitive therapy in early stages. The rate of success of establishing

G.T. Krishnamurthy and S. Krishnamurthy, *Nuclear Hepatology*,
DOI 10.1007/978-3-642-00648-7_11, © Springer-Verlag Berlin Heidelberg 2009

Table 11.1.1 Causes of persistent jaundice beyond 2 weeks after birth

1. Neonatal hepatitis
Viral
Cytomegalo virus
Hepatitis B
Rubella
Herpes
Coxsackie
Bacterial
E. coli
Klebsiella
Pseudomonas
Proteus
Bacteroids
Streptococcus
Treponema pallidum
Parasitic
Toxoplasma gondii
2. Biliary atresia
Extra-hepatic ducts (congenital biliary atresia)
Intra-hepatic ducts.
Congenital rubella
Trisomy 17
Trisomy 18
Alagille's syndrome (arterio-hepatic dysplasia)
3. Genetic or metabolic
Alpha 1 anti-trypsin
Galactosemia
Hereditary fructosemia
Hypothyroidism

an adequate bile flow by the Kasai procedure depends very much on the duct size at birth and the time interval between birth and hepatoportoenterostomy (HPE). Effective bile flow is established in 77–82% of the infants when HPE is performed within 60 days after birth. The success rate decreases to 45–59% when HPE is delayed for 60–90 days and decreases further to 10–28% when HPE is delayed for 3–4 months. The success rate increases to 92% when the duct lumen is greater than 150 μm in size [4]. Early diagnosis, therefore, plays a critical role in determining the outcome of therapy (Table 11.1.2).

Etiology

The exact etiology of CBA is unknown. Two theories have been proposed; one theory is that of metaplasia of the hepatocytes, and the other is that of faulty metaplasia combined with ingrowth from extrahepatic ducts [5, 6]. Ischemia, toxins, and duct injury are well

Table 11.1.2 Effect of timing and duct size on rate of success of hepatoportoenterostomy (HPE) for congenital biliary atresia [4]

Age at HPE	Success rate
<60 days	77–82%
61–90 days	45–59%
90–120 days	10–28%
Duct size	
>151 μm	92%
50–150 μm	81%
No patent ducts	18%

recognized risk factors. Recent studies suggest that atresia may be due to a failure of remodeling at the hepatic hilum with a continuation of the fetal-type bile leak due to poor mesenchymal support. Bile leak through the ducts initiates an intense inflammatory reaction with a subsequent obliteration of the bile duct lumen. The characteristic findings on liver biopsy include ductal proliferation, canalicular and cellular bile stasis, periportal edema, and fibrosis. The title "atresia" is reserved for patients with complete obliteration of the duct lumen. Hypoplasia is a transition phase before complete obliteration of the duct lumen [7].

Congenital biliary atresia is divided into two clinical forms, fetal and perinatal. The perinatal form is the most common and is characterized by late-onset neonatal jaundice, with a jaundice-free time interval after birth. There are no other accompanying congenital abnormalities. Remnants of the bile duct are found within the hepatoduodenal ligament [4]. The fetal form is less frequent and accounts for less than 25% of the cases. It is characterized by an early onset of neonatal jaundice, with no clearance of physiologic jaundice (no jaundice-free time interval). It is frequently associated with other congenital anomalies, including polysplenia, asplenia, cardiovascular defects, or abdominal situs inversus, etc. No bile duct remnants are found in the hepato-duodenal ligament.

Clinical Presentation

Infants with CBA are usually born at full term with a normal birth weight and show normal growth pattern in the immediate neonatal period. It is more common in girls than boys. Jaundice usually starts 2 weeks after birth with acholic stool. Serum shows nonspecific elevation of direct bilirubin, alanine aminotransferase (ALT), and gamma- glutamyl transferase (GGT). About 90% of infants show a serum conjugated bilirubin (direct bilirubin) level greater than 4 mg dl^{-1} [8, 9]. Aspiration of bile through a naso-duodenal tube (after instillation of 25% magnesium sulfate into the duodenum to stimulate gallbladder contraction and bile emptying) establishes patency of the bile ducts and thus excludes the diagnosis of congenital biliary atresia and confirms the diagnosis of neonatal hepatitis. Bile is aspirated from the duodenum in more than 80% of the infants with neonatal hepatitis, but

not from infants with biliary atresia [10]. Intubation and duodenal bile aspiration are relatively invasive in a newborn, and a negative test (no bile aspiration) is not always specific for congenital biliary atresia.

Hepatomegaly is unusual at birth and begins to develop 6–8 weeks later. Cholestasis, fibrosis, and cirrhosis develop as the infant grows. The incidence of biliary atresia is higher among Chinese and Filipinos (2–3 per 10,000) than in Japanese and Caucasians [11]. Serial liver function tests provide an indication of the severity of the disease. Serum values of total bilirubin, direct bilirubin, GGT, and alkaline phosphatase, and the alkaline phosphatase/GGT ratio do not reliably distinguish congenital biliary atresia from neonatal hepatitis [12]. Laparoscopy has no diagnostic role as it cannot assess the patency of the bile ducts. Cholangiography is invasive and technically difficult to do because of the small size of the ducts.

Cholescintigraphy

The indication for cholescintigraphy in a neonate is persistent jaundice beyond the 2nd week of life or new jaundice that develops 3 weeks after birth. An ideal patient preparation includes treatment with 5 mg kg^{-1} per day of phenobarbital, in two equally divided doses, for 5–7 days prior to cholescintigraphy. Phenobarbital stimulates bile production [13] and increases the secretion of the radiotracer into bile, enabling better delineation of bile ducts and duodenum in infants with neonatal hepatitis, but not in those with CBA [14–16]. Cholestyramine or ursodeoxycholic acid also promotes bile secretion. The infant should not be fed for an hour before and an hour after injection of the radiotracer. The duration of fasting prior to cholescintigraphy should be increased in older children in proportion to their age.

Data Collection

The agent of choice in neonatal cholestasis is Tc-99-m mebrofenin, because it competes with serum bilirubin for hepatocyte uptake much more effectively than Tc-99m disofenin or any other Tc-99m-HIDA agent [17]. A dose of 100 μCi kg^{-1} (1 mCi minimum) of Tc-99-m-mebrofenin is injected intravenously. A gamma camera, preferably with a small field of view, fitted with a low-energy, parallel-hole, all-purpose collimator, is positioned anteriorly over the upper abdomen. The computer data are collected on a 64 × 64 word mode matrix at one frame per minute for 60 min (Fig. 11.1.1). Delayed images are obtained between 2–4 h and 20–24 h when intestinal activity is not seen in early images.

Data Analysis

A normal neonate shows rapid liver uptake and excretion compared to the infant with CBA or hepatitis (Fig. 11.1.1). For quantification, three regions of interest are drawn, and time-activity curves are generated separately over the (1) heart, (2) right upper lobe of the liver,

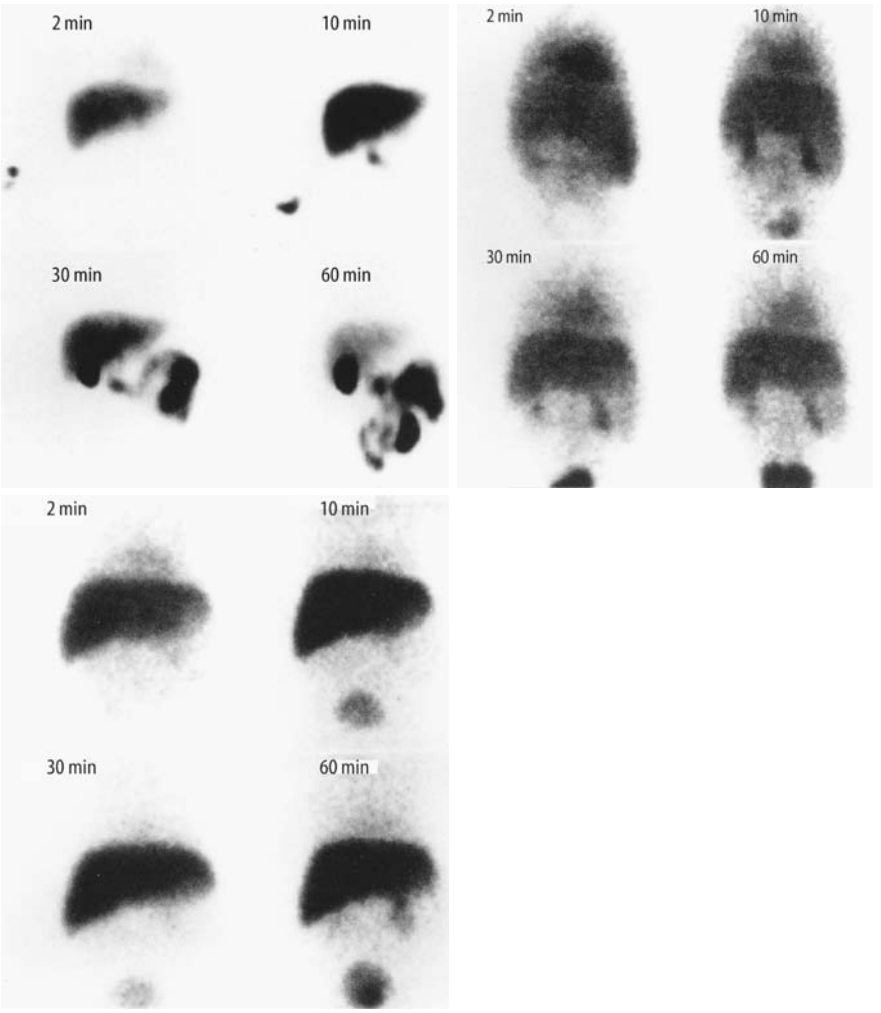

Fig. 11.1.1 Cholescintigraphy in the neonate. There is normal extraction and rapid excretion of 99mTc-HIDA in a normal neonate (*top left*). Extraction is decreased (persistent heart activity), and there is delayed excretion in neonatal hepatitis (*top right*). In biliary atresia, extraction is good, but no excretion into small bowel is seen (*bottom left*). Kidneys form the alternate route of excretion [19]

and (3) spleen. The spleen ROI is used for blood background. Because both the hepatic and splenic arteries arise from the same celiac artery, the spleen serves as an ideal organ to represent the liver blood background. The hepatic extraction fraction and excretion half times are obtained by subjecting data to deconvolutional analysis, very similar to the procedure for adults (Fig. 11.1.2) [18, 19]. Measurement of the hepatic extraction fraction by deconvolutional analysis is equivalent to measuring the first pass extraction by injecting the tracer directly into the hepatic artery or portal vein. The hepatic extraction fraction

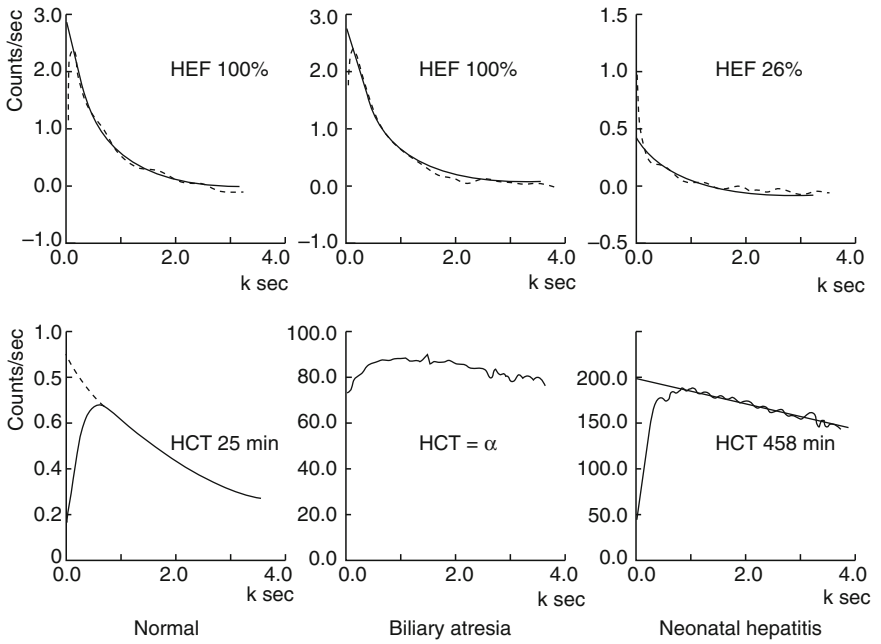

Fig. 11.1.2 Quantitative biliary dynamic studies in pediatrics. Hepatic extraction fraction (*HEF*) and excretion half-time (*HCT*) in a normal neonate (*left*), congenital biliary atresia (*middle*), and neonatal hepatitis (*right*). HEF remains relatively normal in biliary atresia, whereas both HEF and HCT are abnormal in neonatal hepatitis (modified from [19])

provides an objective criterion for separating biliary atresia from neonatal hepatitis in early cases of CBA. The liver extraction fraction and excretion half time provide a measure of the severity of hepatobiliary disease. For a comparable level of serum bilirubin, infants with congenital biliary atresia show a relatively higher hepatic extraction fraction than infants with neonatal hepatitis [19, 20]. Obstruction over a longer period of time ultimately compromises hepatocyte function, and the hepatic extraction fraction begins to decrease and loses its power to differentiate biliary from hepatocyte decrease. The diagnosis of congenital biliary atresia or neonatal hepatitis is also made by assessing both the images and the shape and direction of the curves (Fig. 11.1.3).

Normal Neonate

Cholescintigraphy in a normal neonate is characterized by rapid hepatocyte uptake and secretion of Tc-99 m-HIDA. Peak hepatic uptake occurs within 5 min, the gallbladder appears within 10 min, and intestinal activity is seen between 20–30 min. Unlike in adults and older children, the common hepatic duct, common bile duct, and the cystic ducts are not seen in a neonate [15]. After reaching the peak within 5 min, the liver shows a rapid decline. Peak cardiac counts occur in the first frame (1 min) followed by a rapid decline,

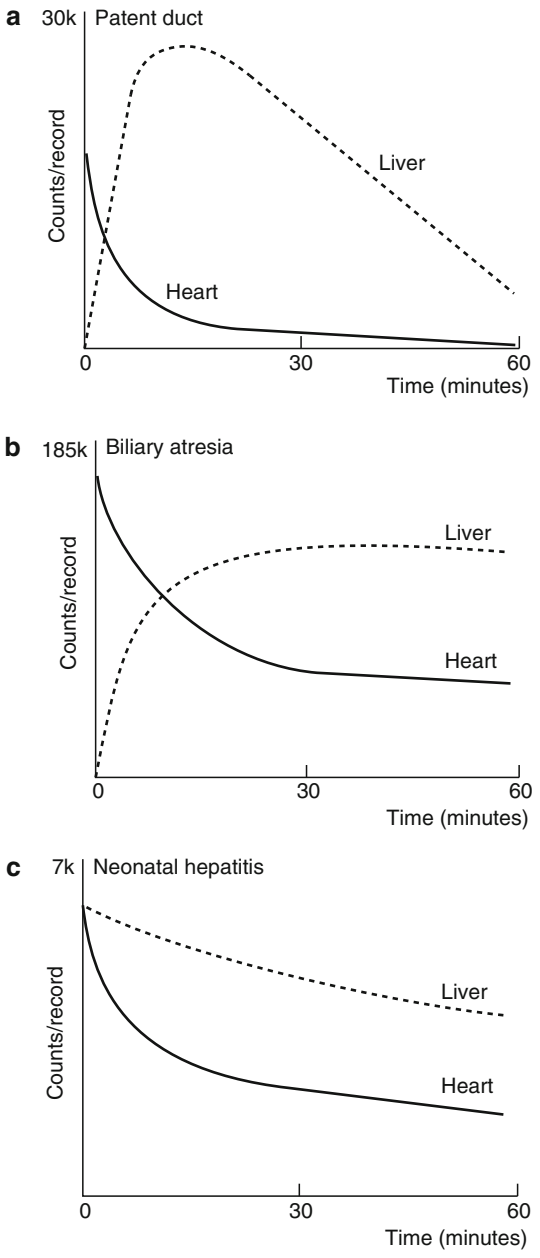

Fig. 11.1.3 Heart and liver simple time-activity curves in three children. In a normal child (**a**), both heart and liver curves show a rapid decline. In biliary atresia (**b**), the liver curve shows slow uptake and no excretion. In neonatal hepatitis (**c**), the liver curve shows slow excretion without an uptake peak, indicating mainly background reduction [12]

reaching a background activity level within 5 min. Both liver and heart curves converge towards the end [12]. A subjective analysis of the shape of the curves helps to separate normal infant from congenital biliary atresia or neonatal hepatitis (Fig. 11.1.3). Calculation of the hepatic extraction fraction and excretion half time provide better and more powerful objective functional parameters than a simple subjective analysis of the curves (Fig. 11.1.2). Two of the commercial vendors now are planning to provide hepatobiliary software for routine clinical use on their gamma camera and computer systems, but for others, the users have to develop their own software and database for clinical application.

In a normal neonate, the hepatic extraction fraction value ranges between 87 and 100% with an average of 99.0 ± 3.6% (Table 11.1.3). A value below 92% (mean, 2 SD) is considered abnormal. Mean excretion half time with Tc-99 m disofenin is 23.6 ± 7.7 min; a value above 40 min is considered abnormal. An artifact in the calculation of the hepatic extraction fraction due to an abrupt truncation of data collection is avoided by adding an appendage at the end of the curve [21].

Congenital Biliary Atresia

Neonates with congenital biliary atresia maintain a relatively high extraction Tc-99m-HIDA with clear delineation of the hepatic morphology with well-defined borders and contour. Major abnormalities are confined to bile secretion. Despite a good extraction by the hepatocytes, there is total lack of secretion of Tc-99m-HIDA into the bile, resulting in non-visualization of the entire biliary tree. The liver image appears much like a radiocolloid scan without the spleen. Delayed images at 24 h do not show any evidence of bile entry into the small intestine [15, 16]. The liver time-activity curve shows good uptake, but no excretion. Excretion half time values often indicate infinity (Fig. 11.1.2). The hepatic extraction fraction value is maintained at a high level despite high serum bilirubin, especially when cholescintigraphy is obtained within 45 days after birth. When the extraction fraction value begins to decline in patients with CBA, however, it indicates functional compromise because of persistent bile duct obstruction over a longer period of time [20]. A diagnosis of congenital biliary atresia is highly probable in a neonate with conjugated (direct) hyper-bilirubinemia, a relatively high hepatic extraction fraction in association with non-visualization of the entire biliary tree and the small intestine. Cholescintigraphy is unable to differentiate intrahepatic (Alagille's syndrome) from extrahepatic (congenital biliary atresia) ductal obstruction.

Table 11.1.3 Hepatic extraction fraction and excretion half time (mean ± SD) in normal subjects and children with congenital biliary atresia, hepatitis, and miscellaneous hepatobiliary diseases [18]

Parameter	Normal	CBA	Hepatitis	Miscellaneous
Number	12	9	16	8
Hepatic extraction fraction (%)	99.0 ± 3.6	79.3 ± 25.5	51.5 ± 20.6	87.8 ± 13.3
Hepatic excretion halftime (min)	23.6 ± 7.7	183.1 ± 201.1	101.9 ± 77.0	44.8 + 35.7

The incidence of persistent jaundice beyond 2 weeks after birth, in general, is estimated to be 1 in 5,000 live births; neonatal hepatitis occurs 1 in 8,000, and biliary atresia, 1 in 10,000–15,000 live births. Pure intrahepatic biliary atresia or hypoplasia is rare and occurs in 1 in 70,000 births [22]. The extrahepatic bile ducts are patent in most patients with intrahepatic biliary atresia. Intrahepatic biliary atresia is commonly associated with intrauterine infection and genetic abnormalities as listed in Table 10.1.1. Alagille's syndrome is a form of intrahepatic biliary hypoplasia or atresia in association with pulmonary stenosis, vertebral body abnormalities, sexual and mental underdevelopment, and a typical facial feature [23].

Neonatal Hepatitis

Neonatal hepatitis is usually caused by viral, fungal, or bacterial infection (Table 10.1.1). Jaundice persists beyond 2 weeks after birth, and the liver function tests show non-specific elevation of enzymes with conjugated hyper-bilirubinemia [11]. Cholescintigraphic features depend upon the severity of hepatocellular disease at the time of imaging. Uptake of Tc-99m-HIDA by the hepatocyte is delayed and decreased. Both the time-to-peak hepatic uptake and excretion half time are increased. Intestinal and gallbladder visualization time may be either normal or markedly delayed. Due to the marked reduction in hepatocyte extraction of Tc-99m HIDA, the liver morphology is poorly defined with indistinct borders and contour. Heart and liver time-activity curves run in parallel, indicating mostly background reduction (Fig. 11.1.3). The hepatic extraction fraction value shows an inverse relationship with the serum bilirubin level. Extraction fraction values as low as 30% are common [19]. Intestinal activity is seen by 24 h. An apparent appearance of good uptake by the liver is merely a reflection of hepatic blood pool radioactivity and is not due to true uptake by the hepatocytes, as reflected by low hepatic extraction fraction value.

The success of cholescintigraphy is variable, depending upon the time interval between birth and imaging (Table 11.1.4). A sensitivity of 100%, specificity of 80%, and accuracy of 93% have been reported from some centers with technetium-99m mebrofenin [24]. High accuracy is attributed partly to the agent's ability to compete effectively with serum bilirubin for uptake by the hepatocytes. One cannot always separate congenital biliary atresia from neonatal hepatitis solely on the basis of the HEF value, emphasizing the importance of combining quantification with the image pattern to increase diagnostic accuracy [20].

Table 11.1.4 Efficacy of cholescintigraphy, ultrasonography, and liver biopsy in the differential diagnosis of congenital biliary atresia from neonatal hepatitis [24]

Parameter	Cholescintigraphy	Ultrasonography	Liver biopsy
Sensitivity (%)	100	70	95
Specificity (%)	80	70	100
Accuracy (%)	93	70	97
Positive predictive value	91	82	100
Negative predictive value	100	54	91

Management of Neonatal Cholestasis

Neonatal hepatitis is treated medically with good nutrition, anti-viral, anti-bacterial, or anti-parasitic agents, depending upon its etiology. Most patients recover uneventfully (Fig. 11.1.4A). The American Academy of Pediatrics recommends phototherapy for healthy term infants [24]. The Kasai procedure is the treatment of choice for congenital biliary atresia [26, 27]. The neonate is prepared for surgery with preoperative antibiotic prophylaxis, optimal hydration, and good nutrition. The abdomen is explored through a high transverse incision, and a fine catheter is inserted into the gallbladder by piercing the fundus. Fibrosis of the wall with no bile within the gallbladder or obliteration of the common bile duct lumen confirms biliary atresia. The presence of bile inside the gallbladder with patency of the common bile duct, on the other hand, indicates neonatal hepatitis. A cholangiogram is obtained by injecting the radiocontrast through the catheter.

In the original Kasai procedure, the jejunum is cut beyond the ligament of Trietz, and a portoenterostomy is established. The proximal part of the jejunum is anastomosed to the side wall of the Roux-en-Y limb, below the portoenterostomy. The most common complication of portoenterostomy is acute ascending cholangitis due to reflux of intestinal contents into bile ducts. Several modifications to the original portoenterostomy were made mainly with the hope of preventing acute ascending cholangitis (Fig. 11.1.5). The temporary jejunostomy stoma created for decompression is usually closed at 3 months after confirming adequacy of bile flow. Most pediatric surgeons now seem to prefer the original Kasai procedure (Kasai 1) and avoid creating an external fistula. Administration

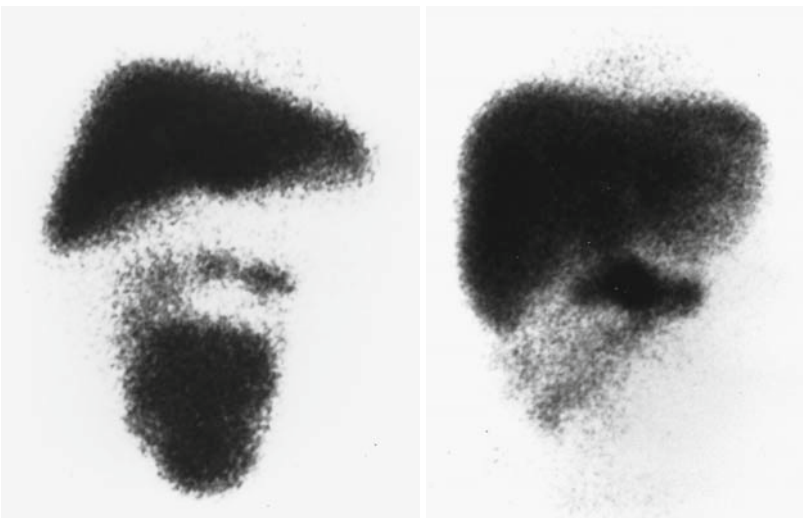

Fig. 11.1.4 Response to therapy in neonatal cholestasis. An infant with giant cell neonatal hepatitis responds to medical therapy and shows bile secretion into intestine (*left*). An infant with congenital biliary atresia (*right*) shows bile secretion into the intestine after a Kasai procedure. (Courtesy of Dr. Vasundara Tolia, Detroit, MI [20])

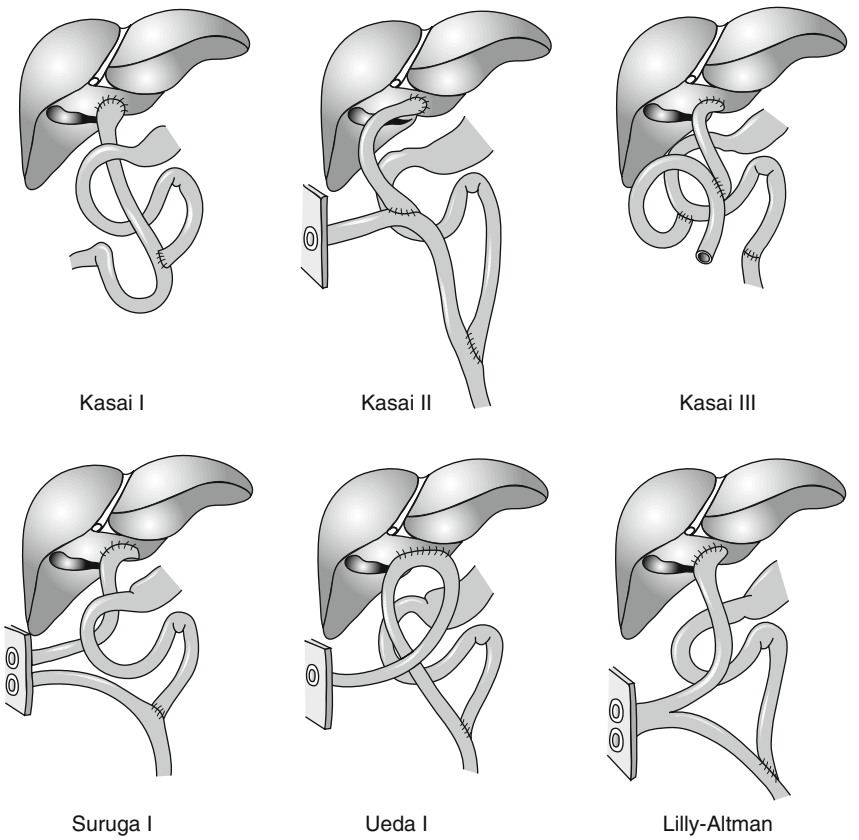

Fig. 11.1.5 Portoenterostomy for congenital biliary atresia. In Kasai I, an open end of a loop of the jejunum is attached directly to the undersurface of the liver to serve as a bile conduit. In Kasai II and Kasai III, a temporary external fistula is created. Other types of anastomoses include Segura I, Ueda I, and Lilly-Altman (modified from [11])

of appropriate antibiotics reduces the incidence of acute or recurrent cholangitis. A successful Kasai procedure establishes free bile flow into the small intestine (Fig. 11.1.4B)

The rate of success of portoenterostomy for congenital biliary atresia depends primarily upon the time interval between birth and surgery and also upon the size of the duct lumen at birth (Table 11.1.2). Poor results are generally attributed to delayed portoenterostomy. A success rate of 89% and a 10-year survival rate of 33–74% are obtained when the neonate with congenital biliary atresia receives portoenterostomy within 60 days after birth (Table 11.1.5).

Liver transplantation is the ultimate therapy when HPE fails. The usual cause for HPE failure is continued fibrosis secondary to recurrent cholangitis. Approximately 65% of infants who receive HPE for biliary atresia ultimately require liver transplantation [28, 29]. Biliary atresia is the most common indication and accounts for 54% of all liver transplantation in children. Other indications include metabolic diseases (14%), acute hepatic necrosis

(11%), autoimmune and other cirrhosis (7%), malignancy, and other miscellaneous conditions [30]. Split liver and living donor liver transplantations have helped to overcome, to some extent, the shortages of donor livers in the pediatric population [31, 32]. The high cost and limited availability of donors still remain two of major factors limiting liver transplantation in children (see Chap. 12). The Kasai operation remains the first choice of treatment, and its application early at experienced centers reduces the need for liver transplantation [33]. Non-invasive functional imaging with quantification is ideal for children, for evaluation of both native and transplant livers. Congenital biliary atresia, metabolic diseases, and acute hepatic necrosis all together account for nearly 80% of all transplants in children (Fig. 11.1.6). In the case of congenital biliary atresia, cholescintigraphy is suitable not only for diagnosis, but also for assessing function after the Kasai procedure or transplant liver function when the Kasai procedure fails [34].

Table 11.1.5 Clinical outcome after Kasai procedure for congenital biliary atresia [3]

Parameter	Success rate (%)
Effective bile excretion	89
Clearance of jaundice	62
Jaundice-free survival	53–62
10-year survival	33–74
Onset of esophageal varices	29–73

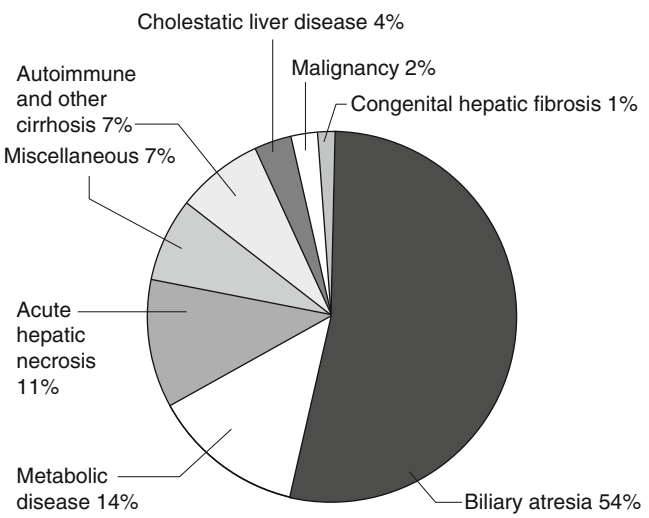

Fig. 11.1.6 Indications for liver transplantation in children. Congenital biliary atresia is the most common indication, followed by metabolic diseases, acute hepatic necrosis, and others [33]

References

1. Jangaard KA, Fell DB, Dodds L, Allen AC. Outcome in a population of healthy term and near-term infants with serum bilirubin levels of ≥325 μmol/l (>19 mg/dl) who were born in Nova Scotia, Canada, between 1994 and 2000. Pediatrics 2008;122:119–124
2. Croen LA, Yoshida CK, Odouli R, Newman TB. Neonatal hyperbilirubinemia and risk of autism spectrum disorders. Pediatrics 2005;115(2):e135–e138
3. Balistreri WF. Neonatal cholestasis. J Pediatr 1985;106:171–184
4. Balistreri WF, Grand R, Hoofnagle JH, Suchy FJ, Ryckman FC, Perlmutter DH, Sokol RJ. Biliary atresia: current concepts and research directions. Summary of a symposium. Hepatology 1996;23:1682–1692
5. Cocjin J, Rosenthal P, Buslon V, Luk L Jr, Barajas L, Geller SA, Ruebner B, French S. Bile ductule formation in fetal, neonatal, and infant livers compared with extrahepatic biliary atresia. Hepatology 1996;24:568–574
6. Desmet VJ. Congenital diseases of intrahepatic bile ducts: variations on the theme "ductal plate malformation". Hepatology 1992;16:1069–1083
7. Tan CEL, Davenport M, Driver M, Howard ER. Does the morphology of the extrahepatic biliary remnant in biliary atresia influence survival? A review of 205 cases. J Pediatr Surg 1994;29:1459–1464
8. Mieli-Vergani G, Howard ER, Portman B, Mowat AP. Late referral for biliary atresia-missed opportunities for effective surgery. Lancet 1989;1:421–423
9. Mowat AP, Davidson LL, Dick MC. Earlier identification of biliary atresia and hepatobiliary disease: selective screening in the third week. Arch Dis Child 1995;72:90–92
10. Greene HL, Helinek GL, Moran R, O'Neill J. A diagnostic approach to prolonged obstructive jaundice by 24-hour collection of duodenal fluid. J Pediatr 1979;95:412–414
11. De Lorimier AA, Harrison MR. Congenital biliary atresia. In: Way LW, Pelligrini CA (eds). Surgery of the gallbladder and bile ducts. WB Saunders, Philadelphia, 1987, pp 581–607
12. Leonard JC, Hitch DC, Manion CV. The use of diethyl-IDA Tc-99m clearance curves in the differentiation of biliary atresia from other forms of neonatal jaundice. Radiology 1982;142:773–776
13. Jaffe SJ, Jachau MR. Perinatal pharmacology. Ann Rev Pharmacology 1974;14:219–238
14. Thaler MM. Effect of phenobarbital on hepatic transport and excretion of 131 I-rose bengal in children with cholestasis. Pediatr Res 1972;6:100–110
15. Majd M, Reba RC, Altman RP. Effect of phenobarbital on 99mTc-IDA scintigraphy in the evaluation of neonatal jaundice. Semin Nucl Med 1981;11:194–204
16. Majd M, Reba RC, Altman RP. Hepatobiliary scintigraphy with 99mTc-PIPIDA in the evaluation of neonatal jaundice. Pediatrics 1981;67:140–145
17. Krishnamurthy S, Krishnamurthy GT. Technetium-99m-iminodiacetic acid organic anions: review of biokinetics and clinical application in hepatology. Hepatology 1989;9:139–153
18. Brown PH, Juni JE, Lieberman DA, Krishnamurthy GT. Hepatocyte versus biliary disease: a distinction by deconvolutional analysis of technetium-99m IDA time-activity curves. J Nucl Med 1988;29:623–630
19. Howman-Giles R, Moase A, Gaskin K, Uren R. Hepatobiliary scintigraphy in a pediatric population: determination of hepatic extraction fraction by deconvolution analysis. J Nucl Med 1993;34:214–221
20. Tolia V, Kottamasu SR, Tabassum D, Simpson P. The use of hepatocyte extraction fraction to evaluate neonatal cholestasis. Clin Nucl Med 1999;24:655–659
21. Juni JE, Thrall JH, Froelich JW, Wiggins RC, Campbell DA Jr, Tuscan M. The appended curve for deconvolutional analysis-method and validation. Eur J Nucl Med 1988;14:403–407
22. Shim WKT, Kasai M, Spence MA. Racial influence on the incidence of biliary atresia. In: Bill MA, Kasai M (eds) Progress in pediatric surgery, Urban, Scharzenberg, 1979

23. Alagille D, Odievre M, Gautier M, Dommergues JP. Hepatic ductular hypoplasia associated with characteristic facies, vertebral malformation, retarded physical, mental, and sexual development, and cardiac murmur. J Pediatr 1975;56:63–71
24. Maini A, Khanduri A, Gambhir S, Yacha SK, Das BK. Role of Tc-99 m-mebrofenin in evaluation of neonatal cholestasis syndrome. Indian J Nucl Med 1997;12:84–87
25. American Academy of Pediatrics, provisional committee for quality improvement and subcommittee on hyperbilirunemia. Practice parameter: management of hyperbilirunemia in the healthy term newborn. Pediatrics 1994;94(4):558–562
26. Kasai M, Kimura S, Asakura Y. Surgical treatment of biliary atresia. J Pediatr Surg 1968;3:665–668
27. Kasai M, Suzuki H, Ohashi F, Ohi R, Chiba T, Okamoto A. Technique and results of operative management of biliary atresia. World J Surg 1978;2:571–579
28. Otte JB, deVille de Goyet J, Reding R, Hausleithner V, Sokal E, Chardot C, Debande B. Sequential treatment of biliary atresia with Kasai portoenterostomy and liver transplantation: a review. Hepatology 1994;20:41S–48S (suppl)
29. Ryckman F, Fisher R, Pedersen S, Dittrich V, Heubi J, Farrell M, Balistreri W, Ziegler M. Improved survival in biliary atresia patients in the present era of liver transplantation. J Pediatr Surg 1993;28:382–385
30. Reyes J, Mazariegos GV. Pediatric transplantation. Surg Clin North Am 1999;79:163–189
31. Egawa H, Uemoto S, Inomata Y, Shapiro J, Asonuma K, Kiuchi T, Okajima H, Itou K, Tanaka K. Biliary complications in pediatric living related liver transplantation. Surgery 1998;124:901–910
32. Reding R, Goyet J, Delbeke I, Sokal E, Jamart J, Janssen M, Otte J. Pediatric liver transplantation with cadaveric or living related donors: comparative results in 90 elective recipients of primary grafts. J Pediatr 1999;134:280–286
33. Chardot C, Carton M, Spire-Bendelac, Pommelet CL, Golmard J, Auvert B. Prognosis of biliary atresia in the era of liver transplantation: French national study from 1986 to 1996. Hepatology 1999;30:606–611
34. Reyes J, Mazariegos GV. Pediatric transplantation. Surg Clin North Am 1999;79:163–189

11.2 Cystic Diseases of the Hepatobiliary System

Cysts are abnormal spaces within the liver parenchyma or along the biliary tract (choledochal cysts). They vary in size and location and contain mostly clear liquid. Choledochal cysts are rare, occurring in 1 in 100,000–150,000 live births. About 80% of choledochal cysts become symptomatic early and are diagnosed before the age of 10. Cysts are classified in many ways, and the classification provided in Table 11.2.1 is primarily for diagnostic purposes using various imaging techniques, including ultrasound, CT, MRCP, and cholescintigraphy. Cystic diseases due to parasites (hydatid cyst) and bacteria (abscess) are covered separately under space-occupying lesions of the liver in Chap. 4. This section deals primarily with those congenital cysts that have direct communication with the bile ducts and hence fill in with radiolabeled bile. The diagnosis of a non-communicating cyst is inferred when radioactive bile does not enter the cyst.

Cysts are either solitary or multiple. Solitary cysts are rare, found at all ages, and most remain asymptomatic [1]. The cysts occur mostly along the hepatobiliary tract, starting at the smallest intralobular duct to the termination of the common bile duct into the duodenum.

Table 11.2.1 Classification of cystic diseases of the hepatobiliary system

1. Parasitic (hydatid cyst)
2. Non-parasitic cystic disease
a) Intrahepatic
1) Solitary or multiple intrahepatic cysts with no communication with the bile ducts (adult polycystic liver disease)
2) Mixed variety where few cysts communicate with the bile ducts
3) Diffuse or segmental cystic dilatation of the bile ducts (Caroli's disease)
b) Extrahepatic.
1) Choledochal cyst
a) Cystic
b) Fusiform
c) Cylindrical
d) Rosary (multiple cysts)
e) Diverticular
f) Choledochocele

Most of the cysts are congenital, but a few of the acquired cysts follow an infection, trauma, or obstruction of a duct. The cyst may be entirely extrahepatic or intrahepatic in location.

The occurrence of both intrahepatic and extrahepatic cysts in a patient is rare, but is well recognized [2].

Etiology

The exact cause of cystic dilatation of the bile ducts is unknown. Various hypotheses have been proposed, including weakness of the duct wall, angulation of the duct, presence of a valve-like structure within the lumen, inflammation, or sphincter dysfunction, all of which increase in intraductal pressure with impedance to bile flow [3]. The dilatation is initiated by an irregular and unequal proliferation of duct cells during recanalization of the solid core during early intrauterine life. Cysts are relatively more common in the Japanese and other Asians than in people elsewhere in the western hemisphere. An incidence of 1 in 13,000 hospital admissions has been reported in Japanese children [4]. The cyst wall ranges in thickness from 1 to 10 mm and consists mostly of fibrous tissue lined with cuboidal cells, or often with no lining cells at all. The cyst wall lacks mucous glands and a muscle layer. The cyst volume varies from a few milliliters to several liters [3].

Classification of Choledochal Cysts

Cysts are classified mainly into the intrahepatic and extrahepatic variety. Kami et al. and Todani et al. recommend classification based upon the shape, size, extent, and location of the cyst [5, 6]. The cystic type is the most common variety and accounts for 54% of all choledochal cysts (Fig. 11.2.1). Fusiform is the next most common (24%), followed by the

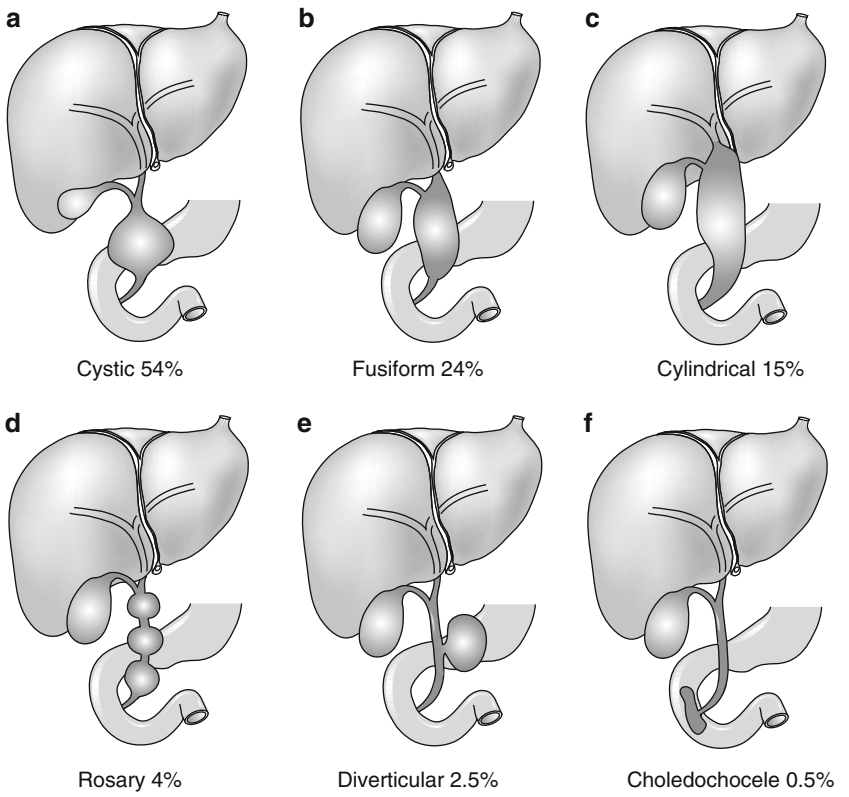

Fig. 11.2.1 Classification of extrahepatic bile duct cysts. Cystic type is the most common (54%), followed by fusiform (24%), cylindrical type (15%), rosary (4%), and diverticular form (2.5%). Choledochocele is cystic dilatation of the intraduodenal part of the common bile duct before its entrance into the duodenum

cylindrical (15%) and rosary type (4%). Together, these four account for nearly 97% of all cystic lesions. The diverticular type arises from one side of the duct wall, consists of a narrow opening, and may compress the adjoining structures, manifesting clinical symptoms of obstruction. A cyst at the distal end of the common bile duct, situated within the duodenal wall close to the ampulla of Vater, is called a choledochocele and is the rarest type (0.5%). The gallbladder remains normal in size, and gallstones are relatively rare in patients with choledochal cysts [3].

Intrahepatic Cystic Dilatation (Caroli's Disease)

Caroli et al. in 1958 first described an entity of pure intrahepatic cystic dilatation [2]. Numerous authors have since described frequent association of intrahepatic cysts with cysts of the extrahepatic ducts. Studies from Japan report as many as 28–42% of patients

with extrahepatic cysts having simultaneous intrahepatic cysts [3, 5, 7]. The fusiform and cylindrical types are more common in patients with intrahepatic cysts (Fig. 11.2.2).

Diagnosis

Choledochal cysts are three times more common in women than men, and more common in Asia and the Orient than in the western hemisphere [3]. Cysts remain asymptomatic for many years. When symptoms occur, more than one half of the patients present with a triad of abdominal pain, abdominal mass, and jaundice. Pain is usually localized to the right upper quadrant. The onset of symptoms usually coincides with the enlargement of the cyst, and the symptoms subside when the cyst decreases in size or drains spontaneously into the duodenum. Liver function tests show mild non-specific elevation. Ultrasonography or CT is the initial diagnostic procedure of choice. Once a cyst is identified with one of the imaging modalities, cholescintigraphy confirms the diagnosis. A cyst by ultrasound or CT in the vicinity of the biliary tract that fills with radiolabeled bile is specific for a choledochal cyst (Fig. 11.2.3). Choledochal cysts must be differentiated from cysts in other nearby organs, including cystic lesions of the kidney (renal cyst, hydronephrosis, and Wilm's tumor), pancreas (pseudocyst), or duodenum (diverticulum), etc. The malignant potential of a choledochal cyst is about 2.4% [6].

Cholescintigraphy

The imaging study is obtained 4–6 h after fasting. Usually there is no need for pretreatment with phenobarbital, unless the child is severely jaundiced. Any one of the Tc-99m-HIDA agents may be chosen when serum bilirubin is within normal range. Routinely 1 min per

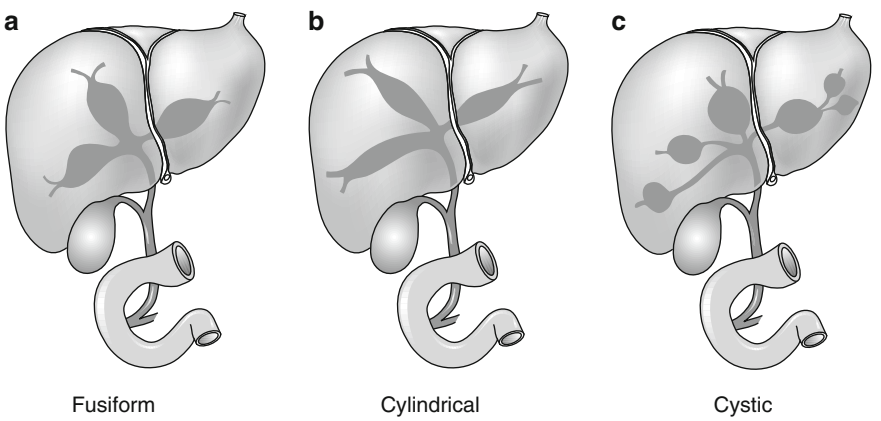

Fig. 11.2.2 Classification of intrahepatic bile duct cysts. Fusiform and cylindrical types are typical examples of Caroli's disease. Cystic type may affect both the intrahepatic and extrahepatic ducts. Simultaneous involvement of both intrahepatic and extrahepatic ducts is found in 28–42% of patients

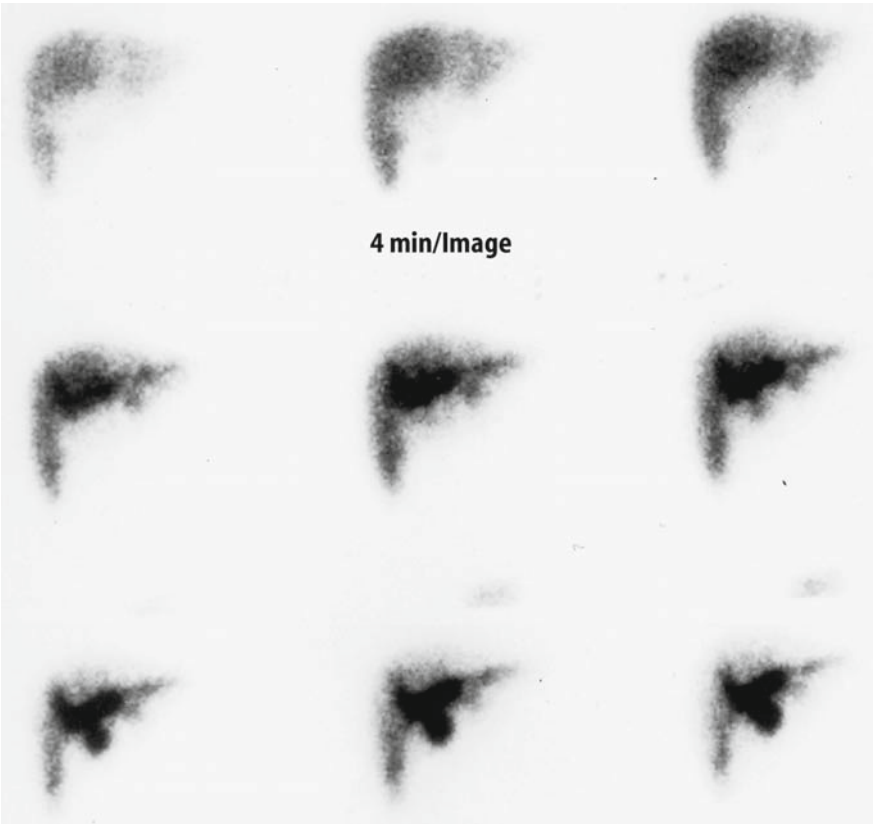

Fig. 11.2.3 Cholescintigraphic features of a choledochal cyst. A choledochal cyst fills in with radiolabeled bile and appears as a round structure in the middle of the common duct. The gallbladder is not seen

frame images are obtained for 60 min (Fig. 11.2.3). Delayed images are obtained at 4 and 24 h when necessary.

The most common cholescintigraphic feature of a choledochal cyst is that of an early defect (90%) in the vicinity of the common hepatic or common bile duct that fills with radioactive bile at 4 or 24 h (Table 11.2.2). Intrahepatic ductal prominence or bile pooling is seen in 22% [8]. The gallbladder usually appears late. Only about 25% of the gallbladders are seen within 60 min, and up to 25% remain nonvisualized, even at 24 h [8, 9, 10].

Delayed filling or non-filling of the native gallbladder in a patient with choledochal cyst suggests that the cyst may act as a low pressure reservoir for bile. Gallbladder histopathological changes indicative of acute cholecystitis are found in 7% and those of chronic cholecystitis in 59% of patients with choledochal cysts [8]. This raises the possibility that the presenting symptoms may be due to onset of cholecystitis and not the choledochal cyst itself. Large cysts (one measured 400 ml) may compress adjoining structures and present clinically as an acute emergency [11]. Combined application of ultrasound and

Table 11.2.2 Cholescintigraphic features of choledochal cyst

Parameter	Frequency (%)
1. Prolonged intrahepatic ductal prominence	22
2. Visualization of the gallbladder within 1 h	25
3. Non-visualization of the gallbladder by 2–4 h	71
4. Non-visualization of the gallbladder by 24 h	25
5. Filling defect in the region of the cyst in early images	90
6. Filling of the defect with the radiolabel in late images	89

Tc-99m-HIDA cholescintigraphy is the most cost-effective approach in the diagnosis of choledochal cysts [12].

Management of Choledochal Cysts

Surgical excision of the cyst is the treatment of choice [13]. The cyst is excised with the hepatic duct Roux-en-Y jejunal anastomosis. This approach results in the most favorable postsurgical outcome, with a low incidence of ascending cholangitis. Total excision of the cyst is recommended because of its high malignant potential, which is 20 times higher than in the general population [3]. Surgical management of pure intrahepatic cysts (Caroli's disease) remains controversial. Lobectomy is advocated when cysts involve only one lobe of the liver. In the severe form of Caroli's disease, recurrent ascending cholangitis often leads to fibrosis and portal hypertension. About 20% of the choledochal cysts diagnosed in adults are treated much like those in children with total surgical excision [14].

Cystic Disease of the Liver Parenchyma

Liver cysts can be either solitary or multiple. Solitary cysts are uncommon, non-hereditary, and not associated with cysts in other organs. The Mayo Clinic reported only 38 solitary asymptomatic liver cysts during a follow-up period of 47 years [15]. Frequent use of abdominal ultrasound examination now can detect many more asymptomatic liver cysts than before. Symptomatic solitary liver cysts are four times more common in women than men and are found more frequently in the anterior-inferior area of the right lobe [16]. The cyst surface is usually smooth with wall thickness less than a centimeter. The cyst size varies from a few milliliters to several liters. One reported cyst contained 17 l of fluid [17]. Most of the cysts contain clear fluid. Some cysts may contain blood, mucin, proteins, and cholesterol. Bile is rarely found in a solitary cyst, indicating its non-communication with the bile ducts. A solitary cyst on ultrasound or CT that does not fill with radiolabeled bile indicates a non-communicating simple liver cyst (Fig. 11.2.4A).

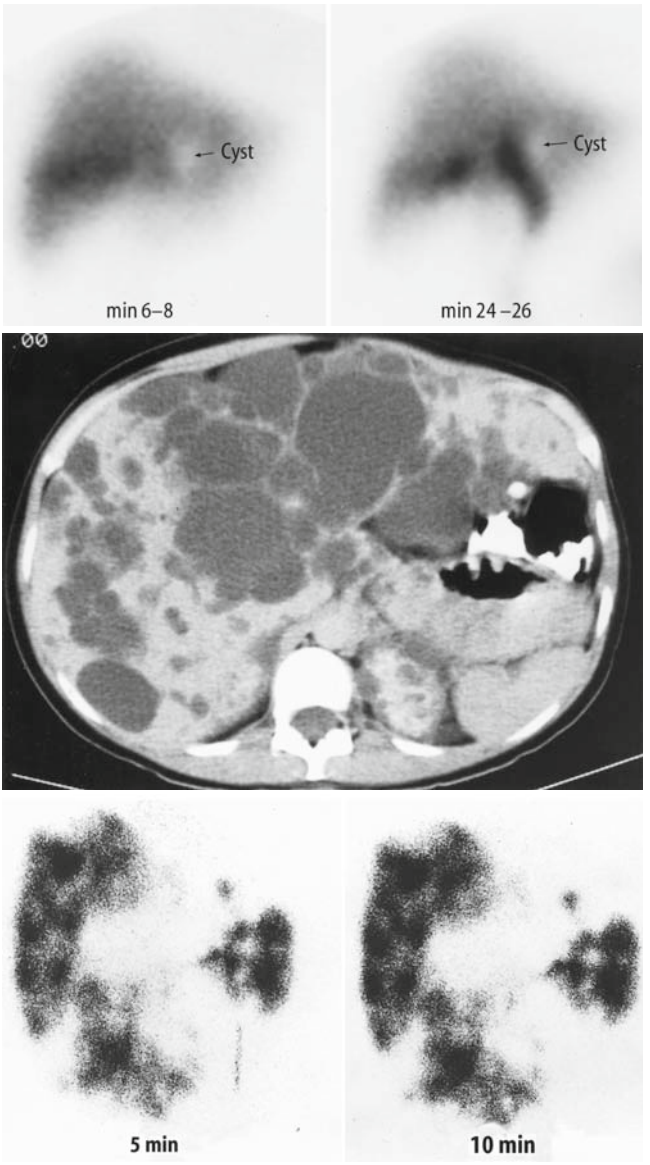

Fig. 11.2.4 Liver cyst. A simple liver cyst appears as a round defect early and does not fill in with radiolabeled bile later (*top*). A polycystic liver shows multiple small and large liver cysts on CT (*middle*). Cholescintigraphy in polycystic liver disease shows functioning liver tissue along the margins of right and left lobes (*bottom*). No filling of the cysts occurs. The cyst fills in only when there is wall rupture

Polycystic Liver Disease

Polycystic liver disease is classified into two main categories, non-communicating, and communicating. Non-communicating cysts are usually multiple, common in adults (adult polycystic liver disease), and show an autosomal dominant pattern of inheritance. It is associated with cysts in other organs, especially of the kidneys [18]. Cysts become symptomatic when they rupture or get infected. Tc-99m-HIDA cholescintigraphy can establish reliably whether or not the abdominal pain is due to rupture of the liver cyst [19]. In patients with polycystic liver disease on CT or ultrasound, non-filling with radiolabeled bile indicates a non-rupture (Fig. 11.2.4B, C).

References

1. Witzleben C. Cystic disease of the liver. In: Zakim D, Boyer TD (eds) Hepatology. A textbook of liver disease, vol 2. WB Saunders, Philadelphia, 1996, pp 1630–1649
2. Caroli J, Soupault R, Kossakowski J et al. La dilatation polycystic congenitale des voies biliares intra-hepatiques. Sem Hop Paris 1958;34:488–491
3. Fonkalsrud E. Biliary cystic disease in children and adults. In: Way LW, Pelligrini CA (eds) Surgery of the gallbladder and bile ducts. WB Saunders, Philadelphia, 1987, pp 609–629
4. Kimura K, Tsugawa C, Ogawa K, Matsumoto Y, Yamamoto T, Kubo M, Asada S, Nishiyama S, Ito H. Choledochal cysts. Etiological considerations and surgical management in 22 cases. Arch Surg 1978;113:159
5. Komi N, Udaka H, Ikeda N, Kashiwagi Y. Congenital dilatation of the biliary tract; new classification and study with particular reference to anomalous arrangement of the pancreaticobiliary ducts. Gastroenterol JPN 1977;12:293–304
6. Todani T, Watanabe Y, Narusue M, Tabuchi K, Okajima K. Congenital bile duct cysts: classification, operative procedure, and review of 37 cases including cancer arising from choledochal cyst. Am J Surg 1977;134:263–269
7. Saito S. Surgical treatment and long-term follow-up results of congenital dilatation of the biliary duct. Presented at the International Symposium on Cholestasis in Infancy-Its pathogenesis, diagnosis, and treatment. Sendai, Japan, 1978, June 7–9
8. Kao PF, Huang MJ, Tzen KY, You DL, Liaw YF. The clinical significance of gall-bladder nonvisualization in cholescintigraphy of patients with choledochal cysts. Eur J Nucl Med 1996;23:1468–1472
9. Camponovo E, Buck JL, Drane WE. Scintigraphic features of choledochal cyst. J Nucl Med 1989;30:622–628
10. Padhy AK, Gopinath PG, Basu AK, Upadhyay P. Hepatobiliary scintigraphy in congenital cystic dilatation of biliary tract. Clin Nucl Med 1985;10:703–707
11. Williams LE, Fisher JH, Courtney RA, Darling DB. Preoperative diagnosis of choledochal cyst by hepatoscintigraphy. N Engl J Med 1970;283:85–86
12. Gates GF, Miller JH. Combined radionuclide and ultrasonic assessment of upper abdominal masses in children. AJR Am J Roentgenol 1977;128:773–780
13. Tsardakas E, Rdonett AH. Congenital cystic dilatation of the common bile duct. Arch Surg 1956;72:311–315
14. Weyant MJ, Maluccio MA, Bertagnolli MM, Daly JM. Choledochal cysts in adults. A report of two cases and review of the literature. Am J Gastroenterol 1998;93:2580–2583
15. Henson SW Jr, Gray HK, Dockery MB. Benign tumors of the liver III. Solitary cysts. Surg Gynecol Obstet 1956;103:607–609

16. Caplan LH, Simon M. Nonparasitic cysts of the liver. Am J Roentgenol Radium Ther Nucl Med 1966;96:421–428
17. Flagg RS, Robinson DW. Solitary nonparasitic hepatic cysts. Report of oldest known case and review of the literature. Arch Surg 1967;95:964–973
18. Gabow PA, Ikle DW, Holmes JH. Polycystic kidney disease: prospective analysis of non-azotemic patients and family members. Ann Intern Med 1984;101:238–247
19. Salam M, Keeffe EB. Liver cysts associated with polycystic kidney disease: role of Tc-99m hepatobiliary imaging. Clin Nucl Med 1989;14:803–807

Malignant Liver Lesions

12

The liver is a common site for both primary and metastatic malignant lesions. Although the metastatic lesions are the most common, primary malignancies like hepatocellular carcinoma (HCC) and cholangiocarcinoma (CC) have become increasingly more common in recent years in the United States [1]. HCC arises from the hepatic parenchymal cells, the hepatocytes, and CC from the cells lining the major bile ducts and gallbladder, the cholangiocytes. In Asian countries like China, Taiwan, and Japan, HCC is one of the three most common causes of death due to malignancy. HCC has a serum marker in the form of α-fetoprotein, and no such marker exists for CC. Gallium-67 citrate, which has been an imaging agent for HCC over the years, still remains popular in places where F-18 fluorodeoxyglucose (F-18 FDG) is not readily available. A filling defect on a radiocolloid liver scan (Fig. 12.1.1) associated with intense Ga-67 uptake (Fig. 12.1.2) and increased serum α-fetoprotein in a patient is more likely to be HCC than any other type of malignancy. F-18 FDG shows avidity for CC, HCC, metastatic lesions, and abscesses. Being a common imaging agent for many different types of liver lesions, F-18 FDG imaging provides no specificity for any one particular type of malignancy.

Detection of primary and metastatic malignancy depends upon uptake and retention of F-18 FDG by the normal liver and tumor (Fig. 12.1.3). Uptake is dependent upon the enzyme glucokinase, which facilitates F-18 FDG uptake and immediate conversion into F-18 FDG-6 phosphate inside the cell. High levels of FDG-6 phosphatase enzyme in the hepatocyte promote conversion of F-18 FDG-6 phosphate back into F-18 FDG, which may exit the hepatocyte rapidly, especially in delayed images taken beyond an hour after injection. The balance between uptake and exit determines the sensitivity for tumor imaging. The serum level of α-fetoprotein and tumor stage greatly influence the sensitivity of F-18 FDG PET/CT imaging (Fig. 12.1.4). Patients with a serum α-fetoprotein level of less than 20 ng ml^{-1} show a sensitivity of 44%, whereas those with levels greater than 400 ng gl^{-1} show a sensitivity of 86%. Stage II and III tumors show F-18 FDG PET/CT sensitivity of 31–62%, whereas stage IVa and IVb show much higher sensitivity at 68–85%. Overall sensitivity of F-18 FDG PET/CT for HCC is 61% and for metastatic lesions 86%. Higher sensitivity for metastatic lesions is related to the slow rate of conversion of F-18 FDG-6-phosphate back into F-18 FDG. Although colon cancer frequently metastasizes to the liver, other types of cancer, including breast and lung, also involve the liver (Fig. 12.1.5). Primary liver tumors less than 2 cm in size are rarely detected, and 78% of tumors ≥5 cm are readily identified with PET/CT [2]. Risk factors for HCC include primary sclerosing cholangitis,

G.T. Krishnamurthy and S. Krishnamurthy, *Nuclear Hepatology*,
DOI 10.1007/978-3-642-00648-7_12, © Springer-Verlag Berlin Heidelberg 2009

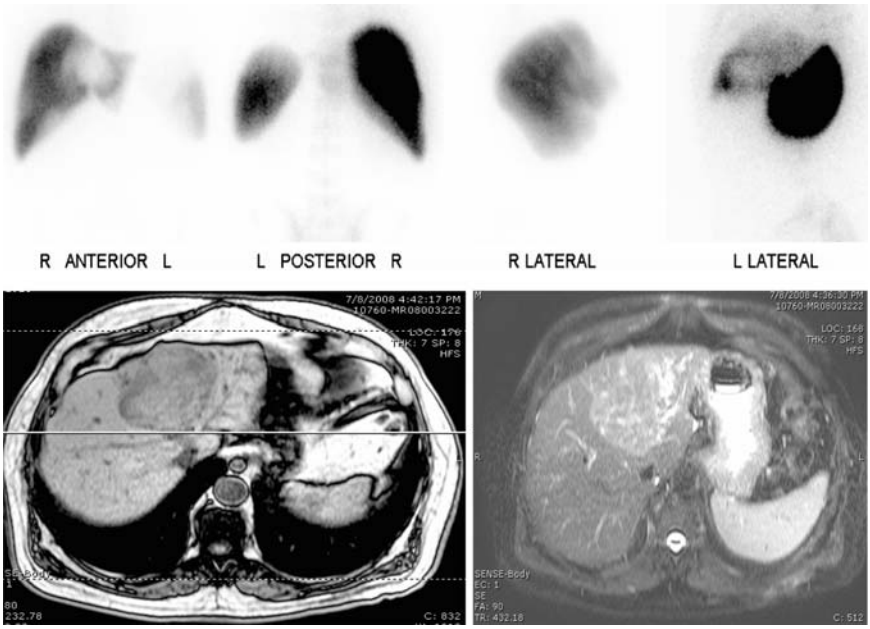

Fig. 12.1.1 Tc-99m radiocolloid scan (*top*) shows HCC as a filling defect in segment 4A and 4B of the left lobe. A CT (*bottom left*) shows it as a low density lesion and MRI with contrast (*bottom right*) shows the lesion as hypervascular

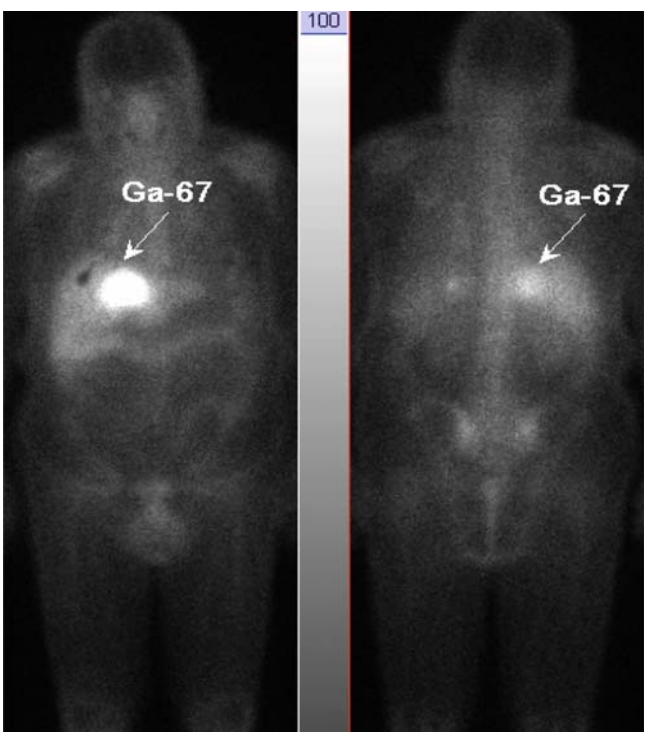

Fig. 12.1.2 Gallium-67 citrate scan of patient shown in Fig. 12.1.1 shows high intensity uptake in segment 4A and 4B of the left lobe. As the lesion is anterior in location, it is seen better in the anterior (*left*) than in the posterior view (*right*). Bone marrow and transverse colon activity below the liver is normal. Patient had increased serum alpha-fetoprotein, and surgical resection confirmed hepatocellular carcinoma

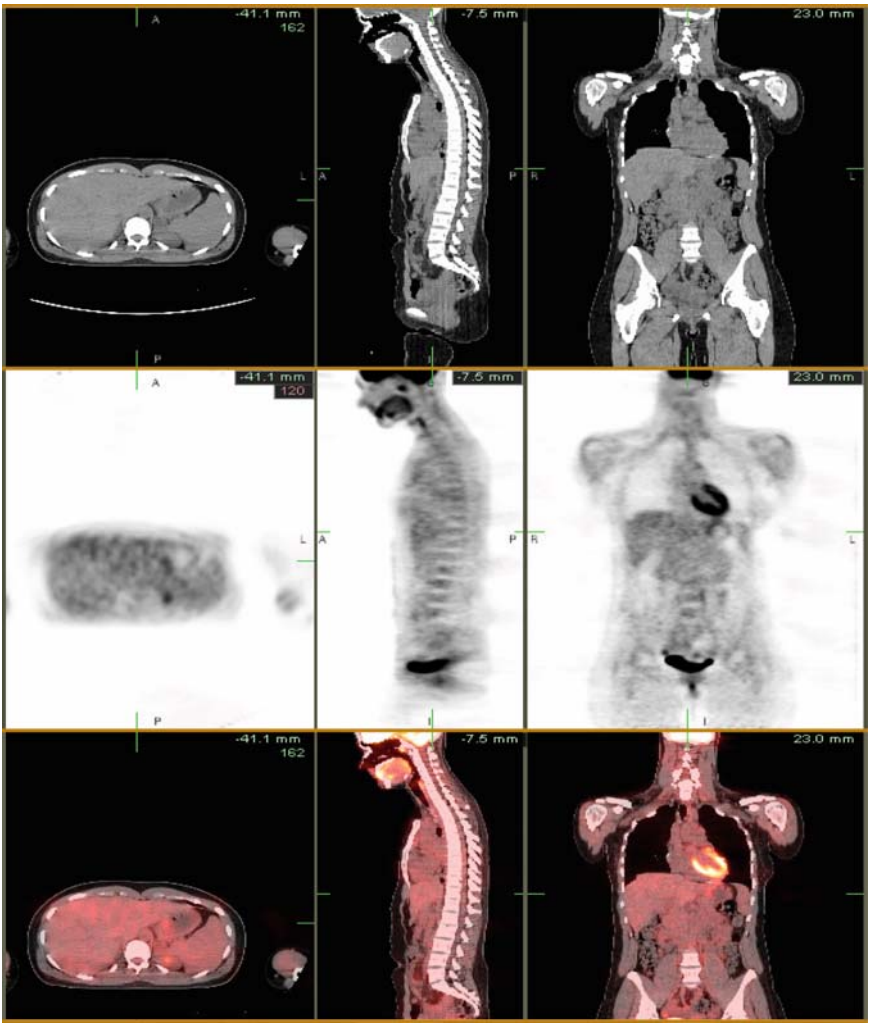

Fig. 12.1.3 Normal PET/CT. Brain and heart show the highest F-18 FDG uptake (*middle panel*). Liver, spleen, kidneys, and bone marrow show low uptake, and lungs show no uptake. *Top* (CT) and *middle* (PET) *panel* images are fused in the *bottom panel*

hepatolithiasis, chronic infections, including typhoid and parasites, drug exposure, and genetic influence.

CC is a malignant epithelial tumor of the biliary tree and is less common than HCC [3]. About 60% of CC tumors arise from the extrahepatic part of the biliary tree and spread upwards to invade the liver parenchyma (Klatskin tumor). Hilar lesions are classified into five different types, depending upon the extent of the tumor (see Chap. 8.2). Hilar tumors progress slowly, and the diagnosis is often delayed for weeks or months. Although the

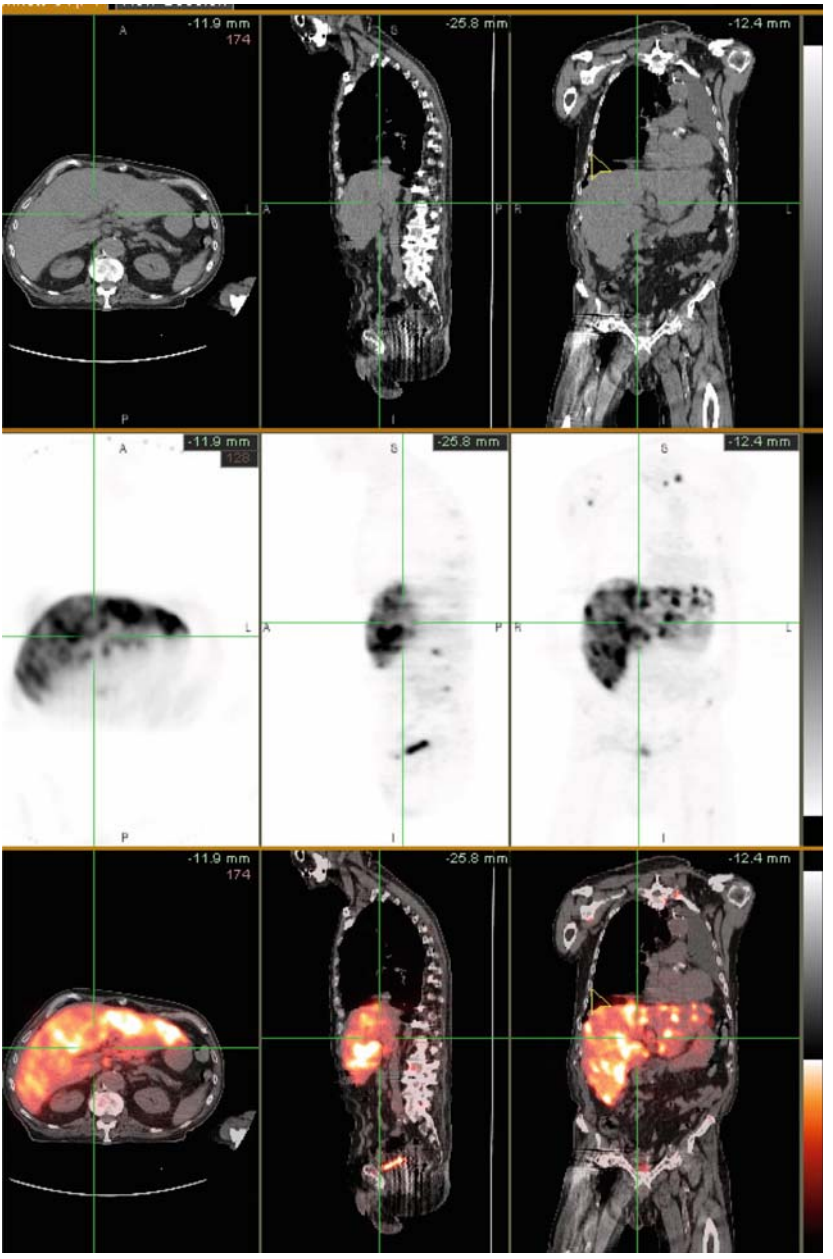

Fig. 12.1.4 Colon CA with liver metastases. Multiple metastatic lesions are found in both liver lobes

sensitivity for detection of the primary cholangiocarcinoma with F-18 FDG is slightly higher than for HCC, metastatic lesions show no difference between the two types (Table 12.1.1). CT remains the primary diagnostic procedure of choice, and PET/CT adds valuable

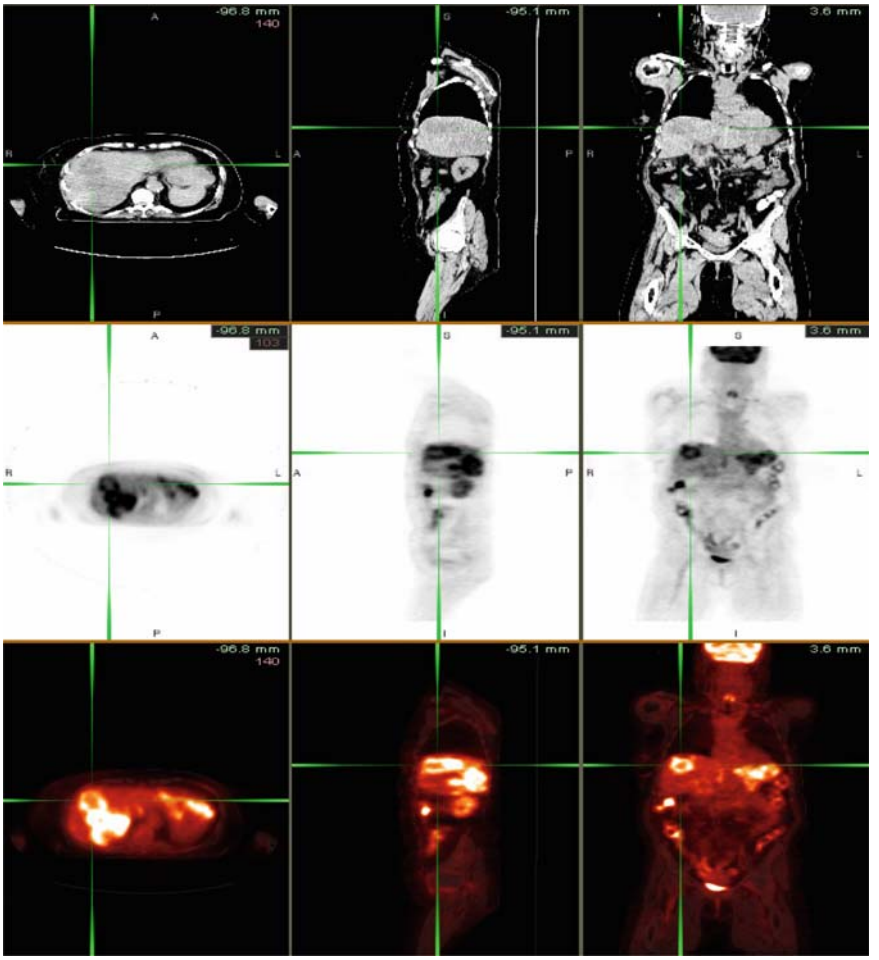

Fig. 12.1.5 Breast CA with metastases to both lobes of the liver. *Right lobe* involves segments 5, 7, and 8. Segment 7 lesion shows central necrosis with no uptake in the center. *Left lobe* has lesions in segments 2 and 3

Table 12.1.1 Sensitivity and accuracy (%) of F-18 FDG PET/CT imaging in the detection of hepatocellular carcinoma and cholangicarcinoma

	Hepatocellular carcinoma [1]		Cholangicarcinoma [3]	
	Primary	Metastatic	Primary	Metastatic
Sensitivity	61	86	84	83
Accuracy			61	79

information with regard to the extent of the primary tumor and its resectability, especially in separating intrahepatic from common bile duct lesions [4, 5].

Early detection of metastatic liver lesions plays a crucial role in the proper management of the patient. A single lesion in either lobe is locally resected, whereas multiple lesions in one or both lobes call for more aggressive surgery and require clear delineation of involvement of each of eight segments of the liver. Couinaud's classification divides the liver into eight segments [6], and Bismuth divides the liver into nine segments by separating Couinaud's segment 4 into 4A and 4B [7]. Resection of four or more lesions followed by chemotherapy frequently results in 3-year survival [8].

12.1 Management

The therapy for early uncomplicated primary tumor is surgical resection. Five-year survival for margin-negative resections ranges from 30 to 45 years. Margin-positive lesions show poor 5-year survival, ranging from 0 to 13 years [3].Only segments 6 and 7 (posterior half of the right lobe) are left behind in cases where other segments show metastatic involvement. Other forms of therapy include photodynamic therapy, intraductal high-intensity ultrasonography, radiofrequency ablation, and chemo-embolization. Liver transplantation, which was considered in the past as a contraindication for HCC and CC, is now accepted as a life-saving measure for both.

References

1. Wood CB, Gillis CR, Blumgart LH. Retrospective study of the natural history of patients with liver metastases from locorectal cancer. Clin Oncol 1976;2:285–288
2. Park JW, Kim JH, Kim SK, Kang KW, Park KW, Choi JI, Lee WJ, Kim CM, Nam BH. A prospective evaluation of ^{18}F-FDG and ^{11}C-Acetate PET/CT for detection of primary and metastatic hepatocellular carcinoma. J Nucl Med 2008;49:1912–1921
3. Ustundag Y, Bayraktar. Cholangicarcinoma: a compact review of the literature. World J Gastroenterol 2008;14(42):6458–6466
4. Kim JY, Kim MH, Lee TY, Hwang CY, Kim JS, Yun SC, Lee SS, Seo DW, Lee SK. Clinical role of 18F-FDG PET/CT in suspected and potentially operable cholangiocarcinoma: a prospective study compared with conventional imaging. Am J Gastroenterol 2008;103:1145–1151
5. Moon CM, Bang S, Chung JB, Park SW, Song SY, Yun M, Doo J. Usefulness of F18-fluodeoxyglucose positron emission tomography in the differential diagnosis and staging of cholangiocarcinomas. J Gastroenterol Hepatol 2007;23(5):759–765
6. Couinaud C. Le foie etudes anatomiques et chirurgicales. Masson, Paris, 1957
7. Bismuth H. Surgical anatomy and anatomical surgery of the liver. World J Surg 1982;6:3–9
8. Tanaka K, Shimada H, Ueda M, Matsuo K, Endo I, Togo S. Role of hepatectomy in treating bilobar colorectal cancer metastases. Surgery 2008;143:259–270

Liver Transplantation 13

Liver transplantation is an optimal therapy for various types of end-stage liver disease [1]. The first liver transplantation was performed in a dog by Welch in 1955, and the first human liver transplantation was performed by Starzl et al. in 1963 [2, 3]. Although the early clinical results were disappointing, modern immunosuppressive agents have improved survival rates in both children and adults. The survival rates in children at 1, 3, 5, and 10 years are 82%, 80%, 78%, and 76%, respectively [4]. In the Model for End-Stage Liver Disease (MELD) survey, the 5-year survival rate after liver transplantation has now increased to 88% [5]. The indications for liver transplantation for various end-stage liver diseases are shown in Table 13.1.1.

13.1 Types of Liver Transplantation

There are essentially three types of liver transplantation: (1) cadaver liver, (2) living-donor liver, and (3) auxiliary liver. In cadaver liver transplantation, the recipient's entire liver is removed and replaced (orthotopic) by a cadaver liver (Fig. 13.1.1). In the case of a living-donor liver transplantation, either the lateral segment (segments 2 and 3) or the entire left lobe (segments 4A, 4B, 2, and 3), anterior section (segments 5 and 8), or posterior section (segments 6 and 7) of the right lobe or the entire right lobe (segments 5, 6, 7, and 8) from the donor liver replaces the entire native liver of the recipient. In the case of an auxiliary liver transplantation for patients with fulminant hepatic failure, the donor liver acts as a transient bridge until the native liver recovers its function. The donor liver is placed either adjacent to the native liver or replaces the left lobe of the recipient liver [6–8]. The transplantation procedure usually involves four stages: (1) hepatectomy of the diseased native liver, (2) the anhepatic stage, which is the time interval between liver removal and interruption of blood flow through the vena cava, portal vein, and hepatic artery, (3) the reperfusion stage when the donor liver is being revascularized in the recipient, and (4) the biliary reconstruction stage in which a choledochocholedochostomy (adults) or a choledochojejunostomy (in children less than 35 lbs) is performed.

Nuclear medicine procedures are used for the evaluation of liver function both in the pre- and post-transplant period. In the case of a living-donor liver transplantation, both the donor and the recipient may undergo pre-transplant evaluation, which generally includes assessment of the functional reserve of the donor liver and determination of the ideal time

G.T. Krishnamurthy and S. Krishnamurthy, *Nuclear Hepatology*,
DOI 10.1007/978-3-642-00648-7_13, © Springer-Verlag Berlin Heidelberg 2009

Table 13.1.1 Indications for liver transplantation

Parenchymal diseases
Post-necrotic cirrhosis
Primary biliary cirrhosis
Primary sclerosing cholangitis
Alcoholic liver failure
Viral hepatitis
Inborn errors of metabolism
Fulminant hepatic failure
Autoimmune hepatitis
Cystic fibrosis
Neonatal hepatitis
Cholestatic diseases
Biliary atresia
Cystic fibrosis
Biliary cirrhosis
Sclerosing cholangitis
Familial cholestasis
Graft vs. host disease
Chronic hepatic rejection
Tumors
Hepatoma
Hepatoblastoma
Apudomas
Miscellaneous
Budd-Chiari syndrome
Trauma

for transplantation in the recipient [9]. It is essential to establish end-stage liver disease in the recipient prior to considering transplantation. Since no single test is adequate for either determining end-stage liver disease or indicating the ideal time for transplantation, serial imaging and non-imaging diagnostic procedures are performed over many months or years. Persistent poor function over many months or years despite appropriate therapy is an indication of end-stage liver disease. Just prior to liver transplantation, a multiple-gated acquisition (MUGA) study is obtained for evaluating the left ventricular ejection fraction and wall motion and a myocardial perfusion study for testing the adequacy of the coronary circulation in the recipient. After the transplantation, nuclear medicine studies are used to detect immediate and late postoperative complications (Table 13.1.2) and also for the assessment of functional recovery of the donor liver (Fig. 13.1.1). In the immediate post-operative period, cholescintigraphy is used to exclude bile leak or to assess transplant function. Blood pool studies are obtained to identify vascular complications, such as bleeding and thrombosis [10, 11]. Post-transplant chronic ischemia of the liver causes diffuse bile duct stenoses, manifesting as a vanishing bile duct syndrome in some patients [12].

In the case of living-donor liver transplantation, the volume of the donor liver and its segmental morphology are measured with a single or multi-detector spiral CT. For a multi-detector spiral CT study, 750 ml of water is ingested as a negative contrast, and 120–150 ml of a non-ionic contrast is injected intravenously at 4–5 ml s^{-1} using scanning collimation of 1 mm, and 1-mm-thick

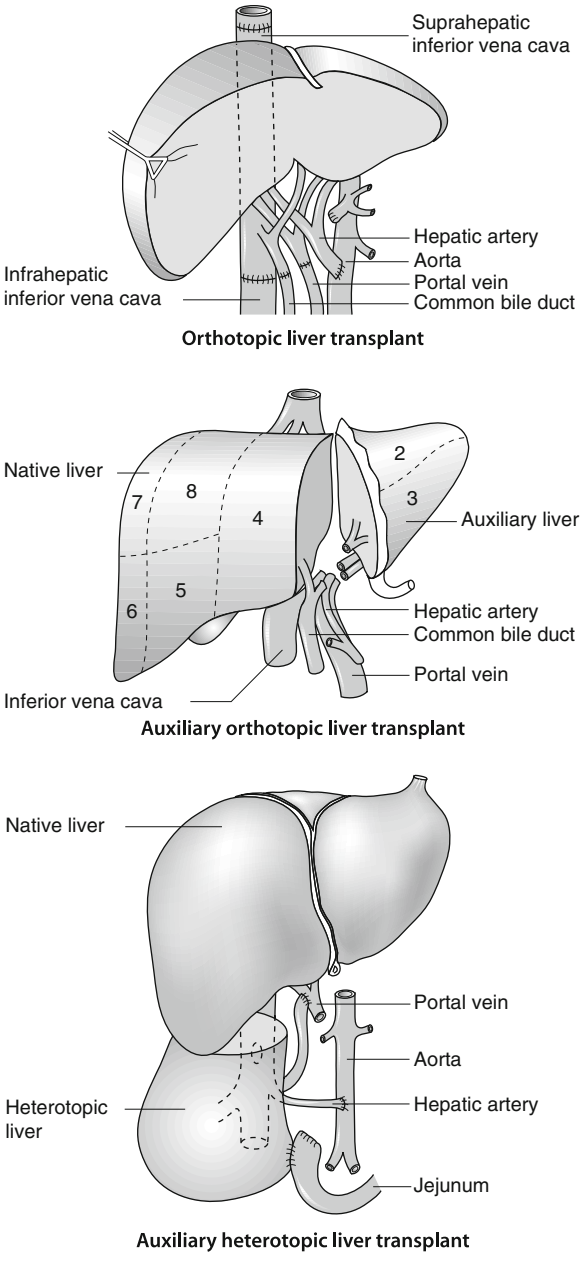

Fig.13.1.1 Liver transplantation. Orthotopic liver transplant with end-to-end anastomosis is the most common type. In auxiliary transplantation, the donor liver is placed in either an orthotopic or heterotopic position

Table 13.1.2 Complications of liver transplantation [10]

Complication	Frequency (%)
Infections	30.0–60.0
Biliary obstruction	15.0–25.0
Rejection	10.0–15.0
Bile leak	7.5–10.0
Bleeding	5.5–6.5
Renal failure (requiring dialysis)	5.0
Arterial thrombosis	3.0–5.0
Lymphoproliferative disorder	2.0–2.5
Portal vein thrombosis	1.0–2.0

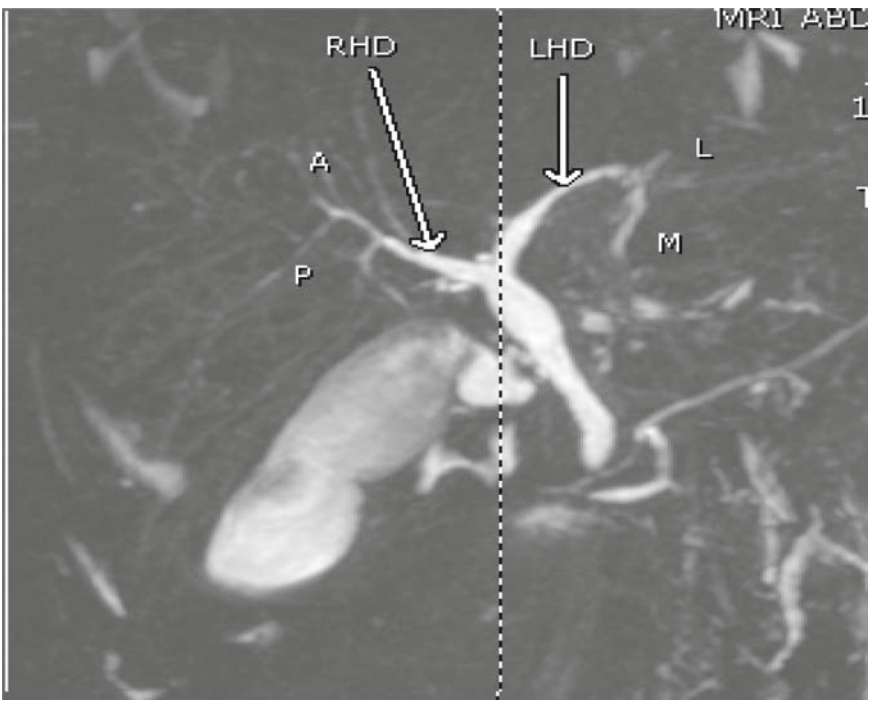

Fig.13.1.2 Magnetic resonance cholangiopancreatogram (*left*) shows the gallbladder, common bile duct, right hepatic duct (*RHD*), and left hepatic duct (*LHD*) and their segmental branches. RHD receives bile from anterior (*A*) and posterior (*P*) and LHD from medial (*M*) and lateral (*L*) segmental branches

images are reconstructed for interpretation [13]. The intraoperative volume in milliliters and weight in grams of the right lobe are estimated by using the preoperative volume [14]:

Intraoperative volume = 0.656 × preoperative volume + 87.629 ml

Intraoperative weight = 0.678 g/ml × preoperative volume + 143.704

Since one or two segments from an adult are adequate for a child, living-donor liver transplantation for post-Kasai biliary atresia has gained widespread acceptance with 5-year

survival of nearly 90% [15]. Currently, hepatitis C infection is the most common cause of chronic liver disease in adults and accounts for 42% of cases, followed by hepatitis C and alcohol in 22%, alcohol alone in 8%, non-alcoholic fatty liver disease in 9%, hepatitis B in 3%, and other causes in 16% [16]. Hepatitis C in adults and congenital biliary atresia in children are the two most common indications for liver transplantation.

13.2 Normal Functioning Liver Transplant

Transplant liver maintains its normal shape and size in the right upper quadrant and functions much like a native normal liver. The gallbladder is usually absent as cholecystectomy is routinely performed as an integral part of transplantation to the prevent formation of as well as future complications from gallstones. The hepatic extraction fraction and excretion half time values of the transplant liver are maintained within the normal range established for the normal native liver. Common hepatic and common bile ducts show normal features. Duodeno-gastric bile reflux is rare (Figs. 13.1.3 and 13.1.4).

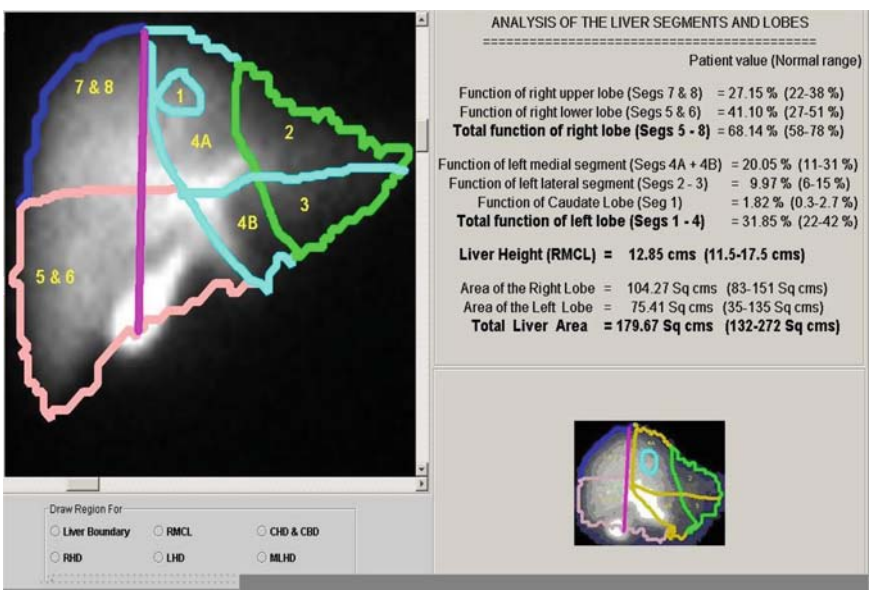

Fig. 13.1.3 Liver segments derived from a planar Tc-99m-HIDA study. A line passing through the common bile duct (*CBD*) and common hepatic duct (*CHD*) when extended upwards to meet the superior margin divides the liver into right and left lobes. A line passing through the right hepatic duct and left hepatic duct divides each lobe into superior and inferior segments. In a planar image, segment 5 is superimposed on segment 6 and segment 7 on segment 8 of the right lobe. The segments are clearly separated in the left lobe. The caudate lobe (*segment 1*) is added to the right or left lobe depending upon user preference. Normal values for segments are shows within parentheses. *Planar image* depicts the biliary anatomy similar to MRCP shown in Fig. 13.1.2

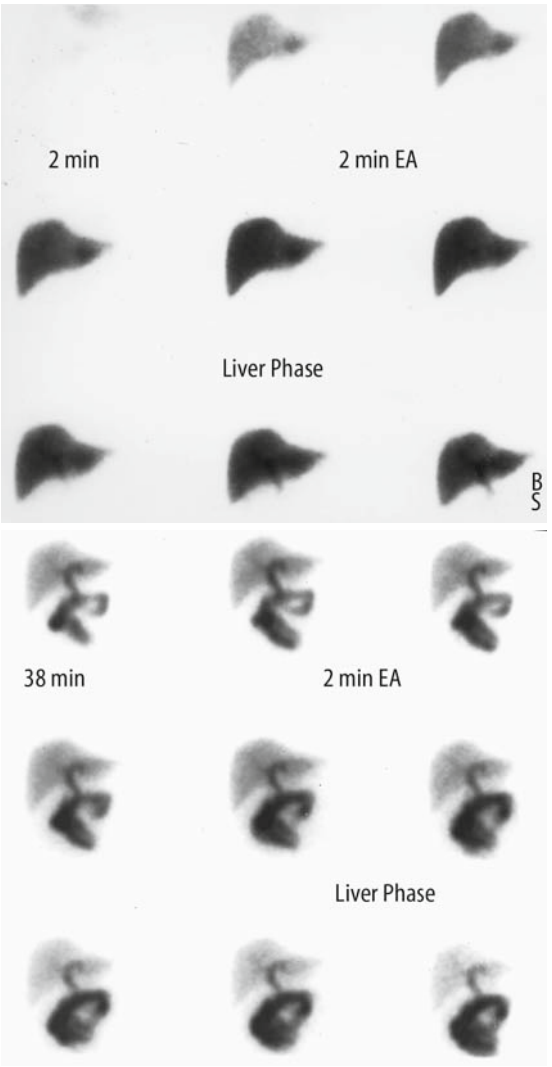

Fig. 13.1.4 Normal liver transplant. Early images beginning at 2 min show normal morphology and bile formation (*top*). Late images beginning at 38 min show free bile flow into intestine. Gallbladder is absent due to cholecystectomy (*bottom*). Hepatic extraction fraction and excretion half time are normal

Complications

Liver transplant complications occur both in the immediate and delayed postoperative period (Table. 13.1.2). Immediate complications include bile leak and arterial or venous thrombosis, and delayed complications (rejection) are immunological in nature.

Bile Leak

Leak is inferred when bile enters an unanticipated region or an anticipated region at an unanticipated time [17]. Bile leak at the anastomotic site is relatively common and accounts for 10% of all complications. The leak may occur into the liver parenchymam or into the subhepatic space forming a biloma, or the leak may enter the peritoneal space, causing bile peritonitis. Biloma produces a filling defect within the liver in early images and fills in with Tc-99m-HIDA-radiolabeled bile in late images. In contrast, a benign or malignant space-occupying lesion remains a "cold" defect throughout. Bile enters an abscess cavity when the abscess connects with a bile duct. Healing of the abscess cavity is demonstrated with serial imaging (Fig. 13.1.5). Bile leak at the anastomotic site (choledocho-choledochal) is usually small in size and closes spontaneously. Bile leak at the choledocho-duodenal junction, on the other hand, tends to be large in volume and carries a much higher morbidity and mortality due to simultaneous leakage of intestinal contents into the peritoneal space. In the supine position, leaked bile gravitates to the right or left paracolic gutter and later enters the pelvic cavity. Opioids prescribed for pain control often increase the volume of bile leak because of their constrictive effect on the sphincter of Oddi.

Bile Duct Stricture

Stricture is a late complication and accounts for 15 to 25% of the total complications of liver transplantation. Stricture is attributed to bile duct ischemia caused by arterial stenosis or thrombosis. Cholescintigraphy shows bile pooling in ducts proximal to the stricture. Segmental and area ducts are seen with unusual prominence [18]. Denervation during transplant surgery alters sympathetic-parasympathetic-hormonal control over the ducts and sphincter of Oddi. Nervous and hormonal imbalance may cause biliary dyskinesia. Distinction between anatomic stricture and biliary dyskinesia is made with the use of amyl nitrite or a calcium channel blocker (nefidapine), very similar to studies obtained in non-transplant patients [19, 20].

Primary Non-Function Versus Rejection

Primary non-function is non-recovery of donor liver function in the recipient despite good surgical technique establishing adequate portal vein and hepatic artery blood flow. Clinically, it presents as liver failure in association with encephalopathy, persistent acidosis, and severe coagulopathy, and requires retransplantation. Acute rejection occurs within 3 months of transplantation, and chronic rejection follows later. Unlike the kidneys, the liver does not manifest a hyperacute rejection. Rejection is a microvascular phenomenon where fibrin, immune and inflammatory cells deposit within and around the capillaries, manifesting an obliterative angiopathy and chronic ischemia. Chronic ischemia leads to obliteration of the bile ducts (vanishing bile duct syndrome) and intrahepatic cholestasis. Both rejection and intrahepatic cholestasis resulting from other causes manifest similar cholescintigraphic

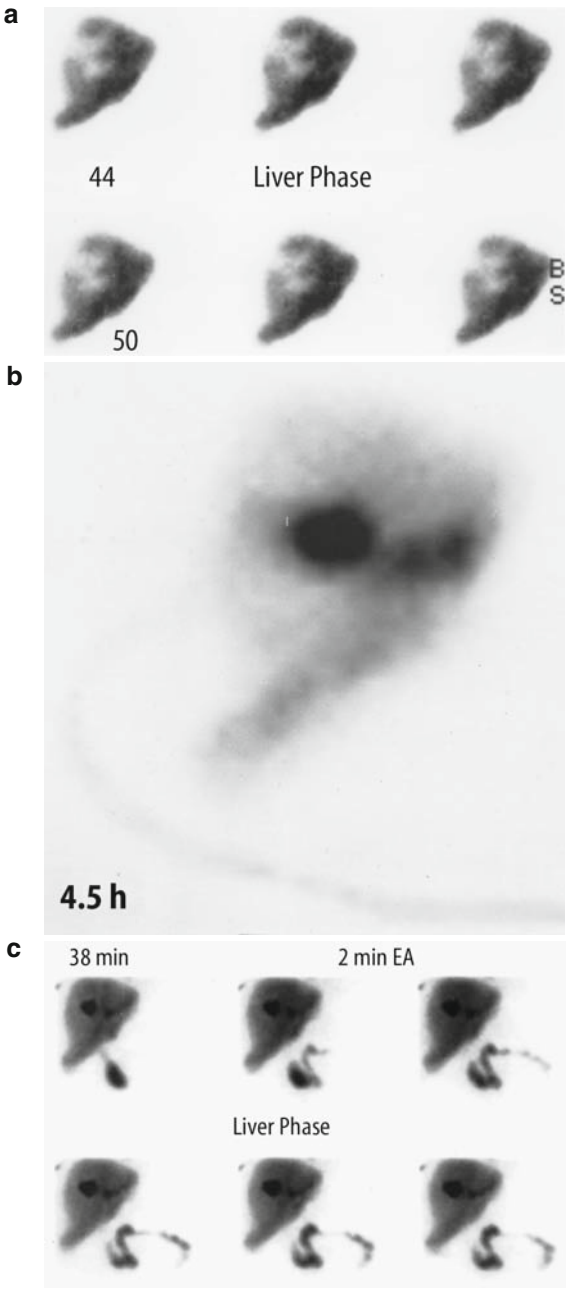

Fig. 13.1.5 Abscess in a transplant liver. An abscess causes a large filling defect within liver parenchyma (**a**) and fills with bile at 4.5 h (**b**). A repeat study 3 months later shows shrinkage of the abscess, but fistula persists

findings, and hence one entity cannot be separated from the other [21]. Rejection is managed with immunosuppressive agents like cyclosporine and tacrolimus [22]. Serial studies enable evaluation of liver function and aid in the adjustment of the immunosuppressant dosage [23].

Cholescintigraphy

The data are collected with a large field of view gamma camera fitted with a low-energy, all-purpose, parallel-hole collimator using 3-8 mCi of Tc-99m-HIDA. Technetium-99m mebrofenin is the best agent both in normal as well as jaundiced patients. Liver perfusion images are obtained at 2 s per frame during the first 1 min, followed by functional images at 1 min per frame for 59 min, for a total of 1 h, and recorded on a 128 × 128 word mode matrix. A short imaging interval is essential for location of the exact site of the bile leak. The first place of unexpected bile radioactivity usually indicates the site of origin of the leak. Once there is collection of a large volume of bile, it becomes difficult to identify the exact site of the bile leak.

Auxiliary Liver Transplantation

In an auxiliary transplant, the donor liver is placed in a heterotopic position adjacent to the native liver or in the space created by partial hepatectomy of the native liver (Fig. 13.1.6). Auxiliary liver transplantation is restricted mostly to patients with fulminant hepatic failure where the native liver has the potential for full functional recovery if the patient survives the acute episode. Fulminant hepatic failure consists of liver failure and encephalopathy occurring within a 2–8 week period in a previously healthy person. Fulminant hepatic failure is relatively rare, and accounts for 6% of all adult liver transplants and 11% of all pediatric liver transplants each year in the United States [24]. Mortality is 100% in untreated patients. Full functional recovery is due to the generous regeneration capacity of the native liver in those patients who can withstand an acute insult [25].

Fulminant hepatic failure heals slowly over several months to attain full functional recovery (Table 13.1.3). When serum liver function tests show either an improvement or deterioration in a patient with auxiliary liver transplantation, it is not clear from the serum levels whether the changes reflect the function of the native or the donor liver. The immunosuppressive dose needs to be increased if there is rejection of the donor liver. An improvement of the native liver function, on the other hand, calls for either a reduction in dosage or total discontinuation of immunosuppressive agents. The donor liver undergoes spontaneous regression and atrophy when the native liver recovers its full function, and steroids are withdrawn safely at this time. The donor liver is surgically removed if it does not undergo spontaneous atrophy and interferes with the function of the native liver [26].

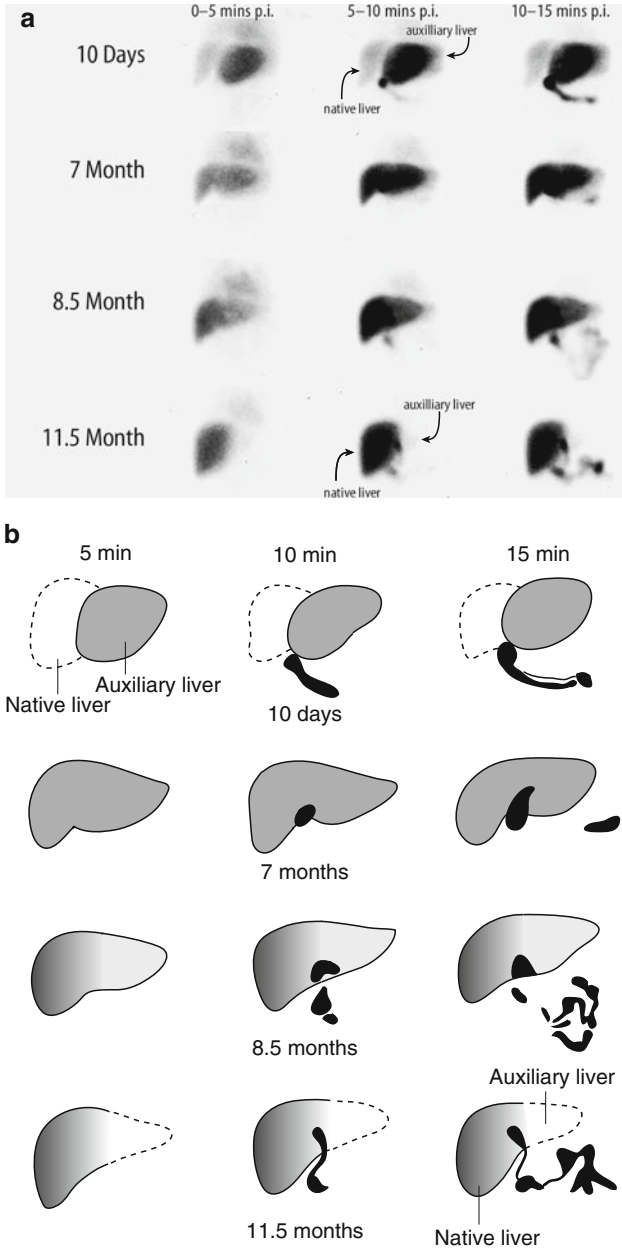

Fig. 13.1.6a,b Pattern of recovery of native liver function following auxiliary liver transplantation. Cholescintigram (**a**) and a corresponding schematic diagram (**b**) are shown in a 2-year-old child with auxiliary liver transplant for fulminant hepatic failure. At 10 days, the native liver shows poor uptake, and the auxiliary liver has good uptake of 99mTc-HIDA. Function appears equal by 7 months. Function of the auxiliary liver begins to decrease by 8.5 months and disappears completely at 11.5 months. The native liver recovers its function completely with 100% extraction fraction. (Courtesy of Dr. Muriel Buxton-Thomas, Kings College Hospital, London, UK)

Table 13.1.3 Differentiation of the native from donor liver function following auxiliary liver transplantation for fulminant hepatic failure

Study no.	Time post-transplant	Native liver function			Auxiliary liver function		
		HEF (%)	Ex. $T^{½}$ (min)	function (%)	HEF (%)	Ex. $T^{½}$ (min)	function (%)
1	10 days	37	27	15	73	21	85
2	7 months	51	18	44	54	17	56
3	8.5 months	78	16	64	50	53	36
4	11.5 months	100	8	>99	–	–	<1

(Courtesy Dr. Muriel Buxton-Thomas, Kings College Hospital, London)

Differentiation of Native vs. Donor Liver Function

Cholescintigraphy is able to measure the total as well as the function of the donor and native liver separately. The differential liver function information helps the clinician in adjusting the dose of immunosuppressive agents.

Cholescintigraphy is obtained in adults with a large field of view and in children with a standard or even small field of view gamma camera, fitted with a low-energy, general-purpose, parallel-hole collimator. With the patient in a supine position, the camera is positioned anteriorly to cover the entire native and the donor liver. A dynamic 60-frame image at minute intervals are obtained with 4 to 6 mCi of Tc-99m HIDA, and recorded on a 128 × 128 computer matrix. The preferred imaging agent in jaundiced patients is Tc-99m mebrofenin, which has superior biokinetic behavior in patients with hyperbilirubinemia [27]. One can obtain a liver scan with Tc-99m-S colloid to outline the liver borders, but it is not essential in most cases, as early Tc-99m-HIDA images, obtained within the first 5 to 6 min, provide similar morphologic information (Fig. 13.1.2).

Quantification

Many different methods have been used for quantification of transplant function. Deconvolutional analysis (Chap. 5) is applied to measure the extraction fraction of the native and auxiliary liver separately, by choosing heart for the input and liver for the output function. Excretion half time is measured with a monoexponential fit. Some express the function as uptake of the injected dose by the native versus donor liver. Four regions of interest are drawn; two ROIs over the liver (one over the entire native liver and the other over the entire donor liver) and two ROIs for background just lateral to each liver. Background counts (from Tc-99m-S colloid when a preliminary scan is obtained) are subtracted from the liver counts, and the net liver counts and curve are displayed. From the net liver curve, three functional parameters are generated [28].

(1) T-max = time to maximum liver counts.
(2) $T_{1/2}$ = clearance half time using a mono-exponential fit to the data points from peak counts.

(3) Relative uptake (RU) by the liver. RU is obtained by noting the area under the time-activity curves of the native and graft livers between 2 and 10 min.

$$\text{RU by native liver} = \frac{\text{Native liver area between 2–10 min} \times 100}{\text{Native liver area between 2–10 min + donor liver area between 2–10 min.}}$$

$$\text{RU by graft liver} = \frac{\text{Graft liver area between 2–10 min} - 100}{\text{Graft liver area between 2–10 min + native liver area between 2–10 min.}}$$

In one study, authors followed patient recovery for up to 30 months and calculated the percent uptake by the native liver by using the area under the curve between the 2nd and 10th min, and validated the scintigraphic method in the management of the patient with auxiliary liver transplantation [28].

Deconvolutional analysis is applied when the software is available. In children, where the liver physiology is much faster than in adults, the data are collected at a much shorter interval, 30 s per frame for 30 min. Hepatic extraction fraction calculation uses only the first 30 frames (15 min), and the excretion $T_{1/2}$ is calculated using all 60 frames. Native and donor liver HEF and excretion half times are measured separately for both. The contribution of each liver towards total function is calculated and expressed as percent (Table 13.1.3).

Recovery Pattern in Auxiliary Liver Transplantation

Immediately after the transplantation, the function of the native liver remains depressed with a median uptake value of 27% (range 4%–36%) during the first 4 weeks. The median uptake value increases gradually to twice the baseline value 6–12 months after transplantation. When serum liver function tests show stable normal values, the uptake by the native liver raises to above 90%. The native liver T-max value may normalize within a month, but the excretion T1/2 value usually remains elevated for a much longer period of time. The immunosuppressive drug dose may be decreased when the relative uptake value raises above 30%, and the drug may be withdrawn completely when the uptake value reaches above 90% [28]. The pattern of recovery of native liver function following an auxiliary liver transplantation in a 2-year-old child is shown in Table 13.1.3. The hepatic extraction fraction and excretion half time of the native liver and auxiliary liver are measured separately for each liver (Fig. 13.1.6). As the function of the native liver improves gradually and recovers fully, the auxiliary liver function deteriorates with regression of functional liver volume.

Living-donor Liver Transplantation

Although the liver is one solid organ, its distinct segmental and lobar anatomy and physiology allow resection into smaller portions for transplantation [29]. Resection of the donor liver is performed along the physiological planes (Fig. 1.1.3, Chap. 1). The lateral segment

of the left lobe (areas 2 and 3) or the entire left lobe (areas 2, 3, 4A, and 4B) is resected from the donor for transplantation in the recipient (Fig. 13.1.1). The first living-donor liver transplantation was performed by Raia et al. in Brazil in 1989 [30]. The left lobe of the liver from a mother was transplanted successfully into her son in Australia in 1989 [31]. There are numerous centers around the world performing living-donor liver transplantations [32–34]. Major advantages of living-donor liver transplantation are: (1) reduction in waiting time, (2) high quality of the donor liver, and (3) immunological similarity in haplo-identical donors.

Complications

Postoperative complications are a major concern both in the donor and the recipient. Among the first 100 living-donor liver donor transplantations performed at the University of Chicago, 91 donors had resection of the lateral segment of the left lobe (areas 2 and 3), and the remaining 9 had resection of the entire left lobe (areas 2, 3, 4A, and 4B). Thirteen of the 100 donors had complications, including bile leaks, infection, injury to the bile ducts and spleen, etc., as listed in Table 13.1.4 [35]. Bile leak, bleeding, thrombosis, or infection may occur in either the recipient or the donor, or both. Rejection is an additional complication in the recipient. The living-donor liver transplantation procedure has been found to be safe both for the donor and the recipient. Donor survival is 100%, and the recipient survival ranges from 80 to 94% in centers that perform more than 15 living-donor transplantations in a year [22]. Common complications within 30 days after transplantation include bleeding, extrinsic obstruction, hemobilia, and bile leak around the T-tube or at the anastomotic site. Bile leaks around the T-tube usually close spontaneously, and those that continue to leak may require sphincterotomy or insertion of a biliary stent. Complications occurring after 30 days include stricture at or proximal to the site of anastomosis [36]. Viral, bacterial, and fungal infections are always a concern in an immunocompromised liver transplant patient [37].

Future Directions

The major advantage of hepatobiliary imaging is the opportunity to detect functional abnormality early before irreversible morphological changes take place. Simultaneous quantification of function provides a measure of the severity of disease and enables the

Table 13.1.4 Complications in living-liver donors [31]

Bile leak from cut end
Injury to bile ducts
Injury to spleen
Stricture of the common bile duct
Ileus
Wound infection
Urinary tract infection
Hepatic artery thrombosis
Abscess

clinician to determine the appropriate time to intervene with therapy, and also to test later whether or not the chosen therapy has achieved the intended goals. Following a thorough clinical evaluation and analysis of liver function tests, Tc-99m-HIDA cholescintigraphy is an appropriate initial imaging procedure for detection of most pathophysiologic changes associated with bile formation and flow [38]. Cholescintigraphic results can guide the clinician in developing a management strategy and also aid in determining the need for other imaging (CT or MR) or non-imaging procedures that will lead to the ultimate diagnosis. Liver biopsy is the most appropriate next step for patients with intrahepatic cholestasis. For extrahepatic cholestasis, the clinician may choose percutaneous transhepatic cholagiography for obstruction at or proximal to the union of the right hepatic and left hepatic ducts. ERCP is preferred for obstructions in the common hepatic or common bile duct. Magnetic resonance cholangiopancreatography (MRCP) is being used more often as a non-invasive alternative to invasive ERCP [39]. Receptor-based imaging may enable the selection of a receptor-specific therapy. Quantitative asialoglycoprotein receptor imaging with Tc-99m DTPA galactosyl human serum albumin enables to predict residual liver function after resection of hepatocellular cancer and cholangiocarcinoma and to forecast prognosis of liver cirrhosis [40–42]. A somatostatin receptor-positive metastatic gastrinoma may respond to therapy with octreotide.

References

1. National Institute of Health Consensus Development Conference statement: Liver transplantation. June 20–23, 1983, Hepatology 1983;3:(Suppl) 107S–110S
2. Welch CS. A note on transplantation of whole liver in dogs. Transplant Bull 1955;2:54
3. Starzl TE, Marchioro TL, Von Kaulla KN, Hermann G, Brittain RS, Waddell UR. Homotransplantation of the liver in humans. Surg Gynecol Obstet 1963;117:659–676
4. Goss JA, Shackleton CR, McDiarmid SV, Maggard M, Swenson K, Seu P, Vargas J, Martin M, Ament M, Brill J, Harrison R, Busuttil RW. Long-term results of pediatric liver transplantation. An analysis of 569 transplants. Ann Surg 1998;228:411–420
5. Pfitzmann R, Schwenger J, Rayes N, et al. Long-term survival and predictors of relapse after orthoptic liver transplantation for alcoholic liver disease. Liver Transpl 2007;13:197–205
6. Starzl TE, Demetris AJ, Van Thiel D. Liver transplantation (1). N Engl J Med 1989;321: 1014–1022
7. Kawasaki S, Makuuchi M, Matsunami H, Hashihura Y, Ikegami T, Nakazawa Y, Chisuwa H, Terada M, Miyagawa S. Living related liver transplantation in adults. Ann Surg 1998;227:269–274
8. Sudan DL, Shaw BW Jr, Fox IJ, Langnas AN. Long-term follow-up of auxiliary orthotopic liver transplantation for the treatment of fulminant hepatic failure. Surgery 1997;122:771–778
9. Shah AN, Dodson F, Fung J. Role of nuclear medicine in liver transplantation. Semin Nucl Med 1995;25:36–48
10. Stieber AC, Gordon RD, Galloway JR. Orthotopic liver transplantation. In: Zakim D, Boyer TD (eds). Hepatology. A text book of liver disease. WB Saunders, Philadelphia, 1996, pp 1759–1780
11. Brown RK, Memsic LD, Busuttil RW, Pusey E, Ray RA, Kangarloo H, Hawkins RA. Accurate demonstration of hepatic infarction in liver transplant recipients. J Nucl Med 1986;27:1428–1431
12. Sanchez-Urdazpal L, Gores GJ, Ward EM, Maus TP, Wahlstrom HE, Moore SB, Wiesner RH, Krom RA. Ischemic-type biliary complication after orthotopic liver transplantation. Hepatology 1992;16:49–53

13. Pannu HK, Warren WR, Fishman EK. Liver transplantation: preoperative CT evaluation. RadioGraphics 2001;21:S133–S146
14. Lamke AJ, Brinkman MJ, Schott T, Niehaus P, Felix R. Living donor right liver lobes: Preoperative CT volumetric measurement for calculation of intraoperative weight and volume. Radiology 2006;240:736–742
15. Kyoden Y, Tamura S, Sugawara Y, Yamashiki N, Matsui Y, Togashi J, Kaneko J, Kokudo N, Makuuchi M. Outcome of living donor liver transplantation for post-Kasai biliary atresia in adults. Liver Transpl 2008;14:186–192
16. Bell BP, Manos M, Zaman A, Terrault N, Thomas A, Navarro VJ, Dhotre KB, et al. The epidemiology of newly diagnosed chronic liver disease in gastroenterology practices in the United States: Results from population-based surveillance. Am J Gastroenterol 2008;103:2727–2736
17. Von Moll LK, Juni JE, Merion RM. Scintigraphic demonstration of accessory hepatic duct leak following liver transplantation. J Nucl Med 1988;29:259–262
18. Lantsberg S, Lanchbury EE, Drolc ZA. Evaluation of bile duct complications after orthotopic liver transplantation by hepatobiliary scanning. Nucl Med Commun 1990;11:761–769
19. Madacsy L, Velosy B, Lonovics J, Csernay L. Differentiation between organic stenosis and functional dyskinesia of the sphincter of Oddi with amyl nitrite-augmented quantitative hepatobiliary scintigraphy. Eur J Nucl Med 1994;21:203–208
20. Bhatnagar A. Nifedipine interventional cholescintigraphy. A new method for assessing sphincter of Oddi? Indian J Nucl Med 1997;12:93–96
21. Jain A, Khanna A, Molmenti EP, Rishi N, Fung JJ. Immunosuppressive therapy. Surg Clin North Am 1999;79:59–76
22. Parker BM, Cywinski JB, Alster JM, Irefin SA, Popovich M, Beven M, Fung JJ. Predicting immunosuppressant dosing in the early postoperative period with noninvasive indicyanine green elimination following orthoptopic liver transplantation. Liver Transpl 2008;14:46–52
23. Hawkins RA, Hall T, Gambhir SS, Busuttil RW, Huang SC, Glickman S, Marciano D, Brown RK, Phelps ME. Radionuclide evaluation of liver transplant. Semin Nucl Med 1988;18:199–212
24. Shakil AO, Mazariegos GV, Kramer DJ. Fulminant hepatic failure. Surg Clin North Am 1999;79:77–108
25. Boudjema K, Cherqui D, Jaeck D, Chenard-Neu MP, Steib A, Freis G, Becmeur F, Brunot B, Simeoni U, Bellocq JP, et al. Auxiliary liver transplantation for fulminant and subfulminant hepatic failure. Transplantation 1995;59:218–223
26. Metselaar HJ, Hesselink EJ, de Rave S, ten Kate FJ, Lameris JS, Groenland TH, Reuvers CB, Weimar W, Terpstra OT, Schalm SW. Recovery of failing liver after auxiliary heterotopic transplantation. Lancet 1990;335:1156–1157
27. Krishnamurthy S, Krishnamurthy GT. Technetium-99m-iminodiacetic acid organic anions: review of biokinetics and clinical application in hepatology. Hepatology 1989;9:139–153
28. Buyck D, Bonnin F, Bernuau J, Belghiti J, Bok B. Auxiliary liver transplantation in patients with fulminant hepatic failure: hepatobiliary scintigraphy follow-up. Eur J Nucl Med 1997;24:138–142
29. Bismuth H, Houssin D. Reduced-size orthotopic liver graft in hepatic transplantation in children. Surgery 1984;95:367–372
30. Raia S, Nery JR, Mies S. Liver transplantation from live donors. Lancet 1989;2:497
31. Strong RW, Lynch SV, Ong TH, et al. Successful liver transplantation from a living donor to her son. N Eng J Med 1990;322:1505–1507
32. Emond JC. Clinical application of living-related liver transplantation. Gastroenterol Clin North Am 1993;22:301–315
33. Donovan J. Nonsurgical management of biliary tract disease after liver transplantation. Gastroenterol Clin North Am 1993;22:317–336
34. Reding R, Goyet JV, Delbeke I, Sokal E, Jamart J, Janssen M, Otte J. Pediatric liver transplantation with cadaveric or living related donors: comparative results in 90 elective recipients of primary grafts. J Pediatr 1999;134:280–286

35. Grewal HP, Thistlethhwaite JR Jr, Loss GE, Fisher JS, Cronin DC, Siegel CT, Newell KA, Bruce DS, Woodle ES, Brady L, Kelly S, Boone P, Oswald K, Millis JM. Complications in 100 living-liver donors. Ann Surg 1998;228:214–219
36. Stratta RJ, Wood RP, Langnas AN, Hollins RR, Bruder KJ, Donovan JP, Burnett DA, Lieberman RP, Lund GB, Pillen TJ, et al. Diagnosis and treatment of biliary tract complications after orthotopic liver transplantation. Surgery 1989;106:675–684
37. Mazariegos GV, Molmenti EP, Kramer DJ. Early complications after orthotopic liver transplantation. Surg Clin North Am 1999;79:109–129
38. Krishnamurthy S, Krishnamurthy GT. Nuclear hepatology: where is it heading now? J Nucl Med 1988;29:1144–1149
39. Fulcher AS, Turner MA, Capps GW, Zfass AM, Baker KM. Half-Fourier RARE MR cholangiopancreatography: experience in 300 subjects. Radiology 1998;207:21–32
40. Sasaki N, Shiomi S, Iwata Y, Nishiguchi S, Kuroki T, Kawabw J, Ochi H. Clinical usefulness of scintigraphy with Tc-99m Galactosyl-human serum albumin for prognosis of cirrhosis of the liver. J Nucl Med 1999;40:1652–1656
41. Hwang E, Taki J, Shuke N, Nakajima K, Kinuya S, Konoshi S, Michigishi T, Aburano T, Tonami N. Preoperative assessment of residual hepatic functional reserve using Tc-99m-DTPA-galactosyl-human serum albumin dynamic SPECT. J Nucl Med 1999;40:1644–1651
42. Uetake M, Koizumi K, Yagawa A, Nogata H, Tezuka T, Kono H, Ozawa T, Kusano T, Miyabukuro M, Hosaka M. Use of Tc-99m DTPA galactosyl human serum albumin to predict postoperative residual liver function. Clin Nucl Med 1999;24:428–434

Index